International CLIMATE CHANGE ADAPTATION Initiative

Pacific Climate Change Science Program

Climate Change in the Pacific: Scientific Assessment and New Research

Volume 2: Country Reports

Australian Government

Australian AID

National Library of Australia Cataloguing-in-Publication entry

Climate change in the Pacific: scientific assessment and new research. Volume 2. Country reports / Australian Bureau of Meteorology, Commonwealth Scientific and Industrial Research Organisation.

ISBN: 9780643107137 (pbk.: Vol. 2)
ISBN: 9780643107144 (ebook: Vol. 2)

Includes index.

Climatic changes--Pacific Region.
Climate change mitigation--Pacific Region.

551.691823

This publication should be cited as:

Australian Bureau of Meteorology and CSIRO, 2011. Climate Change in the Pacific: Scientific Assessment and New Research. Volume 1: Regional Overview. Volume 2: Country Reports.

Contents

Abbreviations

CCAM	Conformal Cubic Atmospheric Model
CliCom	CLImate COMputing Project (of the World Meteorological Organization)
CliDE	Climate Data for the Environment
CMAP	Climate Prediction Centre Merged Analysis of Precipitation
CMIP3	Coupled Model Intercomparison Project (Phase 3)
CSIRO	Commonwealth Scientific and Industrial Research Organisation
ECMWF	European Centre for Medium-Range Weather Forecasts
EMI	ENSO Modoki Index
ENSO	El Niño-Southern Oscillation
GCM	Global Climate Model
GPCP	Global Precipitation Climatology Project
IOD	Indian Ocean Dipole
IPCC	Intergovernmental Panel on Climate Change
IPO	Interdecadal Pacific Oscillation
ITCZ	Intertropical Convergence Zone
MJO	Madden Julian Oscillation
NMS	National Meteorological Services
PCCSP	Pacific Climate Change Science Program
PDO	Pacific Decadal Oscillation
SAM	Southern Annular Mode
SPCZ	South Pacific Convergence Zone
SRES	Special Report on Emission Scenarios
TCLV	Tropical cyclone-like vortices
TRMM	Tropical Rainfall Measuring Mission
UNFCCC	United Nations Framework Convention on Climate Change
WMO	World Meteorological Organization
WPM	West Pacific Monsoon

Acknowledgements

This scientific assessment and new research has benefitted from the high degree of cooperation that exists between the implementing agencies: Australian Bureau of Meteorology and the Commonwealth Scientific and Industrial Research Organisation, other contributors from the region and beyond, and colleagues from our Partner Countries and regional/international organisations.

Authors

Coordinating Lead Author:
Jillian Rischbieth

Lead Authors: Simon McGree, Brad Murphy, Damien Irving, Jaclyn Brown

Contributing Authors: Deborah Abbs, Josephine Brown, Gillian Cambers, Belinda Campbell, Dev Capey, John Church, Dean Collins, Kevin Hennessy, Ron Hoeke, Andrew Lenton, Kathleen McInnes, Aurel Moise, Les Muir, Sarah Perkins, Skye Platten, Alexander Sen Gupta, Neil White, Xuebin Zhang

Chapter 2 (Cook Islands): Arona Ngari, Maarametua Vaiimene, David Maihia, Nitoro Bates, Pasha Carruthers

Chapter 3 (East Timor): Terencio Fernandes Moniz, Sebastião da Silva

Chapter 4 (Federated States of Micronesia): David Aranug, Johannes Berdon, Eden Skilling

Chapter 5 (Fiji): Alipate Waqaicelua, Areita B Daphne, Bipendra Prakash, Varanisese Vuniyayawa, Ravind Kumar

Chapter 6 (Kiribati): Ueneta Toorua, Tebwaau Tetabo Riibeta Abeta, Nakibae Teuatabo

Chapter 7 (Marshall Islands): Reginald White, Lee Z. Jacklick, Ned Lobwij

Chapter 8 (Nauru): Andrew Kaierua, Franklin Teimitsi, Douglas Audoa, Russ Kun

Chapter 9 (Niue): Rossylynn Pulehetoa-Mitiepo, Adorra Misikea, Felicia Pihigia Talagi

Chapter 10 (Palau): Maria Ngemaes, Dirutelchii Ngirengkoi, Godwin Sisior

Chapter 11 (Papua New Guinea): Kasis Inape, Maino Virobo

Chapter 12 (Samoa): Fata Lagomauitumua Sunny K. Seuseu, Tumau Faasaoina

Chapter 13 (Solomon Islands): David Hiriasia, Lloyd Tahani

Chapter 14 (Tonga): Ofa Fa'anunu, Mele Lakai

Chapter 15 (Tuvalu): Hilia Vavae, Kilateli Epu

Chapter 16 (Vanuatu): Salesa Kaniaha, Philip Malsale

Other contributors

Other contributors: John Clarke, Gillian Cook, Francois Delage, Timothy Erwin, Andrew Howard and Rod Hutchinson

All staff involved in the Pacific Climate Change Science Program

Sub-contractors: Geoscience Australia, Iowa State University, National Institute of Water and Atmospheric Research (New Zealand), University of Melbourne, University of New South Wales

The modelling groups, the Program for Climate Model Diagnosis and Intercomparison and the World Climate Research Programme's Working Group on Coupled Modelling for their roles in making available the World Climate Research Programme's CMIP3 multi-model dataset. Support of this dataset is provided by the Office of Science, U.S. Department of Energy

Regional and International Organisations: National Institute of Water and Atmospheric Research (New Zealand), National Oceanic and Atmospheric Administration (NOAA), Secretariat of the Pacific Regional Environment Programme (SPREP), Secretariat of the Pacific Community (SPC), United Nations Development Programme (UNDP), University of the South Pacific (USP)

Peer Review

Anthony Chen, University of the West Indies, Graeme Pearman, Graeme Pearman Consulting Pty Ltd

Other Reviewers

Australian Agency for International Development, Department of Climate Change and Energy Efficiency, John Clarke, Ian Cresswell, Peter May, Netatua Pelesikoti

Scientific Editors

Kevin Hennessy, Scott Power, Gillian Cambers

Volume Editors

Volume 1: Stephanie Baldwin, Jillian Rischbieth

Volume 2: Jillian Rischbieth

Other Editors

Karen Pearce (Bloom Communication), Whitehorne Communication and Design

Coordination

Stephanie Baldwin, Bernadette Barlow, Gillian Cambers, Gillian Cook, Dev Capey, Lily Frencham, Mandy Hopkins, Lucy Manne, Zarif Raman, Jillian Rischbieth

Design and Layout

Siobhan Duffy, Lea Crosswell, Carl Davies, Soussanith Nokham, Louise Bell

Funafuti Atoll, Tuvalu

Executive Summary

Introduction and Background

Islanders, especially in the Pacific region, have a strong relationship with the land and ocean so changes in climate can represent a threat not only to the physical environment but also to their culture and customs. Already, people living in Pacific Islands and East Timor are experiencing changes in their climate such as higher temperatures, shifts in rainfall patterns, changing frequencies of extreme events and rising sea levels. These changes are affecting peoples' lives and livelihoods, as well as important industries such as agriculture and tourism. In recognition of this, leaders of the Pacific Island Countries and Territories developed the Pacific Islands Framework for Action on Climate Change 2006-2015 to guide the building of resilience to the risks and impacts of climate change.

In 2008, the Australian Government launched the International Climate Change Adaptation Initiative to meet high priority adaptation needs of vulnerable countries within the Asia-Pacific region. Improved understanding of the physical climate system is required to inform effective adaptation and this is being addressed through a component of the International Climate Change Adaptation Initiative called the Pacific Climate Change Science Program (PCCSP). The PCCSP is a collaborative research partnership between Australian Government agencies, East Timor and 14 Pacific Island countries (Cook Islands, Federated States of Micronesia, Fiji, Kiribati, Marshall Islands, Nauru, Niue, Palau, Papua New Guinea, Samoa, Solomon Islands, Tonga, Tuvalu and Vanuatu), carried out in collaboration with regional and international organisations (Figure ES.1).

The Fourth Assessment Report of the Intergovernmental Panel on Climate Change (IPCC, 2007) identified significant research gaps which needed to be filled to better inform climate change adaptation and resilience building in small-island developing States. The report identified a number of information gaps and research priorities, noting in particular that many small islands lacked adequate observational data, and that output from global climate models was not of sufficiently fine resolution to provide specific information for islands. These regional and Partner Country climate change science needs formed the basis for the development of the research of the PCCSP.

The 15 Partner Countries are immensely diverse in terms of their history, geography, climate, natural resource base and culture. As part of the group of small island developing States, they share many similar sustainable development challenges such as small populations, limited resources, remoteness, susceptibility to natural disasters, vulnerability to external shocks and dependence on international trade.

Guided by the Australian Agency for International Development and the Australian Department of Climate Change and Energy Efficiency, the PCCSP is delivered by the Australian Bureau of Meteorology and the Commonwealth Scientific and Industrial Research Organisation, through their research partnership in the Centre for Australian Weather and Climate Research. The PCCSP's objectives are to:

- Conduct a comprehensive climate change science research program aimed at providing in-depth information about past, present and future climate in Partner Countries.
- Build the capacity of Partner Countries' national meteorological services and scientific organisations to undertake scientific research.
- Disseminate the information to Partner Countries' stakeholders and other parties.

Climate is defined as the average weather over 30 years or more. In different chapters in this publication, different averaging periods, such as 20 years, are also used. Climate change is defined as a change in the state of the climate, identified by changes in the mean and/or the variability of its properties, and that persists for an extended period, typically decades or longer (IPCC, 2007).

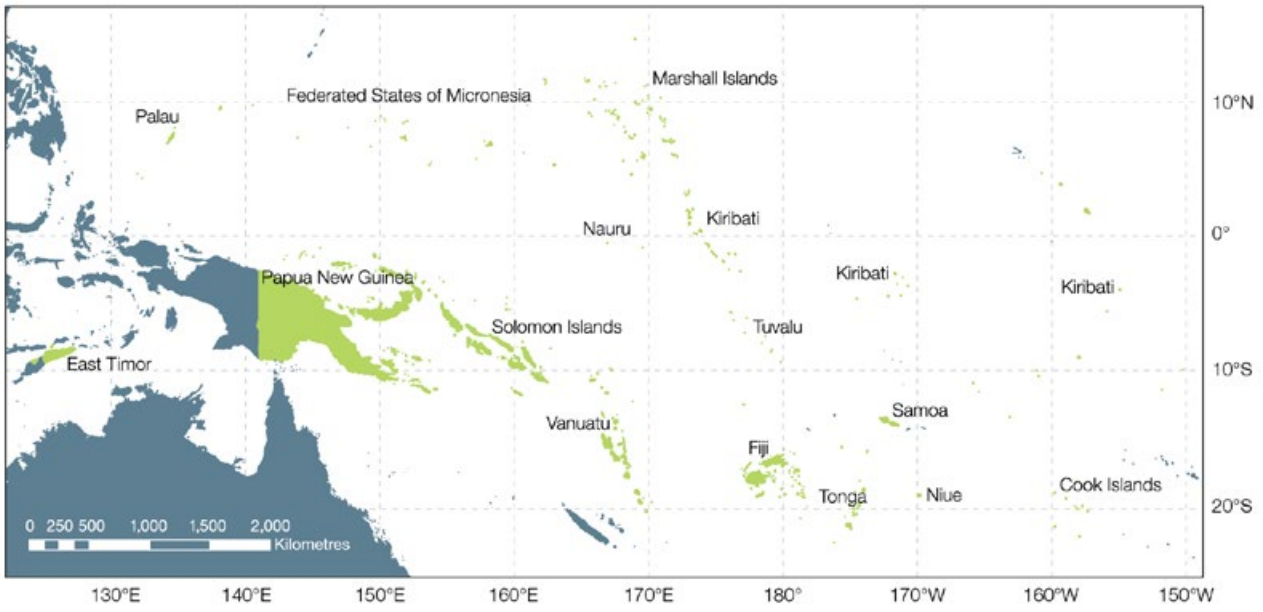

Figure ES.1: PCCSP region, defined by the coordinates: 25°S-20°N and 120°E-150°W (excluding the Australian region south of 10°S and west of 155°E), and Partner Countries: Cook Islands, East Timor, Federated States of Micronesia, Fiji, Kiribati, Marshall Islands, Nauru, Niue, Palau, Papua New Guinea, Samoa, Solomon Islands, Tonga, Tuvalu and Vanuatu

About this Publication

Building on the Fourth Assessment Report of the Intergovernmental Panel on Climate Change (IPCC, 2007), this publication draws on recent research conducted by the PCCSP as well as other research, such as the recently published 'Vulnerability of Tropical Pacific Fisheries and Aquaculture to Climate Change' (Bell et al., 2011). It is anticipated that this PCCSP publication and associated products and capacity-building activities will provide senior decision makers and other stakeholders in the Partner Countries, as well as the wider scientific community, with up-to-date, robust, climate change science information for the region and the individual countries.

This publication has two volumes. The first volume presents a detailed assessment and analysis of the PCCSP region encompassing latitudes 25°S-20°N and longitudes 120°E-150°W, excluding the Australian region south of 10°S and west of 155°E. Climate change reports for each Partner Country are presented in the second volume. Each of the 15 reports has four main sections which present and discuss (1) seasonal cycles, (2) climate variability, (3) observed annual trends, and (4) projections for atmospheric and oceanic variables. Projections are provided for temperature, rainfall, extreme events, (including tropical cyclones, extreme hot days and heavy rainfall days), sea-surface temperature, ocean acidification, and sea-level rise for three future 20-year periods centred on 2030, 2055 and 2090, and for three different scenarios of greenhouse gas and aerosol emissions: B1 (low), A1B (medium) and A2 (high).

Current Climate of the PCCSP Region

The PCCSP region is characterised by three extensive bands of large-scale wind convergence and associated rainfall: the Intertropical Convergence Zone (ITCZ), the South Pacific Convergence Zone (SPCZ) and the West Pacific Monsoon (WPM) (Figure ES.2).

The ITCZ lies just north of the equator and influences climate in the Federated States of Micronesia, Kiribati, Marshall Islands, Nauru, Palau and Papua New Guinea. These same countries, together with East Timor, also experience very high seasonal rainfall variations associated with the WPM, although in Nauru and the Marshall Islands this only occurs in some years.

The SPCZ has a significant impact on most of the Partner Countries in the South Pacific: Cook Islands, Fiji, Nauru, Niue, Samoa, Solomon Islands, Tonga, Tuvalu and Vanuatu; and Kiribati in some years.

Many of the Partner Countries experience marked seasonal rainfall variations, but little variation in temperature. However, they may experience extreme events including tropical cyclones, storm surges, heat waves, drought and heavy rainfall. Tropical cyclones produce damaging winds, heavy rainfall and storm surges which can have devastating impacts.

Large-scale atmospheric circulation patterns influence ocean currents and sea-surface temperature patterns, while the ocean in turn also affects atmospheric winds, temperatures and rainfall. For example, the equatorial trade winds push warm water to the west, giving rise to the Warm Pool, and drive the upwelling of cooler water in the eastern Pacific; while the warmer water near the equator and the Warm Pool in particular, drive strong convection in the overlying atmosphere which helps to draw the trade winds across the Pacific Ocean.

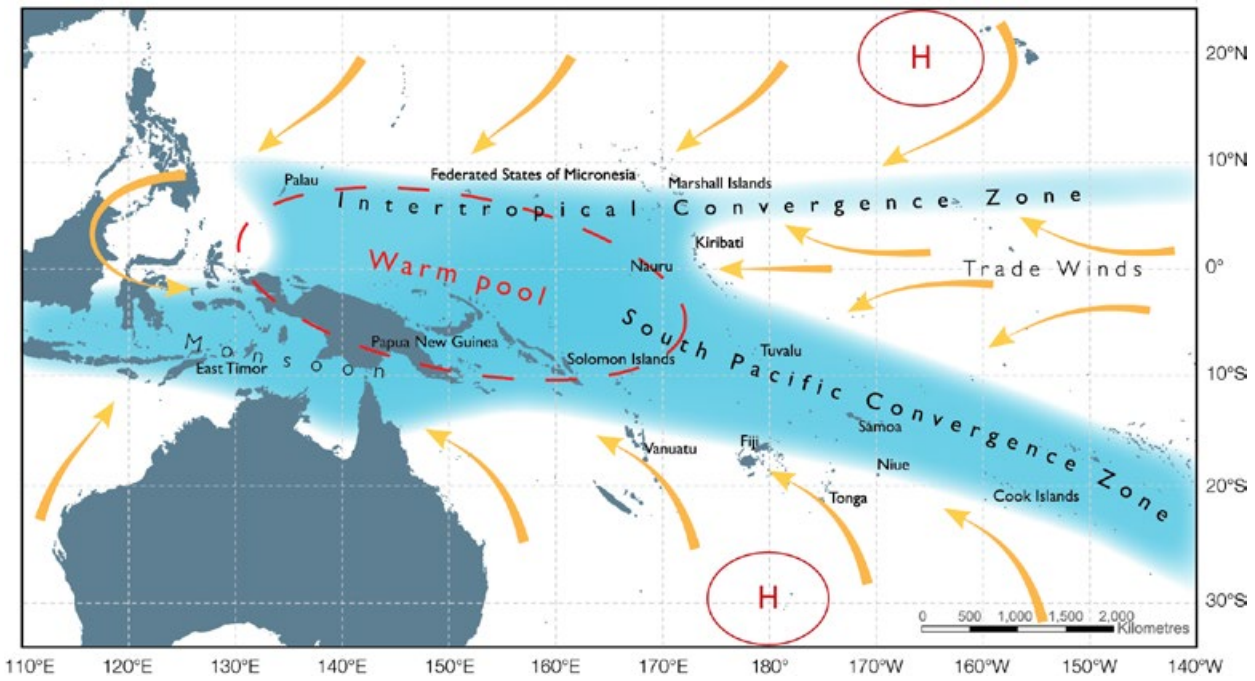

Figure ES.2: The average positions of the major climate features of the PCCSP region in November to April. The yellow arrows show near surface winds, the blue shading represents the bands of rainfall (convergence zones with relatively low pressure), and the red dashed oval indicates the West Pacific Warm Pool. H represents the typical positions of moving high pressure systems.

Climate Variability and Trends

Climate variability in the PCCSP region occurs on a wide range of time scales. Palaeoclimatic records indicate that during the millennia before the Industrial Revolution (around 1750), the climate of the Pacific underwent large variations, primarily associated with changes in the intensity and frequency of the El Niño-Southern Oscillation (ENSO). These climate shifts were driven by natural mechanisms, whereas some of the changes observed over the past decades are also partially driven by human influences. Consequently, it is important to understand the range of climate variability experienced in the past in order to provide a context in which to interpret projections of future climate change.

The major pattern of climate variability in the PCCSP region is ENSO. This is a coupled atmosphere-ocean phenomenon, with time scales of about two to seven years. The term El Niño is identified with a basin-wide warming of the tropical Pacific Ocean east of the dateline. The term La Niña is a basin-wide cooling of the tropical Pacific Ocean east of the dateline. This event is associated with a fluctuation of a global-scale tropical and sub-tropical pressure pattern called the Southern Oscillation.

ENSO is strongly linked with variations in climatic features such as the ITCZ, the SPCZ and the WPM. During El Niño events the SPCZ tends to shift towards the north-east, while the ITCZ tends to shift closer to the equator. These shifts have a profound influence on rainfall, sea level and the risk of tropical cyclones in the region. All PCCSP Partner Countries are affected by ENSO in some way, although the magnitude and timing of this influence varies.

As well as ENSO there are other natural patterns of climate variability that influence the region, including the Interdecadal Pacific Oscillation and the closely related Pacific Decadal Oscillation.

The climate trends for the PCCSP region that are presented in this publication are based on updated and improved climate datasets. This work has involved significant collaboration with Partner Country meteorological services and has resulted in improved data access and security, and enhanced scientific and technical capacity in the region.

All updated temperature records from Pacific Island observation stations show warming over the past 50 years, with trends mostly between 0.08 to 0.20°C per decade, consistent with global warming over this time. Unlike temperature, rainfall across the Pacific Islands displays large year-to-year and decade-to-decade changes in response to natural climate variability. Over the past 50 years, rainfall has increased north-east of the SPCZ, and declined to the south.

Over the 1981-2007 period of satellite measurement there are no significant trends in the overall number of tropical cyclones, or in the number of intense tropical cyclones, in the South Pacific Ocean. However, this is a short period of time for the analysis of infrequent extreme events such as tropical cyclones. Determining trends over longer periods is difficult due to the lack of adequate data prior to satellite measurements.

Sea-surface temperatures of the Pacific Ocean have generally increased since 1950. In addition, the western tropical Pacific Ocean has become significantly less salty, while regions to the east have generally become saltier. In combination, these changes have driven an increase in the stratification of the upper ocean in this region.

A distinctive pattern of intensified warming of surface waters and cooling of sub-surface equatorial waters centred near a depth of 200 m is also apparent over the past 50 years in the Pacific Ocean. These patterns of observed change in the ocean are reproduced in climate model simulations that include increased atmospheric greenhouse gases.

Sea level has been rising globally including in the PCCSP region over recent decades. Extreme high sea levels are also increasing, primarily as a result of increases in mean sea level. There is significant interannual variability of sea level in the region related to ENSO and other natural variability.

As a consequence of higher carbon dioxide (CO_2) concentrations in the atmosphere, the oceans are absorbing more CO_2. The CO_2 taken up by the ocean reacts in water and causes a decrease in the pH of the seawater that is referred to as ocean acidification. Acidification is accompanied by a decrease in the seawater saturation state of carbonate minerals that are secreted as shells and skeletal material by many key species in reef ecosystems. Aragonite is the form of calcium carbonate precipitated by reef building corals and studies have shown that coral growth declines as the aragonite saturation state of seawater decreases.

Aragonite saturation states above a value of 4 are considered optimal for coral growth and for the development of healthy reef ecosystems. Throughout most of the sub-tropical and tropical Pacific Island region, the saturation state in pre-industrial times exceeded 4. By the mid 1990s, the uptake of anthropogenic CO_2 had resulted in a widespread decline in the aragonite saturation state.

Climate Modelling

The complexity of the climate system means that past trends cannot be simply extrapolated to forecast future conditions. Instead, mathematical representations of the Earth's climate system, based on the laws of physics, are used to simulate the fundamental processes affecting weather and climate. Global climate models calculate variables such as temperature and rainfall at points over the globe spaced 100–400 km apart, with about 30 layers in the ocean and 30 layers in the atmosphere. They are run on supercomputers and have been used extensively over recent decades to not only estimate future climate change, but also to help better understand the present and past climate.

Emissions of greenhouse gases and aerosols have played a major role in the climate of the past century. In order to make future climate projections, it is necessary to make plausible estimates of how these emissions will evolve into the future. To assist in modelling the future climate, the IPCC has prepared 40 greenhouse gas and sulphate aerosol emissions scenarios for the 21st century that combine a variety of plausible assumptions about demographic, economic and technological factors likely to influence future emissions. Such estimates can then be put into climate models to provide projections of future climate change. Climate model projections in this publication are based on three of the most widely used emissions scenarios, B1 (low), A1B (medium) and A2 (high).

Performance of Climate Models

To make projections of future climate, it first has to be demonstrated that climate models are sufficiently realistic in simulating the observed climate. This depends on the model's ability to represent several different aspects of climate, including:

- The long-term average pattern of various atmospheric and oceanic characteristics, e.g. temperature, rainfall, wind, salinity and sea level.
- Important regional climate features, e.g. ITCZ, SPCZ and WPM.
- Major patterns of climate variability on various timescales, e.g. ENSO.
- Extreme weather events, e.g. heat waves, tropical cyclones.
- Long-term trends.

How well the models agree with the observed present climate is used to assess model reliability, with the underlying assumption that a model which adequately simulates the present climate will provide more reliable projections of the future. No single model is the 'best' in representing all aspects of climate so a range of models should be considered when making projections of future climate.

After analysing data from 24 global climate models from around the world, the PCCSP identified a set of 18 models which provide a reasonable representation of observed climate over the PCCSP region. These 18 models were used to construct projections of future climate for the PCCSP region and the individual Partner Countries.

These 18 global climate models can simulate many aspects of climate, and generally give a reasonable representation of climate in the Pacific region. Most models, however, show biases, such as a tendency to underestimate sea-surface temperatures and rainfall along the equator. The representation of ENSO in climate models has improved over the years but remains a challenge at the regional scale. For example, sea-surface temperature variability associated with ENSO tends to be too narrowly focused on the equator and extends too far to the west.

Global climate models do not have sufficiently fine resolution to represent small islands and important small-scale climate processes. Downscaling techniques are used to represent important small island effects, however, these techniques are very computer intensive.

Global Climate Model Projections

The IPCC Fourth Assessment Report (2007) presents broad-scale projections for the Pacific. Annual-mean temperature and rainfall projections are averaged over two large Pacific regions (the North Pacific and the South Pacific), for three 30-year periods (2010–2039, 2040–2069 and 2070–2099), based on results from seven global climate models and four emissions scenarios.

The PCCSP provides a more detailed set of climate change projections, building on the IPCC assessment. The projections for the PCCSP region are based on simulations from up to 18 global climate models for three emissions scenarios; B1 (low), A1B (medium) and A2 (high), and three future 20-year periods centred on 2030, 2055 and 2090, relative to a 20-year period centred on 1990. The selection of years and emissions scenarios is limited by data availability.

A summary of the key climate projections for the PCCSP region is outlined on the following pages. Volume 2 of this publication provides detailed discussion on the range of possible futures simulated for each country.

Projected Changes in Major Climate Features and Patterns of Variability

South Pacific Convergence Zone

In the wet season (November-April), the SPCZ is not expected to shift position, but there is some evidence for a projected equatorward shift in the dry season (May-October). Increased rainfall is projected within the SPCZ in the wet season in particular, due to increased atmospheric moisture content in a warmer climate. Many models also suggest that islands located near the eastern edge of the SPCZ will become drier in the wet season as the trade winds in the south-east Pacific become stronger.

Intertropical Convergence Zone

Changes in rainfall averaged over the ITCZ show a general increase in June-August, with little change in December-February, thereby amplifying the current seasonal cycle. There is an increase in the area of the ITCZ in all models in June-August, and in all but three in December-February. Models suggest the ITCZ may shift equatorward in March-May and June-August, although displacement is small.

West Pacific Monsoon

There is a general tendency for rainfall to increase in the WPM region throughout the year, but with an amplification of the seasonal cycle of rainfall. There is no significant projected change in the east-west winds over the region.

El Niño-Southern Oscillation

Year-to-year variability in the region will continue to be strongly affected by ENSO. However, climate models do not provide consistent projections of changes in the frequency, intensity and patterns of future El Niño and La Niña events. As climate changes, however, aspects of climate experienced in some regions during El Niño and La Niña events may differ from the past. For example, if El Niño tends to warm a particular region now, then temperatures experienced during future El Niño events may tend to be higher than those experienced during past El Niño events.

Indian Ocean Dipole

The IOD influences climate both locally and in remote regions, mainly affecting East Timor. It also affects the Indian and Australian monsoons, however, the IOD is a much weaker source of climate variability for the Pacific region than ENSO. Climate models suggest that a more positive IOD mean state will exist with easterly wind trends and a shallowing thermocline (a zone in the ocean separating warm surface waters from cold deep waters) over the eastern Indian Ocean, associated with a weakening of the Walker Circulation.

Atmospheric Projections

Temperature

The magnitude of the projected warming over the PCCSP region is about 70% as large as the magnitude of global average warming for all emissions scenarios. This is linked to the fact that the oceans have been warming, and are projected to warm into the future at a lower rate than land areas. As the PCCSP region is dominated by the ocean, it follows that temperature increases in the region will be less than those seen globally. The projections centred on the three 20-year periods (relative to 1990 baseline temperatures) show that:

- By **2030**, the projected regional warming is around +0.5 to 1.0°C, regardless of the emissions scenario.
- By **2055**, the warming is generally +1.0 to 1.5°C with regional differences depending on the emissions scenario.
- By **2090**, the warming is around:
  - +1.5 to 2.0°C for B1 (low emissions scenario).
  - +2.0 to 2.5°C for A1B (medium emissions scenario).
  - +2.5 to 3.0°C for A2 (high emissions scenario) (Figure ES.3).

Large increases in the incidence of extremely hot days and warm nights are also projected.

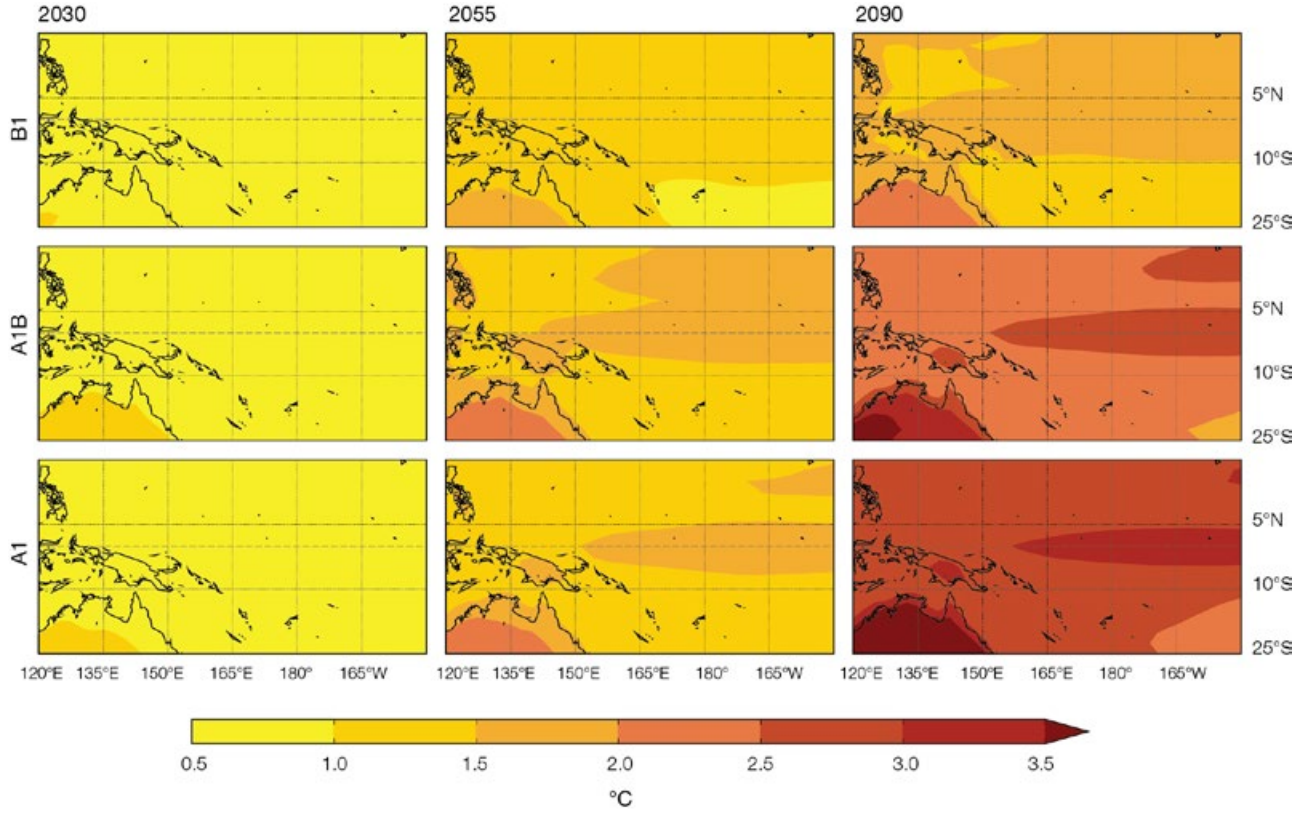

Figure ES.3: Projected multi-model mean changes in annual mean surface air temperature for 2030, 2055 and 2090, relative to 1990, under the A2 (high), A1B (medium) and B1 (low) emissions scenarios. All models agree on warming in all locations.

Rainfall

In the PCCSP region, increases in annual mean rainfall are projected to be most prominent near the SPCZ and ITCZ, with little change in the remainder of the region (Figure ES.4). The annual numbers of rain days (over 1 mm), light rain days (10–10 mm) and moderate rain days (10–20 mm) are projected to increase near the equator, with little change elsewhere in the region. There is a widespread increase in the number of heavy rain days (20–50 mm). Extreme rainfall events that currently occur once every 20 years on average are generally simulated to occur four times per 20-year period, on average, by 2055 and seven times per 20-year period, on average, by 2090 under the A2 (high) scenario. Droughts are projected to occur less often.

Potential Evapotranspiration

Evapotranspiration is the sum of evaporation and plant transpiration from the Earth's land surface to the atmosphere. Potential evapotranspiration is a reflection of the energy available to evaporate water, and of the wind available to transport the water vapour from the ground up into the lower atmosphere. Potential evapotranspiration is highest in hot, sunny, dry (arid), and windy conditions. Increases in potential evapotranspiration are expected in the PCCSP region.

The ratio of annual average rainfall to potential evapotranspiration is a measure of aridity. Aridity increases in most, but not all, of the PCCSP region (i.e. the projected increase in potential evapotranspiration is not being matched by sufficient increases in rainfall).

Humidity and Solar Radiation

Projected changes in humidity and solar radiation are relatively small in the PCCSP region, i.e. less than 5% by 2090.

Wind

Surface wind speed is generally expected to decrease in the equatorial and northern parts of the PCCSP region, while increases are indicated in the south. However these changes are projected to be relatively small in most locations.

Ocean Projections

Salinity and Stratification

Sea-surface salinity is expected to decrease, with regional differences closely matching projected changes in net rainfall (rainfall minus evaporation). The intensified warming and freshening at the surface is projected to make the surface ocean less dense compared to the deep ocean, so the ocean becomes more stratified. This increase in stratification acts to inhibit mixing, thereby reducing the supply of nutrients from the deep to the surface ocean. This has consequences for biological productivity, particularly fisheries.

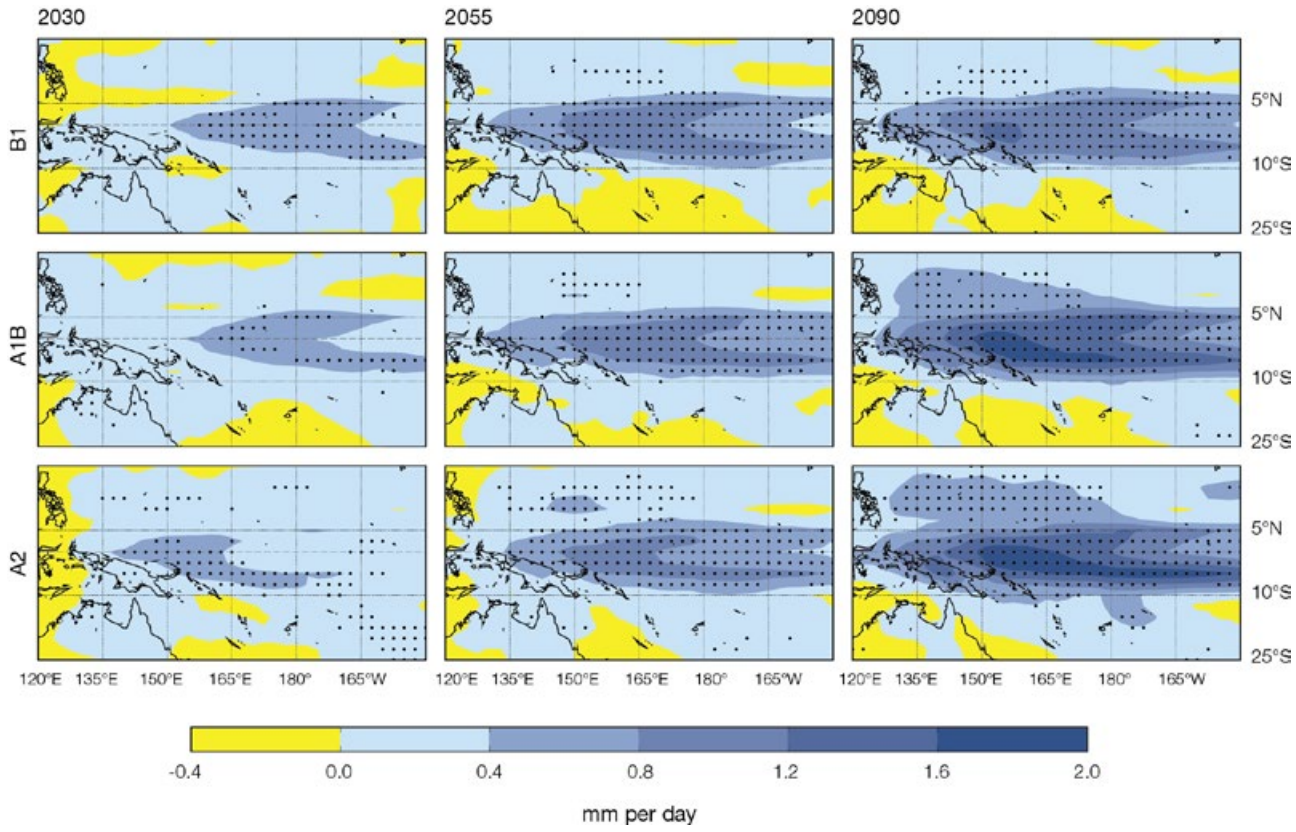

Figure ES.4: Projected multi-model mean changes in annual rainfall (mm/day) for 2030, 2055 and 2090, relative to 1990, under the A2 (high), A1B (medium) and B1 (low) emissions scenarios. Regions where at least 80% of models agree on the direction of change are stippled.

Sea Level

Global climate models reproduce the observed pattern of the regional distribution of sea level reasonably well. Models indicate that the rise will not be geographically uniform. However, deviations between models make regional estimates uncertain (Figure ES.5). In current projections, the sea-level rise in the PCCSP region is similar to the global average.

Projections of sea-level rise require consideration of ocean thermal expansion, the melting of glaciers and ice caps, the surface mass balance and dynamic response of the ice sheets of Antarctica and Greenland, and changes in terrestrial water storage. Current projections indicate sea levels are expected to continue to rise, on average, during this century. The Fourth Assessment Report of the IPCC (IPCC, 2007) states that global average sea level is projected to rise by 0.18 to 0.59 m by 2080-2099, relative to 1980-1999, with an additional potential contribution from the dynamic response of the ice sheets. By scaling to global temperature changes this additional rise was estimated to be 10 to 20 cm but larger increases could not be ruled out. Observations indicate sea level is currently rising at near the upper end of the projected range. Larger rises than in the IPCC projections have been argued by some but one recent study suggests that global-mean sea-level rise greater than 2 m by 2100 is physically untenable and that a more plausible estimate is about 80 cm, consistent with the upper end of the IPCC estimates and the present rate of rise. However, improved understanding of the processes responsible for ice sheet changes are urgently required to improve estimates of the rate and timing of 21st century and longer-term sea-level rise.

Ocean Acidification

The projected growth in atmospheric CO_2 concentration is expected to cause further ocean acidification. Aragonite saturation values below 3.5 are projected to become more widespread and have the potential to disrupt the health and sustainability of reef ecosystems. The lowest values of aragonite saturation in the region of the Partner Countries are projected to occur in the eastern equatorial Pacific, to the east of longitude 160°W, affecting the easternmost islands of Kiribati, with the highest values in the region of the South Equatorial Current, affecting the islands of Cook Islands, Samoa and Tuvalu.

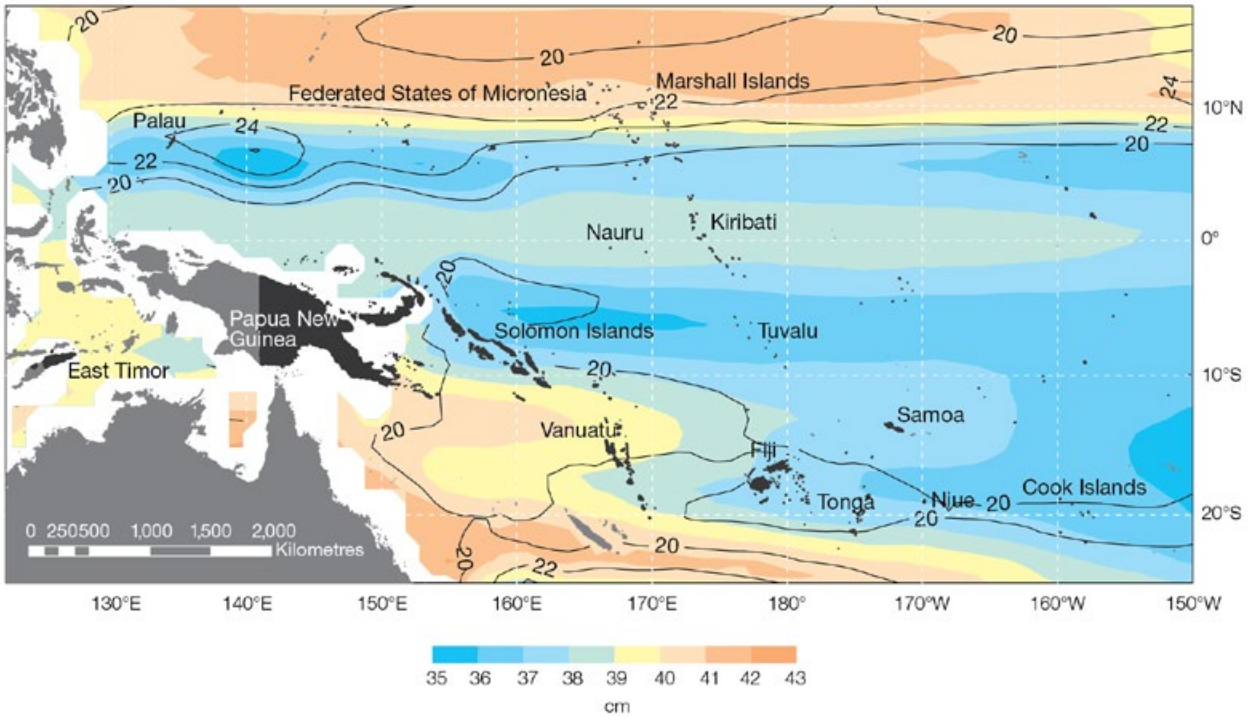

Figure ES.5: Sea-level rise projections for the A1B (medium) emissions scenario in the PCCSP region for 2081-2100 relative to 1981-2000 are indicated by the shading with the uncertainty indicated by the contours (in centimetres). The distribution of the projections of sea-level change is estimated by combining the global average sea-level projections, the dynamic ocean departure from the global average and the regional changes associated with the changing ice-mass distribution. Note that white areas indicate no model data are available for that area.

Downscaled Projections

Dynamical and statistical downscaling techniques were used to provide small-scale (i.e. country-scale and/or individual island-scale) climate projections. The output from six global climate models was downscaled to 60 km over the PCCSP region, and to 8 km for selected islands. The 60 km downscaled projections are broadly consistent with those of the global climate models, however, some differences are noted such as bands of rainfall decrease around latitudes 8°N and 8°S.

The 8 km downscaled projections complement the projections from the global climate models and show regional variations of the climate change signal, largely related to the topography of the islands where significant changes in elevation exist.

Tropical Cyclone Projections

It is difficult to make projections of tropical cyclone activity for two reasons. First, the features of a tropical cyclone occur at a smaller spatial scale than can be represented by most climate models. Second, climate models vary in their ability to simulate large-scale environmental conditions that are known to influence tropical cyclones including patterns of variability such as ENSO and large-scale climate features such as the SPCZ.

Three methods were used by the PCCSP to diagnose tropical cyclones from global climate models. While large uncertainty still remains, the results from this study indicate that the frequency of tropical cyclones in the PCCSP region is projected to decrease by the late 21st century. There is a moderate level of confidence in this direction of change, however, there is little consistency in the magnitude of changes between either the models or the analysis methods.

For the Partner Countries in the south Pacific sub-basins (latitudes 0-35ºS; longitudes 130°E-130ºW), most models indicate a decrease in the frequency of tropical cyclones by the late 21st century and an increase in the proportion of more intense storms. For the Partner Countries in the North Pacific sub-basin (latitudes 0-15ºN; longitudes 130º-180ºE), there is a decrease in the frequency of tropical cyclones and a decrease in the proportion of more intense storms. This decrease in occurrence is more robust in the Southern Hemisphere than in the Northern Hemisphere, and may be due to a combination of increased vertical wind shear in the Southern Hemisphere, and changes in the thermodynamic characteristics of the atmosphere which are associated with tropical storm activity and intensity.

Uncertainties in Climate Model Projections

While climate models are all based on the same physical laws, they are not perfect representations of the real world. As such, there will always be a range of uncertainty in climate projections. The existence of uncertainty is common to all areas of science and does not negate the usefulness of model projections. Uncertainty exists in the projections provided in this publication and it is expected to exist for future projections, so reducing and achieving greater clarity on the uncertainties is still required. It is important that this uncertainty is understood and incorporated into any future impact assessments based on climate model projections. Box ES.1 summarises key uncertainties associated with climate projections (IPCC, 2007).

Box ES.1: Climate Projection Uncertainties

- Since it is uncertain how society will evolve over this century, it is not possible to know exactly how anthropogenic emissions of greenhouse gases and aerosols will change. Each of the 40 emissions scenarios produced by the IPCC is considered plausible, with the range of uncertainty increasing over the 21st century. Subtle differences between models associated with the representation of key physical processes result in a range of climate projections for a given emissions scenario.
- Models differ in their estimates of the strength of different feedbacks in the climate system, particularly cloud feedbacks, oceanic heat uptake and carbon cycle feedbacks.
- Direct and indirect aerosol impacts on the magnitude of the temperature response, on clouds and on precipitation remain uncertain.
- Future changes in the Greenland and Antarctic ice sheet mass are a major source of uncertainty that affect sea-level rise projections.
- Confidence in projections is higher for some variables (e.g. temperature) than for others (e.g. precipitation), and it is higher for larger spatial scales and longer averaging periods. Conversely, confidence is lower for smaller spatial scales, which represents a particular challenge for projections for Partner Countries in the PCCSP region.
- Some of the most difficult aspects of understanding and projecting changes in regional climate relate to possible changes in the circulation of the atmosphere and oceans, and their patterns of variability.
- When interpreting projected changes in the mean climate, it is important to remember that natural climate variability (e.g. the state of ENSO) will be superimposed and can cause conditions to vary substantially from the long-term mean from one year to the next, and sometimes from one decade to the next.
- It is not currently possible to determine if downscaled projections provide more reliable future climate projections than those from the coarser resolution global models. For this reason, dynamically downscaled projections can provide complementary information, but should be interpreted in conjunction with global climate models over the same region.

Future Research to Advance Climate Science in the PCCSP Region

Better understanding the past climate helps to inform more robust projections of future climate which are essential for underpinning climate change adaptation strategies and contributing to the sustainable development of the Partner Countries.

While there has been excellent progress on many fronts to monitor, document, understand and project climate change relevant to Partner Countries, there are still many challenges. Further work to strengthen the scientific understanding of climate change is required to inform adaptation and mitigation. The following areas have been identified as priorities.

The geographical spread of Partner Countries means that the land- and ocean-based climate observation network in the PCCSP region is sparse. Expanding atmospheric data measurements in the PCCSP region will strengthen the ability of Partner Countries to monitor climate. Enhancing and, in some cases, creating oceanic observation networks is equally important. The rescue and rehabilitation of historical climate data is also needed to extend the climate data record in the PCCSP region. Further analysis of palaeoclimate data will enhance the understanding of climate variability on a wide variety of time scales.

A better understanding of the state of climate features in the PCCSP region, including the SPCZ, ITCZ and WPM, and patterns of variability in the climate, including ENSO, is needed to advance climate science. Determining the extent to which climate trends are attributable to natural variability and to human activities is also a priority. Greater clarity on these issues and more reliable estimates of past variability in the atmosphere and the ocean, including extreme events, will help strengthen the credibility and communication of climate projections.

Analysing the ability of the next generation of climate models to simulate climate in the PCCSP region is essential. This will provide for improved projections for rainfall, extreme weather events, ENSO, sea level and ocean acidification, among other variables. Work needs to continue to improve the global climate models and to rigorously verify downscaling methods so as to provide finer resolution projections over smaller areas.

Sunshine recorder, Samoa Meteorology Division

Chapter 1
Introduction to the Country Reports

The first volume of Climate Change in the Pacific: Scientific Assessment and New Research provides a regional overview of climate change across the Pacific Climate Change Science Program (PCCSP) region, and includes annual and seasonal climatology, variability and long-term trends, methodology, climate model evaluation, and projected changes in atmospheric and oceanic variables from global and downscaled climate models.

This second and final volume contains individual reports for all 15 Partner Countries. The reports are largely based on the information contained in Volume 1, although some additional country-specific information is also presented. Chapters 2–16 all follow a similar format (Table 1.1) that starts with a brief introduction, a country description and summary of the current and future climate. This is followed by further details on data availability, seasonal cycles, climate variability, observed trends and climate projections.

The following sections provide information about the data sources, methodology and interpretation of country-specific detail provided in Chapters 2–16. It is important background information for understanding the country reports.

Table 1.1: Format for each country chapter

Chapter subsection	Subject	Content
	Introduction	Chapter outline
1	Climate summary	Summary of the current climate and climate trends including temperature, rainfall, sea-level rise, and extreme events, and future climate projections for temperature, rainfall, tropical cyclones, ocean acidification and sea-level rise.
2	Country description	Details of country location, size, population and major geographical features.
3	Data availability	Information about observation networks, data records and data availability.
4	Seasonal cycles	Average rainfall, maximum, minimum and mean air temperatures and the influence of large scale climate features such as the South Pacific Convergence Zone.
5	Climate variability	Influence of patterns of variability, such as the El Niño-Southern Oscillation, and analysis of indices characterising their impact.
6	Observed trends	Analysis of observed climate and trends for temperature, rainfall, extreme events, sea-surface temperature, ocean acidification, mean sea level, extreme sea-level events.
7	Climate projections	Analysis of projections for temperature, rainfall, extreme events, ocean acidification and sea level, followed by a projection summary. Climate projections for these climatic variables are based on up to 18 CMIP3 global climate models (Volume 1, Section 5.5.1 and Appendix 1).

1.1 Climate Summary

This section provides summaries of the current observed climate and projected future climate for each country.

1.2 Country Description

This section provides details of country location, size, population and major geographical features.

1.3 Data Availability

This section provides information about the observation network and data record availability in each country. The length, completeness and quality of historical data records differ from country to country. For many observing sites there have been changes in station position, instrumentation and local environment that have produced artificial changes (inhomogeneities) in the data over time. Where possible, these inhomogeneities have been identified for rainfall and temperature and corrected using statistical techniques.

Monthly-averaged in situ sea-level data (tide gauge data) are available through international archives (e.g. Permanent Service for Mean Sea Level at http://www.psmsl.org/ and Australia's National Tidal Centre at http://www.bom.gov.au/oceanography/projects/spslcmp/spslcmp.shtml). Satellite-altimeter data are available from 1993 to the present from National Aeronautics and Space Administration (NASA) and Centre National d'Etudes Spaciales (CNES). Both satellite (from 1993) and in situ sea-level data (1950–2009) on a regular grid are available from CSIRO. Figure 1.1 shows all the climate observation sites and tide gauges used.

Long-term locally-monitored sea-surface temperature data are unavailable for the this region. As a result large-scale sea-surface temperature (SST) gridded datasets have been used. A gridded data set is a set of climate data that are given for the same time or average period on a regular grid in space. This gives a complete coverage of a particular region (or the whole globe) at regularly spaced points. Data at each grid point represent the average value over a grid box, of which the size is determined by the spacing between the grid points.

Figures in the seasonal cycles section of each chapter show the seasonal variation of the key meteorological factors (1950–2000) from the HadISST dataset. Figures in the climate projections section of each chapter show the 1950–2000 sea-surface changes (relative to a reference year of 1990) from three large-scale, sea-surface temperature gridded datasets (HadSST2, ERSST and Kaplan Extended SST V2; Volume 1, Table 2.3).

1.4 Seasonal Cycles

Total rainfall and average daily maximum, minimum and mean air temperatures for each month of the year are discussed in this section, along with the influence of large-scale features of the climate system. The three main climate features in the PCCSP region are:

West Pacific Monsoon

The West Pacific Monsoon (WPM) refers to the seasonal switch from easterly winds to westerly winds and the onset of very wet conditions. It moves north to mainland Asia during the Northern Hemisphere summer and south to Australia in the Southern Hemisphere summer. It affects countries in the far western Pacific and the Maritime Continent.

Intertropical Convergence Zone

The Intertropical Convergence Zone (ITCZ) is a band of high rainfall stretching across the Pacific just north of the equator and is strongest in the Northern Hemisphere summer. It affects most countries on, or north of, the equator.

South Pacific Convergence Zone

The South Pacific Convergence Zone (SPCZ) is a band of high rainfall that stretches approximately from the Solomon Islands to east of the Cook Islands. It is strongest in the Southern Hemisphere summer and affects most countries in the South Pacific.

For most countries two sites are discussed to reflect regional climate differences, except where data are only available for one site or the country is small, e.g. Niue and Nauru. It is recognised that in other cases two sites may not adequately represent the whole country, e.g. Papua New Guinea and Kiribati, and in future research, additional sites should be included particularly for these countries. The monthly average sea-surface temperature is also included, showing its influence on seasonal air temperature variations.

Climate averages for the period 1961–1990 are used, unless otherwise specified. For example, other longer periods may be used if there is a longer complete data record.

1.5 Climate Variability

The patterns of climate variability that result in changes from one year to the next are discussed in this section. Indices that monitor these patterns of climate variability are used to determine their influence on temperature and rainfall at sites in each Partner Country. These influences are determined by calculating the strength of the relationship (correlation coefficients) between the indices and temperature and rainfall. The standard indices used are explained in Section 1.5.1.

1.5.1 Climate Indices

El Niño-Southern Oscillation Indices

Year-to-year variations in the climate of all Partner Countries are influenced by the El Niño-Southern Oscillation (ENSO). ENSO events involve basin-wide changes of the tropical Pacific Ocean temperatures. These oceanic events are associated with a fluctuation of a global-scale tropical and sub-tropical surface pressure pattern called the Southern Oscillation. El Niño is the warm phase of the El Niño-Southern Oscillation, while La Niña is the cold phase. It also has a neutral phase. The typical pattern in an El Niño is warming of the ocean east of the International Date Line. This is known as a Canonical El Niño. A variation of El Niño with warming centred near the International Date Line is known as El Niño Modoki. For some regions the impacts of these two types of El Niño events differ. Indices used to monitor the phases of ENSO are:

Niño3.4

One of three indices used to describe ENSO, the Niño3.4 index is the average sea-surface temperature anomaly in the central Pacific (5°N–5°S, 170°W–120°W), as determined using the HadISST dataset (Volume 1, Section 2.2.2; Rayner et al., 2003).

Southern Oscillation Index

Also used to describe ENSO, the Southern Oscillation Index (SOI) is based on the mean sea level pressure difference between Tahiti and Darwin, using data from the Australian Bureau of Meteorology (Troup, 1965).

ENSO Modoki Index

The ENSO Modoki Index (EMI) represents variations in a type of ENSO that is focused more in the western Pacific than canonical ENSO (which is more in the eastern Pacific). Like Niño3.4, the EMI is an average sea-surface temperature anomaly, but over three areas: (A) 10ºN–10ºS, 165ºE–140ºW, (B) 5ºN–15ºS, 110ºW–70ºW and (C) 20ºN–10ºS, 125ºE– 145ºE. The EMI = A–0.5*B– 0.5*C. The EMI is calculated using the HadISST dataset.

Interdecadal Pacific Oscillation Index

The Interdecadal Pacific Oscillation (IPO) is a multi-decadal ENSO-like oscillation in the ocean and atmosphere centred in the Pacific (Volume 1, Section 3.4.2) which affects climate in the South Pacific, the North Pacific, and Australasia and beyond (Power et al., 1999; Folland et al., 1999; Parker et al., 2007). The Pacific Decadal Oscillation can be regarded as the North Pacific manifestation of the IPO. Data for the IPO index were provided by the UK Meteorological Office. The data are based on the analysis method described by Parker et al. (2007).

Indian Ocean Dipole Index

The Indian Ocean Dipole (IOD) is a pattern of interannual variability in sea-surface temperatures in the Indian Ocean (Volume 1, Section 3.4.8). It usually features opposite changes in temperatures from normal conditions in the western and eastern tropical Indian Ocean. The IOD index measures the difference in sea-surface temperatures between the western tropical Indian Ocean (50°E–70°E and 10°S–10°N) and the eastern tropical Indian Ocean (90°E–110°E and 10°S–0°S). Averages over each of these regions are the monthly-mean anomalies in sea-surface temperature. Thus, a positive IOD event is when the western Indian Ocean is warmer than normal and/or the eastern Indian Ocean is cooler than normal.

Southern Annual Mode Index

The Southern Annular Mode (SAM) is the major mode of atmospheric variability in the southern extra-tropics (Volume 1, Section 2.4.4). It features a north-south shift in the mid-latitude westerly winds and an oscillation in mass and pressure between the mid and high latitudes. The SAM is represented by an index measuring the difference in surface pressure between 50ºS–65ºS. A positive SAM index corresponds to a southward movement and intensification of the extra-tropical westerly winds. Data are from the British Antarctic Survey (Marshall, 2003).

1.5.2 Calculating Relationships between Indices and Climate Variables

The correlation coefficient is a measure of how well year-to-year variations in a climate variable (e.g. rainfall) match the year-to-year variations in the index (e.g. the SOI). The closer the correlation is to 1 or -1, the stronger the relationship. A positive correlation coefficient indicates that the two variables tend to increase or decrease in the same direction together. A negative correlation coefficient indicates that one variable will tend to increase while the other decreases. A correlation near zero means the climate variable and the index do not vary together in any consistent way and therefore are not (linearly) related. Correlations are calculated for wet and dry seasons (usually November-April and May-October) or the reverse in the Northern Hemisphere countries. The statistical significance of correlation coefficients is assessed using the method described by Power et al. (1998), which takes persistence into account.

In this analysis the relationship of interest is between interannual variations in indices and climate variables. However, if there are strong linear trends in the time series of some indices and climate variables this may also result in a significant correlation coefficient between them. Therefore, linear trends have been removed from all data before calculating the correlation coefficients.

The SAM is directly affected by ENSO, and so correlation coefficients between climate variables and the SAM index may simply be relating the ENSO relationship to the variable via the SAM. Thus the partial correlation coefficient between the variables and the SAM index are given, which means the linear

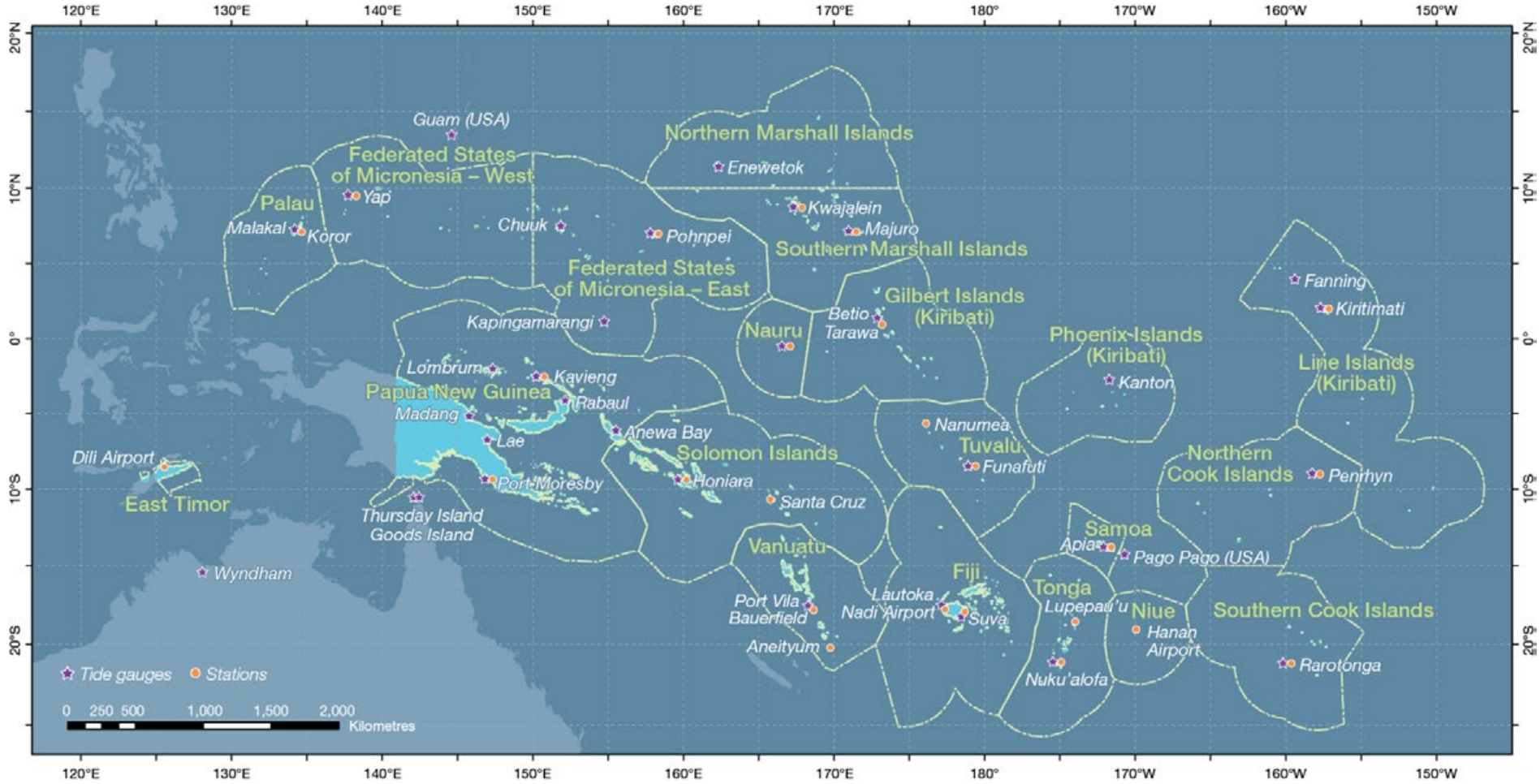

Figure 1.1: Meteorological observation stations, tide gauges and climate projections regions. The green dashed lines represent the regions used for climate projections for each country or country subregion. The tide gauges are indicated by the purple stars and observation stations by the orange circles.

relationship between the variable and Niño3.4 has been removed.

1.6 Observed Trends

This section provides analysis of observed climate and trends for annual and seasonal air temperature and rainfall, extreme events (particularly tropical cyclones), sea-surface temperature, ocean acidification and mean and extreme sea level.

1.6.1 Air Temperature and Rainfall

Sections X.6.1 and X.6.2 in each chapter provide information on trends in annual and seasonal air temperature and rainfall for the period 1950–2009 where data are available. A time series of annual mean air temperatures and total rainfall is presented for each country. A linear trend is fitted to the data record where more than 80% of the data record is available, and colour-coding is used to show the influence of ENSO: light blue columns indicate El Niño years, dark blue columns are La Niña years and grey columns are neutral years. El Niño and La Niña years are defined using the June-December SOI: a La Niña year is when the June-December SOI is greater than 5; an El Niño year is when December-June SOI is less than -5 (Power and Smith, 2007; Callaghan and Power, 2010). The expected ENSO influence from the climate variability section (X.5) of each chapter may not always be clear in the observed record presented in these sections because: (1) these events often start in the middle of one year and continue into the next; and (2) the impact of ENSO on local rainfall and air temperature is not always simultaneous, i.e. there can be a lag of a few months between ENSO development and impact at some locations.

1.6.3 Extreme Events

This section presents information on the number of tropical cyclones that have passed within 400 km of the capital town or city between the 1969/70 and 2009/10 cyclone seasons for countries in the South Pacific and East Timor. Year-to-year changes in tropical cyclone occurrences are described. These are largely characterised by phases of ENSO. Numbers of tropical cyclones within 400 km of a particular town or city are sourced from the PCCSP's Pacific Tropical Cyclone Data Portal (http://www.bom.gov.au/cyclone/history/tracks/). This Portal contains tropical cyclone best track data for the Southern Hemisphere. Trends in tropical cyclone frequency are not analysed in this publication as the data record in the 1970s is not homogeneous with that from the early 1980s to present day. This is for the most part due to the improvement in satellite coverage over the South Pacific Ocean from the early 1980s (Kuleshov et al., 2010). In addition, on a country scale the interannual variability in the number of tropical cyclones is large. This high variability and no cyclones in some seasons make it impossible at present to identify any long-term trends in cyclone frequency. A graph with annual occurrences and an 11-year running mean is provided to display interannual behaviour of tropical cyclones in the South Pacific and East Timor region.

Other extreme climate and weather events are described where information is available.

1.6.4 Sea-Surface Temperature

This section discusses sea-surface temperature trends between the 1950s and the present. These changes are important as they can affect changes in air temperatures, wind and rainfall and the position of climate features like the SPCZ. They also affect marine ecosystems through, for example, coral bleaching and nutrient supply.

1.6.5 Ocean Acidification

This section discusses changes in aragonite saturation (an indicator of ocean acidification) between the late 18th century and the present. Ocean acidification occurs in response to the continuing uptake of anthropogenic carbon dioxide from the atmosphere by the ocean, causing a decrease in seawater pH (a measure of the acidity or alkalinity level of a solution). The pH changes are accompanied by a decrease in the aragonite saturation state of the seawater. Aragonite is the form of calcium carbonate used by many organisms in reef ecosystems, including reef-building corals, to build their shells and skeletal material. Studies indicate that coral growth rates typically decline as the seawater aragonite saturation state decreases. However, not all coral species show the same response and the long-term adaptive capacity of corals to the changes is unknown. The crustose coralline algae, which precipitate calcium carbonate as high-magnesium calcite and act to cement corals into strong reef structures, may be even more susceptible to ocean acidification (Kuffner et al., 2008). By considering the large-scale distribution of coral reefs through the Pacific and the seawater chemistry, Guinotte et al. (2003) suggested that seawater aragonite saturation states above 4 were optimal for coral growth and for the development of healthy reef ecosystems, with values from 3.5 to 4 adequate for coral growth, and values between 3 and 3.5, marginal. Coral reef ecosystems were not found at seawater aragonite saturation state below 3 and these conditions were classified as extremely marginal for supporting coral growth.

1.6.6 Mean Sea Level

This section provides information on changes in mean sea level measured by historical tide gauge and satellite-mounted altimeters (since 1993) and gridded (reconstructed) sea level (since 1950). Information about tide gauges used is provided in the data availability section of each report.

1.6.7 Extreme Sea-Level Events

This section presents a discussion of extreme sea-level events and how they are related to patterns of variability,

tidal variations, interannual sea-level variability and extreme events such as tropical cyclones.

Extreme high sea levels are generally caused by a combination of three components: tides; seasonal or longer-term fluctuations due to changing wind, pressure and ocean temperature patterns (such as ENSO); and short-term events due to weather (such as storm surges). To better understand the relative contributions of these components to extreme sea levels, hourly tide gauge data are used to construct annual climatologies of high water levels (Merrifield et al., 2007). These annual extreme sea-level climatologies provide location-specific insight into the causes of high water levels and indicate times of the year when high sea levels and inundation events are most likely to occur.

The climatologies are constructed by performing a harmonic analysis of the hourly tide gauge data, which gives the tidal constants and allows the tide-only component of the measured sea level to be calculated. From this, the highest daily tide for each day is stored and the 95th percentile tide (exceedence level) is estimated from these values. After removal of tides from the hourly tide gauge data, the seasonal component is calculated by identifying month-to-month changes (using a low-pass filter) in the non-tidal water level. These results indicate the influence of steric (temperature driven) sea-level variability and large scale atmospheric circulation on the sea levels. The short-term (high frequency) component is the remainder of the non-tidal water level, after the seasonal component is removed. The highest short-term level for each year day is stored and the 95th percentile short-term component (exceedence level) is estimated from these values. These components are calculated using all years available in a particular tide gauge record. In addition, seasonal and short-term components are also calculated for El Niño and La Niña events, defined as water levels occurring when the monthly multivariate ENSO index (MEI) is greater than 0.5 or less than -0.5 respectively (Wolter and Timlin, 1998). This allows for better identification of interannual variability in extreme water levels.

The MEI combines six observed variables over the tropical Pacific. These six variables are: sea-level pressure, zonal and meridional components of the surface wind, sea-surface temperature, surface air temperature, and total cloudiness fraction of the sky. The MEI is calculated as the first unrotated principal component of all six observed fields combined (Wolter and Timlin, 1993).

Depending on the length of record for the tide gauge station, these annual climatologies may not accurately capture the likelihood of rare cyclone-related storm surge, and do not capture the likelihood of extremely rare tsunamis (which are not considered to be climate related). Therefore the top 10 extreme water-level events in each tide gauge record are also identified, and their relationship to the annual climatology components is discussed in the individual country reports.

1.7 Climate Projections

Climate projections that are presented for each PCCSP Partner Country were derived using output from global climate model simulations of the future climate, performed as part of the international Coupled Model Intercomparison Project (CMIP3; Volume 1, Section 4.3.1; Meehl et al., 2007a). Projections are given for surface air temperature, sea-surface temperature, rainfall, extreme weather events (including temperature, rainfall, drought and tropical cyclones), ocean acidification and sea level. Substantial and additional analysis of CMIP3 output was undertaken to determine many of these projections (Section 1.7.3).

Important information to consider in interpreting the projections and presentation of the projections (including the confidence levels) are explained in the following sections.

1.7.1 Understanding Climate Model Projections

The following issues need to be considered when interpreting projections from climate models:

- **Model Differences**
  Many research institutions around the world develop and maintain their own global climate model. While these models are based on the same physical laws, there are subtle differences between them associated with grid characteristics (e.g. spatial resolution), the representation of small-scale physical processes, and model sub-components (e.g. some models include a representation of atmospheric chemistry, while others do not (Volume 1, Section 4.3)). As a consequence of these differences, each model projects a slightly different future climate.
- **Model Skill**
  Due to model differences, not all climate models are equally skilful. A rigorous evaluation of the ability of the CMIP3 models to simulate the present western tropical Pacific climate revealed that while it is not possible to identify a single best climate model, it is possible to identify a small subset of models that perform consistently poorly across many aspects of a climate model simulation, or that perform poorly on critical aspects (Volume 1, Chapter 5; Irving et al., in press). These poor performing models were eliminated from the original set of 24 CMIP3 models, leaving 18 acceptable models for use in determining projections for each Partner Country (Volume 1, Section 5.5.1).
  While these remaining 18 models are generally able to capture the broad-scale features of the western tropical Pacific climate, a number of systematic deficiencies exist across the models (Volume 1, Chapter 5). For instance, the South Pacific Convergence Zone is typically

too east-west oriented and the westward extent of the Equatorial Cold Tongue is exaggerated. When a country is located in a region with model deficiencies, less confidence can be placed on model projections.

- **Emissions Scenarios**
  Since it is uncertain how society will evolve over the next century, it is difficult to know exactly how emissions of greenhouse gases and aerosols resulting from human activities will change in the future. To assist in modelling the future climate, the Intergovernmental Panel on Climate Change (IPCC) prepared 40 greenhouse gas and sulphate aerosol emissions scenarios for the 21st century that combine a variety of plausible assumptions about demographic, economic and technological factors likely to influence future emissions (Volume 1, Section 4.2; IPCC, 2000). Three of the most widely used scenarios are the B1, A1B and A2, which represent a low, medium and high greenhouse gas emissions future, respectively.
- **Multiple Possible Futures**
  As it is not possible to identify a single 'best' climate model, nor a single scenario that will best approximate the future evolution of greenhouse gas emissions, it is not possible to isolate one single projected future climate. Instead, a range of possible futures exist. In the context of the CMIP3 output analysed in this publication, this range of possibilities spans the futures simulated by all 18 acceptably skilful models for the A2 (high), A1B (medium), and B1 (low) emissions scenarios. Possible futures beyond the range simulated by these models and emissions scenarios may exist, however they represent our best estimate of that range at the present time.
- **Natural Variability**
  When interpreting projected changes in the mean climate it is important to keep in mind that natural climate variability, e.g. the state of ENSO, can cause conditions to vary substantially from the long-term mean from one year to the next. For example, within a warming trend it is still possible to experience cold years, however these would be likely to become less frequent (Figure 1.2).
- **Small-Scale Spatial Variability**
  Global climate models have relatively coarse spatial resolution (100 to 400 km between grid-points) and can therefore only make projections on a broad scale. As a result of island topography and other local features, there may be considerable deviation from these large-scale projections at small scales. This small-scale spatial variability that the global climate models are unable to capture may, in some cases, explain why observed trends at individual meteorological stations can be inconsistent with the large-scale projections provided by the models.

For information on other issues and uncertainties associated with climate model projections, see Volume 1, Box 5.2 and Box 6.1.

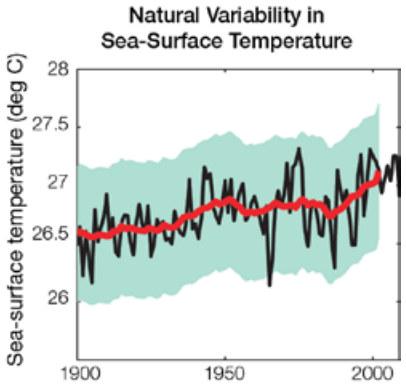

Figure 1.2: Annual mean sea-surface temperature record for an unspecified country. The black line shows the actual values recorded for each year, while the red line is the 20-year running average (i.e. the long-term mean). The deviation of the black line from the red in any given year represents the influence of natural variability. The blue shading is a measure of the interannual variability based on two standard deviations (approximately 95% of the years will fall within this range). It can be seen that the annual mean temperature for any given year can vary substantially from the long term mean.

1.7.2 Presentation of Projections

In order to systematically consider the issues noted in Section 1.7.1, a consistent approach was taken in presenting the projections for each PCCSP Partner Country (Section 1.7.2.1). This approach includes the use of multiple emissions scenarios, downscaling techniques and the assignment of confidence levels:

- **Multiple Emissions Scenarios**
  In general, projections are given for the A2 (high), A1B (medium), and B1 (low) emissions scenarios, for three 20-year time periods centred on 2030, 2055 and 2090 (Figure 1.3).
- **Downscaling**
  Given the fact that global climate models are unable to adequately capture small-scale climate influences, e.g. complex topography, a technique known as dynamical downscaling has been used to enhance the resolution of the CMIP3 output locally (Volume 1, Section 4.5). For this technique, high resolution atmospheric model simulations were conducted, driven by the changes in sea-surface temperature simulated by six of the CMIP3 models. The high resolution model used is the Conformal Cubic Atmospheric Model (CCAM; McGregor and Dix, 2008). It was run at 60 km resolution for all Partner Countries, and at 8 km resolution for seven selected countries. Dynamical downscaling results are only discussed in the presentation of projections for each Partner Country when they highlight small-scale details not present in the global climate model projections. It should be noted that while dynamical downscaling provides more detail at the local level, this does not guarantee increased reliability in representing the future climate (Volume 1, Section 5.3).

- **Confidence Levels**
  The level of confidence associated with a given projection is described as very high, high, moderate, low or very low. The determination of an appropriate confidence level depends upon expert judgement by PCCSP scientists, which takes into account various lines of evidence. These include agreement amongst model simulations (including both the global CMIP3 and dynamical downscaling simulations), model ability in simulating the current climate (including any consistent model biases) and the physical plausibility of the projection (Figure 1.4).

In general, the projections discussed for each Partner Country are not specific to any actual location, such as a town or city. Instead, they refer to an average change over the broad geographic region encompassing the country of interest and the surrounding ocean (Figure 1.1 identifies the regions used for all but the tropical cyclone projections). This is another reason why observed trends at individual meteorological stations may in some cases be different to the projections provided in this publication. Four countries were divided into sub-regions (Cook Islands, Federated States of Micronesia, Kiribati and Marshall Islands) due to the differing influences of large-scale climate features across the country. It should be noted that many research institutions participating in CMIP3 did not provide output for all the model variables and future emissions scenarios requested by the project organisers. As such, the actual number of models used differed between projections (Volume 1, Appendix 1).

1.7.2.1 Approach to Presenting the Projections

The following approach was adopted for projections of each climate variable (surface air temperature, sea-surface temperature, rainfall, extreme weather events, ocean acidification and sea level):

- **Projected Direction of Change**
  Each section begins with a statement of whether the climate variable in question is projected to increase, decrease or show little change over the course of the 21st century. This projected direction of change was determined by considering how projections from the CMIP3 models progress over the next century, for each of the three emissions scenarios. For instance, if 12 models simulate a progressive increase in wet season rainfall and six simulate a decrease for each of the three scenarios, the statement would say that wet season rainfall is projected to increase over the course of the 21st century, i.e. the statement represents the most likely climate future. The statement is followed by a quoted confidence level, which is supported by one or more dot points. Based on multiple lines of evidence (Figure 1.5), this level indicates the confidence PCCSP scientists have in the ability of the models to capture the true most likely direction of change.

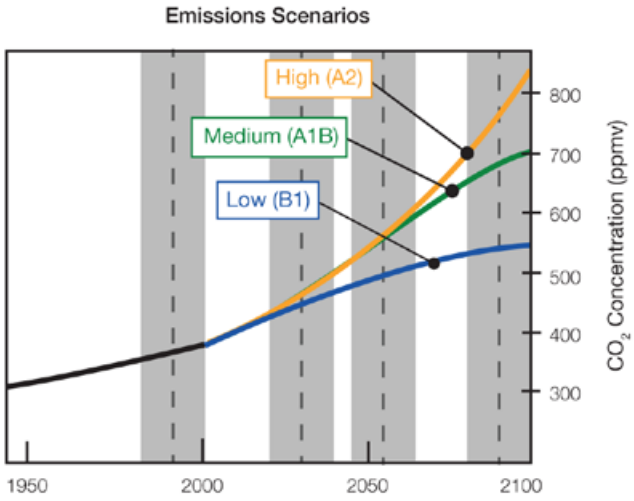

Figure 1.3: Projections in this publication are based on three emissions scenarios: B1 (low), A1B (medium) and A2 (high). The carbon dioxide (CO_2) concentrations projected for each scenario are shown as blue, green and orange lines, respectively. Projections for 2030, 2055 and 2090 (relative to 1990) were calculated using the average value of the 20-year periods 2020–2039, 2046–2065, 2080–2099 (relative to 1980–1999) to minimise the effect of natural variability. The grey bars represent the 20-year periods.

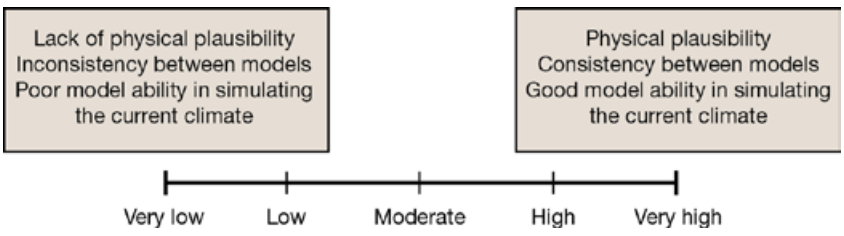

Figure 1.4: Lines of evidence and consequent labels used in describing the confidence associated with climate projections.

- **Range and Distribution of Projections**
  A detailed description of the range and distribution of projections across all three time periods and emissions scenarios is provided next. For instance, the models may simulate little change in annual rainfall by 2030, however by 2090 under the A1B (medium) and A2 (high) emissions scenarios, two-thirds of the models may simulate an increase (>5%) in annual rainfall, while one-third may simulate a decrease (< -5%). The description of the range and distribution of possible futures is followed by a quoted confidence level, which is supported by one or more dot points. Based on multiple lines of evidence (Figure 1.4), this level indicates the confidence PCCSP scientists have in the ability of the models to capture the true range of possible futures.
  It should be noted that the confidence associated with the range and distribution of possible futures need not necessarily be the same as that for the projected direction of change. For instance, if expert judgement suggests that an increase in wet season rainfall is most likely, confidence in a model projected increase in the direction of change might be high. However, if the models are known to systematically underestimate rainfall in the country of interest, then the confidence in the range of the projections might be low.
- **Additional Information**
  At the end of each section, additional information such as projected small-scale changes from dynamical downscaling or possible changes in interannual variability is discussed.

1.7.3 Detailed Projection Methods

For a number of climate variables, substantial analysis of CMIP3 and/or dynamically downscaled output was required to produce climate projections. Important features of these analyses are discussed in the following sections, while a more detailed account is available in Volume 1, Chapter 4.

1.7.3.1 Extreme Daily Temperature and Rainfall

Projected changes in days of extreme temperature and rainfall were made relative to the event that occurs on average once every 20 years. This 1-in-20-year event was calculated using the using the Generalised Extreme Value distribution (Volume 1, Section 6.2.7; Coles et al., 2001; Kharin et al., 2005). In general, two types of projection are given:

- The change in the magnitude of the 1-in-20-year event. For instance, in a warming climate the temperature experienced on the 1-in-20-year hot day may increase by 2°C by 2055 (i.e. 2046–2065), relative to 1990 (i.e. 1980–1999).
- The change in the frequency of the present day 1-in-20-year event. For instance, in a climate of increasing rainfall the current (i.e. 1980–1999) 1-in-20-year daily rainfall total may be projected to be exceeded once every three years by 2090 (i.e. 2080–2099).

1.7.3.2 Drought

Projected changes in the frequency of mild, moderate and severe drought were made using the Standardised Precipitation Index (SPI; Volume 1, Section 6.2.7.3; Lloyd-Hughes and Saunders, 2002). It should be noted that this index is based solely on rainfall (i.e. extended periods of low rainfall are classified as a drought) and does not take into account factors such as evaporation or soil moisture content.

1.7.3.3 Tropical Cyclones

Three separate methods were used to determine projections of tropical cyclone activity, known as the Genesis Potential Index (GPI), Curvature Vorticity Parameter (CVP) and the CSIRO Direct Detection Scheme (CDD) (Volume 1, Section 4.8). All were applied to CMIP3 output, while the latter was also applied to the CCAM 60 km resolution output.

Projections of changes in the statistics of tropical cyclone behaviour, especially at the individual country scale, are subject to greater uncertainty than projections of more uniform atmospheric properties such as temperature. This is because tropical cyclones are relatively compact weather systems that are not well represented in global climate models. Furthermore, global climate models show limited agreement on detailed aspects of atmospheric structure, such as the vertical wind shear and vorticity across the monsoon trough, which are both important determinants for tropical cyclone development and motion. Due to this uncertainty, the PCCSP region is divided into three sub-basins (Table 1.2). In addition, the region 0–20ºS, 100ºE–130ºE has been used for East Timor tropical cyclone projections.

1.7.3.4 Ocean Acidification

Projected changes in aragonite saturation state were calculated using empirical relationships between ocean carbonate chemistry and salinity, projections of ocean temperature and salinity from the CMIP3 models, and predicted changes in atmospheric carbon dioxide (Volume 1, Section 4.9). This information was used as input to an offline carbonate chemistry model. Particular reference is made to when aragonite saturation levels are first projected to fall below 3.5, since values below 3.5 are considered to be increasingly marginal for supporting healthy coral reef growth (Volume 1, Section 3.6.5; Guinotte et al., 2003).

1.7.3.5 Sea Level

Sea-level projections include estimates of ocean thermal expansion, melting of glaciers and ice caps, modelled ice-sheet contributions and an allowance for the estimated contribution from the potential rapid ice-sheet response (Volume 1, Section 4.7; Meehl et al., 2007b). The possibility of larger rates of rise than those projected in this publication cannot be excluded, but adequate understanding of the relevant physical processes is currently too limited to provide a best estimate or an upper bound (IPCC, 2007). To estimate regional sea-level changes, changes in ocean circulation and the associated sea levels, and the redistribution of mass due to changes in ice sheets, glaciers and ice caps have also been taken into account (Volume 1, Section 4.7; Church et al., 2011). The projected changes in sea level are relative to the land, except for local issues such as sediment compaction. In addition to the regional variations in sea level associated with ocean and mass changes, there are ongoing changes in relative sea level associated with changes in surface loading over the last glacial cycle (glacial isostatic adjustment) and local tectonic motions. The glacial isostatic motions are relatively small for the PCCSP region.

Table 1.2: Division of the PCCSP region for tropical cyclone projections

South-east basin 0–40°S, 170°E–130°W	South-west basin 0–40°S, 130°E–170°E	Northern basin 0–15°N, 130°E–180°E
Cook Islands Fiji Niue Samoa Tonga Tuvalu	Papua New Guinea Solomon Islands Vanuatu	Federated States of Micronesia Marshall Islands Palau

1.7.6 Projection Summaries

A summary table of projections is included at the end of each chapter. In some cases there are two tables for different country regions and imperial units are included for the Federated States of Micronesia, the Marshall Islands and Palau.

Rarotonga

Chapter 2
Cook Islands

The contributions of Arona Ngari, Maarametua Vaiimene, David Maihia and Nitoro Bates from the Cook Islands Meteorological Service and Pasha Carruthers from the National Enviroment Service are gratefully acknowledged

Introduction

This chapter provides a brief description of the Cook Islands, its past and present climate as well as projections for the future. The climate observation network and the availability of atmospheric and oceanic data records are outlined. Seasonal cycles are described, and the influences of large-scale climate features (e.g. the South Pacific Convergence Zone) and patterns of climate variability (e.g. the El Niño-Southern Oscillation) are analysed and discussed. Observed trends and analysis of air temperature, rainfall, extreme events (including tropical cyclones), sea-surface temperature, ocean acidification, sea level and extreme sea level are presented. Projections for air and sea-surface temperature, rainfall, extreme events, ocean acidification and sea level for the 21st century are provided. These projections are presented along with confidence levels based on expert judgement by Pacific Climate Change Science Program (PCCSP) scientists. The chapter concludes with summary tables of projections for the Northern Cook Islands and the Southern Cook Islands (Tables 2.4 and 2.5). Important background information including an explanation of methods and models is provided in Chapter 1. For definitions of other terms refer to the Glossary.

2.1 Climate Summary

2.1.1 Current Climate

- In the Northern Cook Islands temperatures are fairly constant throughout the year, while in the Southern Cook Islands there is a difference of around 4°C between the warmest and coolest months.
- The wet season in the Cook Islands is usually from late November to April or May but is longer in the Southern Cook Islands.
- Year-to-year rainfall variations are high in both the Northern and Southern Cook Islands, and much of this is due to the El Niño-Southern Oscillation, particularly in the wet season. El Niño years tend to be drier and La Niña years wetter than normal.
- Warming trends are evident in annual and seasonal mean air temperatures at Rarotonga for the period 1950–2009.
- Annual and seasonal rainfall trends for Rarotonga and Penrhyn for the period 1950–2009 are not statistically significant.
- The sea-level rise measured by satellite altimeters since 1993 is about 4 mm per year.
- On average Rarotonga experiences 11 tropical cyclones per decade, with most occurring between November and April. The high interannual variability in tropical cyclone numbers makes it difficult to identify any long-term trends in frequency.

2.1.2 Future Climate

Over the course of the 21st century:

- Surface air temperature and sea-surface temperature are projected to continue to increase (*very high* confidence).
- Annual and seasonal mean rainfall is projected to increase (*low* confidence)
- The intensity and frequency of days of extreme heat are projected to increase (*very high* confidence).
- The intensity and frequency of days of extreme rainfall are projected to increase (*high* confidence).
- The incidence of drought is projected to decrease (*moderate* confidence).
- Tropical cyclone numbers are projected to decline in the south-east Pacific Ocean basin (0–40ºS, 170ºE–130ºW) (*moderate* confidence).
- Ocean acidification is projected to continue (*very high* confidence).
- Mean sea-level rise is projected to continue (*very high* confidence).

2.2 Country Description

The Cook Islands consist of 15 islands spread over 2.2 million km^2 in the South Pacific between 9°S–22°S and 157°–166°W (Cook Islands First National Communication under the UNFCCC, 2000). The Cook Islands are divided geographically into the Northern Group and the Southern Group. The Northern Group consists of six low-lying atolls (most of which are about one to two metres above mean sea level), while the Southern Group comprises nine elevated islands, including volcanic islands and raised atolls. The Cook Islands has an Exclusive Economic Zone of 1.8 million km^2 of which only 237 km^2 is land area. Te Manga (652 m above sea level) on Rarotonga is the highest peak in the Cook Islands (Cook Islands Country Profile, SOPAC, 2000).

Rarotonga is also home to the capital, Avarua and the majority of the Cook Islands' resident population of 11 500 (2010 estimate) (Cook Islands Statistics Office, 2010).

The largest economic sector is tourism which has brought significant revenue and development to both Rarotonga and Aitutaki. Other sources of revenue in the Cook Islands are financial services, black pearl exports, fisheries and agriculture (Cook Islands Country Profile, SOPAC, 2000).

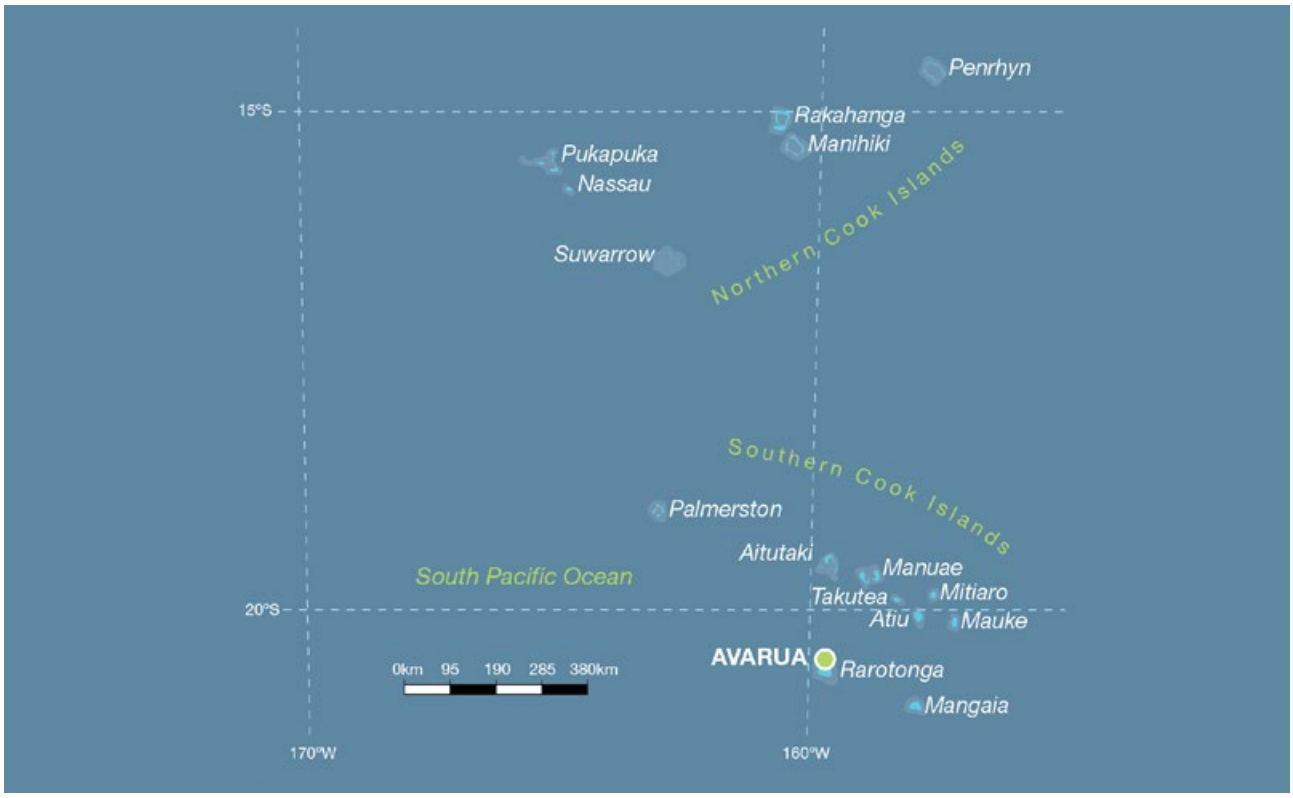

Figure 2.1: Cook Islands

2.3 Data Availability

The Cook Islands Meteorological Service is responsible for monitoring weather and climate in the Cook Islands. It currently operates six automatic weather stations on three islands in the Southern Cook Islands (Mangaia, Mauke, Aitutaki) and three islands in the Northern Cook Islands (Pukapuka, Penryhn, Manihiki).

Good quality historical meteorological data exist for six stations until the mid-1990s when manual observations were replaced by automatic weather stations. Since the mid-1990s observations have been sporadic, with the exception of Rarotonga and Penrhyn, the main observation stations in the Southern and Northern Groups respectively. Multiple observations within a 24-hour period are conducted at both stations. The Rarotonga climate station is located at Nikao, near the western end of the Rarotonga International Airport runway, on the north-western side of the island. Data are available here from 1899 to present for rainfall and 1907 to present for air temperature. For Penrhyn, rainfall data are available from 1937 to present and air temperature data from 1950 to 1995. Data from 1950 have been used for both sites. Both records are homogeneous and more than 95% complete (up to 1995 for temperature at Penrhyn).

Oceanographic records do not cover such a long time period. Monthly-averaged sea-level data are available from the late 1970s at Rarotonga (1977–2001 and 2001– present) and since 1993 with an acoustic gauge at Rarotonga. A global positioning system instrument to estimate vertical land motion was deployed at Rarotonga in 2001 and will provide valuable direct estimates of local vertical land motion in future years. Monthly-averaged sea-level data are available from 1977–present at Penrhyn. Both satellite (from 1993) and in situ sea-level data (1950–2009; termed reconstructed sea level; Volume 1, Section 2.2.2.2) are available on a global 1° x 1° grid.

Long-term locally-monitored sea-surface temperature data are unavailable for the Cook Islands, so large-scale gridded sea-surface temperature datasets have been used (HadISST, HadSST2, ERSST and Kaplan Extended SST V2; Volume 1, Table 2.3).

Measuring evaporation, Cook Islands Meteorological Service

2.4 Seasonal Cycles

Seasonal temperatures differ greatly between Rarotonga in the Southern Group and Penrhyn in the Northern Group (Figure 2.2). Being close to the equator Penrhyn has fairly constant temperatures throughout the year, with average maxima around 30ºC and average minima around 26ºC. In Rarotonga the monthly average temperatures peak in March and are about 4ºC warmer than the winter months (June-September). The colder winter temperatures are due to weaker solar radiation and the influence of colder air from higher latitudes in winter. At both stations, sea-surface temperature changes with the season in the same way as air temperature, and there is a strong linkage between sea-surface temperature and air temperature on the small islands.

Rainfall follows similar seasonal patterns at the two sites. The wet season is from late November to April or May but persists by approximately one month longer at Rarotonga. The South Pacific Convergence Zone (SPCZ) is very important for rainfall in the Cook Islands. The SPCZ is centred close to or over the Southern Cook Islands from November to May. This is when the SPCZ is most active and furthest south. From November to March the SPCZ is wide and strong enough for the Northern Cook Islands to also receive significant rainfall.

The driest months of the year in the Cook Islands are from June to October. In this season, the SPCZ is mostly weak and inactive over the Cook Islands, although occasionally convection and rainfall occur. The Southern Group is also affected by rain systems from the sub- and extra-tropics, such as cold fronts, especially in winter.

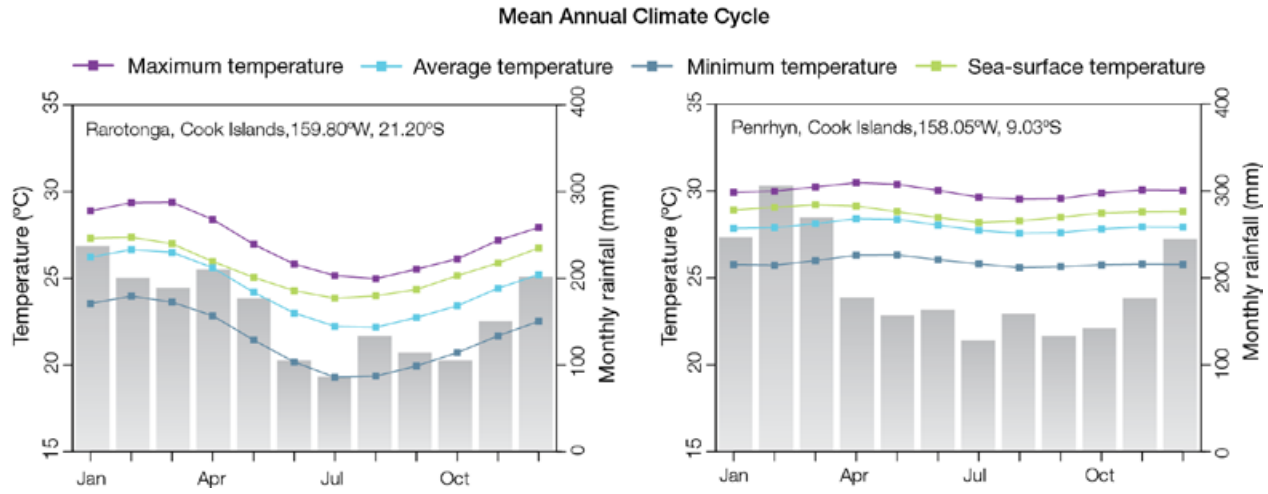

Figure 2.2: Mean annual cycle of rainfall (grey bars) and daily maximum, minimum and mean air temperatures at Rarotonga (left) and at Penrhyn (right), and local sea-surface temperatures derived from the HadISST dataset (Volume 1, Table 2.3).

2.5 Climate Variability

Year-to-year rainfall variations are high in both the Northern and Southern Groups, and much of this is due to the El Niño-Southern Oscillation (ENSO), particularly in the wet season. This is substantiated by the significant correlations between wet and dry season rainfall and ENSO indices. ENSO also affects maximum and minimum air temperatures. ENSO has opposite effects on Penrhyn compared to Rarotonga, which is partly caused by the position and strength of the SPCZ. During an El Niño event rainfall decreases in Rarotonga as the SPCZ moves away to the north-east, an effect that is stronger in the wet season. Temperatures also decrease in Rarotonga during an El Niño event as the waters around the Southern Cook Islands cool. In Penrhyn, however, an El Niño usually brings wetter conditions as the SPCZ moves over the Northern Group. Ocean temperatures warm in this region during an El Niño so air temperatures also warm. At Penrhyn the effect of ENSO appears to be stronger on maximum temperatures than minimum air temperatures, whereas in Rarotonga minimum air temperatures are more strongly affected by ENSO. In both the Southern and Northern Groups the influence of ENSO is greatest in the wet season. ENSO Modoki events (Volume 1, Section 3.4.1) also affect rainfall at both sites, more in the wet than the dry season, with similar influences but to a lesser degree than canonical ENSO events. Wet season air temperatures are also affected by ENSO Modoki events.

The only other significant correlations between climate indices and interannual climate variations found in the Cook Islands (Tables 2.1 and 2.2) are the weak relationship between the Interdecadal Pacific Oscillation and the maximum air temperatures at Rarotonga, and the effect of the Southern Annular Mode on wet season minimum air temperatures in Penrhyn. This suggests the Southern Annular Mode is related to the position of sub-tropical high pressure systems so that only in some years is there a relationship with the temperatures in the Northern Group, whereas these high pressure systems influence the Southern Group in all years. Most of the interannual climate variability in the Cook Islands related to large-scale climate variability seems therefore to come from ENSO, with the SPCZ playing an important role in bringing about this variability.

Table 2.1: Correlation coefficients between indices of key large-scale patterns of climate variability and minimum and maximum temperatures (Tmin and Tmax) and rainfall at Rarotonga. Only correlation coefficients that are statistically significant at the 95% level are shown.

Climate feature/index		Dry season (May-October)			Wet season (November-April)		
		Tmin	Tmax	Rain	Tmin	Tmax	Rain
ENSO	Niño3.4	-0.70	-0.42	-0.35			-0.52
	Southern Oscillation Index	0.67	0.42	0.24	0.33	0.27	0.49
Interdecadal Pacific Oscillation Index						-0.25	
Southern Annular Mode Index							
ENSO Modoki Index						-0.25	-0.21
Number of years of data		77	79	108	78	78	108

Table 2.2: Correlation coefficients between indices of key large-scale patterns of climate variability and minimum and maximum temperatures (Tmin and Tmax) and rainfall at Penrhyn. Only correlation coefficients that are statistically significant at the 95% level are shown.

Climate feature/index		Dry season (May-October)			Wet season (November-April)		
		Tmin	Tmax	Rain	Tmin	Tmax	Rain
ENSO	Niño3.4		0.73		0.45	0.85	0.63
	Southern Oscillation Index		-0.74	-0.28		-0.71	-0.72
Interdecadal Pacific Oscillation Index							
Southern Annular Mode Index					0.40		
ENSO Modoki Index				0.30	0.35	0.54	0.40
Number of years of data		46	46	70	44	45	70

2.6 Observed Trends

2.6.1 Air Temperature

Warming trends (Figure 2.3 top) of similar magnitude have been identified in both annual and seasonal mean air temperatures at Rarotonga for the period 1950–2009. Annual and seasonal minimum air temperature trends are greater than those observed for maximum air temperatures at Rarotonga (Table 2.3). Figure 2.3 (bottom) shows that for the period 1950–1995 there was no trend in annual mean air temperature at Penrhyn. Data are not available for the period 1996–2009.

2.6.2 Rainfall

Annual and seasonal rainfall trends for Rarotonga and Penrhyn for the period 1950–2009 are not statistically significant (Table 2.3 and Figure 2.4).

2.6.3 Extreme Events

Tropical cyclone season in the Cook Islands is between November and April. Occurrences outside this period are rare. The tropical cyclone archive for the Southern Hemisphere indicates that between the 1969/70 and 2009/10 seasons, the centre of 47 tropical cyclones passed within approximately 400 km of Rarotonga. This represents an average of 11 cyclones per decade. Tropical cyclones were most frequent in El Niño years (15 cyclones per decade) and least frequent in La Niña years (six cyclones per decade). The neutral year average is 11 per decade. The interannual variability in the number of tropical cyclones in the vicinity of Rarotonga is large, ranging from zero in some cyclone seasons to six in the 2005/06 cyclone season (Figure 2.5). This high variability makes it difficult to identify any long-term trends in frequency.

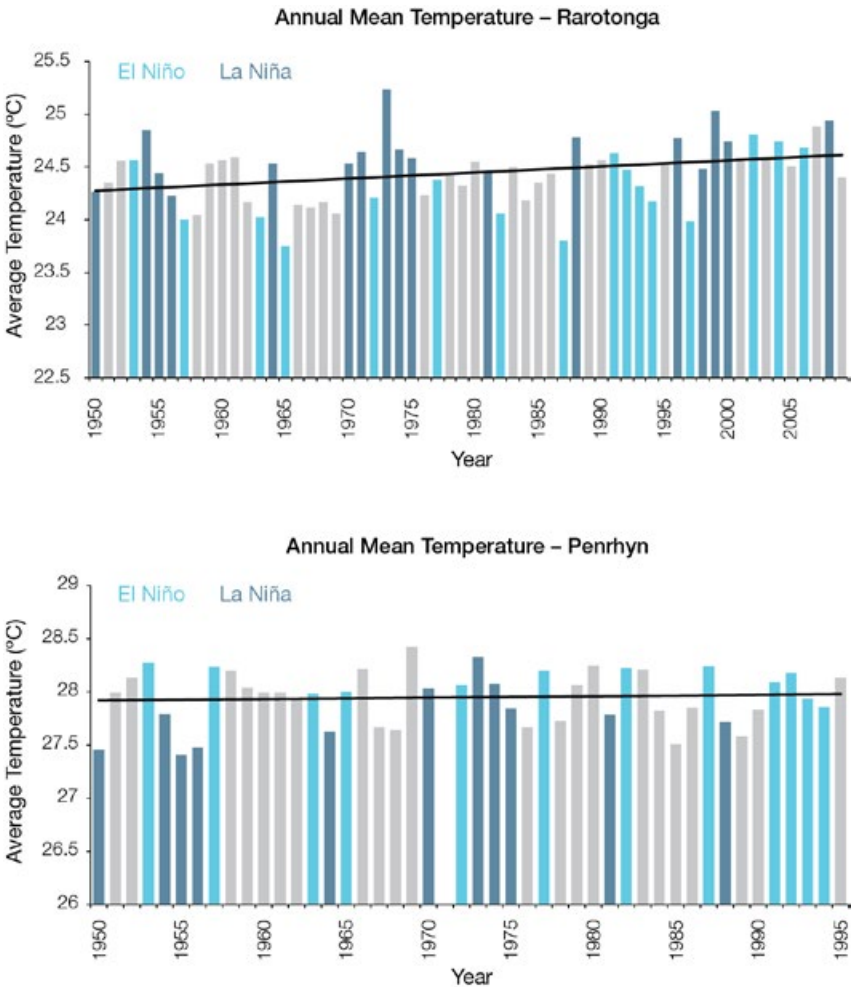

Figure 2.3: Annual mean air temperature for Rarotonga (top) and Penrhyn (bottom). Light blue, dark blue and grey bars denote El Niño, La Niña and neutral years respectively.

Table 2.3: Annual and seasonal trends in maximum, minimum and mean air temperature (Tmax, Tmin and Tmean) and rainfall at Rarotonga (and rainfall only at Penrhyn) for the period 1950–2009. Asterisks indicate significance at the 95% level. Persistence is taken into account in the assessment of significance as in Power and Kociuba (in press). The statistical significance of the air temperature trends is not assessed.

	Rarotonga Tmax (°C per 10 yrs)	Rarotonga Tmin (°C per 10 yrs)	Rarotonga Tmean (°C per 10 yrs)	Rarotonga Rain (mm per 10 yrs)	Penrhyn Rain (mm per 10 yrs)
Annual	+0.05	+0.07	+0.06	-35	+137
Wet season	+0.05	+0.08	+0.06	-28	+69
Dry season	+0.04	+0.08	+0.06	-13	+29

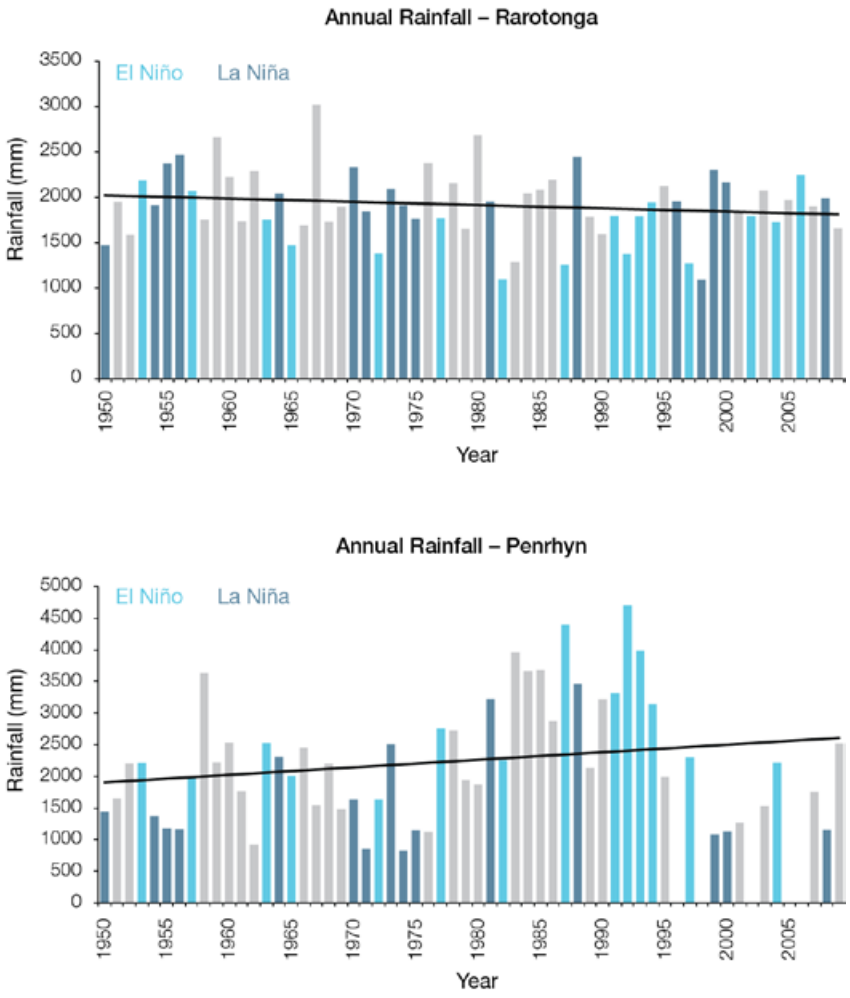

Figure 2.4: Annual rainfall at Rarotonga (top) and Penrhyn (bottom). Light blue, dark blue and grey bars denote El Niño, La Niña and neutral years respectively.

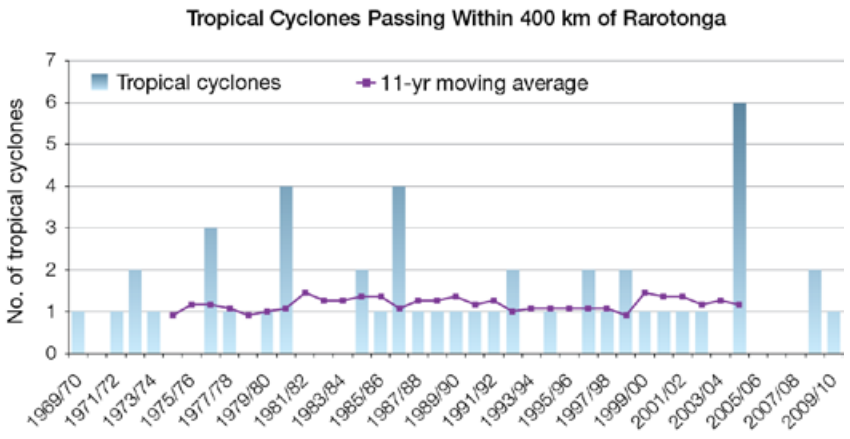

Figure 2.5: Tropical cyclones passing within 400 km of Rarotonga per season. The 11-year moving average is in purple.

2.6.4 Sea-Surface Temperature

Historical changes in sea-surface temperature around the Cook Islands are consistent with the broad-scale changes for the wider PCCSP region. Water temperatures remained relatively constant from the 1950s to the late 1980s. This was followed by a period of more rapid warming (approximately 0.12°C per decade for 1970–present). At these regional scales, natural variability plays a large role in determining sea-surface temperature making it difficult to identify long-term trends. Figure 2.8 shows the 1950–2000 sea-surface temperature changes (relative to a reference year of 1990) from three large-scale, sea-surface temperature gridded datasets (HadSST2, ERSST and Kaplan Extended SST V2; Volume 1, Table 2.3).

2.6.5 Ocean Acidification

Based the large-scale distribution of coral reefs across the Pacific and the seawater chemistry, Guinotte et al. (2003) suggested that seawater aragonite saturation states above 4 were optimal for coral growth and for the development of healthy reef ecosystems, with values from 3.5 to 4 adequate for coral growth, and values between 3 and 3.5 marginal. Coral reef ecosystems were not found at seawater aragonite saturation states below 3 and these conditions were classified as extremely marginal for supporting coral growth.

In the Cook Islands region, the aragonite saturation state has declined from about 4.5 in the late 18th century to an observed value of about 4.1 ± 0.2 by 2000.

2.6.6 Sea Level

Monthly averages of the historical tide gauge, satellite (since 1993) and gridded sea-level (since 1950) data that are co-located have similar variability after 1993 and indicate year-to-year variability in sea levels of about 19 cm (estimated 5–95% range) after removal of the seasonal cycle (Figure 2.10). The sea-level rise near the Cook Islands, measured by satellite altimeters (Figure 2.6) since 1993, is about 4 mm per year, similar to the global average of 3.2 ± 0.4 mm per year. This rise is partly linked to a pattern related to climate variability from year to year and decade to decade (Figure 2.10).

2.6.7 Extreme Sea-Level Events

The annual climatology of the highest daily sea levels has been evaluated using hourly tide gauge measurements at Avarua, Rarotonga and Penrhyn (Tongareva) Atoll (Figure 2.7). Maximum tides tend to occur between March and April at Rarotonga and February and March at Penrhyn. These higher tides and short-term raised water levels combine to produce the highest likelihood of extreme water levels between January and April, peaking in March, at both locations. Seasonal water levels tend to be lower during La Niña years at Penrhyn, but generally higher during La Niña years at Rarotonga. Despite the generally lower seasonal component during El Niño years, the higher short-term components during December-April in El Niño years at Rarotonga result in a tendency for higher water levels during these periods (Volume 1, Section 3.6.3 and Figures 3.20 and 3.21). Seven of the 10 highest water levels recorded occurred during an El Niño at both locations and these events tend to cluster between the months of November to March, especially at Rarotonga. Many of these 10 highest recorded water levels are significantly higher than the total (combined) high water level climatology (grey lines in Figures 2.7). Indeed the five highest sea-level events at Rarotonga and four events at Penrhyn (including the top three) were associated with named tropical cyclones. These results strongly indicate that extreme sea-level events in the Cook Islands are more often associated with tropical cyclones or high wave events than with tides or interannual sea level variability.

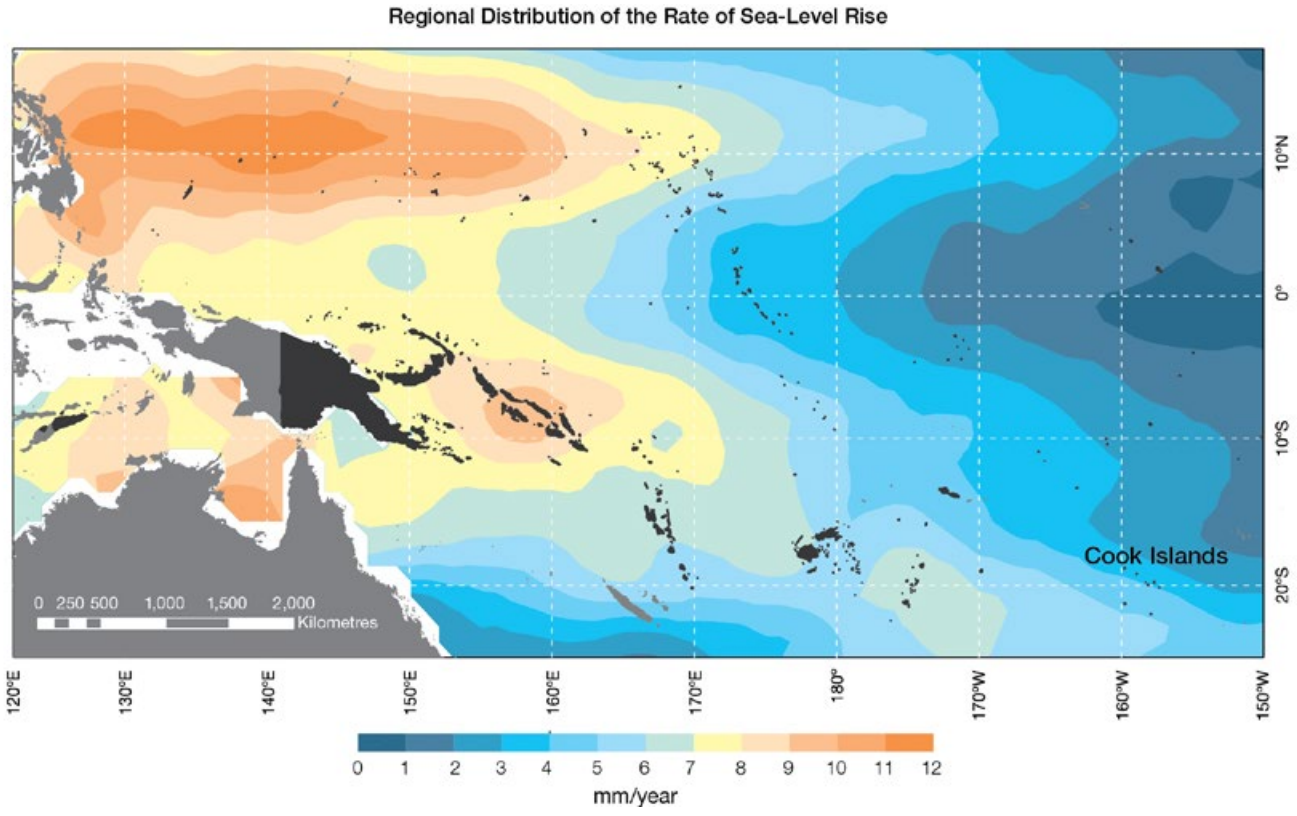

Figure 2.6: The regional distribution of the rate of sea-level rise measured by satellite altimeters from January 1993 to December 2010, with the location of Cook Islands indicated. Further detail about the regional distribution of sea-level rise is provided in Volume 1, Section 3.6.3.2.

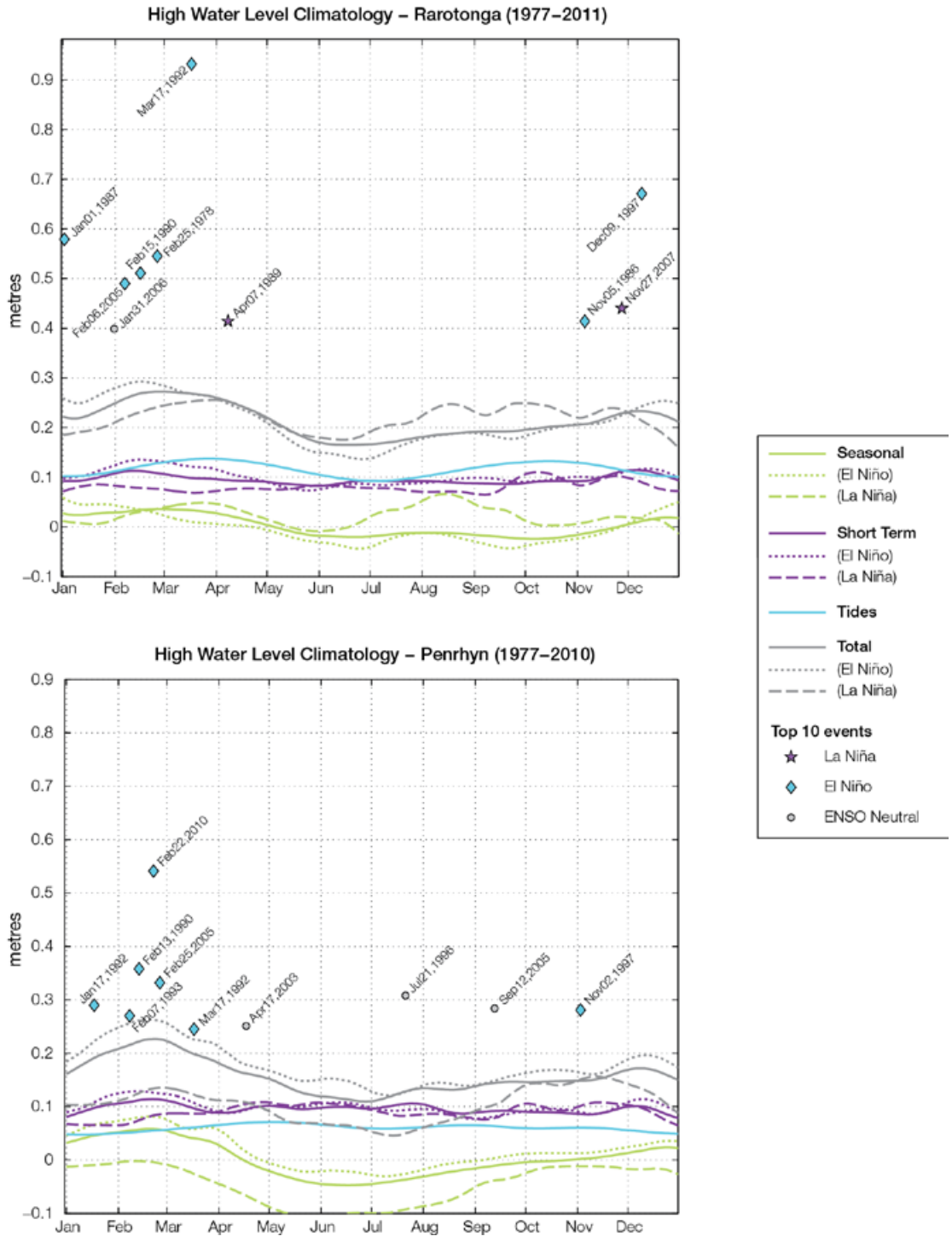

Figure 2.7: The annual cycle of high waters relative to Mean Higher High Water (MHHW) due to tides, short-term fluctuations (most likely associated with storms) and seasonal variations for Rarotonga (top) and Penryhn (bottom). The tides and short-term fluctuations are respectively the 95% exceedence levels of the astronomical high tides relative to MHHW and the short-term sea level anomaly fluctuations. Components computed only for El Niño and La Niña years are shown by dotted and dashed lines, and grey lines are the sum of the tide, short-term and seasonal components. The 10 highest sea level events in the record relative to MHHW are shown, and coded to indicate the phase of ENSO at the time of the extreme event.

2.7 Climate Projections

Climate projections have been derived from up to 18 global climate models from the CMIP3 database, for up to three emissions scenarios (B1 (low), A1B (medium) and A2 (high)) and three 20-year periods centred on 2030, 2055 and 2090, relative to 1990. These models were selected based on their ability to reproduce important features of the current climate (Volume 1, Section 5.2.3), so projections from each of the models may be considered a plausible representation of the future climate. This means there is not one single projected future for the Cook Islands, but rather a range of possible futures. The full range of these futures is discussed in the following sections.

These projections do not represent a value specific to any actual location, such as a town or city in the Cook Islands. Instead, they refer to an average change over the broad geographic region encompassing the Cook Islands and the surrounding ocean. Projections refer to the entire Cook Islands unless otherwise stated. In some instances, given that there are some differences between the climate of the Northern and Southern Cook Islands (Section 2.4), projections are given separately for these two regions (Figure 1.1 shows the region boundaries). Section 1.7 provides important information about interpreting climate model projections.

2.7.1 Temperature

Surface air temperature and sea-surface temperature are projected to continue to increase over the course of the 21st century. There is *very high* confidence in this direction of change because:

- Warming is physically consistent with rising greenhouse gas concentrations.
- All CMIP3 models agree on this direction of change.

The majority of CMIP3 models simulate a slight increase (< 1°C) in annual and seasonal mean surface air temperature by 2030, however by 2090 under the A2 (high) emissions scenario increases of greater than 2.5°C are simulated by almost all models (Tables 2.4 and 2.5). Given the close relationship between surface air temperature and sea-surface temperature, a similar (or slightly weaker) rate of warming is projected for the surface ocean (Figure 2.8). There is *moderate* confidence in this range and distribution of possible futures because:

- There is generally some discrepancy between modelled and observed temperature trends over the past 50 years in the vicinity of the Cook Islands, although this may be partly due to limited observational records (Figure 2.8).

Interannual variability in surface air temperature and sea-surface temperature over the Cook Islands is strongly influenced by ENSO in the current climate (Section 2.5). As there is no consistency in projections of future ENSO activity (Volume 1, Section 6.4.1), it is not possible to determine whether interannual variability in temperature will change in the future. However, it is expected that ENSO will continue to be an important source of variability for the Cook Islands.

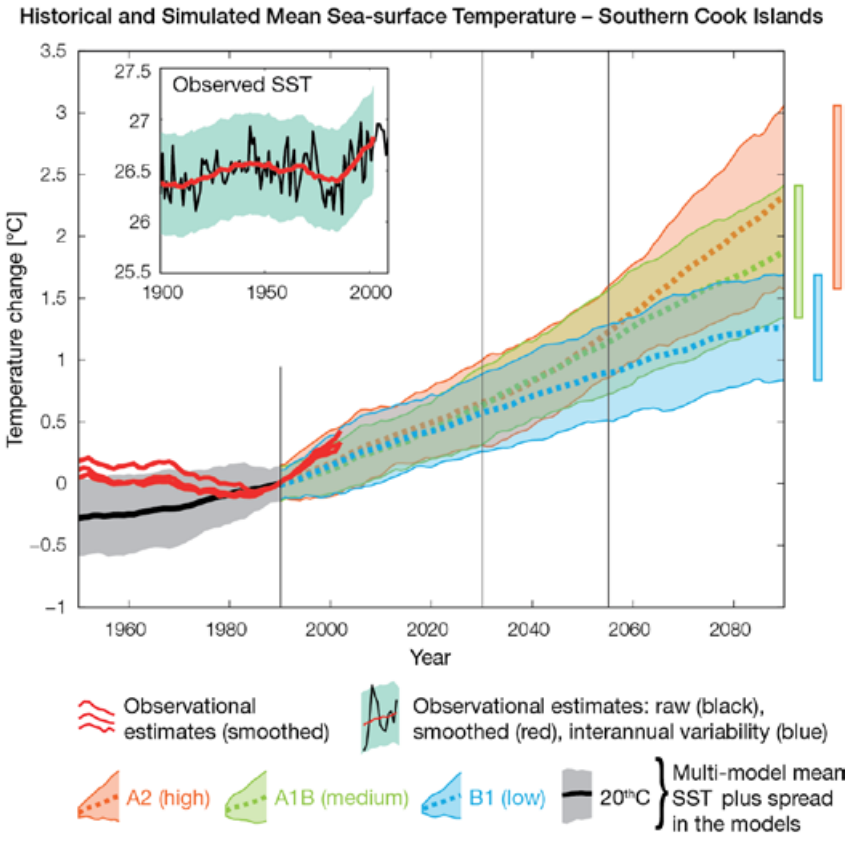

Figure 2.8: Historical climate (from 1950 onwards) and simulated historical and future climate for annual mean sea-surface temperature (SST) over the region surrounding the Southern Cook Islands, for the CMIP3 models. Shading represents approximately 95% of the range of model projections (twice the inter-model standard deviation), while the solid lines represent the smoothed (20-year running average) multi-model mean temperature. Projections are calculated relative to the 1980–1999 period (which is why there is a decline in the inter-model standard deviation around 1990). Observational estimates in the main figure (red lines) are derived from the HadSST2, ERSST and Kaplan Extended SST V2 datasets (Volume 1, Section 2.2.2). Annual average (black) and 20-year running average (red) HadSST2 data is also shown inset. Projections for the Northern Cook Islands closely resemble those for the south and are therefore not shown.

2.7.2 Rainfall

Wet season (November-April), dry season (May-October), and annual average rainfall is projected to increase over the course of the 21st century. There is *moderate* confidence in this direction of change because:

- An increase in rainfall is consistent with the projected likely increase in the intensity of the South Pacific Convergence Zone (SPCZ) (Volume 1, Section 6.4.5) which has a large influence on rainfall in the Cook Islands.
- The majority of CMIP3 models agree on this direction of change by 2090.

The majority of CMIP3 models simulate little change (-5% to 5%) in rainfall by 2030, however by 2090 the majority simulate an increase (>5%) in wet season, dry season and annual rainfall, with up to a third simulating a large increase (>15%) for the Northern Cook Islands under the A2 (high) emissions scenario (Table 2.4 and 2.5). There is *low* confidence in this range and distribution of possible futures because:

- In simulations of the current climate, the CMIP3 models generally do not locate the SPCZ in the correct location relative to the Cook Islands (Brown et al., 2011).
- The CMIP3 models are unable to resolve many of the physical processes involved in producing rainfall. As a consequence, they do not simulate rainfall as well as other variables such as temperature (Volume 1, Chapter 5).

Interannual variability in rainfall over the Cook Islands is strongly influenced by ENSO in the current climate, particularly via its influence on the movement of the SPCZ (Section 2.5). As there is no consistency in projections of future ENSO activity (Volume 1, Section 6.4.1), it is not possible to determine whether interannual variability in rainfall will change in the future.

2.7.3 Extremes

Temperature

The intensity and frequency of days of extreme heat are projected to increase over the course of the 21st century. There is *very high* confidence in this direction of change because:

- An increase in the intensity and frequency of days of extreme heat is physically consistent with rising greenhouse gas concentrations.
- All CMIP3 models agree on the direction of change for both intensity and frequency.

For both the Northern and Southern Cook Islands, the majority of CMIP3 models simulate an increase of approximately 1°C in the temperature experienced on the 1-in-20-year hot day by 2055 under the B1 (low) emissions scenario, with an increase of over 2.5°C simulated by the majority of models by 2090 under the A2 (high) emissions scenario (Tables 2.4 and 2.5). There is *low* confidence in this range and distribution of possible futures because:

- In simulations of the current climate, the CMIP3 models tend to underestimate the intensity and frequency of days of extreme heat (Volume 1, Section 5.2.4).
- Smaller increases in the frequency of days of extreme heat are projected by the CCAM 60 km simulations.

Rainfall

The intensity and frequency of days of extreme rainfall are projected to increase over the course of the 21st century. There is *high* confidence in this direction of change because:

- An increase in the frequency and intensity of extreme rainfall is consistent with larger-scale projections, based on the physical argument that the atmosphere is able to hold more water vapour in a warmer climate (Allen and Ingram, 2002; IPCC, 2007). It is also consistent with the projected likely increase in SPCZ intensity (Volume 1, Section 6.4.5).
- Almost all of the CMIP3 models agree on this direction of change for both intensity and frequency.

For the Northern Cook Islands, the majority of CMIP3 models simulate an increase of at least 20 mm in the amount of rain received on the 1-in-20-year wet day by 2055 under the B1 (low) emissions scenario, with an increase of at least 30 mm simulated by the majority of models by 2090 under the A2 (high) emissions scenario. In the Southern Cook Islands, the majority of CMIP3 models project this increase to be at least 10 mm for the 1-in-20-year wet day by 2055, under the B1 (low) emissions scenario, and 20 mm by 2090 under the A2 (high) emissions scenario. The majority of models project, by 2055 under the B1 (low) emissions scenario, that the current 1-in-20-year extreme rainfall event will occur, on average, four times per 20-year period in the Northern Cook Islands and three times per 20-year period in the Southern Cook Islands. By 2090, under the A2 (high) emissions scenario, the projected frequency remains relatively unchanged in the Northern Cook Islands, and increases to three to four times per 20-year period over the Southern Cook Islands. There is *low* confidence in this range and distribution of possible futures because:

- In simulations of the current climate, the CMIP3 models tend to underestimate the intensity and frequency of extreme rainfall (Volume 1, Section 5.2.4), and generally do not locate the SPCZ in the correct location relative to the Cook Islands (Brown et al., 2011).
- The CMIP3 models are unable to resolve many of the physical processes involved in producing extreme rainfall.

Drought

The incidence of drought is projected to decrease over the course of the 21st century. There is *moderate* confidence in this direction of change because:

- A decrease in drought is consistent with projections of increased rainfall (Section 2.7.2).
- The majority of models agree on this direction of change for most drought categories.

For the Northern and Southern Cook Islands, the majority of CMIP3 models project that mild drought will occur approximately seven to eight times every 20 years in 2030 under all emissions scenarios, decreasing to six to seven times by 2090. The frequency of moderate drought is projected to remain stable at once to twice every 20 years in the Southern Cook Islands, while in the north it is expected to decrease from twice every 20 years in 2030, to once to twice by 2090. The majority of CMIP3 models project that severe droughts will occur approximately once every 20 years across all time periods and scenarios in both the north and south. There is *low* confidence in this range and distribution of possible futures because:

- There is only low confidence in the range of rainfall projections (Section 2.7.2), which directly influences projections of future drought conditions.

Tropical Cyclones

Tropical cyclone numbers are projected to decline in the south-east Pacific Ocean basin (0–40ºS, 170ºE– 130ºW) over the course of the 21st century. There is *moderate* confidence in this direction of change because:

- Many studies suggest a decline in tropical cyclone frequency globally (Knutson et al., 2010).
- Tropical cyclone numbers decline in the south-east Pacific Ocean in the majority assessment techniques.

Based on the direct detection methodologies (Curvature Vorticity Parameter (CVP) and the CSIRO Direct Detection Scheme (CDD) described in Volume 1, Section 4.8.2), 65% of projections show no change or a decrease in tropical cyclone formation when applied to the CMIP3 climate models for which suitable output is available (Volume 1, Appendix 1, Table A2). When these techniques are applied to CCAM, 100% of projections show a decrease in tropical cyclone formation. In addition, the Genesis Potential Index (GPI) empirical technique suggests that conditions for tropical cyclone formation will become less favourable in the south-east Pacific Ocean basin, for all analysed CMIP3 models. There is *moderate* confidence in this range and distribution of possible futures because:

- In simulations of the current climate, the CVP, CDD and GPI methods capture the frequency of tropical cyclone activity reasonably well (Volume 1, Section 5.4).

Despite this projected reduction in total tropical cyclone numbers, five of the six CCAM 60 km simulations show an increase in the proportion of the most severe cyclones. Most models also indicate a reduction in tropical cyclone wind hazard north of 20ºS latitude and regions of increased hazard south of 20ºS latitude. This increase in wind hazard coincides with a poleward shift in the latitude at which tropical cyclones are most intense.

2.7.4 Ocean Acidification

The acidification of the ocean will continue to increase over the course of the 21st century. There is *very high* confidence in this projection as the rate of ocean acidification is driven primarily by the increasing oceanic uptake of carbon dioxide, in response to rising atmospheric carbon dioxide concentrations.

Projections from all analysed CMIP3 models indicate that the annual maximum aragonite saturation state will reach values below 3.5 by about 2050 in the Southern Cook Islands and 2065 in the Northern Cook Islands. The aragonite saturation will continue to decline thereafter (Figure 2.9; Tables 2.4 and 2.5). There is *moderate* confidence in this range and distribution of possible futures because the projections are based on climate models without an explicit representation of the carbon cycle and with relatively low resolution and known regional biases.

The impact of acidification change on the health of reef ecosystems is likely to be compounded by other stressors including coral bleaching, storm damage and fishing pressure.

2.7.5 Sea Level

Mean sea level is projected to continue to rise over the course of the 21st century. There is *very high* confidence in this direction of change because:

- Sea-level rise is a physically consistent response to increasing ocean and atmospheric temperatures, due to thermal expansion of the water and the melting of glaciers and ice caps.
- Projections arising from all CMIP3 models agree on this direction of change.

The CMIP3 models simulate a rise of between approximately 5–15 cm by 2030, with increases of 20–60 cm indicated by 2090 under the higher emissions scenarios (i.e. A1B (medium) and A2 (high); Figure 2.10; Tables 2.4 and 2.5). There is *moderate* confidence in this range and distribution of possible futures because:

- There is significant uncertainty surrounding ice-sheet contributions to sea-level rise and a larger rise than that projected above cannot be excluded (Meehl et al., 2007b).

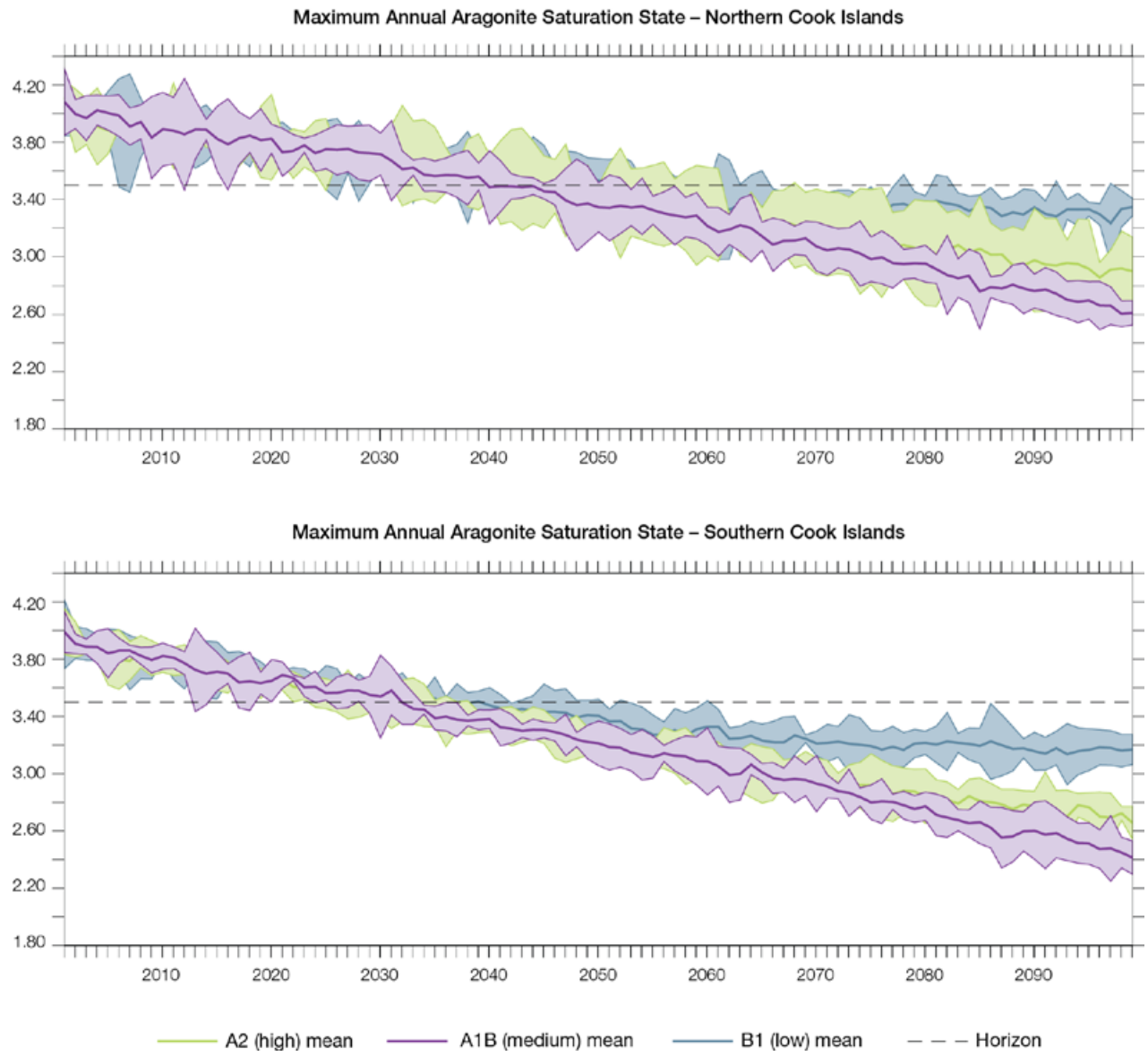

Figure 2.9: Multi-model projections, and their associated uncertainty (shaded area represents two standard deviations), of the maximum annual aragonite saturation state in the sea surface waters of the Northern Cook Islands (top) and the Southern Cook Islands (bottom) under the different emissions scenarios. The dashed black line represents an aragonite saturation state of 3.5.

However, adequate understanding of the processes is currently too limited to provide a best estimate or an upper bound (IPCC, 2007).

- Globally, since the early 1990s, sea level has been rising near the upper end of the above projections. During the 21st century, some studies (using semi-empirical models) project faster rates of sea-level rise.

Interannual variability of sea level will lead to periods of lower and higher regional sea levels. In the past, this interannual variability has been about 19 cm (5–95% range, after removal of the seasonal signal; see dashed lines in Figure 2.10 (a)) and it is likely that a similar range will continue through the 21st century. In addition, winds and waves associated with weather phenomena will continue to lead to extreme sea-level events.

In addition to the regional variations in sea level associated with ocean and mass changes, there are ongoing changes in relative sea level associated with changes in surface loading over the last glacial cycle (glacial isostatic adjustment) and local tectonic motions. The glacial isostatic motions are relatively small for the PCCSP region.

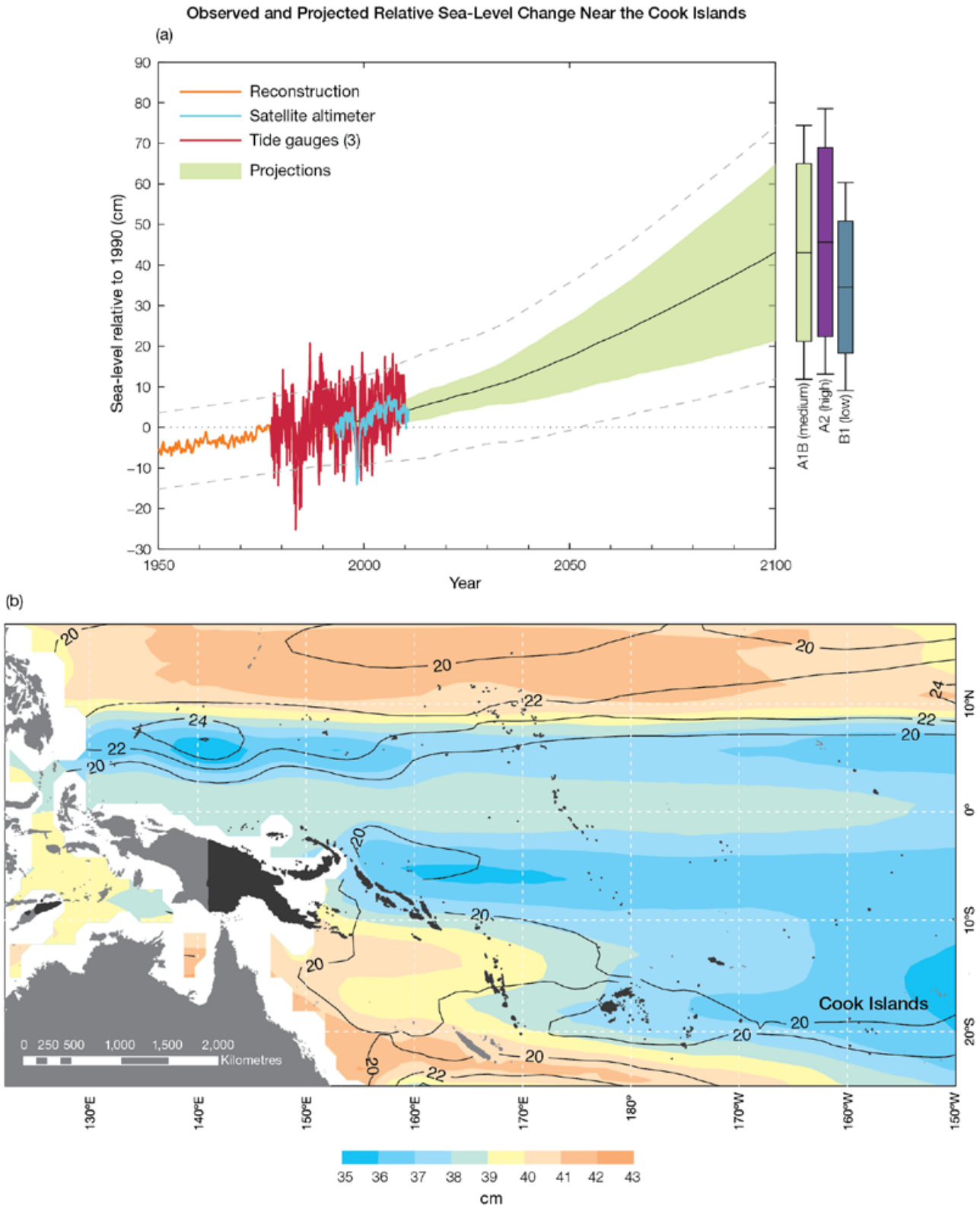

Figure 2.10: Observed and projected relative sea-level change near the Cook Islands. (a) The observed in situ relative sea-level records (since the late 1970s) are indicated in red, with the satellite record (since 1993) in light blue. The gridded (reconstructed) sea level data at the Cook Islands (since 1950, from Church and White (in press)) is shown in orange. The projections for the A1B (medium) emissions scenario (5–95% uncertainty range) are shown by the green shaded region from 1990–2100. The range of projections for the B1 (low), A1B (medium) and A2 (high) emissions scenarios by 2100 are also shown by the bars on the right. The dashed lines are an estimate of interannual variability in sea level (5–95% range about the long-term trends) and indicate that individual monthly averages of sea level can be above or below longer-term averages. (b) The projections for the A1B (medium) emissions scenario for the average over 2081–2100 relative to 1981–2000 are indicated by the shading, with the estimated uncertainty in the projections indicated by the contours (in cm).

2.7.6 Projections Summary

The projections presented in Section 2.7 are summarised in Table 2.4 (Northern Cook Islands) and Table 2.5 (Southern Cook Islands). For detailed information regarding the various uncertainties associated with the table values, refer to the preceding text in Sections 2.7 and 1.7, in addition to Chapters 5 and 6 in Volume 1. When interpreting the differences between projections for the B1 (low), A1B (medium) and A2 (high) emissions scenarios, it is also important to consider the emissions pathways associated with each scenario (Volume 1, Figure 4.1) and the fact that a slightly different subset of models was available for each (Volume 1, Appendix 1).

Table 2.4: Projected change in the annual and seasonal mean climate for the Northern Cook Islands, under the B1 (low; blue), A1B (medium; green) and A2 (high; purple) emissions scenarios. Projections are given for three 20-year periods centred on 2030 (2020–2039), 2055 (2046–2065) and 2090 (2080–2099), relative to 1990 (1980–1999). Values represent the multi-model mean change ± twice the inter-model standard deviation (representing approximately 95% of the range of model projections), except for sea level where the estimated mean change and the 5–95% range are given (as they are derived directly from the Intergovernmental Panel on Climate Change Fourth Assessment Report values). The confidence (Section 1.7.2) associated with the range and distribution of the projections is also given (indicated by the standard deviation and multi-model mean, respectively). See Volume 1, Appendix 1, for a complete listing of CMIP3 models used to derive these projections.

Variable	Season	2030	2055	2090	Confidence
Surface air temperature (°C)	Annual	+0.6 ± 0.4 +0.8 ± 0.4 +0.7 ± 0.2	+1.1 ± 0.4 +1.4 ± 0.5 +1.4 ± 0.4	+1.5 ± 0.6 +2.2 ± 0.8 +2.6 ± 0.6	Moderate
Maximum temperature (°C)	1-in-20-year event	N/A	+1.0 ± 0.6 +1.4 ± 0.6 +1.5 ± 0.5	+1.3 ± 0.7 +2.0 ± 1.1 +2.6 ± 1.3	Low
Minimum temperature (°C)	1-in-20-year event	N/A	+1.3 ± 1.7 +1.6 ± 1.6 +1.4 ± 1.9	+1.7 ± 1.7 +1.9 ± 1.8 +2.3 ± 1.9	Low
Total rainfall (%)*	Annual	+3 ± 8 +4 ± 9 +3 ± 13	+5 ± 12 +6 ± 25 +6 ± 26	+6 ± 22 +8 ± 33 +9 ± 37	Low
Wet season rainfall (%)*	November-April	+4 ± 9 +4 ± 9 +3 ± 9	+5 ± 11 +6 ± 19 +5 ± 19	+6 ± 19 +8 ± 31 +8 ± 31	Low
Dry season rainfall (%)*	May-October	+4 ± 14 +5 ± 13 +5 ± 19	+6 ± 15 +7 ± 35 +8 ± 38	+6 ± 28 +9 ± 42 +10 ± 51	Low
Sea-surface temperature (°C)	Annual	+0.6 ± 0.3 +0.7 ± 0.4 +0.7 ± 0.4	+0.9 ± 0.4 +1.2 ± 0.5 +1.3 ± 0.6	+1.3 ± 0.5 +2.0 ± 0.8 +2.3 ± 0.8	Moderate
Aragonite saturation state (Ωar)	Annual maximum	+3.6 ± 0.2 +3.6 ± 0.2 +3.6 ± 0.1	+3.4 ± 0.2 +3.3 ± 0.2 +3.3 ± 0.2	+3.3 ± 0.1 +2.9 ± 0.3 +2.7 ± 0.1	Moderate
Mean sea level (cm)	Annual	+10 (5–15) +10 (5–15) +10 (4–15)	+18 (10–26) +20 (10–30) +19 (10–29)	+31 (17–45) +38 (19–56) +38 (19–58)	Moderate

*The MIROC3.2(medres) and MIROC3.2(hires) models were eliminated in calculating the rainfall projections, due to their inability to accurately simulate present-day activity of the South Pacific Convergence Zone (Volume 1, Section 5.5.1).

Table 2.5: Projected change in the annual and seasonal mean climate for the Southern Cook Islands, under the B1 (low; blue), A1B (medium; green) and A2 (high; purple) emissions scenarios. Projections are given for three 20-year periods centred on 2030 (2020–2039), 2055 (2046–2065) and 2090 (2080–2099), relative to 1990 (1980–1999). Values represent the multi-model mean change ± twice the inter-model standard deviation (representing approximately 95% of the range of model projections), except for sea level where the estimated mean change and the 5–95% range are given (as they are derived directly from the Intergovernmental Panel on Climate Change Fourth Assessment Report values). The confidence (Section 1.7.2) associated with the range and distribution of the projections is also given (indicated by the standard deviation and multi-model mean, respectively). See Volume 1, Appendix 1, for a complete listing of CMIP3 models used to derive these projections.

Variable	Season	2030	2055	2090	Confidence
Surface air temperature (°C)	Annual	+0.6 ± 0.4 +0.7 ± 0.4 +0.7 ± 0.3	+1.0 ± 0.5 +1.3 ± 0.6 +1.3 ± 0.4	+1.3 ± 0.6 +2.0 ± 0.8 +2.5 ± 0.7	Moderate
Maximum temperature (°C)	1-in-20-year event	N/A	+1.0 ± 0.6 +1.4 ± 0.6 +1.5 ± 0.6	+1.2 ± 0.8 +2.0 ± 0.9 +2.5 ± 1.3	Low
Minimum temperature (°C)	1-in-20-year event	N/A	+1.1 ± 1.6 +1.4 ± 1.6 +1.3 ± 1.6	+1.4 ± 1.5 +2.9 ± 1.8 +2.0 ± 1.9	Low
Total rainfall (%)*	Annual	+1 ± 11 +3 ± 10 +5 ± 9	+2 ± 8 +3 ± 13 +5 ± 11	+5 ± 14 +6 ± 13 +8 ± 24	Low
Wet season rainfall (%)*	November-April	+1 ± 11 +3 ± 11 +3 ± 9	+3 ± 11 +3 ± 13 +5 ± 14	+5 ± 19 +7 ± 15 +10 ± 23	Low
Dry season rainfall (%)*	May-October	+1 ± 15 +5 ± 15 +7 ± 12	+2 ± 12 +4 ± 17 +5 ± 15	+5 ± 13 +6 ± 22 +6 ± 34	Low
Sea-surface temperature (°C)	Annual	+0.6 ± 0.3 +0.6 ± 0.3 +0.7 ± 0.3	+0.9 ± 0.4 +1.1 ± 0.4 +1.2 ± 0.4	+1.3 ± 0.4 +1.9 ± 0.5 +2.3 ± 0.7	Moderate
Aragonite saturation state (Ωar)	Annual maximum	+3.5 ± 0.1 +3.5 ± 0.1 +3.5 ± 0.1	+3.3 ± 0.1 +3.1 ± 0.1 +3.1 ± 0.1	+3.1 ± 0.1 +2.7 ± 0.1 +2.5 ± 0.1	Moderate
Mean sea level (cm)	Annual	+10 (5–15) +10 (5–15) +10 (4–15)	+18 (10–26) +20 (10–30) +19 (10–29)	+31 (17–45) +38 (19–56) +38 (19–58)	Moderate

*The MIROC3.2(medres) and MIROC3.2(hires) models were eliminated in calculating the rainfall projections, due to their inability to accurately simulate present-day activity of the South Pacific Convergence Zone (Volume 1, Section 5.5.1).

Coastline, Dili district

Chapter 3
East Timor (Timor-Leste)

The contributions of Terencio Fernandes Moniz and Sebastião da Silva from the National Directorate of Meteorology and Geophysics are gratefully acknowledged

Introduction

This chapter provides a brief description of East Timor, its past and present climate as well as projections for the future. The climate observation network and the availability of atmospheric and oceanic data records are outlined. Seasonal cycles are described and the influences of large-scale climate features (e.g. the South Pacific Convergence Zone) and patterns of climate variability (e.g. the El Niño-Southern Oscillation) are analysed and discussed. Observed trends and analysis of rainfall, extreme events (including tropical cyclones), sea-surface temperature, ocean acidification, sea level and mean sea level are presented. Projections for air and sea-surface temperature, rainfall, extreme events, ocean acidification and sea level for the 21st century are provided. These projections are presented along with confidence levels based on expert judgement by Pacific Climate Change Science Program (PCCSP) scientists. The chapter concludes with a summary table of projections (Table 3.3). Important background information, including an explanation of methods and models, is provided in Chapter 1. For definitions of other terms refer to the Glossary.

3.1 Climate Summary

3.1.1 Current Climate

- Dili has a very marked wet season from December to May and a dry season from June to November.
- Sea-surface temperatures are closely related to air temperatures and show a weak seasonal cycle with highest temperatures in March and November, about 2.5ºC warmer than those in July, the coolest month.
- Air temperature trends are not presented as there is insufficient data available for the 1950–2009 period.
- Negative trends in annual and dry season rainfall at Dili Airport for the period 1952–2009 are statistically significant.
- The sea-level rise near East Timor measured by satellite altimeters since 1993 is about 9 mm per year.
- On average Dili experiences eight tropical cyclones per decade, with most occurring between November and April, however, the effect is usually weak.

3.1.2 Future Climate

Over the course of the 21st century:

- Surface air temperature and sea-surface temperature are projected to continue to increase (*very high* confidence).
- Wet season rainfall is projected to increase (*moderate* confidence).
- Dry season rainfall is projected to decrease (*moderate* confidence).
- Little change is projected in annual mean rainfall (*low* confidence).
- The intensity and frequency of days of extreme heat are projected to increase (*very high* confidence).
- The intensity and frequency of days of extreme rainfall are projected to increase (*high* confidence).
- Little change is projected in the incidence of drought (*low* confidence).
- Tropical cyclone numbers are projected to decline in the broad region surrounding East Timor (0–20ºS and 100ºE–130ºE) (*moderate* confidence).
- Ocean acidification is projected to continue (*very high* confidence).
- Mean sea-level rise is projected to continue (*very high* confidence).

3.2 Country Description

East Timor lies between 8°S–10°S and 124°E–128°E at the eastern end of the Indonesian archipelago. East Timor comprises the eastern half of Timor Island and includes the exclave of Oecusse-Ambeno as well as the two islands, Atauru and Jaco. A mountain range divides the north and south coasts of Timor-Leste. The highest peak is Mount Ramelau (Timor-Leste Country Statistics, 2011).

The population of East Timor in the 2010 census was 1 066 582, most of which live in, or around, the capital of Dili. East Timor's total land area is 15 007 km^2 which is divided in to 13 administrative districts (Timor-Leste Country Statistics, 2011).

East Timor is a low to middle income economy that continues to suffer the after-effects of decades-long conflict, which damaged infrastructure and displaced thousands of people. Oil and gas deposits are responsible for a large part of East Timor's revenue. Major export commodities include coffee, vanilla, coconut, sandalwood and marble (East Timor Country Brief, 2011).

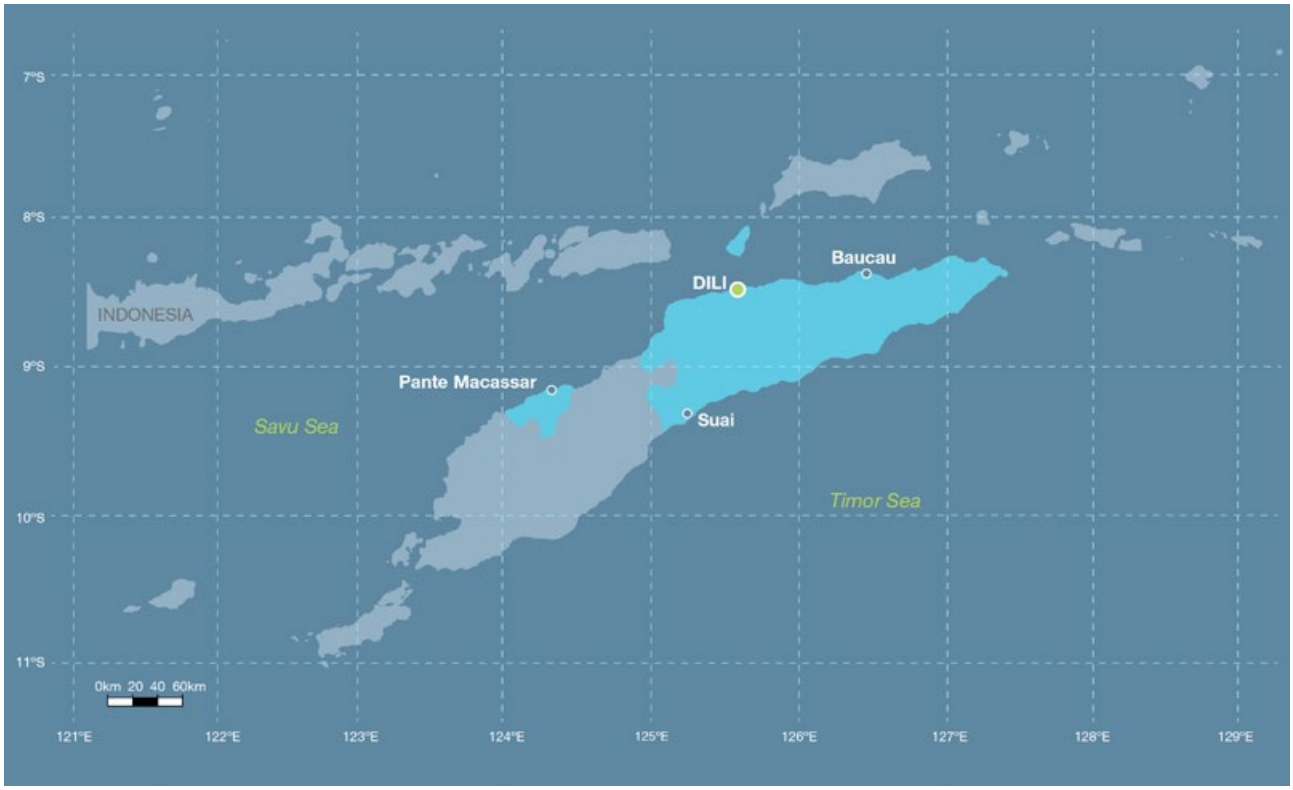

Figure 3.1: East Timor

3.3 Data Availability

There are currently five operational stations in the East Timor national meteorological network. The primary climate station is located at Dili Airport, near the nation's capital, on the northern side of the island of Timor (Figure 3.1). Rainfall and air temperature data are available for Dili Airport from 1952 and 2003 to present respectively. Observations likely began much earlier; however, these records are yet to be located.

Rainfall data for Dili Airport for 1950–2009 have been used. This record is 90% complete and homogeneous. The available temperature data record is not long enough to provide information about trends in temperature.

There are no tide gauge data available for East Timor, so the Wyndham (Western Australia; since 1984) record has been used as the closest available gauge (Figure 3.8). Both satellite (from 1993) and in situ sea-level data (1950–2009; termed reconstructed sea level; Volume 1, Section 2.2.2.2) are available on a global 1° x 1° grid.

Long-term locally-monitored sea-surface temperature data are unavailable for East Timor, so large-scale gridded sea-surface temperature datasets have been used (HadISST, HadSST2, ERSST and Kaplan Extended SST V2; Volume 1, Table 2.3).

3.4 Seasonal Cycles

Temperature records from Dili are not long enough to calculate an accurate climatology for the site. Annual variations in sea-surface temperatures near Dili are likely to be closely related to air temperatures, and show a weak seasonal cycle with highest temperatures in March and November, about 2.5ºC warmer than those in July, the coolest month.

The seasonal cycle of rainfall (Figure 3.2) shows that Dili has a very marked wet season from December to May and a dry season from June to November. The effect of the West Pacific Monsoon is very strong. For most of the wet season average monthly rainfall is above 100 mm while for most of the dry season it is less than 30 mm. With regards to wind flow, south-east trade winds dominate in Dili, except during the monsoon season when the winds are predominately westerlies. The different phases of the Madden-Julian Oscillation (Volume 1, Section 2.4.4) bring active and dry periods within the monsoon season.

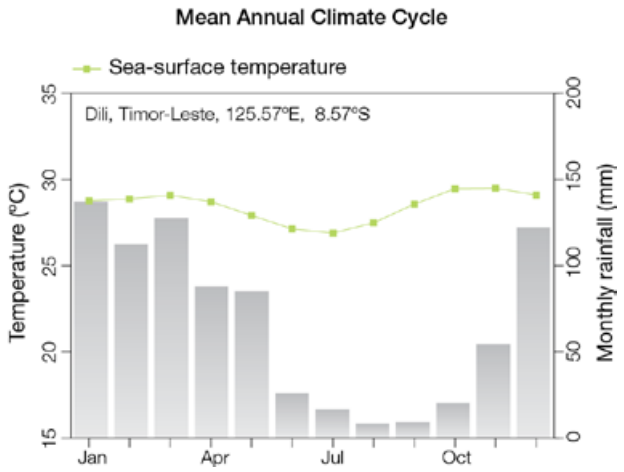

Figure 3.2: Mean annual cycle of rainfall (grey bars) at Dili Airport and local sea-surface temperatures derived from the HadISST dataset (Volume 1, Table 2.3).

3.5 Climate Variability

Due to the short temperature records in Dili, it is not possible to calculate correlation coefficients to determine the impact of large-scale climate variability on temperature. High year-to-year rainfall variability is observed (Figure 3.3). In the dry season there are clear influences on rainfall from a number of components of climate variability, however no significant correlations are found between indicators of this variability in the wet season (Table 3.1). Both the El Niño-Southern Oscillation (ENSO) and the Indian Ocean Dipole (IOD) are related to dry-season rainfall in Dili. El Niño events generally bring drier conditions to Dili, and although they often lead to a late onset and early finish to the wet season, there is no clear influence of ENSO on total wet season rainfall. During La Niña events, dry-season rainfall tends to be above normal, and the wet season often starts earlier and finishes later.

During a positive phase of the IOD, rainfall is lower than normal as seen by the significant correlation between dry season rainfall and the IOD Index (Table 3.1). However, ENSO and IOD are not completely independent. When the relationship between ENSO and the IOD is removed, the correlation is still significant, but weaker (-0.37). The IOD impact is only seen in the dry season, as the IOD is usually not active in the wet season. ENSO Modoki events (Volume1, Section 3.4.1) also affect dry season rainfall but the relationship is slightly weaker than for canonical ENSO events.

Table 3.1: Correlation coefficients between indices of key large-scale climate variability and minimum and maximum temperatures (Tmin and Tmax) and rainfall at Dili Airport. Only correlation coefficients that are statistically significant at the 95% level are shown.

Climate feature/index		Dry season (June-November) Rain	Wet season (December–May) Rain
ENSO	Niño3.4	-0.52	
	Southern Oscillation Index	0.61	
Interdecadal Pacific Oscillation Index			
Indian Ocean Dipole Index		-0.54	
ENSO Modoki Index		-0.45	
Number of years of data		51	48

Climate data management training, National Directorate of Meteorology and Geophysics

3.6 Observed Trends

3.6.1 Air Temperature

There is insufficient data available to provide air temperature trends from 1950 to 2009. Data is only available from 2003 to 2009.

3.6.2 Rainfall

The Dili Airport negative annual and dry season rainfall trends for the period 1952–2009 are statistically significant. The wet season rainfall trend is not statistically significant (Table 3.2 and Figure 3.3).

Table 3.2: Annual and seasonal trends in rainfall at Dili Airport for the period 1952–2009. Asterisks indicate significance at the 95% level. Persistence is taken into account in the assessment of significance as in Power and Kociuba (in press).

	Dili Airport Rain (mm per 10 yrs)
Annual	-41*
Wet season	+14
Dry season	-26*

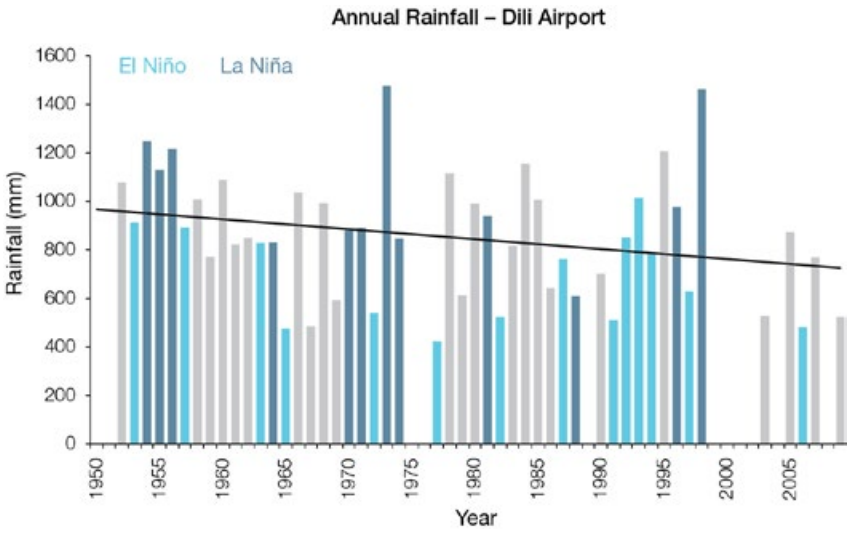

Figure 3.3: Annual rainfall at Dili Airport. Light blue, dark blue and grey bars denote El Niño, La Niña and neutral years respectively.

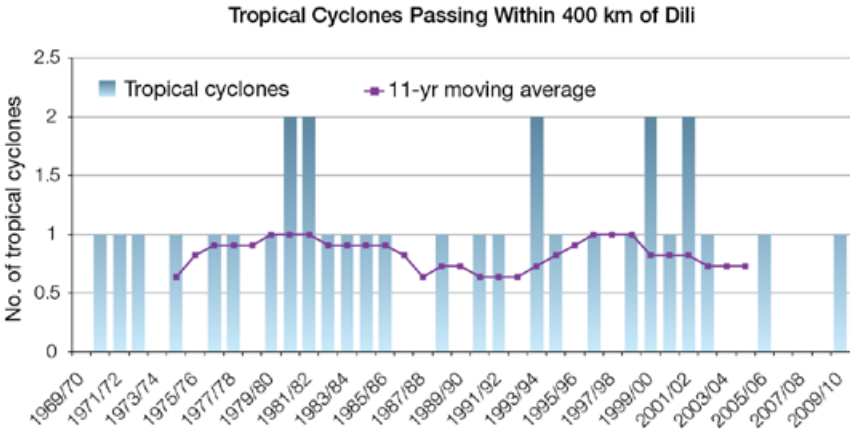

Figure 3.4: Tropical cyclones passing within 400 km of Dili per season. The 11-year moving average is in purple.

3.6.3 Extreme Events

Tropical cyclones can affect East Timor between November and April but their effect has been weak due to East Timor's proximity to the equator. Occurrences outside November to April are rare. The tropical cyclone archive for the Southern Hemisphere indicates that between the 1969/70 and 2009/10 seasons, the centre of 31 tropical cyclones passed within approximately 400 km of Dili (Figure 3.4). This represents an average of eight cyclones per decade. Tropical cyclone occurrences in El Niño, La Niña and neutral years are similar (six, eight and nine cyclones per decade, respectively).

ENSO has a notable effect on East Timor's climate. During La Niña years above-normal rainfall leads to increased frequency of flooding and landslides. El Niño years are associated with droughts. The most significant impact on the population during El Niño years is reduced ground water availability.

3.6.4 Sea-Surface Temperature

Water temperatures around East Timor have risen gradually since the 1950s. Since the 1970s the rate of warming has been approximately 0.16°C per decade. At these regional scales, natural variability plays a large role in determining the sea-surface temperature, making it difficult to identify long-term trends. Figure 3.6 shows the 1950–2000 sea-surface temperature trends (relative to a reference year of 1990) from different large-scale gridded sea-surface temperature datasets (HadISST, HadSST2, ERSST and Kaplan Extended SST V2; Volume 1, Table 2.3).

3.6.5 Ocean Acidification

No data are available for East Timor.

3.6.6 Sea Level

Monthly averages of the closest available tide gauge (Wyndham, since 1984), satellite (since 1993) and gridded sea-level (since 1950) data agree well and indicate interannual variability in sea levels of about 24 cm (estimated 5–95% range) after removal of the seasonal cycle (Figure 3.8). The sea-level rise near East Timor, measured by satellite altimeters (Figure 3.5) since 1993, is about 9 mm per year, larger than the global average of 3.2 ± 0.4 mm per year. This rise is partly linked to of a pattern related to climate variability from year to year and decade to decade (Figure 3.8).

3.6.7 Extreme Sea-Level Events

This analysis could not be undertaken as there are no tide gauge data available for East Timor.

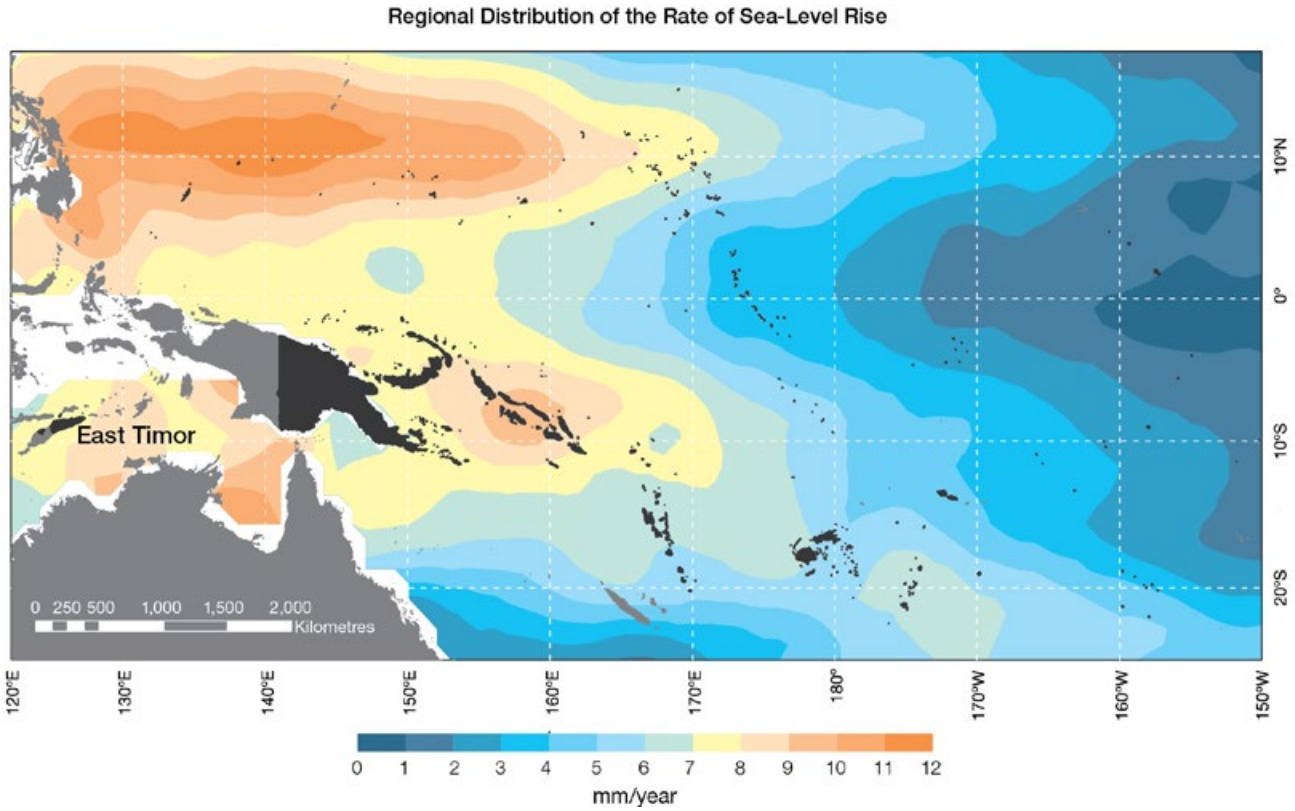

Figure 3.5: The regional distribution of the rate of sea-level rise measured by satellite altimeters from January 1993 to December 2010, with the location of East Timor indicated. Further information on regional distribution of sea-level rise is provided in Volume 1, Section 3.6.3.2.

3.7 Climate Projections

Climate projections have been derived from up to 18 global climate models from the CMIP3 database, for up to three emissions scenarios (B1 (low), A1B (medium) and A2 (high)) and three 20-year periods (centred on 2030, 2055 and 2090, relative to 1990). These models were selected based on their ability to reproduce important features of the current climate (Volume 1, Section 5.2.3), so projections arising from each of the models are a plausible representation of the future climate. This means there is not one single projected future for East Timor, but rather a range of possible futures. The full range of these futures is discussed in the following sections.

These projections do not represent a value specific to any actual location, such as a town or city in East Timor. Instead, they refer to an average change over the broad geographic region encompassing East Timor and the surrounding ocean (Figure 1.1 shows the regional boundaries). Some information regarding dynamical downscaling simulations from the CCAM model (Section 1.7.2) is also provided, in order to indicate how changes in the climate on an individual island-scale may differ from the broad-scale average.

Important information about understanding climate model projections is provided in Section 1.7. A more detailed discussion of East Timor's future climate can also be found in Kirono (2010).

3.7.1 Temperature

Surface air temperature and sea-surface temperature are projected to continue to increase over the course of the 21st century. There is *very high* confidence in this direction of change because:

- Warming is physically consistent with rising greenhouse gas concentrations.
- All CMIP3 models agree on this direction of change.

The majority of CMIP3 models simulate a slight increase (<1°C) in annual and seasonal mean surface air temperature by 2030, however by 2090 under the A2 (high) emissions scenario increases of greater than 2.5°C are simulated by almost all models (Table 3.3). Given the close relationship between surface air temperature and sea-surface temperature, a similar (or slightly weaker) rate of warming is projected for the surface ocean (Figure 3.6). There is *high* confidence in this range and distribution of possible futures because:

- There is generally close agreement between modelled and observed temperature trends (from reanalysis data) over the past 50 years in the vicinity of East Timor, although observational records are limited (Figure 3.8).

The 8 km CCAM simulations suggest that projected changes in surface air temperature over land can be up to 1°C greater than over the surrounding ocean. This suggests that the CMIP3 models may slightly underestimate future increases in land temperature. Inland regions are also projected to warm faster than coastal regions.

Interannual variability in surface air temperature and sea surface temperature over East Timor is strongly influenced by ENSO in the current climate (Section 3.5). Projections of future ENSO activity (Volume 1, Section 6.4.1) are not consistent, so it is not possible to determine whether interannual variability in temperature will change in the future. However, ENSO is expected to continue to be an important source of variability for East Timor and the region.

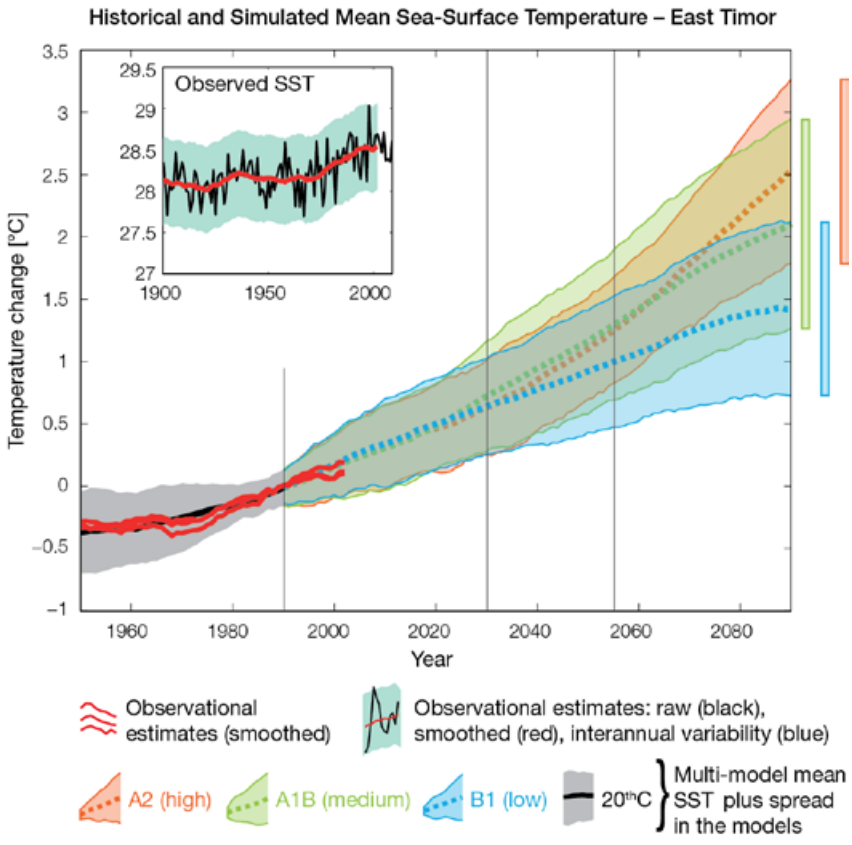

Figure 3.6: Historical climate (from 1950 onwards) and simulated historical and future climate for annual mean sea-surface temperature (SST) in the region surrounding East Timor, for the CMIP3 models. Shading represents approximately 95% of the range of model projections (twice the inter-model standard deviation), while the solid lines represent the smoothed (20-year running average) multi-model mean temperature. Projections are calculated relative to the 1980–1999 period (which is why there is a decline in the inter-model standard deviation around 1990). Observational estimates in the main figure (red lines) are derived from the HadSST2, ERSST and Kaplan Extended SST V2 datasets (Volume 1, Section 2.2.2). Annual average (black) and 20-year running average (red) HadSST2 data is also shown inset.

3.7.2 Rainfall

Wet Season (November-April)

Wet season rainfall is projected to increase over the course of the 21st century. There is *moderate* confidence in this direction of change because:

- An increase in wet season rainfall is consistent with the projected likely amplification of the seasonal rainfall-cycle associated with the West Pacific Monsoon (WPM; Volume 1, Section 6.4.4)
- Approximately half of the CMIP3 models agree on this direction of change by 2090.

The majority of CMIP3 models simulate little change (-5% to 5%) in wet season rainfall by 2030, however by 2090 under the higher emissions scenarios (i.e. A1B (medium) and A2 (high)) the models are approximately equally divided between an increase (>5%) and little change, with only two models suggesting a decline (< -5%) (Table 3.3). There is *moderate* confidence in this range and distribution of possible futures because:

- The majority of CMIP3 models correctly simulate the seasonal cycle of rainfall over East Timor, however the region is subject to large model biases relating to the position of the West Pacific Warm Pool (Volume 1, Section 5.2.2.1).
- The CMIP3 models are unable to resolve many of the physical processes involved in producing rainfall. As a consequence, they do not simulate rainfall as well as other variables such as temperature (Volume 1, Chapter 5).

Dry Season (May-October)

Dry season rainfall is projected to decrease over the course of the 21st century. There is *moderate* confidence in this direction of change because:

- Reduced dry season rainfall is consistent with the projected likely amplification of the seasonal rainfall-cycle associated with the WPM (Volume 1, Section 6.4.4).
- The majority of CMIP3 models agree on this direction of change by 2090.

Approximately half of CMIP3 models simulate little change (-5% to 5%) in dry season rainfall by 2030, however by 2090 under the higher emissions scenarios (i.e. A1B (medium) and A2 (high)) the majority of models simulate a decrease, with the remainder approximately equally divided between a increase (> 5%) and little change (Table 3.3). There is *moderate* confidence in this range and distribution of possible futures because:

- The majority of CMIP3 models correctly simulate the seasonal cycle of rainfall over East Timor, however the region is subject to large model biases relating to the position of the West Pacific Warm Pool (Volume 1, Section 5.2.2.1).
- The CMIP3 models are unable to resolve many of the physical processes involved in producing rainfall.

Annual

Little change is projected in total annual rainfall over the course of the 21st century. There is *low* confidence in this direction of change because:

- Only approximately half of the CMIP3 models suggest this direction of change by 2090.
- There is only moderate confidence in wet and dry season rainfall projections, as discussed.

Interannual variability in rainfall over East Timor is strongly influenced by ENSO in the current climate, via its influence on WPM activity (Section 3.5). As there is no consistency in projections of future ENSO activity (Volume 1, Section 6.4.1), it is not possible to determine whether interannual variability in rainfall will change in the future.

3.7.3 Extremes

Temperature

The intensity and frequency of days of extreme heat are projected to increase over the course of the 21st century. There is *very high* confidence in this direction of change because:

- An increase in the intensity and frequency of days of extreme heat is physically consistent with rising greenhouse gas concentrations.
- All CMIP3 models agree on the direction of change for both intensity and frequency.

The majority of CMIP3 models simulate an increase of approximately 1°C in the temperature experienced on the 1-in-20-year hot day by 2055 under the B1 (low) emissions scenario, with an increase of over 2.5°C simulated by the majority of models by 2090 under the A2 (high) emissions scenario (Table 3.3). There is *low* confidence in this range and distribution of possible futures because:

- In simulations of the current climate, the CMIP3 models tend to underestimate the intensity and frequency of days of extreme heat (Volume 1, Section 5.2.4).
- Smaller increases in the frequency of days of extreme heat are projected by the CCAM 60 km simulations.

Rainfall

The intensity and frequency of days of extreme rainfall are projected to increase over the course of the 21st century. There is *high* confidence in this direction of change because:

- An increase in the frequency and intensity of extreme rainfall is consistent with larger-scale projections, based on the physical argument that the atmosphere is able to hold more water vapour in a warmer climate (Allen and Ingram, 2002; IPCC, 2007). It is also consistent with the projected likely amplification of the seasonal rainfall cycle associated with the WPM (Volume 1, Section 6.4.4).

- Almost all of the CMIP3 models agree on this direction of change for both intensity and frequency.

The majority of CMIP3 models simulate an increase of at least 15 mm in the amount of rain received on the 1-in-20-year wet day by 2055 under a B1 (low) emissions scenario, with an increase of at least 40 mm simulated by all models by 2090 under the A2 (high) emissions scenario. The majority of models project that the current 1-in-20-year extreme rainfall event will occur, on average, four times per 20-year period by 2055 under the B1 (low) emissions scenario and between five and six times per 20-year period by 2090 under the A2 (high) emissions scenario. There is *low* confidence in this range and distribution of possible futures because:

- In simulations of the current climate, the CMIP3 models tend to underestimate the intensity and frequency of extreme rainfall (Volume 1, Section 5.2.4).
- The CMIP3 models are unable to resolve many of the physical processes involved in producing extreme rainfall.

Drought

Little change is projected in the incidence of drought over the course of the 21st century. There is *low* confidence in this direction of change because:

- There is only low confidence in annual rainfall projections (Section 3.7.2), which directly influences projections of future drought conditions.

The majority of CMIP3 models project that mild drought will occur approximately 8–10 times every 20 years across all time periods and emissions scenarios. Moderate drought is projected to occur approximately once to twice every 20 years for all time periods under the A1B (medium) and A2 (high) emissions scenarios, while under the B1 (low) emissions scenario a frequency of two to three times every 20 years is projected by the majority of models for 2030, decreasing to once to twice by 2090. The majority of CMIP3 models project that severe droughts will occur approximately once every 20 years across all time periods and emissions scenarios.

Tropical Cyclones

Tropical cyclone numbers are projected decline for the broad region surrounding East Timor (0–20ºS, 100ºE–130ºE) over the course of the 21st century. There is *moderate* confidence in this direction of change because:

- Many studies suggest a decline in tropical cyclone frequency globally (Knutson et al., 2010).
- Tropical cyclone numbers decline in the East Timor region in the majority of PCCSP assessment techniques.

Projected changes based on the direct detection methodologies (Curvature Vorticity Parameter (CVP) and the CSIRO Direct Detection Scheme (CDD); Volume 1, Section 4.8.2), indicate a decrease in tropical cyclone formation. When these techniques are applied to CCAM, 100% of projections show a decrease in tropical cyclone formation. In addition, the Genesis Potential Index (GPI) empirical technique suggests that conditions for tropical cyclone formation will become less favourable in the East Timor region for almost all analysed CMIP3 models. There is *moderate* confidence in this projection because in simulations of the current climate, the CVP, CDD and GPI methods capture the frequency of tropical cyclone activity reasonably well (Volume 1, Section 5.4).

3.7.4 Ocean Acidification

Aragonite saturation states above about 4 are considered optimal for coral growth and for the development of healthy reef ecosystems. While values between 3.5 and 4 are considered adequate, values between 3 and 3.5 are considered marginal, while values below 3 are considered extremely marginal (Guinotte et al., 2003).

The acidification of the ocean will continue to increase over the course of the 21st century. There is *very high* confidence in this projection as the rate of ocean acidification is driven primarily by the increasing oceanic uptake of carbon dioxide, in response to rising atmospheric carbon dioxide concentrations.

Projections from all analysed CMIP3 models indicate that the annual maximum aragonite saturation state will reach values below 3.5 by about 2025 and continue to decline thereafter (Figure 3.7; Table 3.3). There is *moderate* confidence in this range and distribution of possible futures because the projections are based on climate models without an explicit representation of the carbon cycle and with relatively low resolution and known regional biases.

The impact of acidification change on the health of reef ecosystems is likely to be compounded by other stressors including coral bleaching, storm damage and fishing pressure.

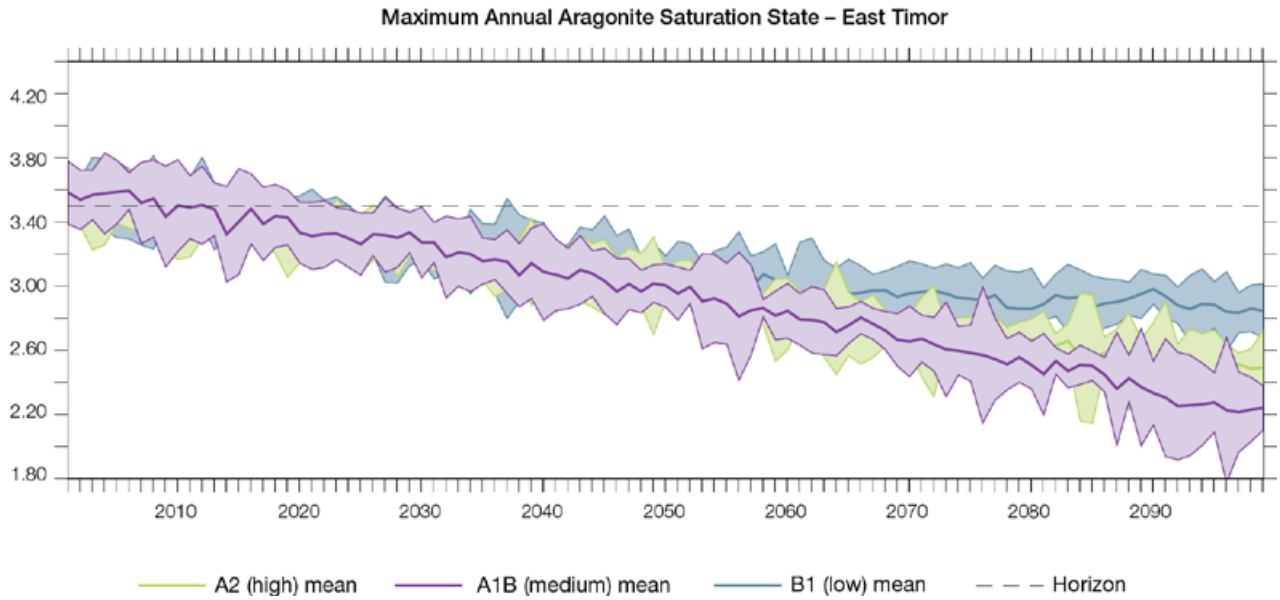

Figure 3.7: Multi-model projections, and their associated uncertainty (shaded area represents two standard deviations), of the maximum annual aragonite saturation state in the sea surface waters of the East Timor region under the different emissions scenarios. The dashed black line represents an aragonite saturation state of 3.5.

3.7.5 Sea Level

Mean sea level is projected to continue to rise over the course of the 21st century. There is *very high* confidence in this direction of change because:

- Sea-level rise is a physically consistent response to increasing ocean and atmospheric temperatures, due to thermal expansion and the melting of glaciers and ice caps.
- Projections from all CMIP3 models agree on this direction of change.

The CMIP3 models simulate a rise of between approximately 5–15 cm by 2030, with increases of 20–60 cm indicated by 2090 under the higher emissions scenarios (i.e. A1B (medium) and A2 (high); Figure 3.8; Table 3.3).

There is *moderate* confidence in this range and distribution of possible futures because:

- There is significant uncertainty surrounding ice-sheet contributions to sea-level rise and a rise larger than projected above cannot be excluded (Meehl et al., 2007b). However, understanding of the processes is currently too limited to provide a best estimate or an upper bound (IPCC, 2007).
- Globally, since the early 1990s, sea level has been rising near the upper end of the above projections. During the 21st century, some studies (using semi-empirical models) project faster rates of sea-level rise.

Interannual variability of sea level will lead to periods of lower and higher regional sea levels. In the past, this interannual variability has been about 24 cm (5–95% range, after removal of the seasonal signal; dashed lines in Figure 3.8 (a)) and it is likely that a similar range will continue through the 21st century. In addition, winds and waves associated with weather phenomena will continue to lead to extreme sea-level events.

In addition to the regional variations in sea level associated with ocean and mass changes, there are ongoing changes in relative sea level associated with changes in surface loading over the last glacial cycle (glacial isostatic adjustment) and local tectonic motions. The glacial isostatic motions are relatively small for the PCCSP region.

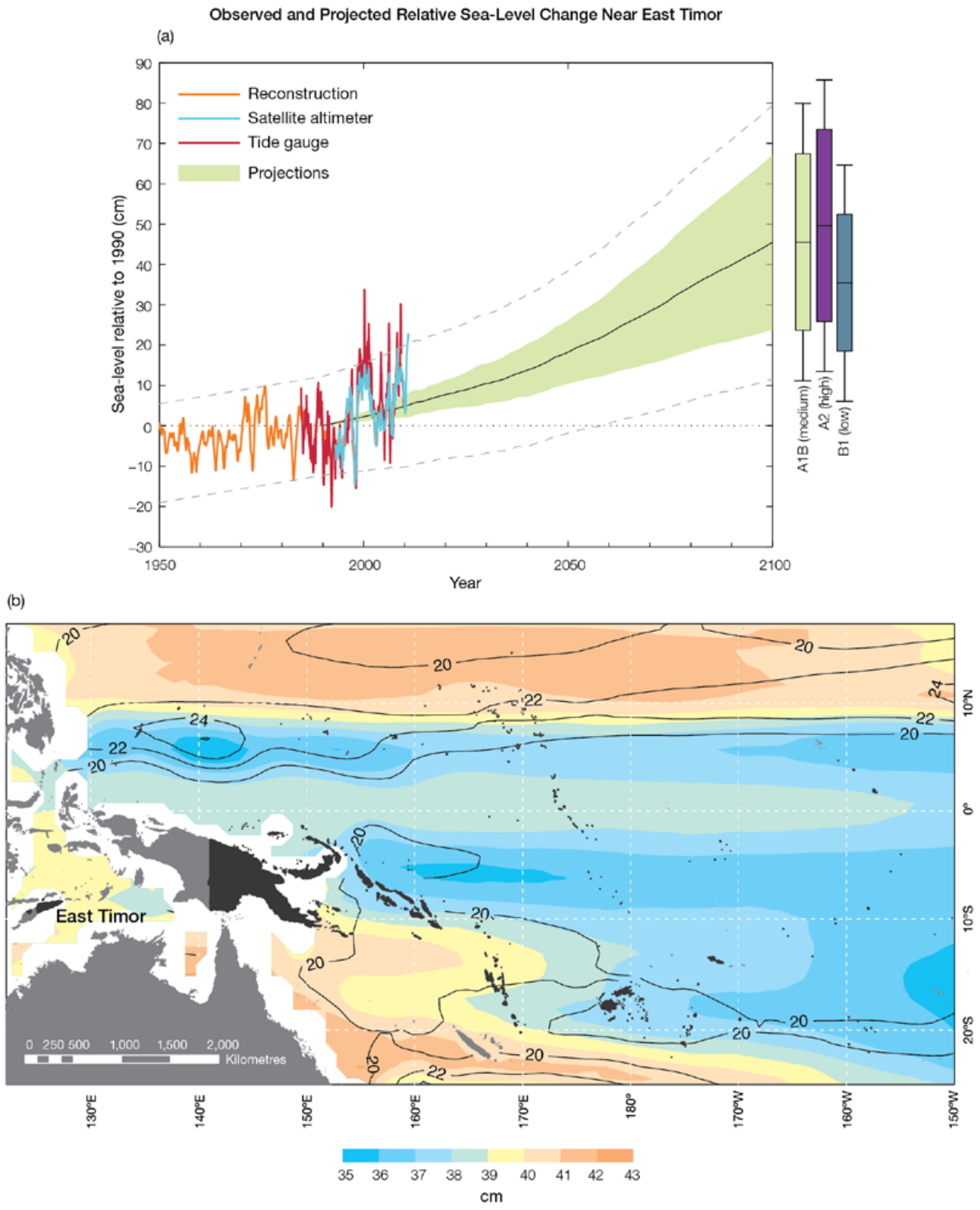

Figure 3.8: Observed and projected relative sea-level change near East Timor. (a) The observed in situ relative sea-level records from the closest available gauge at Wyndham are indicated in red, with the satellite record (since 1993) in light blue. The gridded sea level at East Timor (since 1950, from Church and White (in press)) is shown in orange. The projections for the A1B (medium) emissions scenario (5– 95% uncertainty range) are shown by the green shaded region from 1990–2100. The range of projections for the B1 (low), A1B (medium) and A2 (high) emissions scenarios are also shown by the bars on the right. The dashed lines are an estimate of interannual variability in sea level (5–95% range about the long-term trends) and indicate that individual monthly averages of sea level can be above or below longer-term averages. (b) The projections (in cm) for the A1B (medium) emissions scenario in the East Timor region for the average over 2081–2100 relative to 1981–2000 are indicated by the shading, with the estimated uncertainty in the projections indicated by the contours (in cm).

3.7.6 Projections Summary

The projections presented in Section 3.7 are summarised in Table 3.3. For detailed information regarding the various uncertainties associated with the table values, refer to the preceding text in Sections 3.7 and 1.7, in addition to Chapters 5 and 6 in Volume 1. When interpreting the differences between projections for the B1 (low), A1B (medium) and A2 (high) emissions scenarios, it is also important to consider the emissions pathways associated with each scenario (Volume 1, Figure 4.1) and the fact that a slightly different subset of models was available for each (Volume 1, Appendix 1).

Table 3.3: Projected change in the annual and seasonal mean climate for East Timor, under the B1 (low; blue), A1B (medium; green) and A2 (high; purple) emissions scenarios. Projections are given for three 20-year periods centred on 2030 (2020–2039), 2055 (2046–2065) and 2090 (2080–2099), relative to 1990 (1980–1999). Values represent the multi-model mean change ± twice the inter-model standard deviation (representing approximately 95% of the range of model projections), except for sea level where the estimated mean change and the 5–95% range are given (as they are derived directly from the Intergovernmental Panel on Climate Change Fourth Assessment Report values). The confidence (Section 1.7.2) associated with the range and distribution of the projections is also given (indicated by the standard deviation and multi-model mean, respectively). See Volume 1, Appendix 1, for a complete listing of CMIP3 models used to derive these projections.

Variable	Season	2030	2055	2090	Confidence
Surface air temperature (°C)	Annual	+0.7 ± 0.4 +0.8 ± 0.4 +0.7 ± 0.3	+1.1 ± 0.6 +1.5 ± 0.6 +1.4 ± 0.4	+1.5 ± 0.7 +2.3 ± 0.9 +2.8 ± 0.7	High
Maximum temperature (°C)	1-in-20-year event	N/A	+1.0 ± 0.6 +1.4 ± 0.6 +1.5 ± 0.5	+1.4 ± 0.8 +2.2 ± 1.1 +2.8 ± 1.5	Low
Minimum temperature (°C)	1-in-20-year event	N/A	+1.3 ± 1.6 +1.6 ± 1.8 +1.6 ± 1.7	+1.7 ± 1.6 +2.2 ± 1.8 +2.5 ± 1.8	Low
Total rainfall (%)*	Annual	+1 ± 9 +1 ± 8 0 ± 11	0 ± 15 -1 ± 18 0 ± 16	0 ± 13 0 ± 19 +1 ± 23	Low
Wet season rainfall (%)*	November-April	+1 ± 7 +1 ± 7 0 ± 8	+1 ± 10 +1± 14 +3 ± 10	+2 ± 9 +2 ± 15 +5 ± 16	Moderate
Dry season rainfall (%)*	May-October	+1 ± 20 +3 ± 18 0 ± 23	-2 ± 31 -4 ± 35 -3 ± 31	-4 ± 28 -3 ± 40 -4 ± 51	Moderate
Sea-surface temperature (°C)	Annual	+0.6 ± 0.4 +0.7 ± 0.4 +0.6 ± 0.4	+1.0 ± 0.5 +1.3 ± 0.6 +1.2 ± 0.4	+1.4 ± 0.7 +2.1 ± 0.8 +2.5 ± 0.7	High
Aragonite saturation state (Ωar)	Annual maximum	+3.3 ± 0.2 +3.2 ± 0.1 +3.2 ± 0.2	+3.0 ± 0.2 +2.9 ± 0.2 +2.8 ± 0.2	+2.8 ± 0.2 +2.5 ± 0.2 +2.3 ± 0.2	Moderate
Mean sea level (cm)	Annual	+10 (6–15) +11 (6–15) +10 (6–15)	+18 (10–27) +21 (12–30) +20 (12–29)	+32 (17–47) +40 (21–59) +42 (22–62)	Moderate

*The MIROC3.2 (medres) model was eliminated in calculating the rainfall projections, due to its inability to accurately simulate present-day activity of the West Pacific Monsoon (Volume 1, Section 5.5.1).

Kolonia Harbour, Pohnpei

Chapter 4
Federated States of Micronesia

The contributions of David Aranug, Johannes Berdon and Eden Skilling from the Federated States of Micronesia National Weather Service Office are gratefully acknowledged

Introduction

This chapter provides a brief description of the Federated States of Micronesia, its past and present climate as well as projections for the future. The climate observation network and the availability of atmospheric and oceanic data records are outlined. The annual mean climate, seasonal cycles and the influences of large-scale climate features such as the Intertropical Convergence Zone and patterns of climate variability (e.g. the El Niño-Southern Oscillation) are analysed and discussed. Observed trends and analysis of air temperature, rainfall, extreme events, sea-surface temperature, ocean acidification and mean and extreme sea level are presented. Projections for air and sea-surface temperature, rainfall, sea level and ocean acidification for the 21st century are provided, as are projections for tropical cyclones, drought, extreme rainfall, and extreme temperature. These projections are presented along with confidence levels based on expert judgement by Pacific Climate Change Science Program (PCCSP) scientists. The chapter concludes with summary tables of projections for eastern and western Federated States of Micronesia. Projections are provided in imperial units and metric units (Tables 4.4 and 4.5). Important background information, including an explanation of methods and models, is provided in Chapter 1. For definitions of other terms refer to the Glossary.

4.1 Climate Summary

4.1.1 Current Climate

- There is little seasonal variation in monthly mean maximum and minimum air temperatures, with less than 3ºF (1.5ºC) between the average hottest and coolest months. Sea-surface temperatures around the Federated States of Micronesia influence the seasonal variations in air temperature.
- The wet season occurs from May to September when the Intertropical Convergence Zone is strongest and furthest north.
- The West Pacific Monsoon affects rainfall in the western Federated States of Micronesia, bringing additional rain during the wet season.
- Warming trends are evident at Pohnpei and Yap in annual and seasonal mean air temperatures for the periods 1950–2009 and 1951–2009 respectively.
- Annual and seasonal rainfall trends for Pohnpei for the period 1950–2009 and Yap for the period 1951–2009 are not statistically significant.
- The sea-level rise measured by satellite altimeters since 1993 is over 0.39 inches (10 mm) per year.
- The main extreme events that occur in the Federated States of Micronesia are droughts, typhoons, storm waves, flooding and landslides.

4.1.2 Future Climate

Over the course of the 21st century:

- Surface air temperature and sea-surface temperature are projected to continue to increase (*very high* confidence).
- Annual and seasonal mean rainfall is projected to increase (*high* confidence).
- The intensity and frequency of days of extreme heat are projected to increase (*very high* confidence).
- The intensity and frequency of days of extreme rainfall are projected to increase (*high* confidence).
- The incidence of drought is projected to decrease (*moderate* confidence).
- Tropical cyclone numbers are projected to decline in the tropical North Pacific Ocean basin (0–15ºN, 130ºE –180ºE) (*moderate* confidence).
- Ocean acidification is projected to continue (*very high* confidence).
- Mean sea-level rise is projected to continue (*very high* confidence).

4.2 Country Description

The Federated States of Micronesia is located in the western North Pacific Ocean between the equator and 12°N, stretching from 136°E to 168°E. The country consists of four states: Yap, Chuuk, Pohnpei and Kosrae, listed in sequence from west to east. Of the total 607 islands, some are relatively large and mountainous, while the rest consist of smaller islands, flat coral atolls and raised coralline islands. The total land area comprises 271 square miles (702 km^2) and this contrasts with the size of the Exclusive Economic Zone which totals 1.15 million square miles (2.98 million km^2) (Federated States of Micronesia's First National Communication under the UNFCCC, 1997; Federated States of Micronesia Country Statistics, SOPAC, 2010).

In 2010 the estimated population of the Federated States of Micronesia was 111 364 (Federated States of Micronesia Country Statistics, SOPAC, 2010). The capital city is Palikir in the state of Pohnpei.

Economic activity consists primarily of subsistence farming and agriculture. The Federated States of Micronesia has few mineral deposits except for high-grade phosphate. While the potential exists for a tourism industry, its development is restricted by the country's remote location, few air connections and limited facilities for tourists (Federated States of Micronesia's Pacific Adaptation to Climate Change, 2006). The extensive tuna resources of the Exclusive Economic Zone are mainly exploited by Distant Water Fishing Nations under licence agreements (Federated States of Micronesia's First National Communication under the UNFCCC, 1997).

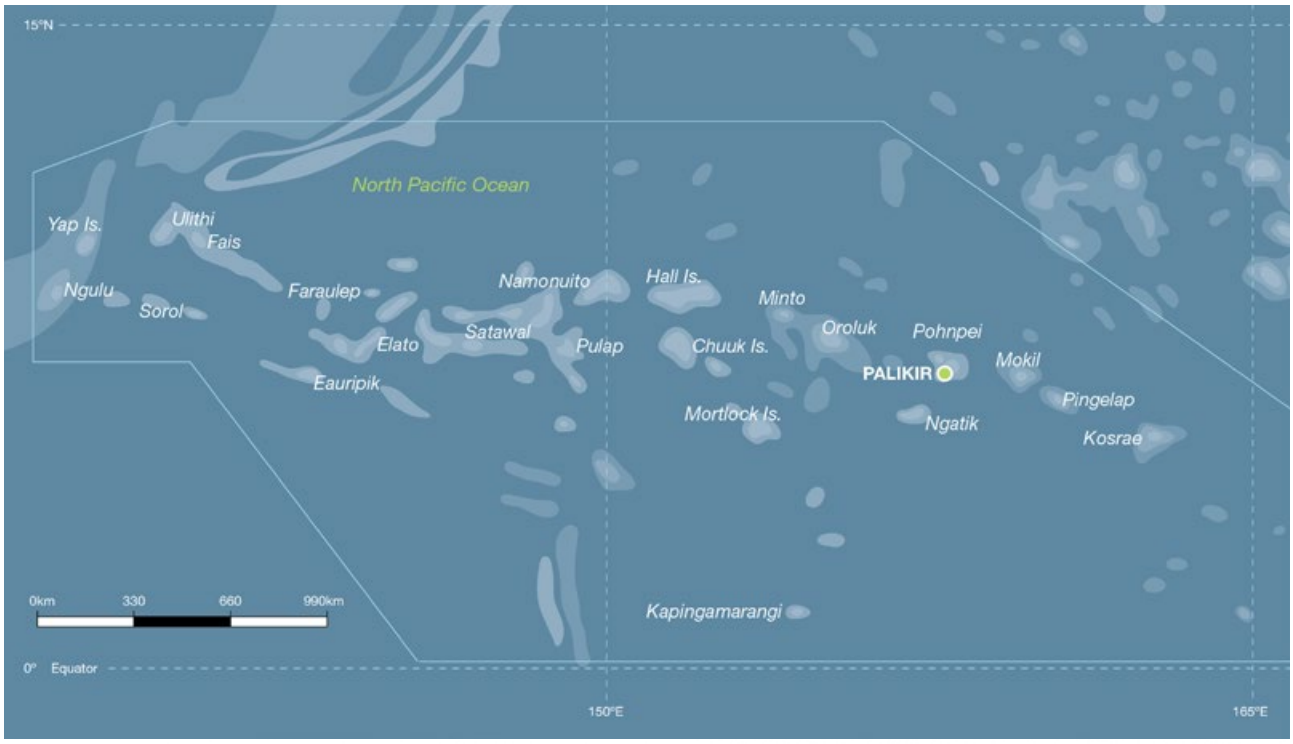

Figure 4.1: Federated States of Micronesia

4.3 Data Availability

There are 23 operational observation meteorological stations in the Federated States of Micronesia. Multiple observations within a 24-hour period are taken at five stations in Chuuk State, six in Pohnpei State (including Kosrae State) and three in Yap State. In addition, there are two single-observation-a-day climate stations in Pohnpei and seven single-observation-a-day rainfall stations in Yap (Figure 4.1).

Rainfall data for Pohnpei are available from 1949 and Yap from 1951. Air temperature data are available from 1950 for Pohnpei and 1951 for Yap. All available data from 1950 to 2009 are used. These records are homogeneous and more than 95% complete.

There are a number of sea-level records relevant for the Federated States of Micronesia. The best appear to be Guam (1948–present), Yap (1969–2005), Chuuk (Moen Island, 1947–1995), Kapingamarangi (1978–2008), Pohnpei-B (1974–2004) and Pohnpei-C (2002–present). A global positioning system instrument to estimate vertical land motion was deployed at Pohnpei in 2003 and will provide valuable direct estimates of local vertical land motion in future years. Both satellite (from 1993) and in situ sea-level data (1950–2009; termed reconstructed sea level; Volume 1, Section 2.2.2.2) are available on a global 1° x 1° grid.

Long-term locally-monitored sea surface-temperature data are unavailable for the Federated States of Micronesia so large-scale gridded sea-surface temperature datasets have been used (HadISST, HadSST2, ERSST and Kaplan Extended SST V2; Volume 1, Table 2.3).

Training in *Pacific Climate Futures*

4.4 Seasonal Cycles

The seasonal variations in monthly mean maximum and minimum air temperatures are very small, with less than 3ºF (1.5ºC) between the average warmest and coolest months (Figure 4.2). In Pohnpei the highest average maximum air temperatures occur when average minimum air temperatures are lowest. However, in Yap average minimum air temperatures are extremely constant and maximum air temperatures are highest in April-May. As a country made up of small islands surrounded by ocean, seasonal variations in air temperatures are driven by sea-surface temperatures around the Federated States of Micronesia.

The monthly mean rainfall cycle shows the distinction between the wet (May–October) and dry (November–April) seasons. The wet season occurs when the Intertropical Convergence Zone (ITCZ) is strongest and furthest north, closest to the Federated States of Micronesia. Pohnpei is close to the average position of the ITCZ, which is active year-round, so each month of the year Pohnpei's average rainfall is above 10 inches (250 mm). Rainfall is lower in Yap as it is further north. During the wet season in Yap there is a more noticeable presence of gusty winds and rainfall in association with the ITCZ. The West Pacific Monsoon (WPM) also affects rainfall in the Federated States of Micronesia, bringing additional rain during the wet season. This influence is strongest in Yap and other islands in the western Federated States of Micronesia and weaker in Pohnpei in the eastern side of the country.

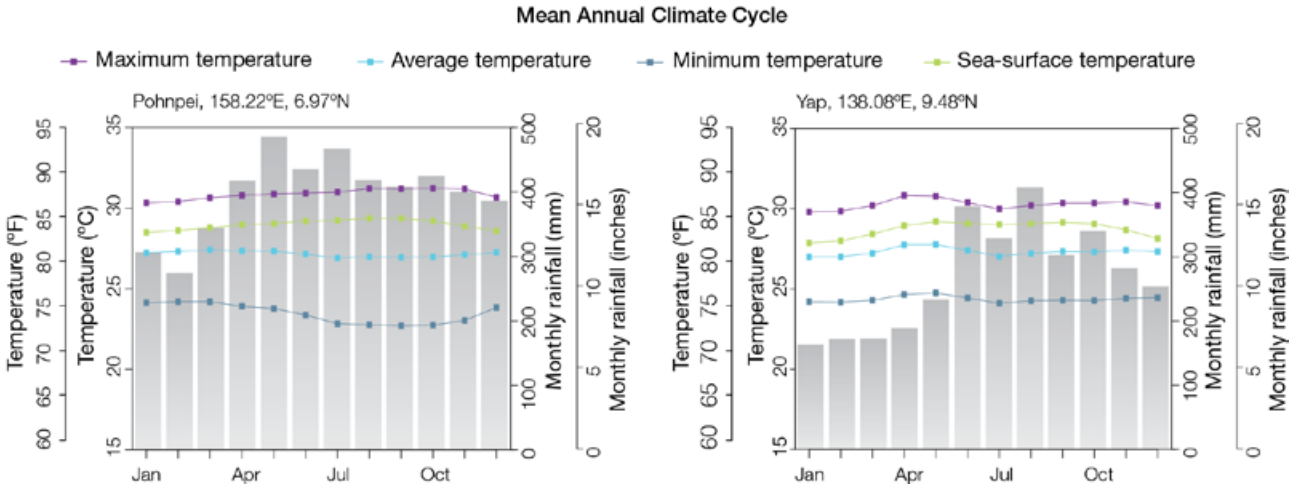

Figure 4.2: Mean annual cycle of rainfall (grey bars) and daily maximum, minimum and mean air temperatures at Pohnpei (left) and Yap (right), and local sea-surface temperatures derived from the HadISST dataset (Volume 1, Table 2.3).

4.5 Climate Variability

The El Niño-Southern Oscillation (ENSO) is the most important influence on the interannual climate variability in the Federated States of Micronesia (Figure 4.4 and correlation coefficients in Table 4.1). ENSO influences the minimum air temperatures in both Yap and Pohnpei in the wet season, but in the dry season there is a weak but significant impact on air minimum temperatures in Pohnpei and maximum air temperatures in Yap (all being warmer in El Niño years and colder in La Niña years).

During the driest years, Pohnpei and Yap receive about half the rainfall of the wettest years. The ENSO influence on rainfall is opposite in the two seasons in Pohnpei. In Yap the ENSO impact on rainfall is only significant in the dry season. In the dry season at both sites El Niño tends to result in drier conditions while La Niña tends to bring above average rainfall.

Although the influence is not as clear or as strong, El Niño brings higher than average rainfall during the wet season to Pohnpei. One mechanism by which this comes about is the position of the WPM. The monsoon tends to be farther east during El Niño, bringing higher wet season rainfall to Pohnpei, and in a more western position during La Niña, bringing lower rainfall. In Yap the ENSO impact is not significant in the wet season, so the WPM affects rainfall there in most years regardless of the phase of ENSO. The ITCZ brings less rainfall during El Niño events and more during La Niña. ENSO Modoki events (Volume1, Section 3.4.1) appear to have only a small effect, with only some weak but significant correlations on temperatures. ENSO Modoki events also have the same but weaker impact on Yap dry season rainfall as canonical ENSO events.

Table 4.1: Correlation coefficients between indices of key large-scale patterns of climate variability and minimum and maximum temperatures (Tmin and Tmax) and rainfall at Pohnpei. Only correlation coefficients that are statistically significant at the 95% level are shown.

Climate feature/index		Wet season (May-October)			Dry season (November-April)		
		Tmin	Tmax	Rain	Tmin	Tmax	Rain
ENSO	Niño3.4	0.26		0.37	0.29		-0.68
	Southern Oscillation Index			-0.33	-0.31		0.66
Interdecadal Pacific Oscillation Index							
ENSO Modoki Index					0.35		
Number of years of data		59	59	59	60	60	60

Table 4.2: Correlation coefficients between indices of key large-scale patterns of climate variability and minimum and maximum temperatures (Tmin and Tmax) and rainfall at Yap. Only correlation coefficients that are statistically significant at the 95% level are shown.

Climate feature/index		Wet season (May-October)			Dry season (November-April)		
		Tmin	Tmax	Rain	Tmin	Tmax	Rain
ENSO	Niño3.4	0.49				0.29	-0.69
	Southern Oscillation Index	-0.41					0.63
Interdecadal Pacific Oscillation Index							
ENSO Modoki Index		0.31					-0.32
Number of years of data		58	58	58	59	59	59

4.6 Observed Trends

4.6.1 Air Temperature

Trends for seasonal and annual mean air temperatures at both Pohnpei (1950–2009) and Yap (1951–2009) are positive (Figure 4.3 and Table 4.3). The strongest trend is seen in Pohnpei in wet season (May-October) mean air temperatures (+0.24°C per decade). At Pohnpei, annual and seasonal trends in minimum air temperature are greater than those observed in maximum air temperature. However, at Yap, the trends in maximum air temperature in annual and dry season (November-April) records are much greater than those observed in minimum air temperatures.

4.6.2 Rainfall

Annual and seasonal rainfall trends for Pohnpei for the period 1950–2009 and Yap for the period 1951–2009 are not statistically significant (Table 4.3 and Figure 4.4).

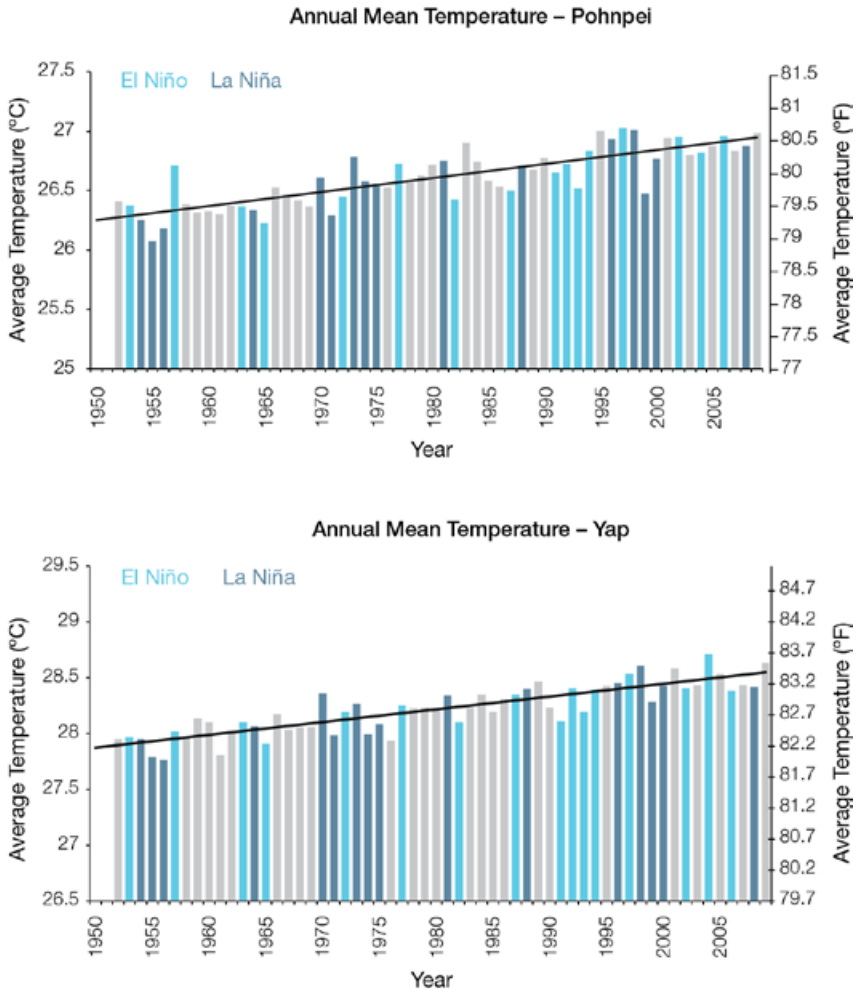

Figure 4.3: Annual mean air temperature in Pohnpei (top) and Yap (bottom). Light blue, dark blue and grey bars denote denote El Niño, La Niña and neutral years respectively.

Table 4.3: Annual and seasonal trends in maximum, minimum and mean air temperature (Tmax, Tmin and Tmean) and rainfall at Pohnpei for the period 1950–2009 and Yap for the period 1951–2009. Asterisks indicate significance at the 95% level. Persistence is taken into account in the assessment of significance as in Power and Kociuba (in press). The statistical significance of the air temperature trends is not assessed.

	Pohnpei Tmax °F per 10 yrs (°C per 10 yrs)	Pohnpei Tmin °F per 10 yrs (°C per 10 yrs)	Pohnpei Tmean °F per 10 yrs (°C per 10 yrs)	Pohnpei Rain inches per 10 yrs (mm per 10 yrs)	Yap Tmax °F per 10 yrs (°C per 10 yrs)	Yap Tmin °F per 10 yrs (°C per 10 yrs)	Yap Tmean °F per 10 yrs (°C per 10 yrs)	Yap Rain inches per 10 yrs (mm per 10 yrs)
Annual	+0.19 (+0.11)	+0.24 (+0.13)	+0.21 (+0.12)	-2.7 (-68)	+0.24 (+0.13)	+0.18 (+0.10)	+0.21 (+0.11)	-0.1 (-3)
Wet season	+0.21 (+0.12)	+0.28 (+0.16)	+0.24 (+0.14)	-2.0 (-52)	+0.15 (+0.08)	+0.23 (+0.12)	+0.19 (+0.10)	+0.6 (+14)
Dry season	+0.17 (+0.10)	+0.19 (+0.10)	+0.18 (+0.10)	-1.0 (-26)	+0.32 (+0.18)	+0.13 (+0.07)	+0.22 (+0.12)	-0.6 (-15)

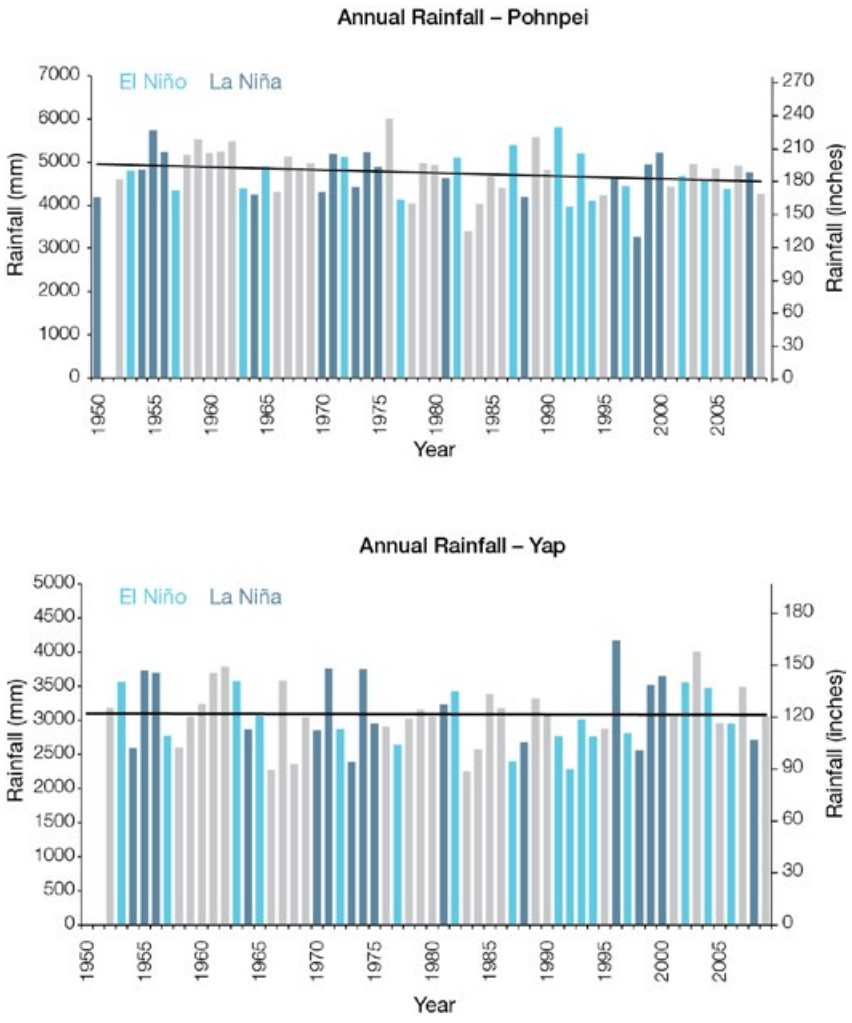

Figure 4.4: Annual rainfall in Pohnpei (top) and Yap (bottom). Light blue, dark blue and grey bars denote denote El Niño, La Niña and neutral years respectively.

4.6.3 Extreme Events

The main extreme events that occur in the Federated States of Micronesia are droughts, typhoons, storm waves, flooding and landslides. El Niño events are associated with less rainfall and occasionally droughts. These severe events have resulted in water and food shortages as well as the occurrence of fires. During La Niña events, above average numbers of tropical storms occur in the Federated States of Micronesia region.

On 2 July 2002, Tropical Storm Chataan struck the islands of Chuuk with 20 inches (~500 mm) of rainfall received in a 24-hour period. Of the 265 landslides attributed to the storm, at least 62 massive landslides occurred on 2 July, resulting in 43 deaths and hundreds of injuries on six islands.

4.6.4 Sea-Surface Temperature

Historical changes around the Federated States of Micronesia are consistent with the broad-scale sea-surface temperature trends for the wider PCCSP region. Warming was relatively weak from the 1950s to the late 1980s. This was followed by a period of more rapid warming (approximately 0.11°C per decade and approximately 0.08°C per decade for 1970–present, in the eastern and western regions respectively). At these regional scales, natural variability plays a large role in determining the sea-surface temperature, making it difficult to identify long-term trends.

4.6.5 Ocean Acidification

Based on the large-scale distribution of coral reefs across the Pacific and seawater chemistry, Guinotte et al. (2003) suggested that aragonite saturation states above 4 were optimal for coral growth and for the development of healthy reef ecosystems, with values from 3.5 to 4 adequate for coral growth, and values between 3 and 3.5, marginal. Coral reef ecosystems were not found at seawater aragonite saturation states below 3 and these conditions were classified as extremely marginal for supporting coral growth.

In the Federated States of Micronesia region, the aragonite saturation state has declined from about 4.5 in the late 18th century to an observed value of about 3.9 ± 0.1 by 2000.

4.6.6 Sea Level

Monthly averages of the historical tide gauge, satellite (since 1993) and gridded sea-level (since 1950) data agree well after 1993 and indicate interannual variability in sea levels of about 10 inches (26 cm) (estimated 5–95% range) after removal of the seasonal cycle (Figure 4.9). The sea-level rise near the Federated States of Micronesia measured by satellite altimeters (Figure 4.5) since 1993 is over 0.39 inches (10 mm) per year, larger than the global average of 0.125 ± 0.015 inches (3.2 ± 0.4 mm) per year. This rise is partly linked to a pattern related to climate variability from year to year and decade to decade (Figure 4.9).

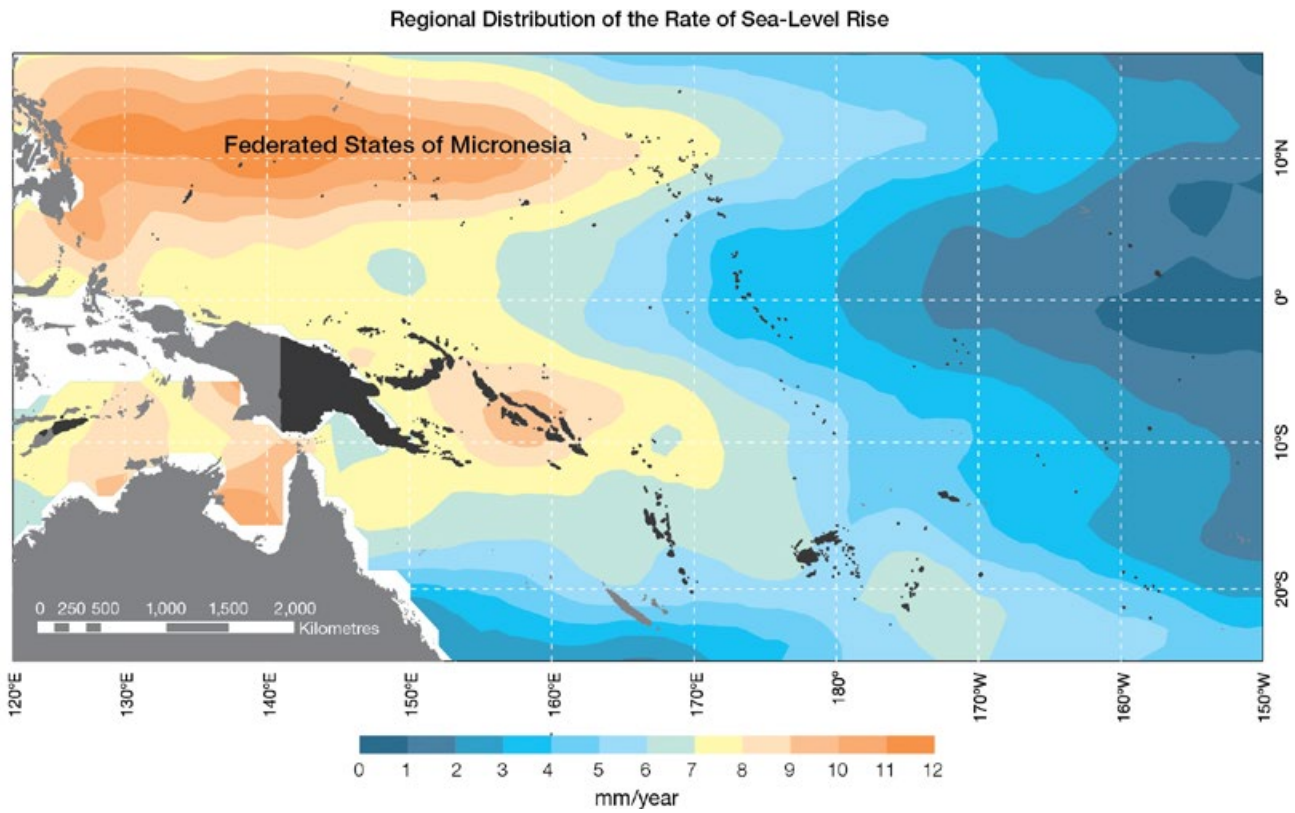

Figure 4.5: The regional distribution of the rate of sea-level rise measured by satellite altimeters from January 1993 to December 2010, with the location of the Federated States of Micronesia indicated. Further detail about the regional distribution of sea-level rise is provided in Volume 1, Section 3.6.3.2.

4.6.7 Extreme Sea-Level Events

The annual climatology of the highest daily sea levels has been evaluated from hourly measurements of tide gauges at Pohnpei and Chuuk (Figure 4.6). Highest tides at both locations tend to occur around the solstices, particularly at Chuuk, where there is a pronounced June maximum. These periods of highest tides lead to the maximum likelihood of high water levels at both locations in mid-April to mid-July and November to January. Seasonal sea levels are significantly lower during El Niño conditions and significantly higher in La Niña conditions, approximately ±0.49 ft (±0.15 m) during October-February. This combination of high solsticial tides with seasonal water levels during October to February in La Niña years is supported by observations of the highest 10 recorded water levels at both sites of which seven of 10 occur during La Niña conditions, and eight occur between late October and January at Pohnpei. None of highest 10 water levels at either location occurred during El Niño conditions. Chuuk, with its higher June tidal maximum, has a higher likelihood of extreme water levels during this month than Pohnpei. This tide gauge information indicates that most occurrences of extreme sea-level events at both Pohnpei and Chuuk are primarily due to a combination extreme tides and La Niña conditions.

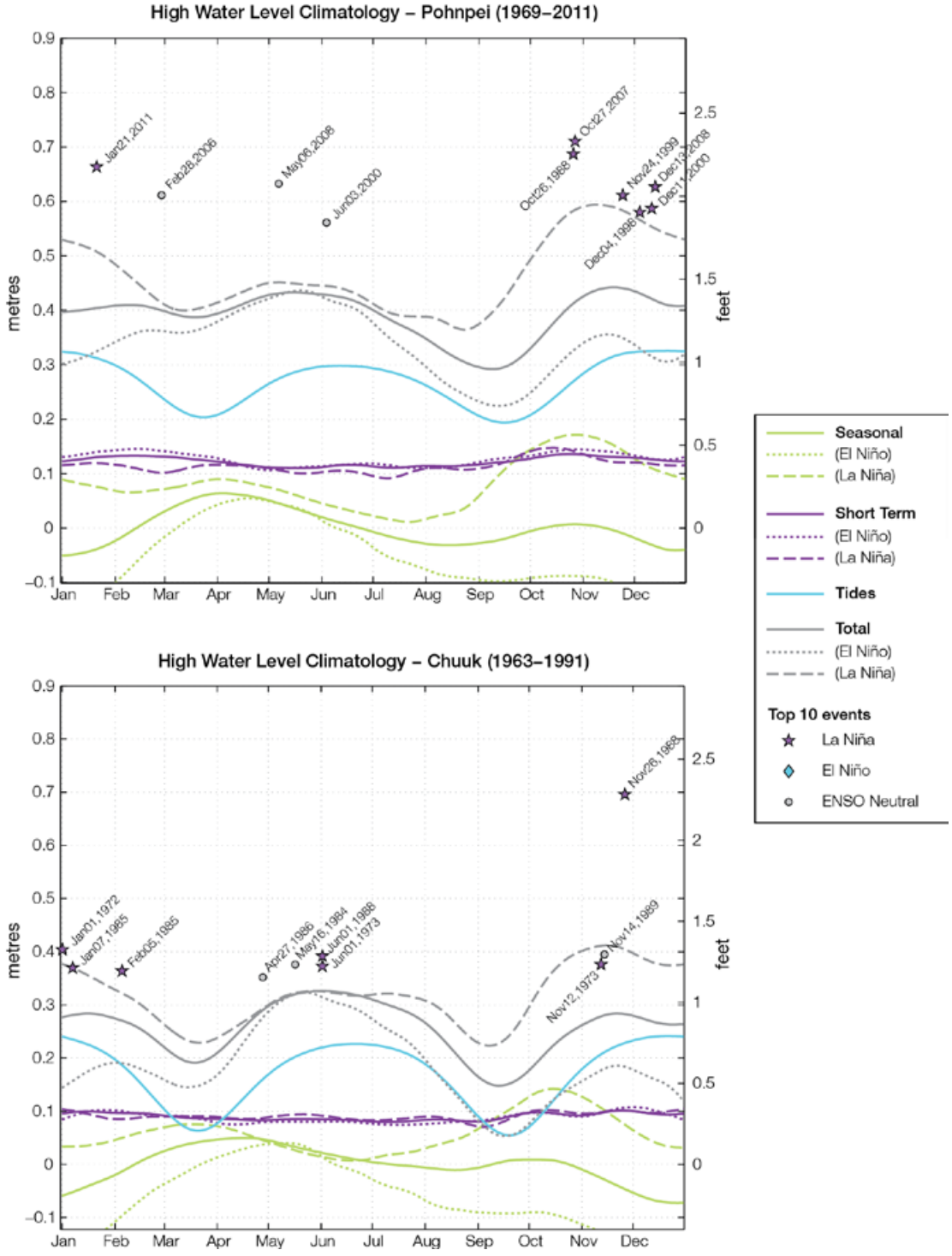

Figure 4.6: The annual cycle of high water levels relative to Mean Higher High Water (MHHW) due to tides, short-term fluctuations (most likely associated with storms) and seasonal variations for Pohnpei (top) and Chuuk (bottom). The tides and short-term fluctuations are respectively the 95% exceedence levels of the astronomical high tides relative to MHHW and short-term sea-level fluctuations. Components computed only for El Niño and La Niña years are shown by dotted and dashed lines, and grey lines are the sum of the tide, short-term and seasonal components. The 10 highest sea-level events in the record relative to MHHW are shown and coded to indicate the phase of ENSO at the time of the extreme event.

4.7 Climate Projections

Climate projections have been derived from up to 18 global climate models from the CMIP3 database, for up to three emissions scenarios (B1 (low), A1B (medium), A2 (high)) and three 20-year periods (centred on 2030, 2055 and 2090, relative to 1990) (Section 1.7.2). These models were selected based on their ability to reproduce important features of the current climate (Volume 1, Section 5.2.3), so projections arising from each of the models are a plausible representation of the future climate. This means there is not one single projected future for the Federated States of Micronesia, but rather a range of possible futures. The full range of these futures is discussed in the following sections.

These projections do not represent a value specific to any actual location, such as a town or city in the Federated States of Micronesia. Instead, they refer to an average change over the broad geographic region encompassing the islands of the Federated States of Micronesia and the surrounding ocean. Projections refer to the entire Federated States of Micronesia unless otherwise stated. In some instances, given there are some differences between the climate of the west (i.e. Yap and the western islands of Chuuk) and east (i.e. Kosrae, Pohnpei and the main island of Chuuk) (Section 4.4), the Federated States of Micronesia projections are given separately for these two regions (Figure 1.1 shows the regional boundaries). Some information regarding dynamical downscaling simulations from the CCAM model (Section 1.7.2) is also provided in order to indicate how changes in the climate on an individual island-scale may differ from the broad-scale average.

Section 1.7 provides important information about interpreting climate model projections.

4.7.1 Temperature

Surface air temperature and sea-surface temperature are projected to continue to increase over the course of the 21st century. There is *very high* confidence in this direction of change because:

- Warming is physically consistent with rising greenhouse gas concentrations.
- All CMIP3 models agree on this direction of change.

The majority of CMIP3 models simulate a slight increase (<1.8°F; <1°C) in annual and seasonal mean surface air temperature by 2030, however by 2090, under the A2 (high) emissions scenario, temperature increases of greater than 4.5°F (2.5°C) are simulated by almost all models (Tables 4.4 and 4.5). Given the close relationship between surface air temperature and sea-surface temperature, a similar (or slightly weaker) rate of warming is projected for the surface ocean (Figure 4.7). There is *high* confidence in this range and distribution of possible futures because:

- There is generally close agreement between modelled and observed temperature trends over the past 50 years in the vicinity of the Federated States of Micronesia, although observational records are limited (Figure 4.7).

The 8 km CCAM simulations did not resolve any spatial variability in the changes to surface air temperature. This result is partially a consequence of the Federated States of Micronesia still being poorly resolved even at 8 km resolution.

Interannual variability in sea-surface temperature and surface air temperature over the Federated States of Micronesia is strongly influenced by ENSO in the current climate (Section 4.5). As there is no consistency in projections of future ENSO activity (Volume 1, Section 6.4.1), it is not possible to determine whether interannual variability in temperature will change in the future. However, ENSO is expected to continue to be an important source of variability for the Federated States of Micronesia and the region.

4.7.2 Rainfall

Wet season (May-October), dry season (November-April) and annual average rainfall is projected to increase over the course of the 21st century. There is *high* confidence in this direction of change because:

- Physical arguments indicate that rainfall will increase in the equatorial Pacific in a warmer climate (IPCC, 2007; Volume 1, Section 6.4.3).
- Almost all of the CMIP3 models agree on this direction of change by 2090.

The majority of CMIP3 models simulate little change (-5% to 5%) in rainfall by 2030, however by 2090 the majority simulate an increase (>5%) in wet season, dry season and annual rainfall, with up to a third simulating a large increase (>15%) for the eastern Federated States of Micronesia under the A2 (high) emissions scenario (Tables 4.4 and 4.5). There is *moderate* confidence in this range and distribution of possible futures because:

- In simulations of the current climate, the CMIP3 models broadly capture the influence of the West Pacific Monsoon and Intertropical Convergence Zone on the rainfall of the western and the entire Federated States of Micronesia regions respectively (Volume 1, Sections 5.2.3.4 and 5.2.3.5), although most models produce monsoon westerly winds that do not extend far enough east into the Pacific basin.

- The CMIP3 models are unable to resolve many of the physical processes involved in producing rainfall. As a consequence, they do not simulate rainfall as well as they simulate other variables such as temperature (Volume 1, Chapter 5).

The inconsistency between the projected increases in rainfall and the recent declining (Pohnpei) or relatively steady (Yap) trends observed at individual meteorological stations (Section 4.6.2) may be related to local factors not captured by the models (e.g. topography), or the fact that the projections presented here represent an average over a very large geographic region (Sections 1.7.1 and 1.7.2).

Interannual variability in rainfall over the Federated States of Micronesia is strongly influenced by ENSO in the current climate (Section 4.5). As there is no consistency in projections of future ENSO activity (Volume 1, Section 6.4.1), it is not possible to determine whether interannual variability in rainfall will change in the future.

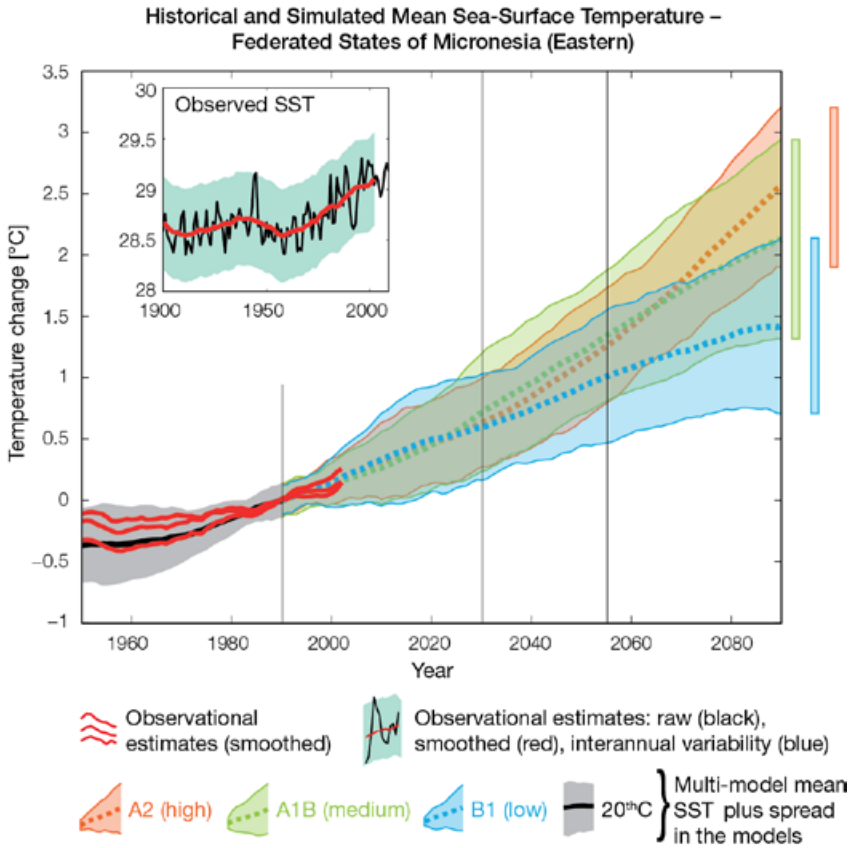

Figure 4.7: Historical climate (from 1950 onwards) and simulated historical and future climate for annual mean sea-surface temperature (SST) in the region surrounding the eastern Federated States of Micronesia for the CMIP3 models. Shading represents approximately 95% of the range of model projections (twice the inter-model standard deviation), while the solid lines represent the smoothed (20-year running average) multi-model mean temperature. Projections are calculated relative to the 1980–1999 period (which is why there is a decline in the inter-model standard deviation around 1990). Observational estimates in the main figure (red lines) are derived from the HadSST2, ERSST and Kaplan Extended SST V2 datasets (Volume 1, Section 2.2.2). Annual average (black) and 20-year running average (red) HadSST2 data is also shown inset. Projections for the western Federated States of Micronesia closely resemble those for the east and are therefore not shown.

4.7.3 Extremes

Temperature

The intensity and frequency of days of extreme heat are projected to increase over the course of the 21st century. There is *very high* confidence in this direction of change because:

- An increase in the intensity and frequency of days of extreme heat is physically consistent with rising greenhouse gas concentrations.
- All CMIP3 models agree on the direction of change for both intensity and frequency.

For both the eastern and western Federated States of Micronesia, the majority of CMIP3 models simulate an increase of approximately 1.8°F (1°C) in the temperature experienced on the 1-in-20-year hot day by 2055 under the B1 (low) emissions scenario, with an increase of over 4.5°F (2.5°C) simulated by the majority of models by 2090 under the A2 (high) emissions scenario (Tables 4.4 and 4.5). There is *low* confidence in this range and distribution of possible futures because:

- In simulations of the current climate, the CMIP3 models tend to underestimate the intensity and frequency of days of extreme heat (Volume 1, Section 5.2.4).
- Smaller increases in the frequency of days of extreme heat are projected by the CCAM 60 km simulations.

Rainfall

The intensity and frequency of days of extreme rainfall are projected to increase over the course of the 21st century. There is *high* confidence in this direction of change because:

- An increase in the frequency and intensity of extreme rainfall is consistent with larger-scale projections, based on the physical argument that the atmosphere is able to hold more water vapour in a warmer climate (Allen and Ingram, 2002; IPCC, 2007). It is also consistent with physical arguments that rainfall will increase in the

deep tropical Pacific in a warmer climate (IPCC, 2007; Volume 1, Section 6.4.3).

- Almost all of the CMIP3 models agree on this direction of change for both intensity and frequency.

For both the eastern and western Federated States of Micronesia, the majority of CMIP3 models simulate an increase of at least 0.4 inches (10 mm) in the amount of rain received on the 1-in-20-year wet day by 2055 under a B1 (low) emissions scenario, with an increase of at least 0.8 inches (20 mm) simulated by all models by 2090 under the A2 (high) emissions scenario. The majority of models project that the current 1-in-20-year extreme rainfall event will occur, on average, two to three times per 20-year period by 2055 under the B1 (low) emissions scenario and between five and six times per 20-year period by 2090 under the A2 (high) emissions scenario. There is *low* confidence in this range and distribution of possible futures because:

- In simulations of the current climate, the CMIP3 models tend to underestimate the intensity and frequency of extreme rainfall (Volume 1, Section 5.2.4).
- The CMIP3 models are unable to resolve many of the physical processes involved in producing extreme rainfall.

Drought

The incidence of drought is projected to decrease over the course of the 21st century. There is *moderate* confidence in this direction of change because:

- A decrease in drought is consistent with projections of increased rainfall (Section 4.7.2).
- The majority of models agree on this direction of change for most drought categories.

For both the eastern and western Federated States of Micronesia, the majority of CMIP3 models project that mild drought will occur approximately eight to nine times every 20 years in 2030. This frequency is projected to decrease to seven to eight times every 20 years by 2090 under the B1 (low) emissions scenario, and six to seven times under the A1B (medium) and A2 (high) scenarios. The frequency of moderate drought is projected to decrease from once to twice every 20 years in 2030, to once every 20 years in 2090 for all emissions scenarios, while the majority of CMIP3 models project that severe droughts will occur approximately once every 20 years across all time periods and scenarios. There is *low* confidence in this range and distribution of possible futures because:

- There is only moderate confidence in the range of rainfall projections (Section 4.7.2), which directly influences projections of future drought conditions.

Tropical Cyclones (Typhoons)

Tropical cyclone numbers are projected to decline in the tropical North Pacific Ocean basin (0–15ºS, 130ºE–180ºE) over the course of the 21st century. There is *moderate* confidence in this direction of change because:

- Many studies suggest a decline in tropical cyclone frequency globally (Knutson et al., 2010).
- Tropical cyclone numbers decline in the tropical North Pacific Ocean basin in the majority assessment techniques.

Based on the direct detection methodologies (Curvature Vorticity Parameter (CVP) and the CSIRO Direct Detection Scheme (CDD) described in Volume 1, Section 4.8.2), 80% of projections show no change or a decrease in tropical cyclone formation when applied to the CMIP3 climate models for which suitable output is available. When these techniques are applied to CCAM, 100% of projections show a decrease in tropical cyclone formation. In addition, the Genesis Potential Index (GPI) empirical technique suggests that conditions for tropical cyclone formation will become less favourable in the North Pacific Ocean basin, for the majority (70%) of analysed CMIP3 models. There is *moderate* confidence in this range and distribution of possible futures because in simulations of the current climate, the CVP, CDD and GPI methods capture the frequency of tropical cyclone activity reasonably well (Volume 1, Section 5.4).

Consistent with this projected reduction in total cyclone numbers, five of the six 60 km CCAM simulations also show a decrease in the proportion of the most severe storms (those stronger than the current climate 90th percentile storm maximum wind speed). Most simulations project an increase in the proportion of storms occurring in the weaker categories. Associated with this is a reduction in cyclonic wind hazard.

4.7.4 Ocean Acidification

The acidification of the ocean will continue to increase over the course of the 21st century. There is *very high* confidence in this projection as the rate of ocean acidification is driven primarily by the increasing oceanic uptake of carbon dioxide, in response to rising atmospheric carbon dioxide concentrations.

Projections from all analysed CMIP3 models indicate that the annual maximum aragonite saturation state will reach values below 3.5 by about 2030 and continue to decline thereafter (Figure 4.8; Tables 4.4 and 4.5). There is *moderate* confidence in this range and distribution of possible futures because the projections are based on climate models without an explicit representation of the carbon cycle and with relatively low resolution and known regional biases.

The impact of acidification change on the health of reef ecosystems is likely to be compounded by other stressors including coral bleaching, storm damage and fishing pressure.

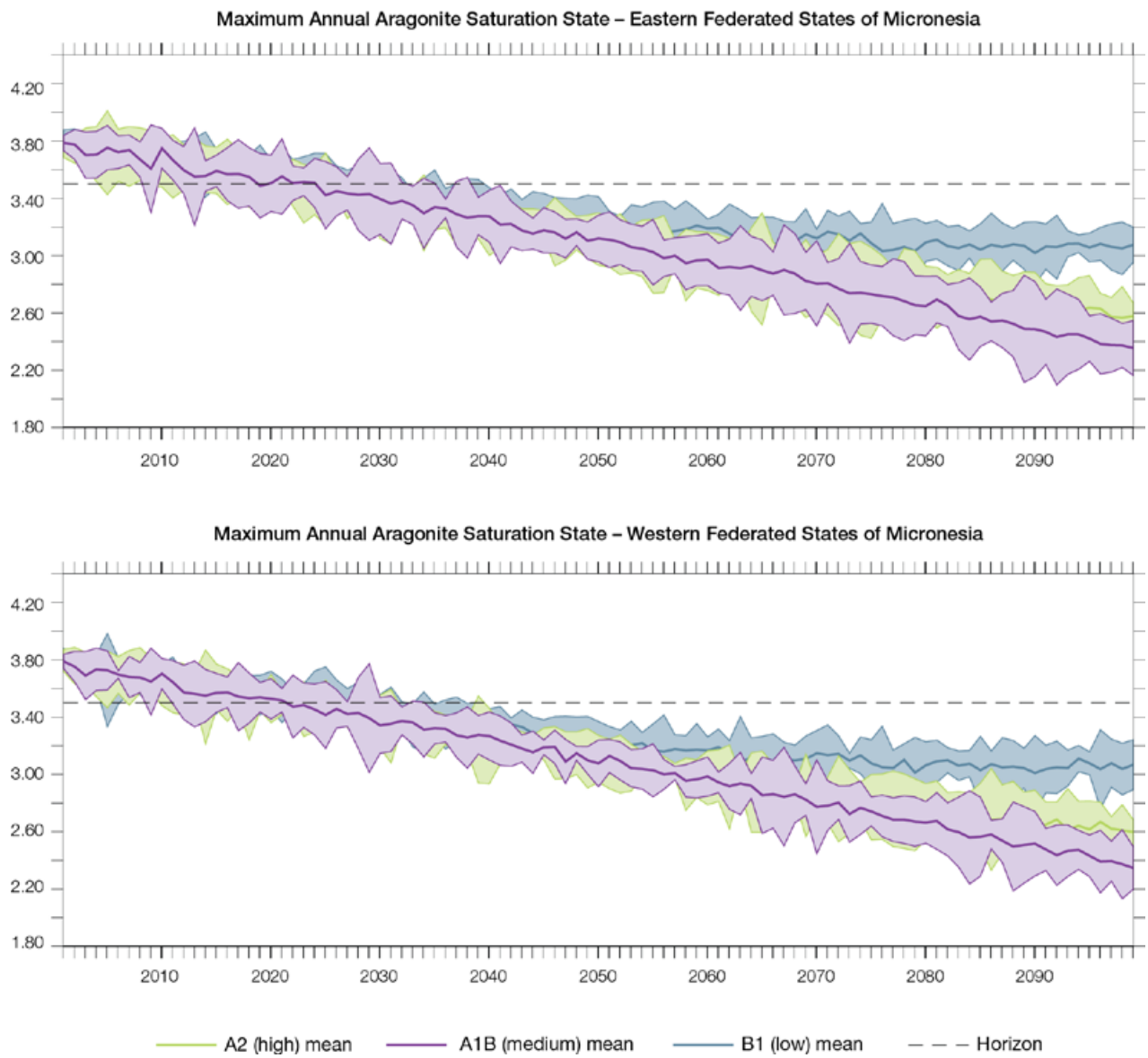

Figure 4.8: Multi-model projections, and their associated uncertainty (shaded area represents two standard deviations), of the maximum annual aragonite saturation state in the sea surface waters of the eastern Federated States of Micronesia (top) and the western Federated States of Micronesia (bottom) under the different emissions scenarios. The dashed black line represents an aragonite saturation state of 3.5.

4.7.5 Sea Level

Mean sea-level is projected to continue to rise over the course of the 21st century. There is *very high* confidence in this direction of change because:

- Sea-level rise is a physically consistent response to increasing ocean and atmospheric temperatures, due to thermal expansion and the melting of glaciers and ice caps.
- Projections arising from all CMIP3 models agree on this direction of change.

The CMIP3 models simulate a rise of between approximately 2–6 inches (5–15 cm) by 2030, with increases of 8–24 inches (20–60 cm) indicated by 2090 under the higher emissions scenarios (i.e. A1B (medium) and A2 (high); Figure 4.9; Tables 4.4 and 4.5). There is *moderate* confidence in this range and distribution of possible futures because:

- There is significant uncertainty surrounding ice-sheet contributions to sea-level rise and a larger rise than that projected above cannot be excluded (Meehl et al., 2007b). However, understanding of the processes is currently too limited to provide a best estimate or an upper bound (IPCC, 2007).
- Globally, since the early 1990s, sea level has been rising near the upper end of the above projections. During the 21st century, some studies (using semi-empirical models) project faster rates of sea-level rise.

Interannual variability of sea level will lead to periods of lower and higher regional sea levels. In the past, this interannual variability has been about 10 inches (26 cm) (5–95% range, after removal of the seasonal signal; dashed lines in Figure 4.9 (a)) and it is likely that a similar range will continue through the 21st century. In addition, winds and waves associated with weather phenomena will continue to lead to extreme sea-level events.

In addition to the regional variations in sea level associated with ocean and mass changes, there are ongoing changes in relative sea level associated with changes in surface loading over the last glacial cycle (glacial isostatic adjustment) and local tectonic motions. The glacial isostatic motions are relatively small for the PCCSP region.

4.7.6 Projections Summary

The projections presented in Section 4.7 are summarised in Table 4.4 (eastern Federated States of Micronesia) and Table 4.5 (western Federated States of Micronesia). Projections are presented in imperial and metric units. For detailed information regarding the various uncertainties associated with the table values, refer to the preceding text in Sections 4.7 and 1.7, in addition to Chapters 5 and 6 in Volume 1. When interpreting the differences between projections for the B1 (low), A1B (medium) and A2 (high) emissions scenarios, it is also important to consider the emissions pathways associated with each scenario (Volume 1, Figure 4.1) and the fact that a slightly different subset of models was available for each (Volume 1, Appendix 1).

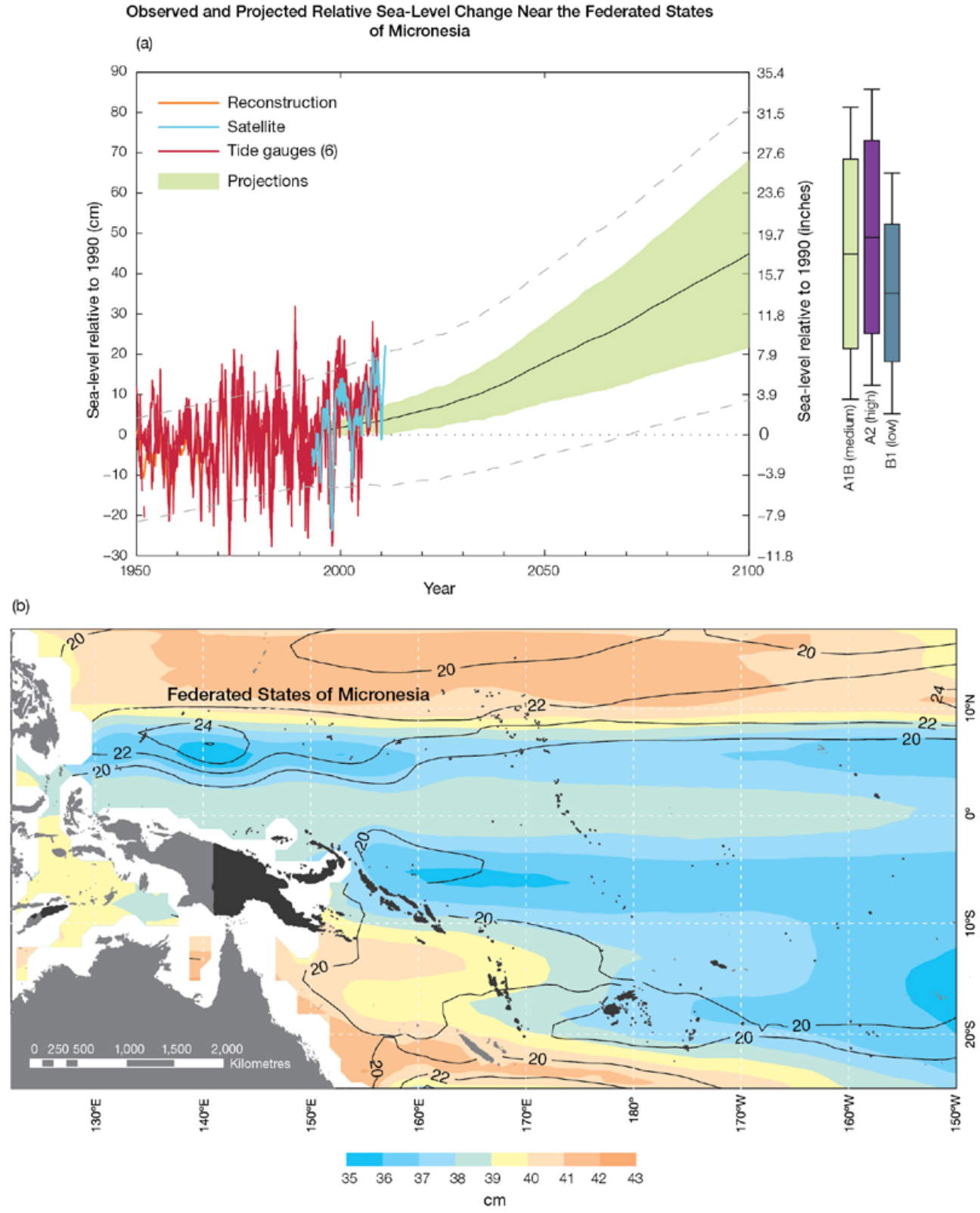

Figure 4.9: Observed and projected relative sea-level change near the Federated States of Micronesia. (a) The average of the observed in situ relative sea-level records is indicated in red, with the satellite record (since 1993) in light blue. The gridded sea-level data at the Federated States of Micronesia (since 1950, from Church and White (in press)) is shown in orange. The projections for the A1B (medium) emissions scenario (5–95% uncertainty range) are shown by the green shaded region from 1990–2100. The range of projections for the B1 (low), A1B (medium) and A2 (high) emissions scenarios by 2100 are also shown by the bars on the right. The dashed lines are an estimate of interannual variability in sea level (5–95% range about the long-term trends) and indicate that individual monthly averages of sea level can be above or below longer-term averages. (b) The projections (in cm) for the A1B (medium) emissions scenario in the Federated States of Micronesia region for the average over 2081–2100 relative to 1981–2000 are indicated by the shading, with the estimated uncertainty in the projections indicated by the contours (in cm).

Table 4.4: Projected change in the annual and seasonal mean climate for the eastern Federated States of Micronesia under the B1 (low; blue), medium A1B (medium; green) and A2 (high; purple) emissions scenarios. Projections are given for three 20-year periods centred on 2030 (2020–2039), 2055 (2046–2065) and 2090 (2080–2099), relative to 1990 (1980–1999). Values represent the multi-model mean change ± twice the inter-model standard deviation (representing approximately 95% of the range of model projections), except for sea level where the estimated mean change and the 5–95% range are given (as they are derived directly from the Intergovernmental Panel on Climate Change Fourth Assessment Report values). The confidence (Section 1.7.2) associated with the range and distribution of the projections is also given (indicated by the standard deviation and multi-model mean, respectively). See Volume 1, Appendix 1 for a complete listing of CMIP3 models used to derive these projections.

Variable	Season	2030	2055	2090	Confidence
Surface air temperature (°F)	Annual	+1.2 ± 0.8 +1.4 ± 0.9 +1.3 ± 0.6	+2.0 ± 0.9 +2.7 ± 1.1 +2.6 ± 0.8	+2.8 ± 1.3 +4.3 ± 1.6 +5.1 ± 1.2	High
Surface air temperature (°C)	Annual	+0.7 ± 0.4 +0.8 ± 0.5 +0.7 ± 0.3	+1.1 ± 0.5 +1.5 ± 0.6 +1.4 ± 0.4	+1.6 ± 0.7 +2.4 ± 0.9 +2.8 ± 0.7	High
Maximum temperature (°F)	1-in-20-year event	N/A	+1.8 ± 0.9 +2.5 ± 1.1 +2.7 ± 0.9	+2.3 ± 1.1 +3.8 ± 1.8 +4.7 ± 2.3	Low
Maximum temperature (°C)	1-in-20-year event	N/A	+1.0 ± 0.5 +1.4 ± 0.6 +1.5 ± 0.5	+1.3 ± 0.6 +2.1 ± 1.0 +2.6 ± 1.3	Low
Minimum temperature (°F)	1-in-20-year event	N/A	+2.2 ± 2.5 +2.7 ± 2.7 +2.5 ± 2.7	+2.7 ± 2.7 +3.8 ± 3.2 +4.3 ± 3.2	Low
Minimum temperature (°C)	1-in-20-year event	N/A	+1.2 ± 1.4 +1.5 ± 1.5 +1.4 ± 1.5	+1.5 ± 1.5 +2.1 ± 1.8 +2.4 ± 1.8	Low
Total rainfall (%)*	Annual	+1 ± 8 +2 ± 9 +4 ± 11	+7 ± 8 +7 ± 14 +7 ± 11	+7 ± 11 +13 ± 16 +12 ± 15	Moderate
Dry season rainfall (%)*	November-April	+1 ± 15 +2 ± 16 +4 ± 14	+7 ± 9 +7 ± 22 +8 ± 18	+7 ± 12 +13 ± 24 +10 ± 19	Moderate
Wet season rainfall (%)*	May-October	+2 ± 10 +2 ± 8 +4 ± 12	+7 ± 12 +8 ± 11 +7 ± 13	+8 ± 14 +13 ± 18 +14 ± 21	Moderate
Sea-surface temperature (°F)	Annual	+1.1 ± 0.7 +1.3 ± 0.9 +1.1 ± 0.7	+1.8 ± 0.9 +2.3 ± 0.9 +2.3 ± 0.9	+2.5 ± 1.3 +3.8 ± 1.4 +4.7 ± 1.3	High
Sea-surface temperature (°C)	Annual	+0.6 ± 0.4 +0.7 ± 0.5 +0.6 ± 0.4	+1.0 ± 0.5 +1.3 ± 0.5 +1.3 ± 0.5	+1.4 ± 0.7 +2.1 ± 0.8 +2.6 ± 0.7	High
Aragonite saturation state (Ωar)	Annual maximum	+3.4 ± 0.1 +3.3 ± 0.2 +3.4 ± 0.2	+3.2 ± 0.1 +3.0 ± 0.2 +3.0 ± 0.2	+3.0 ± 0.1 +2.6 ± 0.2 +2.4 ± 0.2	Moderate
Mean sea level (inches)	Annual	+3.5 (1.2–5.5) +3.5 (1.2–5.9) +3.5 (1.2–5.9)	+6.7 (3.5–10.2) +7.9 (3.5–12.6) +7.9 (3.9–11.8)	+12.2 (6.3–18.1) +15.4 (7.5–23.6) +16.1 (8.3–24.4)	Moderate
Mean sea level (cm)	Annual	+9 (3–14) +9 (3–15) +9 (3–15)	+17 (9–26) +20 (9–32) +20 (10–30)	+31 (16–46) +39 (19–60) +41 (21–62)	Moderate

*The MIROC3.2(hires) model was eliminated in calculating the rainfall projections, due to its inability to accurately simulate present-day activity of the Intertropical Convergence Zone (Volume 1, Section 5.5.1).

Table 4.5: Projected change in the annual and seasonal mean climate for the western Federated States of Micronesia, under the B1 (low; blue), medium A1B (medium; green) and A2 (high; purple) emissions scenarios. Projections are given for three 20-year periods centred on 2030 (2020–2039), 2055 (2046–2065) and 2090 (2080–2099), relative to 1990 (1980–1999). Values represent the multi-model mean change ± twice the inter-model standard deviation (representing approximately 95% of the range of model projections), except for sea level where the estimated mean change and the 5–95% range are given (as they are derived directly from the Intergovernmental Panel on Climate Change Fourth Assessment Report values). The confidence (Section 1.7.2) associated with the range and distribution of the projections is also given (indicated by the standard deviation and multi-model mean, respectively). See Volume 1, Appendix 1 for a complete listing of CMIP3 models used to derive these projections.

Variable	Season	2030	2055	2090	Confidence
Surface air temperature (°F)	Annual	+1.1 ± 0.7 +1.4 ± 0.8 +1.3 ± 0.5	+1.9 ± 0.9 +2.7 ± 1.0 +2.5 ± 0.8	+2.7 ± 1.3 +4.2 ± 1.6 +5.0 ± 1.2	High
Surface air temperature (°C)	Annual	+0.6 ± 0.4 +0.8 ± 0.4 +0.7 ± 0.3	+1.0 ± 0.5 +1.5 ± 0.6 +1.4 ± 0.4	+1.5 ± 0.7 +2.3 ± 0.9 +2.8 ± 0.7	High
Maximum temperature (°F)	1-in-20-year event	N/A	+1.8 ± 0.7 +2.5 ± 0.9 +2.7 ± 1.1	+2.3 ± 1.3 +4.0 ± 1.8 +4.9 ± 2.3	Low
Maximum temperature (°C)	1-in-20-year event	N/A	+1.0 ± 0.4 +1.4 ± 0.5 +1.5 ± 0.6	+1.3 ± 0.7 +2.2 ± 1.0 +2.7 ± 1.3	Low
Minimum temperature (°F)	1-in-20-year event	N/A	+2.3 ± 2.9 +2.9 ± 3.4 +2.5 ± 2.9	+3.1 ± 2.9 +4.1 ± 3.4 +4.7 ± 3.6	Low
Minimum temperature (°C)	1-in-20-year event	N/A	+1.3 ± 1.6 +1.6 ± 1.9 +1.4 ± 1.6	+1.7 ± 1.6 +2.3 ± 1.9 +2.6 ± 2.0	Low
Total rainfall (%)*	Annual	0 ± 8 +1 ± 7 +2 ± 7	+3 ± 8 +5 ± 15 +4 ± 9	+4 ± 6 +9 ± 15 +8 ± 11	Moderate
Dry season rainfall (%)*	November-April	0 ± 9 +1 ± 9 +2 ± 10	+3 ± 9 +6 ± 21 +5 ± 17	+4 ± 7 +9 ± 20 +7 ± 15	Moderate
Wet season rainfall (%)*	May-October	+1 ± 8 +1 ± 7 +2 ± 8	+3 ± 8 +5 ± 11 +4 ± 7	+5 ± 9 +9 ± 14 +9 ± 11	Moderate
Sea-surface temperature (°F)	Annual	+1.1 ± 0.9 +1.3 ± 0.9 +1.3 ± 0.7	+2.0 ± 1.1 +2.5 ± 1.1 +2.3 ± 0.9	+2.7 ± 1.4 +4.0 ± 1.6 +4.7 ± 1.3	High
Sea-surface temperature (°C)	Annual	+0.6 ± 0.5 +0.7 ± 0.5 +0.7 ± 0.4	+1.1 ± 0.6 +1.4 ± 0.6 +1.3 ± 0.5	+1.5 ± 0.8 +2.2 ± 0.9 +2.6 ± 0.7	High
Aragonite saturation state (Ωar)	Annual maximum	+3.4 ± 0.2 +3.3 ± 0.1 +3.3 ± 0.2	+3.1 ± 0.1 +3.0 ± 0.2 +3.0 ± 0.1	+3.0 ± 0.2 +2.6 ± 0.2 +2.5 ± 0.2	Moderate
Mean sea level (inches)	Annual	+3.5 (1.2–5.5) +3.5 (1.2–5.9) +3.5 (1.2–5.9)	+6.7 (3.5–10.2) +7.9 (3.5–12.6) +7.9 (3.9–11.8)	+12.2 (6.3–18.1) +15.4 (7.5–23.6) +16.1 (8.3–24.4)	Moderate
Mean sea level (cm)	Annual	+9 (3–14) +9 (3–15) +9 (3–15)	+17 (9–26) +20 (9–32) +20 (10–30)	+31 (16–46) +39 (19–60) +41 (21–62)	Moderate

*The MIROC3.2(medres) and MIROC3.2(hires) models were eliminated in calculating the rainfall projections, due to their inability to accurately simulate the West Pacific Monsoon and/or the Intertropical Convergence Zone (Volume 1, Section 5.5.1).

Suva

Chapter 5
Fiji Islands

The contributions of Alipate Waqaicelua, Varanisese Vuniyayawa, Ravind Kumar, Arieta Daphne and Bipendra Prakash from the Fiji Meteorological Service are gratefully acknowledged

Introduction

This chapter provides a brief description of the Fiji Islands, its past and present climate as well as projections for the future. The climate observation network and the availability of atmospheric and oceanic data records are outlined. The annual mean climate, seasonal cycles and the influences of large-scale climate features such as the South Pacific Convergence Zone and patterns of climate variability (e.g. the El Niño-Southern Oscillation) are analysed and discussed. Observed trends and analysis in air temperature, rainfall, extreme events including tropical cyclones, sea-surface temperature, ocean acidification and mean and extreme sea level are presented. Projections for air and sea-surface temperature, rainfall, sea level and ocean acidification for the 21st century are provided, as are projections for tropical cyclones, drought, extreme rainfall, and extreme temperature. These projections are presented along with confidence levels based on expert judgement by Pacific Climate Change Science Program (PCCSP) scientists. The chapter concludes with a summary table of projections (Table 5.4). Important background information, including an explanation of methods and models, is provided in Chapter 1. For definitions of other terms refer to the Glossary.

5.1 Climate Summary

5.1.1 Current Climate

- Changes in air temperature from season to season are relatively small and strongly tied to changes in the surrounding ocean temperature. The country has two distinct seasons – a warm wet season from November to April and a cooler dry season from May to October.
- The seasonal cycle is strongly affected by the South Pacific Convergence Zone, which is most intense during the wet season.
- The El Niño-Southern Oscillation is the most important influence on year-to-year climate variations.
- Annual and seasonal mean air temperatures at Suva and Nadi Airport have been increasing, particularly in the wet season over the period 1950–2009.
- Annual and seasonal rainfall trends for Suva and Nadi Airport for the period 1950–2009 are not statistically significant.
- The sea-level rise near Fiji measured by satellite altimeters since 1993 is about 6 mm per year.
- Tropical cyclones usually affect Fiji between November and April. Over the period 1969–2010, the centre of 70 tropical cyclones passed within 400 km of Suva. The high variability in tropical cyclone numbers makes it difficult to identify any long-term trends in frequency.

5.1.2 Future Climate

Over the course of the 21st century:

- Surface air temperature and sea-surface temperature are projected to continue to increase (*very high* confidence).
- Wet season rainfall is projected to increase (*moderate* confidence).
- Dry season rainfall is projected to decrease (*moderate* confidence).
- Little change is projected in annual mean rainfall (*low* confidence).
- The intensity and frequency of days of extreme heat are projected to increase (*very high* confidence).
- The intensity and frequency of days of extreme rainfall are projected to increase (*high* confidence).
- Little change is projected in the incidence of drought (*low* confidence).
- Tropical cyclone numbers are projected to decline in the south-east Pacific Ocean basin (0–40ºS, 170ºE–130ºW) (*moderate* confidence).
- Ocean acidification is projected to continue (*very high* confidence).
- Mean sea-level rise is projected to continue (*very high* confidence).

5.2 Country Description

Fiji is located in the western South Pacific Ocean between 177°E–178°W and 16°S–20°S. The country has 322 islands and a total land area of 18 333 km^2. The Exclusive Economic Zone has an area of 1.3 million km^2. The two largest islands are Viti Levu, 10 429 km^2, and Vanua Levu, 5 556 km^2. They take up 87% of the total land area and are mountainous and of volcanic origin with peaks up to 1 300 m. The other islands consist of small volcanic islands, low-lying atolls and elevated reefs (Fiji's First National Communication under the UNFCCC, 2005; Fiji's Pacific Adaptation to Climate Change, 2009). The estimated population of Fiji in 2010 was 844 420 (Fiji Country Statistics, SOPAC, 2010).

Viti Levu is the economic centre of Fiji, with Suva, the capital, located on the south coast, and Nadi, the tourism centre on the west coast.

Fiji's economy is based on sugar and tourism and over recent years the tourism sector has grown significantly. Most of the rural and urban population of Viti Levu live in the coastal zone where the majority of services, infrastructure, and economic activities are located (Fiji's First National Communication under the UNFCCC, 2005).

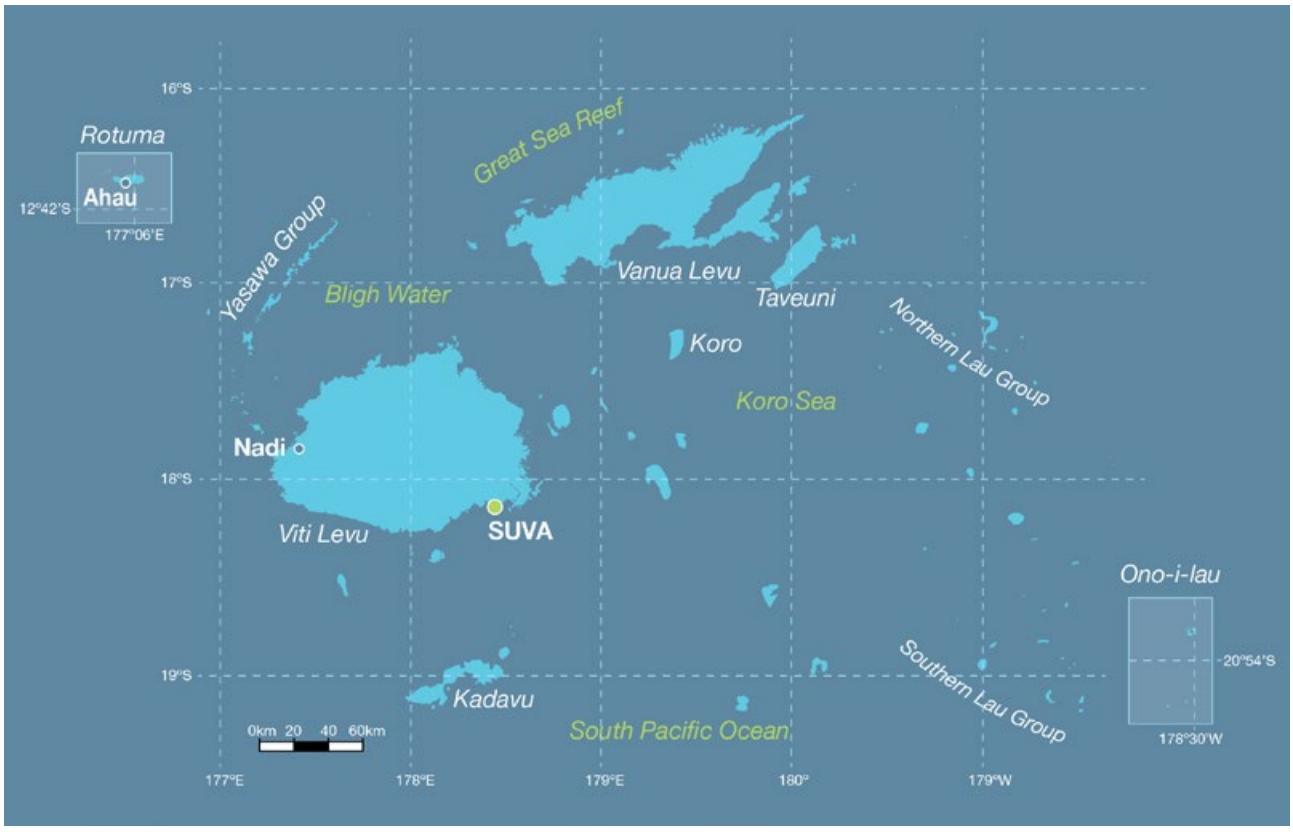

Figure 5.1: Fiji

5.3 Data Availability

There are currently 30 climate (single observation at 9 am), eight synoptic (multiple daily observations) and 52 rainfall-only operational meteorological observation stations in Fiji's meteorological network. Climate records with data available from before 1900 are available for at least six stations or multi-station composites.

Climate records for both Suva (the capital) and Nadi Airport from 1950–2009 have been used (Figure 5.1). Suva and Nadi Airport are located on the south-eastern and western sides of Viti Levu respectively. The records from both sites are homogeneous and more than 99% complete.

Oceanographic records do not cover such a long time period. Monthly-averaged sea-level data are available from Suva (1972–2009 and 1998–present) and Lautoka (1992–present). A global positioning system instrument to estimate vertical land motion was deployed at Lautoka in 2001 and will provide valuable direct estimates of local vertical land motion in future years. Both satellite (from 1993) and in situ sea-level data (1950–2009; termed reconstructed sea level; Volume 1, Section 2.2.2.2) are available on a global 1° x 1° grid.

Long-term locally-monitored sea-surface temperature data are unavailable for Fiji, so large-scale gridded sea-surface temperature datasets have been used (HadISST, HadSST2, ERSST and Kaplan Extended SST V2; Volume 1, Table 2.3).

Barometric pressure meter, Fiji Meteorological Service

5.4 Seasonal Cycles

Average monthly maximum, mean and minimum air temperatures are strongly tied to changes in the surrounding ocean temperature (Figure 5.2). The range in average monthly maximum temperature is about 4ºC for Suva and 3ºC for Nadi Airport. In the cooler/drier half of the year (May-October) less energy is received from the sun, south-east trade winds persist and sub-tropical high pressure systems move north bringing cooler, drier conditions. About 63% of Suva's rain and 77% of Nadi Airport's rain falls in the wet season from November to April.

The seasonal cycle is strongly affected by the South Pacific Convergence Zone (SPCZ), which is most intense during the wet season. The southern edge of the SPCZ usually lies near Fiji. The effects of large-scale climate features such as the SPCZ and trade winds are modified on some islands due to the influence of mountains. Those regions exposed to the trade winds can receive mean annual rainfall in excess of 4000 mm, while leeward regions receive on average less than 2000 mm annually with less than 25% of annual rainfall between May and October. Several weather features have a notable impact on Fiji's climate. Active phases of the Madden-Julian Oscillation (MJO; Volume 1, Section 2.4.4) near Fiji can be associated with significant rainfall for several days in the wet season. In addition, late afternoon convective thunderstorms contribute significant rainfall to the central and western parts of Viti Levu. In the dry season, cold fronts, which are usually weak by the time they reach Fiji's latitude, occasionally merge with troughs in the upper atmosphere resulting in widespread rainfall.

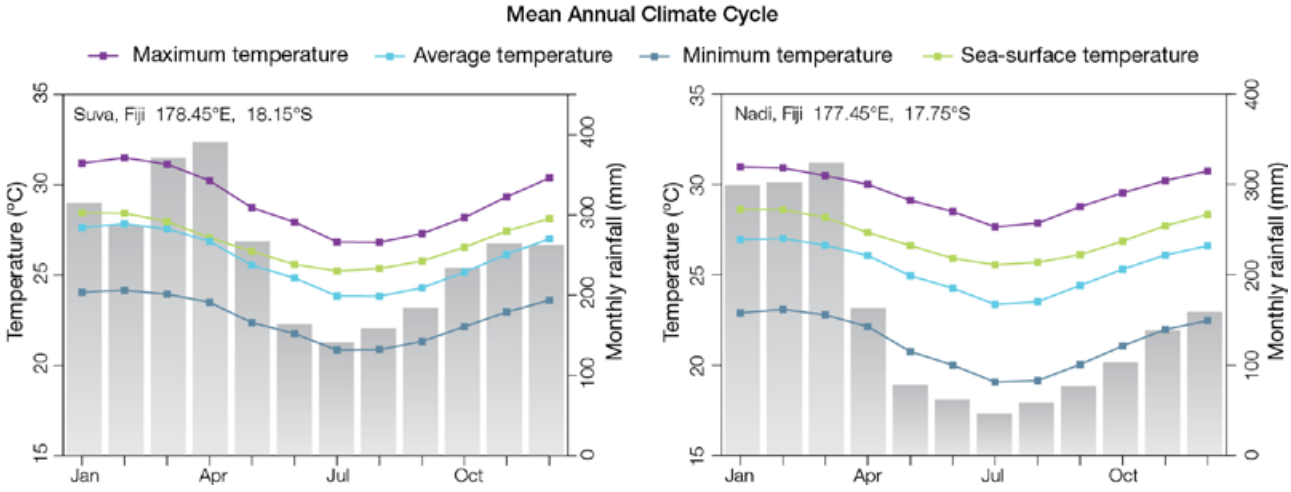

Figure 5.2: Mean annual cycle of rainfall (grey bars) and daily maximum, minimum and mean air temperatures at Suva (left) and at Nadi Airport (right), and local sea-surface temperatures derived from the HadISST dataset (Volume 1, Table 2.3).

5.5 Climate Variability

The El Niño-Southern Oscillation (ENSO) is the most important influence on year-to-year climate variations in Fiji. At Suva (Table 5.1), dry seasons during El Niño tend to be drier and cooler than normal, with the influence of ENSO much stronger on temperature than on rainfall. The opposite changes tend to occur during La Niña events (Figure 5.3). The influence is probably due to the cooler ocean waters around Fiji and more southerly and stronger trade winds (which are cooler and drier) in El Niño years. The Southern Annular Mode (SAM) is related to climate variability in the region, independent of but weaker than ENSO in the dry winter season. When the SAM index is positive, sub-tropical high pressure systems stay further south and temperatures are warmer, and when the SAM index is negative they move north, bringing cooler conditions. In the wet season only ENSO has a clear influence and only on temperature, with warmer nights and cooler days in El Niño years. Modoki El Niño events (Volume 1, Section 3.4.1) bring cooler days in the dry season and warmer nights in the wet season, as do classical El Niño events, but Modoki events have no significant influence on rainfall.

At Nadi Airport (Table 5.2) the dry season in El Niño years also tends to be cooler and drier. In the wet season the impact of ENSO is very strong. In El Niño years Nadi Airport wet seasons are drier (more than 50% of year-to-year rainfall variability can be explained by the central Pacific sea-surface temperature (Niño3.4) and days are warmer. Much of this variability is driven by the SPCZ, which moves to the north-east, away from Fiji, during El Niño events. This brings drier conditions to Nadi Airport, and with the decreased cloud cover this leads to warmer daytime temperatures. The opposite changes tend to occur in La Niña years. Modoki El Niño events have the same but weaker effects as canonical El Niño events in the wet season at Nadi Airport. SAM is correlated with only maximum temperatures at Nadi Airport but in the same way as in Suva.

The differences in climate between Suva and Nadi Airport are primarily due to their different exposure to the trade winds. Differences are greatest during the dry season when the trade winds dominate Fiji's weather. Suva's rainfall during the dry season is more than two and a half times that of Nadi Airport's. Wet season rainfall is similar, 1890 mm and 1385 mm respectively.

Table 5.1: Correlation coefficients between indices of key large-scale patterns of climate variability and minimum and maximum temperatures (Tmin and Tmax) and rainfall at Suva. Only correlation coefficients that are statistically significant at the 95% level are shown.

Climate feature/index		Dry season (May–October)			Wet season (November–April)		
		Tmin	Tmax	Rain	Tmin	Tmax	Rain
ENSO	Niño3.4	-0.53	-0.68	-0.36	0.47	-0.26	
	Southern Oscillation Index	0.45	0.69	0.31	-0.45	0.24	
Interdecadal Pacific Oscillation Index							
Southern Annular Mode Index		-0.33	-0.29				
ENSO Modoki Index			-0.41		0.37		
Number of years of data		68	67	68	68	68	68

Table 5.2: Correlation coefficients between indices of key large-scale patterns of climate variability and minimum and maximum temperatures (Tmin and Tmax) and rainfall at Nadi Airport. Only correlation coefficients that are statistically significant at the 95% level are shown.

Climate feature/index		Dry season (May–October)			Wet season (November–April)		
		Tmin	Tmax	Rain	Tmin	Tmax	Rain
ENSO	Niño3.4	-0.44	-0.57	-0.30		0.63	-0.73
	Southern Oscillation Index	0.33	0.50	0.30		-0.63	0.76
Interdecadal Pacific Oscillation Index							
Southern Annular Mode Index			-0.32			0.29	
ENSO Modoki Index			-0.25			0.37	-0.56
Number of years of data		65	65	67	65	66	66

5.6 Observed Trends

5.6.1 Air Temperature

Warming trends have been identified in annual and seasonal mean air temperatures at Suva and Nadi Airport for the period 1950–2009 (Figure 5.3). Annual and wet season maximum air temperature trends are greater than those observed for minimum air temperatures (Table 5.3) at both Suva and Nadi Airport.

5.6.2 Rainfall

Annual and seasonal rainfall trends for Suva and Nadi Airport for the period 1950–2009 are not statistically significant (Table 5.3 and Figure 5.4).

5.6.3 Extreme Events

The tropical cyclone season in Fiji is usually between November and April, but occasionally tropical cyclones have occurred in October and May in El Niño years. The tropical cyclone archive of the Southern Hemisphere indicates that between the 1969/70 and 2009/10 seasons, the centre of 70 tropical cyclones (Figure 5.5) passed within 400 km of Suva, usually approaching Fiji from the north-west. This represents an average of 17 cyclones per decade. Tropical cyclones were most frequent in El Niño years (19 cyclones per decade) and least frequent in La Niña years (15 cyclones per decade).

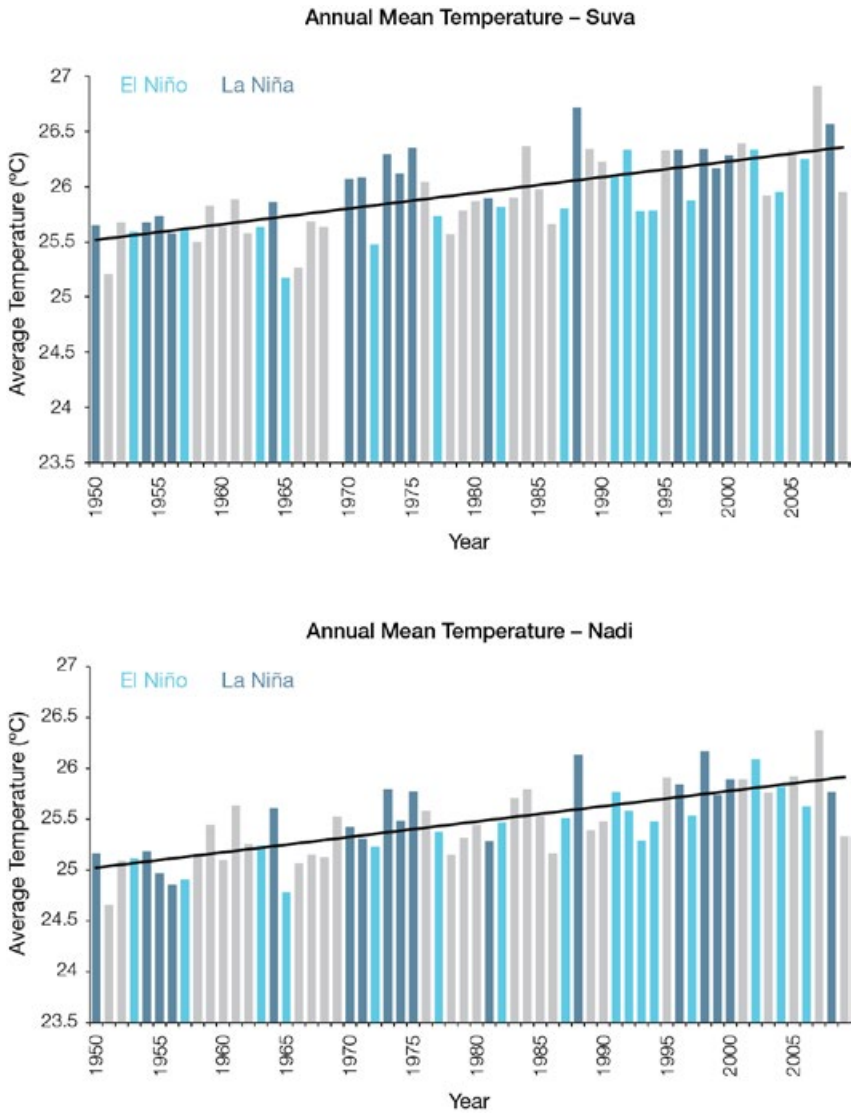

Figure 5.3: Annual mean air temperature for Suva (top) and Nadi Airport (bottom). Light blue, dark blue and grey bars denote El Niño, La Niña and neutral years respectively.

Table 5.3: Annual and seasonal trends in maximum, minimum and mean air temperature (Tmax, Tmin and Tmean) and rainfall at Suva and Nadi Airport for the period 1950–2009. Asterisks indicate significance at the 95% level. Persistence is taken into account in the assessment of significance as in Power and Kociuba (in press). The statistical significance of the air temperature trends is not assessed.

	Suva Tmax (°C per 10 yrs)	Suva Tmin (°C per 10 yrs)	Suva Tmean (°C per 10 yrs)	Suva Rain (mm per 10 yrs)	Nadi Airport Tmax (°C per 10 yrs)	Nadi Airport Tmin (°C per 10 yrs)	Nadi Airport Tmean (°C per 10 yrs)	Nadi Airport Rain (mm per 10 yrs)
Annual	+0.15	+0.14	+0.14	-35	+0.18	+0.12	+0.15	+1
Wet season	+0.20	+0.16	+0.18	-30	+0.20	+0.14	+0.17	+4
Dry season	+0.11	+0.12	+0.11	-2	+0.16	+0.12	+0.14	0

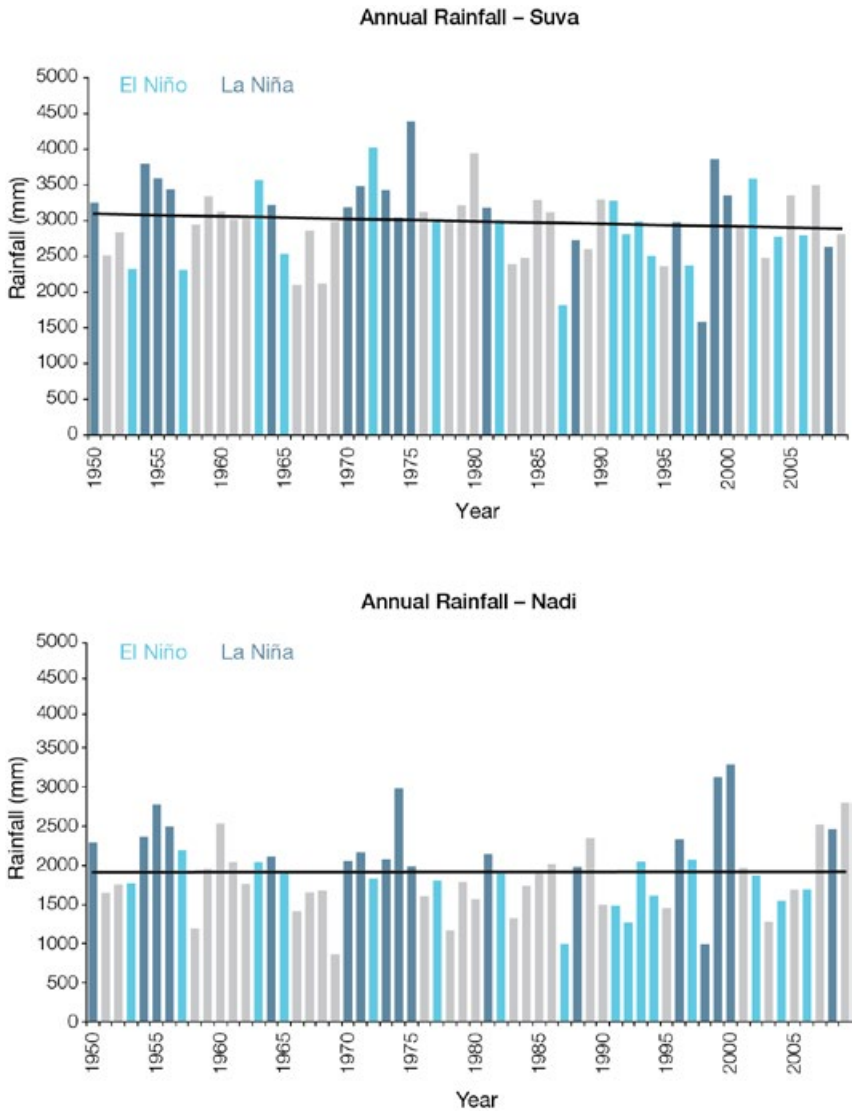

Figure 5.4: Annual rainfall for Suva (top) and Nadi Airport (bottom). Light blue, dark blue and grey bars denote El Niño, La Niña and neutral years respectively.

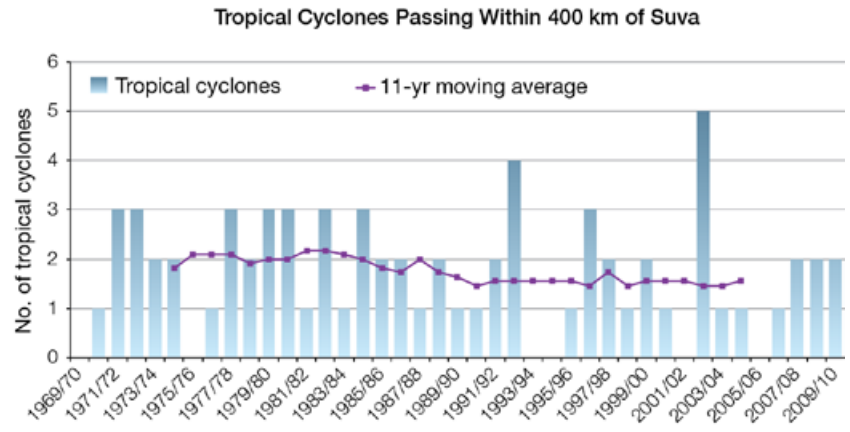

Figure 5.5: The number of tropical cyclones passing within 400 km of Suva per season. The 11-year moving average is in purple.

The neutral season average is 16 cyclones per decade. The interannual variability in the number of tropical cyclones in the vicinity of Suva is large, ranging from zero in some seasons to five in 2002/03. This variability makes it difficult to identify any long-term trends in frequency.

More than 80% of meteorological droughts since 1920 are associated with El Niño events. Severe droughts in recent times occurred in 1987, 1992, 1997/98, 2003 and 2010 (Figure 5.4). A special feature of Fiji droughts is a time lag of several months between the onset/end of moderate to strong El Niño events and the onset/end of droughts.

River flooding occurs almost every wet season and occasionally in the dry season during La Niña events. Most floods occur at the height of the wet season between January and March. Most rivers and streams in Fiji are relatively small and flow from steep mountainous terrain. The short and steep watercourses, together with high intensity rainfall, lead to swiftly rising and falling water levels. The time between rainfall and floods can be as short as a few hours, making prediction difficult.

Fires occasionally occur on the leeward sides of the main islands in the dry season during a significant period without rainfall. Other extreme events include storm surges and waves associated with significant tropical disturbances.

5.6.4 Sea-Surface Temperature

Historical changes in sea-surface temperature around Fiji are consistent with the broad-scale changes in the PCCSP region. Water temperatures remained relatively constant from the 1950s to the late 1980s. This was followed by a period of more rapid warming (approximately 0.07°C per decade for 1970–present). At these regional scales, natural variability plays a large role in changes to sea-surface temperature making it difficult to any identify long-term trends. Figure 5.8 shows the 1950–2000 sea-surface temperature changes (relative to a reference year of 1990) from three different large-scale sea-surface temperature gridded datasets (HadSST2, ERSST and Kaplan Extended SST V2; Volume 1, Table 2.3)

5.6.5 Ocean Acidification

Based the large-scale distribution of coral reefs across the Pacific and the seawater chemistry, Guinotte et al. (2003) suggested that seawater aragonite saturation states above 4 were optimal for coral growth and for the development of healthy reef ecosystems, with values from 3.5 to 4 adequate for coral growth, and values between 3 and 3.5, marginal. Coral reef ecosystems were not found at seawater aragonite saturation states below 3 and these conditions were classified as extremely marginal for supporting coral growth.

In the Fijian maritime boundaries, the aragonite saturation state has declined from about 4.5 in the late 18th century to an observed value of about 3.9 ± 0.1 by 2000.

5.6.6 Sea Level

Monthly averages of the historical tide gauge (both Suva and Lautoka), satellite (since 1993) and gridded sea-level (since 1950) data agree well after 1993 and indicate interannual variability in sea levels of about 18 cm (estimated 5–95% range) after removal of the seasonal cycle (Figure 5.10; Section 5.7.5). Prior to 1990, there are gaps in the Suva time series and changes in instrumentation may have led to data inhomogeneities. The sea-level rise near Fiji measured by satellite altimeters (Figure 5.6) since 1993 is about 6 mm per year, larger than the global average of 3.2 ± 0.4 mm per year. This rise is partly linked to a pattern related to climate variability from year to year and decade to decade (Figure 5.10).

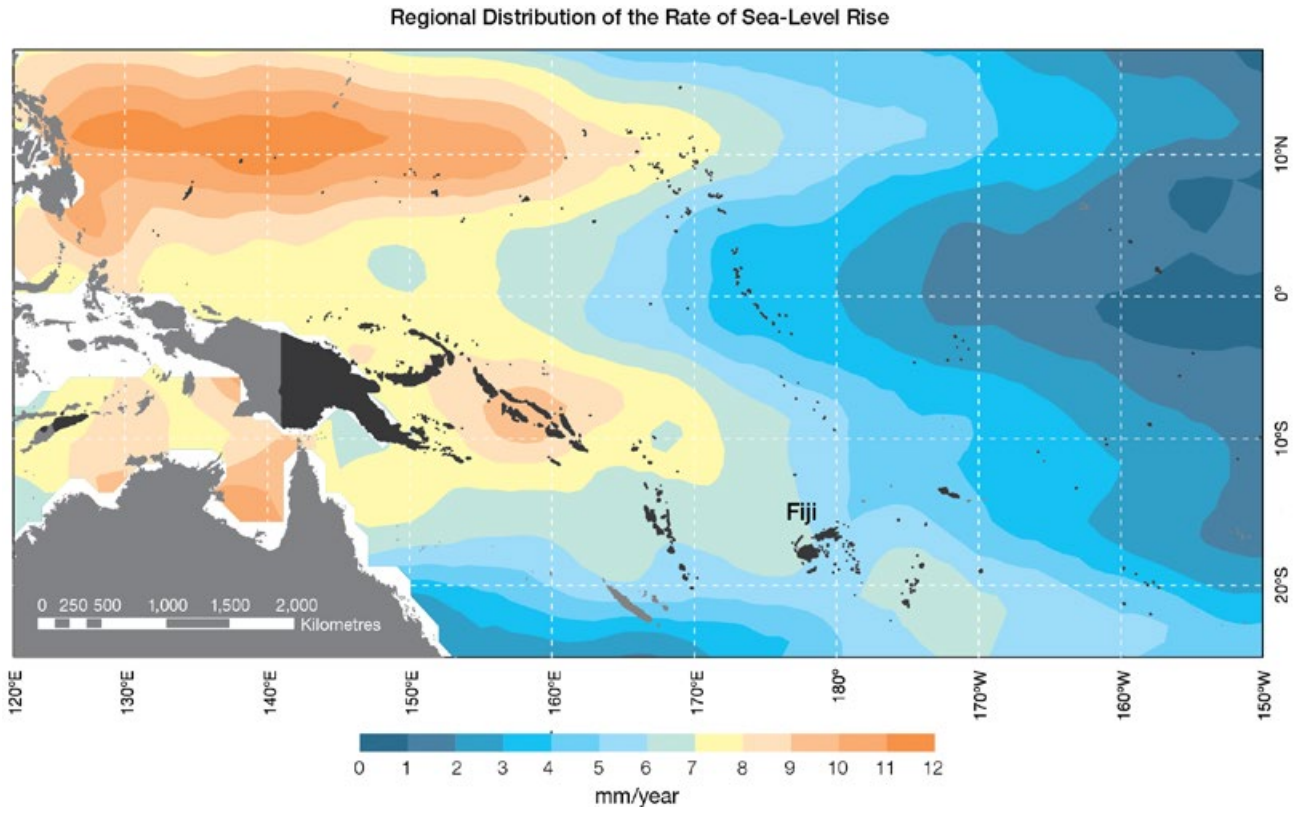

Figure 5.6: The regional distribution of the rate of sea-level rise measured by satellite altimeters from January 1993 to December 2010, with the location of Fiji indicated. Further detail about the regional distribution of sea-level rise is provided in Volume 1, Section 3.6.3.2.

5.6.7 Extreme Sea-Level Events

The annual climatology of the highest daily sea levels has been evaluated from hourly tide gauge measurements at Lautoka and Suva (Figure 5.7). Tidal variations throughout the year lead to highest annual water levels during November-March. Short-term contributions at Lautoka exhibit a weak annual cycle with higher levels during December-March. At Suva, the short-term contributions are higher in December-March as well as June and July which may be partly explained by Suva's south-east exposure to the stronger trade winds and waves at these times of the year. Although the average seasonal signal shows little variability throughout the year, there is a tendency for higher water levels at Suva and Lautoka from March through October during La Niña years whereas during El Niño years there is a tendency for lower seasonal sea levels during these months. The top 10 highest sea levels recorded at both sites mostly occur during the cyclone season. The highest recorded event at each site was associated with Tropical Cyclone Gavin in March 1997 while the second highest event at Lautoka in December 1992 was associated with Tropical Cyclone Joni. Other weather events contributing to the high water levels include tropical depressions and monsoon troughs.

Further research has been undertaken modelling storm surges from a large number of tropical cyclones with varying intensities, speeds and directions of approach, which fit the distributions of the cyclone parameters for cyclones that have affected Fiji in recent decades. This provides more detailed information on how extreme sea levels due to storm surges vary around the coastlines of Viti Levu and Vanua Levu. This modelling indicates that the north-western coastlines of both islands show the greatest risk of storm surges because they face the direction from which tropical cyclones most commonly approach Fiji. The 1-in-100-year storm surge heights along these coastlines were found to be around twice the values at locations situated on the south-west side of the islands (McInnes et al., 2011).

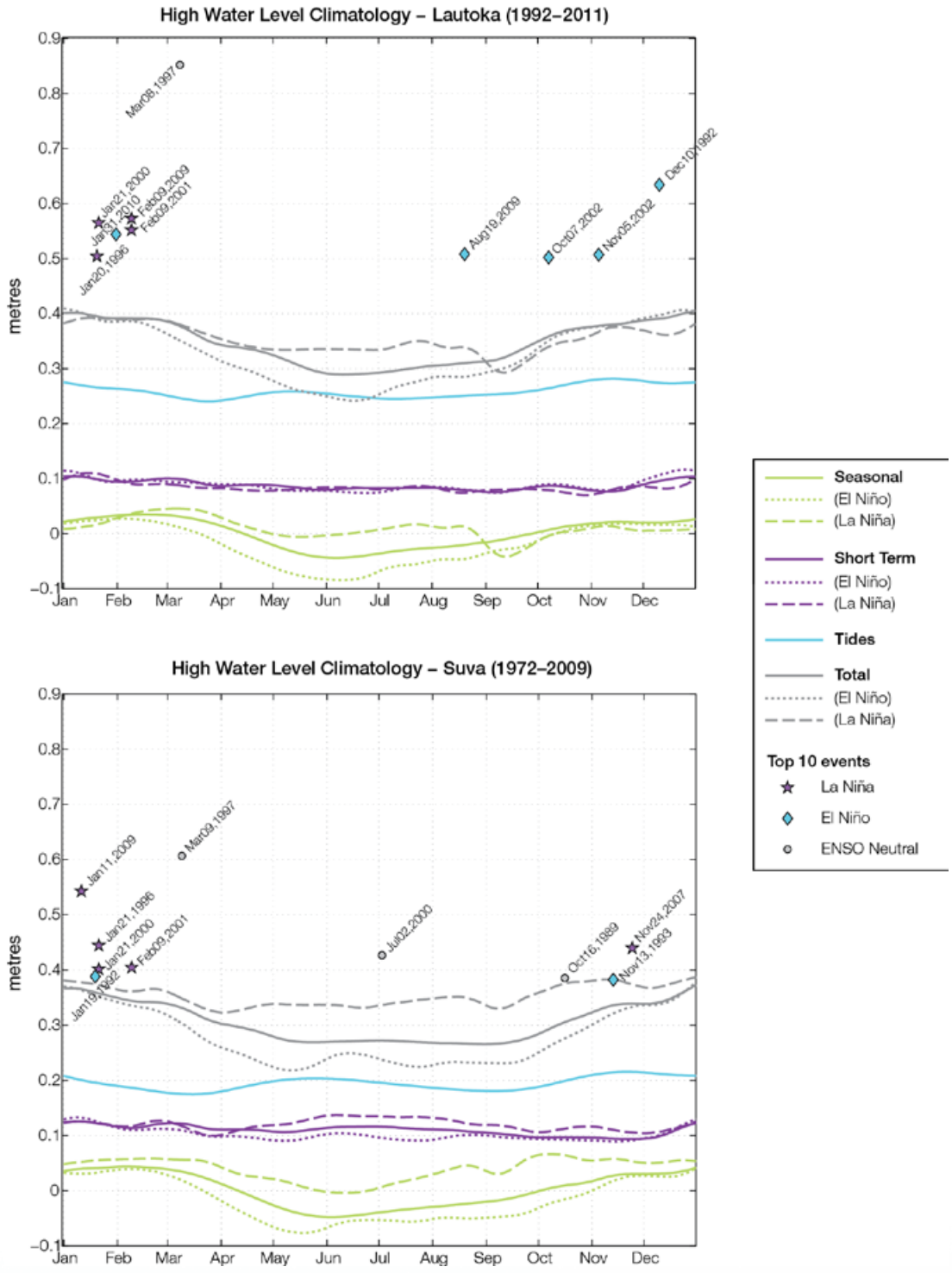

Figure 5.7: The annual cycle of high water relative to the Mean Higher High Water (MHHW) due to tides, short-term fluctuations (most likely associated with storms) and seasonal variations for Lautoka (top) and Suva (bottom). The tides and short-term fluctuations are respectively the 95% exceedence levels of the astronomical high tides relative to MHHW and the short-term sea-level fluctuations. Components computed only for El Niño and La Niña years are shown by dotted and dashed lines and grey lines are the sum of the tide, short-term and seasonal components. The 10 highest sea-level events in the record relative to MHHW are shown and coded to indicate the phase of ENSO at the time of the extreme event.

5.7 Climate Projections

Climate projections have been derived from up to 18 global climate models from the CMIP3 database, for up to three emissions scenarios (B1 (low), A1B (medium) and A2 (high)) and three 20-year periods (centred on 2030, 2055 and 2090, relative to 1990). These models were selected based on their ability to reproduce important features of the current climate (Volume 1, Section 5.2.3), so projections arising from each of the models are plausible representations of the future climate. This means there is not one single projected future for Fiji, but rather a range of possible futures. The full range of these futures is discussed in the following sections.

These projections do not represent a value specific to any actual location, such as a town or city in Fiji. Instead, they refer to an average change over the broad geographic region encompassing the islands of Fiji and the surrounding ocean (Figure 1.1 shows the regional boundaries). Some information regarding dynamical downscaling simulations from the CCAM model (Section 1.7.2) is also provided for temperature and rainfall projections, in order to indicate how changes in the climate on an individual island-scale may differ from the broad-scale average.

Section 1.7 provides important information about interpreting climate model projections.

5.7.1 Temperature

Surface air temperature and sea-surface temperature are projected to continue to increase over the course of the 21st century. There is *very high* confidence in this direction of change because:

- Warming is physically consistent with rising greenhouse gas concentrations.
- All CMIP3 models agree on this direction of change.

The majority of CMIP3 models simulate a slight increase (<1°C) in annual and seasonal mean temperature by 2030, however by 2090 under the A2 (high) emissions scenario temperature increases of greater than 2.5°C are simulated by the majority of models (Table 5.4). Given the close relationship between surface air temperature and sea-surface temperature, a similar (or slightly weaker) rate of warming is projected for the surface ocean (Figure 5.8). There is *moderate* confidence in this range and distribution of possible futures because:

- There is generally a large discrepancy between modelled and observed temperature trends over the past 50 years in the vicinity of Fiji (Figure 5.8).

The 8 km CCAM simulations suggest that warming may be stronger along the west coast of Viti Levu and Vanua Levu. These simulations also typically project an extra 0.5 to 1°C increase in temperature over land, relative to the change in surface air temperature over the ocean (Volume 1, Section 7.2.2.1).

Interannual variability in surface air temperature and sea-surface temperature over Fiji is strongly influenced by ENSO in the current climate (Section 5.5). As there is no consistency in projections of future ENSO activity (Volume 1, Section 6.4.1), it is not possible to determine whether interannual variability in temperature will change in the future. However, ENSO is expected to continue to be an important source of variability for Fiji.

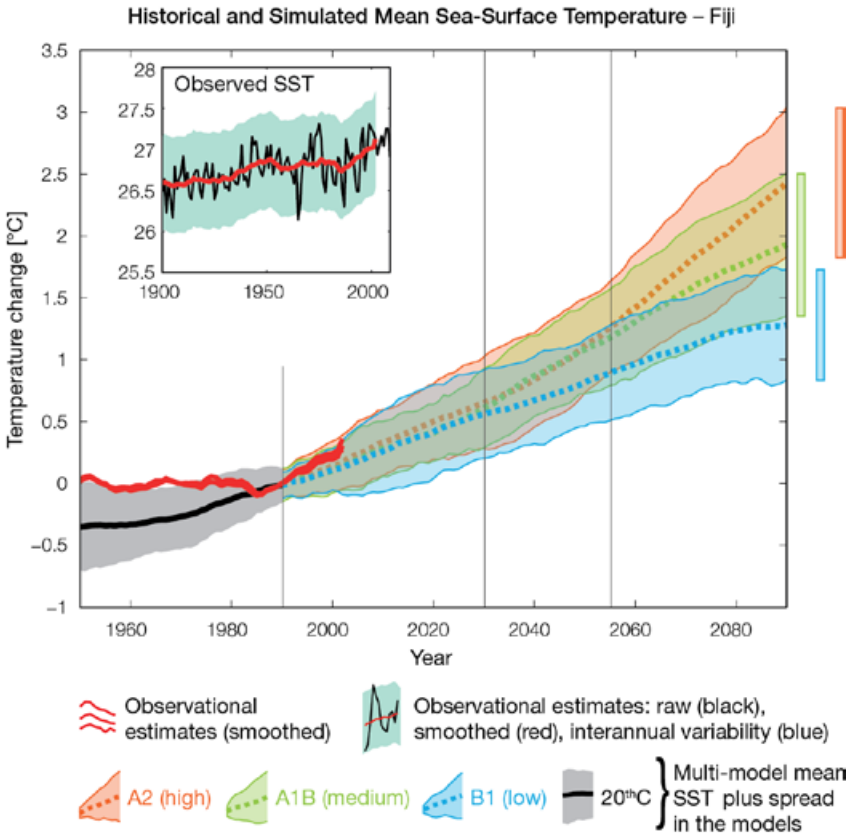

Figure 5.8: Historical climate (from 1950 onwards) and simulated historical and future climate for annual mean sea-surface temperature (SST) in the region surrounding Fiji, for the CMIP3 models. Shading represents approximately 95% of the range of model projections (twice the inter-model standard deviation), while the solid lines represent the smoothed (20-year running average) multi-model mean temperature. Projections are calculated relative to the 1980–1999 period (which is why there is a decline in the inter-model standard deviation around 1990). Observational estimates in the main figure (red lines) are derived from the HadSST2, ERSST and Kaplan Extended SST V2 datasets (Volume 1, Section 2.2.2). Annual average (black) and 20-year running average (red) HadSST2 data is also shown inset.

5.7.2 Rainfall

Wet Season (November-April)

Wet season rainfall is projected to increase over the course of the 21st century. There is *moderate* confidence in this direction of change because:

- An increase in wet season rainfall is consistent with the projected likely increase in the intensity of the South Pacific Convergence Zone (SPCZ), which lies over Fiji in this season (Volume 1, Section 6.4.5).
- The majority of CMIP3 models agree on this direction of change by 2090.

The majority of CMIP3 models simulate little change (-5% to 5%) in wet season rainfall by 2030, however by 2090 the majority simulate an increase (>5%), with approximately one third simulating a large increase (>15%) under the A2 (high) emissions scenario (Table 5.4). There is *moderate* confidence in this range and distribution of possible futures because:

- In simulations of the current climate, the CMIP3 models generally locate the SPCZ in the correct location relative to Fiji in the wet season (Brown et al., 2011).
- The CMIP3 models are unable to resolve many of the physical processes involved in producing rainfall. As a consequence, they do not simulate rainfall as well as other variables such as temperature (Volume 1, Chapter 5).

The 8 km CCAM simulations suggest that rainfall increases may be slightly higher than the large-scale CMIP3 projections along the eastern coastlines of Viti Levu and Vanua Levu. This is a physically plausible response for the windward side of mountainous islands (Volume 1, Section 7.2.2.1).

Dry Season (May-October)

Dry season rainfall is projected to decrease over the course of the 21st century. There is *moderate* confidence in this direction of change because:

- Approximately half of the CMIP3 models agree on this direction of change by 2090.

The majority of CMIP3 models simulate little change (-5% to 5%) in dry season rainfall by 2030, however by 2090 the models are approximately equally divided between a decrease (<-5%) and little change, with only two to three models suggesting an increase (>5%) depending on the emissions scenario (Table 5.4). There is *low* confidence in this range and distribution of possible futures because:

- In simulations of the current climate, some CMIP3 models have an SPCZ that extends too far east during the dry season, with too much rainfall over Fiji (Brown et al., 2011).
- The CMIP3 models are unable to resolve many of the physical processes involved in producing rainfall.

Annual

Little change is projected in total annual rainfall over the course of the 21st century. There is *low* confidence in this direction of change because:

- Only approximately half of the CMIP3 models agree on this direction of change by 2090.
- There is low confidence in the range and distribution of dry season rainfall projections, as discussed.

Interannual variability in rainfall over Fiji is strongly influenced by ENSO in the current climate, via the movement of the SPCZ (Section 5.5). As there is no consistency in projections of future ENSO activity (Volume 1, Section 6.4.1), it is not possible to determine whether interannual variability in rainfall will change in the future.

5.7.3 Extremes

Temperature

The intensity and frequency of days of extreme heat are projected to increase over the course of the 21st century. There is *very high* confidence in this direction of change because:

- An increase in the intensity and frequency of days of extreme heat is physically consistent with rising greenhouse gas concentrations.
- All CMIP3 models agree on the direction of change for both intensity and frequency.

The majority of CMIP3 models simulate an increase of approximately 1°C in the temperature experienced on the 1-in-20-year hot day by 2055 under the B1 (low) emissions scenario, with an increase of over 2.5°C simulated by the majority of models by 2090 under the A2 (high) emissions scenario (Table 5.4). There is *low* confidence in this range and distribution of possible futures because:

- In simulations of the current climate, the CMIP3 models tend to underestimate the intensity and frequency of days of extreme heat (Volume 1, Section 5.2.4).
- Smaller increases in the frequency of days of extreme heat are projected by the CCAM 60 km simulations.

Rainfall

The intensity and frequency of days of extreme rainfall are projected to increase over the course of the 21st century. There is *high* confidence in this direction of change because:

- An increase in the frequency and intensity of extreme rainfall is consistent with larger-scale projections, based on the physical argument that the atmosphere is able to hold more water vapour in a warmer climate (Allen and Ingram, 2002; IPCC, 2007). It is also consistent with the projected likely increase in SPCZ intensity (Volume 1, Section 6.4.5).
- Almost all of the CMIP3 models agree on this direction of change for both intensity and frequency.

The majority of CMIP3 models simulate an increase of at least 10 mm in the amount of rain received on the 1-in-20-year wet day by 2055 under the B1 (low) emissions scenario, with an increase of at least 25 mm simulated by 2090 under the A2 (high) emissions scenario. The majority of models project that the current 1-in-20-year extreme rainfall event will occur, on average, three times

per 20-year period by 2055 under the B1 (low) emissions scenario and four to five times per 20-year period by 2090 under the A2 (high) emissions scenario. There is *low* confidence in this range and distribution of possible futures because:

- In simulations of the current climate, the CMIP3 models tend to underestimate the intensity and frequency of extreme rainfall (Volume 1, Section 5.2.4).
- The CMIP3 models are unable to resolve many of the physical processes involved in producing extreme rainfall.

Drought

Little change is projected in the incidence of drought over the course of the 21st century. There is *low* confidence in this direction of change because:

- There is only low confidence in the range of dry season rainfall projections (Section 5.7.2), which directly influences projections of future drought conditions.

Under the B1 (low) emissions scenario, the majority of CMIP3 models project that the frequency of mild drought will slightly increase from approximately seven to eight times every 20 years in 2030, to eight to nine times every 20 years by 2090. Under the A1B (medium) emissions scenario, the frequency of mild drought remains approximately constant at seven to eight times every 20 years, while under the A2 (high) emissions scenario the frequency is projected to slightly decrease from eight to nine times every 20 years in 2030 to seven to eight times by 2090. The majority of CMIP3 models project that moderate and severe droughts will occur approximately once to twice and once every 20 years respectively, across all time periods and emissions scenarios.

Tropical Cyclones

Tropical cyclone numbers are projected to decline in the south-east Pacific Ocean basin (0–40ºS, 170ºE–130ºW) over the course of the 21st century. There is *moderate* confidence in this direction of change because:

- Many studies suggest a decline in tropical cyclone frequency globally (Knutson et al., 2010).
- Tropical cyclone numbers decline in the south-east Pacific Ocean in the majority assessment techniques.

Based on the direct detection methodologies (Curvature Vorticity Parameter (CVP) and the CSIRO Direct Detection Scheme (CDD) described in Volume 1, Section 4.8.2), 65% of projections show no change or a decrease in tropical cyclone formation when applied to the CMIP3 climate models for which suitable output is available. When these techniques are applied to CCAM, 100% of projections show a decrease in tropical cyclone formation. In addition, the Genesis Potential Index (GPI) empirical technique suggests that conditions for tropical cyclone formation will become less favourable in the south-east Pacific Ocean basin for all analysed CMIP3 models. There is *moderate* confidence in this range and distribution of possible futures because in simulations of the current climate, the CVP, CDD and GPI methods capture the frequency of tropical cyclone activity reasonably well (Volume 1, Section 5.4).

Despite this projected reduction in total cyclone numbers, five of the six CCAM 60 km simulations show an increase in the proportion of the most severe cyclones. Most models also indicate a reduction in tropical cyclone wind hazard north of 20ºS latitude and regions of increased hazard south of 20ºS latitude. This increase in wind hazard coincides with a poleward shift in the latitude at which tropical cyclones are most intense.

5.7.4 Ocean Acidification

The acidification of the ocean will continue to increase over the course of the 21st century. There is *very high* confidence in this projection as the rate of ocean acidification is driven primarily by the increasing oceanic uptake of carbon dioxide, in response to rising atmospheric carbon dioxide concentrations.

Projections from all analysed CMIP3 models indicate that the annual maximum aragonite saturation state will reach values below 3.5 by about 2035 and continue to decline thereafter (Figure 5.9; Table 5.4). There is *moderate* confidence in this range and distribution of possible futures because the projections are based on climate models without an explicit representation of the carbon cycle and with relatively low resolution and known regional biases.

The impact of acidification change on the health of reef ecosystems is likely to be compounded by other stressors including coral bleaching, storm damage and fishing pressure.

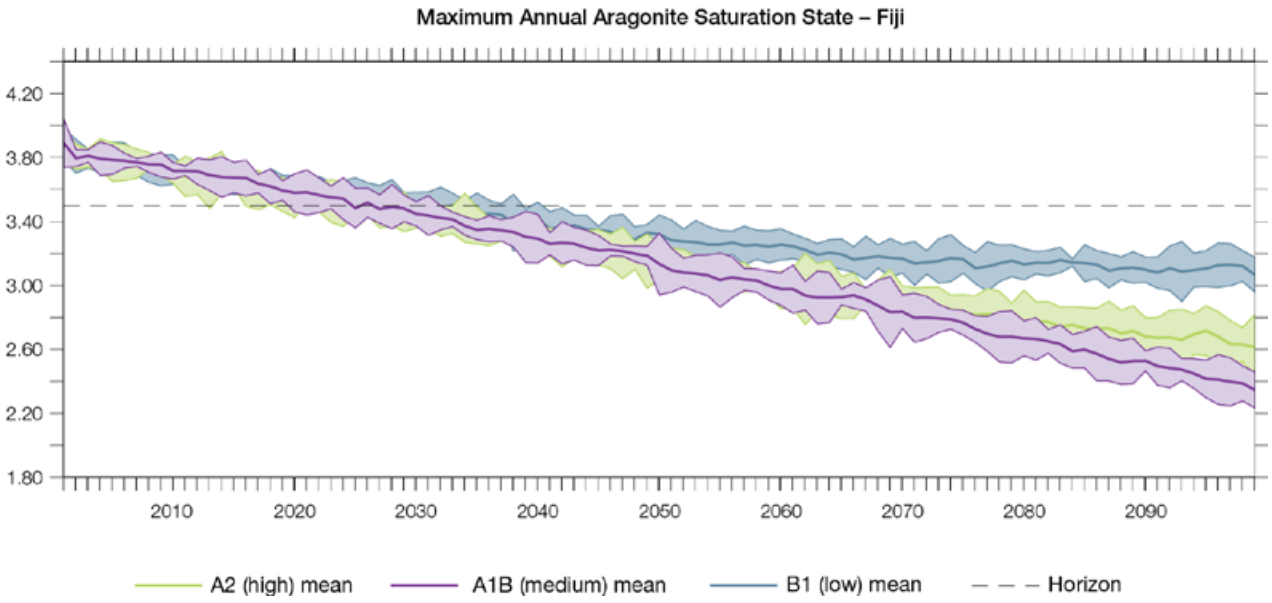

Figure 5.9: Multi-model projections, and their associated uncertainty (shaded area represents two standard deviations), of the maximum annual aragonite saturation state in the sea surface waters of the Fiji region under the different emissions scenarios. The dashed black line represents an aragonite saturation state of 3.5.

5.7.5 Sea Level

Mean sea level is projected to continue to rise over the course of the 21st century. There is *very high* confidence in this direction of change because:

- Sea-level rise is a physically consistent response to increasing ocean and atmospheric temperatures, due to thermal expansion of the water and the melting of glaciers and ice caps.
- Projections arising from all CMIP3 models agree on this direction of change.

The CMIP3 models simulate a rise of between approximately 5–15 cm by 2030, with increases of 20–60 cm indicated by 2090 under the higher emissions scenarios (i.e. A2 (high) and A1B (medium); Figure 5.10; Table 5.4). There is *moderate* confidence in this range and distribution of possible futures because:

- There is significant uncertainty surrounding ice-sheet contributions to sea-level rise and a larger rise than that projected above cannot be excluded (Meehl et al., 2007b). However, understanding of the processes is currently too limited to provide a best estimate or an upper bound (IPCC, 2007).
- Globally, since the early 1990s, sea level has been rising near the upper end of the these projections. During the 21st century, some studies (using semi-empirical models) project faster rates of sea-level rise.

Interannual variability of sea level will lead to periods of lower and higher regional sea levels. In the past, this interannual variability has been about 18 cm (5–95% range, after removal of the seasonal cycle; dashed lines in Figure 5.10 (a)) and a similar range is likely to continue through the 21st century. In addition, winds and waves associated with weather phenomena will continue to lead to extreme sea-level events.

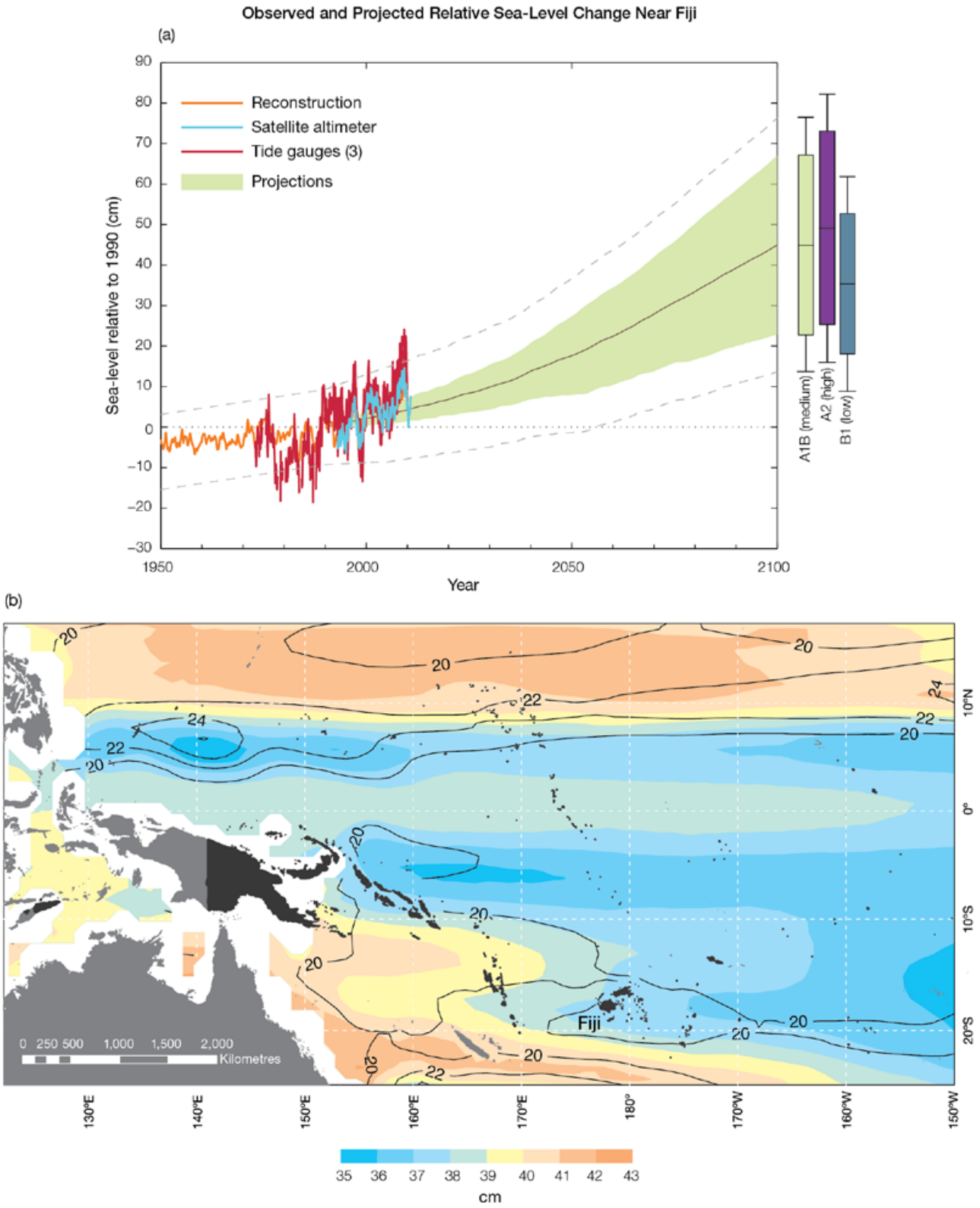

Figure 5.10: Observed and projected relative sea-level change near Fiji. (a) The observed in situ relative sea-level records from Suva (since the early 1970s) and Lautoka (since 1992) are indicated in red, with the satellite record (since 1993) in light blue. The gridded sea-level data at Fiji (since 1950, from Church and White (in press)) is shown in orange. The projections for the A1B (medium) emissions scenario (5–95% uncertainty range) are shown by the green shaded region from 1990–2100. The range of projections for the B1 (low), A1B (medium) and A2 (high) emissions scenarios by 2100 are also shown by the bars on the right. The dashed lines are an estimate of interannual variability in sea level (5–95% range about the long-term trends) and indicate that individual monthly averages of sea level can be above or below longer-term averages. (b) The projections (in cm) for the A1B (medium) emissions scenario in the Fiji region for the average over 2081–2100 relative to 1981–2000 are indicated by the shading, with the estimated uncertainty in the projections indicated by the contours (in cm).

5.7.6 Projections Summary

The projections presented in Section 5.7 are summarised in Table 5.4. For detailed information regarding the various uncertainties associated with the table values, refer to the preceding text in Sections 5.7 and 1.7, in addition to Chapters 5 and 6 in Volume 1. When interpreting the differences between projections for the B1 (low), A1B (medium) and A2 (high) emissions scenarios, it is also important to consider the emissions pathways associated with each scenario (Volume 1, Figure 4.1) and the fact that a slightly different subset of models was available for each (Volume 1, Appendix 1).

Table 5.4: Projected change in the annual and seasonal mean climate for Fiji, under the B1 (low; blue), A1B (medium; green) and A2 (high; purple) emissions scenarios. Projections are given for three 20-year periods centred on 2030 (2020–2039), 2055 (2046–2065) and 2090 (2080–2099), relative to 1990 (1980–1999). Values represent the multi-model mean change ± twice the inter-model standard deviation (representing approximately 95% of the range of model projections), except for sea level where the estimated mean change and the 5–95% range are given (as they are derived directly from the Intergovernmental Panel on Climate Change Fourth Assessment Report values). The confidence (Section 1.7.2) associated with the range and distribution of the projections is also given (indicated by the standard deviation and multi-model mean, respectively). See Volume 1, Appendix 1 for a complete listing of CMIP3 models used to derive these projections.

Variable	Season	2030	2055	2090	Confidence
Surface air temperature (°C)	Annual	+0.6 ± 0.4 +0.7 ± 0.5 +0.7 ± 0.3	+1.0 ± 0.5 +1.4 ± 0.5 +1.4 ± 0.3	+1.4 ± 0.7 +2.1 ± 0.8 +2.6 ± 0.6	Moderate
Maximum temperature (°C)	1-in-20-year event	N/A	+1.0 ± 0.7 +1.4 ± 0.7 +1.5 ± 0.6	+1.3 ± 0.5 +2.1 ± 0.9 +2.6 ± 1.4	Low
Minimum temperature (°C)	1-in-20-year event	N/A	+1.1 ± 1.7 +1.5 ± 1.8 +1.5 ± 1.8	+1.5 ± 1.8 +1.9 ± 2.1 +2.3 ± 1.8	Low
Total rainfall (%)*	Annual	+3 ± 11 +1 ± 12 +2 ± 13	+1 ± 10 +3 ± 14 +4 ± 13	+2 ± 14 +3 ± 16 +7 ± 15	Low
Wet season rainfall (%)*	November-April	+5 ± 10 +3 ± 11 +5 ± 14	+5 ± 12 +6 ± 16 +7 ± 13	+5 ± 18 +8 ± 19 +14 ± 14	Moderate
Dry season rainfall (%)*	May-October	-1 ± 13 -2 ± 17 -2 ± 12	-5 ± 14 -2 ± 16 -1 ± 18	-3 ± 17 -4 ± 19 -1 ± 22	Low
Sea-surface temperature (°C)	Annual	+0.6 ± 0.4 +0.6 ± 0.3 +0.7 ± 0.4	+0.9 ± 0.4 +1.2 ± 0.4 +1.3 ± 0.4	+1.3 ± 0.4 +1.9 ± 0.6 +2.4 ± 0.4	Moderate
Aragonite saturation state (Ωar)	Annual maximum	+3.5 ± 0.1 +3.4 ± 0.1 +3.4 ± 0.1	+3.2 ± 0.1 +3.0 ± 0.1 +3.0 ± 0.1	+3.1 ± 0.1 +2.6 ± 0.1 +2.5 ± 0.1	Moderate
Mean sea level (cm)	Annual	+10 (5–16) +10 (5–15) +10 (3–16)	+18 (10–27) +20 (9–31) +20 (8–31)	+32 (16–47) +39 (20–59) +41 (21–62)	Moderate

*The MIROC3.2(medres) and MIROC3.2(hires) models were eliminated in calculating the rainfall projections, due to their inability to accurately simulate present-day activity of the South Pacific Convergence Zone (Volume 1, Section 5.5.1).

Tarawa Atoll

Chapter 6
Kiribati

The contributions of Ueneta Toorua, Tebwaau Tetabo and Tareti Kireua from the Kiribati Meteorology Service and Riibeta Abeta and Nakibae Teuatabo from the Environment and Conservation Division are gratefully acknowledged

Introduction

This chapter provides a brief description of Kiribati, its past and present climate as well as projections for the future. The climate observation network and the availability of atmospheric and oceanic data records are outlined. The annual mean climate, seasonal cycles and the influences of large-scale climate features such as the Intertropical Convergence Zone and patterns of climate variability (e.g. the El Niño-Southern Oscillation) are analysed and discussed. Observed trends and analysis of air temperature, rainfall, extreme events, sea-surface temperature, ocean acidification, mean and extreme sea levels are presented. Projections for air and sea-surface temperature, rainfall, sea level, ocean acidification and extreme events for the 21st century are provided. These projections are presented along with confidence levels based on expert judgement by Pacific Climate Change Science Program (PCCSP) scientists. The chapter concludes with summary tables of projections for the Gilbert, Phoenix and Line Islands (Tables 6.4, 6.5, 6.6). Important background information, including an explanation of methods and models, is provided in Chapter 1. For definitions of other terms refer to the Glossary.

6.1 Climate Summary

6.1.1 Current Climate

- Kiribati has a hot, humid tropical climate, with air temperatures very closely related to the sea-surface temperature of the surrounding oceans.
- The South Pacific Convergence Zone and the Intertropical Convergence Zone influence Kiribati's wet seasons. The driest and wettest periods in the year vary from location to location.
- High year-to-year variability in rainfall is mostly due to the impact of the El Niño-Southern Oscillation.
- Warming trends are evident in both annual and seasonal mean air temperatures at Tarawa for the period 1950–2009.
- The sea-level rise near Kiribati measured by satellite altimeters since 1993 ranges from 1–4 mm per year.
- The Kiritimati positive annual rainfall trend for the period 1950–2009 is statistically significant; however seasonal trends over the same period are not. Annual and seasonal rainfall trends for Tarawa for 1950–2009 are not statistically significant.
- Droughts, usually associated with La Niña events, are occasionally very severe in Kiribati.

6.1.2 Future Climate

Over the course of the 21st century:

- Surface air temperature and sea-surface temperature are projected to continue to increase (*very high* confidence).
- Annual and seasonal mean rainfall is projected to increase (*high* confidence).
- The intensity and frequency of days of extreme heat are projected to increase (*very high* confidence).
- The intensity and frequency of days of extreme rainfall are projected to increase (*high* confidence).
- The incidence of drought is projected to decrease (*moderate* confidence).
- Ocean acidification is projected to continue (*very high* confidence).
- Mean sea-level rise is projected to continue (*very high* confidence).

6.2 Country Description

Kiribati is located near the equator in the central Pacific Ocean. The country consists of 32 low lying atolls and one raised limestone island, Banaba, also known as Ocean Island. The islands lie in three main groups which are the Gilbert, Phoenix and Line Islands, listed in sequence from west to east. The islands are located between approximately 5°N–12°S and 168°E–152°W. The distance between the most westerly situated island and the most easterly situated island is about 4000 km. For the most part, the islands are no more that three to four metres above sea level. The total land area is 811 km^2, while the area of the Exclusive Economic Zone is 3.6 million km^2 (Kiribati's First National Communication under the UNFCCC, 1999; Kiribati's National Adaptation Plan of Action, 2007). The estimated 2010 population was 100 835 (Kiribati Country Statistics, SOPAC, 2010) and the capital of Kiribati is South Tarawa in the Gilbert Islands.

Many people in Kiribati, especially away from the main population centre in South Tarawa, rely on a subsistence form of livelihood based on harvesting tree crops and marine resources. The main exports are copra and fish (Ministry of Environment and Social Development, 1999).

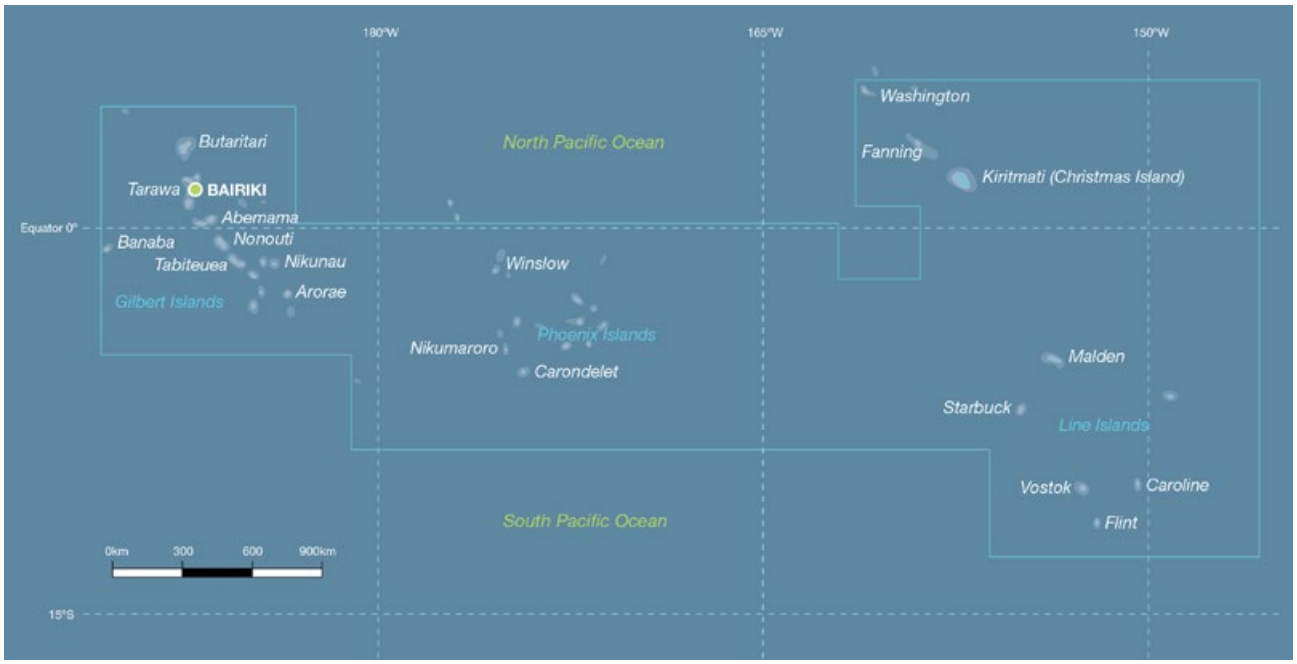

Figure 6.1: Kiribati

6.3 Data Availability

There are currently five operational meteorological stations in Kiribati. Tarawa, the primary station in the Gilbert Islands, is located on the southern side of Tarawa Atoll at Betio. Kiritimati, the primary station in the Line Islands, is situated on the north-west side of the Kiritimati Atoll (Figure 6.1). All five operational stations, including Banaba and Tabuaeran, have rainfall records which began between 1909 and 1945. Banaba has the earliest temperature record which began in 1909 but unfortunately closed in 1993. Tarawa, Beru and Kanton (also known as Canton) have temperature records from 1947. Tarawa and Kiritimati (rainfall only) records from 1950 to 2009 have been used. Both records are homogeneous and more than 95% complete.

Oceanographic records do not cover such a long time period. There are a number of sea-level records available for Kiribati. The best appear to be Tarawa-C (Betio, 1988–2001), Betio (1992–present), Fanning B (1973–1987), Christmas Island (Kiritimati, 1956–1972), Christmas Island II (Kiritimati, 1974–2003), Kanton Island (1949–1974) and Kanton Island-B (1972–2007). A global positioning system instrument to estimate vertical land motion was deployed in Kiribati in 2001 and will provide valuable direct estimates of local vertical land motion in future years. Both satellite (from 1993) and in situ sea-level data (1950–2009; termed reconstructed sea level; Volume 1, Section 2.2.2.2) are available on a global 1° x 1° grid.

Long-term locally-monitored sea-surface temperature data are unavailable for Kiribati, so large-scale gridded sea-surface temperature datasets have been used (HadISST, HadSST2, ERSST and Kaplan Extended SST V2; Volume 1, Table 2.3).

Climate data management training, Kiribati Meteorology Service

6.4 Seasonal Cycles

Kiribati has a hot, humid tropical climate. In Tarawa, average maximum and minimum air temperatures are highly consistent throughout the year, with a range of less than 1°C (Figure 6.2). The air temperatures are very closely related to the sea-surface temperatures. In Kiritimati the seasonal variations in sea-surface temperature are a little higher than near Tarawa, about 1°C between April, the hottest month, and January, the coolest.

The driest and wettest periods in the year vary from location to location. At Tarawa the driest six-month period begins in June, with the lowest mean rainfall in October. This dry season is called *Aumaiaki* in the local language. The peak of the wet season is in January with a mean of almost 268 mm in that month. The wet season, called *Aumeang* in the local language, usually lasts from around November to April. The highest rainfall during the year usually comes from January to March when the Intertropical Convergence Zone (ITCZ) is furthest south and closest to Tarawa, and to a lesser extent when the South Pacific Convergence Zone (SPCZ) is strongest. The marked change in mean monthly rainfall towards the end of the year is common across Kiribati. Some islands have a slight secondary maximum in July when the ITCZ is most intense, although furthest away to the north. Being over 2000 km to the east, Kiritimati has a different seasonal cycle in rainfall. The wet season is from January to June, with the wettest months being March and April. Rainfall there is affected only by the ITCZ.

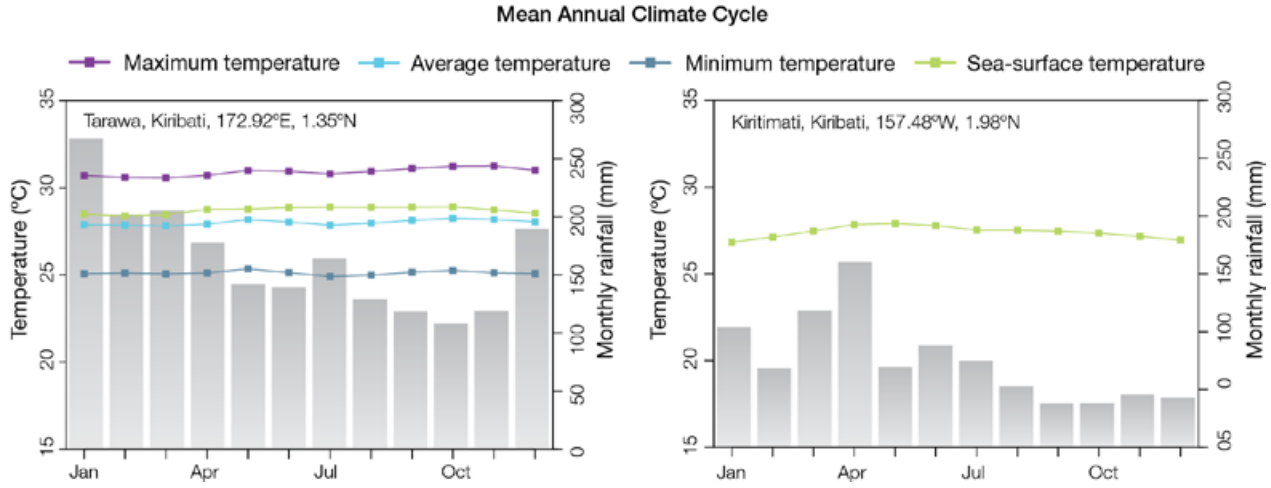

Figure 6.2: Mean annual cycle of rainfall (grey bars) and daily maximum, minimum and mean air temperatures at Tarawa (left), and for rainfall only at Kiritimati (right), as well as local sea-surface temperatures derived from the HadISST dataset (Volume 1, Table 2.3).

6.5 Climate Variability

The climate of Kiribati has high year-to-year variability (Figures 6.3 and 6.4), especially for rainfall. In the driest years, Tarawa received as little as 150 mm, while in the wettest years more than 4000 mm fell. Similar conditions exist in Kiritimati, with huge impacts on water quality and crop production. Most of this year-to-year variability is driven by the El Niño-Southern Oscillation (ENSO; Table 6.1). Many Kiribati islands lie within the equatorial waters that warm significantly during an El Niño event and cool during a La Niña event. As a result rainfall is much higher than normal during an El Niño and much lower during a La Niña. Maximum air temperatures tend to be higher than normal during El Niño years, driven by the warmer oceans surrounding the islands, while in the dry season minimum air temperatures in El Niño years are below normal. ENSO Modoki events (Volume1, Section 3.4.1) have similar impacts to canonical ENSO events, but the influence is only significant on rainfall in the wet season and on maximum air temperatures in both seasons. At Kiritimati, El Niño events also bring wetter conditions in both seasons and La Niña events bring drought.

Table 6.1: Correlation coefficients between indices of key patterns of climate variability and minimum and maximum temperatures (Tmin and Tmax) and rainfall at Tarawa. Only correlation coefficients that are statistically significant at the 95% level are shown.

Climate feature/index		Dry season (May-October)			Wet season (November-April)		
		Tmin	Tmax	Rain	Tmin	Tmax	Rain
ENSO	Niño3.4	-0.31	0.41	0.81		0.53	0.69
	Southern Oscillation Index	0.25	-0.39	-0.74		-0.58	-0.61
Interdecadal Pacific Oscillation Index							
ENSO Modoki Index			0.56			0.57	0.72
Number of years of data		63	60	73	61	61	75

Table 6.2: Correlation coefficients between indices of key patterns of climate variability and minimum and maximum temperatures (Tmin and Tmax) and rainfall at Kiritimati. Only correlation coefficients that are statistically significant at the 95% level are shown.

Climate feature/index		Dry season (May-October)	Wet season (November-April)
ENSO	Niño3.4	0.64	0.67
	Southern Oscillation Index	-0.48	-0.58
Interdecadal Pacific Oscillation Index			
ENSO Modoki Index			
Number of years of data		82	65

6.6 Observed Trends

6.6.1 Air Temperature

Warming trends of a similar magnitude are evident in both annual and seasonal mean air temperatures at Tarawa for 1950–2009. Annual and seasonal minimum air temperature trends are slightly stronger than the trends in maximum air temperatures (Figure 6.3 and Table 6.3).

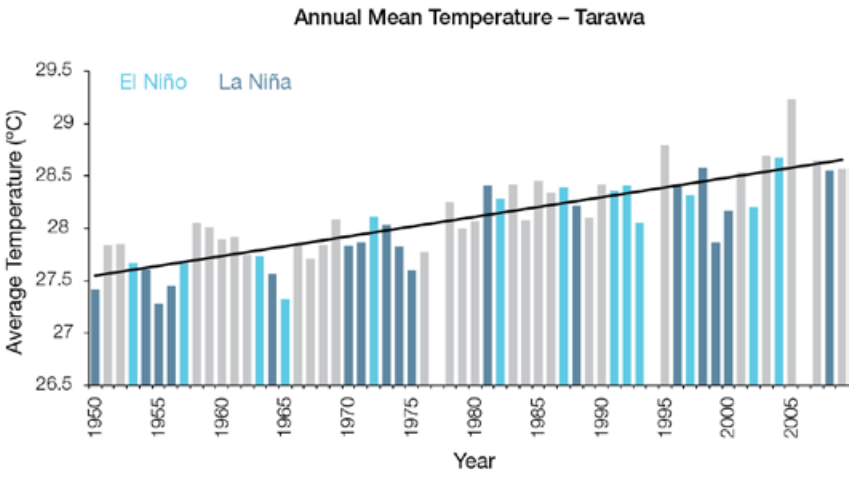

Figure 6.3: Annual mean air temperatures at Tarawa. Light blue, dark blue and grey bars denote El Niño, La Niña and neutral years respectively.

6.6.2 Rainfall

The Kiritimati positive annual rainfall trend for the period 1950–2009 is statistically significant. Annual and seasonal rainfall trends for Tarawa and the seasonal trends for Kiritimati over the same period are not statistically significant (Table 6.3 and Figure 6.4).

Table 6.3: Annual and seasonal trends in maximum, minimum and mean air temperature (Tmax, Tmin and Tmean) and rainfall at Tarawa and rainfall only at Kiritimati for the period 1950–2009. Asterisks indicate significance at the 95% level. Persistence is taken into account in the assessment of significance as in Power and Kociuba (in press). The statistical significance of the air temperature trends is not assessed.

	Tarawa Tmax (°C per 10 yrs)	Tarawa Tmin (°C per 10 yrs)	Tarawa Tmean (°C per 10 yrs)	Tarawa Rain (mm per 10 yrs)	Kiritimati Rain (mm per 10 yrs)
Annual	+0.18	+0.20	+0.19	+60	+115*
Wet season	+0.19	+0.20	+0.19	-15	+60
Dry season	+0.17	+0.20	+0.19	+53	+39

6.6.3 Extreme Events

Droughts, usually associated with La Niña events, are occasionally severe in Kiribati. For example, only 205 mm of rainfall was received over the 18–month period from July 1988 to December 1989, and over the six months from August 1998 to February 1999 total rainfall was only 95 mm. These figures are very much lower than the mean annual rainfall of approximately 2100 mm, and the dry season average of just over 900 mm between May and October.

The recent drought from April 2007 to early 2009 severely affected water supplies in the southern Gilbert Islands and Banaba Island. During this period ground water turned brackish and the leaves of most plants turned yellow. Copra production, the main income source for people in the outer islands, declined. During 1970/71, rainfall suppression was significant across the southern islands of the Gilbert Group. At Kenna on Abemama the drought was severe enough for hardy coconut trees to die.

Tropical cyclones rarely pass within 400 km of the Kiribati Islands. Between 1969/70 and 2009/10 three cyclones passed within 400 km of Arorae Island in western Kiribati and three cyclones within 400 km of Caroline Island in eastern Kiribati. Other important extremes include storm surge and extreme sea levels.

6.6.4 Sea-Surface Temperature

Water temperatures around the Gilbert Island group have risen gradually since the 1950s. Figure 6.7 shows the 1950–2000 sea-surface temperature changes (relative to a reference year of 1990) for the Gilbert Island group region from three different large-scale sea-surface temperature gridded datasets (HadSST2, ERSST and Kaplan Extended SST V2; Volume 1, Table 2.3). Since the 1970s the rate of warming has been approximately 0.15°C per decade. For the Line Island group, historical water temperatures have demonstrated considerable decadal variability. Since the 1970s the rate of warming has been approximately 0.1°C per decade. For the Phoenix Island group water temperatures have risen since the 1950s although considerable decadal variability is evident. Since the 1970s the rate of warming has been approximately 0.12°C per decade. At these regional scales, natural variability plays a large role in determining sea-surface temperatures making it difficult to identify long-term trends.

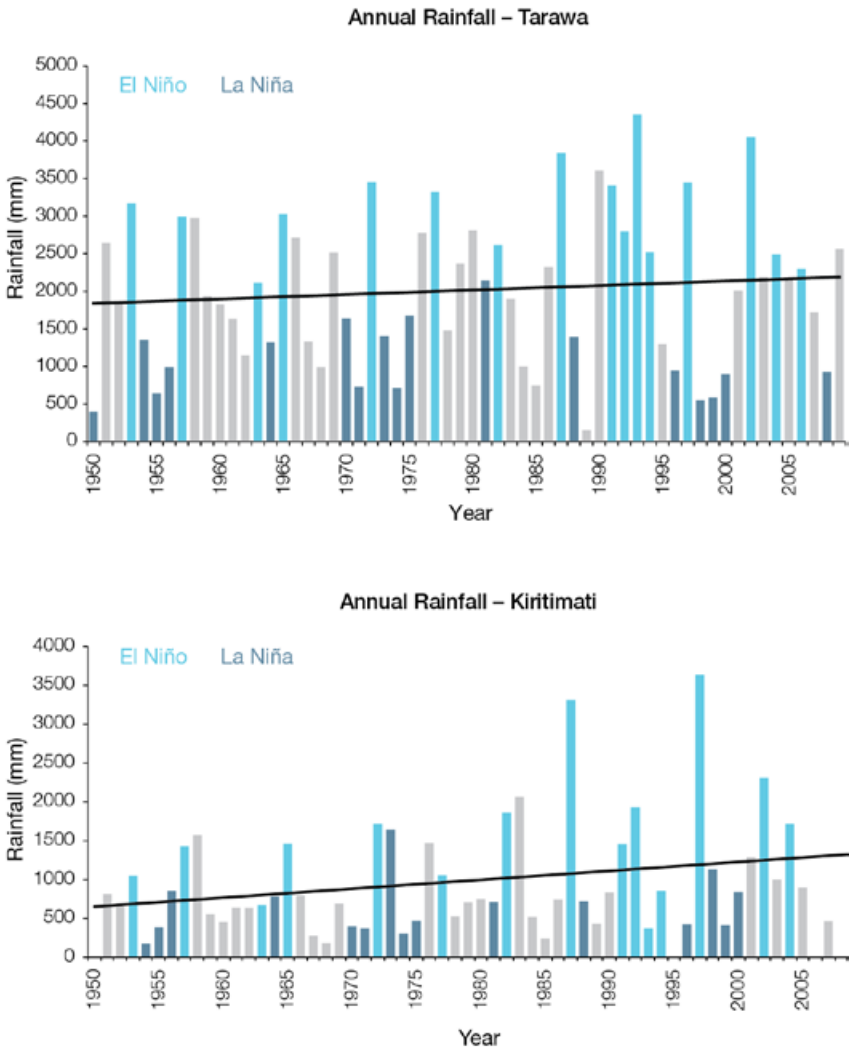

Figure 6.4: Annual rainfall for Tarawa (top) and Kiritimati (bottom). Light blue, dark blue and grey bars denote El Niño, La Niña and neutral years respectively.

6.6.5 Ocean Acidification

Based the large-scale distribution of coral reefs across the Pacific and the seawater chemistry, Guinotte et al. (2003) suggested that seawater aragonite saturation states above 4 were optimal for coral growth and for the development of healthy reef ecosystems, with values from 3.5 to 4 adequate for coral growth, and values between 3 and 3.5, marginal. Coral reef ecosystems were not found at seawater aragonite saturation states below 3 and these conditions were classified as extremely marginal for supporting coral growth.

In the Kiribati region, the aragonite saturation state has declined from about 4.5 in the late 18th century to an observed value of about 3.9 ± 0.1 by 2000.

6.6.6 Sea Level

Monthly averages of the historical tide gauge (since 1950), satellite (since 1993) and gridded sea-level (since 1950) data agree reasonably well after 1993 and indicate year-to-year variability in sea levels of about 26 cm (the estimated 5–95% range) after removal of the seasonal cycle (Figure 6.9). The sea-level rise near Kiribati measured by satellite altimeters (Figure 6.5) since 1993 ranges from 1–4 mm per year, compared with the global average of 3.2 ± 0.4 mm per year. The change is partly linked to a pattern related to climate variability from year to year and decade to decade (Figure 6.9).

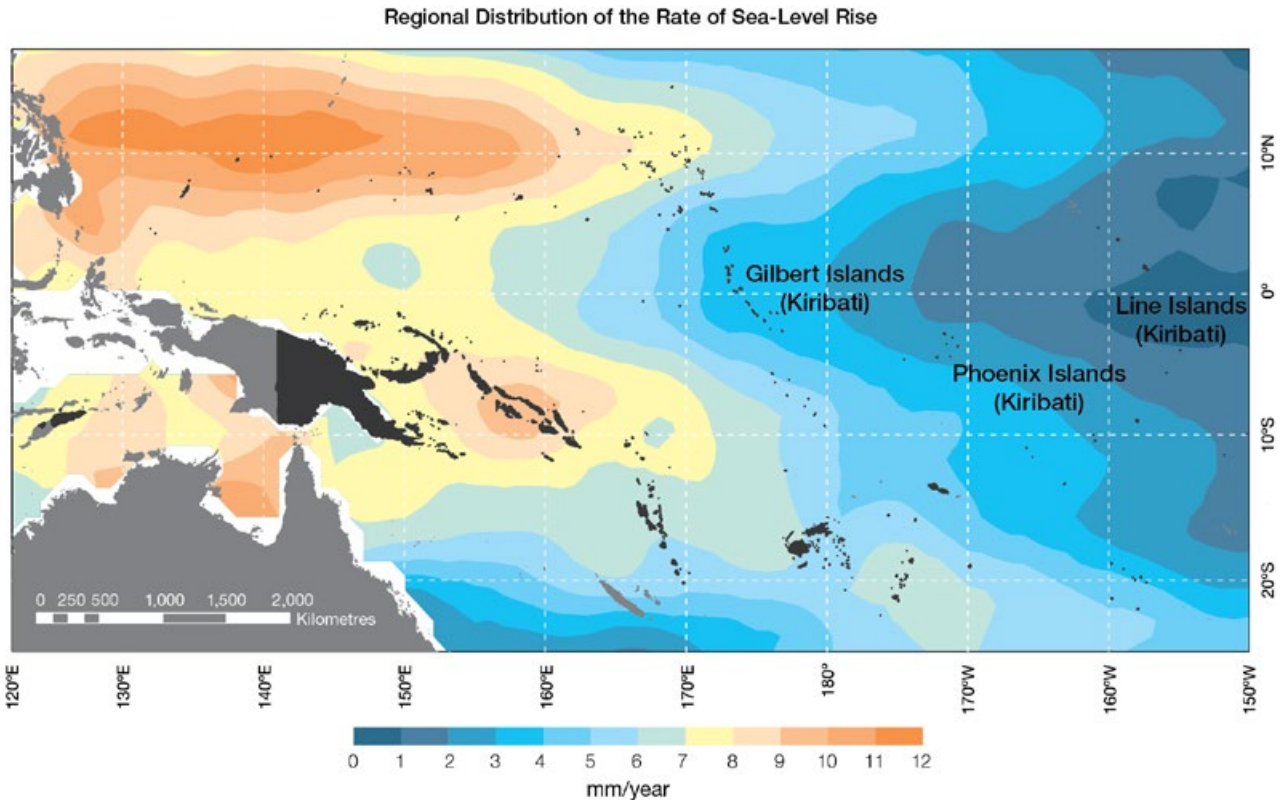

Figure 6.5: The regional distribution of the rate of sea-level rise measured by satellite altimeters from January 1993 to December 2010, with the location of Kiribati indicated. Further detail about the regional distribution of sea-level rise is provided in Volume 1, Section 3.6.3.2.

6.6.7 Extreme Sea-Level Events

The annual climatology of the highest daily sea levels has been evaluated from hourly measurements by tide gauges at Tarawa, Kiritimati and Kanton (Figure 6.6). Highest tides at Tarawa and Kanton are centred on the September equinox, with a secondary peak in February. Kiritimati Island spring tides tend to be greatest near the December solstice. Seasonal and short-term components show relatively little variation throughout the year at all locations, although there is a slight tendency towards higher short-term water levels from November to March at all locations. Sea levels are usually lower in La Niña years and higher during in El Niño years, particularly at Kiritimati. At Kiritimati all of the 10 highest recorded water level events are during El Niño conditions; at Kanton and Tarawa eight and six of the highest occur during El Niño, respectively. These events tend to cluster near the equinoxes at Tarawa and Kanton, and near the December solstice in Kiritimati, indicating that the combination of El Niño conditions and semi-annual tidal variation is the main driver of extreme sea level events, as observed at the respective tidal gauges in Kiribati.

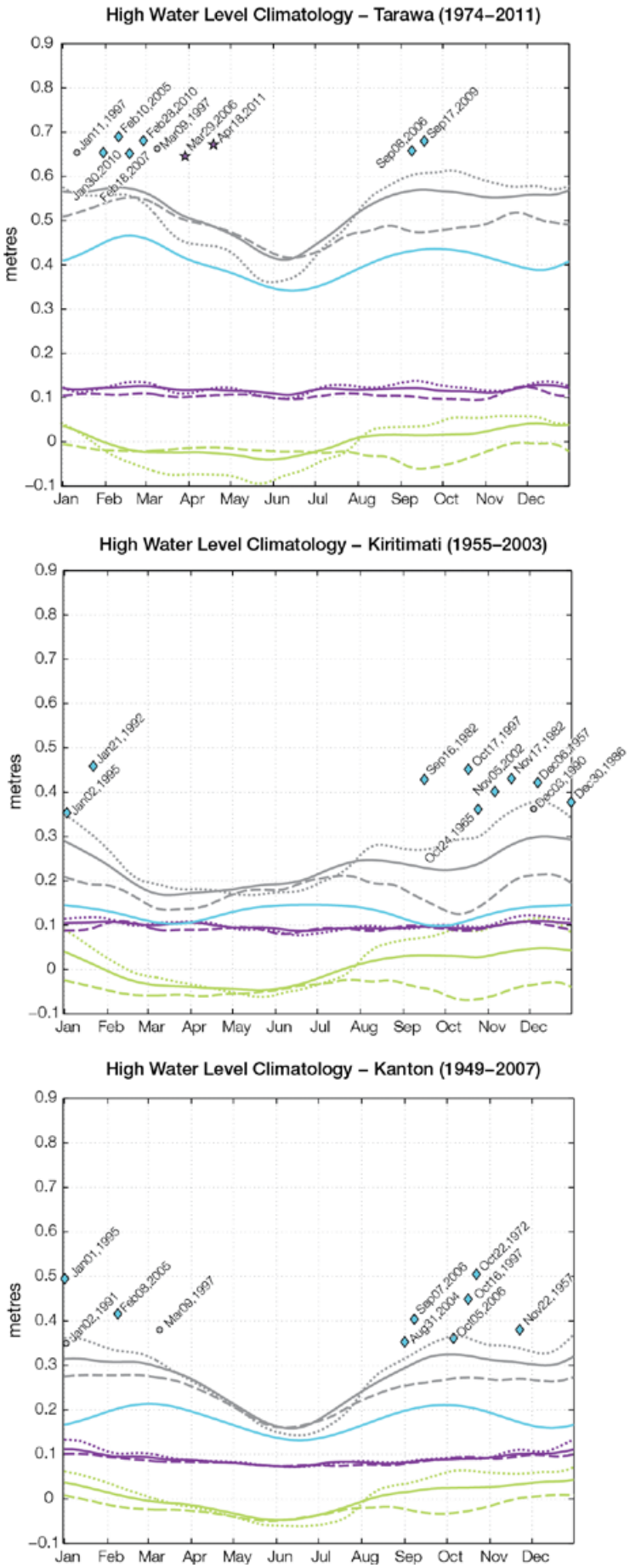

Figure 6.6: The annual cycle of high water relative to Mean Higher High Water (MHHW) due to tides, short-term fluctuations (most likely associated with storms) and seasonal variations for Tarawa (top), Kiritimati (middle) and Kanton (bottom). The tides and short-term fluctuations are respectively the 95% exceedence levels of the astronomical high tides relative to MHHW and short-term sea-level fluctuations. Components computed only for El Niño and La Niña years are shown by dotted and dashed lines, and grey lines are the sum of the tide, short-term and seasonal components. The 10 highest sea-level events in the record relative to MHHW are shown and coded to indicate the phase of ENSO at the time of the extreme event.

6.7 Climate Projections

Climate projections have been derived from up to 18 global climate models from the CMIP3 database, for up to three emissions scenarios (B1 (low), A1B (medium) and A2 (high)) and three 20-year periods (centred on 2030, 2055 and 2090, relative to 1990). These models were selected based on their ability to reproduce important features of the current climate (Volume 1, Section 5.2.3), so projections from each of the models are plausible representations of the future climate. This means there is not one single projected future for Kiribati, but rather a range of possible futures. The full range of these futures is discussed in the following sections.

These projections do not represent a value specific to any actual location, such as a town or city in Kiribati. Instead, they refer to an average change over the broad geographic region encompassing the islands of Kiribati and the surrounding ocean. Projections refer to the whole of Kiribati unless otherwise stated. In some instances, given that there are some differences between the climate of the Gilbert, Phoenix and Line Island groups (Section 6.4), projections are given separately for these three regions (Figure 1.1 shows the regional boundaries). Section 1.7 provides important information about interpreting climate model projections.

6.7.1 Temperature

Surface air temperature and sea-surface temperature are projected to continue to increase over the course of the 21st century. There is *very high* confidence in this direction of change because:

- Warming is physically consistent with rising greenhouse gas concentrations.
- All CMIP3 models agree on this direction of change.

Almost all of CMIP3 models simulate a slight increase (<1°C) in annual and seasonal mean temperature by 2030, however by 2090 under the A2 (high) emissions scenario temperature increases of greater than 3°C are simulated by the majority of models (Tables 6.4, 6.5 and 6.6). Given the close relationship between surface air temperature and sea-surface temperature, a similar (or slightly weaker) rate of warming is projected for the surface ocean (Figure 6.7). There is *moderate* confidence in this range and distribution of possible futures because:

- There is generally close agreement between modelled and observed temperature trends over the past 50 years in the vicinity of Kiribati, although observational records are limited (Figure 6.7).
- In simulations of the current climate, almost all CMIP3 models have a cold temperature bias in the vicinity of Kiribati (known as the 'cold tongue bias'; Volume 1, Section 5.2.2.1).

Interannual variability in surface air temperature and sea-surface temperature over Kiribati is strongly influenced by ENSO in the current climate (Section 6.5). As there is no consistency in projections of future ENSO activity (Volume 1, Section 6.4.1), it is not possible to determine whether interannual variability in temperature will change in the future. However, ENSO is expected to continue to be an important source of variability for Kiribati and the region.

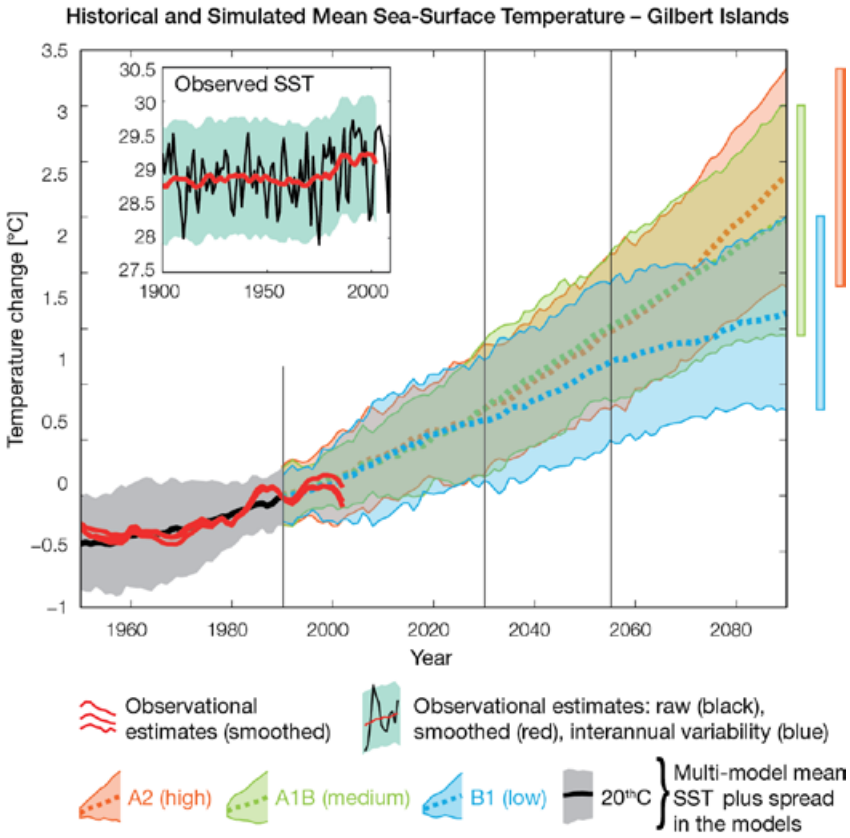

Figure 6.7: Historical climate (from 1950 onwards) and simulated historical and future climate for annual mean sea-surface temperatures (SST) in the region surrounding the Gilbert Islands for the CMIP3 models. Shading represents approximately 95% of the range of model projections (twice the inter-model standard deviation), while the solid lines represent the smoothed (20-year running average) multi-model mean temperature. Projections are calculated relative to the 1980–1999 period (which is why there is a decline in the inter-model standard deviation around 1990). Observational estimates in the main figure (red lines) are derived from the HadSST2, ERSST and Kaplan Extended SST V2 datasets (Volume 1, Section 2.2.2). Annual average (black) and 20-year running average (red) HadSST2 data is also shown inset. Projections for the Phoenix and Line Islands closely resemble those of the Gilbert Islands and are therefore not shown.

6.7.2 Rainfall

Wet season, dry season and annual average rainfall are projected to increase over the course of the 21st century. There is *high* confidence in this direction of change because:

- Physical arguments indicate that rainfall will increase in the equatorial Pacific in a warmer climate (IPCC, 2007; Volume 1, Section 6.4.3).
- Almost all of the CMIP3 models agree on this direction of change.

An increase (>5%) in annual and seasonal mean rainfall is projected by approximately half of the CMIP3 models by as early as 2030, with the majority of models simulating a large increase (>15%) by 2090 (Tables 6.4, 6.5 and 6.6). There is *low* confidence in this range and distribution of possible futures because:

- In simulations of the current climate, almost all CMIP3 models substantially underestimate present day rainfall in the vicinity of Kiribati, in association with the cold tongue bias (Volume 1, Section 5.2.1.2).
- The CMIP3 models are unable to resolve many of the physical processes involved in producing rainfall. As a consequence, they do not simulate rainfall as well as they simulate other variables such as temperature (Volume 1, Chapter 5).

Interannual variability in rainfall over Kiribati is strongly influenced by ENSO in the current climate (Section 6.5). As there is no consistency in projections of future ENSO activity (Volume 1, Section 6.4.1), it is not possible to determine whether interannual variability in rainfall will change in the future.

6.7.3 Extremes

Temperature

The intensity and frequency of days of extreme heat are projected to increase over the course of the 21st century. There is *very high* confidence in this direction of change because:

- An increase in the intensity and frequency of days of extreme heat is physically consistent with rising greenhouse gas concentrations.
- All CMIP3 models agree on the direction of change for both intensity and frequency.

For the Gilbert, Phoenix and Line Islands, the majority of CMIP3 models simulate an increase of approximately 1°C in the temperature experienced on the 1-in-20-year hot day by 2055 under the B1 (low) emissions scenario, with an increase of over 2.5°C simulated by the majority of models by 2090 under the A2 (high) emissions scenario (Tables 6.4, 6.5 and 6.6). There is *low* confidence in this range and distribution of possible futures because:

- In simulations of the current climate, the CMIP3 models tend to underestimate the intensity and frequency of days of extreme heat (Volume 1, Section 5.2.4).
- Smaller increases in the frequency of days of extreme heat are projected by the CCAM 60 km simulations.

Rainfall

The intensity and frequency of days of extreme rainfall are projected to increase over the course of the 21st century. There is *high* confidence in this direction of change because:

- An increase in the frequency and intensity of extreme rainfall is consistent with larger-scale projections, based on the physical argument that the atmosphere is able to hold more water vapour in a warmer climate (Allen and Ingram, 2002; IPCC, 2007). It is also consistent with physical arguments that rainfall will increase in the deep tropical Pacific in a warmer climate (IPCC, 2007; Volume 1, Section 6.4.3).
- Almost all of the CMIP3 models agree on this direction of change for both intensity and frequency.

For the Gilbert, Phoenix and Line Islands, the majority of CMIP3 models simulate an increase of at least 15 mm, 25 mm and 35 mm respectively in the amount of rain received on the 1-in-20-year wet day by 2055 under the B1 (low) emissions scenario, with an increase of at least 40 mm, 65 mm and 80 mm simulated by the majority of models by 2090 under the A2 (high) emissions scenario. The majority of models project that the current 1-in-20-year extreme rainfall event will occur, on average, 5, 10 and 11-12 times per 20-year period by 2055 under the B1 (low) emissions scenario in the Gilbert, Phoenix and Line Islands, respectively. By 2090 under the A2 (high) emissions scenario, the projected frequency increases are 7-8, 18-19 and 22-23 times per 20-year period, respectively. There is *low* confidence in this range and distribution of possible futures because:

- In simulations of the current climate, the CMIP3 models tend to underestimate the intensity and frequency of extreme rainfall (Volume 1, Section 5.2.4), particularly in the vicinity of Kiribati, in association with the cold tongue bias (Volume 1, Section 5.2.1.2).
- The CMIP3 models are unable to resolve many of the physical processes involved in producing extreme rainfall.

Drought

The incidence of drought is projected to decrease over the course of the 21st century. There is *moderate* confidence in this direction of change because:

- A decrease in drought is consistent with projections of increased rainfall (Section 6.7.2).
- The majority of models agree on this direction of change for all drought categories.

For the Gilbert, Phoenix and Line Islands, the majority of CMIP3 models project that mild drought will occur approximately seven to eight times every 20 years in 2030 under all emissions scenarios, decreasing to six to seven times by 2090. The frequency of moderate drought is projected to decrease from two to three times every 20 years in 2030 to once to twice in 2090 for all emissions scenarios, while the majority of CMIP3 models project that severe drought will occur approximately once to twice every 20 years in 2030, decreasing to once every 20 years by 2055 and 2090. There is *low* confidence in this range and distribution of possible futures because:

- There is only low confidence in the range of rainfall projections (Section 6.7.2), which directly influences projections of future drought conditions.

6.7.4 Ocean Acidification

The acidification of the ocean will continue to increase over the course of the 21st century. There is *very high* confidence in this projection as the rate of ocean acidification is driven primarily by the increasing oceanic uptake of carbon dioxide, in response to rising atmospheric carbon dioxide concentrations.

Projections from all analysed CMIP3 models indicate that the annual maximum aragonite saturation state will reach values below 3.5 by about 2045 in the Gilbert Islands, by about 2030 in the Line Islands, and 2055 in the Phoenix Islands. The aragonite saturation will continue to decline thereafter (Figure 6.8; Tables 6.4, 6.5 and 6.6). There is *moderate* confidence in this range and distribution of possible futures because the projections are based on climate models without an explicit representation of the carbon cycle and with relatively low resolution and known regional biases.

The impact of acidification change on the health of reef ecosystems is likely to be compounded by other stressors including coral bleaching, storm damage and fishing pressure.

6.7.5 Sea Level

Mean sea level is projected to continue to rise over the course of the 21st century. There is *very high* confidence in this direction of change because:

- Sea-level rise is a physically consistent response to increasing ocean and atmospheric temperatures, due to thermal expansion of the water and the melting of glaciers and ice caps.
- Projections arising from all CMIP3 models agree on this direction of change.

The CMIP3 models simulate a rise of between approximately 5–15 cm by 2030, with increases of 20–60 cm indicated by 2090 under the higher emissions scenarios (i.e. A2 (high), A1B (medium); Figure 6.9; Tables 6.4, 6.5 and 6.6).

There is *moderate* confidence in this range and distribution of possible futures because:

- There is significant uncertainty surrounding ice-sheet contributions to sea-level rise and a rise larger than projected above cannot be excluded (Meehl et al., 2007b). However, adequate understanding of the processes is currently too limited to provide a best estimate or an upper bound (IPCC, 2007).
- Globally, since the early 1990s, sea level has been rising near the upper end of the above projections. During the 21st century, some studies (using semi-empirical models) project faster rates of sea-level rise.

Interannual variability of sea level will lead to periods of lower and higher regional sea levels. In the past, this interannual variability has been about 23 cm (5–95% range, after removal of the seasonal signal; dashed lines in Figure 6.9 (a)) and it is likely that a similar range will continue through the 21st century. In addition, winds and waves associated with weather phenomena will continue to lead to extreme sea-level events.

In addition to the regional variations in sea level associated with ocean and mass changes, there are ongoing changes in relative sea level associated with changes in surface loading over the last glacial cycle (glacial isostatic adjustment) and local tectonic motions. The glacial isostatic motions are relatively small for the PCCSP region.

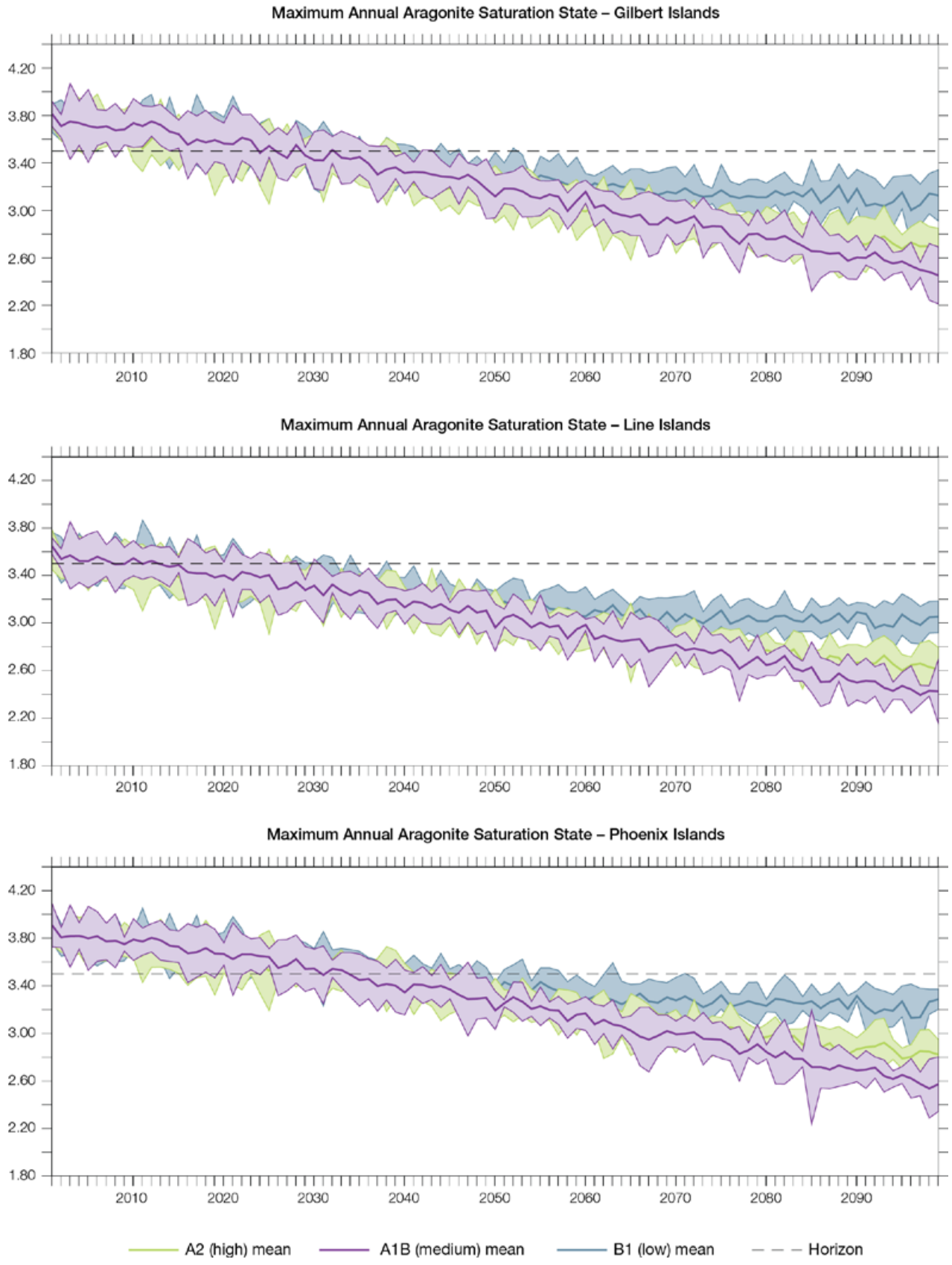

Figure 6.8: Multi-model projections, and their associated uncertainty (shaded area represents two standard deviations), of the maximum annual aragonite saturation state in the sea surface waters of Kiribati (Gilbert Islands, top; the Line Islands, middle; and the Phoenix Islands, bottom) under the different emissions scenarios. The dashed black line represents an aragonite saturation state of 3.5.

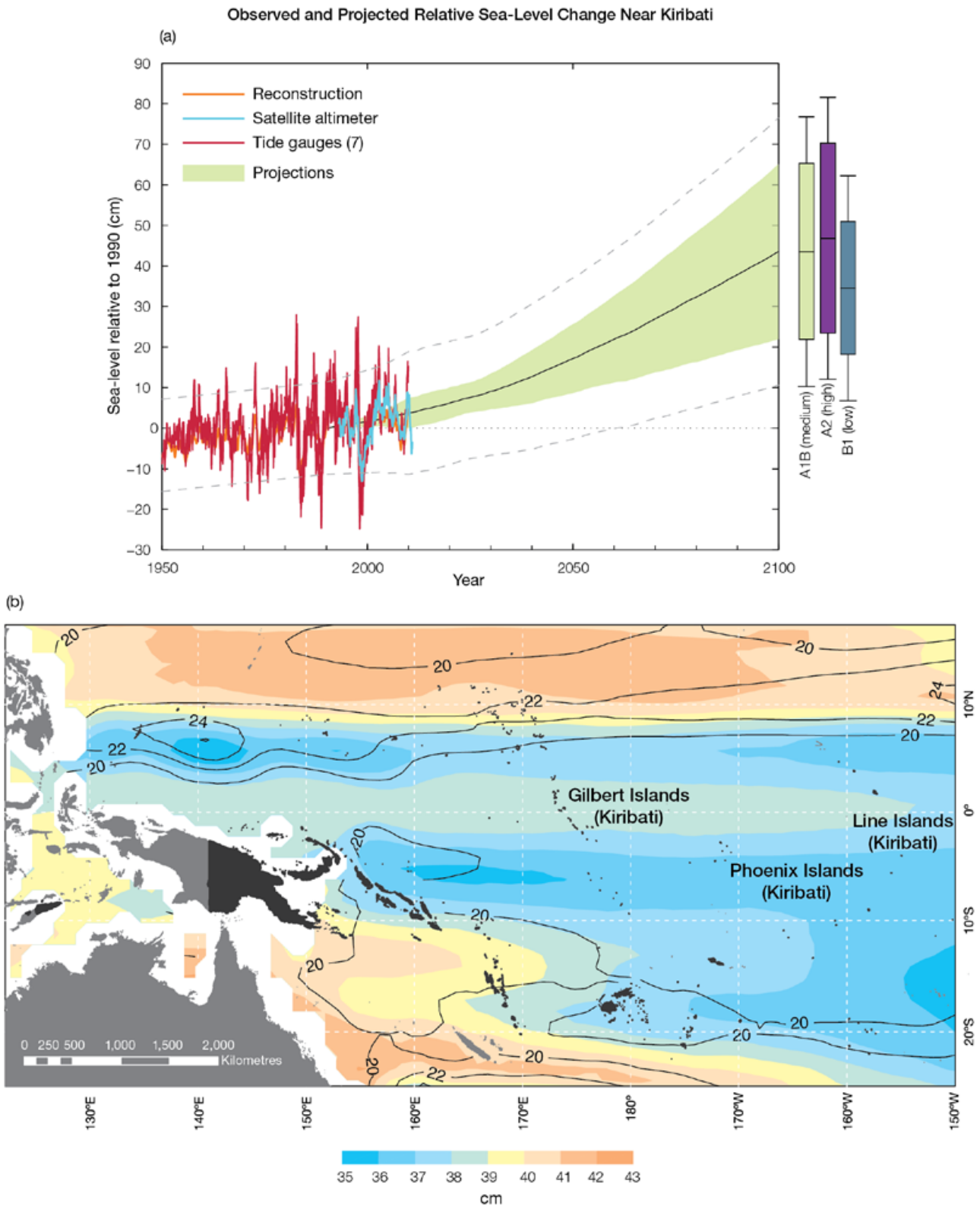

Figure 6.9: Observed and projected relative sea-level change near Kiribati. (a) The observed in situ relative sea-level records are indicated in red, with the satellite record (since 1993) in light blue. The gridded sea level at Kiribati (since 1950, from Church and White (in press)) is shown in orange. The projections for the A1B (medium) emissions scenario (5–95% uncertainty range) are shown by the green shaded region from 1990–2100. The range of projections for the B1 (low), A1B (medium) and A2 (high) emissions scenarios by 2100 are also shown by the bars on the right. The dashed lines are an estimate of interannual variability in sea level (5–95% range about the long-term trends) and indicate that individual monthly averages of sea level can be above or below longer-term averages. (b) The projections (in cm) for the A1B (medium) emissions scenario in the Kiribati region for the average over 2081–2100 relative to 1981–2000 are indicated by the shading, with the estimated uncertainty in the projections indicated by the contours (in cm).

6.7.6 Projections Summary

The projections presented in Section 6.7 are summarised in Table 6.4 (Gilbert Islands), Table 6.5 (Phoenix Islands) and Table 6.6 (Line Islands). For detailed information regarding the various uncertainties associated with the table values, refer to the preceding text in Sections 6.7 and 1.7, in addition to Chapters 5 and 6 in Volume 1. When interpreting the differences between projections for the B1 (low), A1B (medium) and A2 (high) emissions scenarios, it is also important to consider the emissions pathways associated with each scenario (Volume 1, Figure 4.1) and the fact that a slightly different subset of models was available for each (Volume 1, Appendix 1).

Table 6.4: Projected change in the annual and seasonal mean climate for the Gilbert Islands, under the B1 (low; blue), A1B (medium; green) and A2 (high; purple) emissions scenarios. Projections are given for three 20-year periods centred on 2030 (2020–2039), 2055 (2046–2065) and 2090 (2080–2099), relative to 1990 (1980–1999). Values represent the multi-model mean change ± twice the inter-model standard deviation (representing approximately 95% of the range of model projections), except for sea level where the estimated mean change and the 5–95% range are given (as they are derived directly from the Intergovernmental Panel on Climate Change Fourth Assessment Report values). The confidence (Section 1.7.2) associated with the range and distribution of the projections is also given (indicated by the standard deviation and multi-model mean, respectively). See Volume 1, Appendix 1 for a complete listing of CMIP3 models used to derive these projections.

Variable	Season	2030	2055	2090	Confidence
Surface air temperature (°C)	Annual	+0.7 ± 0.5 +0.8 ± 0.6 +0.8 ± 0.5	+1.3 ± 0.6 +1.6 ± 0.7 +1.6 ± 0.6	+1.7 ± 0.7 +2.6 ± 0.9 +3.0 ± 0.8	Moderate
Maximum temperature (°C)	1-in-20-year event	N/A	+1.1 ± 0.6 +1.5 ± 0.6 +1.5 ± 0.6	+1.4 ± 0.9 +2.3 ± 1.3 +2.8 ± 1.5	Low
Minimum temperature (°C)	1-in-20-year event	N/A	+1.4 ± 1.7 +1.7 ± 3.0 +1.5 ± 2.0	+1.8 ± 1.8 +2.6 ± 2.6 +2.8 ± 2.6	Low
Total rainfall (%)*	Annual	+14 ± 25 +12 ± 32 +7 ± 21	+20 ± 37 +23 ± 33 +23 ± 34	+25 ± 36 +37 ± 58 +42 ± 73	Low
Wet season rainfall (%)*	November-April	+10 ± 22 +10 ± 32 +5 ± 25	+14 ± 33 +18 ± 31 +18 ± 40	+19 ± 30 +30 ± 49 +30 ± 59	Low
Dry season rainfall (%)*	May-October	+18 ± 38 +15 ± 42 +12 ± 25	+28 ± 46 +30 ± 49 +31 ± 47	+34 ± 52 +50 ± 84 +57 ± 102	Low
Sea-surface temperature (°C)	Annual	+0.7 ± 0.5 +0.8 ± 0.6 +0.8 ± 0.6	+1.2 ± 0.7 +1.5 ± 0.7 +1.5 ± 0.7	+1.6 ± 0.9 +2.5 ± 1.0 +2.9 ± 1.0	Moderate
Aragonite saturation state (Ωar)	Annual maximum	+3.5 ± 0.2 +3.4 ± 0.2 +3.4 ± 0.2	+3.3 ± 0.1 +3.1 ± 0.2 +3.1 ± 0.1	+3.1 ± 0.2 +2.7 ± 0.2 +2.6 ± 0.2	Moderate
Mean sea level (cm)	Annual	+9 (4–13) +9 (5–14) +9 (5–14)	+17 (9–25) +20 (10–29) +19 (10–28)	+31 (16–45) +38 (19–57) +39 (20–58)	Moderate

*The MIROC3.2(medres) and MIROC3.2(hires) models were eliminated in calculating the rainfall projections, due to their inability to accurately simulate present-day activity of the South Pacific Convergence Zone and the Intertropical Convergence Zone (Volume 1, Section 5.5.1).

Table 6.5: Projected change in the annual and seasonal mean climate for the Phoenix Islands, under the B1 (low; blue), A1B (medium; green) and A2 (high; purple) emissions scenarios. Projections are given for three 20-year periods centred on 2030 (2020–2039), 2055 (2046–2065) and 2090 (2080–2099), relative to 1990 (1980–1999). Values represent the multi-model mean change ± twice the inter-model standard deviation (representing approximately 95% of the range of model projections), except for sea level where the estimated mean change and the 5–95% range are given (as they are derived directly from the Intergovernmental Panel on Climate Change Fourth Assessment Report values). The confidence (Section 1.7.2) associated with the range and distribution of the projections is also given (indicated by the standard deviation and multi-model mean, respectively). See Volume 1, Appendix 1 for a complete listing of CMIP3 models used to derive these projections.

Variable	Season	2030	2055	2090	Confidence
Surface air temperature (°C)	Annual	+0.7 ± 0.5 +0.9 ± 0.5 +0.8 ± 0.4	+1.3 ± 0.6 +1.6 ± 0.6 +1.6 ± 0.5	+1.7 ± 0.7 +2.6 ± 0.9 +3.0 ± 0.7	Moderate
Maximum temperature (°C)	1-in-20-year event	N/A	+1.0 ± 0.9 +1.5 ± 0.9 +1.5 ± 0.8	+1.4 ± 1.2 +2.2 ± 1.5 +2.8 ± 1.4	Low
Minimum temperature (°C)	1-in-20-year event	N/A	+1.3 ± 2.0 +1.6 ± 2.3 +1.5 ± 2.1	+2.0 ± 1.8 +2.5 ± 2.2 +2.7 ± 2.3	Low
Total rainfall (%)*	Annual	+14 ± 34 +11 ± 43 +8 ± 21	+18 ± 38 +21 ± 42 +22 ± 41	+22 ± 45 +33 ± 67 +41 ± 76	Low
Wet season rainfall (%)*	November-April	+12 ± 37 +12 ± 64 +6 ± 31	+14 ± 47 +20 ± 49 +20 ± 54	+18 ± 39 +30 ± 74 +36 ± 71	Low
Dry season rainfall (%)*	May-October	+15 ± 35 +13 ± 40 +12 ± 31	+25 ± 48 +28 ± 74 +29 ± 73	+30 ± 72 +42 ± 105 +53 ± 120	Low
Sea-surface temperature (°C)	Annual	+0.7 ± 0.5 +0.8 ± 0.5 +0.8 ± 0.5	+1.2 ± 0.6 +1.5 ± 0.5 +1.5 ± 0.6	+1.6 ± 0.7 +2.5 ± 0.9 +2.8 ± 0.8	Moderate
Aragonite saturation state (Ωar)	Annual maximum	+3.5 ± 0.2 +3.4 ± 0.2 +3.4 ± 0.2	+3.3 ± 0.1 +3.1 ± 0.2 +3.1 ± 0.1	+3.1 ± 0.2 +2.7 ± 0.2 +2.6 ± 0.2	Moderate
Mean sea level (cm)	Annual	+9 (4–13) +9 (5–14) +9 (5–14)	+17 (9–25) +20 (10–29) +19 (10–28)	+31 (16–45) +38 (19–57) +39 (20–58)	Moderate

*The MIROC3.2 (medres) and MIROC3.2(hires) models were eliminated in calculating the rainfall projections, due to their inability to accurately simulate present-day activity of the South Pacific Convergence Zone and the Intertropical Convergence Zone (Volume 1, Section 5.5.1).

Table 6.6: Projected change in the annual and seasonal mean climate for the Line Islands, under the B1 (low; blue), A1B (medium; green) and A2 (high; purple) emissions scenarios. Projections are given for three 20-year periods centred on 2030 (2020–2039), 2055 (2046–2065) and 2090 (2080–2099), relative to 1990 (1980–1999). Values represent the multi-model mean change ± twice the inter-model standard deviation (representing approximately 95% of the range of model projections), except for sea level where the estimated mean change and the 5–95% range are given (as they are derived directly from the Intergovernmental Panel on Climate Change Fourth Assessment Report values). The confidence (Section 1.7.2) associated with the range and distribution of the projections is also given (indicated by the standard deviation and multi-model mean, respectively). See Volume 1, Appendix 1 for a complete listing of CMIP3 models used to derive these projections.

Variable	Season	2030	2055	2090	Confidence
Surface air temperature (°C)	Annual	+0.7 ± 0.5 +0.8 ± 0.5 +0.8 ± 0.4	+1.2 ± 0.6 +1.6 ± 0.6 +1.5 ± 0.5	+1.7 ± 0.7 +2.5 ± 0.9 +2.9 ± 0.6	Moderate
Maximum temperature (°C)	1-in-20-year event	N/A	+1.1 ± 0.8 +1.5 ± 0.9 +1.6 ± 0.9	+1.5 ± 1.1 +2.2 ± 1.5 +2.9 ± 1.3	Low
Minimum temperature (°C)	1-in-20-year event	N/A	+1.3 ± 2.0 +1.7 ± 2.2 +1.5 ± 2.1	+1.9 ± 2.0 +2.5 ± 2.6 +2.6 ± 2.2	Low
Total rainfall (%)*	Annual	+9 ± 22 +9 ± 30 +6 ± 19	+11 ± 22 +14 ± 38 +13 ± 40	+14 ± 33 +19 ± 49 +23 ± 53	Low
Wet season rainfall (%)*	November-April	+9 ± 22 +9 ± 35 +6 ± 23	+9 ± 25 +13 ± 38 +13 ± 41	+13 ± 30 +17 ± 45 +19 ± 41	Low
Dry season rainfall (%)*	May-October	+8 ± 23 +8 ± 26 +6 ± 18	+12 ± 22 +15 ± 38 +13 ± 41	+16 ± 35 +21 ± 53 +26 ± 68	Low
Sea-surface temperature (°C)	Annual	+07 ± 0.4 +0.8 ± 0.5 +0.7 ± 0.4	+1.1 ± 0.5 +1.5 ± 0.6 +1.4 ± 0.6	+1.6 ± 0.7 +2.4 ± 0.9 +2.7 ± 0.7	Moderate
Aragonite saturation state (Ωar)	Annual maximum	+3.5 ± 0.2 +3.4 ± 0.2 +3.4 ± 0.2	+3.3 ± 0.1 +3.1 ± 0.2 +3.1 ± 0.1	+3.1 ± 0.2 +2.7 ± 0.2 +2.6 ± 0.2	Moderate
Mean sea level (cm)	Annual	+9 (4–13) +9 (5–14) +9 (5–14)	+17 (9–25) +20 (10–29) +19 (10–28)	+31 (16–45) +38 (19–57) +39 (20–58)	Moderate

*The MIROC3.2 (medres) and MIROC3.2(hires) models were eliminated in calculating the rainfall projections, due to their inability to accurately simulate present-day activity of the South Pacific Convergence Zone and the Intertropical Convergence Zone (Volume 1, Section 5.5.1).

Islet, Majuro Atoll

Chapter 7
Marshall Islands

The contributions of Reginald White and Lee Z. Jacklick from the Marshall Islands National Weather Service Office and Ned Lobwij from the Office of Environmental Planning and Policy Coordination are gratefully acknowledged

Introduction

This chapter provides a brief description of the Marshall Islands, its past and present climate as well as projections for the future. The climate observation network and the availability of atmospheric and oceanic data records are outlined. The annual mean climate, seasonal cycles and the influences of large-scale climate features such as the Intertropical Convergence Zone and patterns of climate variability (e.g. the El Niño-Southern Oscillation) are analysed and discussed. Observed trends and analysis of air temperature, rainfall, extreme events, sea-surface temperature, ocean acidification, mean and extreme sea levels are presented. Projections for air and sea-surface temperature, rainfall, sea level, ocean acidification and extreme events for the 21st century are provided. These projections are presented along with confidence levels based on expert judgement by Pacific Climate Change Science Program (PCCSP) scientists. The chapter concludes with summary tables of projections for the northern and southern Marshall Islands (Tables 7.4 and 7.5). Important background information including an explanation of methods and models is provided in Chapter 1. For definitions of other terms refer to the Glossary.

7.1 Climate Summary

7.1.1 Current Climate

- Air temperatures show very little seasonal variation, with the mean maximum temperatures in the warmest months less than 2ºF (1ºC) warmer than those in the coldest months.
- The Marshall Islands experiences a wet season from May to November and a dry season from December to April, but rainfall varies greatly from north to south.
- The Intertropical Convergence Zone brings rainfall to the Marshall Islands throughout the year. It is strongest and furthest north and closest to the Marshall Islands during the wet season, and it is weakest and furthest away from the islands to the south in the dry season.
- The main influence on year-to-year natural climate variability in the Marshall Islands is the El Niño-Southern Oscillation.
- Warming trends are evident in both annual and seasonal mean air temperatures at Majuro for the period 1956–2009 and at Kwajalein for the period 1960–2009.
- The Majuro (1954–2009) and Kwajalein (1950–2009) negative annual and dry season rainfall trends are statistically significant. Wet season rainfall trends over the respective periods for both sites are not significant.
- The sea-level rise, measured by satellite altimeters since 1993, is about 0.3 inches (7 mm) per year.
- Droughts and storm waves are the main extreme events that impact the Marshall Islands. Tropical cyclones (typhoons) usually form between September and November but are often weak when they pass through the Marshall Islands' region.

7.1.2 Future Climate

Over the course of the 21st century:

- Surface air temperature and sea-surface temperature are projected to continue to increase (*very high* confidence).
- Annual and seasonal mean rainfall is projected to increase (*high* confidence).
- The intensity and frequency of days of extreme heat are projected to increase (*very high* confidence).
- The intensity and frequency of days of extreme rainfall are projected to increase (*high* confidence).
- The incidence of drought is projected to decrease (*moderate* confidence).
- Tropical cyclone numbers are projected to decline in the tropical North Pacific Ocean basin (0–15ºN, 130ºE –180ºE) (*moderate* confidence).
- Ocean acidification is projected to continue (*very high* confidence).
- Mean sea-level rise is projected to continue (*very high* confidence).

7.2 Country Description

Located near the equator in the central North Pacific Ocean, the Marshall Islands lie between 4°N–14°N and 160°E–173°E. The country consists of 29 low-lying atolls and five low-elevation islands, with a total land area of 70 square miles (181 km^2). This is in contrast to the 700 000 square miles of ocean (1.81 million km^2) which forms the country's Exclusive Economic Zone.

The atolls and islands lie in two parallel chains: Ratak (Sunrise) to the east; and Ralik (Sunset), to the west (Marshall Islands' First National Communication under the UNFCCC, 2000; Marshall Islands' Pacific Adaptation to Climate Change, 2010). The capital is Majuro in the Ratak island chain. The 2010 estimated population was 54 439 (Marshall Islands Country Statistics, SOPAC, 2010).

Key economic sectors are services, agriculture and fisheries, and industry. The main industries are copra, tuna processing, tourism and handicrafts (Office of Environmental Policy Coordination, 2005).

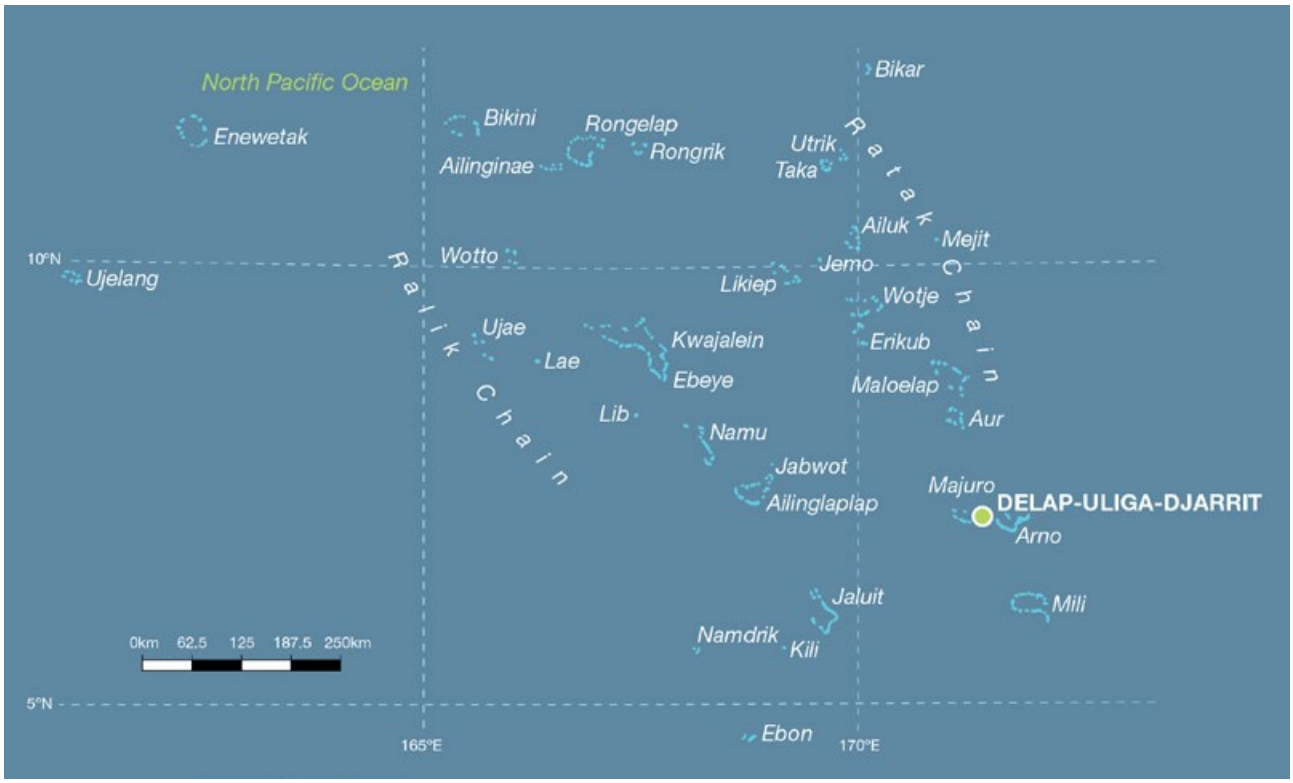

Figure 7.1: Marshall Islands

7.3 Data Availability

There are currently ten operational meteorological stations in the Marshall Islands. Multiple observations within a 24-hour period are taken at eight of these stations (Majuro, Utirik, Ailinglaplap, Jaluit, Wotje, Mili, Amata Kabua International Airport and Kwajalein) and a single daily observation is taken at Laura and Arno. The primary stations are located at Majuro (the capital) on the southern end of the Ratak chain and at Kwajalein near the centre of the Ralik chain (Figure 7.1). Observations began at Majuro in 1951 and at Kwajalein in 1949.

Records from 1951 for rainfall and from 1956 for temperature at Majuro have been used, as well as records from 1950 for rainfall and from 1960 for air temperature at Kwajalein. Both records are homogeneous and more than 99% complete.

There are a number of sea-level records available for the Marshall Islands. The best appear to be Enewetok (1951–1972), Kwajalein (1946–present), Majuro-B (1968–2001) and Majuro-C (1993–2009). A global positioning system instrument to estimate vertical land motion was deployed in the Marshall Islands in 2007 and will provide valuable direct estimates of local vertical land motion in future years. Both satellite (from 1993) and in situ sea-level data (1950–2009; termed reconstructed sea level; Volume 1, Section 2.2.2.2) are available on a global 1° x 1° grid.

Long-term locally-monitored sea-surface temperature data are unavailable for the Marshall Islands, so large-scale gridded sea-surface temperature datasets have been used (HadISST, HadSST2, ERSST and Kaplan Extended SST V2; Volume 1, Table 2.3).

Weather balloon launch, Marshall Islands National Weather Service

7.4 Seasonal Cycles

Temperatures at both Majuro and Kwajalein are constant year-round because the amount of solar radiation does not vary significantly throughout the year (Figure 7.2). The mean maximum air temperatures in the warmest months are less than 2ºF (1ºC) warmer than those in the coldest months. The sea-surface temperature surrounding the small islands influences the seasonal cycles in air temperature.

The rainfall of the Marshall Islands varies greatly from north to south. The atolls at 10ºN and further north receive less than 50 inches (1250 mm) of rain annually and are very dry in the dry season. Atolls 7ºN and equatorward receive more than 100 inches (2500 mm) of rain annually. Both Majuro and Kwajalein have a dry season from around December to April and a wet season from May to November. The difference between the seasons is more marked at Kwajalein where the driest months (January–March) receive about 4 inches (100 mm) on average and the wettest months (September–October) receive on average around 12 inches (300 mm).

The Intertropical Convergence Zone (ITCZ) brings rainfall to the Marshall Islands throughout the year. The ITCZ is strongest and furthest north, and therefore closest to the Marshall Islands, during the wet season, and it is weakest and furthest away from the islands to the south in the dry season. The West Pacific Monsoon (WPM) affects the Marshall Islands in some years. Rainfall during a given year can be influenced by trade wind troughs, the Madden Julian-Oscillation (Volume 1, Section 2.4.4), the tropical upper tropospheric trough and the North Pacific sub-tropical high.

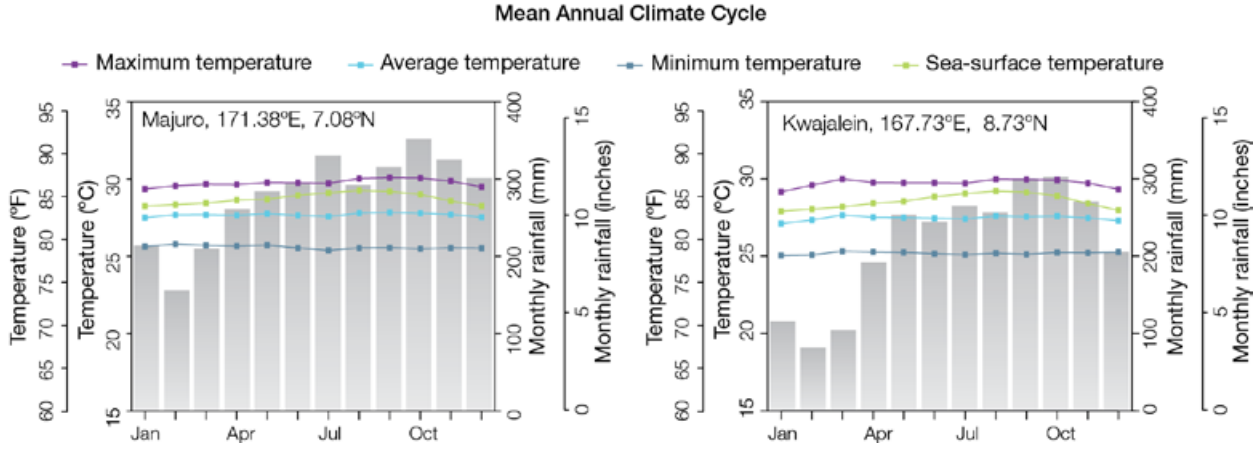

Figure 7.2: Mean annual cycle of rainfall (grey bars) and daily maximum, minimum and mean air temperatures at Majuro (left) and Kwajalein (right), and local sea-surface temperatures derived from the HadISST dataset (Volume 1, Table 2.3).

7.5 Climate Variability

The main influence on the year-to-year natural climate variability in the Marshall Islands is the El Niño-Southern Oscillation (ENSO), as seen in the correlation coefficients between climate indices and rainfall and air temperatures at Majuro (Table 7.1) and Kwajalein (Table 7.2). Rainfall variability is high at both sites, with the wettest years bringing up to twice as much rain as the driest years. The influence of ENSO in producing this variability can be clearly seen (Figure 7.4) with La Niña events being significantly wetter than El Niño years. At both sites wet season maximum and minimum air temperatures are influenced by ENSO. El Niño events tend to bring above average wet season air temperatures. During the dry season the influence of El Niño is to bring warmer than average minimum air temperatures as well as below average rainfall. The reason for these changes is that El Niño results in the ITCZ moving to the south of the Marshall Islands which leads to lower rainfall when El Niño is firmly established. There is also the competing influence of the WPM in the wet season which is able to reach the Marshall Islands in El Niño years when easterly trade winds are weak. ENSO Modoki events (Volume 1, Section 3.4.1) have similar influences but only on temperature.

Table 7.1: Correlation coefficients between indices of key large-scale patterns of climate variability and minimum and maximum temperatures (Tmin and Tmax) and rainfall at Majuro. Only correlations statistically different from zero (95% level) are shown.

Climate feature/index		Wet season (May-October)			Dry season (November-April)		
		Tmin	Tmax	Rain	Tmin	Tmax	Rain
ENSO	Niño3.4	0.31	0.59		0.41		-0.49
	Southern Oscillation Index	-0.27	-0.51		-0.30		0.48
Interdecadal Pacific Oscillation Index							
ENSO Modoki Index			0.44		0.37		
Number of years of data		54	54	56	54	54	56

Table 7.2: Correlation coefficients between indices of key large-scale patterns of climate variability and minimum and maximum temperatures (Tmin and Tmax) and rainfall at Kwajalein. Only correlations statistically different from zero (95% level) are shown.

Climate feature/index		Wet season (May-October)			Dry season (November-April)		
		Tmin	Tmax	Rain	Tmin	Tmax	Rain
ENSO	Niño3.4	0.36	0.48			0.37	-0.37
	Southern Oscillation Index	-0.32	-0.47			-0.35	0.33
Interdecadal Pacific Oscillation Index							
ENSO Modoki Index			0.53			0.46	
Number of years of data		50	50	65	49	49	65

7.6 Observed Trends

7.6.1 Air Temperature

Warming trends of a similar magnitude are evident in both annual and seasonal mean air temperatures at Majuro (1956–2009) and Kwajalein (1960–2009). Annual and seasonal minimum air temperature trends are stronger than those for maximum air temperatures at Majuro (Figure 7.3 and Table 7.3).

7.6.2 Rainfall

The Majuro (1954–2009) and Kwajalein (1950–2009) negative annual and dry season rainfall trends are statistically significant. Wet season rainfall trends over the respective periods for both sites are not significant (Table 7.3 and Figure 7.4).

7.6.3 Extreme Events

Droughts and storm waves are the main extreme events that impact the Marshall Islands. Droughts generally occur in the first four to six months of the year following an El Niño. During severe El Niño events, rainfall can be suppressed by as much as 80%. The dry season begins earlier and ends much later than normal. ENSO events also modulate sea level, and this modulation can significantly hamper ground water extraction.

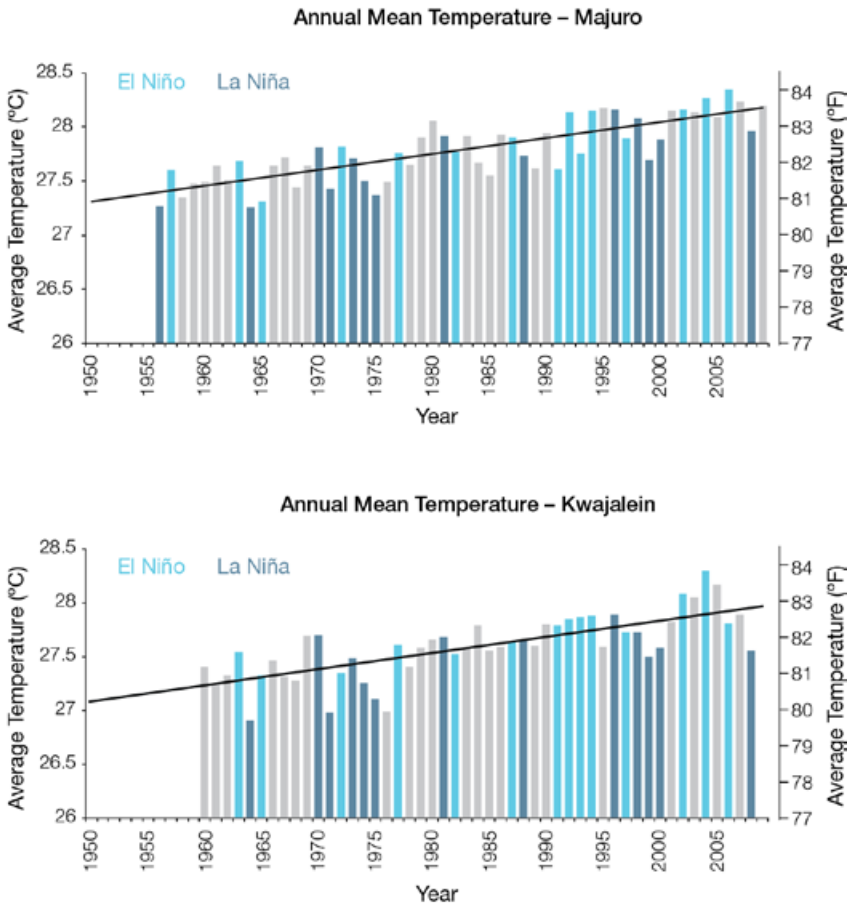

Figure 7.3: Annual mean air temperature at Majuro (top) and Kwajalein (bottom). Light blue, dark blue and grey bars denote El Niño, La Niña and neutral years respectively.

Table 7.3: Annual and seasonal trends in maximum, minimum and mean air temperature (Tmax, Tmin and Tmean) and rainfall at Majuro and Kwajalein for the period 1950–2009[a]. Asterisks indicate significance at the 95% level. Persistence is taken into account in the assessment of significance as in Power and Kociuba (in press). The statistical significance of the air temperature trends is not assessed.

	Majuro Tmax °F per 10 yrs (°C per 10 yrs)	Majuro Tmin °F per 10 yrs (°C per 10 yrs)	Majuro Tmean °F per 10 yrs (°C per 10 yrs)	Majuro Rain inches per 10 yrs (mm per 10 yrs)	Kwajalein Tmax °F per 10 yrs (°C per 10 yrs)	Kwajalein Tmin °F per 10 yrs (°C per 10 yrs)	Kwajalein Tmean °F per 10 yrs (°C per 10 yrs)	Kwajalein Rain inches per 10 yrs (mm per 10 yrs)
Annual	+0.21 (+0.12)	+0.31 (+0.17)	+0.26 (+0.15)	-4.18* (-106)	+0.29 (+0.16)	+0.25 (+0.14)	+0.27 (+0.15)	-3.31* (-84)
Wet season	+0.20 (+0.11)	+0.35 (+0.20)	+0.28 (+0.16)	-2.79 (-71)	+0.33 (+0.18)	+0.25 (+0.14)	+0.29 (+0.16)	-1.86 (-47)
Dry season	+0.23 (+0.13)	+0.27 (+0.15)	+0.25 (+0.14)	-1.48* (-38)	+0.24 (+0.13)	+0.26 (+0.14)	+0.25 (+0.14)	-1.47* (-37)

[a] Majuro rainfall from 1954 and air temperature from 1956, Kwajalein air temperature from 1960.

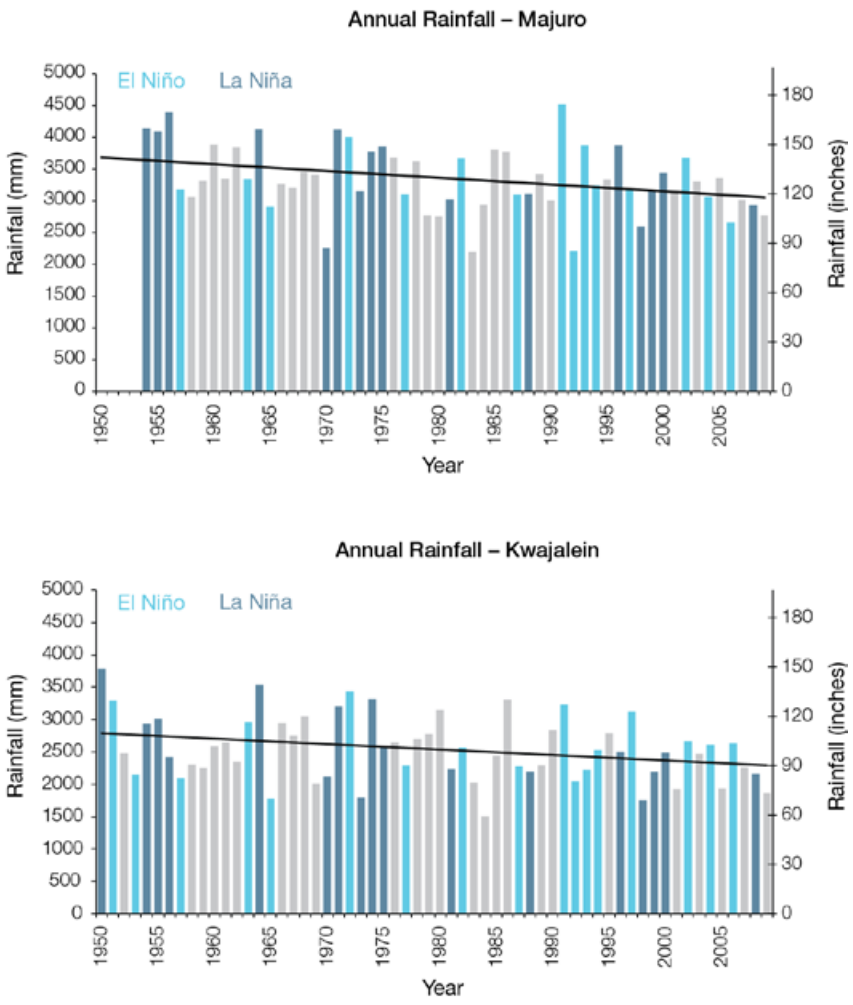

Figure 7.4: Annual rainfall at Majuro (top) and Kwajalein (bottom). Light blue, dark blue and grey bars denote El Niño, La Niña and neutral years respectively.

In December 2008 the islands were impacted several times in quick succession by long-period swell waves generated by an extra-tropical storm. These extreme waves, combined with high tides, caused widespread flooding in Majuro and other urban centres, which are located about a metre above sea level. A state of emergency was declared on Christmas morning.

Tropical cyclones usually form between September and November and are often weak when they pass through the region. During El Niño years, however, sea-surface temperatures increase to the east of the Marshall Islands. This favours more intense tropical cyclones in the Marshall Islands region.

7.6.4 Sea-Surface Temperature

Historical changes in sea-surface temperature around the Marshall Islands show considerable decadal variability. Figure 7.7 shows the 1950–2000 sea-surface temperature changes (relative to a reference year of 1990) from three different large-scale sea-surface temperature gridded datasets (HadSST2, ERSST and Kaplan Extended SST V2; Volume 1, Table 2.3). Water temperatures remained relatively constant from the 1950s to the late 1980s around the southern islands, while they declined slightly around the northern islands.

Since the 1970 both regions have shown warming trends (approximately 0.07°C per decade in the north and approximately 0.09°C per decade in the south). At these regional scales, natural variability may play a large role in the sea-surface temperature trends making it difficult to identify any long-term trends.

7.6.5 Ocean Acidification

Based the large-scale distribution of coral reefs across the Pacific and the seawater chemistry, Guinotte et al. (2003) suggested that seawater aragonite saturation states above 4 were optimal for coral growth and for the development of healthy reef ecosystems, with values from 3.5 to 4 adequate for coral growth, and values between 3 and 3.5, marginal. Coral reef ecosystems were not found at seawater aragonite saturation states below 3 and these conditions were classified as extremely marginal for supporting coral growth.

In the Marshall Islands region, the aragonite saturation state has declined from about 4.5 in the late 18th century to an observed value of about 3.9 ± 0.1 by 2000.

7.6.6 Sea Level

Monthly averages of the historical tide gauge, satellite (since 1993) and gridded sea-level (since 1950) data agree well after 1993 and indicate interannual variability in sea levels of about 20 cm (estimated 5–95% range) after removal of the seasonal cycle (Figure 7.9). The sea-level rise near the Marshall Islands measured by satellite altimeters (Figure 7.5) since 1993 is about 0.3 inches (7 mm) per year, more than the global average of 0.125 ± 0.015 inches (3.2 ± 0.4 mm) per year. This rise is partly linked to a pattern related to climate variability from year to year and decade to decade (Figure 7.9).

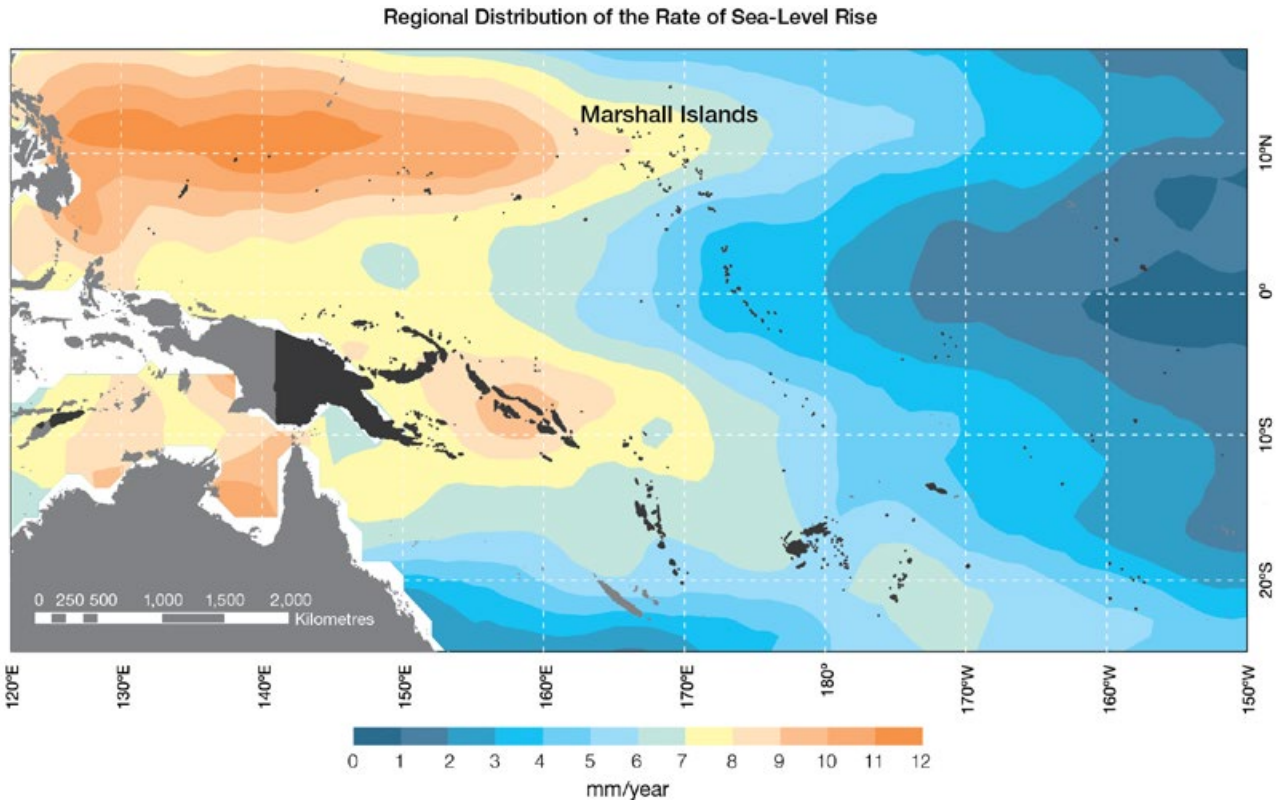

Figure 7.5: The regional distribution of the rate of sea-level rise measured by satellite altimeters from January 1993 to December 2010, with the location of the Marshall Islands indicated. Further information on regional distribution of sea-level rise is provided in Volume 1, Section 3.6.3.2.

7.6.7 Extreme Sea-Level Events

The annual climatology of the highest daily sea levels has been evaluated from hourly measurements by tide gauges at Majuro and Kwajalein (Figure 7.6). Highest tides at both locations tend to occur around the equinoxes, with lower high tides tending to occur towards the solstices. This interannual (spring) tidal height variability is more pronounced at Majuro than at Kwajalein. Seasonal and short-term components show relatively little variation throughout the year at both locations. Sea levels are usually lower in El Niños and higher in La Niñas. The top 10 recorded water levels at both locations cluster around the equinoxial tidal peaks, especially at Majuro. Of these, six occur during La Niña conditions and only one during El Niño conditions at Majuro. At Kwajalein, three of the top 10 water levels occur during La Niña and none during El Niño. At both locations, the relatively strong annual variability in tidal heights recorded by the tide gauges indicates this is a significant component of observed high water level events.

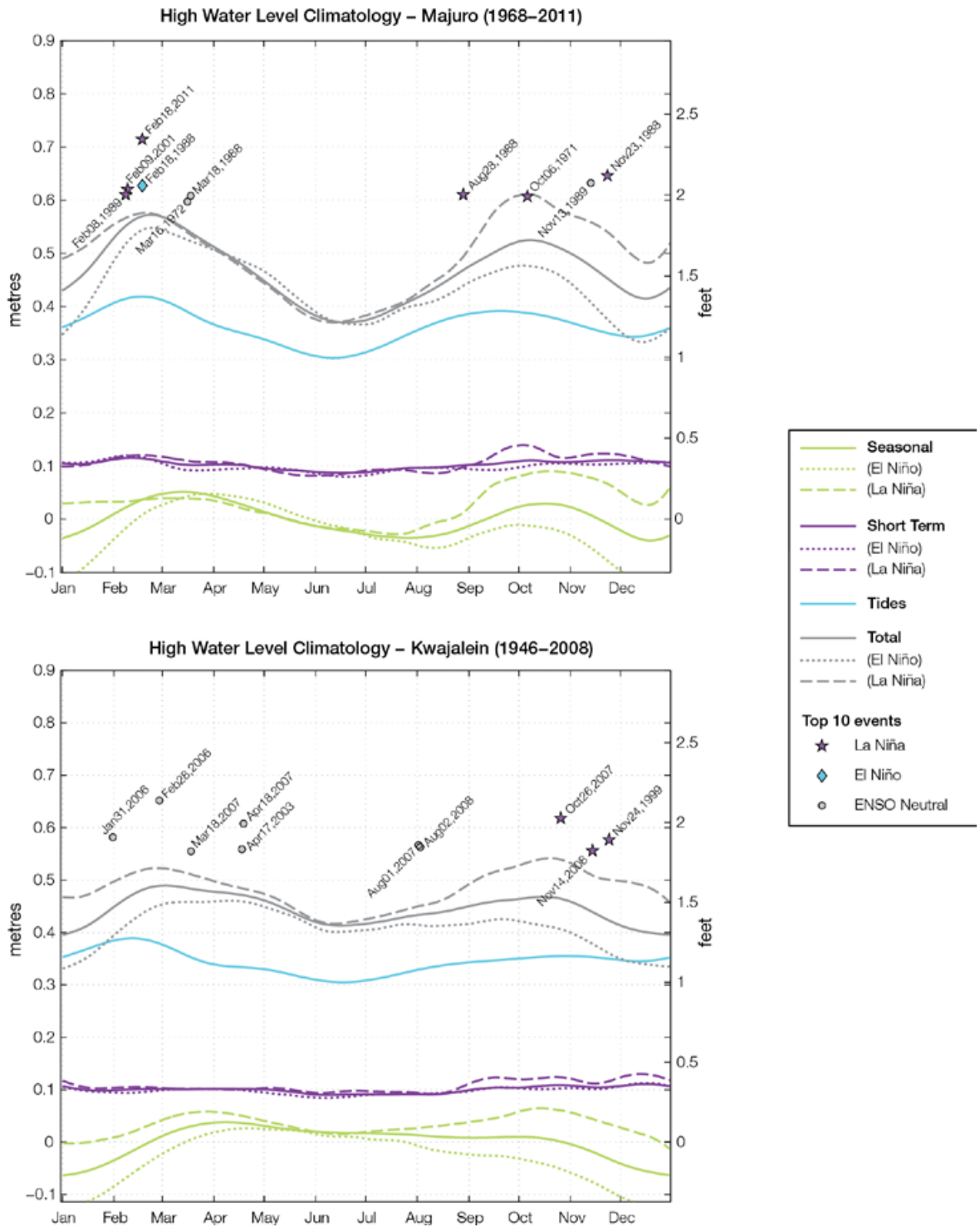

Figure 7.6: The annual cycle of high water relative to Mean Higher High Water (MHHW) due to tides, short-term fluctuations (most likely associated with storms) and seasonal variations for Majuro (top) and Kwajalein (bottom). The tides and short-term fluctuations are respectively the 95% exceedence levels of the astronomical high tides relative to MHHW and short-term sea-level fluctuations. Components computed only for El Niño and La Niña years are shown by dotted and dashed lines, and grey lines are the sum of the tide, short-term and seasonal components. The 10 highest sea-level events in the record relative to MHHW are shown and coded to indicate the phase of ENSO at the time of the extreme event.

7.7 Climate Projections

Climate projections have been derived from up to 18 global climate models from the CMIP3 database, for up to three emissions scenarios (B1 (low), A1B (medium) and A2 (high)) and three 20-year periods (centred on 2030, 2055 and 2090, relative to 1990). These models were selected based on their ability to reproduce important features of the current climate (Volume 1, Section 5.2.3), so projections from each of the models are plausible representations of the future climate. This means there is not one single projected future for the Marshall Islands, but rather a range of possible futures. The full range of these futures is discussed in the following sections.

These projections do not represent a value specific to any actual location, such as a town or city in the Marshall Islands. Instead, they refer to an average change over the broad geographic region encompassing the Marshall Islands and the surrounding ocean. Projections refer to the entire Marshall Islands unless otherwise stated. In some instances, given that there are some differences between the climate of the northern and southern Marshall Islands (Section 7.4), projections are given separately for these two regions (Figure 1.1 shows the regional boundaries). Section 1.7 provides important information about interpreting climate model projections.

7.7.1 Temperature

Surface air temperature and sea-surface temperature are projected to continue to increase over the course of the 21st century. There is *very high* confidence in this direction of change because:

- Warming is physically consistent with rising greenhouse gas concentrations.
- All CMIP3 models agree on this direction of change.

The majority of CMIP3 models simulate a slight increase (<1.8°F; <1°C) in annual and seasonal mean temperature by 2030, however by 2090 under the A2 (high) emissions scenario temperature increases of greater than 4.5°F (2.5°C) are simulated by almost all models (Tables 7.4 and 7.5). Given the close relationship between surface air temperature and sea-surface temperature, a similar (or slightly weaker) rate of warming is projected for the surface ocean (Figure 7.7). There is *moderate* confidence in this range and distribution of possible futures because:

- There is generally a large discrepancy between modelled and observed temperature trends over the past 50 years in the vicinity of the Marshall Islands, although this may be partly due to limited observational records (Figure 7.7).

Interannual variability in surface air temperature and sea-surface temperature over the Marshall Islands is strongly influenced by ENSO in the current climate (Section 7.5). As there is no consistency in projections of future ENSO activity (Volume 1, Section 6.4.1), it is not possible to determine whether interannual variability in temperature will change in the future. However, ENSO is expected to continue to be an important source of variability for the Marshall Islands and the region.

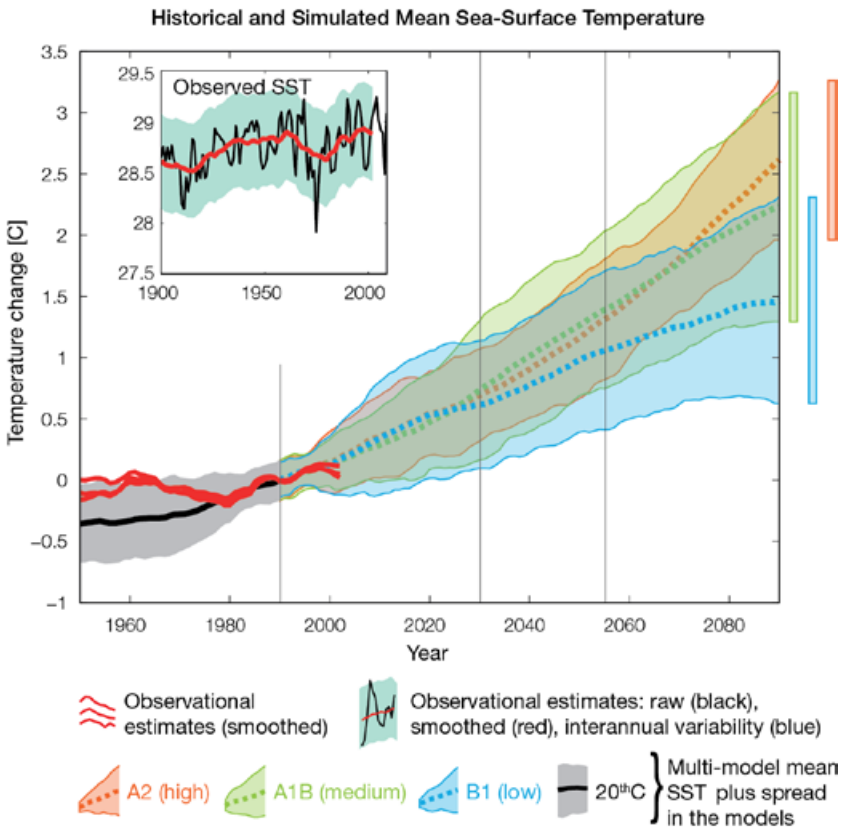

Figure 7.7: Historical climate (from 1950 onwards) and simulated historical and future climate for annual mean sea-surface temperature (SST) in the region surrounding the southern Marshall Islands, for the CMIP3 models. Shading represents approximately 95% of the range of model projections (twice the inter-model standard deviation), while the solid lines represent the smoothed (20-year running average) multi-model mean temperature. Projections are calculated relative to the 1980–1999 period (which is why there is a decline in the inter-model standard deviation around 1990). Observational estimates in the main figure (red lines) are derived from the HadSST2, ERSST and Kaplan Extended SST V2 datasets (Volume 1, Section 2.2.2). Annual average (black) and 20-year running average (red) HadSST2 data is also shown inset. Projections for the northern Marshall Islands closely resemble those for the south and are therefore not shown.

7.7.2 Rainfall

Wet season (May-October), dry season (November-April) and annual average rainfall is projected to increase over the course of the 21st century. There is *high* confidence in this direction of change because:

- Physical arguments indicate that rainfall will increase in the equatorial Pacific in a warmer climate (IPCC, 2007; Volume 1, Section 6.4.3).
- Almost all of the CMIP3 models agree on this direction of change by 2090.

The majority of CMIP3 models simulate little change (-5% to 5%) in rainfall by 2030, however by 2090 the majority simulate an increase (>5%) in wet season, dry season and annual rainfall. In fact, approximately one third of models simulate a large increase (>15%) in rainfall under the higher (i.e. A1B (medium) and A2 (high)) emissions scenarios, for the dry season in the northern Marshall Islands and on both a seasonal and annual basis in the south (Tables 7.4 and 7.5). There is *moderate* confidence in this range and distribution of possible futures because:

- In simulations of the current climate, the CMIP3 models broadly capture the influence of the ITCZ on the rainfall of the Marshall Islands (Volume 1, Sections 5.2.3.4 and 5.2.3.5).
- The CMIP3 models are unable to resolve many of the physical processes involved in producing rainfall. As a consequence, they do not simulate rainfall as well other variables, such as temperature (Volume 1, Chapter 5).

The inconsistency between the projected increase in annual and seasonal rainfall and the recent declining trends observed for Majuro and Kwajalein (Section 7.6.2) may be related to local factors not captured by the models (e.g. topography), or the fact that the projections presented here represent an average over a very large geographic region (Sections 1.7.1 and 1.7.2).

Interannual variability in rainfall over the Marshall Islands is strongly influenced by ENSO in the current climate (Section 7.5). As there is no consistency in projections of future ENSO activity (Volume 1, Section 6.4.1), it is not possible to determine whether interannual variability in rainfall will change in the future.

7.7.3 Extremes

Temperature

The intensity and frequency of days of extreme heat are projected to increase over the course of the 21st century. There is *very high* confidence in this direction of change because:

- An increase in the intensity and frequency of days of extreme heat is physically consistent with rising greenhouse gas concentrations.
- All CMIP3 models agree on the direction of change for both intensity and frequency.

For both the northern and southern Marshall Islands, the majority of CMIP3 models simulate an increase of approximately 2°F (1°C) in the temperature experienced on the 1-in-20-year hot day by 2055 under the B1 (low) emissions scenario, with an increase of over 4.5°F (2.5°C) simulated by the majority of models by 2090 under the A2 (high) emissions scenario (Tables 7.4 and 7.5). There is *low* confidence in this range and distribution of possible futures because:

- In simulations of the current climate, the CMIP3 models tend to underestimate the intensity and frequency of days of extreme heat (Volume 1, Section 5.2.4).
- Smaller increases in the frequency of days of extreme heat are projected by the CCAM 60 km simulations.

Rainfall

The intensity and frequency of days of extreme rainfall are projected to increase over the course of the 21st century. There is *high* confidence in this direction of change because:

- An increase in the frequency and intensity of extreme rainfall is consistent with larger-scale projections, based on the physical argument that the atmosphere is able to hold more water vapour in a warmer climate (Allen and Ingram, 2002; IPCC, 2007). It is also consistent with physical arguments that rainfall will increase in the deep tropical Pacific in a warmer climate (IPCC, 2007; Volume 1, Section 6.4.3).
- Almost all of the CMIP3 models agree on this direction of change for both intensity and frequency.

For the northern and southern Marshall Islands, the majority of CMIP3 models simulate an increase of at least 0.8 inches (20 mm) in the amount of rain received on the 1-in-20-year wet day by 2055 under the B1 (low) emissions scenario, with an increase of at least 1.8 inches (45 mm) simulated by the majority of models by 2090 under the A2 (high) emissions scenario. The majority of models project that the current 1-in-20-year extreme rainfall event will occur, on average, three to four times per 20-year period in the northern Marshall Islands by 2055 under the B1 (low) emissions scenario, and four to five times per 20-year period in the southern Marshall Islands. By 2090, under the A2 (high) emissions scenario, the projected frequency increases to five to six times per 20-year period in the northern Marshall Islands and seven to eight times per 20-year period in the southern Marshall Islands. There is *low* confidence in this range and distribution of possible futures because:

- In simulations of the current climate, the CMIP3 models tend to underestimate the intensity and frequency of extreme rainfall (Volume 1, Section 5.2.4).

- The CMIP3 models are unable to resolve many of the physical processes involved in producing extreme rainfall.

Drought

The incidence of drought is projected to decrease over the course of the 21st century. There is *moderate* confidence in this direction of change because:

- A decrease in drought is consistent with projections of increased rainfall (Section 7.7.2).
- The majority of models agree on this direction of change for most drought categories.

For both the northern and southern Marshall Islands, the majority of CMIP3 models project that mild drought will occur approximately eight to nine times every 20 years in 2030 under all emissions scenarios, decreasing to six to seven times by 2090. The frequency of moderate drought over the northern Marshall Islands is projected to decrease from two to three times every 20 years under the A1B (medium) and A2 (high) emissions scenarios to once to twice by 2090, while under the B1 (low) emissions scenario the frequency of moderate drought remains approximately stable at once to twice every 20 years. Over the southern Marshall Islands, the frequency of moderate drought is projected to remain approximately stable at once to twice every 20 years under all emissions scenarios. The majority of CMIP3 models project that severe droughts will occur approximately once every 20 years across all time periods and emissions scenarios. There is *low* confidence in this range and distribution of possible futures because:

- There is only moderate confidence in the range of rainfall projections (Section 7.7.2), which directly influences projections of future drought conditions.

Tropical Cyclones (typhoons)

Tropical cyclone numbers are projected to decline in the tropical North Pacific Ocean basin (0–15ºS, 130ºE–180ºE) over the course of the 21st century. There is *moderate* confidence in this direction of change because:

- Many studies suggest a decline in tropical cyclone frequency globally (Knutson et al., 2010).
- Tropical cyclone numbers decline in the tropical North Pacific Ocean basin in the majority of assessment techniques.

Based on the direct detection methodologies (Curvature Vorticity Parameter (CVP) and the CSIRO Direct Detection Scheme (CDD) described in Volume 1, Section 4.8.2), 80% of projections show no change or a decrease in tropical cyclone formation when applied to the CMIP3 climate models for which suitable output is available. When these techniques are applied to CCAM, 100% of projections show a decrease in tropical cyclone formation. In addition, the Genesis Potential Index (GPI) empirical technique suggests that conditions for tropical cyclone formation will become less favourable in the North Pacific Ocean basin, for the majority (70%) of analysed CMIP3 models. There is *moderate* confidence in this range and distribution of possible futures because in simulations of the current climate, the CVP, CDD and GPI methods capture the frequency of tropical cyclone activity reasonably well (Volume 1, Section 5.4).

Consistent with this projected reduction in total cyclone numbers, five of the six 60 km CCAM simulations also show a decrease in the proportion of the most severe storms (those stronger than the current climate 90th percentile storm maximum wind speed). Most simulations project an increase in the proportion of storms occurring in the weaker categories. Associated with this is a reduction in cyclonic wind hazard.

7.7.4 Ocean Acidification

The acidification of the ocean will continue to increase over the course of the 21st century. There is *very high* confidence in this projection as the rate of ocean acidification is driven primarily by the increasing oceanic uptake of carbon dioxide, in response to rising atmospheric carbon dioxide concentrations.

Projections from all analysed CMIP3 models indicate that the annual maximum aragonite saturation state will reach values below 3.5 by about 2035 and continue to decline thereafter (Figure 7.8; Tables 7.4 and 7.5). There is *moderate* confidence in this range and distribution of possible futures because the projections are based on climate models without an explicit representation of the carbon cycle and with relatively low resolution and known regional biases.

The impact of acidification change on the health of reef ecosystems is likely to be compounded by other stressors including coral bleaching, storm damage and fishing pressure.

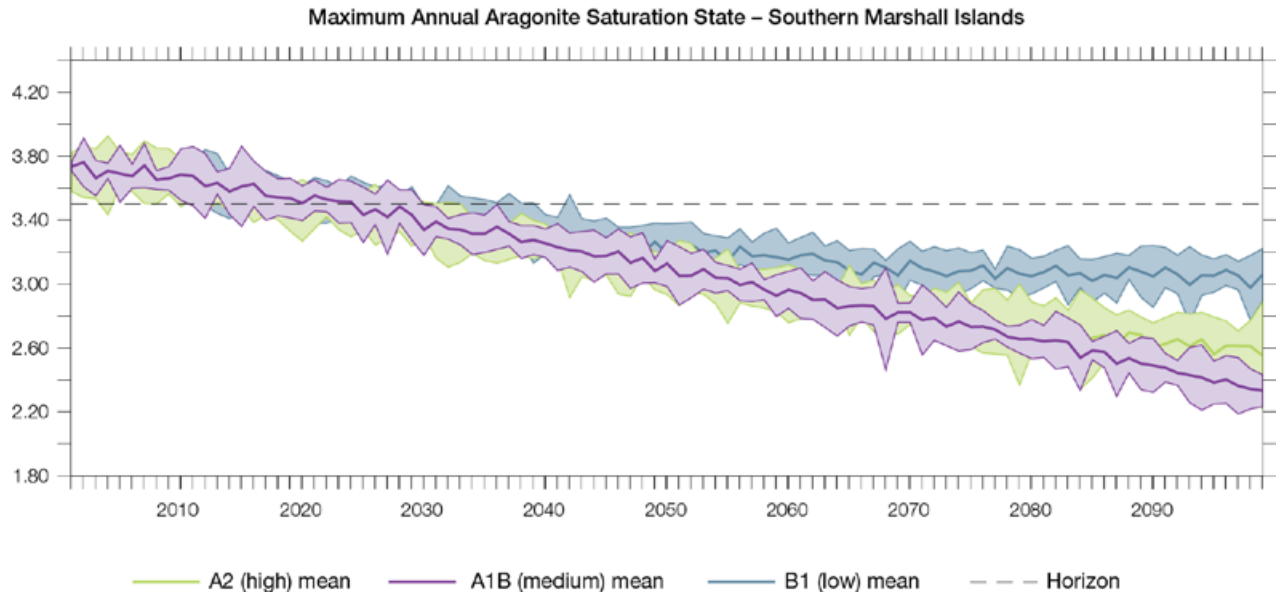

Figure 7.8: Multi-model projections, and their associated uncertainty (shaded area represents two standard deviations), of the maximum annual aragonite saturation state in the sea surface waters of the southern Marshall Islands under the different emissions scenarios. The dashed black line represents an aragonite saturation state of 3.5. Projections for the northern Marshall Islands closely resemble those for the south and are therefore not shown.

7.7.5 Sea Level

Mean sea level is projected to continue to rise over the course of the 21st century. There is *very high* confidence in this direction of change because:

- Sea-level rise is a physically consistent response to increasing ocean and atmospheric temperatures, due to thermal expansion of the water and the melting of glaciers and ice caps.
- Projections arising from all CMIP3 models agree on this direction of change.

The CMIP3 models simulate a rise of between approximately 2–6 inches (5–15 cm) by 2030, with increases of 8–24 inches (20–60 cm) indicated by 2090 under the higher emissions scenarios (i.e. A2 (high), A1B (medium); Figure 7.9; Tables 7.4 and 7.5).

There is *moderate* confidence in this range and distribution of possible futures because:

- There is significant uncertainty surrounding ice-sheet contributions to sea-level rise and a larger rise than that projected above cannot be excluded (Meehl et al., 2007b). However, understanding of the processes is currently too limited to provide a best estimate or an upper bound (IPCC, 2007).
- Globally, since the early 1990s, sea level has been rising near the upper end of the above projections. During the 21st century, some studies (using semi-empirical models) project faster rates of sea-level rise.

Interannual variability of sea level will lead to periods of lower and higher regional sea levels. In the past, this interannual variability has been about 8 inches (20 cm) (5–95% range, after removal of the seasonal cycle; dashed lines in Figure 7.9 (a)) and it is likely that a similar range will continue through the 21st century. In addition, winds and waves associated with weather phenomena will continue to lead to extreme sea-level events.

In addition to the regional variations in sea level associated with ocean and mass changes, there are ongoing changes in relative sea level associated with changes in surface loading over the last glacial cycle (glacial isostatic adjustment) and local tectonic motions. The glacial isostatic motions are relatively small for the PCCSP region.

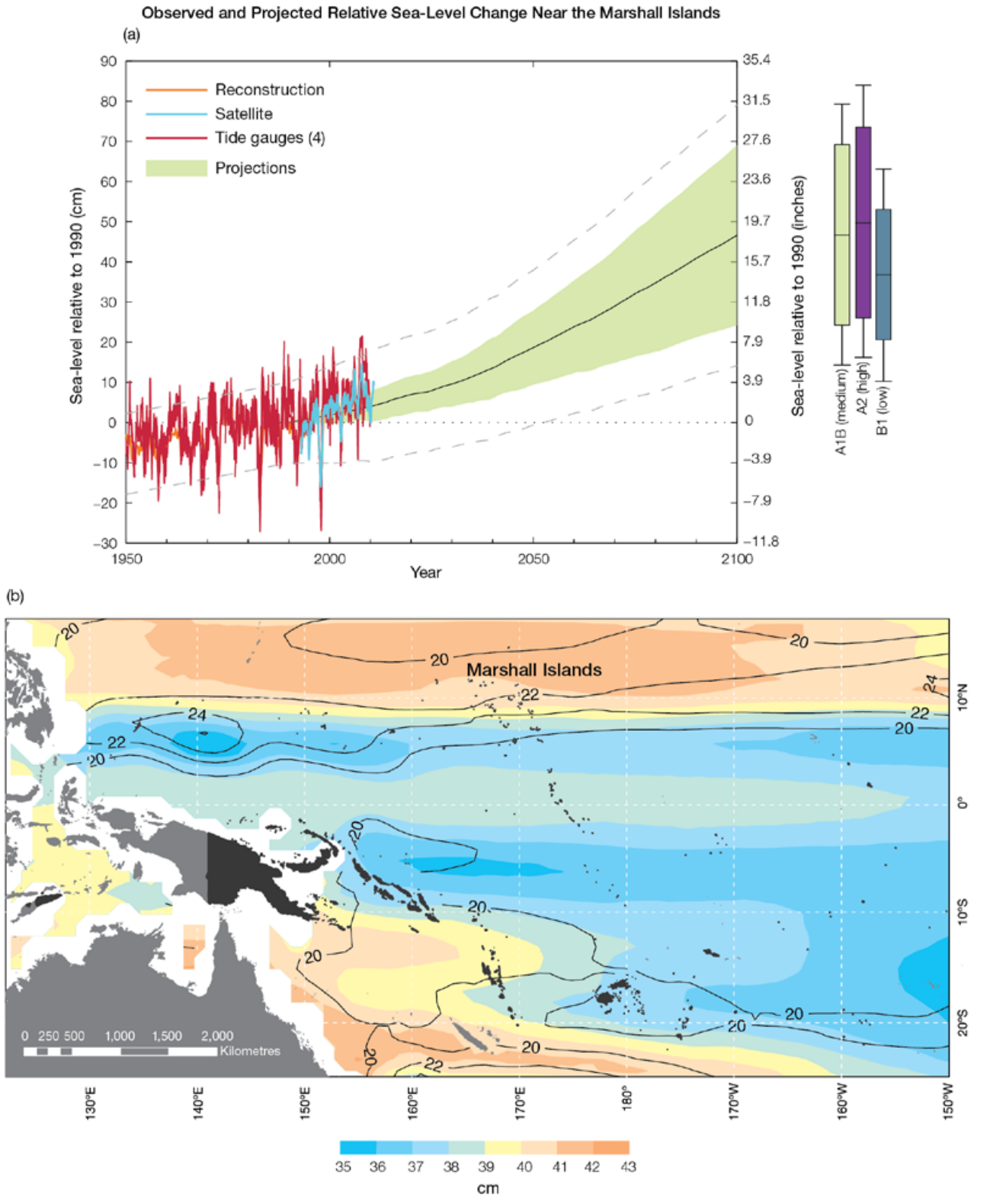

Figure 7.9: Observed and projected relative sea-level change near the Marshall Islands. (a) The observed in situ relative sea-level records are indicated in red, with the satellite record (since 1993) in light blue. The gridded sea level at the Marshall Islands (since 1950, from Church and White (in press)) is shown in orange. The projections for the A1B (medium) emissions scenario (5–95% uncertainty range) are shown by the green shaded region from 1990–2100. The range of projections for the B1 (low), A1B (medium) and A2 (high) emissions scenarios by 2100 are also shown by the bars on the right. The dashed lines are an estimate of interannual variability in sea level (5–95% range about the long-term trends) and indicate that individual monthly averages of sea level can be above or below longer-term averages. (b) The projections (in cm) for the A1B (medium) emissions scenario in the Marshall Islands region for the average over 2081–2100 relative to 1981–2000 are indicated by the shading, with the estimated uncertainty in the projections indicated by the contours (in cm).

7.7.6 Projections Summary

The projections presented in Section 7.7 are summarised in Table 7.4 (northern Marshall Islands) and Table 7.5 (southern Marshall Islands). For detailed information regarding the various uncertainties associated with the table values, refer to the preceding text in Sections 7.7 and 1.7, in addition to Chapters 5 and 6 in Volume 1. When interpreting the differences between projections for the B1 (low), A1B (medium) and A2 (high) emissions scenarios, it is also important to consider the emissions pathways associated with each scenario (Volume 1, Figure 4.1) and the fact that a slightly different subset of models was available for each (Volume 1, Appendix 1).

Table 7.4: Projected change in the annual and seasonal mean climate for the northern Marshall Islands, under the B1 (low; blue), A1B (medium; green) and A2 (high; purple) emissions scenarios. Projections are given for three 20-year periods centred on 2030 (2020–2039), 2055 (2046–2065) and 2090 (2080–2099), relative to 1990 (1980–1999). Values represent the multi-model mean change ± twice the inter-model standard deviation (representing approximately 95% of the range of model projections), except for sea level where the estimated mean change and the 5–95% range are given (as they are derived directly from the Intergovernmental Panel on Climate Change Fourth Assessment Report values). The confidence (Section 1.7.2) associated with the range and distribution of the projections is also given (indicated by the standard deviation and multi-model mean, respectively). See Volume 1, Appendix 1 for a complete listing of CMIP3 models used to derive these projections.

Variable	Season	2030	2055	2090	Confidence
Surface air temperature (°F)	Annual	+1.1 ± 0.7 +1.4 ± 0.8 +1.3 ± 0.5	+1.9 ± 0.9 +2.7 ± 1.0 +2.5 ± 0.8	+2.7 ± 1.3 +4.2 ± 1.6 +5.0 ± 1.2	High
Surface air temperature (°C)	Annual	+0.6 ± 0.4 +0.8 ± 0.4 +0.7 ± 0.3	+1.0 ± 0.5 +1.5 ± 0.6 +1.4 ± 0.4	+1.5 ± 0.7 +2.3 ± 0.9 +2.8 ± 0.7	High
Maximum temperature (°F)	1-in-20-year event	N/A	+1.8 ± 1.3 +2.5 ± 1.4 +2.5 ± 0.9	+2.3 ± 1.4 +4.0 ± 2.2 +4.9 ± 2.3	Low
Maximum temperature (°C)	1-in-20-year event	N/A	+1.0 ± 0.7 +1.4 ± 0.8 +1.4 ± 0.5	+1.3 ± 0.8 +2.2 ± 1.2 +2.7 ± 1.3	Low
Minimum temperature (°F)	1-in-20-year event	N/A	+2.2 ± 2.9 +2.7 ± 2.9 +2.5 ± 4.5	+3.1 ± 2.9 +4.1 ± 3.4 +4.9 ± 2.9	Low
Minimum temperature (°C)	1-in-20-year event	N/A	+1.2 ± 1.6 +1.5 ± 1.6 +1.4 ± 2.5	+1.7 ± 1.6 +2.3 ± 1.9 +2.7 ± 1.6	Low
Total rainfall (%)*	Annual	+3 ± 14 +1 ± 9 +3 ± 13	+2 ± 4 +5 ± 12 +7 ± 24	+3 ± 9 +11 ± 45 +12 ± 25	Moderate
Dry season rainfall (%)*	November-April	+2 ± 21 +4 ± 14 +5 ± 24	+4 ± 18 +9 ± 32 +13 ± 42	+2 ± 25 +16 ± 64 +20 ± 49	Moderate
Wet season rainfall (%)*	May-October	+3 ± 14 -1 ± 13 +3 ± 10	+2 ± 7 +4 ± 10 +6 ± 18	+3 ± 7 +9 ± 39 +9 ± 21	Moderate
Sea-surface temperature (°F)	Annual	+1.3 ± 0.9 +1.4 ± 1.1 +1.3 ± 0.7	+2.0 ± 1.3 +2.5 ± 1.3 +2.5 ± 1.1	+2.7 ± 1.6 +4.1 ± 1.8 +4.9 ± 1.3	Moderate
Sea-surface temperature (°C)	Annual	+0.7 ± 0.5 +0.8 ± 0.6 +0.7 ± 0.4	+1.1 ± 0.7 +1.4 ± 0.7 +1.4 ± 0.6	+1.5 ± 0.9 +2.3 ± 1.0 +2.7 ± 0.7	Moderate
Aragonite saturation state (Ωar)	Annual maximum	+3.4 ± 0.1 +3.3 ± 0.1 +3.4 ± 0.1	+3.2 ± 0.1 +3.0 ± 0.1 +3.0 ± 0.1	+3.0 ± 0.1 +2.6 ± 0.2 +2.4 ± 0.1	Moderate
Mean sea level (inches)	Annual	+3.5 (1.6–5.9) +3.5 (1.6–5.9) +3.9 (1.2–6.3)	+7.5 (3.9–10.6) +8.3 (4.3–12.6) +7.9 (4.3–11.8)	+13.0 (7.1–18.5) +16.1 (8.3–23.6) +16.5 (8.7–24.4)	Moderate
Mean sea level (cm)	Annual	+10 (4–15) +10 (4–15) +9 (3–16)	+19 (10–27) +21 (11–32) +20 (11–30)	+33 (18–47) +41 (21–60) +42 (22–62)	Moderate

*The MIROC3.2(hires) model was eliminated in calculating the rainfall projections, due to its inability to accurately simulate present-day activity of the Intertropical Convergence Zone (Volume 1, Section 5.5.1).

Table 7.5: Projected change in the annual and seasonal mean climate for the southern Marshall Islands, under the B1 (low; blue), A1B (medium; green) and A2 (high; purple) emissions scenarios. Projections are given for three 20-year periods centred on 2030 (2020–2039), 2055 (2046–2065) and 2090 (2080–2099), relative to 1990 (1980–1999). Values represent the multi-model mean change ± twice the inter-model standard deviation (representing approximately 95% of the range of model projections), except for sea level where the estimated mean change and the 5–95% range are given (as they are derived directly from the Intergovernmental Panel on Climate Change Fourth Assessment Report values). The confidence (Section 1.7.2) associated with the range and distribution of the projections is also given (indicated by the standard deviation and multi-model mean, respectively). See Volume 1, Appendix 1 for a complete listing of CMIP3 models used to derive these projections.

Variable	Season	2030	2055	2090	Confidence
Surface air temperature (°F)	Annual	+1.2 ± 0.8 +1.4 ± 0.9 +1.3 ± 0.5	+2.0 ± 1.0 +2.7 ± 1.2 +2.6 ± 0.8	+2.8 ± 1.4 +4.3 ± 1.7 +5.1 ± 1.2	Moderate
Surface air temperature (°C)	Annual	+0.7 ± 0.4 +0.8 ± 0.5 +0.7 ± 0.3	+1.1 ± 0.6 +1.5 ± 0.7 +1.4 ± 0.4	+1.6 ± 0.8 +2.4 ± 0.9 +2.8 ± 0.7	Moderate
Maximum temperature (°F)	1-in-20-year event	N/A	+1.8 ± 0.9 +2.5 ± 1.4 +2.5 ± 0.7	+2.3 ± 1.4 +4.0 ± 2.2 +4.9 ± 2.7	Low
Maximum temperature (°C)	1-in-20-year event	N/A	+1.0 ± 0.5 +1.4 ± 0.8 +1.4 ± 0.4	+1.3 ± 0.8 +2.2 ± 1.2 +2.7 ± 1.5	Low
Minimum temperature (°F)	1-in-20-year event	N/A	+2.3 ± 2.7 +2.7 ± 2.9 +2.7 ± 2.7	+3.2 ± 2.7 +4.1 ± 3.2 +4.9 ± 3.2	Low
Minimum temperature (°C)	1-in-20-year event	N/A	+1.3 ± 1.5 +1.5 ± 1.6 +1.5 ± 1.5	+1.8 ± 1.5 +2.3 ± 1.8 +2.7 ± 1.8	Low
Total rainfall (%)*	Annual	+2 ± 8 +2 ± 7 +3 ± 9	+5 ± 9 +5 ± 11 +6 ± 13	+7 ± 11 +10 ± 16 +10 ± 19	Moderate
Dry season rainfall (%)*	November-April	0 ± 13 +2 ± 13 +3 ± 14	+5 ± 12 +5 ± 21 +7 ± 19	+5 ± 14 +10 ± 25 +9 ± 27	Moderate
Wet season rainfall (%)*	May-October	+3 ± 10 +3 ± 9 +3 ± 10	+6 ± 11 +5 ± 9 +6 ± 14	+8 ± 13 +10 ± 17 +11 ± 23	Moderate
Sea-surface temperature (°F)	Annual	+0.6 ± 0.5 +0.7 ± 0.6 +0.7 ± 0.4	+1.1 ± 0.6 +1.4 ± 0.6 +1.3 ± 0.5	+1.5 ± 0.8 +2.2 ± 0.9 +2.6 ± 0.7	Moderate
Sea-surface temperature (°C)	Annual	+0.3 ± 0.3 +0.4 ± 0.3 +0.4 ± 0.2	+0.6 ± 0.3 +0.8 ± 0.3 +0.7 ± 0.3	+0.8 ± 0.4 +1.2 ± 0.5 +1.4 ± 0.4	Moderate
Aragonite saturation state (Ωar)	Annual maximum	+3.4 ± 0.2 +3.3 ± 0.1 +3.3 ± 0.2	+3.1 ± 0.1 +3.0 ± 0.2 +3.0 ± 0.1	+3.0 ± 0.2 +2.6 ± 0.2 +2.4 ± 0.2	Moderate
Mean sea level (inches)	Annual	+3.5 (1.6–5.9) +3.5 (1.6–5.9) +3.9 (1.2–6.3)	+7.5 (3.9–10.6) +8.3 (4.3–12.6) +7.9 (4.3–11.8)	+13.0 (7.1–18.5) +16.1 (8.3–23.6) +16.5 (8.7–24.4)	Moderate
Mean sea level (cm)	Annual	+10 (4–15) +10 (4–15) +9 (3–16)	+19 (10–27) +21 (11–32) +20 (11–30)	+33 (18–47) +41 (21–60) +42 (22–62)	Moderate

*The MIROC3.2(hires) model was eliminated in calculating the rainfall projections, due to its inability to accurately simulate present-day activity of the Intertropical Convergence Zone (Volume 1, Section 5.5.1).

Anibare Bay

Chapter 8
Nauru

The contributions of Andrew Kaierua, Russ Kun, Franklin Teimitsi and Douglas Audoa from the Department of Commerce, Industry and Environment are gratefully acknowledged

Introduction

This chapter provides a brief description of Nauru, its past and present climate as well as projections for the future. The climate observation network and the availability of atmospheric and oceanic data records are outlined. The annual mean climate, seasonal cycles and the influences of large-scale climate features such as the South Pacific Convergence Zone and patterns of climate variability (e.g. the El Niño-Southern Oscillation) are analysed and discussed. Observed trends and analysis of rainfall, extreme events, sea-surface temperature, ocean acidification, mean and extreme sea levels are presented. Projections for air and sea-surface temperature, rainfall, sea level, ocean acidification and extreme events for the 21st century are provided. These projections are presented along with confidence levels based on expert judgement by Pacific Climate Change Science Program (PCCSP) scientists. The chapter concludes with a summary table of projections (Table 8.3). Important background information including an explanation of methods and models is provided in Chapter 1. For definitions of other terms refer to the Glossary.

8.1 Climate Summary

8.1.1 Current Climate

- Air temperatures in Nauru are fairly constant throughout the year and are closely related to sea-surface temperatures.
- The wet season usually starts in November and continues to April of the next calendar year. Drier conditions occur during the months of May to October.
- Rainfall in Nauru is affected by both the Intertropical Convergence Zone, and the South Pacific Convergence Zone.
- Annual and seasonal rainfall trends for Nauru for the period 1950–2009 are not statistically significant.
- The main influence on interannual climate variability in Nauru is the El Niño-Southern Oscillation.
- The sea-level rise near Nauru measured by satellite altimeters since 1993 is about 5 mm per year.
- The main climate extreme experienced by Nauru is drought, which can last as long as three years. Nauru does not experience tropical cyclones.

8.1.2 Future Climate

Over the course of the 21st century:

- Surface air temperature and sea-surface temperature are projected to continue to increase (*very high* confidence).
- Annual and seasonal mean rainfall is projected to increase (*high* confidence).
- The intensity and frequency of days of extreme heat are projected to increase (*very high* confidence).
- The intensity and frequency of days of extreme rainfall are projected to increase (*high* confidence).
- The incidence of drought is projected to decrease (*moderate* confidence).
- Ocean acidification is projected to continue (*very high* confidence).
- Mean sea-level rise is projected to continue (*very high* confidence).

8.2 Country Description

Located just south of the equator in the western South Pacific Ocean, Nauru lies at approximately 0.5°S and 167°E. It is a raised atoll with an area of 21 km^2. Approximately 6 km long (NE-SW) and 4 km wide (NW-SE), Nauru has a maximum elevation of 71 m. The island has been mined extensively in the past for phosphate. The Exclusive Economic Zone has an area of 320 000 km^2. There is no official capital but the Yaren District is the largest settlement and where the Government offices are located (Nauru's First National Communication under the UNFCCC, 1999; Nauru's Pacific Adaptation to Climate Change, 2006). The estimated population in 2010 was 9976 (Nauru Country Statistics, SOPAC, 2010).

The main economic sector was the mining and export of phosphate, which is now virtually exhausted. Few other resources exist and most necessities are imported from Australia. There is only small scale subsistence agriculture (Nauru's National Committee on Climate Change, 1999; PACC, 2005).

Figure 8.1: Island of Nauru

8.3 Data Availability

Historical climate data exist for several stations in Nauru, and have been merged into a single station composite. Meteorological observations were initially conducted by the British Phosphate Corporation then later taken at the old wireless radio station and Nauru Airport. Currently observations are taken by an automatic weather station near Yaren. Data are available here from 1893 to present for rainfall and 1951 to present for air temperature, however there are significant gaps in the air temperature record. Rainfall data from 1950 to 2009 have been used. This record is homogeneous and more than 99% complete. There are insufficient air temperature data from 1950 to 2009 for air temperature trend analyses. The search for historical hard copy and digitised climate data for Nauru is ongoing.

Monthly-averaged sea-level data are available from the 1970s (1974–1994 and 1993–present). A global positioning system instrument to estimate vertical land motion was deployed at Nauru in 2003 and will provide valuable direct estimates of local vertical land motion in future years. Both satellite (from 1993) and in situ sea-level data (1950–2009; termed reconstructed sea level; Volume 1, Section 2.2.2.2) are available on a global 1° x 1° grid.

Long-term locally-monitored sea-surface temperature data are unavailable for Nauru, so large-scale gridded sea-surface temperature datasets have been used (HadISST, HadSST2, ERSST and Kaplan Extended SST V2; Volume 1, Table 2.3).

8.4 Seasonal Cycles

Nauru has consistent monthly mean air temperatures throughout the year (Figure 8.2). Its air temperatures are closely related to the sea-surface temperatures, which also are fairly constant throughout the year.

The wet season usually starts in November and continues to April of the next calendar year. Drier conditions occur during the months of May to October. Both the Intertropical Convergence Zone (ITCZ), which sits to the north of Nauru for most of the year, and the South Pacific Convergence Zone (SPCZ), which sits to the south, bring rainfall to Nauru. The higher rainfall in the wet seasons is caused by the ITCZ moving south and the SPCZ strengthening and expanding north at that time of year.

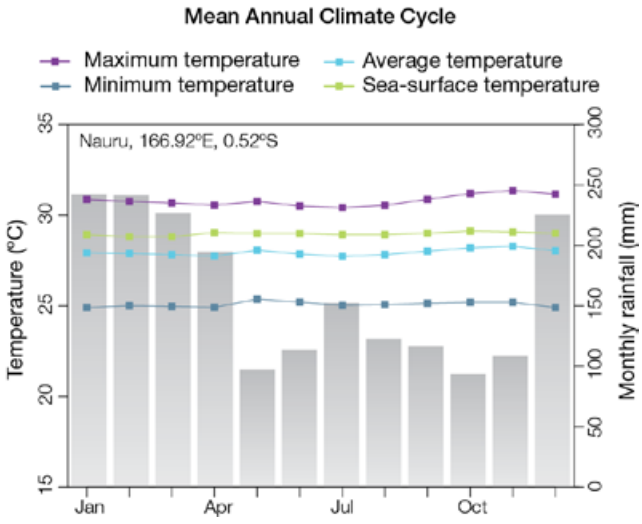

Figure 8.2: Mean annual cycle of rainfall (grey bars) and daily maximum, minimum and mean air temperatures at Nauru, and local sea-surface temperatures derived from the HadISST dataset (Volume 1, Table 2.3). Average air temperatures are calculated from 1951–1980, average rainfall and sea-surface temperatures from 1961–1990.

8.5 Climate Variability

As described earlier, gaps in the climate record of Nauru prevent the calculation of up-to-date trends. There is, however, sufficient historical data to determine rainfall variability.

The annual rainfall of Nauru has extremely high variability (standard deviation is 1151 mm) and the main influence on this climate variability is the El Niño-Southern Oscillation (ENSO) (Table 8.1). During El Niño years, Nauru is warmer and usually much wetter than average, receiving up to 4500 mm of rainfall. La Niña years are associated with a delayed onset of the wet season and drier than normal conditions, often resulting in an extended drought. In some La Niña years, Nauru only receives around 500 mm of rainfall.

Table 8.1: Correlation coefficients between indices of key large-scale patterns of climate variability and minimum and maximum temperatures (Tmin and Tmax) and rainfall at Nauru. Only correlation coefficients that are statistically significant at the 95% level are shown.

Climate feature/index		Dry season (May-October)			Wet season (November-April)		
		Tmin	Tmax	Rain	Tmin	Tmax	Rain
ENSO	Niño3.4			0.76			0.66
	Southern Oscillation Index			-0.77		0.46	-0.62
Interdecadal Pacific Oscillation Index							
ENSO Modoki Index			0.41	0.25			0.66
Number of years of data		29	29	60	28	27	63

Weather station maintenance, Tropical Western Pacific Climate Research Station

8.6 Observed Trends

8.6.1 Air Temperature

Due to incomplete historical air temperature records, observed air temperature trends for Nauru for the period 1950–2009 are unable to be calculated.

8.6.2 Rainfall

Annual and seasonal rainfall trends for Nauru for the period 1950–2009 are not statistically significant (Figure 8.3).

Table 8.2: Annual and seasonal trends in rainfall at Nauru for the period 1950–2009. Asterisks indicate significance at the 95% level. Persistence is taken into account in the assessment of significance as in Power and Kociuba (in press).

	Nauru Rain (mm per 10 yrs)
Annual	+11
Wet season	-37
Dry season	+38

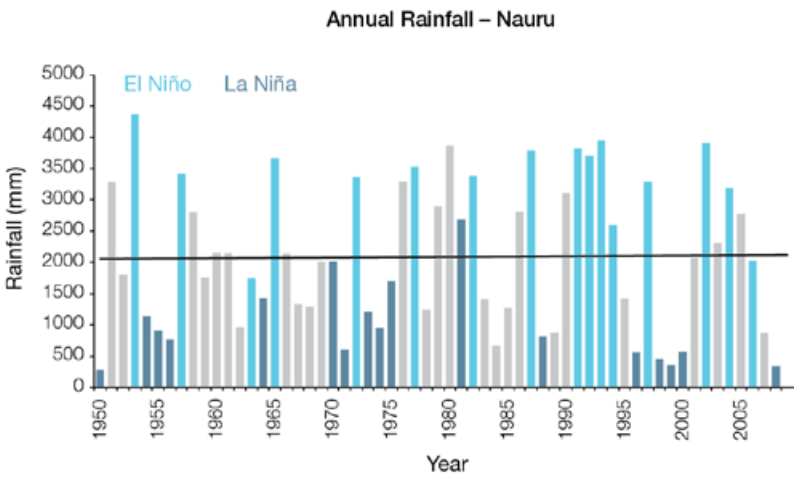

Figure 8.3: Annual rainfall at Nauru. Light blue, dark blue and grey bars denote El Niño, La Niña and neutral years respectively.

8.6.3 Extreme Events

Being so close to the equator, Nauru does not experience tropical cyclones. The main climate extreme experienced by Nauru is drought, which can last as long as three years. Droughts occur when La Niña events decrease the surrounding sea-surface temperature, resulting in less cloud and rainfall. Prolonged droughts cause a lowering of the underground freshwater lens, resulting in water supply problems and severe stress on natural systems.

8.6.4 Sea-Surface Temperature

Water temperatures around Nauru have risen gradually since the 1950s. Since the 1970s the rate of warming has been approximately 0.12°C per decade. Figure 8.6 shows the 1950–2000 sea-surface temperature changes (relative to a reference year of 1990) from three different large-scale sea-surface temperature gridded datasets (HadSST2, ERSST and Kaplan Extended SST V2; Volume 1, Table 2.3). At these regional scales, natural variability may play a large role in the sea-surface temperature trends making it difficult to identify any long-term trends.

8.6.5 Ocean Acidification

Based the large-scale distribution of coral reefs across the Pacific and the seawater chemistry, Guinotte et al. (2003) suggested that seawater aragonite saturation states above 4 were optimal for coral growth and for the development of healthy reef ecosystems, with values from 3.5 to 4 adequate for coral growth, and values between 3 and 3.5, marginal. Coral reef ecosystems were not found at seawater aragonite saturation states below 3 and these conditions were classified as extremely marginal for supporting coral growth.

In the Nauru region, the aragonite saturation state has declined from about 4.5 in the late 18th century to an observed value of about 3.9 ± 0.1 by 2000.

8.6.6 Sea Level

Monthly averages of the historical tide gauge, satellite (since 1993) and gridded sea-level (since 1950) data agree well after 1993 and indicate interannual variability in sea levels of about 23 cm (estimated 5–95% range) after removal of the seasonal cycle (Figure 8.8). The sea-level rise near Nauru measured by satellite altimeters (Figure 8.4) since 1993 is about 5 mm per year, slightly larger than the global average of 3.2 ± 0.4 mm per year. This rise is partly linked to a pattern related to climate variability from year to year and decade to decade (Figure 8.8).

8.6.7 Extreme Sea-Level Events

The annual climatology of the highest daily sea levels has been evaluated from hourly tide gauge measurements at Nauru (Figure 8.5). High tides show relatively small variation throughout the year maximising in December and January. There is no variation in the seasonal component of sea level, possibly due to Nauru's nearly equatorial position (0.5°S). The short-term component varies throughout the year and tends to indicate the occurrence of extreme water levels from November to March with distinct peaks centred on March and December. Consistent with this the top 10 sea-level events in the record all occur from November to March. The La Niña years are associated with near average sea levels from January to July and lower sea levels from July to December. On the other hand the short-term water levels tend to be higher during El Niño years and this is reflected in the top 10 sea-level events for which the majority occurred in El Niño or ENSO-neutral years.

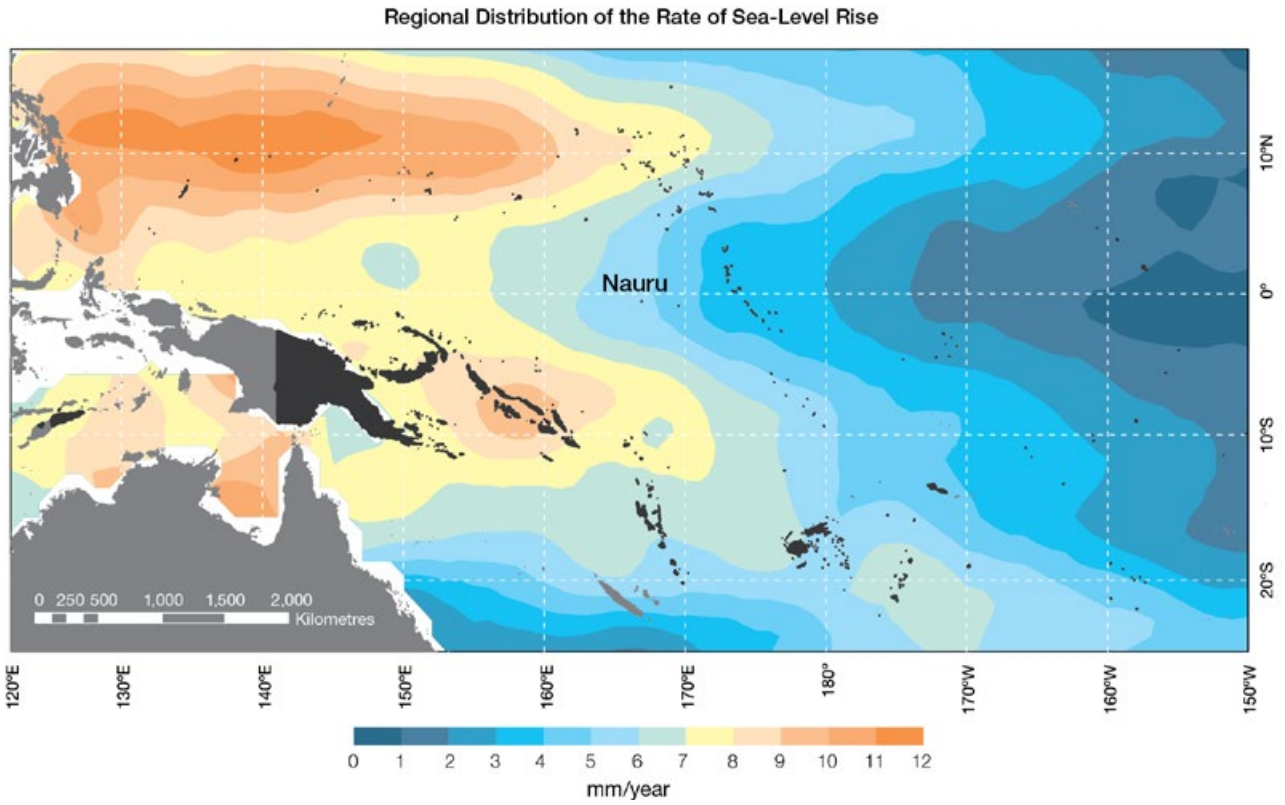

Figure 8.4: The regional distribution of the rate of sea-level rise measured by satellite altimeters from January 1993 to December 2010, with the location of Nauru indicated. Further detail about the regional distribution of sea-level rise is provided in Volume 1, Section 3.6.3.2.

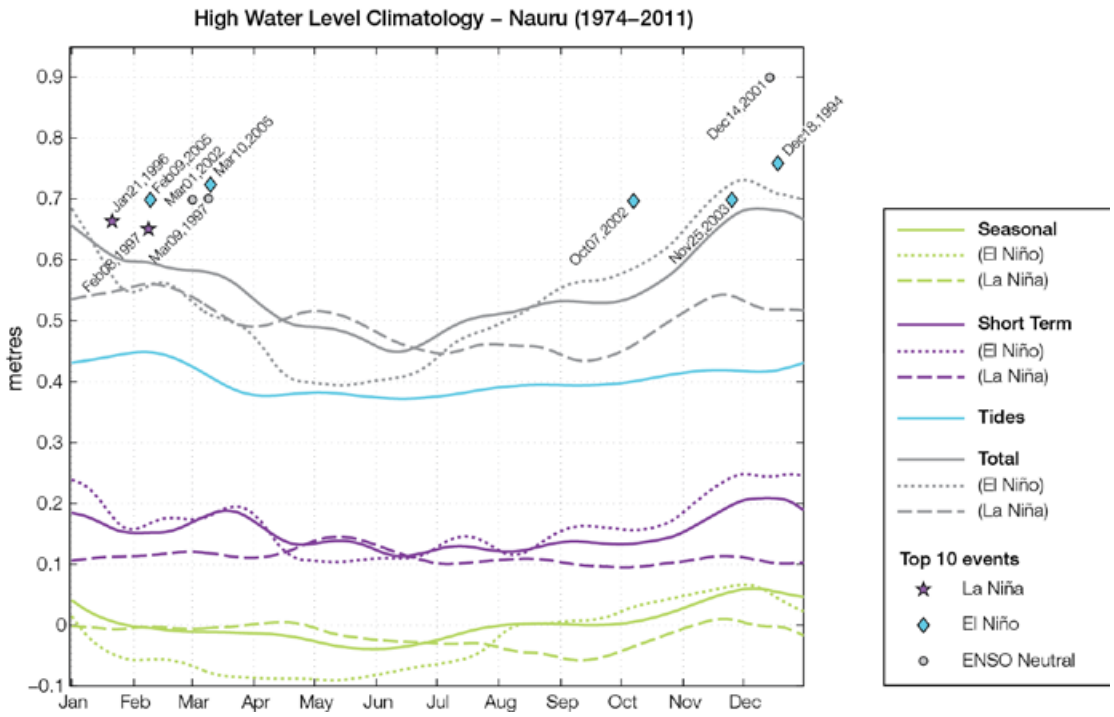

Figure 8.5: The annual cycle of high waters relative to Mean Higher High Water (MHW) due to tides, short-term fluctuations (most likely associated with storms) and seasonal variations for Nauru. The tides and short-term fluctuations are respectively the 95% exceedence levels of the astronomical high tides relative to MHHW and short-term sea level fluctuations. Components computed only for El Niño and La Niña years are shown by dotted and dashed lines, and grey lines are the sum of the tide, short-term and seasonal components. The 10 highest sea-level events in the record relative to MHHW are shown and coded to indicate the phase of ENSO at the time of the extreme event.

8.7 Climate Projections

Climate projections have been derived from up to 18 global climate models from the CMIP3 database, for up to three emissions scenarios (B1 (low), A1B (medium) and A2 (high)) and three 20-year periods (centred on 2030, 2055 and 2090, relative to 1990). These models were selected based on their ability to reproduce important features of the current climate (Volume 1, Section 5.2.3) so projections from each of the models are plausible representations of the future climate. This means there is not one single projected future for Nauru, but rather a range of possible futures. The full range of these futures is discussed in the following sections.

These projections do not represent a value specific to any actual location, such as a town in Nauru. Instead, they refer to an average change over the broad geographic region encompassing Nauru and the surrounding ocean (Figure 1.1 shows the regional boundaries). Section 1.7 provides important information about interpreting the climate model projections.

8.7.1 Temperature

Surface air temperature and sea-surface temperature are projected to continue to increase over the course of the 21st century. There is *very high* confidence in this direction of change because:

- Warming is physically consistent with rising greenhouse gas concentrations.
- All CMIP3 models agree on this direction of change.

Almost all of CMIP3 models simulate a slight increase (<1°C) in annual and seasonal mean temperature by 2030, however by 2090 under the A2 (high) emissions scenario temperature increases of greater than 3°C are simulated by the majority of models (Table 8.3). Given the close relationship between surface air temperature and sea-surface temperature, a similar (or slightly weaker) rate of warming is projected for the surface ocean (Figure 8.6). There is *moderate* confidence in this range and distribution of possible futures because:

- There is generally close agreement between modelled and observed temperature trends over the past 50 years in the vicinity of Nauru, although observational records are limited (Figure 8.6).
- In simulations of the current climate, almost all CMIP3 models have a cold temperature bias in the vicinity of Nauru (known as the 'cold tongue bias'; Volume 1, Section 5.2.2.1).

Interannual variability in surface air temperature and sea-surface temperature over Nauru is strongly influenced by ENSO in the current climate. As there is no consistency in projections of future ENSO activity (Volume 1, Section 6.4.1) it is not possible to determine whether interannual variability in temperature will change in the future. However, ENSO is expected to continue to be an important source of variability for the region.

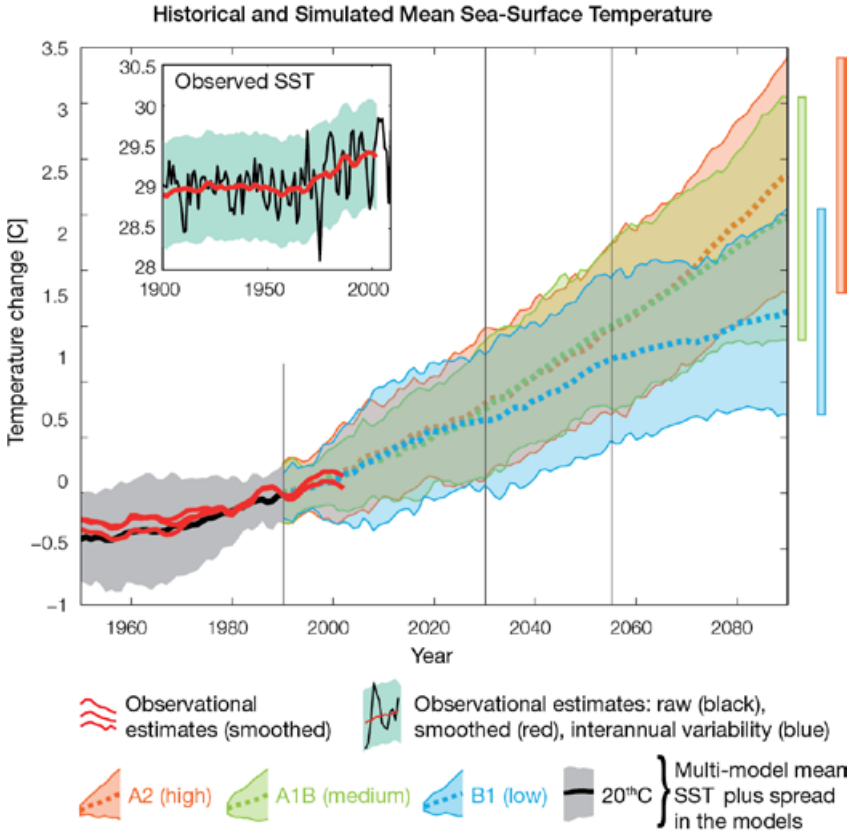

Figure 8.6: Historical climate (from 1950 onwards) and simulated historical and future climate for annual mean sea-surface temperature (SST) in the region surrounding Nauru, for the CMIP3 models. Shading represents approximately 95% of the range of model projections (twice the inter-model standard deviation), while the solid lines represent the smoothed (20-year running average) multi-model mean temperature. Projections are calculated relative to the 1980–1999 period (which is why there is a decline in the inter-model standard deviation around 1990). Observational estimates in the main figure (red lines) are derived from the HadSST2, ERSST and Kaplan Extended SST V2 datasets (Volume 1, Section 2.2.2). Annual average (black) and 20-year running average (red) HadSST2 data is also shown inset.

8.7.2 Rainfall

Wet season (November-April), dry season (May-October) and annual average rainfall are projected to increase over the course of the 21st century. There is *high* confidence in this direction of change because:

- Physical arguments indicate that rainfall will increase in the equatorial Pacific in a warmer climate (IPCC, 2007; Volume 1, Section 6.4.3).
- Almost all of the CMIP3 models agree on this direction of change.

The majority of CMIP3 models simulate an increase (>5%) in annual and seasonal mean rainfall by 2030, with almost all models simulating a large increase (>15%) by 2090 (Table 8.3). There is *low* confidence in this range and distribution of possible futures because:

- In simulations of the current climate, almost all CMIP3 models substantially underestimate present day rainfall in the vicinity of Nauru, in association with the cold tongue bias (Volume 1, Section 5.2.1.2).
- The CMIP3 models are unable to resolve many of the physical processes involved in producing rainfall. As a consequence, they do not simulate rainfall as well as other variables such as temperature (Volume 1, Chapter 5).

Interannual variability in rainfall over Nauru is strongly influenced by ENSO in the current climate (Section 8.5). As there is no consistency in projections of future ENSO activity (Volume 1, Section 6.4.1), it is not possible to determine whether interannual variability in rainfall will change in the future.

8.7.3 Extremes

Temperature

The intensity and frequency of days of extreme heat are projected to increase over the course of the 21st century. There is *very high* confidence in this direction of change because:

- An increase in the intensity and frequency of days of extreme heat is physically consistent with rising greenhouse gas concentrations.
- All CMIP3 models agree on the direction of change for both intensity and frequency.

The majority of CMIP3 models simulate an increase of approximately 1°C in the temperature experienced on the 1-in-20-year hot day by 2055 under the B1 (low) emissions scenario, with an increase of over 2.5°C simulated by the majority of models by 2090 under the A2 (high) emissions scenario (Table 8.3). There is *low* confidence in this range and distribution of possible futures because:

- In simulations of the current climate, the CMIP3 models tend to underestimate the intensity and frequency of days of extreme heat (Volume 1, Section 5.2.4).

Smaller increases in the frequency of days of extreme heat are projected by the CCAM 60 km simulations.

Rainfall

The intensity and frequency of days of extreme rainfall are projected to increase over the course of the 21st century. There is *high* confidence in this direction of change because:

- An increase in the frequency and intensity of extreme rainfall is consistent with larger-scale projections, based on the physical argument that the atmosphere is able to hold more water vapour in a warmer climate (Allen and Ingram, 2002; IPCC, 2007). It is also consistent with physical arguments that rainfall will increase in the deep tropical Pacific in a warmer climate (IPCC, 2007; Volume 1, Section 6.4.3).
- Almost all of the CMIP3 models agree on this direction of change for both intensity and frequency.

The majority of CMIP3 models simulate an increase of at least 15 mm in the amount of rain received on the 1-in-20-year wet day by 2055 under the B1 (low) emissions scenario, with an increase of at least 35 mm simulated by 2090 under the A2 (high) emissions scenario. The majority of models project that the current 1-in-20-year extreme rainfall event will occur, on average, three to four times per 20-year period by 2055 under the B1 (low) emissions scenario and six to seven times per 20-year period by 2090 under the A2 (high) emissions scenario. There is *low* confidence in this range and distribution of possible futures because:

- In simulations of the current climate, the CMIP3 models tend to underestimate the intensity and frequency of extreme rainfall (Volume 1, Section 5.2.4), particularly in the vicinity of Nauru, in association with the cold tongue bias (Volume 1, Section 5.2.1.2).
- The CMIP3 models are unable to resolve many of the physical processes involved in producing extreme rainfall.

Drought

The incidence of drought is projected to decrease over the course of the 21st century. There is *moderate* confidence in this direction of change because:

- A decrease in drought is consistent with projections of increased rainfall (Section 8.7.2).
- The majority of models agree on this direction of change for all drought categories.

The majority of CMIP3 models project that mild drought will occur approximately seven to eight times every 20 years in 2030 under the B1 (low) and A1B (medium) emissions scenarios, decreasing to six to seven times by 2090. For the A2 (high) emissions scenario, a more pronounced decline from eight to nine times every 20 years in 2030 to five to six times by 2090 is projected. The frequency of moderate drought is projected to decline from two to three times every 20 years in 2030 to once to twice every 20 years in 2090 for all emissions scenarios, while severe droughts are expected to decline from once to twice to once every 20 years over the same periods. There is *low* confidence in this range and distribution of possible futures because:

- There is only low confidence in the range of rainfall projections (Section 8.7.2), which directly influences projections of future drought conditions.

8.7.4 Ocean Acidification

The acidification of the ocean will continue to increase over the course of the 21st century. There is *very high* confidence in this projection as the rate of ocean acidification is driven primarily by the increasing oceanic uptake of carbon dioxide, in response to rising atmospheric carbon dioxide concentrations.

Projections from all analysed CMIP3 models indicate that the annual maximum aragonite saturation state will reach values below 3.5 by about 2040 and continue to decline thereafter (Figure 8.7; Table 8.3). There is *moderate* confidence in this range and distribution of possible futures because the projections are based on climate models without an explicit representation of the carbon cycle and with relatively low resolution and known regional biases.

The impact of acidification change on the health of reef ecosystems is likely to be compounded by other stressors including coral bleaching, storm damage and fishing pressure.

8.7.5 Sea Level

Mean sea level is projected to continue to rise over the course of the 21st century. There is *very high* confidence in this direction of change because:

- Sea-level rise is a physically consistent response to increasing ocean and atmospheric temperatures, due to thermal expansion of the water and the melting of glaciers and ice caps.
- Projections arising from all CMIP3 models agree on this direction of change.

The CMIP3 models simulate a rise of between approximately 5–15 cm by 2030, with increases of 20–60 cm indicated by 2090 under the higher emissions scenarios (i.e. A2 (high), A1B (medium); Figure 8.8; Table 8.3). There is *moderate* confidence in this range and distribution of possible futures because:

- There is significant uncertainty surrounding ice-sheet contributions to sea-level rise and a rise larger than projected above cannot be excluded (Meehl et al., 2007b). However, understanding of the processes is currently too limited to provide a best estimate or an upper bound (IPCC, 2007).
- Globally, since the early 1990s, sea level has been rising near the upper end of these projections. During the 21st century, some studies (using semi-empirical models) project faster rates of sea-level rise.

Interannual variability of sea level will lead to periods of lower and higher regional sea levels. In the past, this interannual variability has been about 23 cm (5–95% range, after removal of the seasonal cycle; dashed lines in Figure 8.8 (a)) and it is likely that a similar range will continue through the 21st century. In addition, winds and waves associated with weather phenomena will continue to lead to extreme sea-level events.

In addition to the regional variations in sea level associated with ocean and mass changes, there are ongoing changes in relative sea level associated with changes in surface loading over the last glacial cycle (glacial isostatic adjustment) and local tectonic motions. The glacial isostatic motions are relatively small for the PCCSP region.

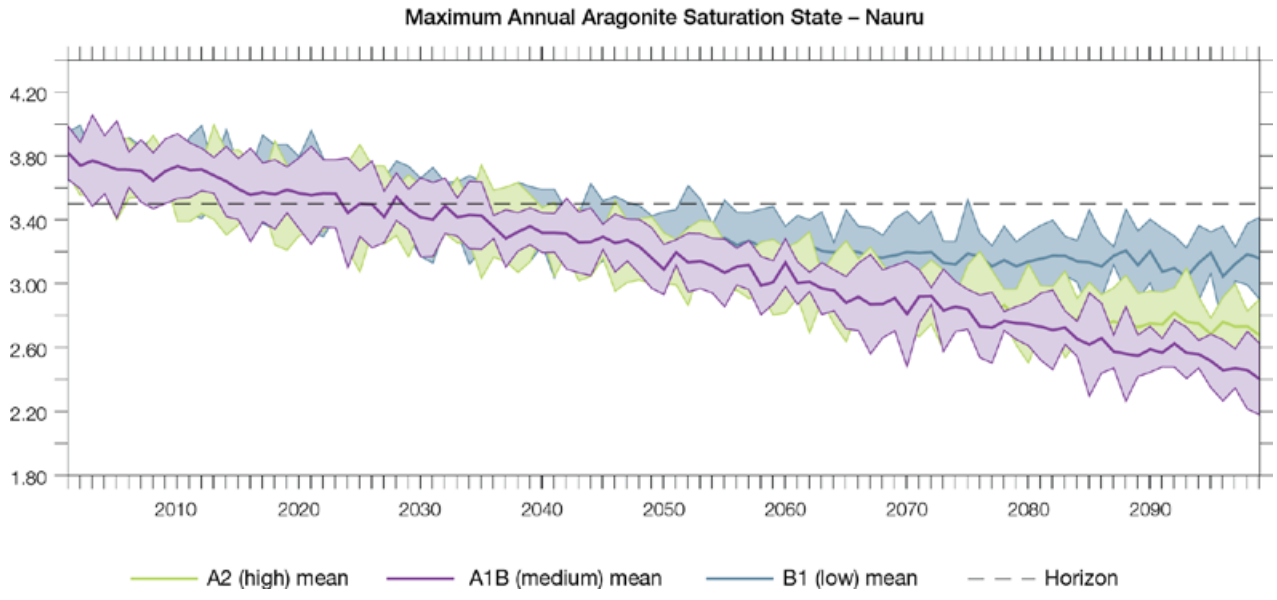

Figure 8.7: Multi-model projections, and their associated uncertainty (shaded area represents two standard deviations), of the maximum annual aragonite saturation state in the sea surface waters of the Nauru region under the different emissions scenarios. The dashed black line represents an aragonite saturation state of 3.5.

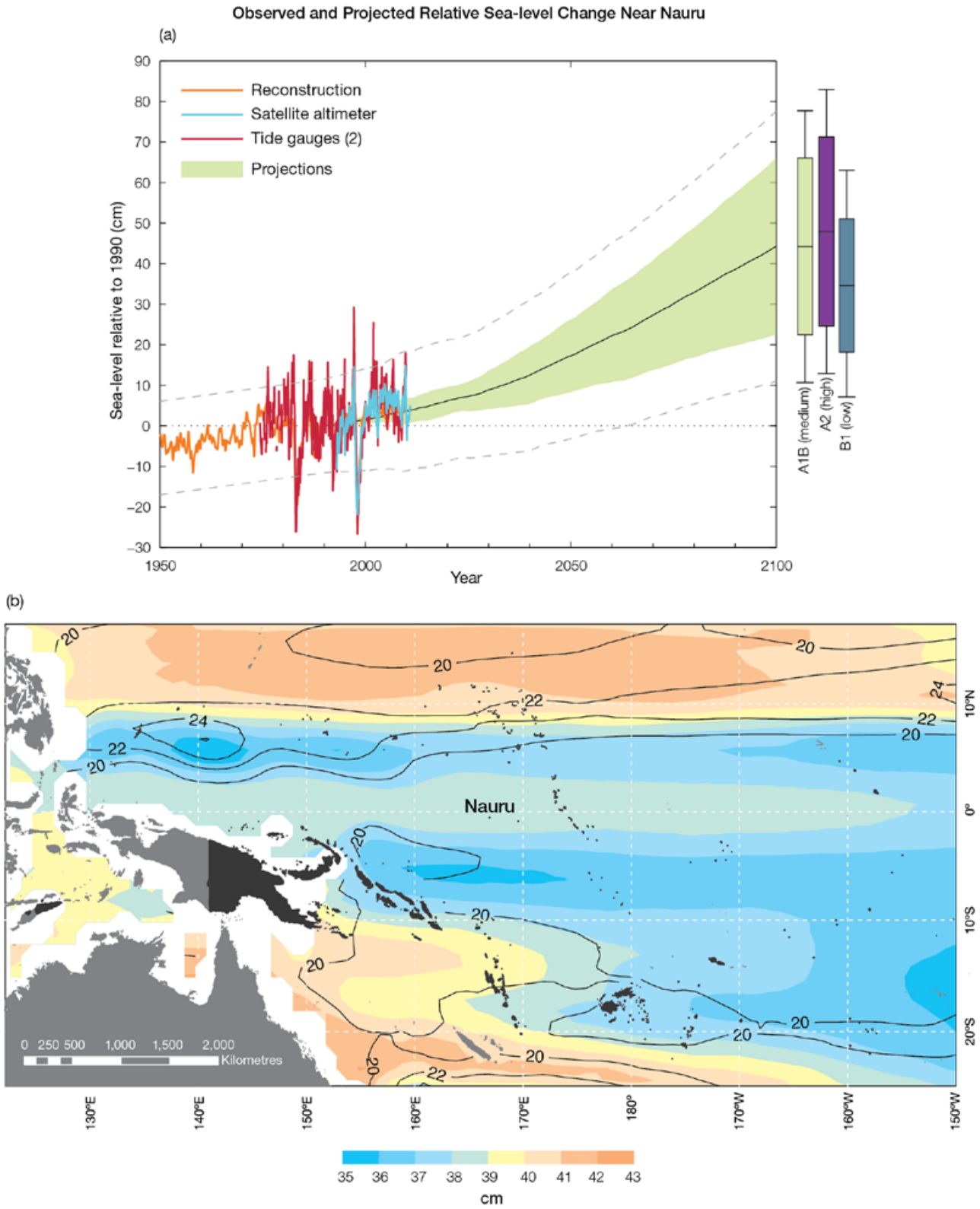

Figure 8.8: Observed and projected relative sea-level change near Nauru. (a) The observed in situ relative sea-level records are indicated in red, with the satellite record (since 1993) in light blue. The gridded sea level at Nauru (since 1950, from Church and White (in press)) is shown in orange. The projections for the A1B (medium) emissions scenario (5–95% uncertainty range) are shown by the green shaded region from 1990–2100. The range of projections for the B1 (low), A1B (medium) and A2 (high) emissions scenarios by 2100 are also shown by the bars on the right. The dashed lines are an estimate of interannual variability in sea level (5–95% range about the long-term trends) and indicate that individual monthly averages of sea level can be above or below longer-term averages. (b) The projections (in cm) for the A1B (medium) emissions scenario in the Nauru region for the average over 2081–2100 relative to 1981–2000 are indicated by the shading, with the estimated uncertainty in the projections indicated by the contours (in cm).

8.7.6 Projections Summary

The projections presented in Section 8.7 are summarised in Table 8.3. For detailed information regarding the various uncertainties associated with the table values, refer to the preceding text in Sections 8.7 and 1.7, in addition to Chapters 5 and 6 in Volume 1. When interpreting the differences between projections for the B1 (low), A1B (medium) and A2 (high) emissions scenarios, it is also important to consider the emissions pathways associated with each scenario (Volume 1, Figure 4.1) and the fact that a slightly different subset of models was available for each (Volume 1, Appendix 1).

Table 8.3: Projected change in the annual and seasonal mean climate for Nauru, under the B1 (low; blue), A1B (medium; green) and A2 (high; purple) emissions scenarios. Projections are given for three 20-year periods centred on 2030 (2020–2039), 2055 (2046–2065) and 2090 (2080–2099), relative to 1990 (1980–1999). Values represent the multi-model mean change ± twice the inter-model standard deviation (representing approximately 95% of the range of model projections), except for sea level where the estimated mean change and the 5–95% range are given (as they are derived directly from the Intergovernmental Panel on Climate Change Fourth Assessment Report values). The confidence (Section 1.7.2) associated with the range and distribution of the projections is also given (indicated by the standard deviation and multi-model mean, respectively). See Volume 1, Appendix 1 for a complete listing of CMIP3 models used to derive these projections.

Variable	Season	2030	2055	2090	Confidence
Surface air temperature (°C)	Annual	+0.7 ± 0.5 +0.8 ± 0.6 +0.8 ± 0.5	+1.3 ± 0.6 +1.6 ± 0.7 +1.6 ± 0.6	+1.7 ± 0.8 +2.6 ± 0.9 +3.0 ± 0.8	Moderate
Maximum temperature (°C)	1-in-20-year event	N/A	+1.0 ± 0.6 +1.4 ± 0.5 +1.5 ± 0.6	+1.3 ± 0.7 +2.2 ± 1.1 +2.7 ± 1.4	Low
Minimum temperature (°C)	1-in-20-year event	N/A	+1.4 ± 2.1 +1.6 ± 3.0 +1.2 ± 2.1	+1.9 ± 2.0 +2.6 ± 2.6 +2.7 ± 2.5	Low
Total rainfall (%)*	Annual	+13 ± 25 +10 ± 24 +11 ± 26	+11 ± 30 +25 ± 33 +25 ± 41	+27 ± 38 +43 ± 64 +45 ± 71	Low
Wet season rainfall (%)*	November-April	+10 ± 27 +10 ± 28 +9 ± 29	+19 ± 27 +21 ± 36 +21 ± 50	+22 ± 34 +35 ± 67 +35 ± 59	Low
Dry season rainfall (%)*	May-October	+16 ± 37 +12 ± 35 +14 ± 34	+30 ± 51 +30 ± 46 +32 ± 49	+35 ± 54 +54 ± 78 +59 ± 97	Low
Sea-surface temperature (°C)	Annual	+0.7 ± 0.6 +0.7 ± 0.6 +0.8 ± 0.7	+1.2 ± 0.7 +1.5 ± 0.7 +1.5 ± 0.8	+1.6 ± 0.9 +2.5 ± 1.1 +2.9 ± 1.1	Moderate
Aragonite saturation state (Ωar)	Annual maximum	+3.5 ± 0.2 +3.4 ± 0.2 +3.4 ± 0.2	+3.2 ± 0.2 +3.1 ± 0.2 +3.1 ± 0.1	+3.1 ± 0.2 +2.7 ± 0.2 +2.5 ± 0.2	Moderate
Mean sea level (cm)	Annual	+8 (4–13) +9 (4–14) +9 (4–14)	+17 (9–25) +20 (10–30) +19 (10–29)	+31 (17–45) +39 (20–57) +40 (21–60)	Moderate

*The MIROC3.2(medres) and MIROC3.2(hires) models were eliminated in calculating the rainfall projections, due to their inability to accurately simulate the South Pacific Convergence Zone and/or the Intertropical Convergence Zone (Volume 1, Section 5.5.1).

Coastline, Alofi

Chapter 9
Niue

The contributions of Rossylynn Pulehetoa-Mitiepo, Adorra Misikea and Felicia Pihigia Talagi from the Niue Department of Meteorology and Climate Change are gratefully acknowledged

Introduction

This chapter provides a brief description of Niue, its past and present climate as well as projections for the future. The climate observation network and the availability of atmospheric and oceanic data records are outlined. The annual mean climate, seasonal cycles and the influences of large-scale climate features such as the South Pacific Convergence Zone and patterns of climate variability (e.g. the El Niño-Southern Oscillation) are analysed and discussed. Observed trends and analysis of air temperature, rainfall, extreme events (including tropical cyclones), sea-surface temperature, ocean acidification and mean sea level are presented. Projections for air and sea-surface temperature, rainfall, sea level, ocean acidification and extreme events for the 21st century are provided. These projections are presented along with confidence levels based on expert judgement by Pacific Climate Change Science Program (PCCSP) scientists. The chapter concludes with a summary table of projections (Table 9.3). Important background information including an explanation of methods and models is provided in Chapter 1. For definitions of other terms refer to the Glossary.

9.1 Climate Summary

9.1.1 Current Climate

- Niue has a tropical maritime climate, with a seasonal range in air temperatures of about 4°C between the warmest and coolest months.
- Niue experiences two distinct seasons: a wet season from November to April and dry season from May to October. The timing of the wet season is influenced by the movement of the South Pacific Convergence Zone.
- Year-to-year variability in Niue's climate is strongly associated with the El Niño-Southern Oscillation.
- Warming trends are evident in both annual and seasonal mean air temperatures at Hanan Airport for the period 1950–2009.
- Annual and seasonal rainfall trends for Hanan Airport for the period 1950–2009 are not statistically significant.
- The sea-level rise near Niue measured by satellite altimeters since 1993 is about 5 mm per year.
- On average, Niue experiences 15 tropical cyclones per decade, with most occurring between November and April. The high interannual variability of tropical cyclone numbers makes it difficult to identify any long-term trends in frequency.

9.1.2 Future Climate

Over the course of the 21st century:

- Surface air temperature and sea-surface temperature are projected to continue to increase (*very high* confidence).
- Wet season and annual mean rainfall is projected to increase (*moderate* confidence).
- Little change is projected in dry season rainfall (*low* confidence).
- The intensity and frequency of days of extreme heat are projected to increase (*very high* confidence).
- The intensity and frequency of days of extreme rainfall are projected to increase (*high* confidence).
- Little change is projected in the incidence of drought (*low* confidence).
- Tropical cyclone numbers are projected to decline in the south-east Pacific Ocean basin (0–40ºS, 170ºE–130ºW) (*moderate* confidence).
- Ocean acidification is projected to continue (*very high* confidence).
- Mean sea-level rise is projected to continue (*very high* confidence).

9.2 Country Description

Niue is located in the western South Pacific Ocean and lies at 19°S and 169°W. The island is a raised coral atoll with three reef terraces; the highest terrace averages 69 m above sea level. The land area is 259 km^2 and the Exclusive Economic Zone has an area of 390 000 km^2. In addition to the main island, two reef atolls, Antiope and Beveridge, are located within its Exclusive Economic Zone. These are visible only at low tide. The capital of Niue is Alofi (Niue's First National Communication under the UNFCCC, 2000; Niue's Pacific Adaptation to Climate Change, 2006). The estimated population in 2010 was 1470 (Niue Country Statistics, SOPAC, 2010).

There is subsistence agriculture with some small-scale raising of livestock. There are small factories to process passionfruit, lime oil, honey, and coconut cream, and vanilla is being developed as an export crop (Niue's Pacific Adaptation to Climate Change, 2006). There is a very small tourism industry.

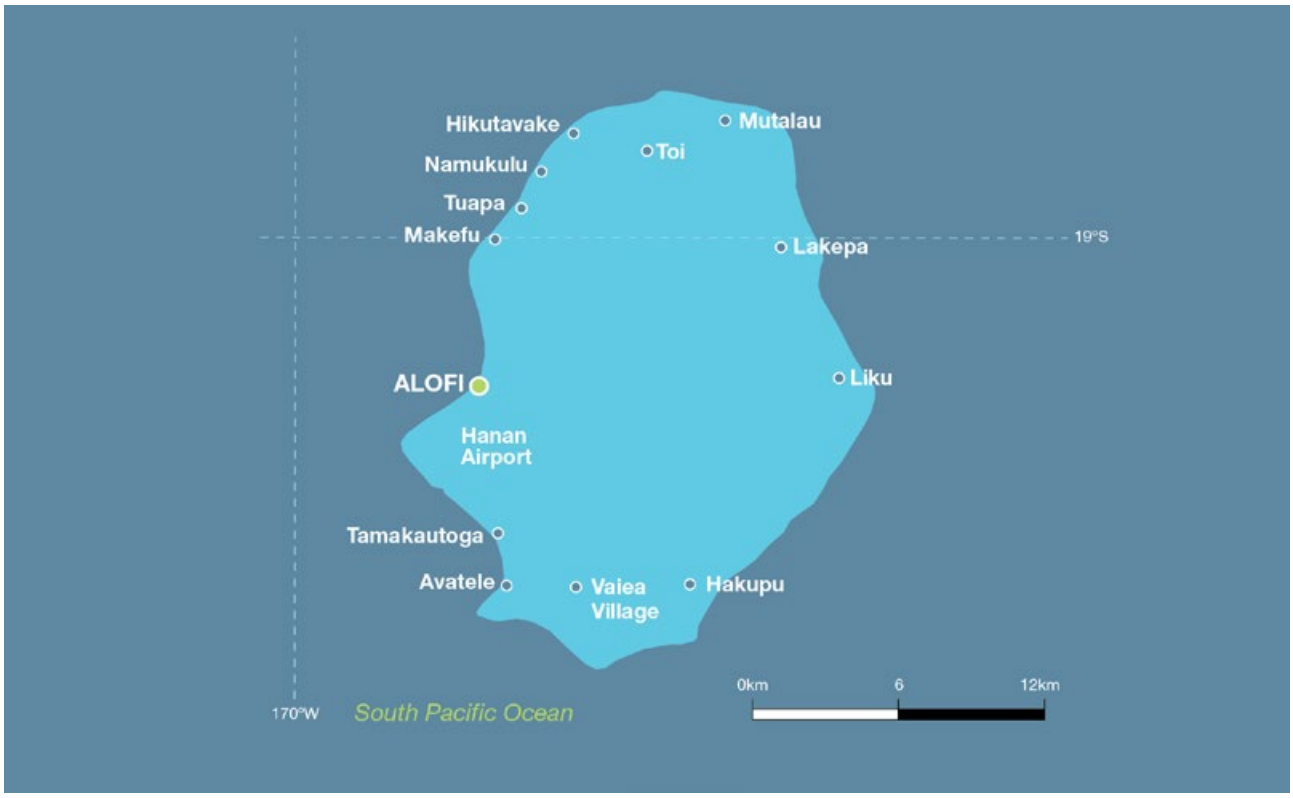

Figure 9.1: Niue

9.3 Data Availability

There are currently two operational meteorological observation stations on Niue. The primary station, where multiple observations are conducted on a daily basis, is located at Hanan Airport, south of Alofi on the western side of the island (Figure 9.1). A single daily observation rainfall station is located at Liku on the eastern side of the island. Observations began at Liku in 1990.

A composite record for Hanan Airport, Alofi and Kaimiti has been used. Observations were taken at Alofi from 1905–1971 and 1977–1996. Between 1971 and 1976 observations were taken at Kaimiti, 2.4 km south of Alofi. The Hanan Airport-Alofi-Kaimiti rainfall and air temperature composite records from 1950–2009 are homogeneous and more than 99% complete.

There are no tide gauge data available for Niue. The Rarotonga (Cook Islands) gauge is the closest available and has been used. Both satellite (from 1993) and in situ sea-level data (1950–2009; termed reconstructed sea level; Volume 1, Section 2.2.2.2) are available on a global 1° x 1° grid.

Long-term locally-monitored sea-surface temperature data are unavailable for Niue, so large-scale gridded sea-surface temperature datasets have been used (HadISST, HadSST2, ERSST and Kaplan Extended SST V2; Volume 1, Table 2.3).

9.4 Seasonal Cycles

Niue has a tropical maritime climate with an average mean temperature of 24°C at Hanan Airport and a seasonal range of just over 4°C between the warmest months (February and March) and the coolest months (July and August) (Figure 9.2). Being a small island, monthly air temperatures in Niue are closely linked to the sea-surface temperatures surrounding the island.

Niue experiences two distinct seasons: a wet season from November to April when the South Pacific Convergence Zone (SPCZ) is closest to the island, and a dry season from May to October when the SPCZ is occasionally inactive and displaced north-eastward. Average annual rainfall for Hanan Airport is 2052 mm.

Niue's climate is also influenced by sub-tropical high pressure systems and trade winds, which blow mainly from the south-east.

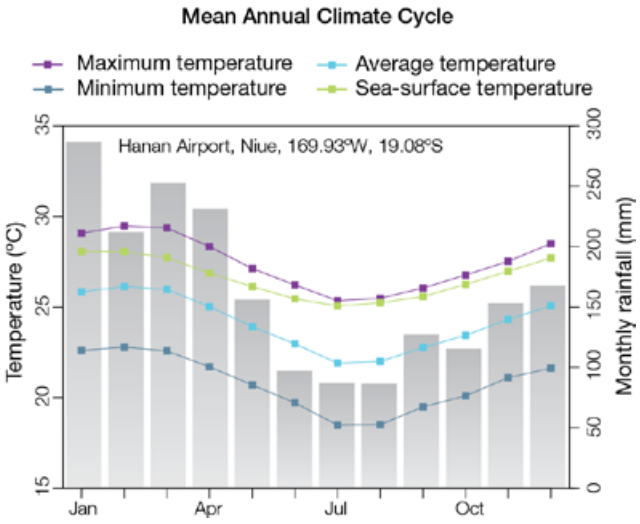

Figure 9.2: Mean annual cycle of rainfall (grey bars) and daily maximum, minimum and mean air temperatures at Hanan Airport, and local sea-surface temperatures derived from the HadISST dataset (Volume 1, Table 2.3).

9.5 Climate Variability

Year-to-year variability in Niue's climate is strongly associated with the El Niño-Southern Oscillation (ENSO). Annual rainfall in the wettest years can be almost four times the rainfall in the driest years. Severe droughts have occurred, with dry season rainfall less than 400 mm, received in 1983, 1991 and 1998, compared with the mean of about 700 mm. The influence of ENSO can be seen in the strong correlation coefficients between Hanan rainfall and ENSO indices (Table 9.1). El Niño events tend to bring below average rainfall, particularly in the wet season, but also cooler conditions during the dry season. The drier conditions in El Niño years are often caused by the SPCZ moving away to the north-east, while in La Niña years the SPCZ moves south-east, bringing more rainfall. ENSO Modoki events (Volume 1, Section 3.4.1) only seem to have an influence on wet season rainfall, but the drier El Niño Modoki and wetter La Niña Modoki events have less of an impact than canonical ENSO events.

Interdecadal variability can be seen in both air temperatures and rainfall at Hanan Airport (Figures 9.3 and 9.4) but the only significant correlation with the Interdecadal Pacific Oscillation (IPO, Table 9.1) is with maximum air temperatures in the wet season.

Table 9.1: Correlation coefficients between indices of key large-scale patterns of climate variability and minimum and maximum temperatures (Tmin and Tmax) and rainfall at Hanan Airport. Only correlation coefficients that are statistically significant at the 95% level are shown.

Climate feature/index		Dry season (May-October)			Wet season (November-April)		
		Tmin	Tmax	Rain	Tmin	Tmax	Rain
ENSO	Niño3.4	-0.37	-0.48	-0.33			-0.61
	Southern Oscillation Index	0.30	0.56	0.30			0.62
Interdecadal Pacific Oscillation Index						0.33	
Southern Annular Mode Index							
ENSO Modoki Index							-0.35
Number of years of data		68	69	100	69	69	103

Training in *Pacific Climate Futures*

9.6 Observed Trends

9.6.1 Air Temperature

Warming trends are evident in both annual and seasonal mean air temperatures at Hanan Airport for the period 1950–2009 (Figure 9.3). The strongest trend is in wet season maximum air temperature, which is more than twice that of minimum air temperature for the same season, and maximum air temperature in the dry season (Table 9.2).

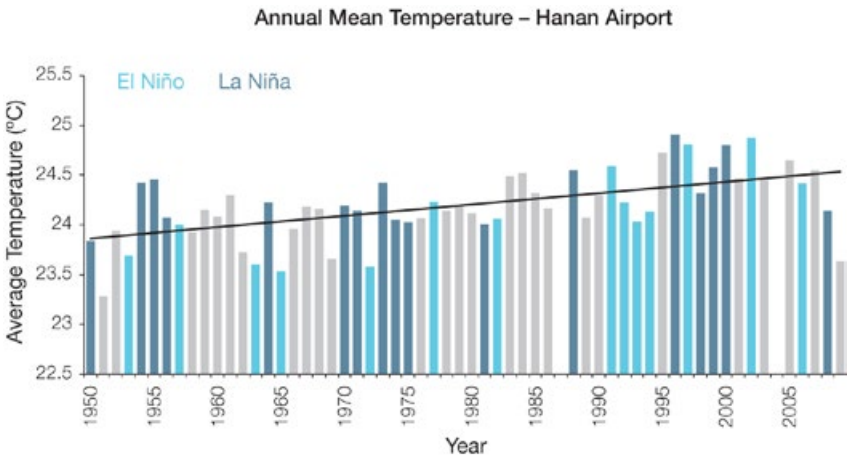

Figure 9.3: Annual mean air temperature at Hanan Airport. Light blue, dark blue and grey bars denote El Niño, La Niña and neutral years respectively.

9.6.2 Rainfall

Annual and seasonal rainfall trends for Hanan Airport for the period 1950–2009 are not statistically significant (Table 9.2 and Figure 9.4).

9.6.3 Extreme Events

The tropical cyclone season in the Niue region is between November and April. Occurrences outside this period are rare. The tropical cyclone archive for the Southern Hemisphere indicates that between the 1969/70 and 2006/07 seasons, the centre of 63 tropical cyclones passed within approximately 400 km of Alofi. This represents an average of 15 cyclones per decade. Tropical cyclones were most frequent in El Niño years (19 per decade) and least frequent in La Niña years (9 per decade). The ENSO-neutral average is 15 cyclones per decade. The interannual variability in the number of tropical cyclones in the vicinity of Alofi is large, ranging from zero in some seasons to five in the 1981/82 and 2002/03 seasons (Figure 9.5). This high variability makes it difficult to identify any long-term trends in frequency of tropical cyclones.

Table 9.2: Annual and seasonal trends in maximum, minimum and mean air temperature (Tmax, Tmin and Tmean) and rainfall at Hanan Airport for the period 1950–2009. Asterisks indicate significance at the 95% level. Persistence is taken into account in the assessment of significance as in Power and Kociuba (in press). The statistical significance of the air temperature trends is not assessed.

	Hanan Airport Tmax (°C per 10 yrs)	Hanan Airport Tmin (°C per 10 yrs)	Hanan Airport Tmean (°C per 10 yrs)	Hanan Airport Rain (mm per 10 yrs)
Annual	+0.15	+0.08	+0.11	+25
Wet season	+0.21	+0.08	+0.15	+4
Dry season	+0.09	+0.09	+0.10	+24

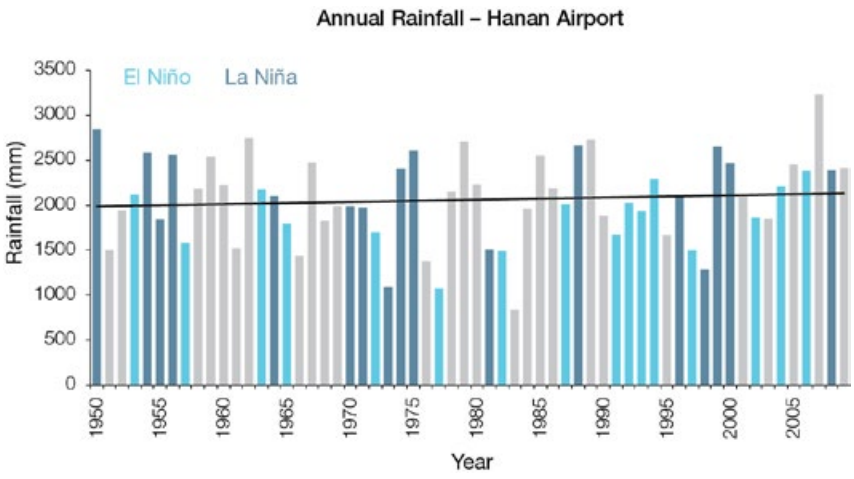

Figure 9.4: Annual rainfall at Hanan Airport. Light blue, dark blue and grey bars denote El Niño, La Niña and neutral years respectively.

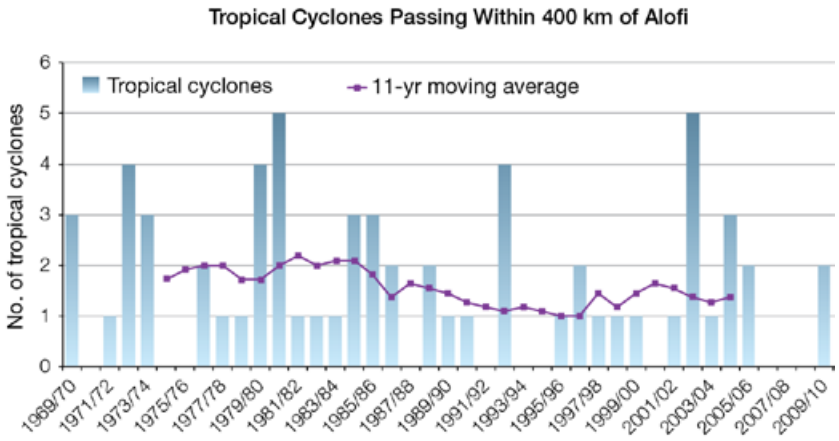

Figure 9.5: Tropical cyclones passing within 400 km of Alofi per season. The 11-year moving average is in purple.

Niue's economy suffered significantly from high winds, storm surge and intense rainfall associated with Tropical Cyclone Heta on 4 January 2004. In total, the storm caused over NZ$37.7 million damage, three times Niue's Gross Domestic Product.

Agriculture is very important to the lifestyle of Niueans and the economy. Nearly all households have plantations of taro. These gardens are mainly rain-fed, making them prone to El Niño associated drought. Conversely, Niue is occasionally affected by prolonged periods of above normal rainfall associated with La Niña, which can result in outbreaks of yam disease (*Yam anthranose*) and mosquito-borne diseases such as dengue fever.

9.6.4 Sea-Surface Temperature

Historical sea-surface temperature changes around Niue show considerable decadal variability. Water temperatures declined slightly around the island from the 1950s to the late 1980s. This was followed by a period of warming (approximately 0.08°C per decade for 1970–present). Figure 9.7 shows the 1950–2000 sea-surface temperature changes (relative to a reference year of 1990) from three different large-scale sea-surface temperature gridded datasets (HadSST2, ERSST and Kaplan Extended SST V2; Volume 1, Table 2.3). At these regional scales, natural variability plays a large role in determining sea-surface temperature, making it difficult to identify long-term trends.

9.6.5 Ocean Acidification

Based the large-scale distribution of coral reefs across the Pacific and the seawater chemistry, Guinotte et al. (2003) suggested that seawater aragonite saturation states above 4 were optimal for coral growth and for the development of healthy reef ecosystems, with values from 3.5 to 4 adequate for coral growth, and values between 3 and 3.5, marginal. Coral reef ecosystems were not found at seawater aragonite saturation states below 3 and these conditions were classified as extremely marginal for supporting coral growth.

In the Niue region, the aragonite saturation state has declined from about 4.5 in the late 18th century to an observed value of about 4.0 ± 0.1 by 2000.

9.6.6 Sea Level

Monthly averages of the historical tide gauge (Rarotonga, Cook Islands; 1977–2001 and 1993–present), satellite (since 1993) and gridded sea-level (since 1950) data agree well after 1993 and indicate interannual variability in sea levels of about 17 cm (estimated 5–95% range) after removal of the seasonal cycle (Figure 9.9). The sea-level rise near Niue measured by satellite altimeters (Figure 9.6) since 1993 is about 5 mm per year, larger than the global average of 3.2 ± 0.4 mm per year. This rise is part of a pattern related to climate variability from year to year and decade to decade (Figure 9.9).

9.6.7 Extreme Sea-Level Events

As there is no tide gauge in Niue, this analysis could not be undertaken.

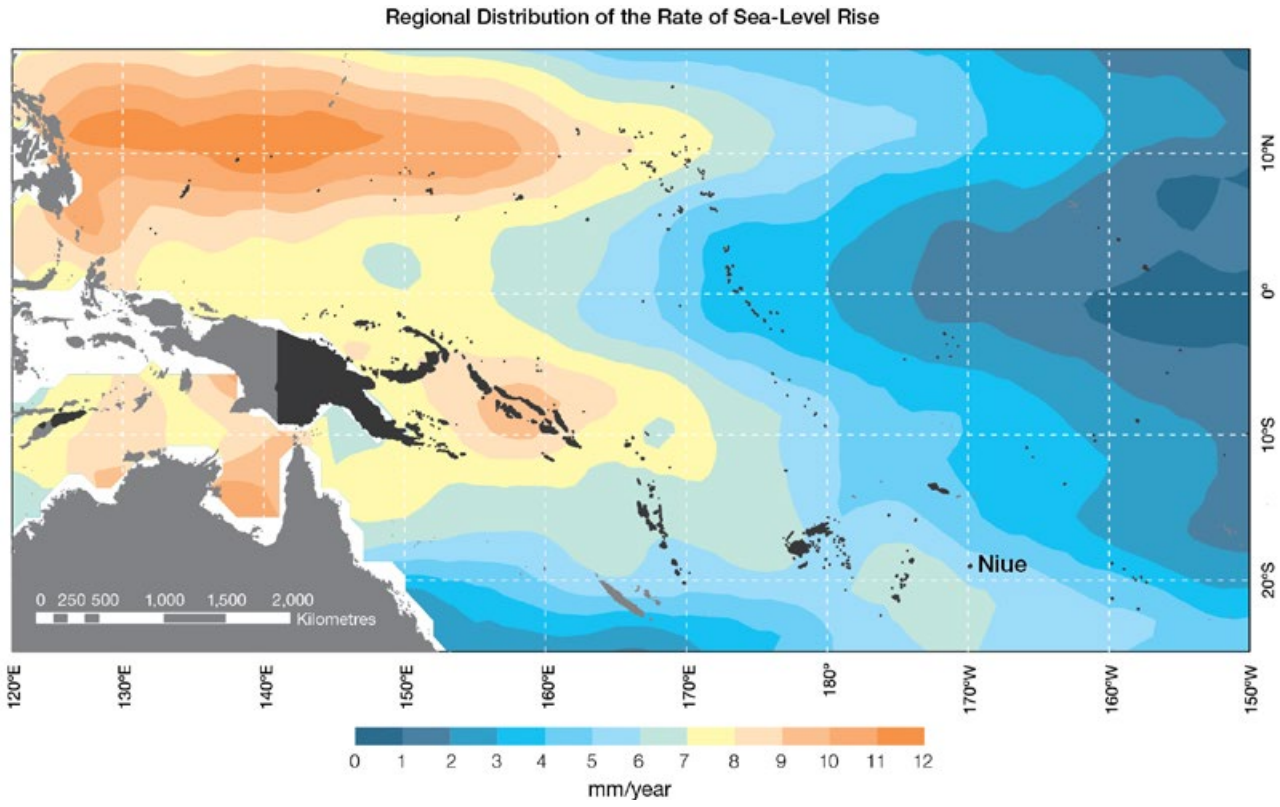

Figure 9.6: The regional distribution of the rate of sea-level rise measured by satellite altimeters from January 1993 to December 2010, with the location of Niue indicated. Further information on regional distribution of sea-level rise is provided in Volume 1, Section 3.6.3.2.

9.7 Climate Projections

Climate projections have been derived from up to 18 global climate models from the CMIP3 database, for up to three emissions scenarios (B1 (low), A1B (medium) and A2 (high)) and three 20-year periods (centred on 2030, 2055 and 2090, relative to 1990). These models were selected based on their ability to reproduce important features of the current climate (Volume 1, Section 5.2.3) so projections from each of the models are plausible representations of the future climate. This means there is not one single projected future for Niue, but rather a range of possible futures. The full range of these futures is discussed in the following sections.

These projections do not represent a value specific to any actual location, such as a town in Niue. Instead, they refer to an average change over the broad geographic region encompassing Niue and the surrounding ocean (Figure 1.1 shows the regional boundaries). Section 1.7 provides important information about interpreting climate model projections.

9.7.1 Temperature

Surface air temperature and sea-surface temperature are projected to continue to increase over the course of the 21st century. There is *very high* confidence in this direction of change because:

- Warming is physically consistent with rising greenhouse gas concentrations.
- All CMIP3 models agree on this direction of change.

The majority of CMIP3 models simulate a slight increase (<1°C) in annual and seasonal mean temperature by 2030, however by 2090 under the A2 (high) emissions scenario temperature increases of greater than 2.5°C are simulated by almost all models (Table 9.3). Given the close relationship between surface air temperature and sea-surface temperature, a similar (or slightly weaker) rate of warming is projected for the surface ocean (Figure 9.7).

There is *moderate* confidence in this range and distribution of possible futures because:

- There is generally a large discrepancy between modelled and observed temperature trends over the past 50 years in the vicinity of Niue, although this may be partly due to limited observational records (Figure 9.7).

Interannual variability in surface air temperature and sea-surface temperature over Niue is strongly influenced by ENSO in the current climate (Section 9.5). As there is no consistency in projections of future ENSO activity (Volume 1, Section 6.4.1) it is not possible to determine whether interannual variability in temperature will change in the future. However, ENSO is expected to continue to be an important source of variability for the region.

9.7.2 Rainfall

Wet Season (November-April)

Wet season rainfall is projected to increase over the course of the 21st century. There is *moderate* confidence in this direction of change because:

- An increase in wet season rainfall is consistent with the projected likely increase intensity of the South Pacific Convergence Zone (SPCZ), which lies over Niue in this season (Volume 1, Section 6.4.5).

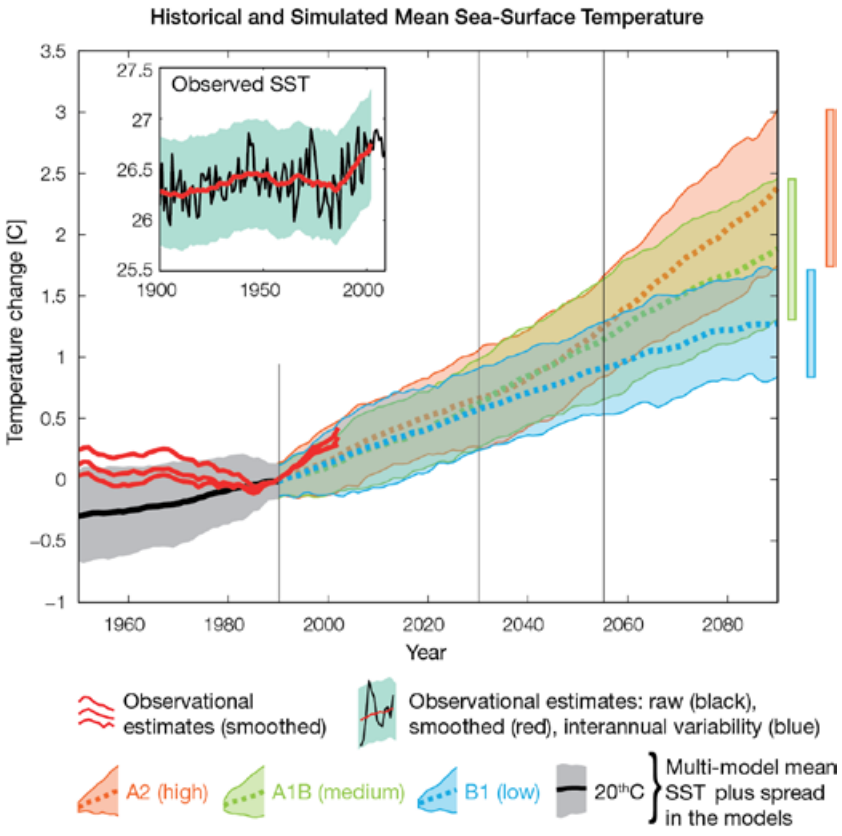

Figure 9.7: Historical climate (from 1950 onwards) and simulated historical and future climate for annual mean sea-surface temperature (SST) in the region surrounding Niue, for the CMIP3 models. Shading represents approximately 95% of the range of model projections (twice the inter-model standard deviation), while the solid lines represent the smoothed (20-year running average) multi-model mean temperature. Projections are calculated relative to the 1980–1999 period (which is why there is a decline in the inter-model standard deviation around 1990). Observational estimates in the main figure (red lines) are derived from the HadSST2, ERSST and Kaplan Extended SST V2 datasets (Volume 1, Section 2.2.2). Annual average (black) and 20-year running average (red) HadSST2 data is also shown inset.

- The majority of CMIP3 models agree on this direction of change by 2090.

The majority of CMIP3 models simulate little change (-5% to 5%) in wet season rainfall by 2030, however by 2090 the majority simulate an increase (>5%), with approximately one third simulating a large increase (>15%) under the A2 (high) emissions scenario (Table 9.3). There is *moderate* confidence in this range and distribution of possible futures because:

- In simulations of the current climate, the CMIP3 models generally locate the SPCZ in the correct location relative to Niue in the wet season (Brown et al., 2011).
- The CMIP3 models are unable to resolve many of the physical processes involved in producing rainfall. As a consequence, they do not simulate rainfall as well as other variables such as temperature (Volume 1, Chapter 5).

Dry Season (May-October)

Little change is projected in dry season rainfall over the course of the 21st century. There is *low* confidence in this direction of change because:

- There is little agreement amongst the models, with approximately equal numbers simulating an increase (>5%), decrease (<-5%) or little change (-5% to 5%) by 2090 across the B1 (low), A1B (medium) and A2 (high) emissions scenarios.
- In simulations of the current climate, some CMIP3 models have an SPCZ that extends too far east during the dry season, with too much rainfall over Niue (Brown et al., 2011).
- The CMIP3 models are unable to resolve many of the physical processes involved in producing rainfall.

Annual

Total annual rainfall is projected to increase over the course of the 21st century. There is *moderate* confidence in this direction of change because:

- Approximately half (A1B (medium) emissions scenario) and the majority (A2 (high) emissions scenario) of CMIP3 models agree on this direction of change by 2090.
- There is moderate and low confidence in wet and dry season rainfall projections respectively, as discussed above.

Interannual variability in rainfall over Niue is strongly influenced by ENSO in the current climate, via the movement of the SPCZ (Section 9.5). As there is no consistency in projections of future ENSO activity (Volume 1, Section 6.4.1) it is not possible to determine whether interannual variability in rainfall will change in the future.

9.7.3 Extremes

Temperature

The intensity and frequency of days of extreme heat are projected to increase over the course of the 21st century. There is *very high* confidence in this direction of change because:

- An increase in the intensity and frequency of days of extreme heat is physically consistent with rising greenhouse gas concentrations.
- All CMIP3 models agree on the direction of change for both intensity and frequency.

The majority of CMIP3 models simulate an increase of approximately 1°C in the temperature experienced on the 1-in-20-year hot day by 2055 under the B1 (low) emissions scenario, with an increase of over 2.5°C simulated by the majority of models by 2090 under the A2 (high) emissions scenario (Table 9.3). There is *low* confidence in this range and distribution of possible futures because:

- In simulations of the current climate, the CMIP3 models tend to underestimate the intensity and frequency of days of extreme heat (Volume 1, Section 5.2.4).
- Smaller increases in the frequency of days of extreme heat are projected by the CCAM 60 km simulations.

Rainfall

The intensity and frequency of days of extreme rainfall are projected to increase over the course of the 21st century. There is *high* confidence in this direction of change because:

- An increase in the frequency and intensity of extreme rainfall is consistent with larger-scale projections, based on the physical argument that the atmosphere is able to hold more water vapour in a warmer climate (Allen and Ingram, 2002; IPCC, 2007). It is also consistent with the projected likely increase in SPCZ intensity (Volume 1, Section 6.4.5).
- Almost all of the CMIP3 models agree on this direction of change for both intensity and frequency.

The majority of CMIP3 models simulate an increase of at least 5 mm in the amount of rain received on the 1-in-20-year wet day by 2055 under the B1 (low) emissions scenario, with an increase of at least 25 mm simulated by 2090 under the A2 (high) emissions scenario. The majority of models project that the current 1-in-20-year extreme rainfall event will occur, on average, two to three times per 20-year period by 2055 under the B1 (low) emissions scenario and three to four times per 20-year period by 2090 under the A2 (high) emissions scenario. There is *low* confidence in this range and distribution of possible futures because:

- In simulations of the current climate, the CMIP3 models tend to underestimate the intensity and frequency of extreme rainfall (Volume 1, Section 5.2.4).
- The CMIP3 models are unable to resolve many of the physical processes involved in producing extreme rainfall.

Drought

Little change is projected in the incidence of drought over the course of the 21st century. There is *low* confidence in this direction of change because:

- There is only low confidence in the range of dry season rainfall projections (Section 9.7.2), which

directly influences projections of future drought conditions.

The majority of CMIP3 models project that the frequency of mild drought will remain approximately stable at six to seven times every 20 years, under all emissions scenarios. The frequency of moderate and severe drought is also projected to remain stable, at once to twice and once every 20 years, respectively

Tropical Cyclones

Tropical cyclone numbers are projected to decline in the south-east Pacific Ocean basin (0–40ºS, 170ºE–130ºW) over the course of the 21st century. There is *moderate* confidence in this direction of change because:

- Many studies suggest a decline in tropical cyclone frequency globally (Knutson et al., 2010).
- Tropical cyclone numbers decline in the south-east Pacific Ocean in the majority assessment techniques.

Based on the direct detection methodologies (Curvature Vorticity Parameter (CVP) and the CSIRO Direct Detection Scheme (CDD) described in Volume 1, Section 4.8.2), 65% of projections show no change or a decrease in tropical cyclone formation when applied to the CMIP3 climate models for which suitable output is available. When these techniques are applied to CCAM, 100% of projections show a decrease in tropical cyclone formation. In addition, the Genesis Potential Index (GPI) empirical technique suggests that conditions for tropical cyclone formation will become less favourable in the south-east Pacific Ocean basin, for all analysed CMIP3 models. There is moderate confidence in this range and distribution of possible futures because in simulations of the current climate, the CVP, CDD and GPI methods capture the frequency of tropical cyclone activity reasonably well (Volume 1, Section 5.4).

Despite this projected reduction in total cyclone numbers, five of the six CCAM 60 km simulations show an increase in the proportion of the most severe cyclones. Most models also indicate a reduction in tropical cyclone wind hazard north of 20ºS latitude and regions of increased hazard south of 20ºS latitude. This increase in wind hazard coincides with a poleward shift in the latitude at which tropical cyclones are most intense.

9.7.4 Ocean Acidification

The acidification of the ocean will continue to increase over the course of the 21st century. There is *very high* confidence in this projection as the rate of ocean acidification is driven primarily by the increasing oceanic uptake of carbon dioxide, in response to rising atmospheric carbon dioxide concentrations.

Projections from all analysed CMIP3 models indicate that the annual maximum aragonite saturation state will reach values below 3.5 by about 2040 and continue to decline thereafter (Figure 9.8; Table 9.3). There is *moderate* confidence in this range and distribution of possible futures because the projections are based on climate models without an explicit representation of the carbon cycle and with relatively low resolution and known regional biases.

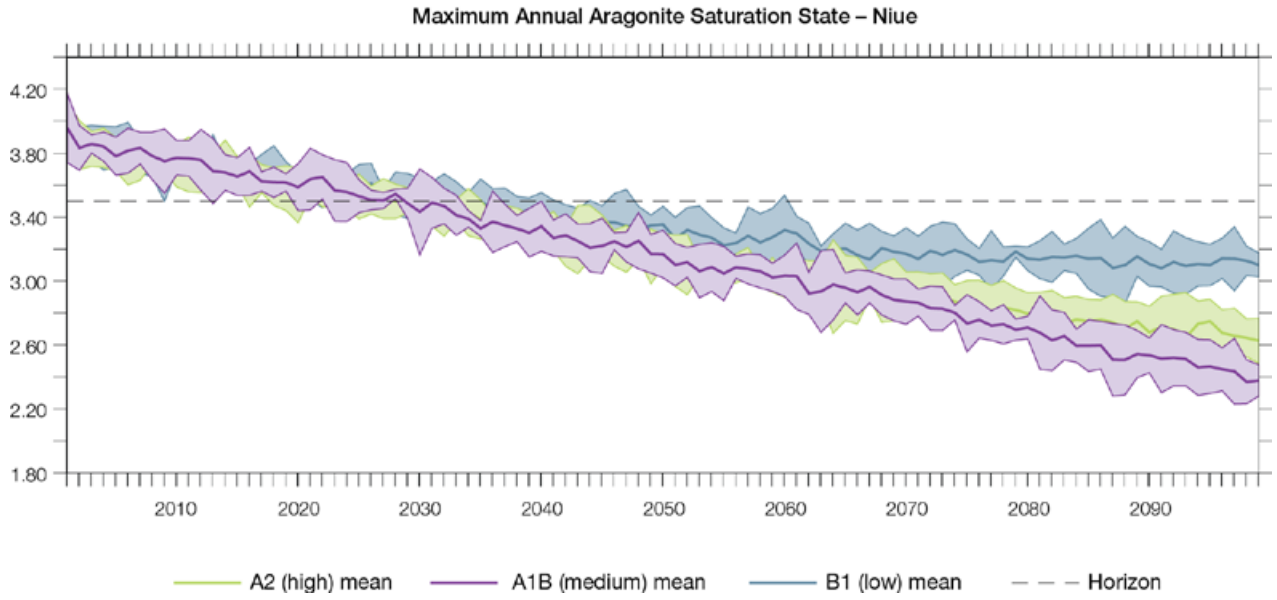

The impact of acidification change on the health of reef ecosystems is likely to be compounded by other stressors including coral bleaching, storm damage and fishing pressure.

Figure 9.8: Multi-model projections, and their associated uncertainty (shaded area represents two standard deviations), of the maximum annual aragonite saturation state in the sea surface waters of Niue under the different emissions scenarios. The dashed black line represents an aragonite saturation state of 3.5.

9.7.5 Sea Level

Mean sea level is projected to continue to rise over the course of the 21st century. There is *very high* confidence in this direction of change because:

- Sea-level rise is a physically consistent response to increasing ocean and atmospheric temperatures, due to thermal expansion of the water and the melting of glaciers and ice caps.
- Projections arising from all CMIP3 models agree on this direction of change.

The CMIP3 models simulate a rise of between approximately 5–15 cm by 2030, with increases of 20–60 cm indicated by 2090 under the higher emissions scenarios (i.e. A2 (high) and A1B (medium); Figure 9.9; Table 9.3). There is *moderate* confidence in this range and distribution of possible futures because:

- There is significant uncertainty surrounding ice-sheet contributions to sea-level rise and a rise larger than projected above cannot be excluded (Meehl et al., 2007b). However, understanding of the processes is currently too limited to provide a best estimate or an upper bound (IPCC, 2007).
- Globally, since the early 1990s, sea level has been rising near the upper end of the above projections. During the 21st century, some studies (using semi-empirical models) project faster rates of sea-level rise.

Interannual variability of sea level will lead to periods of lower and higher regional sea levels. In the past, this interannual variability has been about 17 cm (5–95% range, after removal of the seasonal signal; dashed lines in Figure 9.9 (a)) and it is likely that a similar range will continue through the 21st century. In addition, winds and waves associated with weather phenomena will continue to lead to extreme sea-level events.

In addition to the regional variations in sea level associated with ocean and mass changes, there are ongoing changes in relative sea level associated with changes in surface loading over the last glacial cycle (glacial isostatic adjustment) and local tectonic motions. The glacial isostatic motions are relatively small for the PCCSP region.

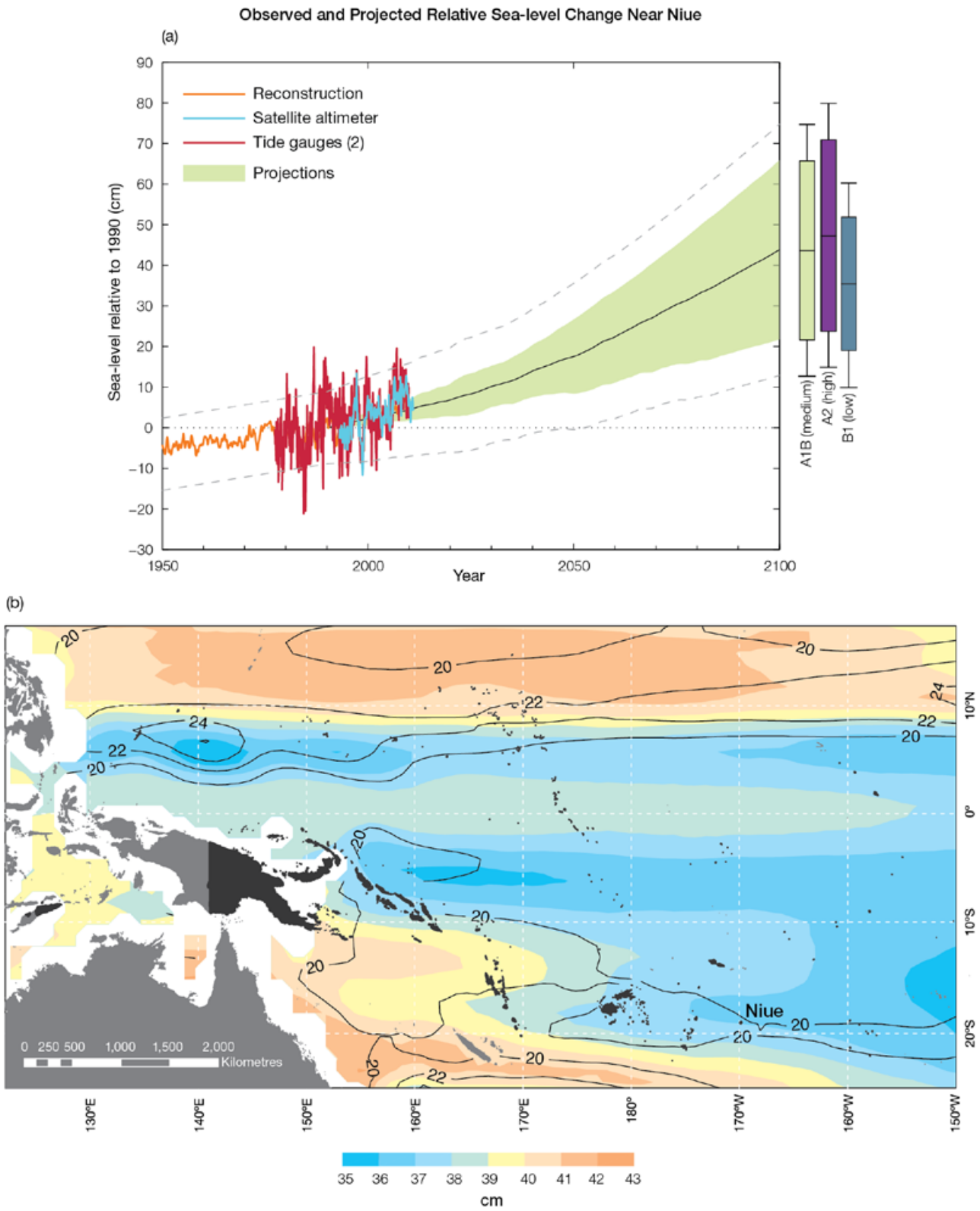

Figure 9.9: Observed and projected relative sea-level change near Niue. (a) The observed in situ relative sea-level records from Rarotonga (Cook Islands) are indicated in red, with the satellite record (since 1993) in light blue. The gridded sea level at Niue (since 1950, from Church and White (in press)) is shown in orange. The projections for the A1B (medium) emissions scenario (5–95% uncertainty range) are shown by the green shaded region from 1990–2100. The range of projections for the B1 (low), A1B (medium) and A2 (high) emissions scenarios by 2100 are also shown by the bars on the right. The dashed lines are an estimate of interannual variability in sea level (5–95% range about the long-term trends) and indicate that individual monthly averages of sea level can be above or below longer-term averages. (b) The projections (in cm) for the A1B (medium) emissions scenario in the Niue region for the average over 2081–2100 relative to 1981–2000 are indicated by the shading, with the estimated uncertainty in the projections indicated by the contours (in cm).

9.7.6 Projections Summary

The projections presented in Section 9.7 are summarised in Table 9.3. For detailed information regarding the various uncertainties associated with the table values, refer to the preceding text in Sections 9.7 and 1.7, in addition to Chapters 5 and 6 in Volume 1. When interpreting the differences between projections for the B1 (low), A1B (medium) and A2 (high) emissions scenarios, it is also important to consider the emissions pathways associated with each scenario (Volume 1, Figure 4.1) and the fact that a slightly different subset of models was available for each (Volume 1, Appendix 1).

Table 9.3: Projected change in the annual and seasonal mean climate for Niue, under the B1 (low; blue), A1B (medium; green) and A2 (high; purple) emissions scenarios. Projections are given for three 20-year periods centred on 2030 (2020–2039), 2055 (2046–2065) and 2090 (2080–2099), relative to 1990 (1980–1999). Values represent the multi-model mean change ± twice the inter-model standard deviation (representing approximately 95% of the range of model projections), except for sea level where the estimated mean change and the 5–95% range are given (as they are derived directly from the Intergovernmental Panel on Climate Change Fourth Assessment Report values). The confidence (Section 1.7.2) associated with the range and distribution of the projections is also given (indicated by the standard deviation and multi-model mean, respectively). See Volume 1, Appendix 1 for a complete listing of CMIP3 models used to derive these projections.

Variable	Season	2030	2055	2090	Confidence
Surface air temperature (°C)	Annual	+0.6 ± 0.4 +0.7 ± 0.5 +0.7 ± 0.4	+1.0 ± 0.5 +1.3 ± 0.6 +1.3 ± 0.4	+1.3 ± 0.6 +2.0 ± 0.8 +2.5 ± 0.7	Moderate
Maximum temperature (°C)	1-in-20-year event	N/A	+1.0 ± 0.7 +1.4 ± 0.6 +1.5 ± 0.6	+1.2 ± 0.7 +2.0 ± 1.0 +2.6 ± 1.4	Low
Minimum temperature (°C)	1-in-20-year event	N/A	+1.2 ± 1.7 +1.5 ± 1.6 +1.5 ± 1.7	+1.4 ± 1.8 +1.9 ± 2.0 +2.2 ± 1.7	Low
Total rainfall (%)*	Annual	+2 ± 15 +1 ± 12 +5 ± 12	+2 ± 11 +5 ± 14 +6 ± 13	+5 ± 13 +5 ± 13 +10 ± 20	Moderate
Wet season rainfall (%)*	November-April	+3 ± 15 +1 ± 12 +5 ± 13	+3 ± 14 +6 ± 15 +7 ± 17	+6 ± 19 +8 ± 17 +14 ± 20	Moderate
Dry season rainfall (%)*	May-October	+1 ± 17 +3 ± 21 +5 ± 13	0 ± 13 +3 ± 21 +5 ± 17	+3 ± 16 +2 ± 22 +4 ± 30	Low
Sea-surface temperature (°C)	Annual	+0.6 ± 0.3 +0.6 ± 0.4 +0.7 ± 0.4	+0.9 ± 0.4 +1.1 ± 0.5 +1.3 ± 0.4	+1.3 ± 0.4 +1.9 ± 0.6 +2.4 ± 0.6	Moderate
Aragonite saturation state (Ωar)	Annual maximum	+3.5 ± 0.1 +3.4 ± 0.1 +3.4 ± 0.1	+3.2 ± 0.1 +3.0 ± 0.1 +3.0 ± 0.1	+3.1 ± 0.1 +2.7 ± 0.2 +2.5 ± 0.2	Moderate
Mean sea level (cm)	Annual	+10 (5–16) +10 (5–15) +10 (4–17)	+18 (10–27) +20 (10–30) +20 (10–30)	+32 (17–46) +38 (19–57) +40 (20–60)	Moderate

*The MIROC3.2(medres) and MIROC3.2(hires) models were eliminated in calculating the rainfall projections, due to their inability to accurately simulate present-day activity of the South Pacific Convergence Zone (Volume 1, Section 5.5.1).

Rock Islands

Chapter 10
Palau

The contributions of Maria Ngemaes, Godwin Sisior and Dirutelchii Ngirengkoi from the Palau National Weather Service Office are gratefully acknowledged

Introduction

This chapter provides a brief description of Palau, its past and present climate as well as projections for the future. The climate observation network and the availability of atmospheric and oceanic data records are outlined. The annual mean climate, seasonal cycles and the influences of large-scale climate features such as the West Pacific Monsoon and patterns of climate variability (e.g. the El Niño-Southern Oscillation) are analysed and discussed. Observed trends and analysis of air temperature, rainfall, extreme events (including tropical cyclones), sea-surface temperature, ocean acidification, mean and extreme sea levels are presented. Projections for air and sea-surface temperature, rainfall, sea level, ocean acidification and extreme events for the 21st century are provided. These projections are presented along with confidence levels based on expert judgement by Pacific Climate Change Science Program (PCCSP) scientists. The chapter concludes with a summary table of projections (Table 10.3). Important background information including an explanation of methods and models is provided in Chapter 1. For definitions of other terms refer to the Glossary.

10.1 Climate Summary

10.1.1 Current Climate

- Air temperatures in Palau show very little seasonal variation with less than 1°C difference between the warmest and coolest months.
- February, March and April are the driest months of the year in Koror, and the main wet season is from May to October.
- Rainfall is influenced by the West Pacific Monsoon, the Intertropical Convergence Zone and Palau's location within the Pacific Warm Pool region.
- Year-to-year variability in Palau's climate is strongly associated with El Niño-Southern Oscillation.
- Warming trends are evident in both annual and seasonal mean air temperatures at Koror for the period 1953–2009.
- Annual and seasonal rainfall trends for Koror for the period 1950–2009 are not statistically significant.
- The sea-level rise measured by satellite altimeters since 1993 is over 0.35 inches (9 mm) per year.
- Tropical cyclones (typhoons) are rare as Palau is south of the main typhoon zone. However, tropical storms and typhoons which pass to the north of Palau occasionally bring heavy rains and strong winds to the Palau Islands.

10.1.2 Future Climate

Over the course of the 21st century:

- Surface air temperature and sea-surface temperature are projected to continue to increase (*very high* confidence).
- Annual and seasonal mean rainfall is projected to increase (*moderate* confidence).
- The intensity and frequency of days of extreme heat are projected to increase (*very high* confidence).
- The intensity and frequency of days of extreme rainfall are projected to increase (*high* confidence).
- The incidence of drought is projected to decrease (*moderate* confidence).
- Tropical cyclone numbers are projected to decline in the tropical North Pacific Ocean basin (0–15ºN, 130ºE –180ºE) (*moderate* confidence).
- Ocean acidification is projected to continue (*very high* confidence).
- Mean sea-level rise is projected to continue (*very high* confidence).

10.2 Country Description

Located between 3°N–9°N and 131°E–135°E, Palau is a small country in the north-west tropical Pacific, 500 miles (800 km) east of the Philippines. There are over 500 islands in Palau most of which are small, uninhabited rock Islands. Total land area is 206 square miles (535 km^2) making Palau one of the smallest nations in the world (Palau's First National Communication under the UNFCCC, 2002).

Palau is divided into 16 states and the estimated population in 2010 was 20 518 (Palau Country Statistics, SOPAC, 2010). About 80% of its population live in Koror (both an island and state) (Office of Environmental Response and Coordination, 2002). Melekeok, on the bigger but less developed island of Babeldaob to the north, replaced Koror as the capital in October 2006.

The economy in Palau consists of tourism, subsistence agriculture and fishing and is relatively large when compared with other countries in Micronesia (Palau's Pacific Adaptations to Climate Change, 2010).

Figure 10.1: Palau

10.3 Data Availability

Palau has five operational meteorological observation stations. Multiple observations within a 24-hour period are taken at Koror and at the Palau International Airport. Climate observations are taken once a day at Kayangel, Nekken and Peleliu. Data are available for Koror (Figure 10.1) from 1948 for rainfall and 1953 for air temperature. Data from 1950 have been used. Koror data are homogeneous and more than 95% complete.

Monthly-averaged sea-level data are available from 1969 at Malakal-B (1969–present). Both satellite (from 1993) and in situ sea-level data (1950–2009; termed reconstructed sea level; Volume 1, Section 2.2.2.2) are available on a global 1° x 1° grid.

Long-term locally-monitored sea-surface temperature data are unavailable for Palau, so large-scale gridded sea-surface temperature datasets have been used (HadISST, HadSST2, ERSST and Kaplan Extended SST V2; Volume 1, Table 2.3).

10.4 Seasonal Cycles

Temperatures in Palau have very little seasonal variation. In Koror (Figure 10.2) the mean daily air temperature is about 82ºF (28°C) throughout the year and there is only a 1.5ºF (0.8°C) difference between the hottest and coolest month. The average relative humidity is 82%. Being on a small island surrounded by ocean, air temperatures in Koror are closely related to the sea-surface temperatures (Figure 10.2).

February, March and April are the driest months in Koror (Figure 10.2), and the main wet season is from May to October. The West Pacific Monsoon is usually most active and brings heavy rainfall between June and August. Average rainfall remains above 8 inches (200 mm) in all months of the year due to the Palau's location within the West Pacific Warm Pool and the year-long influence of the Intertropical Convergence Zone (ITCZ). Winds are generally moderate, and the north-easterly trades prevail from December through to March. During April, the frequency of trade winds decreases, and there is an increase in frequency of easterly winds. In May, the winds are predominantly from south-east to north-east.

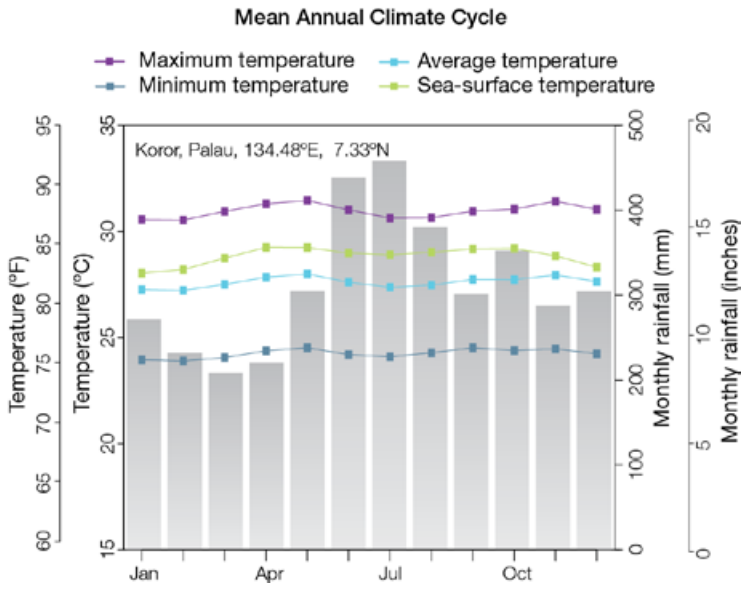

Figure 10.2: Mean annual cycle of rainfall (grey bars) and daily maximum, minimum and mean air temperatures at Koror, and local sea-surface temperatures derived from the HadISST dataset (Volume 1, Table 2.3).

10.5 Climate Variability

The interannual variability in rainfall at Koror is high and is mainly influenced by the El Niño-Southern Oscillation (ENSO). Generally, El Niño years are drier than average and La Niña years are wetter (Figure 10.4). A shortened wet season is usual for Koror during El Niño and prolonged wet season is normal during La Niña years. The dry season can extend to a six-month period with little rainfall during El Niño so the dry season rainfall amounts are much lower (see the correlation coefficients with ENSO indices in Table 10.1). This can lead to water rationing, as was the case during El Niño events in 1997/98 and the first half of 2010. During the El Niño event in 2002, however, the drought was not as severe and no water restrictions were required.

ENSO also influences air temperatures in Koror during the wet season (Table 10.1). In El Niño years wet season minimum air temperatures are usually above average while maximum air temperatures are below average.

ENSO Modoki events (Volume 1, Section 3.4.1) have similar impacts to canonical ENSO events, although the relationship is generally weaker for Modoki events (Table 10.1).

Table 10.1: Correlation coefficients between indices of key large-scale patterns of climate variability and minimum and maximum temperatures (Tmin and Tmax) and rainfall at Koror. Only correlation coefficients that are statistically significant at the 95% level are shown.

Climate feature/index		Wet season (May-October)			Dry season (November-April)		
		Tmin	Tmax	Rain	Tmin	Tmax	Rain
ENSO	Niño3.4	0.50	-0.28				-0.76
	Southern Oscillation Index	-0.38	0.41				0.70
Interdecadal Pacific Oscillation Index							
ENSO Modoki Index		0.36	-0.32				-0.41
Number of years of data		53	53	61	53	53	60

Training in *Pacific Climate Futures*, Palau National Weather Service

10.6 Observed Trends

10.6.1 Air Temperature

Warming trends are evident in both annual and seasonal mean air temperatures at Koror for the period 1953–2009 (Figure 10.3). Stronger mean air temperature trends are found in the dry season (November-April) when compared with the wet season (May-October) (Table 10.2).

10.6.2 Rainfall

Annual and seasonal rainfall trends for Koror for the period 1950–2009 are not statistically significant (Table 10.2 and Figure 10.4).

10.6.3 Extreme Events

Tropical cyclones (typhoons) are rare, as Palau is south of the main typhoon zone. However, tropical storms and typhoons which pass to the north of Palau occasionally bring heavy rains and strong winds to the Palau Islands. Typically, if a large typhoon or tropical storm passes between Guam and Yap (Federated States of Micronesia), a heavy swell is generated that may have sufficient strength to damage reefs.

10.6.4 Sea-Surface Temperature

Historical sea-surface temperature changes around Palau are consistent with the broad-scale sea-surface temperature changes for the PCCSP region. Water temperatures remained relatively constant from the 1950s to the late 1980s (although there is some disagreement between datasets). This was followed by a period of more rapid warming (approximately 0.23°F (0.13°C) per decade for 1970–present). Figure 10.6 shows the 1950–2000 sea-surface temperature changes (relative to a reference year of 1990) from three different large-scale sea-surface temperature gridded datasets (HadSST2, ERSST and Kaplan Extended SST V2; Volume 1, Table 2.3). At these regional scales, natural variability may play a large role in determining the sea-surface temperature making it difficult to identify any long-term trends.

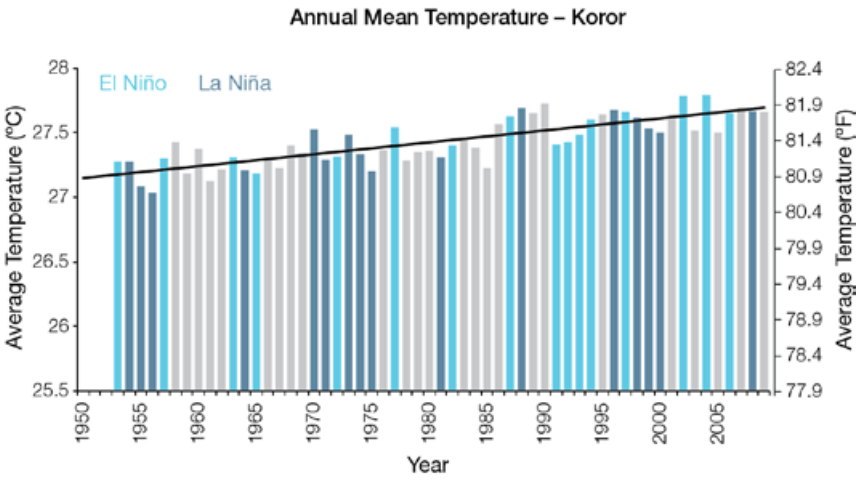

Figure 10.3: Annual mean air temperature at Koror. Light blue, dark blue and grey bars denote El Niño, La Niña and neutral years respectively.

Table 10.2: Annual and seasonal trends in maximum, minimum and mean air temperature (Tmax, Tmin and Tmean; 1953–2009) and rainfall (1950–2009) at Koror. Asterisks indicate significance at the 95% level. Persistence is taken into account in the assessment of significance as in Power and Kociuba (in press). The statistical significance of the air temperature trends is not assessed.

	Koror Tmax °F per 10 yrs (°C per 10 yrs)	Koror Tmin °F per 10 yrs (°C per 10 yrs)	Koror Tmean °F per 10 yrs (°C per 10 yrs)	Koror Rain inches per 10 yrs (mm per 10 yrs)
Annual	+0.19 (+0.11)	+0.14 (+0.08)	+0.17 (+0.09)	+0.21 (+5)
Wet season	+0.11 (+0.06)	+0.13 (+0.07)	+0.12 (+0.07)	-0.52 (-13)
Dry season	+0.29 (+0.16)	+0.16 (+0.09)	+0.22 (+0.12)	+0.87 (+22)

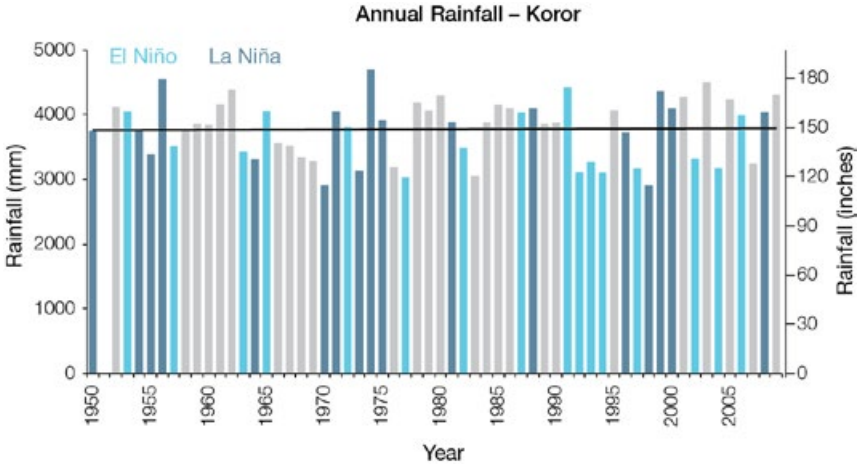

Figure 10.4: Annual rainfall for Koror. Light blue, dark blue and grey bars denote El Niño, La Niña and neutral years respectively.

10.6.5 Ocean Acidification

Based the large-scale distribution of coral reefs across the Pacific and the seawater chemistry, Guinotte et al. (2003) suggested that seawater aragonite saturation states above 4 were optimal for coral growth and for the development of healthy reef ecosystems, with values from 3.5 to 4 adequate for coral growth, and values between 3 and 3.5, marginal. Coral reef ecosystems were not found at seawater aragonite saturation states below 3 and these conditions were classified as extremely marginal for supporting coral growth.

In the Palau region, the aragonite saturation state has declined from about 4.5 in the late 18th century to an observed value of about 3.9 ± 0.1 by 2000.

10.6.6 Sea Level

Monthly averages of the historical tide gauge (since 1969), satellite (since 1993) and gridded sea-level (since 1950) data agree well after 1993 and indicate interannual variability in sea levels of about 14 inches (36 cm) (estimated 5–95% range) after removal of the seasonal cycle (Figure 10.9).

The sea-level rise near Palau measured by satellite altimeters (Figure 10.5) since 1993 is over 0.3 inches (9 mm) per year, larger than the global average of 0.125 ± 0.015 inches (3.2 ± 0.4 mm) per year. This rise is partly linked to a pattern related to climate variability from year to year and decade to decade (Figure 10.9).

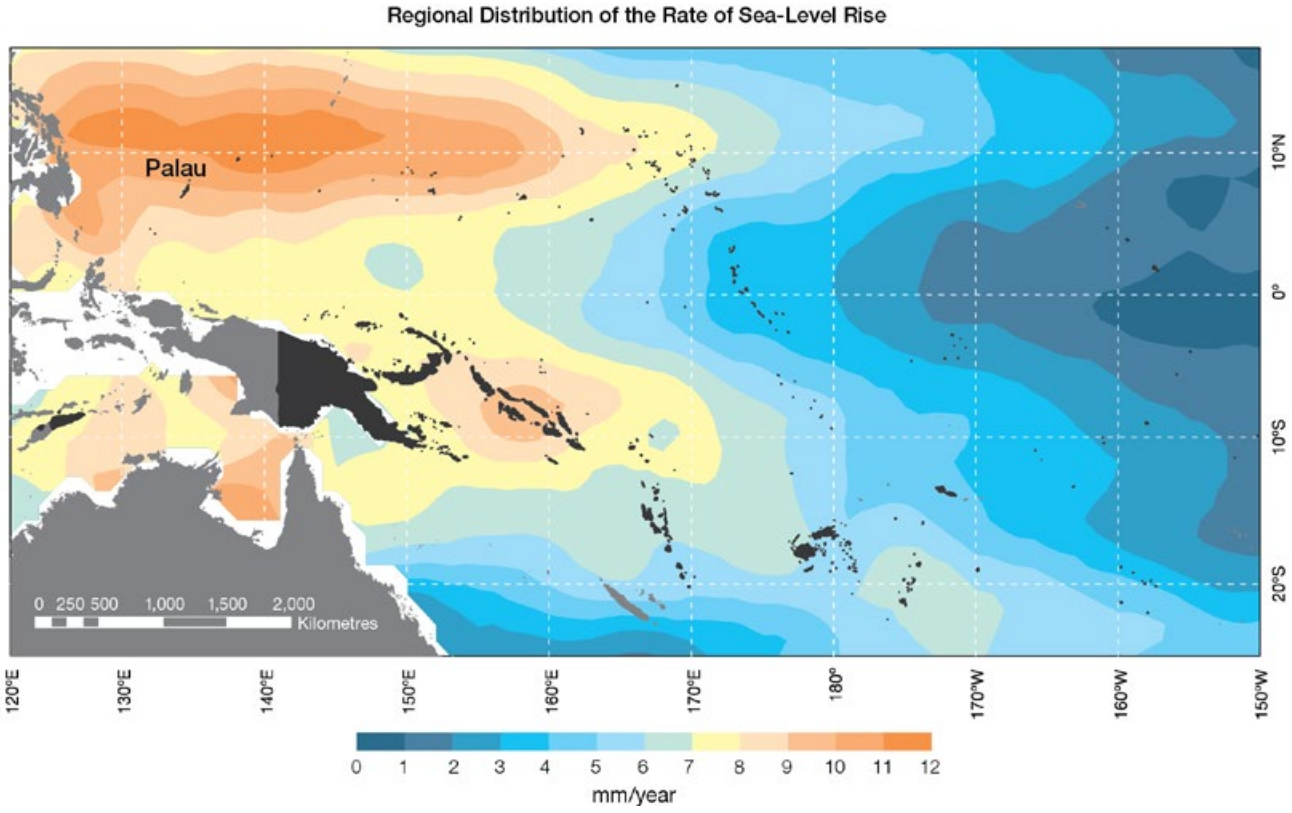

Figure 10.5: The regional distribution of the rate of sea-level rise measured by satellite altimeters from January 1993 to December 2010, with the location of Palau indicated. Further detail about the regional distribution of sea-level rise is provided in Volume 1, Section 3.6.3.2.

10.6.7 Extreme Sea-Level Events

The annual climatology of the highest daily sea levels has been evaluated from hourly measurements by tide gauges at Malakal Harbor, Palau (Figure 10.6). Highest tides tend to occur around the equinoxes, with the September peak the larger of the two. The average seasonal cycle shows little variation throughout the year. However, there is a strong ENSO influence with sea levels higher by over 0.3 ft (0.1 m) during La Niña years and the increase is most pronounced from July to January. The short-term components show little variation throughout the year and exhibit a small increase during La Niña years in January and February. The seasonal and tidal components combine to create a highest likelihood of extreme water levels from August through October. Five of the top 10 water levels recorded at Malakal cluster around the September maximum in tidal levels, indicating the strong influence of tides on extreme sea level occurrence, however, the remaining five are spread throughout the remainder of the year. Six of the 10 extreme events occurred during La Niña conditions, with the remaining four occurring during ENSO-neutral conditions, indicating the additional influence of ENSO on seasonal sea levels.

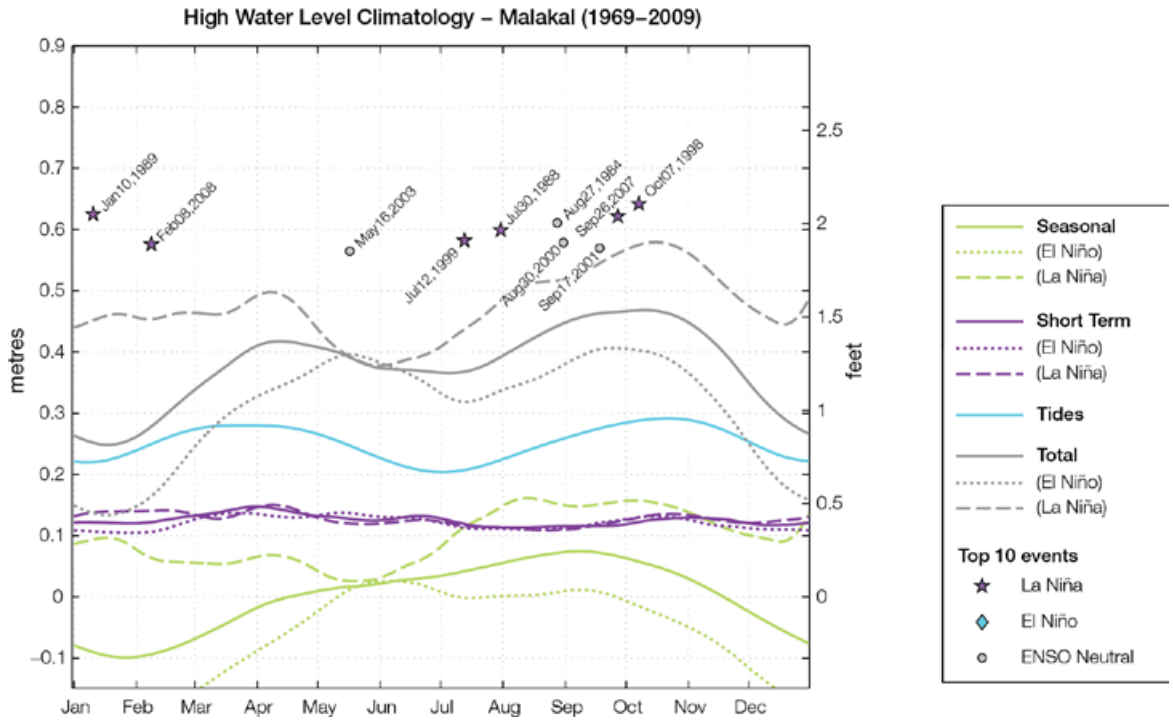

Figure 10.6: The annual cycle of high waters relative to Mean Higher High Water (MHHW) due to tides, short-term fluctuations (most likely associated with storms) and seasonal variations for Palau. The tides and short-term fluctuations are respectively the 95% exceedence of the astronomical high tides relative to MHHW and short-term sea level fluctuations. Components computed only for El Niño and La Niña years are shown by dotted and dashed lines, and grey lines are the sum of the tide, short-term and seasonal components. The 10 highest sea-level events in the record relative to MHHW are shown and coded to indicate the phase of ENSO at the time of the extreme event.

10.7 Climate Projections

Climate projections have been derived from up to 18 global climate models from the CMIP3 database, for up to three emissions scenarios (B1 (low), A1B (medium) and A2 (high)) and three 20-year periods (centred on 2030, 2055 and 2090, relative to 1990). These models were selected based on their ability to reproduce important features of the current climate (Volume 1, Section 5.2.3), so projections from each of the models are plausible representations of the future climate. This means there is not one single projected future for Palau, but rather a range of possible futures. The full range of these futures is discussed in the following sections.

These projections do not represent a value specific to any actual location, such as a town in Palau. Instead, they refer to an average change over the broad geographic region encompassing the islands of Palau and the surrounding ocean (Figure 1.1 shows the regional boundaries). Section 1.7 provides important information about understanding climate model projections.

10.7.1 Temperature

Surface air temperature and sea-surface temperature are projected to continue to increase over the course of the 21st century. There is *very high* confidence in this direction of change because:

- Warming is physically consistent with rising greenhouse gas concentrations.
- All CMIP3 models agree on this direction of change.

The majority of CMIP3 models simulate a slight increase (<1.8°F; <1°C) in annual and seasonal mean temperature by 2030, however by 2090 under the A2 (high) emissions scenario temperature increases of greater than 4.5°F (2.5°C) are simulated by almost all models (Table 10.3). Given the close relationship between surface air temperature and sea-surface temperature, a similar (or slightly weaker) rate of warming is projected for the surface ocean (Figure 10.7). There is *high* confidence in this range and distribution of possible futures because:

- There is generally close agreement between modelled and observed temperature trends over the past 50 years in the vicinity of Palau, although observational records are limited (Figure 10.7).

Interannual variability in surface air temperature and sea-surface temperature over Palau is strongly influenced by El Niño-Southern Oscillation (ENSO) in the current climate (Section 10.5). As there is no consistency in projections of future ENSO activity (Volume 1, Section 6.4.1) it is not possible to determine whether interannual variability in temperature will change in the future. However, ENSO is expected to continue to be an important source of variability for the region.

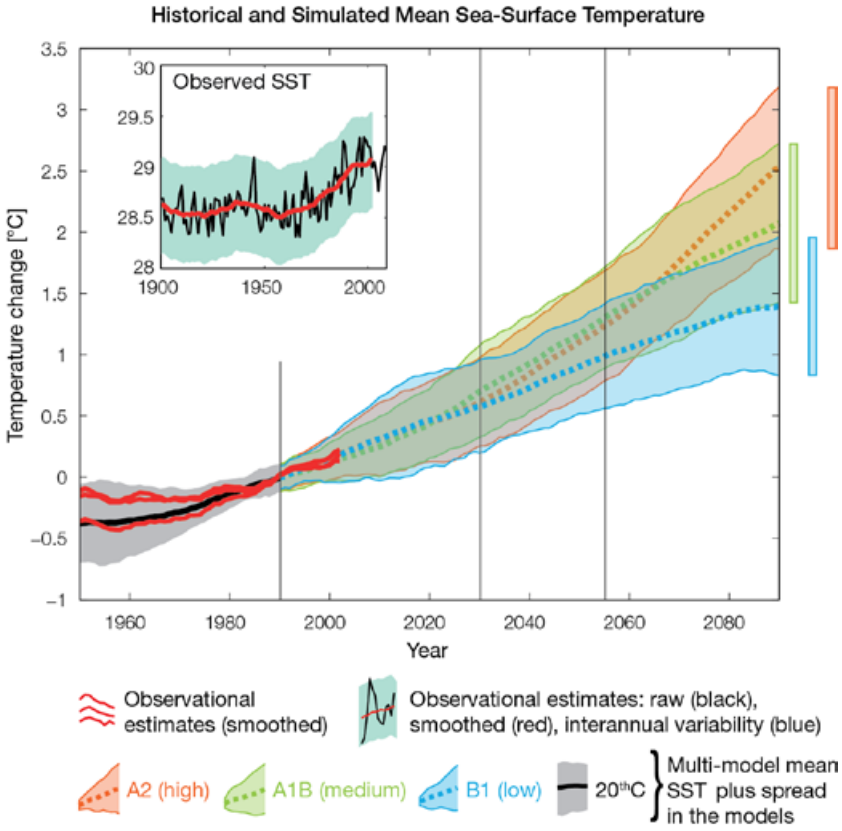

Figure 10.7: Historical climate (from 1950 onwards) and simulated historical and future climate for annual mean sea-surface temperature (SST) in the region surrounding Palau, for the CMIP3 models. Shading represents approximately 95% of the range of model projections (twice the inter-model standard deviation), while the solid lines represent the smoothed (20-year running average) multi-model mean temperature. Projections are calculated relative to the 1980–1999 period (which is why there is a decline in the inter-model standard deviation around 1990). Observational estimates in the main figure (red lines) are derived from the HadSST2, ERSST and Kaplan Extended SST V2 datasets (Volume 1, Section 2.2.2). Annual average (black) and 20-year running average (red) HadSST2 data is also shown inset.

10.7.2 Rainfall

Wet season (May-October), dry season (November-April) and annual average rainfall are projected to increase over the course of the 21st century. There is *moderate* confidence in this direction of change because:

- Physical arguments indicate that rainfall will increase in the equatorial Pacific in a warmer climate (IPCC, 2007; Volume 1, Section 6.4.3).
- Approximately half of the CMIP3 models agree on this direction of change by 2090.

The majority of CMIP3 models simulate little change (-5% to 5%) in rainfall by 2030, however by 2090 the models tend to be equally divided between an increase (>5%) and little change, with very few models simulating a decrease (<-5%) (Table 10.3). There is *moderate* confidence in this range and distribution of possible futures because:

- In simulations of the current climate, the CMIP3 models broadly capture the influence of the West Pacific Monsoon and Intertropical Convergence Zone on the rainfall in Palau (Volume 1, Sections 5.2.3.4 and 5.2.3.5), although most models produce monsoon westerly winds that do not extend far enough east into the Pacific basin.
- The CMIP3 models are unable to resolve many of the physical processes involved in producing rainfall. As a consequence, they do not simulate rainfall as well as other variables such as temperature (Volume 1, Chapter 5).

Interannual variability in rainfall over Palau is strongly influenced by ENSO in the current climate (Section 10.5). As there is no consistency in projections of future ENSO activity (Volume 1, Section 6.4.1), it is not possible to determine whether interannual variability in rainfall will change in the future.

10.7.3 Extremes

Temperature

The intensity and frequency of days of extreme heat are projected to increase over the course of the 21st century. There is *very high* confidence in this direction of change because:

- An increase in the intensity and frequency of days of extreme heat is physically consistent with rising greenhouse gas concentrations.
- All CMIP3 models agree on the direction of change for both intensity and frequency.

The majority of CMIP3 models simulate an increase of approximately 1.8°F (1°C) in the temperature experienced on the 1-in-20-year hot day by 2055 under the B1 (low) emissions scenario, with an increase of over 4.5°F (2.5°C) simulated by the majority of models by 2090 under the A2 (high) emissions scenario (Table 10.3). There is *low* confidence in this range and distribution of possible futures because:

- In simulations of the current climate, the CMIP3 models tend to underestimate the intensity and frequency of days of extreme heat (Volume 1, Section 5.2.4).
- Smaller increases in the frequency of days of extreme heat are projected by the CCAM 60 km simulations.

Rainfall

The intensity and frequency of days of extreme rainfall are projected to increase over the course of the 21st century. There is *high* confidence in this direction of change because:

- An increase in the frequency and intensity of extreme rainfall is consistent with larger-scale projections, based on the physical argument that the atmosphere is able to hold more water vapour in a warmer climate (Allen and Ingram, 2002; IPCC, 2007). It is also consistent with physical arguments that rainfall will increase in the deep tropical Pacific in a warmer climate (IPCC, 2007; Volume 1, Section 6.4.3).
- Almost all of the CMIP3 models agree on this direction of change for both intensity and frequency.

The majority of CMIP3 models simulate an increase of at least 0.4 inches (10 mm) in the amount of rain received on the 1-in-20-year wet day by 2055 under the B1 (low) emissions scenario, with an increase of at least 0.8 inches (20 mm) simulated by 2090 under the A2 (high) emissions scenario. The majority of models project that the current 1-in-20-year extreme rainfall event will occur, on average, two to three times per 20-year period by 2055 under the B1 (low) emissions scenario and four times per 20-year period by 2090 under the A2 (high) emissions scenario. There is *low* confidence in this range and distribution of possible futures because:

- In simulations of the current climate, the CMIP3 models tend to underestimate the intensity and frequency of extreme rainfall (Volume 1, Section 5.2.4).
- The CMIP3 models are unable to resolve many of the physical processes involved in producing extreme rainfall.

Drought

The incidence of drought is projected to decrease over the course of the 21st century. There is *moderate* confidence in this direction of change because:

- A decrease in drought is consistent with projections of increased rainfall (Section 10.7.2).
- The majority of models agree on this direction of change for most drought categories.

The majority of CMIP3 models project that mild drought will occur approximately seven to eight times every 20 years in 2030 under all emissions scenarios, decreasing to six to seven times by 2090. The frequency of moderate drought is projected to decrease from once to twice every 20 years in 2030, to once every 20 years in 2090 for all emissions scenarios, while the majority of CMIP3 models project that severe droughts

will occur less than once every 20 years across all time periods and scenarios. There is *low* confidence in this range and distribution of possible futures because:

- There is only moderate confidence in the range of rainfall projections (Section 10.7.2), which directly influences projections of future drought conditions.

Tropical Cyclones (Typhoons)

Tropical cyclone numbers are projected to decline in the tropical North Pacific Ocean basin (0–15ºS, 130ºE–180ºE) over the course of the 21st century. There is *moderate* confidence in this direction of change because:

- Many studies suggest a decline in tropical cyclone frequency globally (Knutson et al., 2010).
- Tropical cyclone numbers decline in the tropical North Pacific Ocean basin in the majority assessment techniques.

Based on the direct detection methodologies (Curvature Vorticity Parameter (CVP) and the CSIRO Direct Detection Scheme (CDD) described in Volume 1, Section 4.8.2), 80% of projections show no change or a decrease in tropical cyclone formation when applied to the CMIP3 climate models for which suitable output is available. When these techniques are applied to CCAM, 100% of projections show a decrease in tropical cyclone formation. In addition, the Genesis Potential Index (GPI) empirical technique suggests that conditions for tropical cyclone formation will become less favourable in the North Pacific Ocean basin, for the majority (70%) of analysed CMIP3 models. There is *moderate* confidence in this range and distribution of possible futures because:

- In simulations of the current climate, the CVP, CDD and GPI methods capture the frequency of tropical cyclone activity reasonably well (Volume 1, Section 5.4).

Consistent with this projected reduction in total cyclone numbers, five of the six 60 km CCAM simulations also show a decrease in the proportion of the most severe storms (those stronger than the current climate 90th percentile storm maximum wind speed). Most simulations project an increase in the proportion of storms occurring in the weaker categories. Associated with this is a reduction in cyclonic wind hazard.

10.7.4 Ocean Acidification

The acidification of the ocean will continue to increase over the course of the 21st century. There is *very high* confidence in this projection as the rate of ocean acidification is driven primarily by the increasing oceanic uptake of carbon dioxide, in response to rising atmospheric carbon dioxide concentrations.

Projections from all analysed CMIP3 models indicate that the annual maximum aragonite saturation state will reach values below 3.5 by about 2040 and continue to decline thereafter (Figure 10.8; Table 10.3). There is *moderate* confidence in this range and distribution of possible futures because the projections are based on climate models without an explicit representation of the carbon cycle and with relatively low resolution and known regional biases.

The impact of acidification change on the health of reef ecosystems is likely to be compounded by other stressors including coral bleaching, storm damage and fishing pressure.

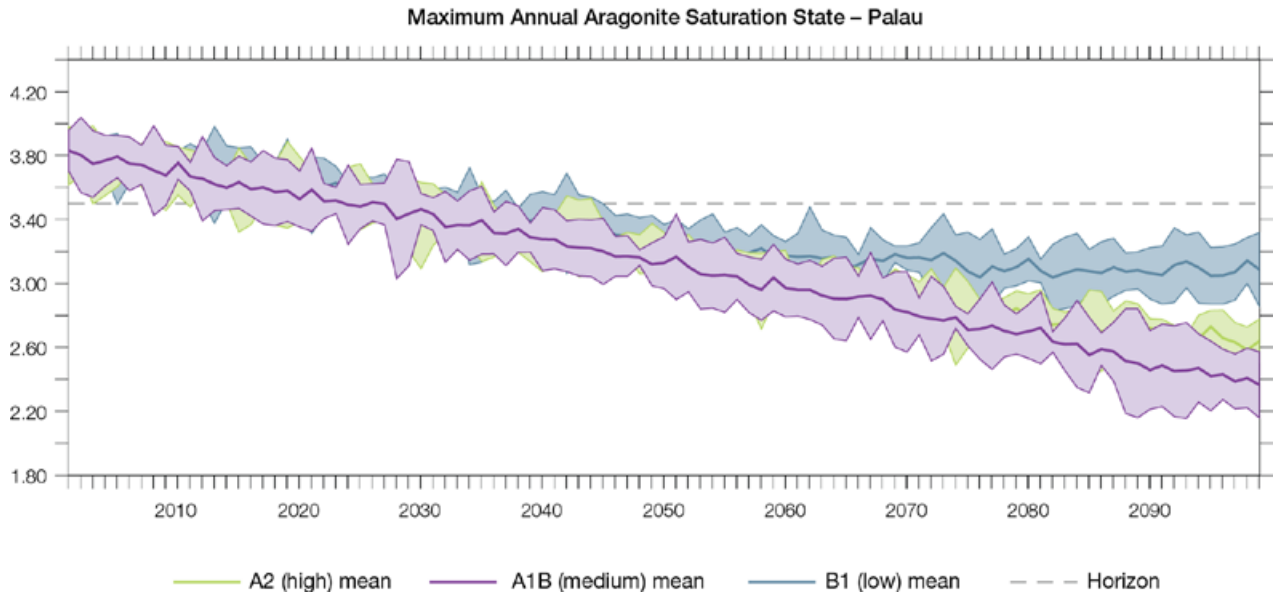

Figure 10.8: Multi-model projections, and their associated uncertainty (shaded area represents two standard deviations), of the maximum annual aragonite saturation state in the sea surface waters of the Palau region under the different emissions scenarios. The dashed black line represents an aragonite saturation state of 3.5.

10.7.5 Sea Level

Mean sea level is projected to continue to rise over the course of the 21st century. There is *very high* confidence in this direction of change because:

- Sea-level rise is a physically consistent response to increasing ocean and atmospheric temperatures, due to thermal expansion of the water and the melting of glaciers and ice caps.
- Projections arising from all CMIP3 models agree on this direction of change.

The CMIP3 models simulate a rise of between approximately 5–15 cm by 2030, with increases of 20–60 cm indicated by 2090 under the higher emissions scenarios (i.e. A2 (high), A1B (medium); Figure 10.9; Table 10.3). There is *moderate* confidence in this range and distribution of possible futures because:

- There is significant uncertainty surrounding ice-sheet contributions to sea-level rise and a rise larger than projected cannot be excluded (Meehl et al., 2007b). However, understanding of the processes is currently too limited to provide a best estimate or an upper bound (IPCC, 2007).
- Globally, since the early 1990s, sea level has been rising near the upper end of the these projections. During the 21st century, some studies (using semi-empirical models) project faster rates of sea-level rise.

Interannual variability of sea level will lead to periods of lower and higher regional sea levels. In the past, this interannual variability has been about 36 cm (5–95% range, after removal of the seasonal signal; dashed lines in Figure 10.9 (a)) and it is likely that a similar range will continue through the 21st century. In addition, winds and waves associated with weather phenomena will continue to lead to extreme sea-level events.

In addition to the regional variations in sea level associated with ocean and mass changes, there are ongoing changes in relative sea level associated with changes in surface loading over the last glacial cycle (glacial isostatic adjustment) and local tectonic motions. The glacial isostatic motions are relatively small for the PCCSP region.

10.7.6 Projections Summary

The projections presented in Section 10.7 are summarised in Table 10.3. For detailed information regarding the various uncertainties associated with the table values, refer to the preceding text in Sections 10.7 and 1.7, in addition to Chapters 5 and 6 in Volume 1. When interpreting the differences between projections for the B1 (low), A1B (medium) and A2 (high) emissions scenarios, it is also important to consider the emissions pathways associated with each scenario (Volume 1, Figure 4.1) and the fact that a slightly different subset of models was available for each (Volume 1, Appendix 1).

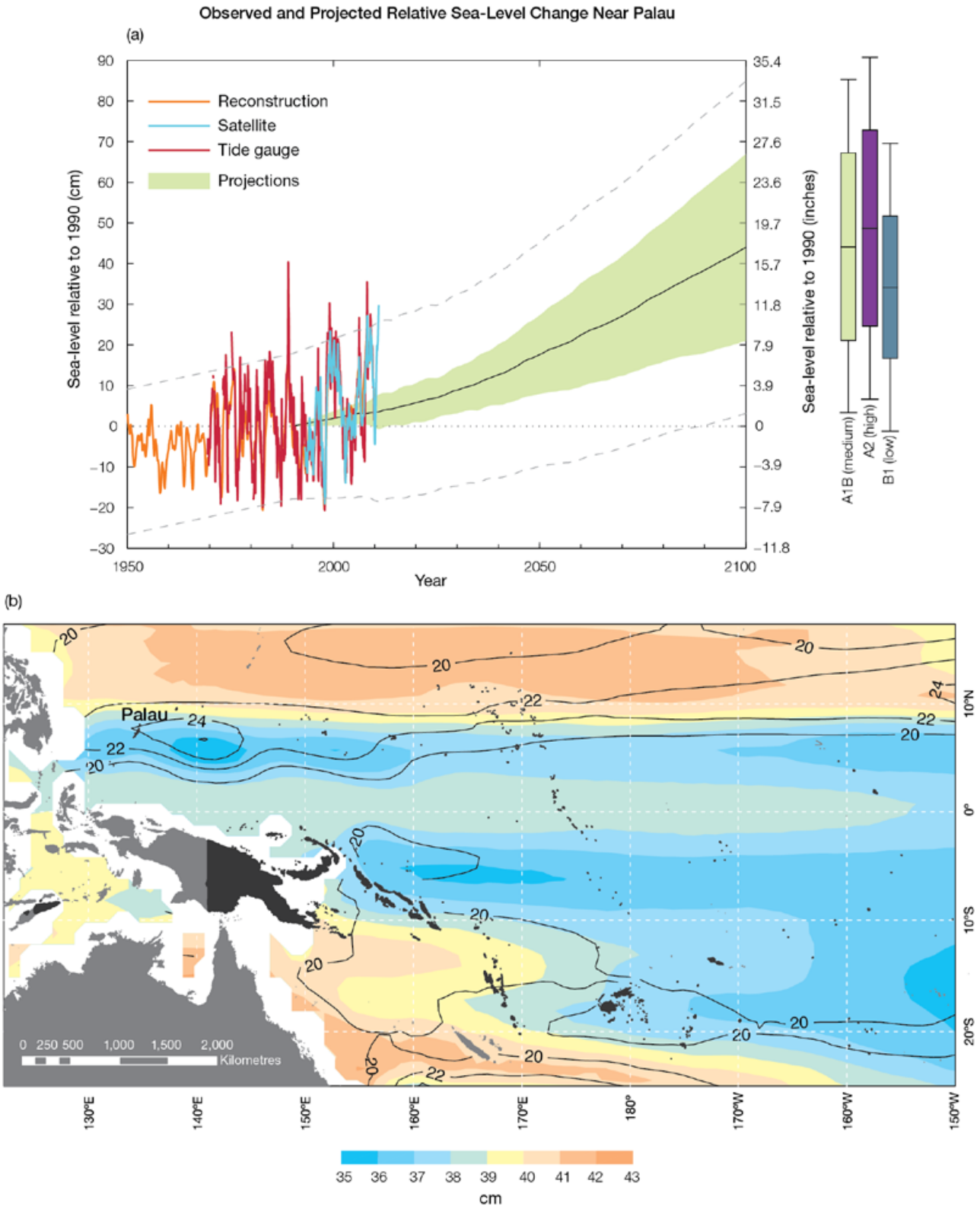

Figure 10.9: Observed and projected relative sea-level change near Palau. (a) The observed in situ relative sea-level records are indicated in red, with the satellite record (since 1993) in light blue. The gridded sea level at Palau (since 1950, from Church and White (in press)) is shown in orange. The projections for the A1B (medium) emissions scenario (5–95% uncertainty range) are shown by the green shaded region from 1990–2100. The range of projections for the B1 (low), A1B (medium), A2 (high) emissions scenarios by 2100 are also shown by the bars on the right. The dashed lines are an estimate of interannual variability in sea level (5–95% range about the long-term trends) and indicate that individual monthly averages of sea level can be above or below longer-term averages. (b) The projections (in cm) for the A1B (medium) emissions scenario in the Palau region for the average over 2081–2100 relative to 1981–2000 are indicated by the shading, with the estimated uncertainty in the projections indicated by the contours (in cm).

Table 10.3: Projected change in the annual and seasonal mean climate for Palau, under the B1 (low; blue), A1B (medium; green) and A2 (high; purple) emissions scenarios. Projections are given for three 20-year periods centred on 2030 (2020–2039), 2055 (2046–2065) and 2090 (2080–2099), relative to 1990 (1980–1999). Values represent the multi-model mean change ± twice the inter-model standard deviation (representing approximately 95% of the range of model projections), except for sea level where the estimated mean change and the 5–95% range are given (as they are derived directly from Intergovernmental Panel on Climate Change Fourth Assessment Report values). The confidence (Section 1.7.2) associated with the range and distribution of the projections is also given (indicated by the standard deviation and multi-model mean, respectively). See Volume 1, Appendix 1 for a complete listing of CMIP3 models used to derive these projections.

Variable	Season	2030	2055	2090	Confidence
Surface air temperature (°F)	Annual	+1.1 ± 0.7 +1.4 ± 0.7 +1.2 ± 0.5	+1.9 ± 0.8 +2.6 ± 0.9 +2.5 ± 0.8	+2.7 ± 1.2 +4.1 ± 1.5 +4.9 ± 1.3	High
Surface air temperature (°C)	Annual	+0.6 ± 0.4 +0.8 ± 0.4 +0.7 ± 0.3	+1.0 ± 0.4 +1.4 ± 0.5 +1.4 ± 0.4	+1.5 ± 0.7 +2.3 ± 0.8 +2.7 ± 0.7	High
Maximum temperature (°F)	1-in-20-year event	N/A	+1.6 ± 1.1 +2.5 ± 1.3 +2.5 ± 0.9	+2.3 ± 1.3 +3.8 ± 1.8 +4.9 ± 2.3	Low
Maximum temperature (°C)	1-in-20-year event	N/A	+0.9 ± 0.6 +1.4 ± 0.7 +1.4 ± 0.5	+1.3 ± 0.7 +2.1 ± 1.0 +2.7 ± 1.3	Low
Minimum temperature (°F)	1-in-20-year event	N/A	+2.2 ± 2.5 +2.7 ± 2.5 +2.5 ± 2.5	+2.9 ± 2.3 +3.8 ± 2.9 +4.1 ± 2.9	Low
Minimum temperature (°C)	1-in-20-year event	N/A	+1.2 ± 1.4 +1.5 ± 1.4 +1.4 ± 1.4	+1.6 ± 1.3 +2.1 ± 1.6 +2.3 ± 1.6	Low
Total rainfall (%)	Annual	0 ± 12 +2 ± 12 +1 ± 11	+3 ± 14 +4 ± 17 +2 ± 10	+5 ± 10 +8 ± 18 +6 ± 16	Moderate
Dry season rainfall (%)	November-April	0 ± 15 +3 ± 13 +1 ± 15	+3 ± 19 +4 ± 23 +2 ± 17	+5 ± 16 +7 ± 24 +4 ± 24	Moderate
Wet season rainfall (%)	May-October	0 ± 12 +2 ± 14 +1 ± 11	+3 ± 12 +5 ± 17 +3 ± 9	+5 ± 11 +9 ± 18 +8 ± 16	Moderate
Sea-surface temperature (°F)	Annual	+1.1 ± 0.7 +1.3 ± 0.7 +1.1 ± 0.7	+1.8 ± 0.7 +2.3 ± 0.7 +2.2 ± 0.7	+2.5 ± 1.1 +3.8 ± 1.1 +4.5 ± 1.3	High
Sea-surface temperature (°C)	Annual	+0.6 ± 0.4 +0.7 ± 0.4 +0.6 ± 0.4	+1.0 ± 0.4 +1.3 ± 0.4 +1.2 ± 0.4	+1.4 ± 0.6 +2.1 ± 0.6 +2.5 ± 0.7	High
Aragonite saturation state (Ωar)	Annual maximum	+3.5 ± 0.1 +3.4 ± 0.1 +3.4 ± 0.2	+3.2 ± 0.2 +3.0 ± 0.1 +3.0 ± 0.2	+3.0 ± 0.2 +2.6 ± 0.1 +2.5 ± 0.2	Moderate
Mean sea level (inches)	Annual	+3.1 (1.6–5.1) +3.5 (1.2–5.9) +3.5 (1.6–5.9)	+6.7 (3.1–10.2) +7.9 (3.5–12.2) +7.9 (4.3–11.4)	+11.8 (5.9–18.1) +15.0 (7.1–23.2) +16.1 (8.3–24.0)	Moderate
Mean sea level (cm)	Annual	+8 (4–13) +9 (3–15) +9 (4–15)	+17 (8–26) +20 (9–31) +20 (11–29)	+30 (15–46) +38 (18–59) +41 (21–61)	Moderate

*The MIROC3.2(medres) and MIROC3.2(hires) models were eliminated in calculating the rainfall projections, due to their inability to accurately simulate present-day activity of the West Pacific Monsoon and the Intertropical Convergence Zone, respectively (Volume 1, Section 5.5.1).

Hanuabada village, Port Moresby

Chapter 11
Papua New Guinea

The contributions of Kasis Inape from the Papua New Guinea National Weather Service and Maino Virobo from the Department of Environment and Conservation are gratefully acknowledged

Introduction

This chapter provides a brief description of Papua New Guinea, its past and present climate as well as projections for the future. The climate observation network and the availability of atmospheric and oceanic data records are outlined. The annual mean climate, seasonal cycles and the influences of large-scale climate features such as the West Pacific Monsoon and patterns of climate variability (e.g. the El Niño-Southern Oscillation) are analysed and discussed. Observed trends and analysis of air temperature, rainfall, extreme events (including tropical cyclones), sea-surface temperature, ocean acidification, mean and extreme sea levels are presented. Projections for air and sea-surface temperature, rainfall, sea level, ocean acidification and extreme events for the 21st century are provided. These projections are presented along with confidence levels based on expert judgement by Pacific Climate Change Science Program (PCCSP) scientists. The chapter concludes with a summary table of projections (Table 11.4). Important background information, including an explanation of methods and models, is provided in Chapter 1. For definitions of other terms refer to the Glossary.

11.1 Climate Summary

11.1.1 Current Climate

- Sites in Papua New Guinea have very weak seasonal variations in temperature. Sea-surface temperatures have a strong influence on average monthly air temperatures.
- The south of Papua New Guinea has a wet season from November to April and a dry season from May to October, while further north rainfall is more consistent throughout the year.
- Rainfall in Papua New Guinea is influenced by the West Pacific Monsoon. High year-to-year variability in rainfall is mostly due to the impact of the El Niño-Southern Oscillation.
- Warming trends are evident in both annual and seasonal mean air temperatures at Port Moresby for the period 1950–2009. These trends are considerably stronger in minimum air temperatures when compared to maximum air temperatures.
- Annual and seasonal rainfall trends for Port Moresby for the period 1950–2009 and Kavieng for the period 1957–2009 are not statistically significant.
- The sea-level rise near Papua New Guinea measured by satellite altimeters since 1993 is about 7 mm per year.
- On average, Port Moresby experiences six tropical cyclones per decade, with most occurring between November and April.

11.1.2 Future Climate

Over the course of the 21st century:

- Surface air temperature and sea-surface temperature are projected to continue to increase (*very high* confidence).
- Annual and seasonal mean rainfall is projected to increase (*high* confidence).
- The intensity and frequency of days of extreme heat are projected to increase (*very high* confidence).
- The intensity and frequency of days of extreme rainfall are projected to increase (*high* confidence).
- The incidence of drought is projected to decrease (*moderate* confidence).
- Tropical cyclone numbers are projected to decline in the south-west Pacific Ocean basin (0–40ºS, 130ºE –170ºE) (*moderate* confidence).
- Ocean acidification is projected to continue (*very high* confidence).
- Mean sea-level rise is projected to continue (*very high* confidence).

11.2 Country Description

Papua New Guinea consists of the eastern half of New Guinea Island and about 700 offshore islands between the equator and 12°S, and 140°E–160°E. At 462 243 km^2, Papua New Guinea is the largest of the 15 PCCSP Partner Countries. The country's geography is diverse and, in places, extremely rugged. A spine of mountains, the New Guinea Highlands, runs the length of New Guinea Island, which is mostly covered with tropical rainforest.

Dense rainforests can also be found in the lowland and coastal areas as well as the very large wetland areas surrounding the Sepik and Fly Rivers. The highest peak is Mount Wilhelm at 4697 m (Papua New Guinea Country Statistics, SOPAC, 2010).

The population of Papua New Guinea is approximately 6 744 955, with 40% living in the highlands and 18% in urban areas. The capital, Port Moresby, is located in the south-east and has a population of approximately 500 000.

Eighty-five percent of the population live a subsistence lifestyle in rural areas. These people depend on traditional agriculture and fishing for their livelihoods. Mining and oil production are the main sources of revenue for Papua New Guinea, accounting for 60% of export earnings and 20% of government revenue. Agricultural crops are still a major source of revenue, in particular copra (Papua New Guinea is the biggest producer in the South Pacific), coffee, palm oil and cocoa. Export of forestry products, once among the country's main sources of revenue, has declined in recent years.

Figure 11.1: Papua New Guinea

11.3 Data Availability

There are currently 39 operational meteorological stations in Papua New Guinea. Multiple observations within a 24-hour period are taken at 18 stations: four synoptic stations in Momase, two in the Highlands, six in the Southern region and six in the New Guinea Islands. In addition there are three single observation climate stations and 18 single observation rainfall stations. The primary climate station is located in Port Moresby (Figure 11.1). Rainfall data for Port Moresby are available from 1890, largely complete from 1905. Air temperature data are available from 1939. Madang, Wewak, Misima, Kavieng and Momote have more than 50 years of rainfall data.

Climate records for Port Moresby from 1950 and Kavieng (an island to the north-east) from 1957 (air temperature from 1962) have been used. Both records are homogeneous and more than 95% complete.

There are a number of sea-level records available for the Papua New Guinea region. The best appear to be Port Moresby II (1984–1994), Rabaul (1966–1997), Lombrum (1994–present), Lae (1984–2000), Anewa Bay (1968–1977), Kavieng (1984–1998), Madang (1984–1998), Goods Island (1989–present) and Thursday Island III (1983–2002). A global positioning system instrument to estimate vertical land motion was deployed at Manus Island in 2002 and will provide valuable direct estimates of local vertical land motion in future years. Both satellite (from 1993) and in situ sea-level data (1950–2009; termed reconstructed sea level; Volume 1, Section 2.2.2.2) are available on a global 1° x 1° grid.

Long-term locally-monitored sea-surface temperature data are unavailable for Papua New Guinea, so large-scale gridded sea-surface temperature datasets have been used (HadISST, HadSST2, ERSST and Kaplan Extended SST V2; Volume 1, Table 2.3).

Training in *Pacific Climate Futures*, Port Moresby

11.4 Seasonal Cycles

Sites in Papua New Guinea have very weak seasonal variations in temperature (Figure 11.2). Port Moresby is further south than Kavieng, so its seasonal temperature cycle is stronger with about 2.5ºC between the warmest month (November) and the coolest (July). Sea-surface temperatures have a strong influence on average monthly air temperatures.

The seasonal cycles of monthly-mean rainfall (Figure 11.2) show a wet season from November to April and a dry season from May to October. However, these seasons are only clearly different in Port Moresby, where about 78% of the yearly average rainfall comes in the wet season. The West Pacific Monsoon is responsible for most of the rainfall in Port Moresby and during the dry season Port Moresby is exposed to dry south-easterly winds. In Kavieng rainfall is more consistent year-round although the peak in rainfall corresponds to the monsoon season from December to April. Kavieng and other sites in the north of Papua New Guinea are affected by the Intertropical Convergence Zone and to a lesser extent the South Pacific Convergence Zone. They lie in the West Pacific Warm Pool, so experience convective rain throughout the year. As a result, Kavieng's average annual rainfall (3150 mm) is much higher than Port Moresby's (1190 mm).

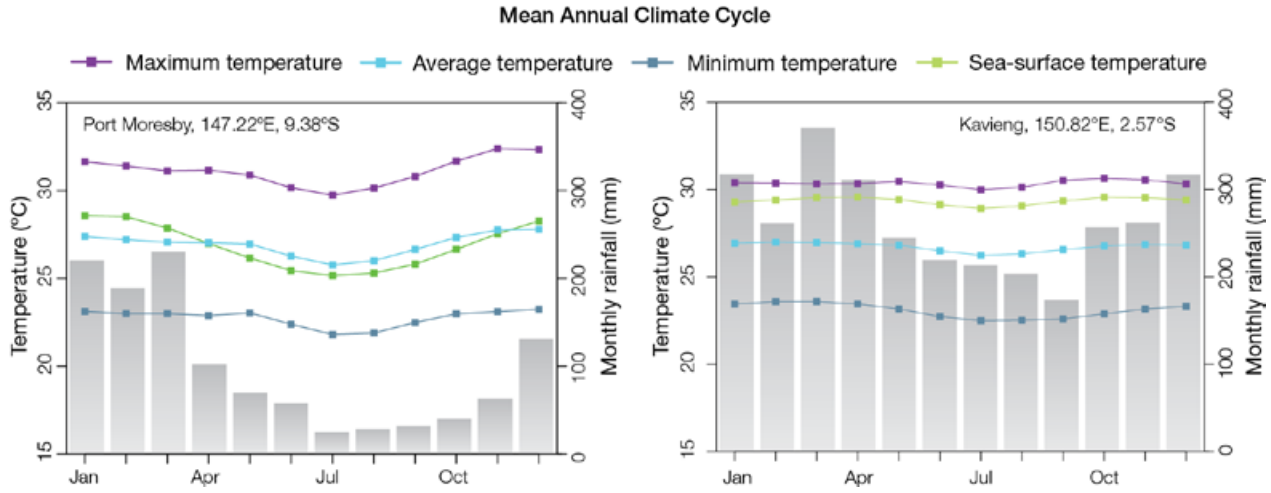

Figure 11.2: Mean annual cycle of rainfall (grey bars) and daily maximum, minimum and mean air temperatures at Port Moresby (left) and Kavieng (right), and local sea-surface temperatures derived from the HadISST dataset (Volume 1, Table 2.3).

11.5 Climate Variability

Year-to-year variability in rainfall is high in Papua New Guinea. At both Port Moresby and Kavieng the wettest years receive up to three times the rainfall of the driest years (Figure 11.4). The El Niño-Southern Oscillation (ENSO) drives much of this variability. Generally, El Niño years are drier than average while La Niña years are wetter than average. Table 11.1 shows that at Port Moresby, the dry season in El Niño years tends to be cooler than normal and warmer in La Niña years, while the wet season is cooler than normal in El Niño years. Another impact of El Niño is a late start to the monsoon season. Modoki ENSO events (Volume 1, Section 3.4.1) appear to have very similar impacts in Port Moresby to canonical ENSO events.

During El Niño events Kavieng tends to have wet seasons that are wetter than normal, and that tend to have warmer nights and cooler days. There is no clear influence of ENSO during the dry season in Kavieng.

Table 11.1: Correlation coefficients between indices of key large-scale patterns of climate variability and minimum and maximum temperatures (Tmin and Tmax) and rainfall at Port Moresby. Only correlation coefficients that are statistically significant at the 95% level are shown.

Climate feature/index		Dry season (May-October)			Wet season (November-April)		
		Tmin	Tmax	Rain	Tmin	Tmax	Rain
ENSO	Niño3.4	-0.66	-0.43		0.42	0.59	-0.51
	Southern Oscillation Index	0.65	-0.61		-0.28	-0.52	0.49
Interdecadal Pacific Oscillation Index							
ENSO Modoki Index		-0.34	-0.43			0.30	-0.29
Number of years of data		67	66	99	69	67	107

Table 11.2: Correlation coefficients between indices of key large-scale patterns of climate variability and minimum and maximum temperatures (Tmin and Tmax) and rainfall at Kavieng. Only correlation coefficients that are statistically significant at the 95% level are shown.

Climate feature/index		Dry season (May-October)			Wet season (November-April)		
		Tmin	Tmax	Rain	Tmin	Tmax	Rain
ENSO	Niño3.4				0.40	-0.38	0.34
	Southern Oscillation Index				-0.35	0.41	-0.27
Interdecadal Pacific Oscillation Index							
ENSO Modoki Index						-0.37	0.40
Number of years of data		46	44	75	45	45	73

11.6 Observed Trends

11.6.1 Air Temperature

Warming trends of a similar magnitude are evident in both annual and seasonal mean air temperatures at Port Moresby for the period 1950–2009. Air temperature trends are generally greater in the wet season than they are in the dry season and minimum air temperature trends are considerably stronger than maximum air temperatures trends (Figure 11.3 and Table 11.3).

11.6.2 Rainfall

Annual and seasonal rainfall trends for Port Moresby for the period 1950–2009 and Kavieng for the period 1957–2009 are not statistically significant (Table 11.3 and Figure 11.4).

11.6.3 Extreme Events

The tropical cyclone season in the south-eastern coastal regions of Papua New Guinea is between November and April. Occurrences outside this period are rare.
The tropical cyclone archive for the Southern Hemisphere indicates that between the 1969/70 and 2009/10 seasons, the centre of 23 tropical cyclones passed within approximately 400 km of Port Moresby (Figure 11.5). This represents an average of six cyclones per decade. Tropical cyclones were most frequent in ENSO-neutral years (eight cyclones per decade) and least frequent in El Niño and La Niña years (four cyclones per decade).

In the southern Papua New Guinea region, prolonged rainfall during La Niña events leads to serious floods and landslides. El Niño events are associated with droughts.

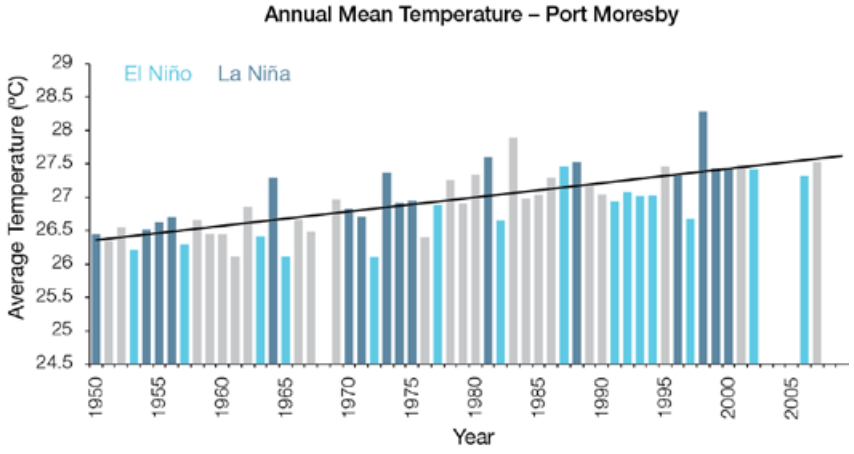

Figure 11.3: Annual mean air temperature at Port Moresby. Light blue, dark blue and grey bars denote El Niño, La Niña and neutral years respectively.

Table 11.3: Annual and seasonal trends in maximum, minimum and mean air temperature (Tmax, Tmin and Tmean) and rainfall at Port Moresby for the period 1950–2009 and rainfall only at Kavieng for the period 1957–2009. Asterisks indicate significance at the 95% level. Persistence is taken into account in the assessment of significance as in Power and Kociuba (in press). The statistical significance of the air temperature trends is not assessed.

	Port Moresby Tmax (°C per 10 yrs)	Port Moresby Tmin (°C per 10 yrs)	Port Moresby Tmean (°C per 10 yrs)	Port Moresby Rain (mm per 10 yrs)	Kavieng Rain (mm per 10 yrs)
Annual	+0.11	+0.31	+0.21	+7	-27
Wet season	+0.14	+0.32	+0.23	-4	-42
Dry season	+0.08	+0.31	+0.20	+4	+13

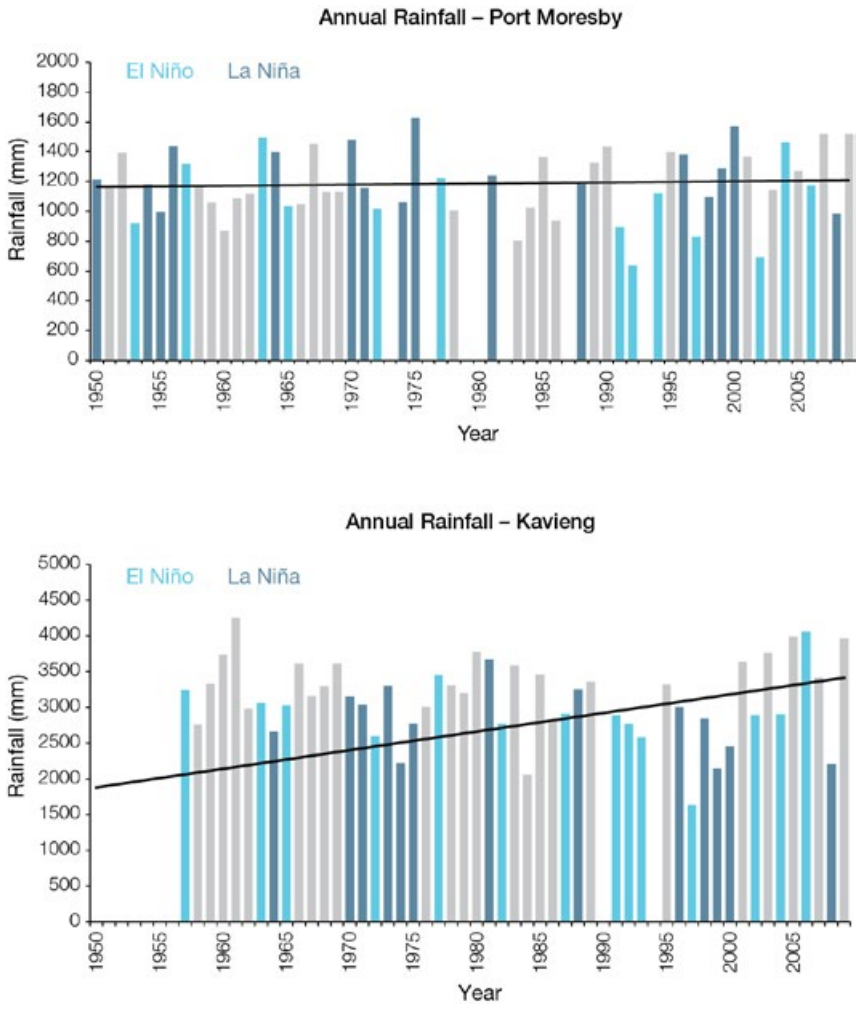

Figure 11.4: Annual rainfall at Port Moresby (top) and Kavieng (bottom). Light blue, dark blue and grey bars denote El Niño, La Niña and neutral years respectively.

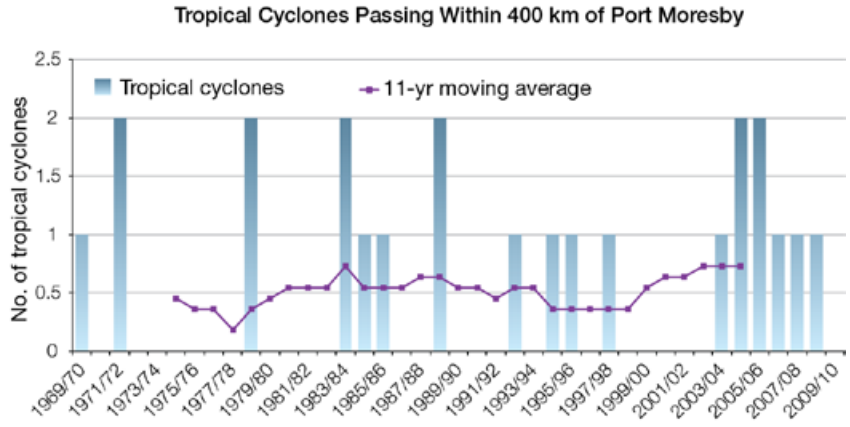

Figure 11.5: Tropical cyclones passing within 400 km of Port Moresby per season. The 11-year moving average is in purple.

11.6.4 Sea-Surface Temperature

Water temperatures in the Papua New Guinea region have risen gradually since the 1950s. Since the 1970s the rate of warming has been approximately 0.11°C per decade. Figure 11.8 shows the 1950–2000 sea-surface temperature changes (relative to a reference year of 1990) from three different large-scale sea-surface temperature gridded datasets (HadSST2, ERSST and Kaplan Extended SST V2; Volume 1, Table 2.3). At these regional scales, natural variability may play a large role in determining the sea-surface temperature making it difficult to any identify long-term trends.

11.6.5 Ocean Acidification

Based the large-scale distribution of coral reefs across the Pacific and the seawater chemistry, Guinotte et al. (2003) suggested that seawater aragonite saturation states above 4 were optimal for coral growth and for the development of healthy reef ecosystems, with values from 3.5 to 4 adequate for coral growth, and values between 3 and 3.5, marginal. Coral reef ecosystems were not found at seawater aragonite saturation states below 3 and these conditions were classified as extremely marginal for supporting coral growth.

In the Papua New Guinea region, the aragonite saturation state has declined from about 4.5 in the late 18th century to an observed value of about 3.9 ± 0.1 by 2000.

11.6.6 Sea Level

Monthly averages of the historical tide gauge, satellite (since 1993) and gridded sea-level (since 1950) data agree well after 1993 and indicate interannual variability in sea levels of about 23 cm (estimated 5–95% range) after removal of the seasonal cycle (Figure 11.10). The sea-level rise near Papua New Guinea measured by satellite altimeters (Figure 11.6) since 1993 is about 7 mm per year, larger than the global average of 3.2 ± 0.4 mm per year. This rise is partly linked to a pattern related to climate variability from year to year and decade to decade (Figure 11.10).

11.6.7 Extreme Sea-Level Events

The annual climatology of the highest daily sea levels has been evaluated from hourly measurements by tide gauges at Lombrum (Manus Province) and Rabaul (East New Britain Province) (Figure 11.7). Highest tides at both locations tend to occur around the solstices, with a higher December maximum, particularly at Rabaul. There is little seasonal cycle throughout the year but seasonal water levels at both locations are significantly higher during La Niña years and lower during El Niño years. The tidal, seasonal, and short-term components combine to create the highest likelihood for extreme water levels between November and February of La Niña years at Lombrum and November to February and April of La Niña years at Rabaul. At Lombrum, the 10 highest recorded water levels all occurred in January or early February and most occurred during La Niña years from November to February. Three events occurred from May to July of ENSO-neutral years. At Rabaul, seven of the top 10 events occurred during La Niña years and all events occurred over the period from November to March. It is important to note that the annual climatology produced by these two tide gauge locations may not be indicative of other coastal areas of Papua New Guinea, particularly the Gulf of Papua.

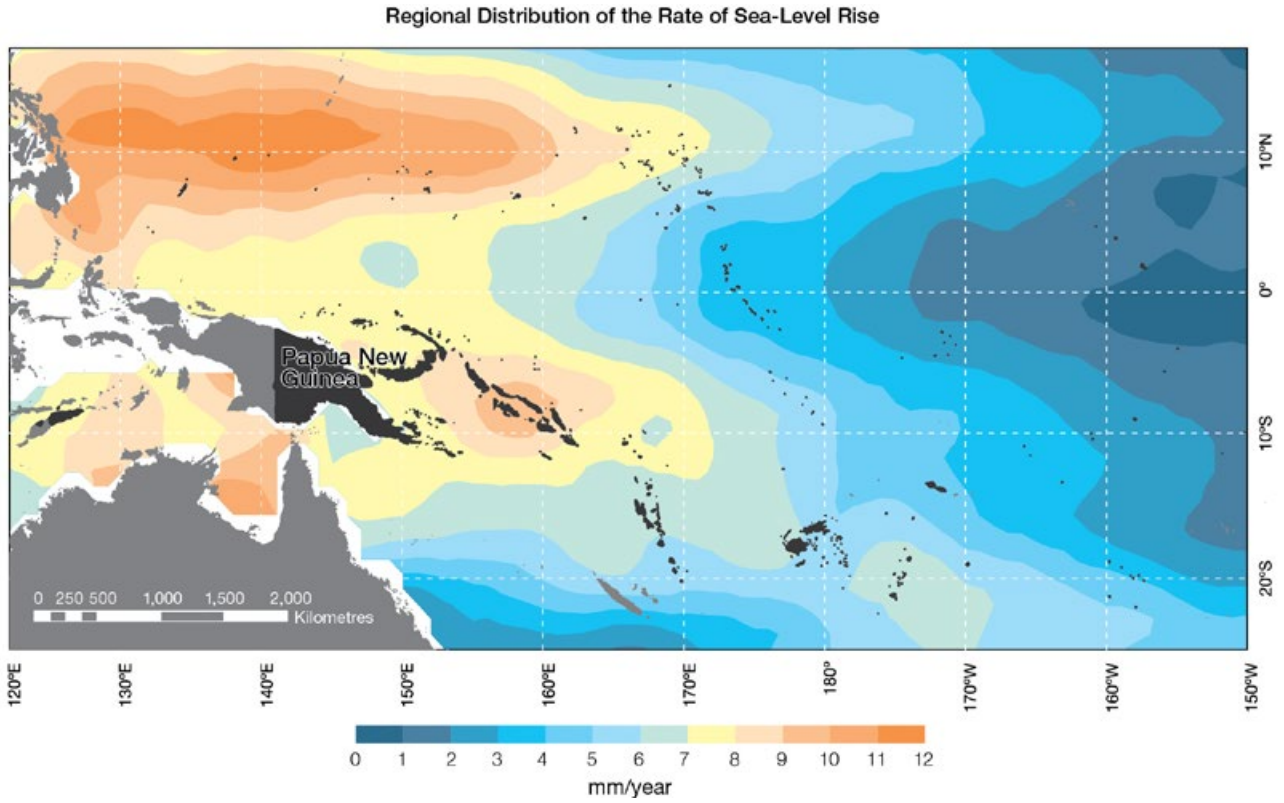

Figure 11.6: The regional distribution of the rate of sea-level rise measured by satellite altimeters from January 1993 to December 2010, with the location of Papua New Guinea indicated. Further detail about the regional distribution of sea-level rise is provided in Volume 1, Section 3.6.3.2.

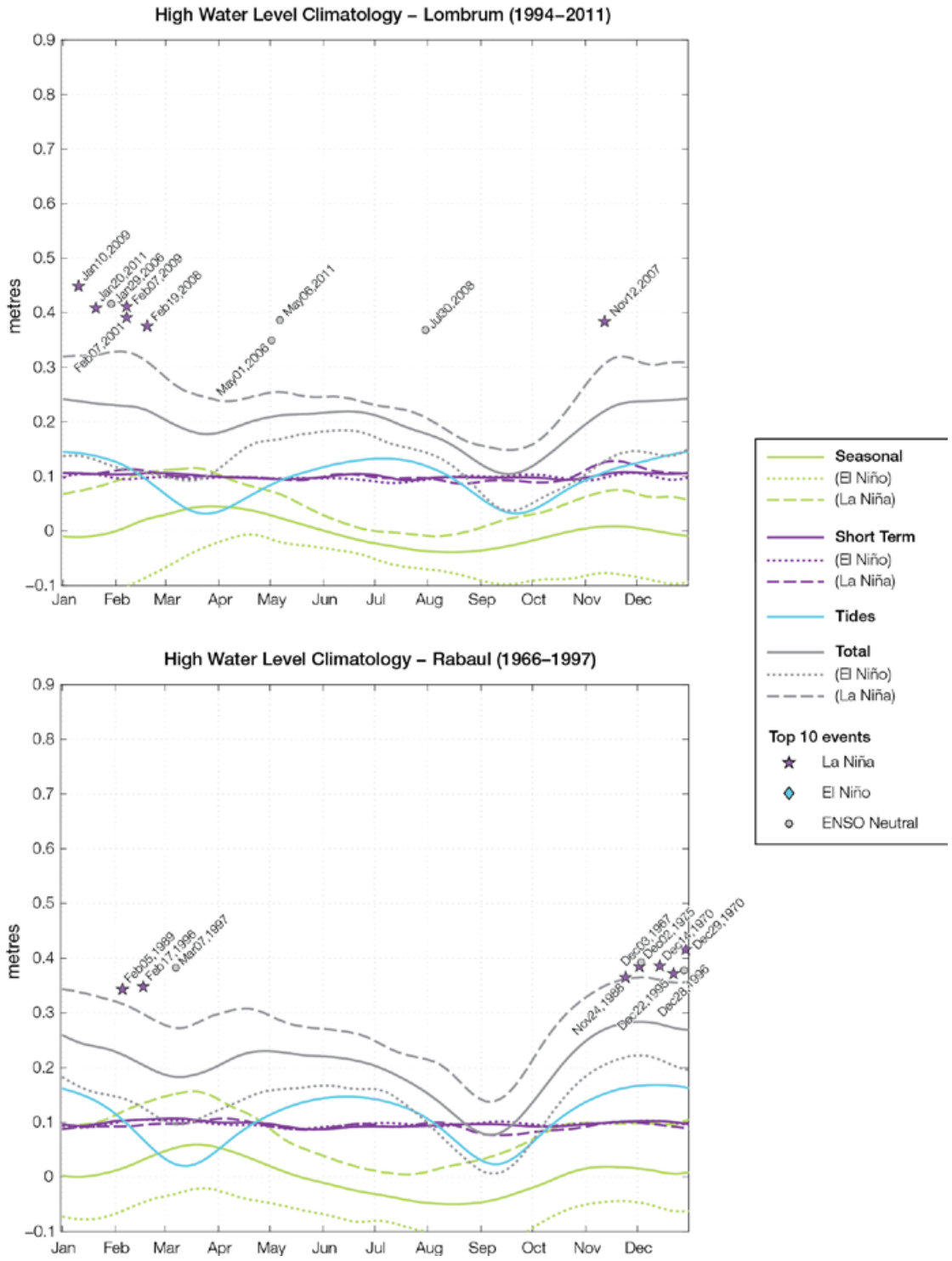

Figure 11.7: The annual cycle of high waters relative to Mean Higher High Water (MHHW) due to tides, short-term fluctuations (most likely associated with storms) and seasonal variations for Lombrum (top) and Rabaul (bottom). The tides and short-term fluctuations are respectively the 95% exceedence levels of the astronomical high tides relative to MHHW and short-term sea level fluctuations. Components computed only for El Niño and La Niña years are shown by dotted and dashed lines, and grey lines are the sum of the tide, short-term and seasonal components. The 10 highest sea level events in the record relative to MHHW are shown and coded to indicate the phase of ENSO at the time of the extreme event.

11.7 Climate Projections

Climate projections have been derived from up to 18 global climate models from the CMIP3 database, for up to three emissions scenarios (B1 (low), A1B (medium) and A2 (high)) and three 20-year periods (centred on 2030, 2055 and 2090, relative to 1990). These models were selected based on their ability to reproduce important features of the current climate (Volume 1, Section 5.2.3), so projections from each of the models are plausible representations of the future climate. This means there is not one single projected future for Papua New Guinea, but rather a range of possible futures. The full range of these futures is discussed in the following sections.

These projections do not represent a value specific to any actual location, such as a town or city in Papua New Guinea. Instead, they refer to an average change over the broad geographic region encompassing the islands of Papua New Guinea and the surrounding ocean (Figure 1.1 shows the regional boundaries). Some information regarding dynamical downscaling simulations from the CCAM model (Section 1.7.2) is also provided, in order to indicate how changes in the climate on an individual island-scale may differ from the broad-scale average.

Section 1.7 provides important information about interpreting climate model projections.

11.7.1 Temperature

Surface air temperature and sea-surface temperature are projected to continue to increase over the course of the 21st century. There is *very high* confidence in this direction of change because:

- Warming is physically consistent with rising greenhouse gas concentrations.
- All CMIP3 models agree on this direction of change.

The majority of CMIP3 models simulate a slight increase (<1°C) in annual and seasonal mean temperature by 2030, however by 2090 under the A2 (high) emissions scenario temperature increases of greater than 2.5°C are simulated by almost all models (Table 11.4). Given the close relationship between surface air temperature and sea-surface temperature, a similar (or slightly weaker) rate of warming is projected for the surface ocean (Figure 11.8). There is *high* confidence in this range and distribution of possible futures because:

- There is generally close agreement between modelled and observed temperature trends over the past 50 years in the vicinity of Papua New Guinea, although observational records are limited (Figure 11.8).

The 8 km CCAM simulations indicate considerable spatial variability in temperature change between 1990 and 2090 (Volume 1, Section 7.2.2.1). For example, the average daily minimum air temperature over inland New Guinea Island can warm up to 1°C more than some coastal regions and small islands, while the average daily maximum can warm up to 4°C more.

Interannual variability in surface temperature over Papua New Guinea is strongly influenced by ENSO in the current climate (Section 11.5). As there is no consistency in projections of future ENSO activity (Volume 1, Section 6.4.1), it is not possible to determine whether interannual variability in temperature will change in the future. However, ENSO is expected to continue to be an important source of variability for the region.

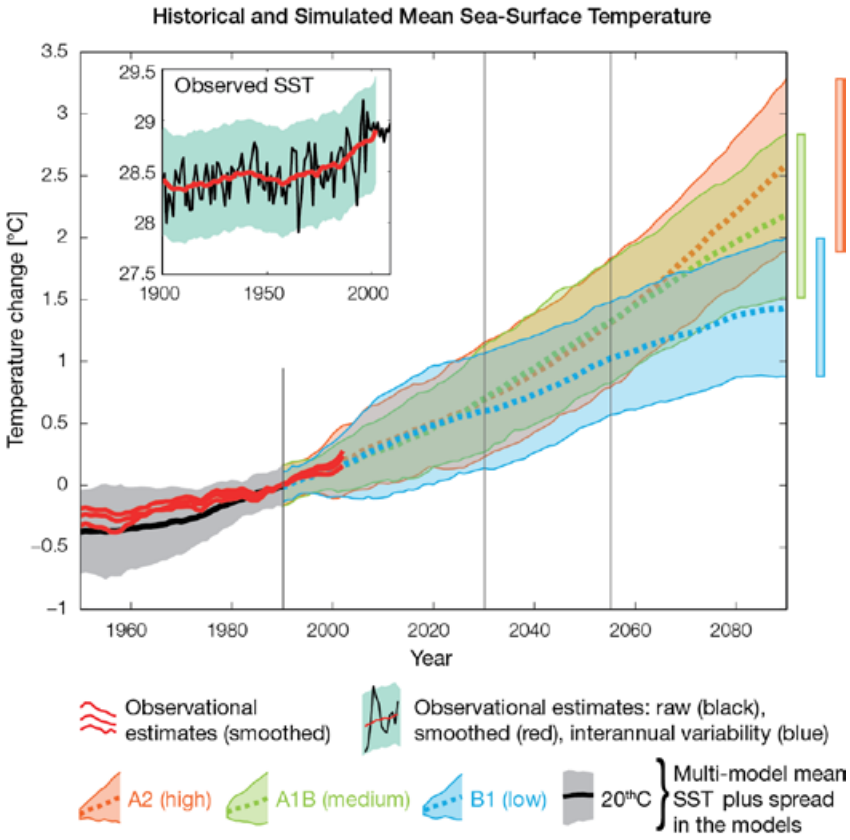

Figure 11.8: Historical climate (from 1950 onwards) and simulated historical and future climate for annual mean sea-surface temperature (SST) in the region surrounding Papua New Guinea, for the CMIP3 models. Shading represents approximately 95% of the range of model projections (twice the inter-model standard deviation), while the solid lines represent the smoothed (20-year running average) multi-model mean temperature. Projections are calculated relative to the 1980–1999 period (which is why there is a decline in the inter-model standard deviation around 1990). This highlights the fact that near-term projections are relatively independent of both model and emissions scenario (although they are significantly affected by natural variability). Observational estimates in the main figure (red lines) are derived from the HadSST2, ERSST and Kaplan Extended SST V2 datasets (Volume 1, Section 2.2.2). Annual average (black) and 20-year running average (red) HadSST2 data is also shown inset.

11.7.2 Rainfall

Wet season (November-April), dry season (May-October) and annual average rainfall are projected to increase over the course of the 21st century. There is *high* confidence in this direction of change because:

- Physical arguments indicate that rainfall will increase in the equatorial Pacific in a warmer climate (IPCC, 2007; Volume 1, Section 6.4.3).
- Almost all of the CMIP3 models agree on this direction of change by 2090.

The CMIP3 models are approximately equally divided between increase (>5%) and little change (-5% to 5%) in annual and seasonal rainfall by 2030, however by 2090 under the higher emissions scenarios (i.e. A2 (high) and A1B (medium)) the majority of the models simulate an increase, with approximately half simulating a large increase (>15%) (Table 11.4). There is *moderate* confidence in this range and distribution of possible futures because:

- In simulations of the current climate, the CMIP3 models broadly capture the influence of the West Pacific Monsoon, Intertropical Convergence Zone and the South Pacific Convergence Zone on the rainfall of Papua New Guinea (Volume 1, Section 5.2.3), although most models produce monsoon westerly winds that do not extend far enough east into the Pacific basin.
- The CMIP3 models are unable to resolve many of the physical processes involved in producing rainfall. As a consequence, they do not simulate rainfall as well as other variables such as temperature (Volume 1, Chapter 5).

The 8 km CCAM simulations indicate considerable spatial variability in rainfall changes across Papua New Guinea associated with the complex topography, with increases in rainfall in some regions and decreases for other regions (Volume 1, Section 7.2.2.1).

These small-scale spatial changes are somewhat correlated with the present day rainfall climatology (e.g. regions that are wettest in the current climate tend to be associated with the highest rainfall increases in the future).

Interannual variability in rainfall over Papua New Guinea is strongly influenced by ENSO in the current climate (Section 11.5). As there is no consistency in projections of future ENSO activity (Volume 1, Section 6.4.1), it is not possible to determine whether interannual variability in rainfall will change in the future.

11.7.3 Extremes

Temperature

The intensity and frequency of days of extreme heat are projected to increase over the course of the 21st century. There is *very high* confidence in this direction of change because:

- An increase in the intensity and frequency of days of extreme heat is physically consistent with rising greenhouse gas concentrations.
- All CMIP3 models agree on the direction of change for both intensity and frequency.

The majority of CMIP3 models simulate an increase of approximately 1°C in the temperature experienced on the 1-in-20-year hot day by 2055 under the B1 (low) emissions scenario, with an increase of over 2.5°C simulated by the majority of models by 2090 under the A2 (high) emissions scenario (Table 11.4). There is *low* confidence in this range and distribution of possible futures because:

- In simulations of the current climate, the CMIP3 models tend to underestimate the intensity and frequency of days of extreme heat (Volume 1, Section 5.2.4).
- Smaller increases in the frequency of days of extreme heat are projected by the CCAM 60 km simulations.

Rainfall

The intensity and frequency of days of extreme rainfall are projected to increase over the course of the 21st century. There is *high* confidence in this direction of change because:

- An increase in the frequency and intensity of extreme rainfall is consistent with larger-scale projections, based on the physical argument that the atmosphere is able to hold more water vapour in a warmer climate (Allen and Ingram, 2002; IPCC, 2007). It is also consistent with physical arguments which indicate that rainfall will increase in the deep tropical Pacific in a warmer climate (IPCC, 2007; Volume 1, Section 6.4.3).
- Almost all of the CMIP3 models agree on this direction of change for both intensity and frequency.

The majority of CMIP3 models simulate an increase of at least 15 mm in the amount of rain received on the 1-in-20-year wet day by 2055 under the B1 (low) emissions scenario, with an increase of at least 30 mm simulated by 2090 under the A2 (high) emissions scenario. The majority of models project that the current 1-in-20-year extreme rainfall event will occur, on average, three to four times per 20-year period by 2055 under the B1 (low) emissions scenario and six times per 20-year period by 2090 under the A2 (high) emissions scenario. There is *low* confidence in this range and distribution of possible futures because:

- In simulations of the current climate, the CMIP3 models tend to underestimate the intensity and frequency of extreme rainfall (Volume 1, Section 5.2.4).
- The CMIP3 models are unable to resolve many of the physical processes involved in producing extreme rainfall.

Drought

The incidence of drought is projected to decrease over the course of the 21st century. There is *moderate* confidence in this direction of change because:

- A decrease in drought is consistent with projections of increased rainfall (Section 11.7.2).
- The majority of models agree on this direction of change for most drought categories.

The majority of CMIP3 models project that mild drought will occur approximately seven to eight times every 20 years in 2030 under all emissions scenarios, decreasing to six to seven times by 2090. The frequency of moderate and severe drought is projected to remain approximately stable, at once to twice and once every 20 years, respectively. There is *low* confidence in this range and distribution of possible futures because:

- There is only moderate confidence in the range of rainfall projections (Section 11.7.2), which directly influences projections of future drought conditions.

Tropical Cyclones

Tropical cyclone numbers are projected to decline in the south-west Pacific Ocean basin (0–40ºS, 130ºE–170ºE) over the course of the 21st century. There is *moderate* confidence in this direction of change because:

- Many studies suggest a decline in tropical cyclone frequency globally (Knutson et al., 2010).
- Tropical cyclone numbers decline in the south-west Pacific Ocean in the majority assessment techniques.

Based on the direct detection methodologies (Curvature Vorticity Parameter (CVP) and the CSIRO Direct Detection Scheme (CDD) described in Volume 1, Section 4.8.2), 55% of projections show no change or a decrease in tropical cyclone formation when applied to the CMIP3 climate models for which suitable output is available. When these techniques are applied to CCAM, 100% of projections show a decrease in tropical cyclone formation. In addition, the Genesis Potential Index (GPI) empirical technique suggests that conditions for tropical cyclone formation will become less favourable in the south-west Pacific Ocean basin, for the majority (80%) of analysed CMIP3 models. There is *moderate* confidence in this range and distribution of possible futures because:

- In simulations of the current climate, the CVP, CDD and GPI methods capture the frequency of tropical cyclone activity reasonably well (Volume 1, Section 5.4).

Despite this projected reduction in total cyclone numbers, five of the six CCAM 60 km simulations show an increase in the proportion of the most severe cyclones. Most models also indicate a reduction in tropical cyclone wind hazard north of 20ºS latitude and regions of increased hazard south of 20ºS latitude. This increase in wind hazard coincides with a poleward shift in the latitude at which tropical cyclones are most intense.

11.7.4 Ocean Acidification

The acidification of the ocean will continue to increase over the course of the 21st century. There is *very high* confidence in this projection as the rate of ocean acidification is driven primarily by the increasing oceanic uptake of carbon dioxide, in response to rising atmospheric carbon dioxide concentrations.

Projections from all analysed CMIP3 models indicate that the annual maximum aragonite saturation state will reach values below 3.5 by about 2040 and continue to decline thereafter (Figure 11.9; Table 11.4). There is *moderate* confidence in this range and distribution of possible futures because the projections are based on climate models without an explicit representation of the carbon cycle and with relatively low resolution and known regional biases.

The impact of acidification change on the health of reef ecosystems is likely to be compounded by other stressors including coral bleaching, storm damage and fishing pressure.

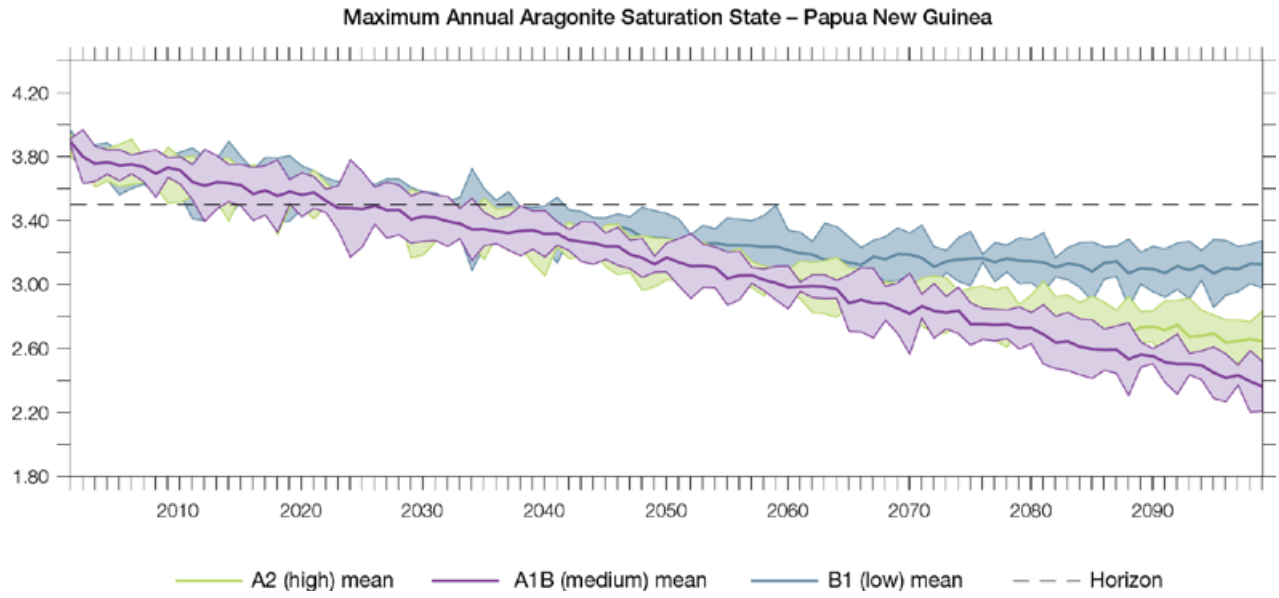

Figure 11.9: Multi-model projections, and their associated uncertainty (shaded area represents two standard deviations), of the maximum annual aragonite saturation state in the sea surface waters of the Papua New Guinea region under the different emissions scenarios. The dashed black line represents an aragonite saturation state of 3.5.

11.7.5 Sea Level

Mean sea level is projected to continue to rise over the course of the 21st century. There is *very high* confidence in this direction of change because:

- Sea-level rise is a physically consistent response to increasing ocean and atmospheric temperatures, due to thermal expansion of the water and the melting of glaciers and ice caps.
- Projections arising from all CMIP3 models agree on this direction of change.

The CMIP3 models simulate a rise of between approximately 5–15 cm by 2030, with increases of 20–60 cm indicated by 2090 under the higher emissions scenarios (i.e. A2 (high) and A1B (medium); Figure 11.10; Table 11.4). There is *moderate* confidence in this range and distribution of possible futures because:

- There is significant uncertainty surrounding ice-sheet contributions to sea-level rise and a rise larger than projected above cannot be excluded (Meehl et al., 2007b). However, understanding of the processes is currently too limited to provide a best estimate or an upper bound (IPCC, 2007).
- Globally, since the early 1990s, sea level has been rising near the upper end of the above projections. During the 21st century, some studies (using semi-empirical models) project faster rates of sea-level rise.

Interannual variability of sea level will lead to periods of lower and higher regional sea levels. In the past, this interannual variability has been about 23 cm (5–95% range, after removal of the seasonal signal; dashed lines in Figure 11.10 (a)) and it is likely that a similar range will continue through the 21st century. In addition, winds and waves associated with weather phenomena will continue to lead to extreme sea-level events.

In addition to the regional variations in sea level associated with ocean and mass changes, there are ongoing changes in relative sea level associated with changes in surface loading over the last glacial cycle (glacial isostatic adjustment) and local tectonic motions. The glacial isostatic motions are relatively small for the PCCSP region.

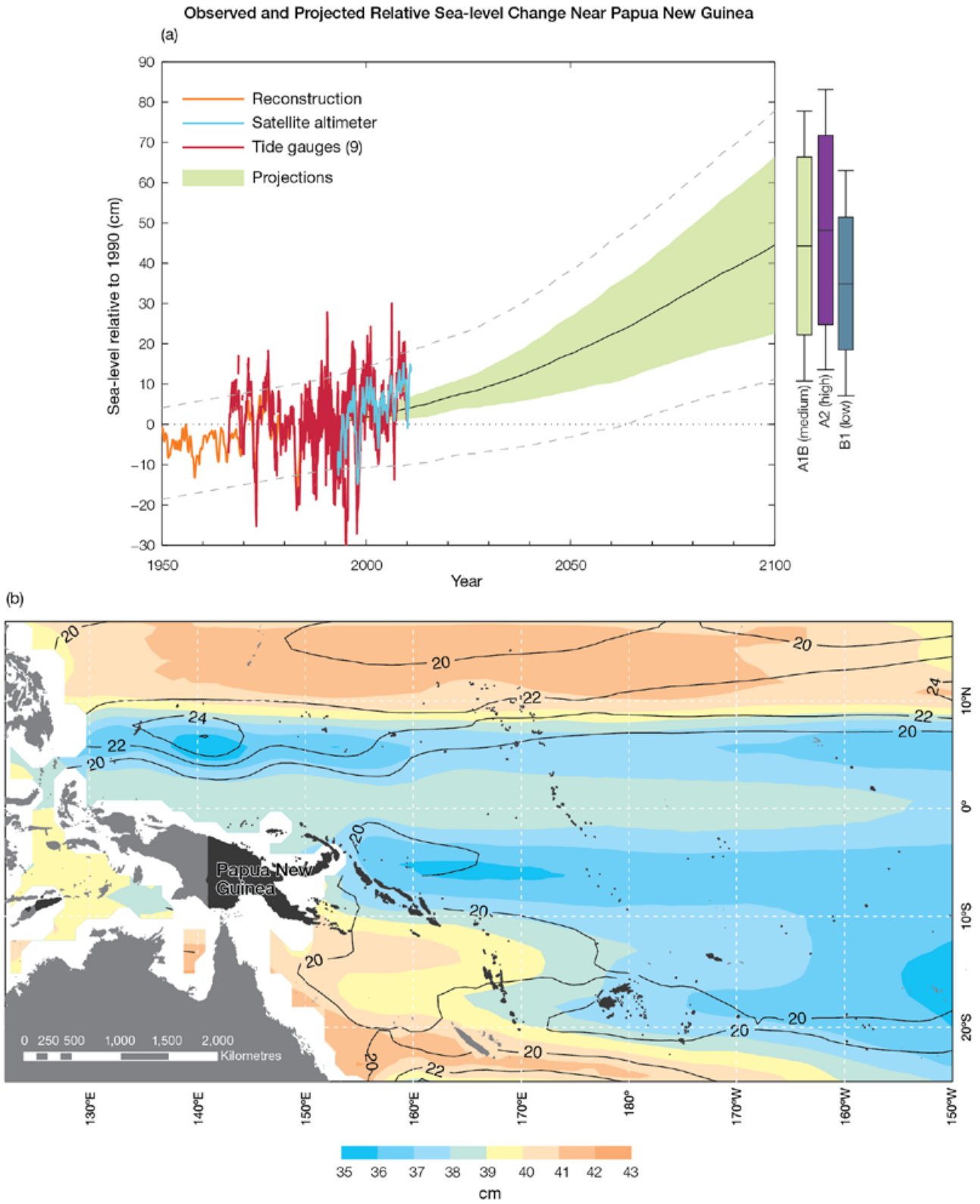

Figure 11.10: Observed and projected relative sea-level change near Papua New Guinea. (a) The observed in situ relative sea-level records are indicated in red, with the satellite record (since 1993) in light blue. The gridded sea level near Papua New Guinea (since 1950, from Church and White (in press)) is shown in orange. The projections for the A1B (medium) emissions scenario (5–95% uncertainty range) are shown by the green shaded region from 1990–2100. The range of projections for the B1 (low), A1B (medium) and A2 (high) emissions scenarios by 2100 are also shown by the bars on the right. The dashed lines are an estimate of interannual variability in sea level (5–95% range about the long-term trends) and indicate that individual monthly averages of sea level can be above or below longer-term averages. (b) The projections (in cm) for the A1B (medium) scenario in the Papua New Guinea region for the average over 2081–2100 relative to 1981–2000 are indicated by the shading, with the estimated uncertainty in the projections indicated by the contours (in cm).

11.7.6 Projections Summary

The projections presented in Section 11.7 are summarised in Table 11.4. For detailed information regarding the various uncertainties associated with the table values, refer to the preceding text in Sections 11.7 and 1.7, in addition to Chapters 5 and 6 in Volume 1. When interpreting the differences between projections for the B1 (low), A1B (medium) and A2 (high) emissions scenarios, it is also important to consider the emissions pathways associated with each scenario (Volume 1, Figure 4.1) and the fact that a slightly different subset of models was available for each (Volume 1, Appendix 1).

Table 11.4: Projected change in the annual and seasonal mean climate for Papua New Guinea, under the B1 (low; blue), A1B (medium; green) and A2 (high; purple) emissions scenarios. Projections are given for three 20-year periods centred on 2030 (2020–2039), 2055 (2046–2065) and 2090 (2080–2099), relative to 1990 (1980–1999). Values represent the multi-model mean change ± twice the inter-model standard deviation (representing approximately 95% of the range of model projections), except for sea level where the estimated mean change and the 5–95% range are given (as they are derived directly from Intergovernmental Panel on Climate Change Fourth Assessment Report values). The confidence (Section 1.7.2) associated with the range and distribution of the projections is also given (indicated by the standard deviation and multi-model mean, respectively). See Volume 1, Appendix 1 for a complete listing of CMIP3 models used to derive these projections.

Variable	Season	2030	2055	2090	Confidence
Surface air temperature (°C)	Annual	+0.7 ± 0.4 +0.8 ± 0.4 +0.7 ± 0.3	+1.1 ± 0.5 +1.5 ± 0.5 +1.5 ± 0.4	+1.6 ± 0.6 +2.4 ± 0.8 +2.8 ± 0.6	High
Maximum temperature (°C)	1-in-20-year event	N/A	+1.0 ± 0.9 +1.4 ± 0.9 +1.5 ± 0.7	+1.3 ± 1.0 +2.2 ± 1.3 +2.7 ± 1.5	Low
Minimum temperature (°C)	1-in-20-year event	N/A	+1.4 ± 1.8 +1.7 ± 2.0 +1.6 ± 1.8	+1.8 ± 1.8 +2.4 ± 1.9 +2.6 ± 2.1	Low
Total rainfall (%)*	Annual	+3 ± 13 +3 ± 13 +5 ± 9	+8 ± 13 +7 ± 17 +7 ± 13	+11 ± 13 +15 ± 20 +15 ± 21	Moderate
Wet season rainfall (%)*	November-April	+4 ± 12 +5 ± 11 +6 ± 10	+10 ± 13 +9 ± 17 +8 ± 12	+12 ± 12 +16 ± 18 +15 ± 20	Moderate
Dry season rainfall (%)*	May-October	+1 ± 15 +1 ± 16 +4 ± 12	+7 ± 16 +5 ± 20 +6 ± 17	+10 ± 16 +15 ± 24 +15 ± 26	Moderate
Sea-surface temperature (°C)	Annual	+0.6 ± 0.5 +0.7 ± 0.4 +0.7 ± 0.5	+1.0 ± 0.5 +1.3 ± 0.5 +1.3 ± 0.5	+1.4 ± 0.6 +2.2 ± 0.7 +2.6 ± 0.7	High
Aragonite saturation state (Ωar)	Annual maximum	+3.5 ± 0.1 +3.4 ± 0.1 +3.4 ± 0.1	+3.2 ± 0.1 +3.0 ± 0.1 +3.0 ± 0.1	+3.1 ± 0.1 +2.7 ± 0.2 +2.5 ± 0.1	Moderate
Mean sea level (cm)	Annual	+9 (4–14) +10 (5–14) +10 (4–15)	+18 (10–26) +20 (9–30) +20 (10–29)	+31 (17–46) +39 (20–58) +41 (22–60)	Moderate

*The MIROC3.2(medres) and MIROC3.2(hires) models were eliminated in calculating the rainfall projections, due to their inability to accurately simulate one or more of the South Pacific Convergence Zone, Intertropical Convergence Zone and the West Pacific Monsoon (Volume 1, Section 5.5.1).

Upolu

Chapter 12
Samoa

The contributions of Fata Lagomauitumua, Sunny K. Seuseu and Tumau Faasaoina from the Samoa Meteorology Division, Ministry of Natural Resources and Environment are gratefully acknowledged

Introduction

This chapter provides a brief description of Samoa, its past and present climate as well as projections for the future. The climate observation network and the availability of atmospheric and oceanic data records are outlined. The annual mean climate, seasonal cycles and the influences of large-scale climate features such as the South Pacific Convergence Zone and patterns of climate variability (e.g. the El Niño-Southern Oscillation) are analysed and discussed. Observed trends and analysis of air temperature, rainfall, extreme events (including tropical cyclones), sea-surface temperature, ocean acidification, mean and extreme sea levels are presented. Projections for air and sea-surface temperature, rainfall, sea level, ocean acidification and extreme events for the 21st century are provided. These projections are presented along with confidence levels based on expert judgement by Pacific Climate Change Science Program (PCCSP) scientists. The chapter concludes with a summary table of projections (Table 12.4). Important background information, including an explanation of methods and models, is provided in Chapter 1. For definitions of other terms refer to the Glossary.

12.1 Climate Summary

12.1.1 Current Climate

- Seasonal temperature differences in Samoa are very small.
- The wet season extends from November to April. Rainfall is greatly influenced by the position and strength of the South Pacific Convergence Zone, which lies between Samoa and Fiji during the wet season.
- There is significant year-to-year variability in rainfall, which is strongly influenced by the El Niño-Southern Oscillation. The impact of the El Niño-Southern Oscillation is more significant in the wet season.
- Positive trends are evident in both annual and seasonal mean air temperatures at Apia for the period 1950–2009.
- Annual and seasonal rainfall trends for Apia for the period 1950–2009 are not statistically significant.
- On average Apia experiences 10 tropical cyclones per decade, usually between November and April. The high variability in tropical cyclone numbers makes it difficult to identify any long-term trends in frequency.
- Droughts and flooding associated with the El Niño-Southern Oscillation have impacted the social and economic livelihoods of the Samoan people on many occasions in the past.
- The sea-level rise near Samoa measured by satellite altimeters since 1993 is about 4 mm per year.

12.1.2 Future Climate

Over the course of the 21st century:

- Surface air temperature and sea-surface temperature are projected to continue to increase (*very high* confidence).
- Wet season and annual mean rainfall is projected to increase (*moderate* confidence).
- Little change is projected in dry season rainfall (*low* confidence).
- The intensity and frequency of days of extreme heat are projected to increase (*very high* confidence).
- The intensity and frequency of days of extreme rainfall are projected to increase (*high* confidence).
- Little change is projected in the incidence of drought (*low* confidence).
- Tropical cyclone numbers are projected to decline in the south-east Pacific Ocean basin (0–40ºS, 170ºE–130ºW) (*moderate* confidence).
- Ocean acidification is projected to continue (*very high* confidence).
- Mean sea-level rise is projected to continue (*very high* confidence).

12.2 Country Description

Samoa consists of four main inhabited islands (Upolu, Savai'i, Manono and Apolima) and six smaller uninhabited islands. The islands lie between 13ºS–14ºS and 170ºW–173ºW and have a total land area of approximately 2934 km^2 (Samoa's First National Communication under the UNFCCC, 2000). Samoa has a rugged and mountainous topography. On Upolu, the central mountain range runs along the length of the island with some peaks rising more than 1000 m above sea level. Savai'i has central volcanic peaks reaching 1860 m (Samoa Country Profile, SOPAC, 2000).

Samoa's 2010 estimated population was 183 123 (Samoa Country Statistics, SOPAC, 2011). More than half of Samoa's resident population live on the island of Upolu, also home to the capital, Apia.

Agriculture and fisheries products have traditionally provided the bulk of Samoa's commodity exports including coconut oil, coconut cream, bananas, taro, kava and fish. Tourism also contributes significantly to Samoa's economy (Samoa's Second National Communication under the UNFCCC, 2010).

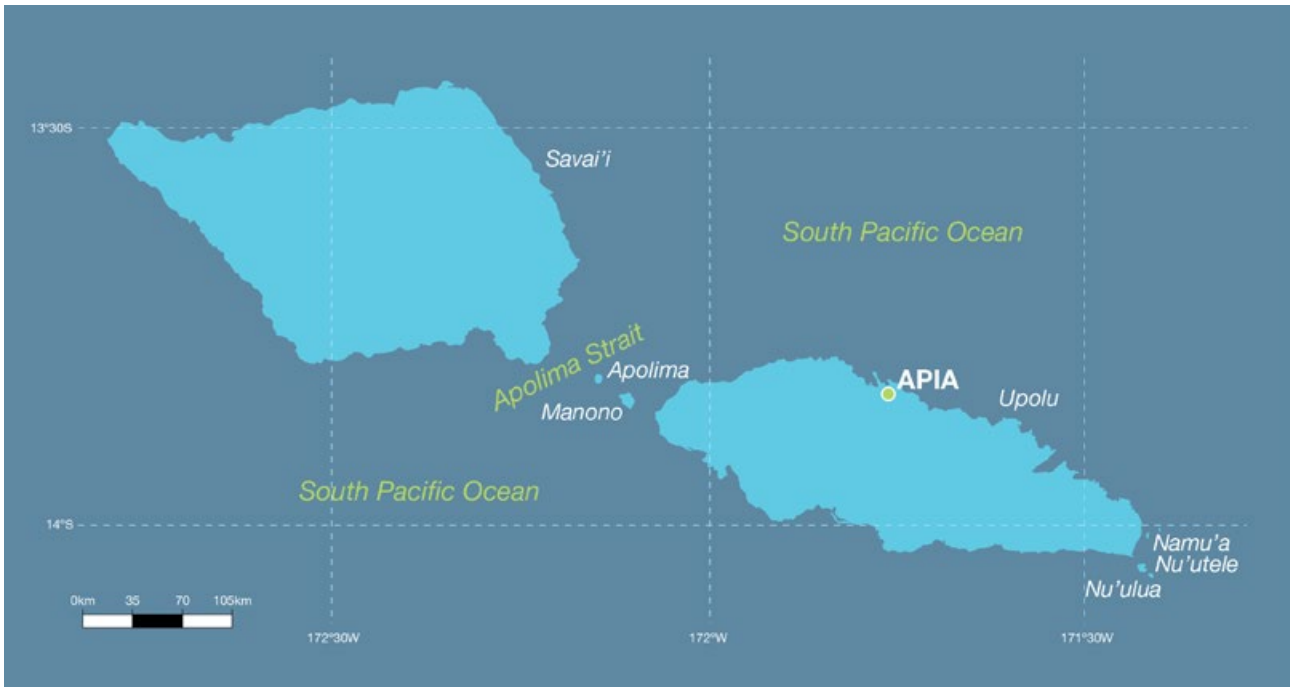

Figure 12.1: Samoa

12.3 Data Availability

There are eight operational meteorological stations in Samoa. The primary meteorological station is located in Apia (Figure 12.1). Apia has rainfall and air temperature data from 1890. Apia, Faleolo and Maota stations take multiple observations within a 24-hour period. The other stations (Afiamalu, Nafanua, Alafua, Togitogiga on Upolu and Asau on Savaii) record rainfall once a day only.

Climate records for Apia from 1950–2009 have been used. The Apia records are homogeneous and more than 98% complete.

Monthly-averaged sea-level data are available from Pago Pago (1948–present, American Samoa) and Apia (1954–1971 and 1993–present). A global positioning system instrument to estimate vertical land motion was deployed at Apia in 2001 and will provide valuable direct estimates of local vertical land motion in future years. Both satellite (from 1993) and in situ sea-level data (1950–2009; termed reconstructed sea level; Volume 1, Section 2.2.2.2) are available on a global 1° x 1° grid.

Long-term locally-monitored sea-surface temperature data are unavailable for Samoa, so large-scale gridded sea-surface temperature datasets have been used (HadISST, HadSST2, ERSST and Kaplan Extended SST V2; Volume 1, Table 2.3).

12.4 Seasonal Cycles

There are only very small seasonal temperature differences in Samoa (Figure 12.2). The coolest month of the year is July. This is also when relatively cool, dry south-east trade winds are strongest. The warmest month is March, which is about 1˚C warmer than July.

Rainfall has a distinct seasonal variation in Samoa. On average 75% of total annual rainfall is received in the wet season, from November to April (Figure 12.2). Average wet season rainfall amounts to approximately 350 mm per month. On average rainfall is about 150 mm per month in the dry season. Samoa's rainfall is greatly influenced by the position and strength of the South Pacific Convergence Zone (SPCZ), which lies between Samoa and Fiji during the wet season. In the dry season the SPCZ is normally to the north-east of Samoa, often weak, inactive and sometimes non-existent. The close proximity of the SPCZ to Samoa during summer results in heavy rainfall throughout the country. Samoa's topography has a significant effect on rainfall distribution. Wet areas are located in the south-east and relatively sheltered, drier areas are in the north-west.

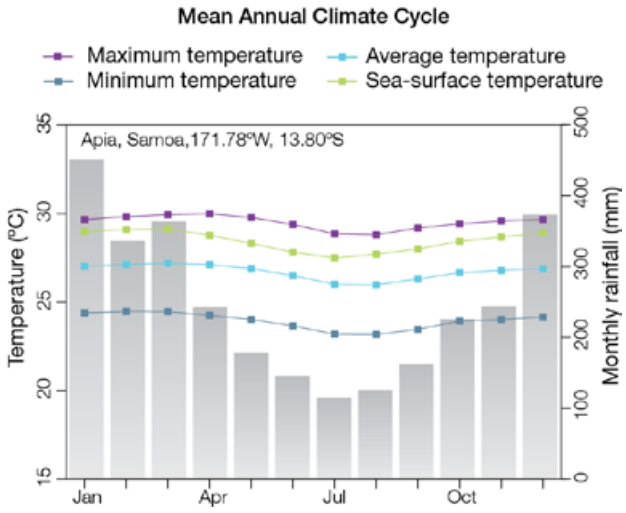

Figure 12.2: Mean annual cycle of rainfall (grey bars) and daily maximum, minimum and mean air temperatures at Apia, and local sea-surface temperatures derived from the HadISST dataset (Volume 1, Table 2.3).

12.5 Climate Variability

There is significant year-to-year variability in rainfall observed in Samoa (Figure 12.4). Annual rainfall in the drier years can be approximately half of that observed in wettest years. This year-to-year variability is strongly influenced by the El Niño-Southern Oscillation (ENSO). The impact of ENSO is more significant in the wet season (Table 12.1). El Niño events tend to bring drier conditions in the wet season due to the SPCZ becoming less active. In La Niña years, rainfall is usually above normal and air temperatures are cooler than normal. ENSO Modoki events (Volume1, Section 3.4.1) have the same impacts but weaker. There is a weaker but still significant correlation between canonical ENSO and ENSO Modoki and dry season rainfall.

A negative correlation exists between the Interdecadal Pacific Oscillation (IPO) and dry season rainfall. This suggests that the El Niño-like pattern of decadal variability that exists in a positive phase of the IPO produces a similar reduction in rainfall as El Niño events, but on longer time periods.

Table 12.1: Correlation coefficients between indices of key large-scale patterns of climate variability and minimum and maximum temperatures (Tmin and Tmax) and rainfall at Apia. Only correlation coefficients that are statistically significant at the 95% level are shown.

Climate feature/index		Dry season (May-October)			Wet season (November-April)		
		Tmin	Tmax	Rain	Tmin	Tmax	Rain
ENSO	Niño3.4			-0.38	0.67	0.68	-0.46
	Southern Oscillation Index		-0.24	0.30	-0.56	-0.65	0.54
Interdecadal Pacific Oscillation Index				-0.23			
Southern Annular Mode Index							
ENSO Modoki Index		0.30	0.29		0.60	0.59	-0.20
Number of years of data		78	75	108	78	77	108

Weather station, Samoa Meterology Division

12.6 Observed Trends

12.6.1 Air Temperature

Positive trends are evident in both annual and seasonal mean air temperatures at Apia for the period 1950–2009. Maximum air temperature trends are considerably greater than minimum air temperature trends. In the wet season, maximum air temperature trends are greater than the trends in the dry season (Figure 12.3 and Table 12.2).

12.6.2 Rainfall

Annual and seasonal rainfall trends for Apia for the period 1950–2009 are not statistically significant (Table 12.2 and Figure 12.4).

12.6.3 Extreme Events

The tropical cyclone season in the Samoa region is between November and April. Between 1969/70 and 2009/10 only Tropical Cyclone Keli occurred outside these months in June 1997. The tropical cyclone archive for the Southern Hemisphere indicates that between the 1969/1970 and 2009/10 seasons, the centre of 52 tropical cyclones passed within approximately 400 km of Apia. This represents an average of 10 cyclones per decade. Tropical cyclones were most frequent in El Niño years (16 cyclones per season) and occurrences in La Niña and neutral years are less frequent (10 cyclones per decade). The interannual variability in the number of tropical cyclones in the vicinity of Apia is large, ranging from zero in some seasons to five in the 1980/81 and 2004/05 seasons (Figure 12.5). This high variability makes it difficult to identify any long-term trends in frequency.

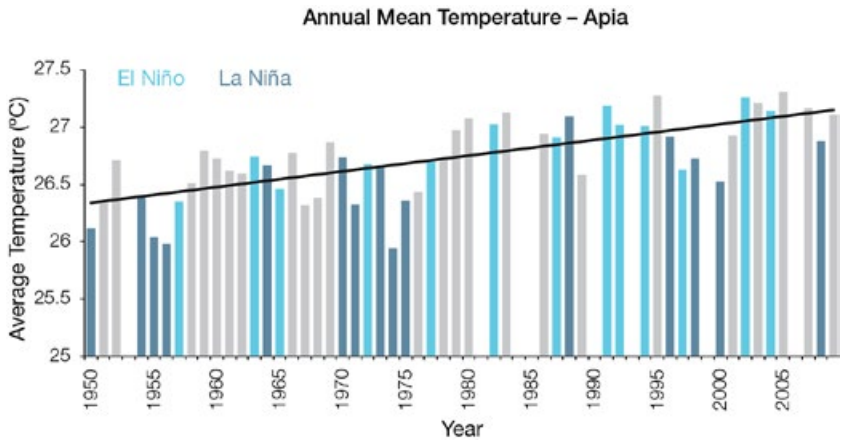

Figure 12.3: Annual mean air temperature at Apia. Light blue, dark blue and grey bars denote El Niño, La Niña and neutral years respectively

Table 12.2: Annual and seasonal trends in maximum, minimum and mean air temperature (Tmax, Tmin and Tmean) and rainfall at Apia for the period 1950–2009. Asterisks indicate significance at the 95% level. Persistence is taken into account in the assessment of significance as in Power and Kociuba (in press). The statistical significance of the air temperature trends is not assessed.

	Apia Tmax (°C per 10 yrs)	Apia Tmin (°C per 10 yrs)	Apia Tmean (°C per 10 yrs)	Apia Rain (mm per 10 yrs)
Annual	+0.22	+0.04	+0.14	+8
Wet season	+0.24	+0.04	+0.14	+22
Dry season	+0.18	+0.04	+0.11	0

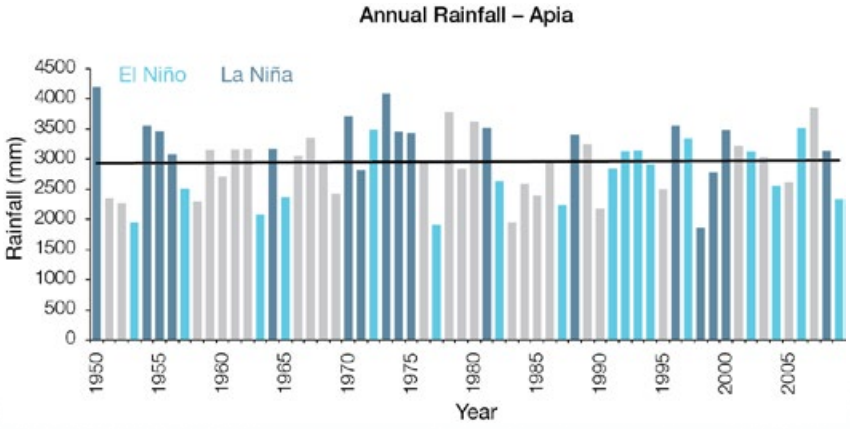

Figure 12.4: Annual rainfall at Apia. Light blue, dark blue and grey bars denote El Niño, La Niña and neutral years respectively

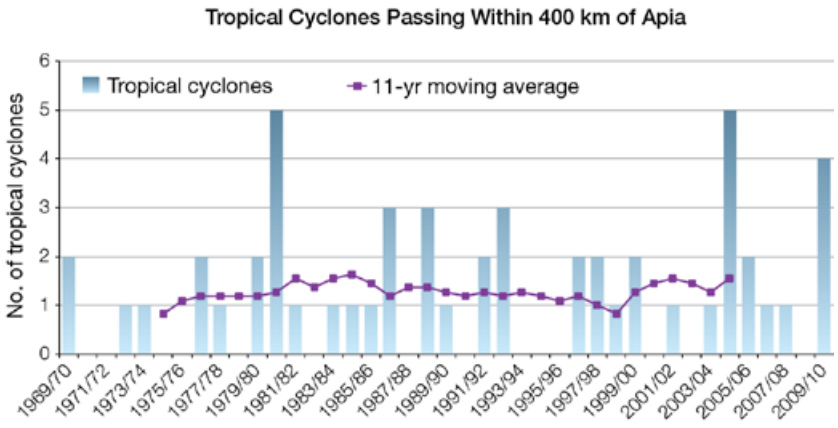

Figure 12.5: Tropical cyclones passing within 400 km of Apia per season. The 11-year moving average is in purple.

Tropical Cyclone Ofa (1990) and Tropical Cyclone Val (1991) caused widespread damage in Samoa, which has been estimated to equal approximately four times the national Gross Domestic Product.

Droughts and flooding associated with ENSO have impacted the social and economic livelihoods of the Samoan people on many occasions in the past. Drought impacts are most notable in the north-west regions of the main islands (Faleolo and Asau) and at times are associated with forest fires. In Asau, there were major forest fires during the dry seasons of 1982/83, 1997/98, 2001/02 and 2002/03.

Flooding associated with tropical cyclones and strong La Niña events has caused widespread damage in Samoa in the past. In early 2008 and 2011, for example, transportation and water infrastructure were severely damaged.

12.6.4 Sea-Surface Temperature

Water temperatures around Samoa declined from the 1950s to about 1980. This was followed by a period of warming (approximately 0.08°C per decade for 1970–present). Figure 12.8 shows the 1950–2000 sea-surface temperature changes (relative to a reference year of 1990) from three different large-scale sea-surface temperature gridded datasets (HadSST2, ERSST and Kaplan Extended SST V2; Volume 1, Table 2.3). At these regional scales, natural variability may play a large role determining sea-surface temperature in the region making it difficult to identify any long-term trends.

12.6.5 Ocean Acidification

Based on the large-scale distribution of coral reefs across the Pacific and the seawater chemistry, Guinotte et al. (2003) suggested that seawater aragonite saturation states above 4 were optimal for coral growth and for the development of healthy reef ecosystems, with values from 3.5 to 4 adequate for coral growth, and values between 3 and 3.5, marginal. Coral reef ecosystems were not found at seawater aragonite saturation states below 3 and these conditions were classified as extremely marginal for supporting coral growth.

In the Samoa region, the aragonite saturation state has declined from about 4.5 in the late 18th century to an observed value of about 4.1 ± 0.1 by 2000.

12.6.6 Sea Level

Monthly averages of the historical tide gauge, satellite (since 1993) and gridded sea-level (since 1950) data agree well after 1993 and indicate interannual variability in sea levels of about 20 cm (estimated 5–95% range) after removal of the seasonal cycle (Figure 12.10). The sea-level rise near Samoa measured by satellite altimeters (Figure 12.6) since 1993 is about 4 mm per year, slightly larger than the global average of 3.2 ± 0.4 mm per year. This rise is partly linked to a pattern related to climate variability from year to year and decade to decade (Figure 12.10).

12.6.7 Extreme Sea-Level Events

The annual climatology of the highest daily sea levels has been evaluated from hourly measurements by the tide gauge at Apia (Figure 12.7). High tides show a small variation throughout the year with an April to May minimum and a July to August maximum. There is no seasonal cycle in the long-term variations in sea level, although during La Niña years sea levels tend to be higher from January to June and during El Niño they tend to be lower from February to September (Volume 1, Section 3.6.3, and Figures 3.20 and 3.21). Short-term variations are slightly higher in December through March. When the tidal, short-term and long-term components are combined, they produce an annual cycle which shows relatively little variation throughout the year. The 10 events in the sea-level record tend occur at different times of the year, however all 10 events occur in either La Niña or ENSO-neutral years.

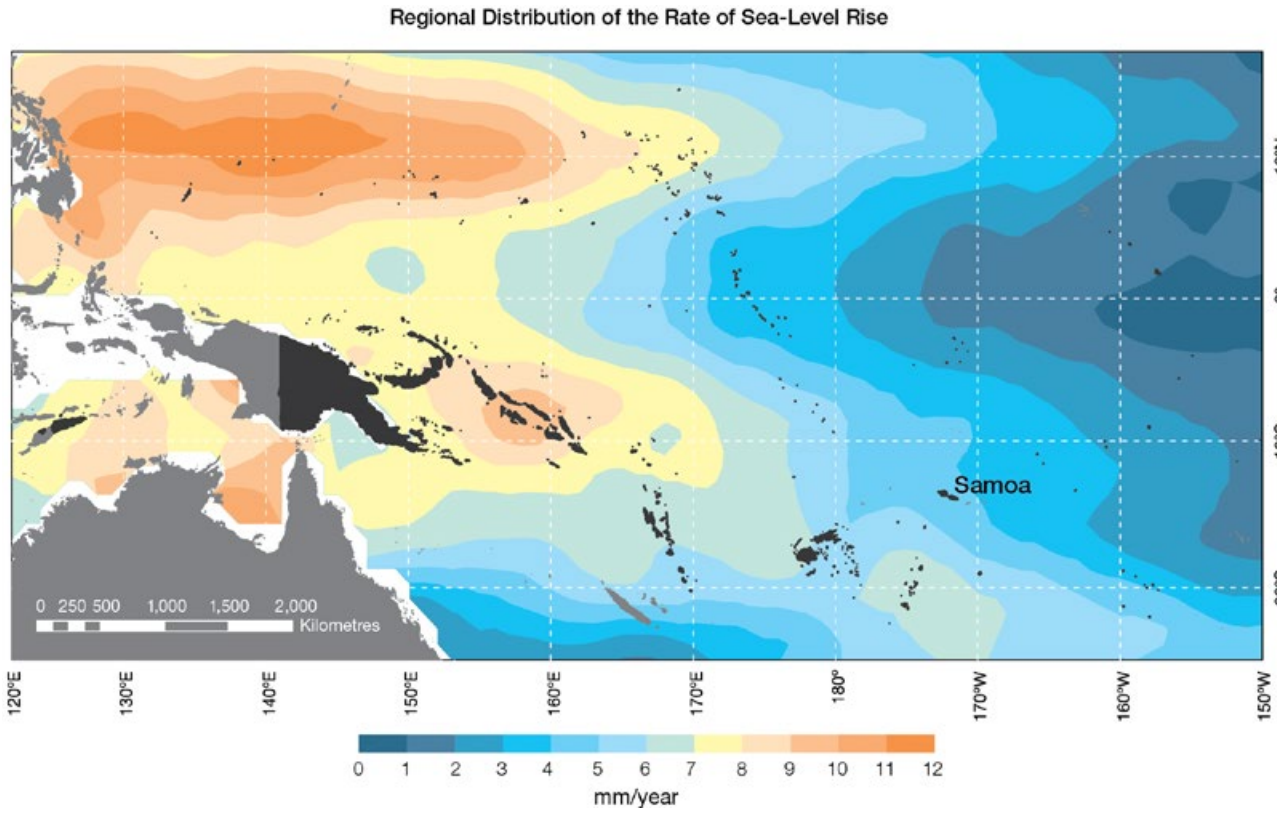

Figure 12.6: The regional distribution of the rate of sea-level rise measured by satellite altimeters from January 1993 to December 2010, with the location of Samoa indicated. Further detail about the regional distribution of sea-level rise is provided in Volume 1, Section 3.6.3.2.

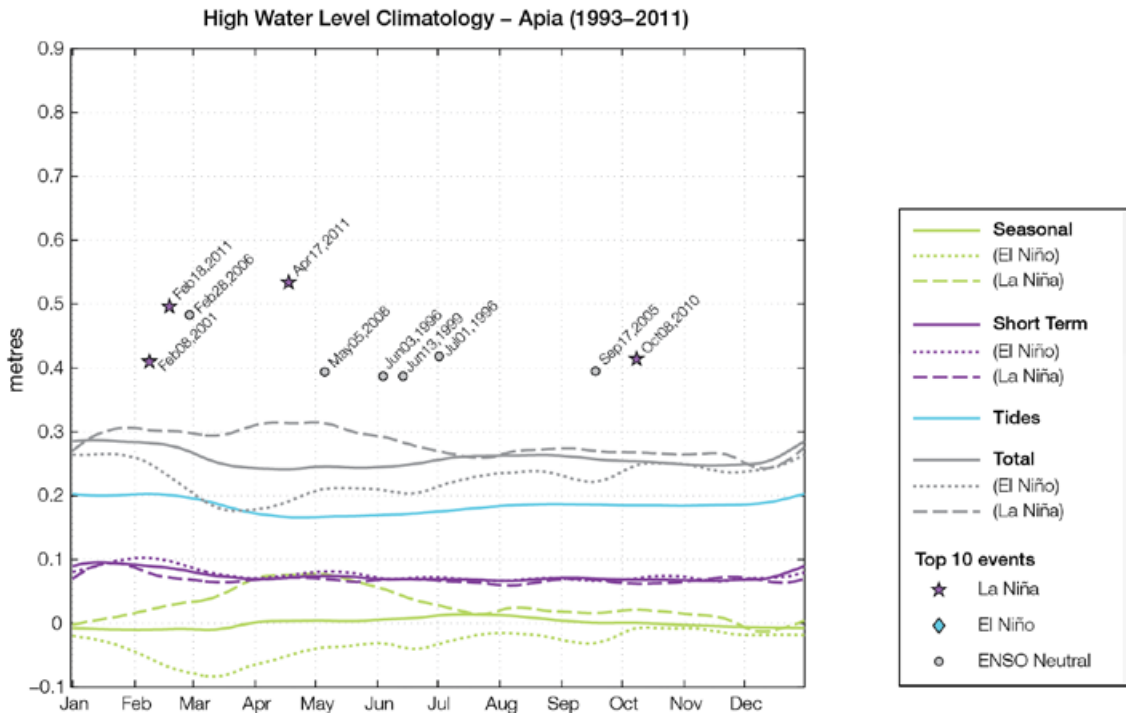

Figure 12.7: The annual cycle of high waters relative to Mean Higher High Water (MHHW) due to tides, short-term fluctuations (most likely associated with storms) and seasonal variations for Apia. The tides and short-term fluctuations are respectively the 95% exceedence levels of the astronomical high tides relative to MHHW and short-term sea level fluctuations. Components computed only for El Niño and La Niña years are shown by dotted and dashed lines, and grey lines are the sum of the tide, short-term and seasonal components. The 10 highest sea level events in the record relative to MHHW are shown and coded to indicate the phase of ENSO at the time of the extreme event.

12.7 Climate Projections

Climate projections have been derived from up to 18 global climate models from the CMIP3 database, for up to three emissions scenarios (B1 (low), A1B (medium) and A2 (high)) and three 20-year periods (centred on 2030, 2055 and 2090, relative to 1990). These models were selected based on their ability to reproduce important features of the current climate (Volume 1, Section 5.2.3), so projections from each of the models are plausible representations of the future climate. This means there is not one single projected future for Samoa, but rather a range of possible futures. The full range of these futures is discussed in the following sections.

These projections do not represent a value specific to any actual location, such as a town or city in Samoa. Instead, they refer to an average change over the broad geographic region encompassing the islands of Samoa and the surrounding ocean (Figure 1.1 shows the regional boundaries). Some information regarding dynamical downscaling simulations from the CCAM model (Section 1.7.2) is also provided, in order to indicate how changes in the climate on an individual island-scale may differ from the broad-scale average.

Section 1.7 provides important information about understanding climate model projections.

12.7.1 Temperature

Surface air temperature and sea-surface temperature is projected to continue to increase over the course of the 21st century. There is *very high* confidence in this direction of change because:

- Warming is physically consistent with rising greenhouse gas concentrations.
- All CMIP3 models agree on this direction of change.

Almost all of the CMIP3 models simulate a slight increase (<1°C) in annual and seasonal mean temperature by 2030, however by 2090 under the A2 (high) emissions scenario temperature increases of greater than 2.5°C are simulated by the majority of models (Table 12.3). Given the close relationship between surface air temperature and sea-surface temperature, a similar (or slightly weaker) rate of warming is projected for the surface ocean (Figure 12.8). There is *moderate* confidence in this range and distribution of possible futures because:

- There is generally a large discrepancy between modelled and observed temperature trends over the past 50 years in the vicinity of Samoa (Figure 12.8).

The 8 km CCAM simulations suggest that projected changes in the average daily minimum air temperature over land can be up to 0.5°C greater than over the surrounding ocean. This suggests that the CMIP3 models may slightly underestimate future increases in daily minimum air temperature.

Interannual variability in surface air temperature and sea-surface temperature over Samoa is strongly influenced by ENSO in the current climate (Section 12.5). As there is no consistency in projections of future ENSO activity (Volume 1, Section 6.4.1) it is not possible to determine whether interannual variability in temperature will change in the future. However, ENSO is expected to continue to be an important source of variability for the region.

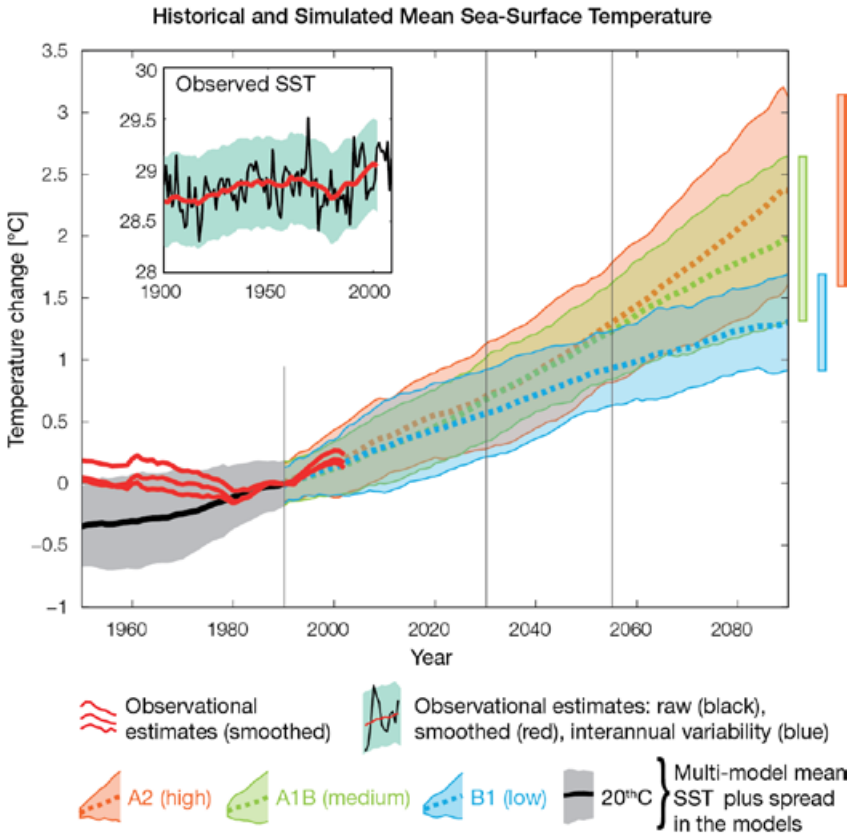

Figure 12.8: Historical climate (from 1950 onwards) and simulated historical and future climate for annual mean sea-surface temperature (SST) in the region surrounding Samoa, for the CMIP3 models. Shading represents approximately 95% of the range of model projections (twice the inter-model standard deviation), while the solid lines represent the smoothed (20-year running average) multi-model mean temperature. Projections are calculated relative to the 1980–1999 period (which is why there is a decline in the inter-model standard deviation around 1990). Observational estimates in the main figure (red lines) are derived from the HadSST2, ERSST and Kaplan Extended SST V2 datasets (Volume 1, Section 2.2.2). Annual average (black) and 20-year running average (red) HadSST2 data is also shown inset.

12.7.2 Rainfall

Wet Season (November-April)

Wet season rainfall is projected to increase over the course of the 21st century. There is *moderate* confidence in this direction of change because:

- An increase in wet season rainfall is consistent with the projected likely increase in the intensity of the South Pacific Convergence Zone (SPCZ) which lies over Samoa in this season (Volume 1, Section 6.4.5).
- The majority of CMIP3 models agree on this direction of change by 2090.

The majority of CMIP3 models simulate little change (-5% to 5%) in wet season rainfall by 2030, however by 2090 under the higher emissions scenarios (i.e. A2 (high) and A1B (medium)) the majority simulate an increase (>5%), with very few models simulating decline (< -5%) (Table 12.3). There is *moderate* confidence in this range and distribution of possible futures because:

- In simulations of the current climate, the CMIP3 models generally locate the SPCZ in the correct location relative to Samoa in the wet season (Brown et al., 2011).
- The CMIP3 models are unable to resolve many of the physical processes involved in producing rainfall. As a consequence, they do not simulate rainfall as well as other variables such as temperature (Volume 1, Chapter 5).

The 8 km CCAM simulations suggest that any changes in wet season rainfall will be relatively uniform across Samoa, with no significant topographic differences indicated between the eastern and western sides of Savai'i or Upolu.

Dry Season (May-October)

Little change is projected in dry season rainfall over the course of the 21st century. There is *low* confidence in this direction of change because:

- There is little agreement amongst the models, with approximately equal numbers simulating an increase (>5%), decrease (<-5%) and little change (-5% to 5%) by 2090 across the three emissions scenarios.
- In simulations of the current climate, some CMIP3 models have an SPCZ that extends too far east during the dry season, with too much rainfall over Samoa (Brown et al., 2011).
- The CMIP3 models are unable to resolve many of the physical processes involved in producing rainfall.

The 8 km CCAM simulations suggest that any changes in dry season rainfall will be enhanced on the eastern side of Savai'i and Upolu. This is a physically consistent response on the windward side of mountainous islands.

Annual

Total annual rainfall is projected to increase over the course of the 21st century. There is *moderate* confidence in this direction of change because:

- Approximately half of the CMIP3 models agree on this direction of change by 2090.
- There is moderate and low confidence in wet and dry season rainfall projections respectively, as discussed above.

Interannual variability in rainfall over Samoa is strongly influenced by ENSO in the current climate, via the movement of the SPCZ (Section 12.5). As there is no consistency in projections of future ENSO activity (Volume 1, Section 6.4.1), it is not possible to determine whether interannual variability in rainfall will change in the future.

12.7.3 Extremes

Temperature

The intensity and frequency of days of extreme heat are projected to increase over the course of the 21st century. There is *very high* confidence in this direction of change because:

- An increase in the intensity and frequency of days of extreme heat is physically consistent with rising greenhouse gas concentrations.
- All CMIP3 models agree on the direction of change for both intensity and frequency.

The majority of CMIP3 models simulate an increase of approximately 1°C in the temperature experienced on the 1-in-20-year hot day by 2055 under the B1 (low) emissions scenario, with an increase of over 2.5°C simulated by the majority of models by 2090 under the A2 (high) emissions scenario (Table 12.3). There is *low* confidence in this range and distribution of possible futures because:

- In simulations of the current climate, the CMIP3 models tend to underestimate the intensity and frequency of days of extreme heat (Volume 1, Section 5.2.4).
- Smaller increases in the frequency of days of extreme heat are projected by the CCAM 60 km simulations.

Rainfall

The intensity and frequency of days of extreme rainfall is projected to increase over the course of the 21st century. There is *high* confidence in this direction of change because:

- An increase in the frequency and intensity of extreme rainfall is consistent with larger-scale projections, based on the physical argument that the atmosphere is able to hold more water vapour in a warmer climate (Allen and Ingram, 2002; IPCC, 2007). It is also consistent with the projected likely increase in SPCZ intensity (Volume 1, Section 6.4.5).

- Almost all of the CMIP3 models agree on this direction of change for both intensity and frequency.

The majority of CMIP3 models simulate an increase of at least 20 mm in the amount of rain received on the 1-in-20-year wet day by 2055 under the B1 (low) emissions scenario, with an increase of at least 25 mm simulated by 2090 under the A2 (high) emissions scenario. The majority of models project that the current 1-in-20-year extreme rainfall event will occur, on average, four times per 20-year period by 2055 under the B1 (low) emissions scenario and three times per 20-year period by 2090 under the A2 (high) emissions scenario. There is *low* confidence in this range and distribution of possible futures because:

- In simulations of the current climate, the CMIP3 models tend to underestimate the intensity and frequency of extreme rainfall (Volume 1, Section 5.2.4).
- The CMIP3 models are unable to resolve many of the physical processes involved in producing extreme rainfall.

Drought

Little change is projected in the incidence of drought over the course of the 21st century. There is *low* confidence in this direction of change because:

- There is only low confidence in the range of dry season rainfall projections (Section 12.7.2), which directly influences projections of future drought conditions.

The majority of CMIP3 models project that mild drought will occur approximately seven to eight times every 20 years in 2030 under all emissions scenarios, decreasing to six to seven times by 2090. The frequency of moderate and severe drought is projected to remain approximately stable, at once to twice and once every 20 years, respectively.

Tropical Cyclones

Tropical cyclone numbers are projected to decline in the south-east Pacific Ocean basin (0–40ºS, 170ºE–130ºW) over the course of the 21st century. There is *moderate* confidence in this direction of change because:

- Many studies suggest a decline in tropical cyclone frequency globally (Knutson et al., 2010).
- Tropical cyclone numbers decline in the south-east Pacific Ocean in the majority assessment techniques.

Based on the direct detection methodologies (Curvature Vorticity Parameter (CVP) and the CSIRO Direct Detection Scheme (CDD) described in Volume 1, Section 4.8.2), 65% of projections show no change or a decrease in tropical cyclone formation when applied to the CMIP3 climate models for which suitable output is available. When these techniques are applied to CCAM, 100% of projections show a decrease in tropical cyclone formation. In addition, the Genesis Potential Index (GPI) empirical technique suggests that conditions for tropical cyclone formation will become less favourable in the south-east Pacific Ocean basin, for all analysed CMIP3 models. There is *moderate* confidence in this range and distribution of possible futures because in simulations of the current climate, the CVP, CDD and GPI methods capture the frequency of tropical cyclone activity reasonably well (Volume 1, Section 5.4).

Despite this projected reduction in total cyclone numbers, five of the six CCAM 60 km simulations show an increase in the proportion of the most severe cyclones. Most models also indicate a reduction in tropical cyclone wind hazard north of 20ºS latitude and regions of increased hazard south of 20ºS latitude. This increase in wind hazard coincides with a poleward shift in the latitude at which tropical cyclones are most intense.

12.7.4 Ocean Acidification

The acidification of the ocean will continue to increase over the course of the 21st century. There is *very high* confidence in this projection as the rate of ocean acidification is driven primarily by the increasing oceanic uptake of carbon dioxide, in response to rising atmospheric carbon dioxide concentrations.

Projections from all analysed CMIP3 models indicate that the annual maximum aragonite saturation state will reach values below 3.5 by about 2060 and continue to decline thereafter (Figure 12.9; Table 12.3). There is *moderate* confidence in this range and distribution of possible futures because the projections are based on climate models without an explicit representation of the carbon cycle and with relatively low resolution and known regional biases.

The impact of acidification change on the health of reef ecosystems is likely to be compounded by other stressors including coral bleaching, storm damage and fishing pressure.

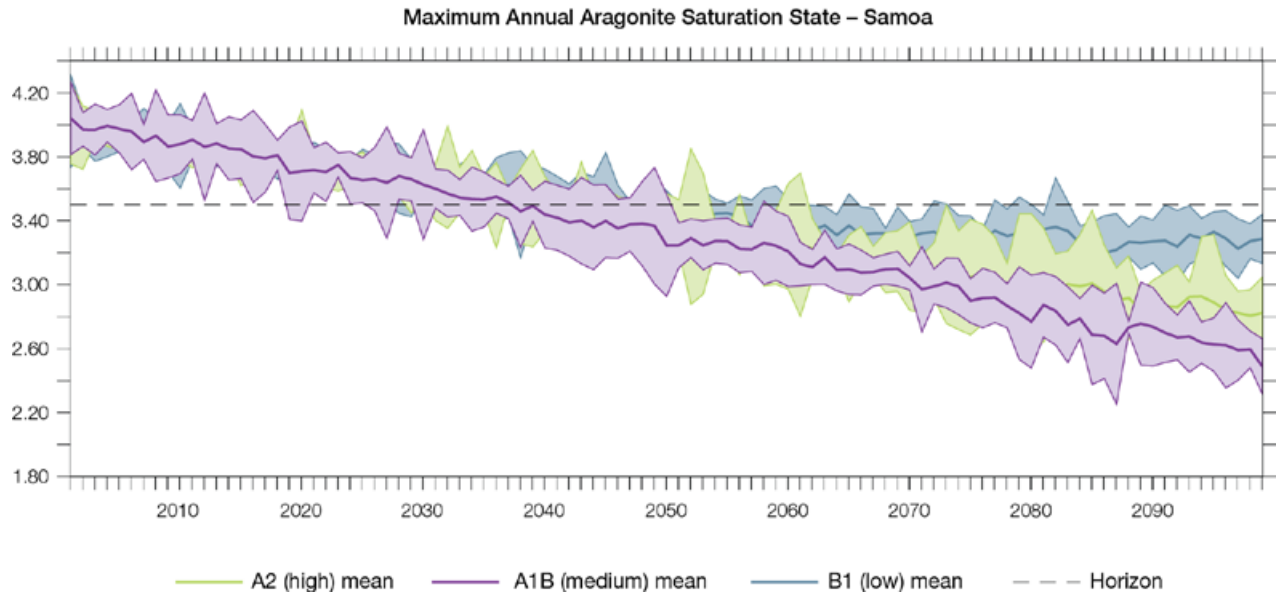

Figure 12.9: Multi-model projections, and their associated uncertainty (shaded area represents two standard deviations), of the maximum annual aragonite saturation state in the sea surface waters of the Samoa region under the different emissions scenarios. The dashed black line represents an aragonite saturation state of 3.5.

12.7.5 Sea Level

Mean sea level is projected to continue to rise over the course of the 21st century. There is *very high* confidence in this direction of change because:

- Sea-level rise is a physically consistent response to increasing ocean and atmospheric temperatures, due to thermal expansion of the water and the melting of glaciers and ice caps.
- Projections arising from all CMIP3 models agree on this direction of change.

The CMIP3 models simulate a rise of between approximately 5–15 cm by 2030, with increases of 20–60 cm indicated by 2090 under the higher emissions scenarios (i.e. A2 (high) and A1B (medium); Figure 12.10; Table 12.3). There is *moderate* confidence in this range and distribution of possible futures because:

- There is significant uncertainty surrounding ice-sheet contributions to sea-level rise and a rise larger than projected above cannot be excluded (Meehl et al., 2007b). However, understanding of the processes is currently too limited to provide a best estimate or an upper bound (IPCC, 2007).
- Globally, since the early 1990s, sea level has been rising near the upper end of these projections. During the 21st century, some studies (using semi-empirical models) project faster rates of sea-level rise.

Interannual variability of sea level will lead to periods of lower and higher regional sea levels. In the past, this interannual variability has been about 20 cm (5–95% range, after removal of the seasonal signal; dashed lines in Figure 12.10 (a)) and it is likely that a similar range will continue through the 21st century. In addition, winds and waves associated with weather phenomena will continue to lead to extreme sea-level events.

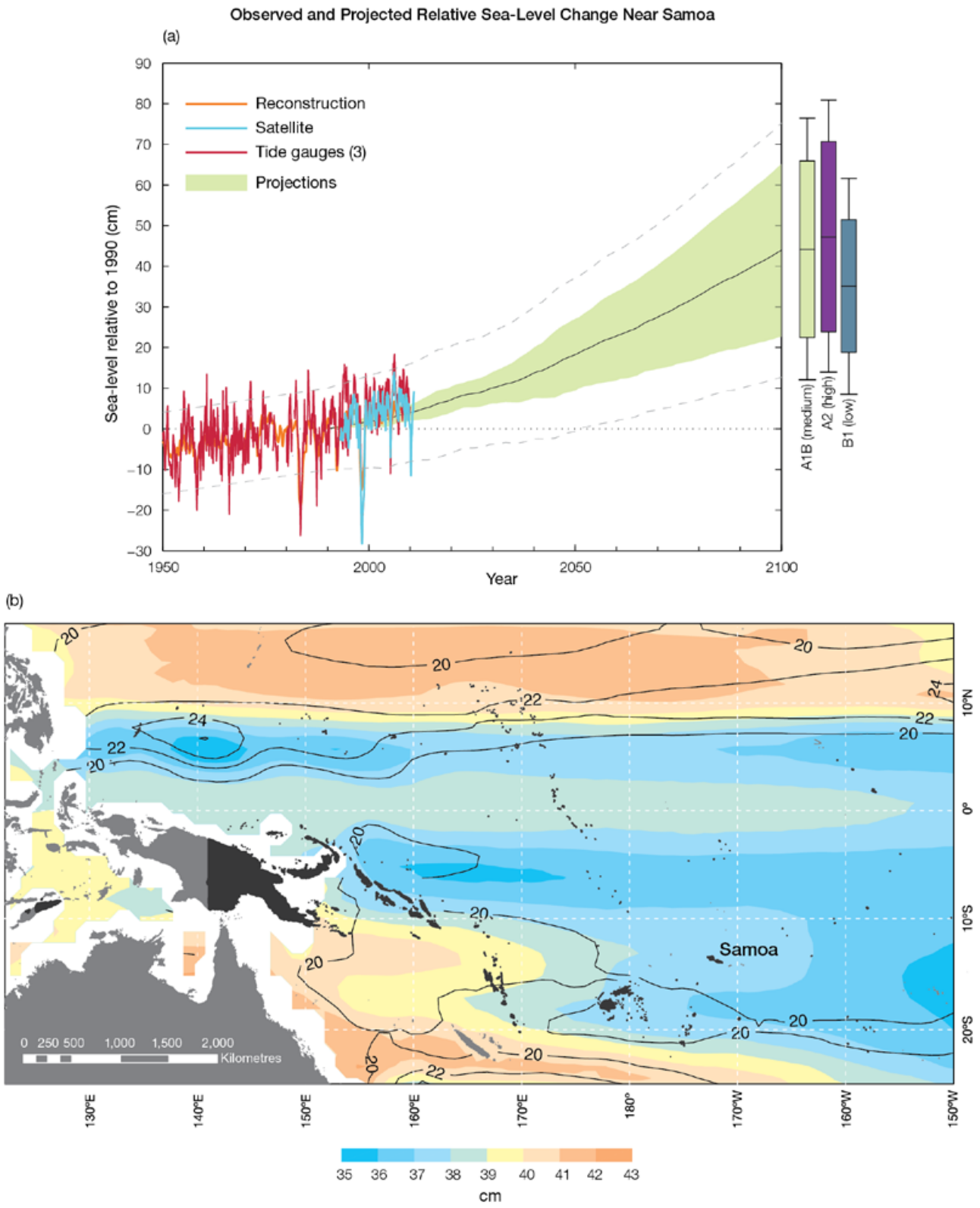

Figure 12.10: Observed and projected relative sea-level change near Samoa. (a) The observed in situ relative sea-level records are indicated in red, with the satellite record (since 1993) in light blue. The gridded sea level at Samoa (since 1950, from Church and White (in press)) is shown in orange. The projections for the A1B (medium) emissions scenario (5–95% uncertainty range) are shown by the green shaded region from 1990–2100. The range of projections for the B1 (low), A1B (medium) and A2 (high) emissions scenarios by 2100 are also shown by the bars on the right. The dashed lines are an estimate of interannual variability in sea level (5–95% range about the long-term trends) and indicate that individual monthly averages of sea level can be above or below longer-term averages. (b) The projections (in cm) for the A1B emissions scenario in the Samoa region for the average over 2081–2100 relative to 1981–2000 are indicated by the shading, with the estimated uncertainty in the projections indicated by the contours (in cm).

12.7.6 Projections Summary

The projections presented in Section 12.7 are summarised in Table 12.3. For detailed information regarding the various uncertainties associated with the table values, refer to the preceding text in Sections 12.7 and 1.7, in addition to Chapters 5 and 6 in Volume 1. When interpreting the differences between projections for the B1 (low), A1B (medium) and A2 (high) emissions scenarios, it is also important to consider the emissions pathways associated with each scenario (Volume 1, Figure 4.1) and the fact that a slightly different subset of models was available for each (Volume 1, Appendix 1).

Table 12.3: Projected change in the annual and seasonal mean climate for Samoa, under the B1 (low; blue), A1B (medium; green) and A2 (high; purple) emissions scenarios. Projections are given for three 20-year periods centred on 2030 (2020–2039), 2055 (2046–2065) and 2090 (2080–2099), relative to 1990 (1980–1999). Values represent the multi-model mean change ± twice the inter-model standard deviation (representing approximately 95% of the range of model projections), except for sea level where the estimated mean change and the 5–95% range are given (as they are derived directly from the Intergovernmental Panel on Climate Change Fourth Assessment Report values). The confidence (Section 1.7.2) associated with the range and distribution of the projections is also given (indicated by the standard deviation and multi-model mean, respectively). See Volume 1, Appendix 1 for a complete listing of CMIP3 models used to derive these projections.

Variable	Season	2030	2055	2090	Confidence
Surface air temperature (°C)	Annual	+0.6 ± 0.4 +0.8 ± 0.4 +0.7 ± 0.3	+1.0 ± 0.4 +1.4 ± 0.5 +1.4 ± 0.4	+1.4 ± 0.6 +2.2 ± 0.7 +2.6 ± 0.7	Moderate
Maximum temperature (°C)	1-in-20-year event	N/A	+1.0 ± 0.5 +1.4 ± 0.6 +1.5 ± 0.4	+1.3 ± 0.5 +2.1 ± 1.0 +2.6 ± 1.3	Low
Minimum temperature (°C)	1-in-20-year event	N/A	+1.2 ± 1.8 +1.6 ± 1.6 +1.5 ± 1.9	+1.5 ± 1.6 +2.0 ± 2.2 +2.3 ± 1.9	Low
Total rainfall (%)*	Annual	+1 ± 6 +2 ± 9 +4 ± 11	+3 ± 9 +4 ± 15 +5 ± 14	+3 ± 13 +5 ± 17 +7 ± 24	Moderate
Wet season rainfall (%)*	November-April	+1 ± 8 +2 ± 10 +3 ± 11	+4 ± 11 +5 ± 15 +5 ± 11	+4 ± 14 +6 ± 16 +8 ± 22	Moderate
Dry season rainfall (%)*	May-October	+2 ± 9 +3 ± 15 +4 ± 14	+3 ± 11 +4 ± 23 +6 ± 23	+2 ± 14 +3 ± 26 +5 ± 36	Low
Sea-surface temperature (°C)	Annual	+0.6 ± 0.4 +0.7 ± 0.3 +0.7 ± 0.4	+0.9 ± 0.3 +1.2 ± 0.4 +1.3 ± 0.5	+1.3 ± 0.4 +2.0 ± 0.7 +2.4 ± 0.8	High
Aragonite saturation state (Ωar)	Annual maximum	+3.6 ± 0.1 +3.6 ± 0.2 +3.6 ± 0.2	+3.4 ± 0.1 +3.2 ± 0.2 +3.2 ± 0.2	+3.2 ± 0.2 +2.9 ± 0.2 +2.6 ± 0.2	High
Mean sea level (cm)	Annual	+10 (5–15) +10 (6–14) +10 (5–15)	+18 (10–26) +21 (11–30) +20 (10–29)	+31 (17–45) +38 (20–57) +40 (21–59)	Moderate

*The MIROC3.2(medres) and MIROC3.2(hires) models were eliminated in calculating the rainfall projections, due to their inability to accurately simulate present-day activity of the South Pacific Convergence Zone (Volume 1, Section 5.5.1).

Village, Central Province

Chapter 13
Solomon Islands

The contributions of David Hiriasia and Lloyd Tahani from the Solomon Islands Meteorological Service are gratefully acknowledged

Introduction

This chapter provides a brief description of the Solomon Islands, its past and present climate as well as projections for the future. The climate observation network and the availability of atmospheric and oceanic data records are outlined. The annual mean climate, seasonal cycles and the influences of large-scale climate features such as the West Pacific Monsoon and patterns of climate variability (e.g. the El Niño-Southern Oscillation) are analysed and discussed. Observed trends and analysis of air temperature, rainfall, extreme events (including tropical cyclones), sea-surface temperature, ocean acidification, mean and extreme sea levels are presented. Projections for air and sea-surface temperature, rainfall, sea level, ocean acidification and extreme events for the 21st century are provided. These projections are presented along with confidence levels based on expert judgement by Pacific Climate Change Science Program (PCCSP) scientists. The chapter concludes with a summary table of projections (Table 13.4). Important background information, including an explanation of methods and models, is provided in Chapter 1. For definitions of other terms refer to the Glossary.

13.1 Climate Summary

13.1.1 Current Climate

- Air temperatures in the Solomon Islands show very little seasonal variation, and are closely linked to sea-surface temperatures.
- In the west there is a marked wet season from November to April, while rainfall is more constant year-round in the east. Rainfall in the Solomon Islands is affected by the West Pacific Monsoon, the South Pacific Convergence Zone and the Intertropical Convergence Zone.
- Rainfall in the Solomon Islands varies greatly from year-to-year, due mainly to the influence of the El Niño-Southern Oscillation.
- Warming trends are evident in both annual and seasonal mean air temperatures at Honiara for the period 1951–2009.
- Annual and seasonal rainfall trends for Honiara for the period 1950–2009 are not statistically significant.
- The sea-level rise near Solomon Islands measured by satellite altimeters since 1993 is mostly over 8 mm per year.
- On average, Honiara experiences 13 tropical cyclones per decade, with most occurring between November and April. The high variability in tropical cyclone numbers makes it difficult to identify any long-term trends in frequency.

13.1.2 Future Climate

Over the course of the 21st century:

- Surface air temperature and sea-surface temperature are projected to continue to increase (*very high* confidence).
- Annual and seasonal mean rainfall is projected to increase (*high* confidence).
- The intensity and frequency of days of extreme heat are projected to increase (*very high* confidence).
- The intensity and frequency of days of extreme rainfall are projected to increase (*high* confidence).
- The incidence of drought is projected to decrease (*moderate* confidence).
- Tropical cyclone numbers are projected to decline in the south-west Pacific Ocean basin (0–40ºS, 130ºE–170ºE) (*moderate* confidence).
- Ocean acidification is projected to continue (*very high* confidence).
- Mean sea-level rise is projected to continue (*very high* confidence).

13.2 Country Description

The Solomon Islands consist of two chains of volcanic islands that lie between 5ºS–13ºS and 155ºE–169ºE. There are 992 islands with a total land area of 28 785 km^2. The islands range from small low-lying atolls to large, volcanic islands with high peaks (Solomon Islands Country Profile, SOPAC, 2000).

Most of the population, which was estimated at 549 574 in 2010, live in small rural communities dispersed over the nine largest islands (Solomon Islands Country Statistics, SOPAC, 2010). The capital, Honiara, is located on the island Guadalcanal.

Timber has long been a mainstay of the Solomon Islands economy and gold deposits may provide an additional source of revenue for the country. Local agriculture consists of both subsistence and commercial components. Key agricultural exports include cocoa, palm oil and coconut products (Solomon Islands First National Communication under the UNFCCC, 2001).

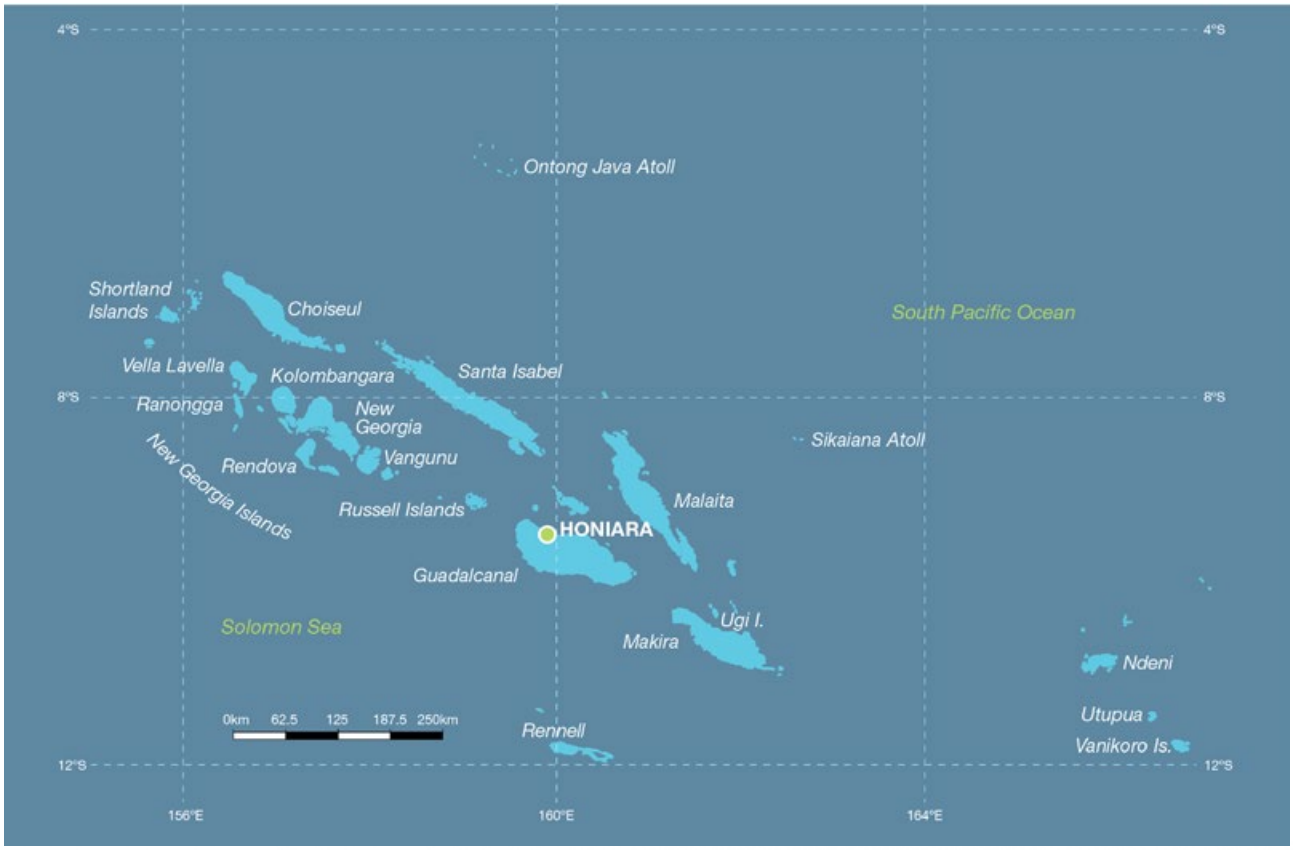

Figure 13.1: Solomon Islands

13.3 Data Availability

There are currently six operational meteorological stations in the Solomon Islands. Multiple observations within a 24-hour period are taken at Taro, Munda, Auki, Honiara, Henderson and Santa Cruz (also known as Lata). A single rainfall observation per day is taken at Kirakira (previously multiple observations). More than 60 volunteer single observation rainfall-only stations have closed in recent years. The primary climate station is located in Honiara on the northern side of Guadalcanal Island (Figure 13.1). Several stations, including Auki and Kirakira, have rainfall data from late the 1910s. Honiara has air temperature data from the early 1950s.

Climate records for a Henderson-Honiara composite (1950–2009) and Santa Cruz (1970–2009) have been used. The Henderson-Honiara and Santa Cruz records are homogeneous and more than 95% and 85% complete respectively.

Monthly-averaged sea-level data are available from 1974 at Honiara (1974–1994 and 1994–present). A global positioning system instrument to estimate vertical land motion was deployed in the Solomon Islands in 2008 and will provide valuable direct estimates of local vertical land motion in future years. Both satellite (from 1993) and in situ sea-level data (1950–2009; termed reconstructed sea level; Volume 1, Section 2.2.2.2) are available on a global 1° x 1° grid.

Long-term locally-monitored sea-surface temperature data are unavailable for the Solomon Islands, so large-scale gridded sea-surface temperature datasets have been used (HadISST, HadSST2, ERSST and Kaplan Extended SST V2; Volume 1, Table 2.3).

Climate data management training, Solomon Islands Meteorological Service

13.4 Seasonal Cycles

The climate in the Solomon Islands is tropical with two seasons: the wet season from November to April and the dry season from May to October. The local names for these seasons, *Komburu* and *Ara*, are based on the prevailing direction of the trade winds.

Air temperatures in the Solomon Islands are fairly constant throughout the year with very weak seasonal variations (Figure 13.2). The most significant variation is from July to August when cooler air blows in from the south. In Honiara a slight decrease in temperature is also evident in January, February and March due to increased cloud cover during the wet season. Monthly air temperatures at both sites are closely linked to sea-surface temperatures in the region.

Many climate features influence rainfall in the Solomon Islands. Honiara has a very marked wet season from November to April (Figure 13.2) when on average almost 70% of the yearly total rain falls. In the dry season (May-October) on average about 600 mm falls compared with upwards of 1800 mm in the wet season. Most rain falls from January to March when the West Pacific Monsoon (WPM) is most active in the region. This feeds moisture into the South Pacific Convergence Zone (SPCZ), which is most active in the wet season, and Intertropical Convergence Zone (ITCZ), which lies closest to the Solomon Islands in the wet season. Being further to the east, Santa Cruz sits in a region where the SPCZ is active year-round and it receives more constant rainfall during the year, averaging between 280 mm and 420 mm per month.

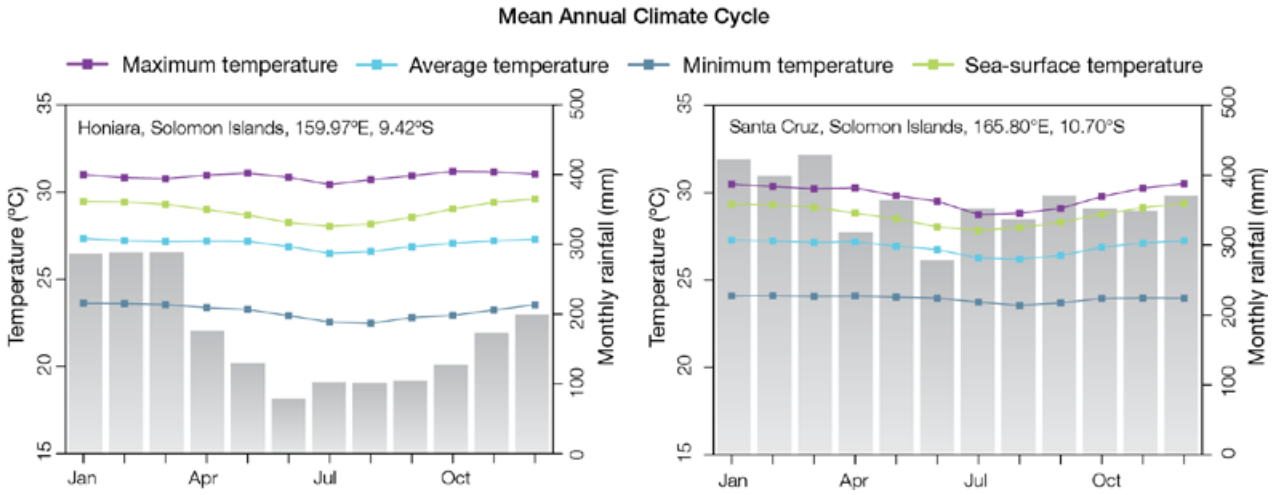

Figure 13.2: Mean annual cycle of rainfall (grey bars) and daily maximum, minimum and mean air temperatures at Honiara (left) and at Santa Cruz (right), and local sea-surface temperatures derived from the HadISST dataset (Volume 1, Table 2.3).

13.5 Climate Variability

Rainfall in the Solomon Islands varies strongly from year-to-year. Annual rainfall in the wettest years can be twice that in the driest years. The El Niño-Southern Oscillation (ENSO) has a strong influence on this year-to-year variability, particularly in the wet season, as seen by the significant correlations between wet season rainfall and ENSO indices in Tables 13.1 and 13.2. The impact of ENSO is stronger in Santa Cruz than Honiara. El Niño events tend to bring drier conditions in the wet season through a delayed onset of the WPM, often until late January or February, and a weaker or displaced SPCZ and ITCZ. During El Niño events wet-season maximum and minimum air temperatures are above normal due to increased solar radiation as a result of reduced cloud cover. During La Niña years wet season rainfall is usually above normal and temperatures are usually lower. ENSO Modoki events (Volume1, Section 3.4.1) also have significant impacts on wet season rainfall and temperatures but the influence is slightly weaker than canonical El Niño and La Niña events. In the dry season canonical ENSO and ENSO Modoki affect only maximum air temperatures. Both types of El Niño bring cooler maximum air temperatures in the dry season, in contrast to them bringing warmer temperatures in the wet season. The effect is due to cooler ocean waters in the region of the Solomon Islands during El Niño events and warmer waters during La Niña events.

Table 13.1: Correlation coefficients between indices of key large-scale patterns of climate variability and minimum and maximum temperatures (Tmin and Tmax) and rainfall at Honiara. Only correlation coefficients that are statistically significant at the 95% level are shown.

Climate feature/index		Dry season (May-October)			Wet season (November-April)		
		Tmin	Tmax	Rain	Tmin	Tmax	Rain
ENSO	Niño3.4		-0.56		0.41	0.55	-0.62
	Southern Oscillation Index		0.68		-0.35	-0.53	0.63
Interdecadal Pacific Oscillation Index							
ENSO Modoki Index			-0.33		0.36	0.45	-0.50
Number of years of data		56	55	58	53	53	58

Table 13.2: Correlation coefficients between indices of key large-scale patterns of climate variability and minimum and maximum temperatures (Tmin and Tmax) and rainfall at Santa Cruz. Only correlation coefficients that are statistically significant at the 95% level are shown.

Climate feature/index		Dry season (May-October)			Wet season (November-April)		
		Tmin	Tmax	Rain	Tmin	Tmax	Rain
ENSO	Niño3.4		-0.73		0.51	0.62	-0.70
	Southern Oscillation Index		0.68		-0.36	-0.56	0.70
Interdecadal Pacific Oscillation Index							
ENSO Modoki Index					0.55	0.70	-0.64
Number of years of data		34	35	39	34	34	39

13.6 Observed Trends

13.6.1 Air Temperature

Warming trends are evident in both annual and seasonal mean air temperatures at Honiara for the period 1951–2009 (Figure 13.3). Annual and seasonal maximum air temperature trends are comparable to those for minimum air temperatures (Table 13.3).

13.6.2 Rainfall

Annual and seasonal rainfall trends for Honiara for the period 1950–2009 are not statistically significant (Table 13.3; Figure 13.4).

13.6.3 Extreme Events

The tropical cyclone season in the Solomon Islands is between November and April. Occurrences outside this period are rare. The tropical cyclone archive for the Southern Hemisphere indicates that between the 1969/70 and 2009/10 cyclone seasons, the centre of 41 tropical cyclones passed within approximately 400 km of Honiara. This represents an average of 10 cyclones per decade. Tropical cyclones were most frequent in El Niño years (13 cyclones per decade) and least frequent in La Niña years (six cyclones per decade). The ENSO-neutral average is nine cyclones per decade. The interannual variability in the number of tropical cyclones in the vicinity of Honiara is large, ranging from zero in some seasons to five in the 1971/72 season (Figure 13.5). This high variability makes it difficult to identify any long-term trends in frequency.

Tropical cyclones result in flooding and wind damage in the Solomon Islands. There have been severe floods on Guadalcanal, Malaita, Makira and Santa Isabel in recent years with a number of lives lost, and severe damage to agriculture and infrastructure.

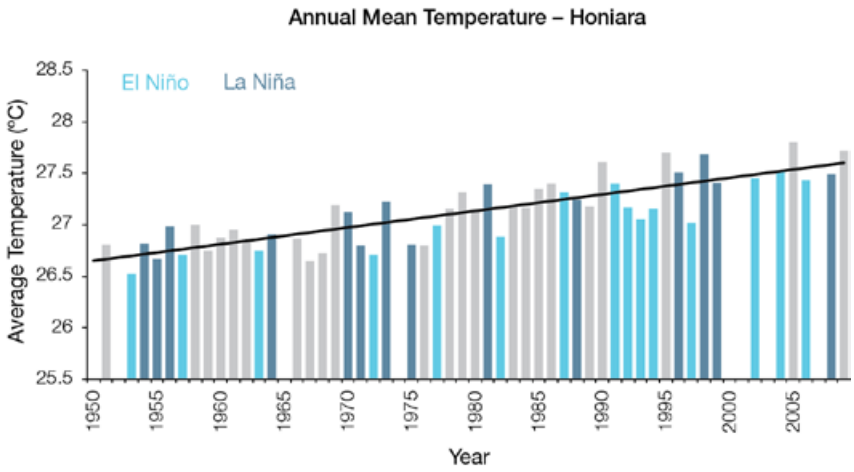

Figure 13.3: Annual mean air temperature for Honiara. Light blue, dark blue and grey bars denote El Niño, La Niña and neutral years respectively.

Table 13.3: Annual and seasonal trends in maximum, minimum and mean air temperature (Tmax, Tmin and Tmean; 1951–2009) and rainfall (1950–2009) at Honiara. Asterisks indicate significance at the 95% level. Persistence is taken into account in the assessment of significance as in Power and Kociuba (in press). The statistical significance of the air temperature trends is not assessed.

	Honiara Tmax (°C per 10 yrs)	Honiara Tmin (°C per 10 yrs)	Honiara Tmean (°C per 10 yrs)	Honiara Rain (mm per 10 yrs)
Annual	+0.16	+0.18	+0.17	-40
Wet season	+0.19	+0.18	+0.18	-32
Dry season	+0.15	+0.18	+0.17	-5

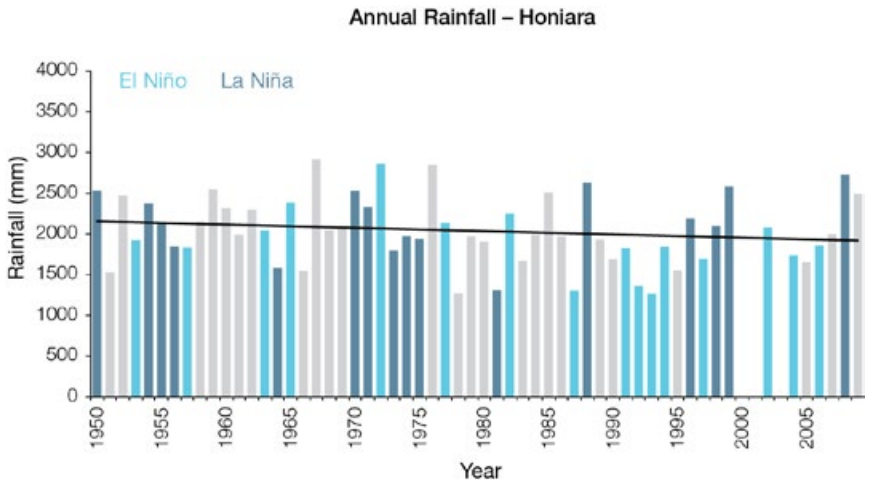

Figure 13.4: Annual rainfall at Honiara. Light blue, dark blue and grey bars denote El Niño, La Niña and neutral years respectively.

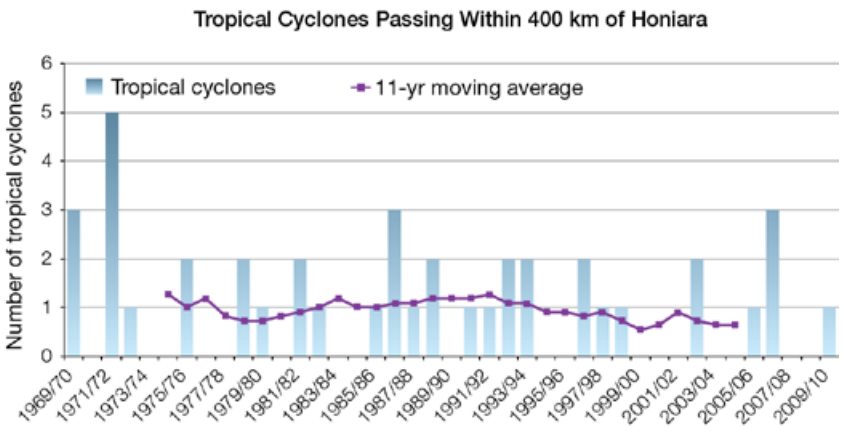

Figure 13.5: Tropical cyclones passing within 400 km of Honiara per season. The 11-year moving average is in purple.

13.6.4 Sea-Surface Temperature

Water temperatures around the Solomon Islands have risen gradually since the 1950s. Since the 1970s the rate of warming has been approximately 0.12°C per decade. Figure 13.7 shows the 1950–2000 sea-surface temperature changes (relative to a reference year of 1990) from three different large-scale sea-surface temperature gridded datasets (HadSST2, ERSST and Kaplan Extended SST V2; Volume 1, Table 2.3). At these regional scales, natural variability may play a large role determining sea-surface temperature in the region making it difficult to identify any long-term trends.

13.6.5 Ocean Acidification

Based the large-scale distribution of coral reefs across the Pacific and the seawater chemistry, Guinotte et al. (2003) suggested that seawater aragonite saturation states above 4 were optimal for coral growth and for the development of healthy reef ecosystems, with values from 3.5 to 4 adequate for coral growth, and values between 3 and 3.5, marginal. Coral reef ecosystems were not found at seawater aragonite saturation states below 3 and these conditions were classified as extremely marginal for supporting coral growth.

In the Solomon Islands region, the aragonite saturation state has declined from about 4.5 in the late 18th century to an observed value of about 3.9 ± 0.1 by 2000.

13.6.6 Sea Level

Monthly averages of the historical tide gauge, satellite (since 1993) and gridded sea-level (since 1950) data agree well after 1993 and indicate interannual variability in sea levels of about 31 cm (estimated 5–95% range) after removal of the seasonal cycle (Figure 13.10). The sea-level rise near Solomon Islands measured by satellite altimeters (Figure 13.6) since 1993 is mostly over 8 mm per year, larger than the global average of 3.2 ± 0.4 mm per year. This rise is partly linked to a pattern related to climate variability from year to year and decade to decade (Figure 13.10).

13.6.7 Extreme Sea-Level Events

The annual climatology of the highest daily sea levels has been evaluated from hourly measurements by the tide gauge at Honiara (Figure 13.7). High tides are largest near the equinoxes, in April–May and November–December. The seasonal cycle curve is fairly flat throughout the year but sea levels in this time frame are strongly modified by ENSO with sea levels higher by around 0.1 m during La Niña seasons and lower by a similar amount during El Niño seasons. Short-term variations (due mainly to weather events) are fairly uniform throughout the year with little influence apparent due to ENSO. The top 10 sea-level events in the record cluster around the tidal maxima and mostly occur during La Niña years. This is further supported by the values of wind speed and pressure which indicate that severe weather was not the cause of the high sea-level events, further supporting the notion that the extremes are mainly the result of other factors such as tides and ENSO.

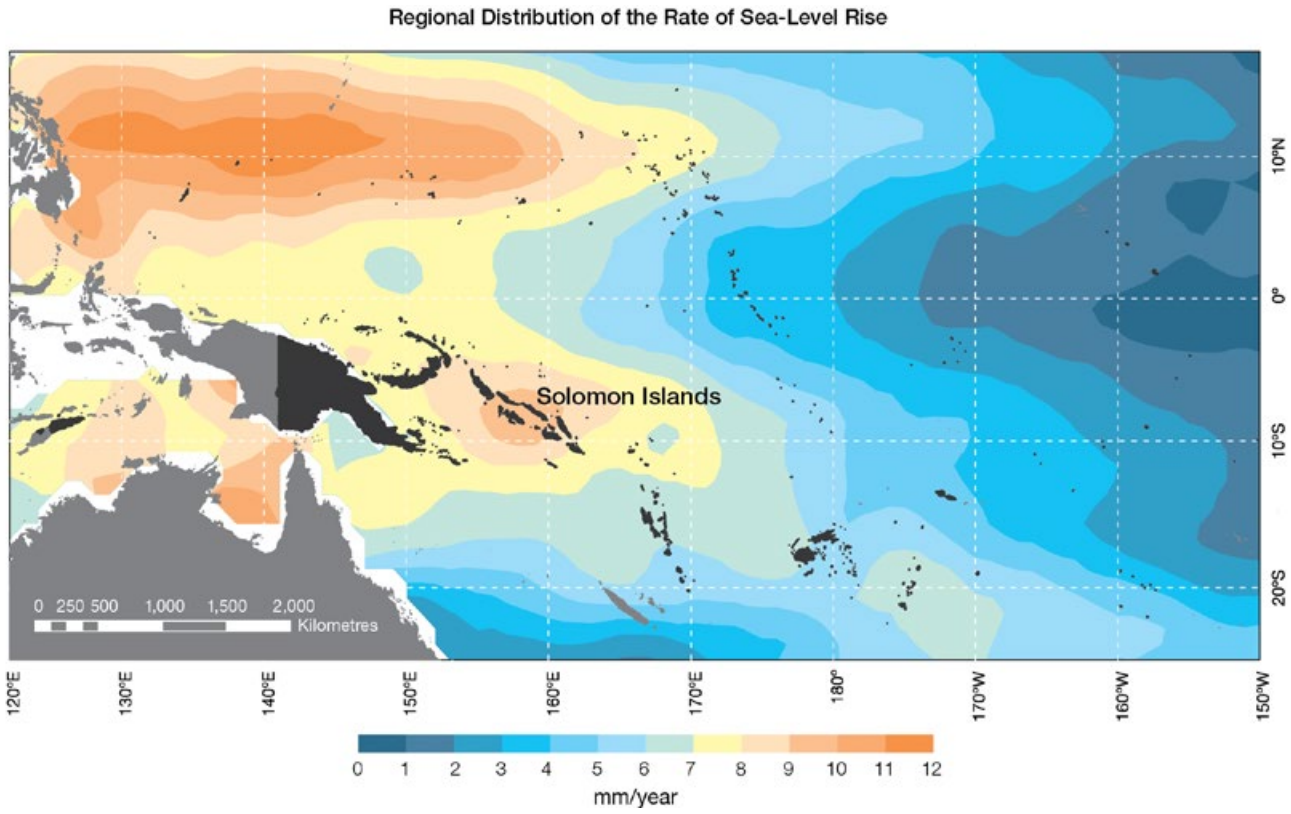

Figure 13.6: The regional distribution of the rate of sea-level rise measured by satellite altimeters from January 1993 to December 2010, with the location of Solomon Islands indicated. Further detail about regional distribution of sea-level rise is provided in Volume 1, Section 3.6.3.2.

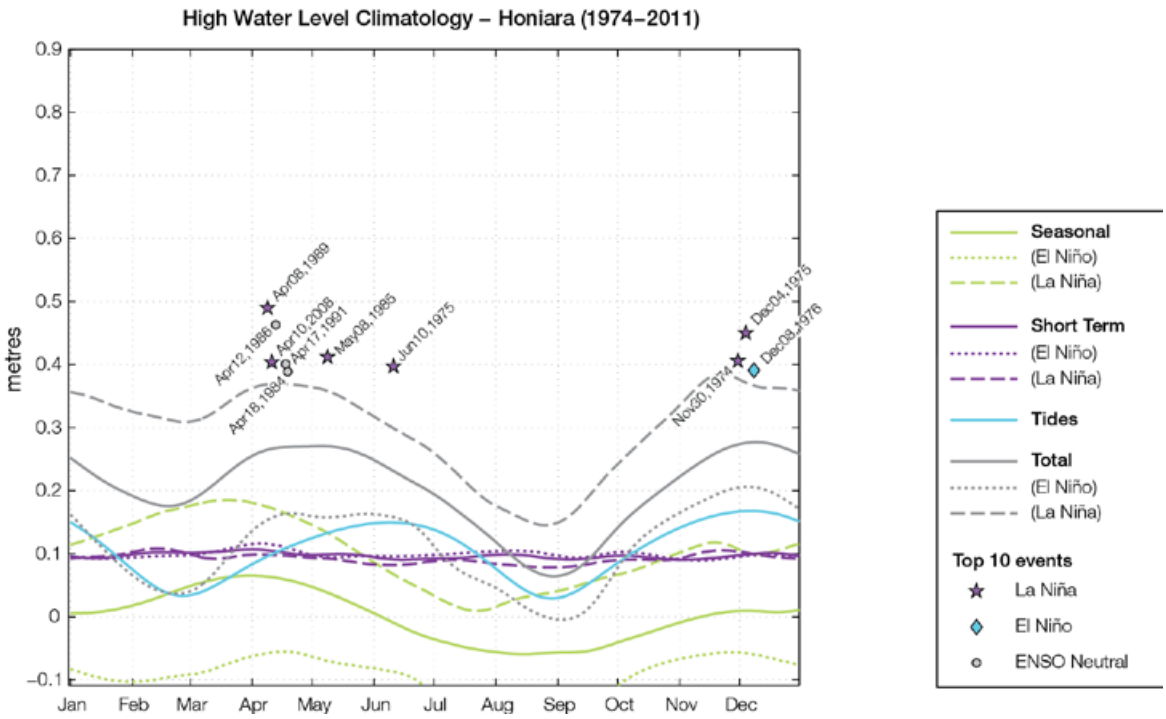

Figure 13.7: The annual cycle of high waters relative to Mean Higher High Water (MHHW) due to tides, short-term fluctuations (most likely associated with storms) and seasonal variations for Honiara. The tides and short-term fluctuations are respectively the 95% exceedence levels of the astronomical high tides relative to MHHW and short-term sea level fluctuations. Components computed only for El Niño and La Niña months are shown by dotted and dashed lines, and grey lines are the sum of the tide, short-term and seasonal components. The 10 highest sea level events in the record relative to MHHW are shown and coded to indicate the phase of ENSO at the time of the extreme event.

13.7 Climate Projections

Climate projections have been derived from up to 18 global climate models from the CMIP3 database, for up to three emissions scenarios (B1 (low), A1B (medium) and A2 (high)) and three 20-year periods (centred on 2030, 2055 and 2090, relative to 1990). These models were selected based on their ability to reproduce important features of the current climate (Volume 1, Section 5.2.3), so projections from each of the models are plausible representations of the future climate. This means there is not one single projected future for the Solomon Islands, but rather a range of possible futures. The full range of these futures is discussed in the following sections.

These projections do not represent a value specific to any actual location, such as a town or city in the Solomon Islands. Instead, they refer to an average change over the broad geographic region encompassing the Solomon Islands and the surrounding ocean (Figure 1.1 shows the regional boundaries). Some information regarding dynamical downscaling simulations from the CCAM model (Section 1.7.2) is also provided, in order to indicate how changes in the climate on an individual island-scale may differ from the broad-scale average.

Section 1.7 provides important information about understanding climate model projections.

13.7.1 Temperature

Surface air temperature and sea-surface temperature are projected to continue to increase over the course of the 21st century. There is *very high* confidence in this direction of change because:

- Warming is physically consistent with rising greenhouse gas concentrations.
- All CMIP3 models agree on this direction of change.

The majority of CMIP3 models simulate a slight increase (<1°C) in annual and seasonal mean temperature by 2030, however by 2090 under the A2 (high) emissions scenario temperature increases of greater than 2.5°C are simulated by almost all models (Table 13.4). Given the close relationship between surface air temperature and sea-surface temperature, a similar (or slightly weaker) rate of warming is projected for the surface ocean (Figure 13.8). There is *high* confidence in this range and distribution of possible futures because:

- There is generally close agreement between modelled and observed temperature trends over the past 50 years in the vicinity of the Solomon Islands, although observational records are limited (Figure 13.8).

The 8 km CCAM simulations suggest that projected changes in the average daily maximum air temperature over land can be up to 0.5°C greater than over the surrounding ocean. This suggests that the CMIP3 models may slightly underestimate future increases in daily maximum air temperature.

Interannual variability in surface air temperature and sea-surface temperature over the Solomon Islands is strongly influenced by ENSO in the current climate (Section 13.5). As there is no consistency in projections of future ENSO activity (Volume 1, Section 6.4.1) it is not possible to determine whether interannual variability in temperature will change in the future. However, ENSO is expected to continue to be an important source of variability for the region.

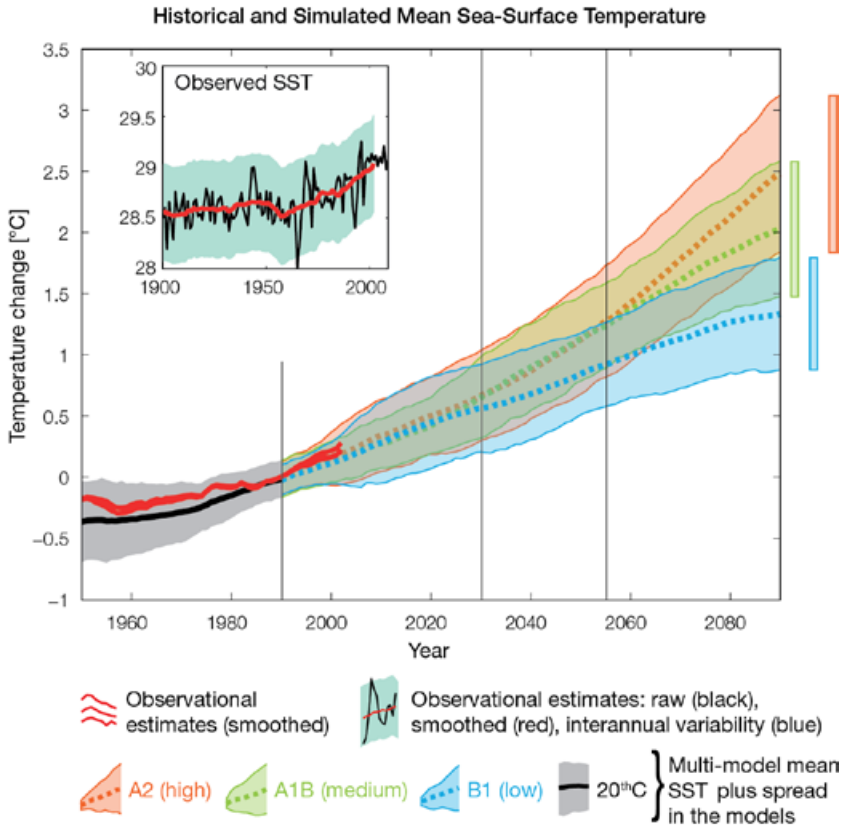

Figure 13.8: Historical climate (from 1950 onwards) and simulated historical and future climate for annual mean sea-surface temperature (SST) in the region surrounding Solomon Islands, for the CMIP3 models. Shading represents approximately 95% of the range of model projections (twice the inter-model standard deviation), while the solid lines represent the smoothed (20-year running average) multi-model mean temperature. Projections are calculated relative to the 1980–1999 period (which is why there is a decline in the inter-model standard deviation around 1990). Observational estimates in the main figure (red lines) are derived from the HadSST2, ERSST and Kaplan Extended SST V2 datasets (Volume 1, Section 2.2.2). Annual average (black) and 20-year running average (red) HadSST2 data is also shown inset.

13.7.2 Rainfall

Wet season (November-April), dry season (May-October) and annual average rainfall are projected to increase over the course of the 21st century. There is *high* confidence in this direction of change because:

- Physical arguments indicate that rainfall will increase in the equatorial Pacific in a warmer climate (IPCC, 2007; Volume 1, Section 6.4.3).
- Almost all of the CMIP3 models agree on this direction of change by 2090.

The majority of CMIP3 models simulate little change (-5% to 5%) in annual and seasonal rainfall by 2030, however by 2090 under the higher emissions scenarios (i.e. A2 (high) and A1B (medium)) the majority simulate an increase (>5%), with very few models simulating a decrease (<-5%) (Table 13.4). There is *moderate* confidence in this range and distribution of possible futures because:

- In simulations of the current climate, the CMIP3 models broadly capture the influence of the West Pacific Monsoon, Intertropical Convergence Zone and South Pacific Convergence Zone on the rainfall of the Solomon Islands (Volume 1, Section 5.2.3), although most models produce monsoon westerly winds that do not extend far enough east into the Pacific basin
- The CMIP3 models are unable to resolve many of the physical processes involved in producing rainfall. As a consequence, they do not simulate rainfall as well as other variables such as temperature (Volume 1, Chapter 5).

The inconsistency between the projected increase in annual rainfall and the recent declining trend observed for Honiara (Section 13.6.2) may be related to local factors not captured by the models (e.g. topography), or the fact that the projections presented here represent an average over a very large geographic region (Sections 1.7.1 and 1.7.2).

Interannual variability in rainfall over the Solomon Islands is strongly influenced by ENSO in the current climate (Section 13.5). As there is no consistency in projections of future ENSO activity (Volume 1, Section 6.4.1) it is not possible to determine whether interannual variability in rainfall will change in the future.

13.7.3 Extremes

Temperature

The intensity and frequency of days of extreme heat are projected to increase over the course of the 21st century. There is *very high* confidence in this direction of change because:

- An increase in the intensity and frequency of days of extreme heat is physically consistent with rising greenhouse gas concentrations.
- All CMIP3 models agree on the direction of change for both intensity and frequency.

The majority of CMIP3 models simulate an increase of approximately 1°C in the temperature experienced on the 1-in-20-year hot day by 2055 under the B1 (low) emissions scenario, with an increase of over 2.5°C simulated by the majority of models by 2090 under the A2 (high) emissions scenario (Table 13.4). There is *low* confidence in this range and distribution of possible futures because:

- In simulations of the current climate, the CMIP3 models tend to underestimate the intensity and frequency of days of extreme heat (Volume 1, Section 5.2.4).
- Smaller increases in the frequency of days of extreme heat are projected by the CCAM 60 km simulations.

Rainfall

The intensity and frequency of days of extreme rainfall are projected to increase over the course of the 21st century. There is *high* confidence in this direction of change because:

- An increase in the frequency and intensity of extreme rainfall is consistent with larger-scale projections, based on the physical argument that the atmosphere is able to hold more water vapour in a warmer climate (Allen and Ingram, 2002; IPCC, 2007). It is also consistent with physical arguments that rainfall will increase in the deep tropical Pacific in a warmer climate (IPCC, 2007; Volume 1, Section 6.4.3).
- Almost all of the CMIP3 models agree on this direction of change for both intensity and frequency.

The majority of CMIP3 models simulate an increase of at least 15 mm in the amount of rain received on the 1-in-20-year wet day by 2055 under the B1 (low) emissions scenario, with an increase of at least 30 mm simulated by 2090 under the A2 (high) emissions scenario. The majority of models project that the current 1-in-20-year extreme rainfall event will occur, on average, three to four times per 20-year period by 2055 under the B1 (low) emissions scenario and five times per 20-year period by 2090 under the A2 (high) emissions scenario. There is *low* confidence in this range and distribution of possible futures because:

- In simulations of the current climate, the CMIP3 models tend to underestimate the intensity and frequency of extreme rainfall (Volume 1, Section 5.2.4).
- The CMIP3 models are unable to resolve many of the physical processes involved in producing extreme rainfall.

Drought

The incidence of drought is projected to decrease over the course of the 21st century. There is *moderate* confidence in this direction of change because:

- A decrease in drought is consistent with projections of increased rainfall (Section 13.7.2).
- The majority of models agree on this direction of change for most drought categories.

The majority of CMIP3 models project that mild drought will occur approximately seven to eight times

every 20 years in 2030 under all emissions scenarios, decreasing to six to seven times by 2090. The frequency of moderate and severe drought is projected to remain approximately stable, at once to twice and once every 20 years, respectively. There is *low* confidence in this range and distribution of possible futures because:

- There is only moderate confidence in the range of rainfall projections (Section 13.7.2), which directly influences projections of future drought conditions.

Tropical Cyclones

Tropical cyclone numbers are projected to decline in the south-west Pacific Ocean basin (0–40ºS, 130ºE–170ºE) over the course of the 21st century. There is *moderate* confidence in this direction of change because:

- Many studies suggest a decline in tropical cyclone frequency globally (Knutson et al., 2010).
- Tropical cyclone numbers decline in the south-west Pacific Ocean in the majority assessment techniques.

Based on the direct detection methodologies (Curvature Vorticity Parameter (CVP) and the CSIRO Direct Detection Scheme (CDD) described in Volume 1, Section 4.8.2), 55% of projections show no change or a decrease in tropical cyclone formation when applied to the CMIP3 climate models for which suitable output is available. When these techniques are applied to CCAM, 100% of projections show a decrease in tropical cyclone formation. In addition, the Genesis Potential Index (GPI) empirical technique suggests that conditions for tropical cyclone formation will become less favourable in the south-west Pacific Ocean basin, for the majority (80%) of analysed CMIP3 models. There is *moderate* confidence in this range and distribution of possible futures because in simulations of the current climate, the CVP, CDD and GPI methods capture the frequency of tropical cyclone activity reasonably well (Volume 1, Section 5.4).

Despite this projected reduction in total cyclone numbers, five of the six CCAM 60 km simulations show an increase in the proportion of the most severe cyclones. Most models also indicate a reduction in tropical cyclone wind hazard north of 20ºS latitude and regions of increased hazard south of 20ºS latitude. This increase in wind hazard coincides with a poleward shift in the latitude at which tropical cyclones are most intense.

13.7.4 Ocean Acidification

The acidification of the ocean will continue to increase over the course of the 21st century. There is *very high* confidence in this projection as the rate of ocean acidification is driven primarily by the increasing oceanic uptake of carbon dioxide, in response to rising atmospheric carbon dioxide concentrations.

Projections from all analysed CMIP3 models indicate that the annual maximum aragonite saturation state will reach values below 3.5 by about 2045 and continue to decline thereafter (Figure 13.9; Table 13.4). There is *moderate* confidence in this range and distribution of possible futures because the projections are based on climate models without an explicit representation of the carbon cycle and with relatively low resolution and known regional biases.

The impact of acidification change on the health of reef ecosystems is likely to be compounded by other stressors including coral bleaching, storm damage and fishing pressure.

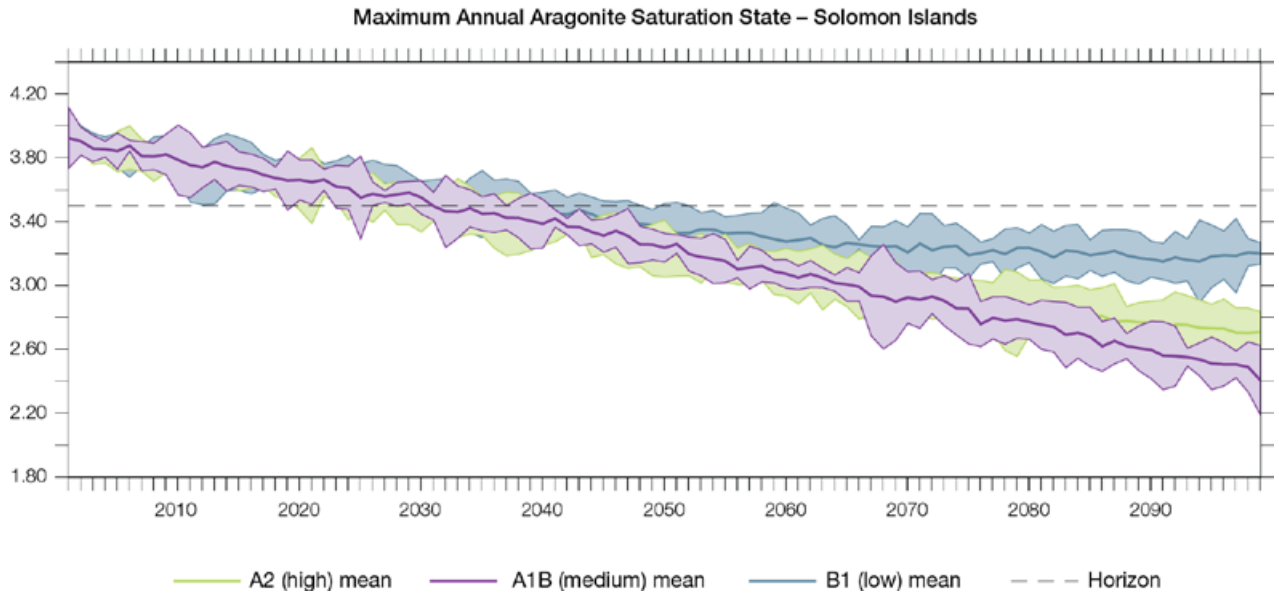

Figure 13.9: Multi-model projections, and their associated uncertainty (shaded area represents two standard deviations), of the maximum annual aragonite saturation state in the sea surface waters of the Solomon Islands region under the different emissions scenarios. The dashed black line represents an aragonite saturation state of 3.5.

13.7.5 Sea Level

Mean sea level is projected to continue to rise over the course of the 21st century. There is *very high* confidence in this direction of change because:

- Sea-level rise is a physically consistent response to increasing ocean and atmospheric temperatures, due to thermal expansion of the water and the melting of glaciers and ice caps.
- Projections arising from all CMIP3 models agree on this direction of change.

The CMIP3 models simulate a rise of between approximately 5–15 cm by 2030, with increases of 20–60 cm indicated by 2090 under the higher emissions scenarios (i.e. A2 (high) and A1B (medium); Figure 13.10; Table 13.4). There is *moderate* confidence in this range and distribution of possible futures because:

- There is significant uncertainty surrounding ice-sheet contributions to sea-level rise and a rise larger than projected above cannot be excluded (Meehl et al., 2007b). However, understanding of the processes is currently too limited to provide a best estimate or an upper bound (IPCC, 2007).
- Globally, since the early 1990s, sea level has been rising near the upper end of the above projections. During the 21st century, some studies (using semi-empirical models) project faster rates of sea-level rise.

Interannual variability of sea level will lead to periods of lower and higher regional sea levels. In the past, this interannual variability has been about 31 cm (5–95% range, after removal of the seasonal signal; dashed lines in Figure 13.10 (a)) and it is likely that a similar range will continue through the 21st century. In addition, winds and waves associated with weather phenomena will continue to lead to extreme sea-level events.

In addition to the regional variations in sea level associated with ocean and mass changes, there are ongoing changes in relative sea level associated with changes in surface loading over the last glacial cycle (glacial isostatic adjustment) and local tectonic motions. The glacial isostatic motions are relatively small for the PCCSP region.

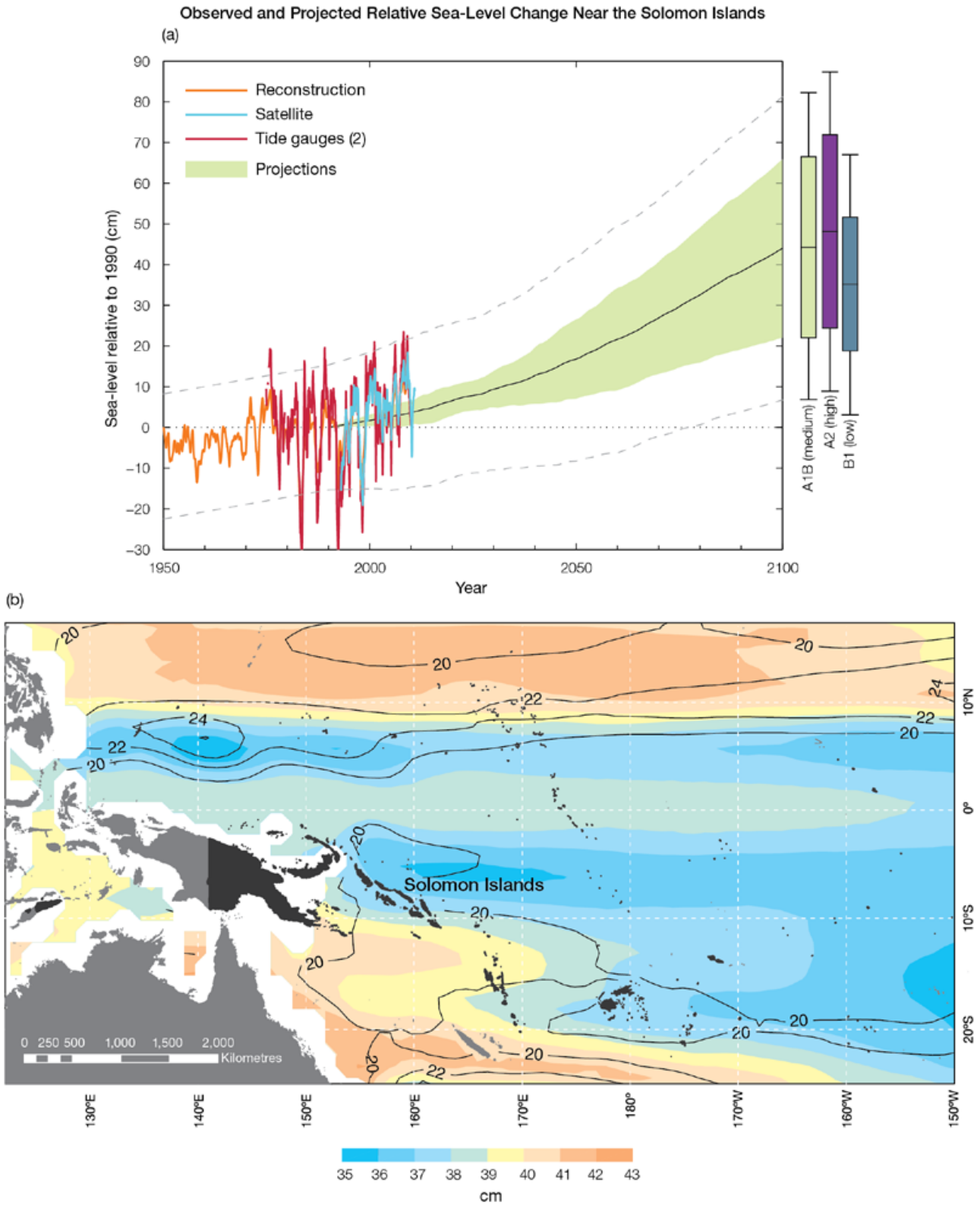

Figure 13.10: Observed and projected relative sea-level change near the Solomon Islands. (a) The observed in situ relative sea-level records are indicated in red, with the satellite record (since 1993) in light blue. The gridded sea level at the Solomon Islands (since 1950, from Church and White (in press)) is shown in orange. The projections for the A1B (medium) emissions scenario (5–95% uncertainty range) are shown by the green shaded region from 1990–2100. The range of projections for the B1 (low), A1B (medium) and A2 (high) emissions scenarios by 2100 are also shown by the bars on the right. The dashed lines are an estimate of interannual variability in sea level (5– 95% range about the long-term trends) and indicate that individual monthly averages of sea level can be above or below longer-term averages. (b) The projections (in cm) for the A1B (medium) emissions scenario in the Solomon Islands region for the average over 2081–2100 relative to 1981–2000 are indicated by the shading, with the estimated uncertainty in the projections indicated by the contours (in cm).

13.7.6 Projections Summary

The projections presented in Section 13.7 are summarised in Table 13.4. For detailed information regarding the various uncertainties associated with the table values, refer to the preceding text in Sections 13.7 and 1.7, in addition to Chapters 5 and 6 in Volume 1. When interpreting the differences between projections for the A2 (high), A1B (medium) and B1 (low) emissions scenarios, it is also important to consider the emissions pathways associated with each scenario (Volume 1, Figure 4.1) and the fact that a slightly different subset of models was available for each (Volume 1, Appendix 1).

Table 13.4: Projected change in the annual and seasonal mean climate for the Solomon Islands, under the B1 (low; blue), A1B (medium; green) and A2 (high; purple) emissions scenarios. Projections are given for three 20-year periods centred on 2030 (2020–2039), 2055 (2046–2065) and 2090 (2080–2099), relative to 1990 (1980–1999). Values represent the multi-model mean change ± twice the inter-model standard deviation (representing approximately 95% of the range of model projections), except for sea level where the estimated mean change and the 5–95% range are given (as they are derived directly from the Intergovernmental Panel on Climate Change Fourth Assessment Report values). The confidence (Section 1.7.2) associated with the range and distribution of the projections is also given (indicated by the standard deviation and multi-model mean, respectively). See Volume 1, Appendix 1 for a complete listing of CMIP3 models used to derive these projections.

Variable	Season	2030	2055	2090	Confidence
Surface air temperature (°C)	Annual	+0.6 ± 0.4 +0.8 ± 0.4 +0.7 ± 0.3	+1.1 ± 0.4 +1.4 ± 0.5 +1.4 ± 0.4	+1.5 ± 0.6 +2.3 ± 0.8 +2.7 ± 0.6	High
Maximum temperature (°C)	1-in-20-year event	N/A	+1.0 ± 0.5 +1.4 ± 0.6 +1.5 ± 0.4	+1.3 ± 0.6 +2.1 ± 1.0 +2.7± 1.2	Low
Minimum temperature (°C)	1-in-20-year event	N/A	+1.2 ± 1.8 +1.5 ± 1.9 +1.6 ± 1.7	+1.7 ± 1.6 +2.2 ± 1.9 +2.5 ± 1.8	Low
Total rainfall (%)*	Annual	+1 ± 9 +2 ± 9 +2 ± 6	+4 ± 8 +5 ± 10 +4 ± 9	+6 ± 9 +9 ± 11 +9 ± 12	Moderate
Wet season rainfall (%)*	November-April	+2 ± 9 +2 ± 9 +2 ± 7	+5 ± 8 +6 ± 11 +4 ± 7	+6 ± 7 +9 ± 11 +9 ± 11	Moderate
Dry season rainfall (%)*	May-October	0 ± 11 +2 ± 13 +2 ± 9	+3 ± 11 +4 ± 12 +5 ± 15	+6 ± 14 +9 ± 16 +10 ± 18	Moderate
Sea-surface temperature (°C)	Annual	+0.6 ± 0.4 +0.7 ± 0.3 +0.7 ± 0.4	+0.9 ± 0.3 +1.2 ± 0.3 +1.3 ± 0.5	+1.3 ± 0.5 +2.0 ± 0.6 +2.5 ± 0.6	High
Aragonite saturation state (Ωar)	Annual maximum	+3.6 ± 0.1 +3.5 ± 0.1 +3.5 ± 0.1	+3.3 ± 0.1 +3.1 ± 0.1 +3.1 ± 0.1	+3.1 ± 0.1 +2.7 ± 0.2 +2.5 ± 0.1	Moderate
Mean sea level (cm)	Annual	+9 (4–14) +9 (5–14) +9 (4–15)	+18 (10–26) +19 (8–30) +19 (8–30)	+31 (17–45) +38 (19–58) +40 (20–60)	Moderate

*The MIROC3.2(medres) and MIROC3.2(hires) models were eliminated in calculating the rainfall projections, due to their inability to accurately simulate one or more of the South Pacific Convergence Zone, Intertropical Convergence Zone and the West Pacific Monsoon (Volume 1, Section 5.5.1).

Nuku'alofa

Chapter 14
Tonga

The contributions of Ofa Fa'anunu and Mele Lakai from the Tonga Meteorological Service are gratefully acknowledged

Introduction

This chapter provides a brief description of Tonga, its past and present climate as well as projections for the future. The climate observation network and the availability of atmospheric and oceanic data records are outlined. The annual mean climate, seasonal cycles and the influences of large-scale climate features such as the South Pacific Convergence Zone and patterns of climate variability (e.g. the El Niño-Southern Oscillation) are analysed and discussed. Observed trends and analysis of air temperature, rainfall, extreme events (including tropical cyclones), sea-surface temperature, ocean acidification, mean and extreme sea levels are presented. Projections for air and sea-surface temperature, rainfall, sea level, ocean acidification and extreme events for the 21st century are provided. These projections are presented along with confidence levels based on expert judgement by Pacific Climate Change Science Program (PCCSP) scientists. The chapter concludes with a summary table of projections (Table 14.4). Important background information including an explanation of methods and models is provided in Chapter 1. For definitions of other terms refer to the Glossary.

14.1 Climate Summary

14.1.1 Current Climate

- Sites in Tonga show some seasonal variations in air temperature due to their position close to the sub-tropics. Part of the seasonal change is driven by the sea-surface temperature of the oceans surrounding the islands.
- Nearly two-thirds of Tonga's rainfall falls in the wet season from November to April. The rainfall is affected by the South Pacific Convergence Zone, which is most intense during the wet season.
- Rainfall in Tonga has high variability from year-to-year due mainly to the El Niño-Southern Oscillation.
- Warming trends are evident in both annual and seasonal mean air temperatures at Nuku'alofa for the period 1950–2009, with the strongest trends in the wet season.
- Annual and seasonal rainfall trends for Nuku'alofa and Lupepau'u for the period 1950–2009 are not statistically significant.
- The sea-level rise near Tonga measured by satellite altimeters since 1993 is over 6 mm per year.
- On average, Nuku'alofa experiences 17 tropical cyclones per decade, with most occurring between November and April. The high interannual variability in the tropical cyclone numbers makes it difficult to identify any long-term trends in frequency.

14.1.2 Future Climate

Over the course of the 21st century:

- Surface air temperature and sea-surface temperature are projected to continue to increase (*very high* confidence).
- Wet season rainfall is projected to increase (*moderate* confidence).
- Dry season rainfall is projected to decrease (*moderate* confidence).
- Little change is projected in annual mean rainfall (*low* confidence).
- The intensity and frequency of days of extreme heat are projected to increase (*very high* confidence).
- The intensity and frequency of days of extreme rainfall are projected to increase (*high* confidence).
- Little change is projected in the incidence of drought (*low* confidence).
- Tropical cyclone numbers are projected to decline in the south-east Pacific Ocean basin (0–40ºS, 170ºE–130ºW) (*moderate* confidence).
- Ocean acidification is projected to continue (*very high* confidence).
- Mean sea-level rise is projected to continue (*very high* confidence).

14.2 Country Description

Tonga is located in the western South Pacific Ocean, between 15°–23.5°S and 173°–177°W. The archipelago is spread over 800 km in a north-south direction. Tonga consists of four groups of islands: Tongatapu and 'Eua in the south, Ha'apai in the middle, Vava'u in the north and Niuafo'ou and Niua Toputapu in the far north. The 172 named islands have an area of 748 km^2. The islands include high volcanic islands, elevated limestone islands and low-lying atolls. The area of the Exclusive Economic Zone is 720 000 km^2. The capital, Nuku'alofa, is situated in Tongatapu in the south (Tonga's Joint National Action Plan, 2010). The 2010 estimated population was 103 365 (Tonga Country Statistics, SOPAC, 2010).

Agricultural production is the main economic sector with squash, coconuts, bananas, and vanilla beans comprising the main crops. Agricultural exports make up two-thirds of total exports. The tourism sector is growing in importance (Tonga's Pacific Adaptation to Climate Change, 2006).

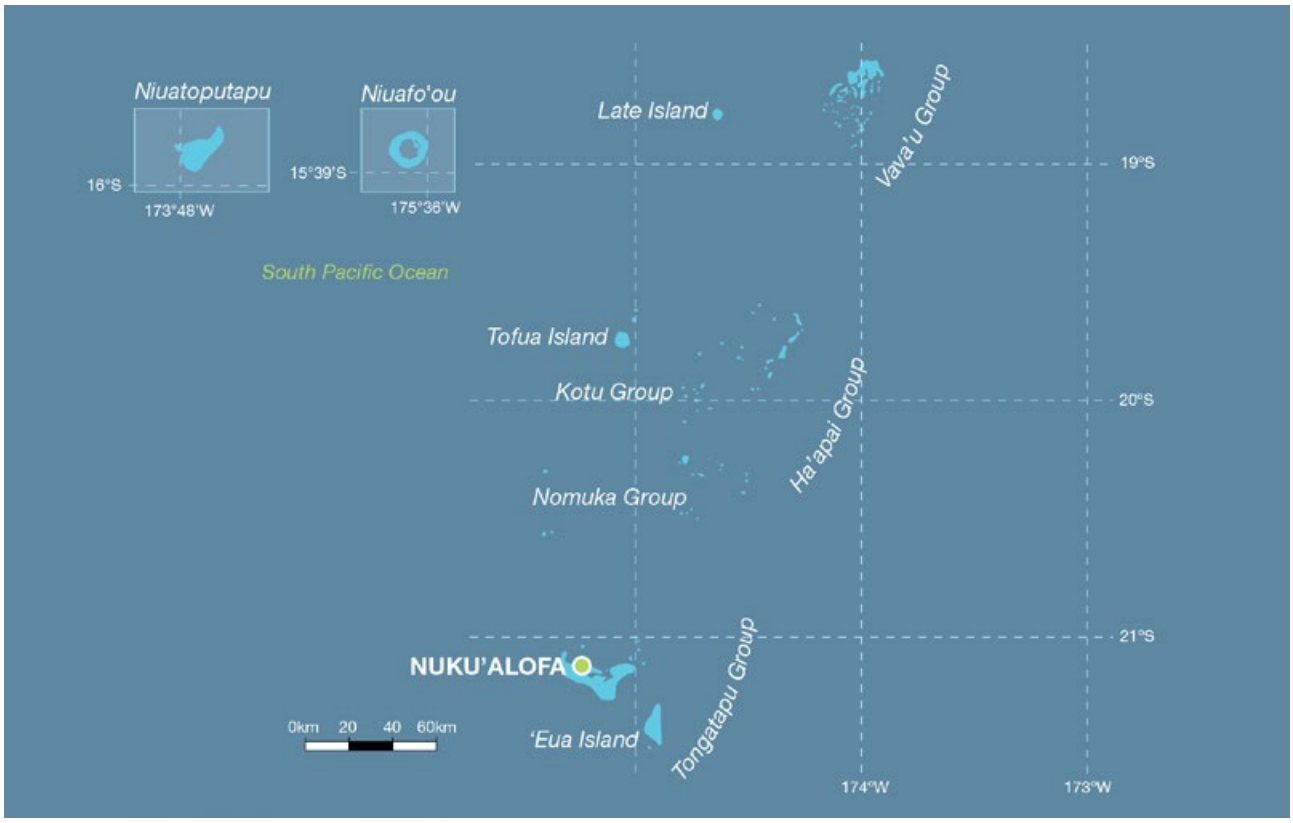

Figure 14.1: Kingdom of Tonga

14.3 Data Availability

There are currently seven operational meteorological stations in Tonga. Multiple observations within a 24-hour period are taken at Fua'amotu, Lupepau'u (also known as Vava'u), Niuatoputapu (also known as Keppel), Ha'apai and Niuafo'ou. A single daily observation is taken at Nuku'alofa and Kaufana. Nuku'alofa and Fua'amotu, the primary stations, are located on the northern and southern side of Tongatapu Island respectively. Nuku'alofa has rainfall data from 1944 and air temperature data from 1945 and Lupepau'u, Ha'apai and Niuatoputapu have rainfall data from 1947 and temperature data from 1950. Additional data for the period 1931–1941 have recently been discovered in the United Kingdom. These data are yet to be digitised.

Nuku'alofa and Lupepau'u rainfall and air temperature records from 1950 (Lupepau'u temperature from 1956) have been used. Both records are homogeneous and more than 95% complete.

Oceanographic records do not cover such a long time period. Monthly-averaged sea-level data are available from 1993 at Nuku'alofa (1993–present). A global positioning system instrument to estimate vertical land motion was deployed at Nuku'alofa in 2002 and will provide valuable direct estimates of local vertical land motion in future years. Both satellite (from 1993) and in situ sea-level data (1950–2009; termed reconstructed sea level; Volume 1, Section 2.2.2.2) are available on a global 1° x 1° grid.

Long-term locally-monitored sea-surface temperature data are unavailable for Tonga, so large-scale gridded sea-surface temperature datasets have been used (HadISST, HadSST2, ERSST and Kaplan Extended SST V2; Volume 1, Table 2.3).

14.4 Seasonal Cycles

Sites in Tonga show some seasonal variations in air temperature due to their position close to the sub-tropics. Being further south, Nuku'alofa has a slightly larger difference in air temperatures (about 5ºC) between the warmest month (February) and the coolest (July-August) months than Lupepau'u. Part of the seasonal change is driven by temperatures of the oceans surrounding the islands of Tonga. Air temperatures in the winter months are also affected by sub-tropical high pressure systems that direct cooler air from the south.

Both Nuku'alofa and Lupepau'u have marked seasonal cycles in rainfall, particularly Lupepau'u. Almost two-thirds of the annual rainfall comes during the wet season from November to April. The remainder falls in the dry season from May to October. This reflects the importance of the South Pacific Convergence Zone (SPCZ) on rainfall in Tonga, which is most intense during the wet season.

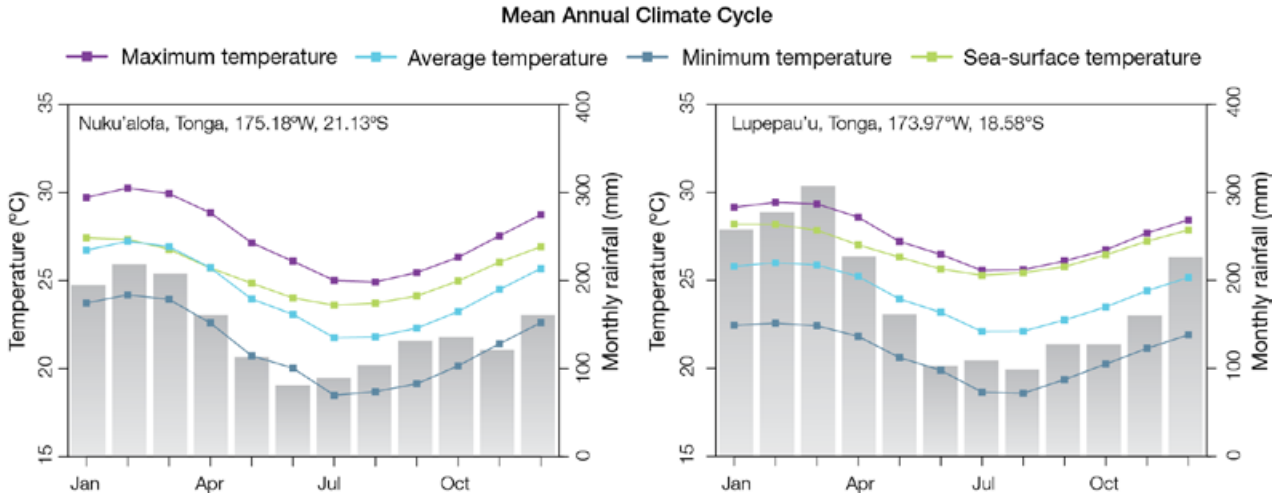

Figure 14.2: Mean annual cycle of rainfall (grey bars) and daily maximum, minimum and mean air temperatures at Nuku'alofa and (left) and Lupepau'u (right), and local sea-surface temperatures derived from the HadISST dataset (Volume 1, Table 2.3).

14.5 Climate Variability

Rainfall in Tonga has high variability from year-to-year. Both Nuku'alofa and Lupepau'u receive about three times as much rain in the wettest years as in the driest years. Much of this variability is driven by El Niño-Southern Oscillation (ENSO), as seen by the correlation coefficients in Table 14.2. In Nuku'alofa, El Niño events tend to bring cooler temperatures, especially in the dry season, most likely because of the cooler sea-surface temperatures around Tonga. El Niño years also tend to bring lower than normal rainfall during the wet season as the SPCZ usually moves away from Tonga to the north-east. In La Niña years the SPCZ moves closer and so wet season rainfall increases. Similar impacts are seen in Lupepau'u except temperatures in the wet season show no clear response to ENSO. Similar impacts are seen in ENSO Modoki events (Volume1, Section 3.4.1) to canonical El Niño and La Niña events but the influence is not as strong.

Some interdecadal variability in rainfall in the wet season can be linked with the Interdecadal Pacific Oscillation. The Southern Annular Mode influences air temperature to some extent in Tonga, and this is independent of the relationship between the Southern Annular Mode and ENSO.

Table 14.1: Correlation coefficients between indices of key large-scale patterns of climate variability and minimum and maximum temperatures (Tmin and Tmax) and rainfall at Nuku'alofa. Only correlation coefficients that are statistically significant at the 95% level are shown.

Climate feature/index		Dry season (May-October)			Wet season (November-April)		
		Tmin	Tmax	Rain	Tmin	Tmax	Rain
ENSO	Niño3.4	-0.72	-0.70		-0.37	-0.33	-0.61
	Southern Oscillation Index	0.66	0.73		0.38	0.35	0.69
Interdecadal Pacific Oscillation Index							-0.30
Southern Annular Mode Index			-0.30				
ENSO Modoki Index		-0.42	-0.36		-0.33	-0.26	-0.45
Number of years of data		58	60	65	58	60	66

Table 14.2: Correlation coefficients between indices of key large-scale patterns of climate variability and minimum and maximum temperatures (Tmin and Tmax) and rainfall at Lupepau'u. Only correlation coefficients that are statistically significant at the 95% level are shown.

Climate feature/Index		Dry Season (May–October)			Wet Season (November–April)		
		Tmin	Tmax	Rain	Tmin	Tmax	Rain
ENSO	Niño3.4	-0.53	-0.69				-0.58
	Southern Oscillation Index	0.40	0.67	0.26			0.66
Interdecadal Pacific Oscillation Index							
Southern Annular Mode Index						0.29	
ENSO Modoki Index					0.34		-0.39
Number of years of data		51	51	63	51	52	62

Taking observations, Tonga Meteorological Service

14.6 Observed Trends

14.6.1 Air Temperature

Trends for seasonal and annual mean air temperatures at Nuku'alofa (1950–2009) are positive (Figure 14.3), with the strongest trend (+0.16°C per decade) seen in wet season mean air temperatures. The trends in wet season maximum and minimum air temperatures are also considerably larger than that observed in the dry season (Table 14.3).

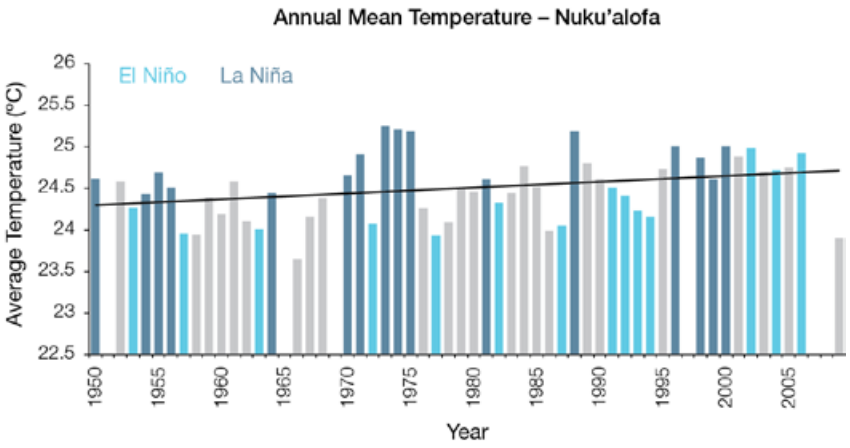

Figure 14.3: Annual mean air temperature at Nuku'alofa. Light blue, dark blue and grey bars denote El Niño, La Niña and neutral years respectively.

14.6.2 Rainfall

Annual and seasonal rainfall trends for Nuku'alofa and Lupepau'u for the period 1950–2009 are not statistically significant (Table 14.3; Figure 14.4).

14.6.3 Extreme Events

The tropical cyclone season in Tonga is between November and April. Occurrences outside this period are rare. The tropical cyclone archive for the Southern Hemisphere indicates that between the 1969/70 and 2009/10 seasons, the centre of 71 tropical cyclones passed within approximately 400 km of Nuku'alofa. This represents an average of 17 cyclones per decade. Tropical cyclones were most frequent in El Niño years (19 cyclones per decade) and least frequent in La Niña and ENSO-neutral years (16 cyclones per season). The interannual variability in the number of tropical cyclones in the vicinity of Nuku'alofa is large, ranging from zero in some seasons to five in the 2003/04 season (Figure 14.5). This high variability makes it difficult to identify any long-term trends in frequency.

Table 14.3: Annual and seasonal trends in maximum, minimum and mean air temperature (Tmax, Tmin and Tmean) and rainfall at Nuku'alofa and rainfall only at Lupepau'u for the period 1950–2009. Asterisks indicate significance at the 95% level. Persistence is taken into account in the assessment of significance as in Power and Kociuba (in press). The statistical significance of the air temperature trends is not assessed.

	Nuku'alofa Tmax (°C per 10 yrs)	Nuku'alofa Tmin (°C per 10 yrs)	Nuku'alofa Tmean (°C per 10 yrs)	Nuku'alofa Rain (mm per 10 yrs)	Lupepau'u Rain (mm per 10 yrs)
Annual	+0.10	+0.07	+0.07	-52	+7
Wet season	+0.14	+0.17	+0.16	-52	-7
Dry season	+0.06	+0.04	+0.05	+2	+20

14.6.4 Sea-Surface Temperature

Water temperatures around Tonga declined from the 1950s to the late 1980s (although there is some disagreement between datasets). This was followed by a period of warming (approximately 0.06°C per decade for 1970–present). Figure 14.8 shows the 1950–2000 sea-surface temperature changes (relative to a reference year of 1990) from three different large-scale sea-surface temperature datasets (HadSST2, ERSST and Kaplan Extended SST V2; Volume 1, Table 2.3). At these regional scales, natural variability may play a large role in the sea-surface temperature changes making it difficult to identify any long-term trends.

14.6.5 Ocean Acidification

Based the large-scale distribution of coral reefs across the Pacific and the seawater chemistry, Guinotte et al. (2003) suggested that seawater aragonite saturation states above 4 were optimal for coral growth and for the development of healthy reef ecosystems, with values from 3.5 to 4 adequate for coral growth, and values between 3 and 3.5, marginal. Coral reef ecosystems were not found at seawater aragonite saturation states below 3 and these conditions were classified as extremely marginal for supporting coral growth.

In the Tonga region, the aragonite saturation state has declined from about 4.5 in the late 18th century to an observed value of about 4.0 ± 0.1 by 2000.

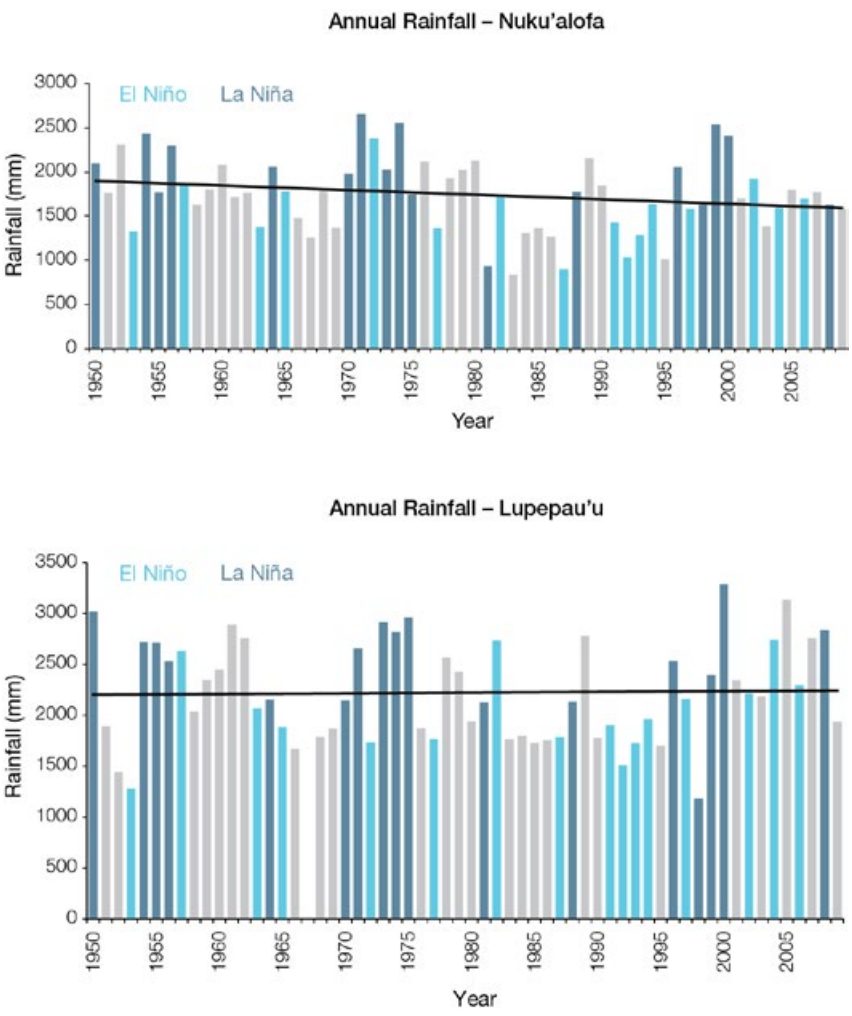

Figure 14.4: Annual rainfall at Nuku'alofa (top) and Lupepau'u (bottom). Light blue, dark blue and grey bars denote El Niño, La Niña and neutral years respectively.

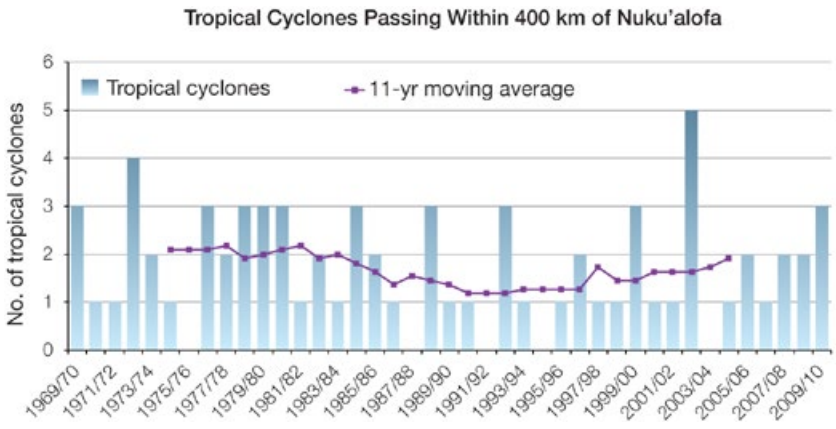

Figure 14.5: Tropical cyclones passing within 400 km of Nuku'alofa per season. The 11-year moving average is in purple.

14.6.6 Sea Level

Monthly averages of the historical tide gauge, satellite (since 1993) and gridded sea-level (since 1950) data agree well after 1993 and indicate interannual variability in sea levels of about 18 cm (estimated 5–95% range) after removal of the seasonal cycle (Figure 14.10). The sea-level rise near Tonga measured by satellite altimeters (Figure 14.6) since 1993 is over 6 mm per year, larger than the global average of 3.2 ± 0.4 mm per year. This rise is partly linked to a pattern related to climate variability from year to year and decade to decade (Figure 14.10).

14.6.7 Extreme Sea-Level Events

The annual climatology of the highest daily sea levels has been evaluated from hourly measurements by tide gauges at Nuku'alofa (Figure 14.7). High tides show relatively small variation throughout the year maximising in December and January. Average seasonal variations throughout the year are minimal. During La Niña years sea levels tend to be higher from May through August. During El Niño years the seasonal signal is negative from March through May and August through November, relative to the average signal, and close to the long-term average for the rest of the year. The top 10 sea-level events in the record occurred from December to March and at least half of these were associated with named tropical cyclones, indicating the importance of weather events in contributing to sea-level extremes.

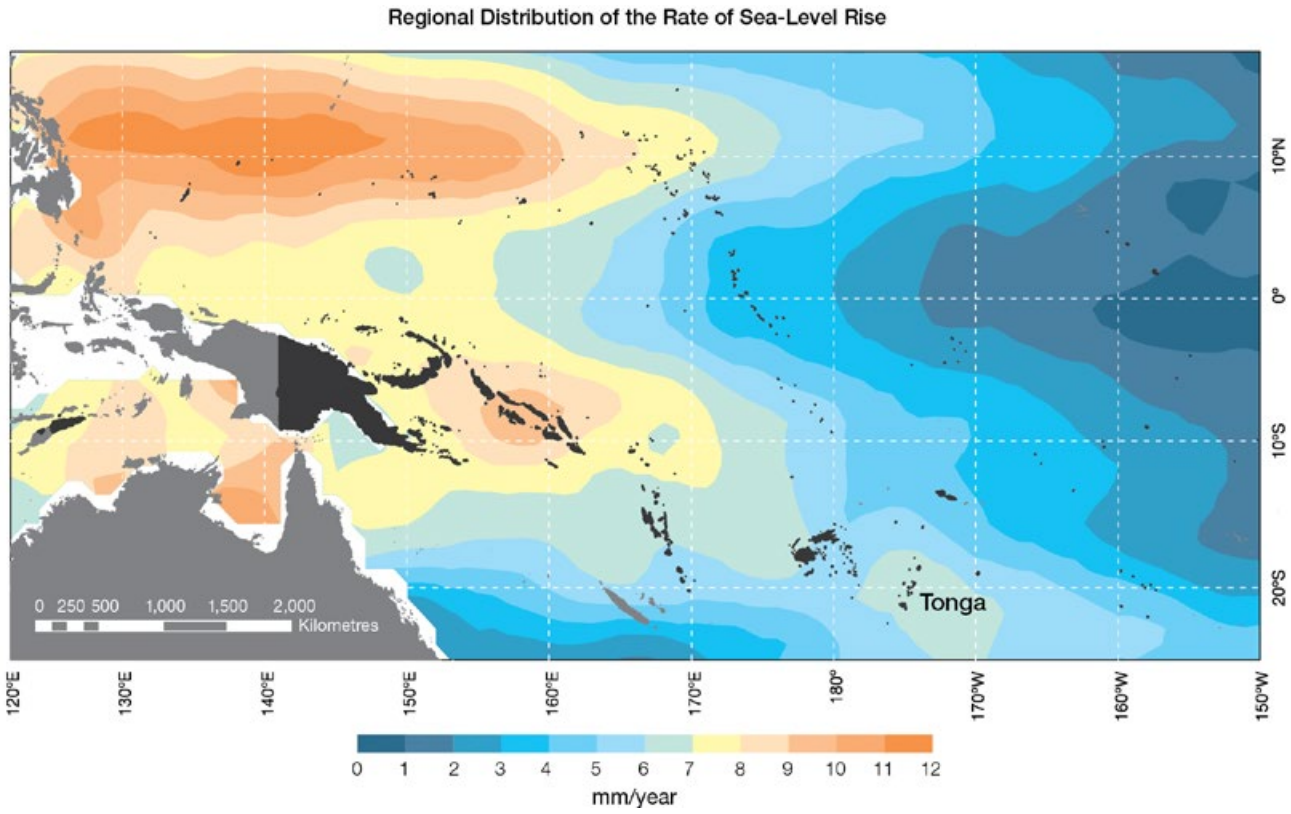

Figure 14.6: The regional distribution of the rate of sea-level rise measured by satellite altimeters from January 1993 to December 2010, with the location of Tonga indicated. Further detail about the regional distribution of sea-level rise is provided in Volume 1, Section 3.6.3.2.

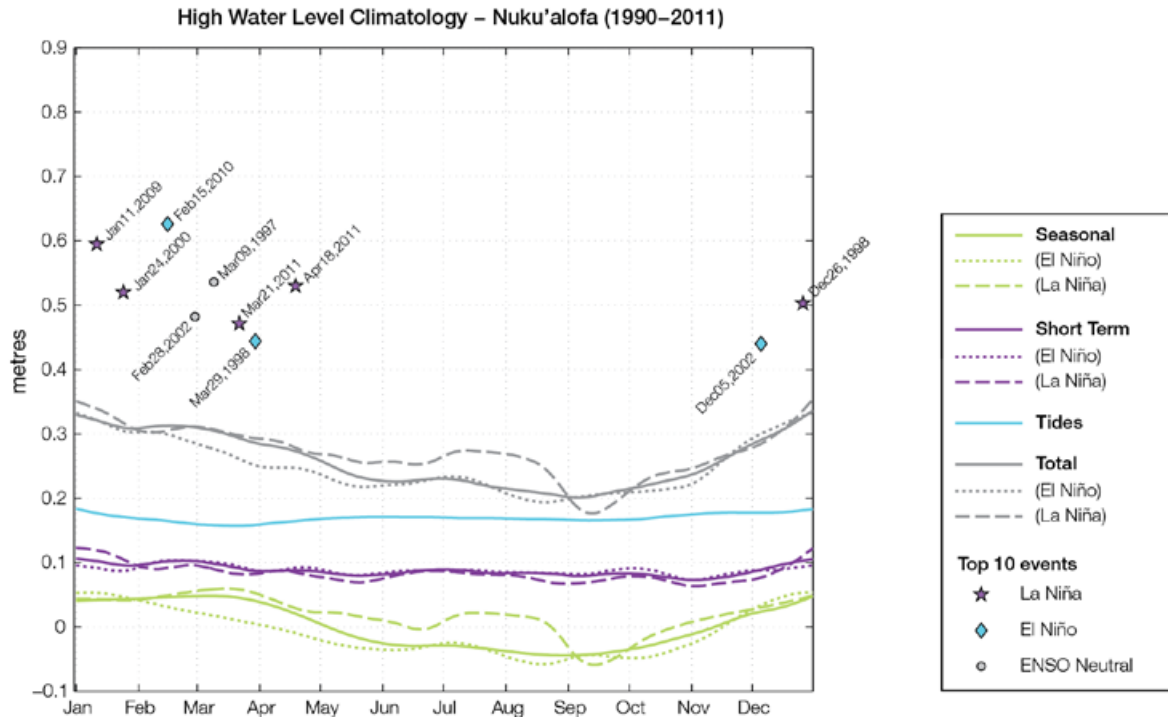

Figure 14.7: The annual cycle of high waters relative to Mean Higher High Water (MHHW) due to tides, short-term fluctuations (most likely associated with storms) and seasonal variations for Nuku'alofa. The tides and short-term fluctuations are respectively the 95% exceedence levels of the astronomical high tides relative to MHHW and short-term sea level anomaly fluctuations. Components computed only for El Niño and La Niña months are shown by dotted and dashed lines, and grey lines are the sum of the tide, short-term and seasonal components. The 10 highest sea-level events in the record relative to MHHW are shown and coded to indicate the phase of ENSO at the time of the extreme event.

14.7 Climate Projections

Climate projections have been derived from up to 18 global climate models from the CMIP3 database, for up to three emissions scenarios (B1 (low), A1B (medium) and A2 (high)) and three 20-year periods (centred on 2030, 2055 and 2090, relative to 1990). These models were selected based on their ability to reproduce important features of the current climate (Volume 1, Section 5.2.3), so projections from each of the models are plausible representations of the future climate. This means there is not one single projected future for Tonga, but rather a range of possible futures. The full range of these futures is discussed in the following sections.

These projections do not represent a value specific to any actual location, such as a town or city in Tonga. Instead, they refer to an average change over the broad geographic region encompassing the islands of Tonga and the surrounding ocean (Figure 1.1 shows the regional boundaries). Section 1.7 provides important information about interpreting climate model projections.

14.7.1 Temperature

Surface air temperature and sea-surface temperature are projected to continue to increase over the course of the 21st century. There is *very high* confidence in this direction of change because:

- Warming is physically consistent with rising greenhouse gas concentrations.
- All CMIP3 models agree on this direction of change.

Almost all of the CMIP3 models simulate a slight increase (<1°C) in annual and seasonal mean temperature by 2030, however by 2090 under the A2 (high) emissions scenario temperature increases of greater than 2.5°C are simulated by the majority of models (Table 14.4). Given the close relationship between surface air temperature and sea-surface temperature, a similar (or slightly weaker) rate of warming is projected for the surface ocean (Figure 14.8). There is *moderate* confidence in this range and distribution of possible futures because:

- There is generally a large discrepancy between modelled and observed temperature trends over the past 50 years in the vicinity of Tonga (Figure 14.8).

Interannual variability in surface air temperature and sea-surface temperature over Tonga is strongly influenced by ENSO in the current climate (Section 14.5). As there is no consistency in projections of future ENSO activity (Volume 1, Section 6.4.1) it is not possible to determine whether interannual variability in temperature will change in the future. However, ENSO is expected to continue to be an important source of variability for the region.

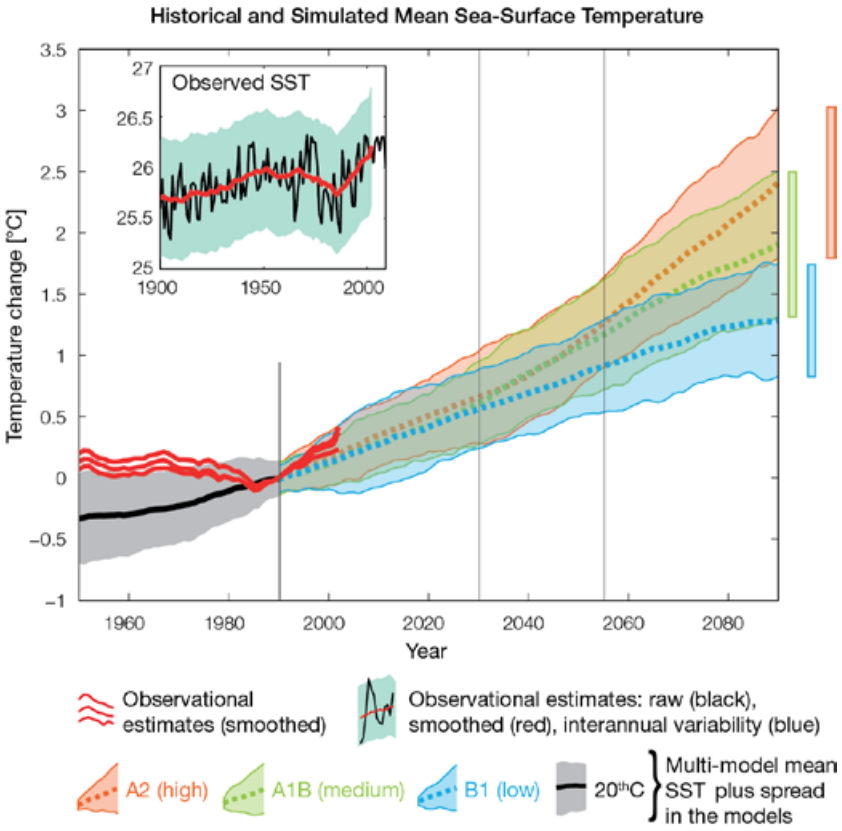

Figure 14.8: Historical climate (from 1950 onwards) and simulated historical and future climate for annual mean sea-surface temperature (SST) in the region surrounding Tonga, for the CMIP3 models. Shading represents approximately 95% of the range of model projections (twice the inter-model standard deviation), while the solid lines represent the smoothed (20-year running average) multi-model mean temperature. Projections are calculated relative to the 1980–1999 period (which is why there is a decline in the inter-model standard deviation around 1990). Observational estimates in the main figure (red lines) are derived from the HadSST2, ERSST and Kaplan Extended SST V2 datasets (Volume 1, Section 2.2.2). Annual average (black) and 20-year running average (red) HadSST2 data is also shown inset.

14.7.2 Rainfall

Wet Season (November-April)

Wet season rainfall is projected to increase over the course of the 21st century. There is *moderate* confidence in this direction of change because:

- An increase in wet season rainfall is consistent with the projected likely increase in the intensity of the South Pacific Convergence Zone (SPCZ), which lies over Tonga in this season (Volume 1, Section 6.4.5).
- The majority of CMIP3 models agree on this direction of change by 2090.

The majority of CMIP3 models simulate little change (-5% to 5%) in wet season rainfall by 2030, however by 2090 the majority simulate an increase (>5%), with a third simulating a large increase (>15%) under the A2 (high) emissions scenario (Table 14.4). There is *moderate* confidence in this range and distribution of possible futures because:

- In simulations of the current climate, the CMIP3 models generally locate the SPCZ in the correct location relative to Tonga in the wet season (Brown et al., 2011).
- The CMIP3 models are unable to resolve many of the physical processes involved in producing rainfall. As a consequence, they do not simulate rainfall as well as other variables such as temperature (Volume 1, Chapter 5).

Dry Season (May-October)

Dry season rainfall is projected to decrease over the course of the 21st century. There is *moderate* confidence in this direction of change because:

- Approximately half of the CMIP3 models agree on this direction of change by 2090.

The majority of CMIP3 models simulate little change (-5% to 5%) in dry season rainfall by 2030, however by 2090 under the higher emissions scenarios (i.e. A2 (high) and A1B (medium)) the models are approximately equally divided between a decrease (<-5%) and little change, with only a few models simulating an increase (>5%) (Table 14.4). There is *low* confidence in this range and distribution of possible futures because:

- In simulations of the current climate, some CMIP3 models have an SPCZ that extends too far east during the dry season, with too much rainfall over Tonga (Brown et al., 2011).
- The CMIP3 models are unable to resolve many of the physical processes involved in producing rainfall.

Annual

Little change is projected in total annual rainfall over the course of the 21st century. There is *low* confidence in this direction of change because:

- Only approximately half of the CMIP3 models agree on this direction of change by 2090.
- There is low confidence in the range and distribution of dry season rainfall projections, as discussed above.

Interannual variability in rainfall over Tonga is strongly influenced by ENSO in the current climate, via the movement of the SPCZ (Section 14.5). As there is no consistency in projections of future ENSO activity (Volume 1, Section 6.4.1) it is not possible to determine whether interannual variability in rainfall will change in the future.

14.7.3 Extremes

Temperature

The intensity and frequency of days of extreme heat are projected to increase over the course of the 21st century. There is *very high* confidence in this direction of change because:

- An increase in the intensity and frequency of days of extreme heat is physically consistent with rising greenhouse gas concentrations.
- All CMIP3 models agree on the direction of change for both intensity and frequency.

The majority of CMIP3 models simulate an increase of approximately 1°C in the temperature experienced on the 1-in-20-year hot day by 2055 under the B1 (low) emissions scenario, with an increase of over 2.5°C simulated by the majority of models by 2090 under the A2 (high) emissions scenario (Table 14.4). There is *low* confidence in this range and distribution of possible futures because:

- In simulations of the current climate, the CMIP3 models tend to underestimate the intensity and frequency of days of extreme heat (Volume 1, Section 5.2.4).
- Smaller increases in the frequency of days of extreme heat are projected by the CCAM 60 km simulations.

Rainfall

The intensity and frequency of days of extreme rainfall are projected to increase over the course of the 21st century. There is *high* confidence in this direction of change because:

- An increase in the frequency and intensity of extreme rainfall is consistent with larger-scale projections, based on the physical argument that the atmosphere is able to hold more water vapour in a warmer climate (Allen and Ingram, 2002; IPCC, 2007). It is also consistent with the projected likely increase in intensity of the SPCZ (Volume 1, Section 6.4.5).
- Almost all of the CMIP3 models agree on this direction of change for both intensity and frequency.

The majority of CMIP3 models simulate an increase of at least 15 mm in the amount of rain received on the 1-in-20-year wet day by 2055 under the B1 (low) emissions scenario, with an increase of at least 30 mm simulated by 2090 under the A2 (high) emissions scenario. The majority of models project that the current 1-in-20-year extreme rainfall event will occur, on average, three to four times per 20-year period by 2055 under the B1 (low) emissions scenario and five times per 20-year period by 2090 under the A2 (high) emissions

scenario. There is *low* confidence in this range and distribution of possible futures because:

- In simulations of the current climate, the CMIP3 models tend to underestimate the intensity and frequency of extreme rainfall (Volume 1, Section 5.2.4).
- The CMIP3 models are unable to resolve many of the physical processes involved in producing extreme rainfall.

Drought

Little change is projected in the incidence of drought over the course of the 21st century. There is *low* confidence in this direction of change because:

- There is only low confidence in the range of dry season rainfall projections (Section 14.7.2), which directly influences projections of future drought conditions.

Under the B1 (low) emissions scenario, the majority of CMIP3 models project that the frequency of mild drought will slightly increase from approximately seven to eight times every 20 years in 2030, to eight to nine times every 20 years by 2090. Under the A1B (medium) emissions scenario, the frequency of mild drought remains approximately constant from 2030 throughout the 21st century at seven to eight times every 20 years, while under the A2 (high) emissions scenario the frequency is projected to slightly decrease from eight to nine times every 20 years in 2030 to six to seven times by 2090. The majority of CMIP3 models project that moderate and severe droughts will occur approximately once to twice and once every 20 years respectively, across all time periods and emissions scenarios.

Tropical Cyclones

Tropical cyclone numbers are projected to decline in the south-east Pacific Ocean basin (0–40ºS, 170ºE–130ºW) over the course of the 21st century. There is *moderate* confidence in this direction of change because:

- Many studies suggest a decline in tropical cyclone frequency globally (Knutson et al., 2010).
- Tropical cyclone numbers decline in the south-east Pacific Ocean in the majority of assessment techniques.

Based on the direct detection methodologies (Curvature Vorticity Parameter (CVP) and the CSIRO Direct Detection Scheme (CDD) described in Volume 1, Section 4.8.2), 65% of projections show no change or a decrease in tropical cyclone formation when applied to the CMIP3 climate models for which suitable output is available. When these techniques are applied to CCAM, 100% of projections show a decrease in tropical cyclone formation. In addition, the Genesis Potential Index (GPI) empirical technique suggests that conditions for tropical cyclone formation will become less favourable in the south-east Pacific Ocean basin, for all analysed CMIP3 models. There is *moderate* confidence in this range and distribution of possible futures because in simulations of the current climate, the CVP, CDD and GPI methods capture the frequency of tropical cyclone activity reasonably well (Volume 1, Section 5.4).

Despite this projected reduction in total cyclone numbers, five of the six CCAM 60 km simulations show an increase in the proportion of the most severe cyclones. Most models also indicate a reduction in tropical cyclone wind hazard north of about 20ºS latitude and regions of increased hazard south of 20ºS latitude. This increase in wind hazard coincides with a poleward shift in the latitude at which tropical cyclones are most intense.

14.7.4 Ocean Acidification

The acidification of the ocean will continue to increase over the course of the 21st century. There is *very high* confidence in this projection as the rate of ocean acidification is driven primarily by the increasing oceanic uptake of carbon dioxide, in response to rising atmospheric carbon dioxide concentrations.

Projections from all analysed CMIP3 models indicate that the annual maximum aragonite saturation state will reach values below 3.5 by about 2035 and continue to decline thereafter (Figure 14.9; Table 14.4). There is *moderate* confidence in this range and distribution of possible futures because the projections are based on climate models without an explicit representation of the carbon cycle and with relatively low resolution and known regional biases.

The impact of acidification change on the health of reef ecosystems is likely to be compounded by other stressors including coral bleaching, storm damage and fishing pressure.

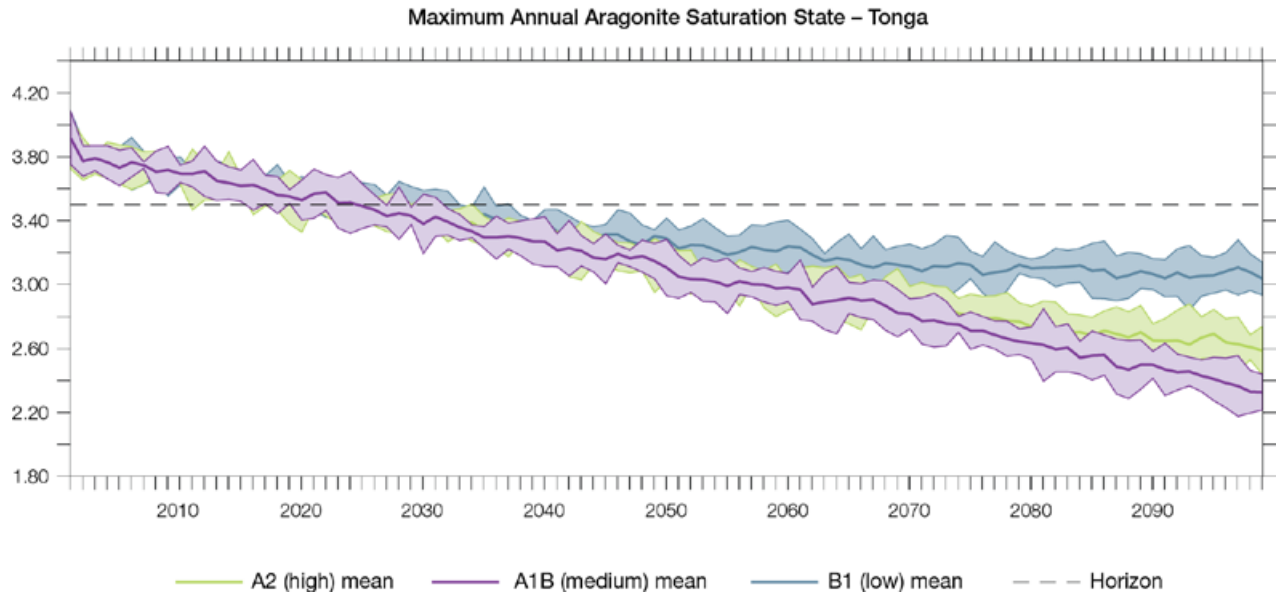

Figure 14.9: Multi-model projections, and their associated uncertainty (shaded area represents two standard deviations), of the maximum annual aragonite saturation state in the sea surface waters of the Tonga region under the different emissions scenarios. The dashed black line represents an aragonite saturation state of 3.5.

14.7.5 Sea Level

Mean sea level is projected to continue to rise over the course of the 21st century. There is *very high* confidence in this direction of change because:

- Sea-level rise is a physically consistent response to increasing ocean and atmospheric temperatures, due to thermal expansion of the water and the melting of glaciers and ice caps.
- Projections arising from all CMIP3 models agree on this direction of change.

The CMIP3 models simulate a rise of between approximately 5–15 cm by 2030, with increases of 20–60 cm indicated by 2090 under the higher-emissions scenarios (i.e. A2 (high), A1B (medium); Figure 14.10; Table 14.4).

There is *moderate* confidence in this range and distribution of possible futures because:

- There is significant uncertainty surrounding ice-sheet contributions to sea-level rise and a rise larger than projected above cannot be excluded (Meehl et al., 2007b). However, understanding of the processes is currently too limited to provide a best estimate or an upper bound (IPCC, 2007).
- Globally, since the early 1990s, sea level has been rising near the upper end of the above projections. During the 21st century, some studies (using semi-empirical models) project faster rates of sea-level rise.

Interannual variability of sea level will lead to periods of lower and higher regional sea levels. In the past, this interannual variability has been about 18 cm (5–95% range, after removal of the seasonal cycle; dashed lines in Figure 14.10 (a)) and it is likely that a similar range will continue through the 21st century. In addition, winds and waves associated with weather phenomena will continue to lead to extreme sea-level events.

In addition to the regional variations in sea level associated with ocean and mass changes, there are ongoing changes in relative sea level associated with changes in surface loading over the last glacial cycle (glacial isostatic adjustment) and local tectonic motions. The glacial isostatic motions are relatively small for the PCCSP region.

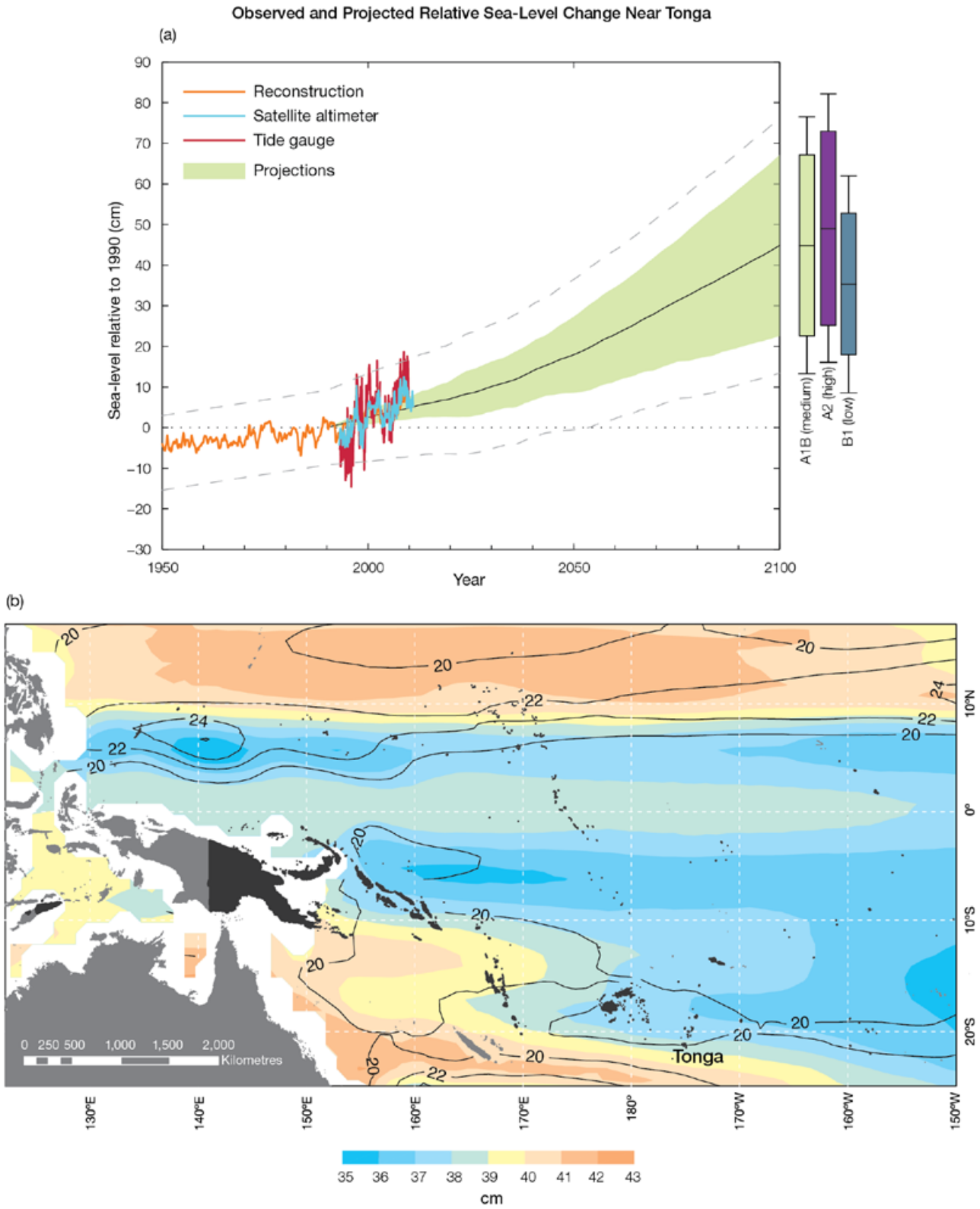

Figure 14.10: Observed and projected relative sea-level change near Tonga. (a) The observed in situ relative sea-level records are indicated in red, with the satellite record (since 1993) in light blue. The gridded sea level at Tonga (since 1950, from Church and White (in press)) is shown in orange. The projections for the A1B (medium) emissions scenario (5–95% uncertainty range) are shown by the green shaded region from 1990–2100. The range of projections for the B1 (low), A1B (medium) and A2 (high) emissions scenarios are also shown by the bars on the right. The dashed lines are an estimate of interannual variability in sea level (5–95% range about the long-term trends) and indicate that individual monthly averages of sea level can be above or below longer-term averages. (b) The projections (in cm) for the A1B (medium) emissions scenario in the Tonga region for the average over 2081–2100 relative to 1981–2000 are indicated by the shading, with the estimated uncertainty in the projections indicated by the contours (in cm).

14.7.6 Projections Summary

The projections presented in Section 14.7 are summarised in Table 14.4. For detailed information regarding the various uncertainties associated with the table values, refer to the preceding text in Sections 14.7 and 1.7, in addition to Chapters 5 and 6 in Volume 1. When interpreting the differences between projections for the A2 (high), A1B (medium), and B1 (low) emissions scenarios, it is also important to consider the emissions pathways associated with each scenario (Volume 1, Figure 4.1) and the fact that a slightly different subset of models was available for each (Volume 1, Appendix 1).

Table 14.4: Projected change in the annual and seasonal-mean climate for Tonga, under the B1 (low; blue), A1B (medium; green) and A2 (high; purple) emissions scenarios. Projections are given for three 20-year periods centred on 2030 (2020–2039), 2055 (2046–2065) and 2090 (2080–2099), relative to 1990 (1980–1999). Values represent the multi-model mean change ± twice the inter-model standard deviation (representing approximately 95% of the range of model projections), except for sea level where the estimated mean change and the 5–95% range are given (as they are derived directly from the Intergovernmental Panel on Climate Change Fourth Assessment Report values). The confidence (Section 1.7.2) associated with the range and distribution of the projections is also given (indicated by the standard deviation and multi-model mean, respectively). See Volume 1, Appendix 1 for a complete listing of CMIP3 models used to derive these projections.

Variable	Season	2030	2055	2090	Confidence
Surface air temperature (°C)	Annual	+0.6 ± 0.4 +0.7 ± 0.5 +0.7 ± 0.4	+1.0 ± 0.5 +1.3 ± 0.6 +1.4 ± 0.4	+1.4 ± 0.6 +2.1 ± 0.8 +2.6 ± 0.7	Moderate
Maximum temperature (°C)	1-in-20-year event	N/A	+1.0 ± 0.7 +1.4 ± 0.7 +1.4 ± 0.6	+1.3 ± 0.6 +2.1 ± 0.9 +2.4 ± 1.4	Low
Minimum temperature (°C)	1-in-20-year event	N/A	+1.1 ± 1.7 +1.5 ± 1.4 +1.4 ± 1.7	+1.5 ± 1.6 +2.0 ± 2.1 +2.3 ± 1.7	Low
Total rainfall (%)*	Annual	+2 ± 13 +1 ± 13 +3 ± 13	+1 ± 10 +3 ± 14 +5 ± 12	+3 ± 14 +3 ± 14 +9 ± 18	Low
Wet season rainfall (%)*	November-April	+4 ± 12 +2 ± 14 +5 ± 15	+4 ± 14 +6 ± 18 +9 ± 15	+6 ± 20 +8 ± 18 +16 ± 19	Moderate
Dry season rainfall (%)*	May-October	0 ± 18 -2 ± 19 +1 ± 13	-3 ± 15 0 ± 21 +1 ± 16	-1 ± 18 -3 ± 20 -1 ± 26	Low
Sea-surface temperature (°C)	Annual	+0.6 ± 0.3 +0.6 ± 0.3 +0.7 ± 0.4	+0.9 ± 0.4 +1.2 ± 0.4 +1.3 ± 0.4	+1.3 ± 0.5 +1.9 ± 0.6 +2.4 ± 0.6	Moderate
Aragonite saturation state (Ωar)	Annual maximum	+3.4 ± 0.1 +3.4 ± 0.1 +3.4 ± 0.1	+3.2 ± 0.1 +3.0 ± 0.1 +3.0 ± 0.1	+3.0 ± 0.1 +2.6 ± 0.1 +2.4 ± 0.1	Moderate
Mean sea level (cm)	Annual	+10 (5–16) +10 (4–16) +10 (3–17)	+19 (10–27) +21 (10–31) +20 (9–31)	+32 (16–47) +39 (20–59) +41 (21–62)	Moderate

*The MIROC3.2(medres) and MIROC3.2(hires) models were eliminated in calculating the rainfall projections, due to their inability to accurately simulate present-day activity of the South Pacific Convergence Zone (Volume 1, Section 5.5.1).

Funafuti Atoll

Chapter 15
Tuvalu

The contributions of Hilia Vavae and Kilateli Epu from the Tuvalu Meteorological Service are gratefully acknowledged

Introduction

This chapter provides a brief description of Tuvalu, its past and present climate as well as projections for the future. The climate observation network and the availability of atmospheric and oceanic data records are outlined. The annual mean climate, seasonal cycles and the influences of large-scale climate features such as the South Pacific Convergence Zone and patterns of climate variability (e.g. the El Niño-Southern Oscillation) are analysed and discussed. Observed trends and analysis of air temperature, rainfall, extreme events (including tropical cyclones), sea-surface temperature, ocean acidification, mean and extreme sea levels are presented. Projections for air and sea-surface temperature, rainfall, sea level, ocean acidification and extreme events for the 21st century are provided. These projections are presented along with confidence levels based on expert judgement by Pacific Climate Change Science Program (PCCSP) scientists. The chapter concludes with a summary table of projections (Table 15.4). Important background information including an explanation of methods and models is provided in Chapter 1. For definitions of other terms refer to the Glossary.

15.1 Climate Summary

15.1.1 Current Climate

- Tuvalu's climate is characterised by two distinct seasons: a wet season from November to April and a dry season from May to October.
- The strong seasonal cycle is driven by the strength of the South Pacific Convergence Zone, which is strongest during the wet season. The West Pacific Monsoon can also bring high rainfall to Tuvalu during the wet season.
- Air temperatures in Tuvalu are relatively constant throughout the year and are closely related to sea-surface temperatures.
- Warming trends are evident in both annual and seasonal mean air temperatures at Funafuti for the period 1950–2009.
- High year-to-year variability in rainfall is mostly due to the impact of the El Niño-Southern Oscillation.
- Annual and seasonal rainfall trends for Funafuti and Nanumea for the period 1950–2009 are not statistically significant.
- The sea-level rise near Tuvalu measured by satellite altimeters since 1993 is about 5 mm per year.
- On average Funafuti experiences eight tropical cyclones per decade, with most occurring between November and April. The high interannual variability in tropical cyclone numbers makes it difficult to identify any long-term trends in frequency.

15.1.2 Future Climate

Over the course of the 21st century:

- Surface air temperature and sea-surface temperature are projected to continue to increase (*very high* confidence).
- Annual and seasonal mean rainfall is projected to increase (*high* confidence).
- The intensity and frequency of days of extreme heat are projected to increase (*very high* confidence).
- The intensity and frequency of days of extreme rainfall are projected to increase (*high* confidence).
- The incidence of drought is projected to decrease (*moderate* confidence).
- Tropical cyclone numbers are projected to decline in the south-east Pacific Ocean basin (0–40ºS, 170ºE–130ºW) (*moderate* confidence).
- Ocean acidification is projected to continue (*very high* confidence).
- Mean sea-level rise is projected to continue (*very high* confidence).

15.2 Country Description

Tuvalu lies is the western South Pacific Ocean between 176°E–180°E and 5°S–11°S. The country consists of five true atolls and four raised limestone reef islands, with a total land area of approximately 26 km^2. The maximum height of the land above mean sea level typically ranges from three to four metres. The area of the Exclusive Economic Zone is 900 000 km^2.

The capital of Tuvalu, Funafuti, is located on the atoll with the same name (Tuvalu's Pacific Adaptation to Climate Change, 2006). The estimated population of Tuvalu in 2010 was 11 149 (Tuvalu Country Statistics, SOPAC, 2010).

Tuvalu's economy is dominated by subsistence farming and fishing activities. Commercial fishing is an expanding economic activity (Tuvalu's First National Communication under the UNFCCC, 1999).

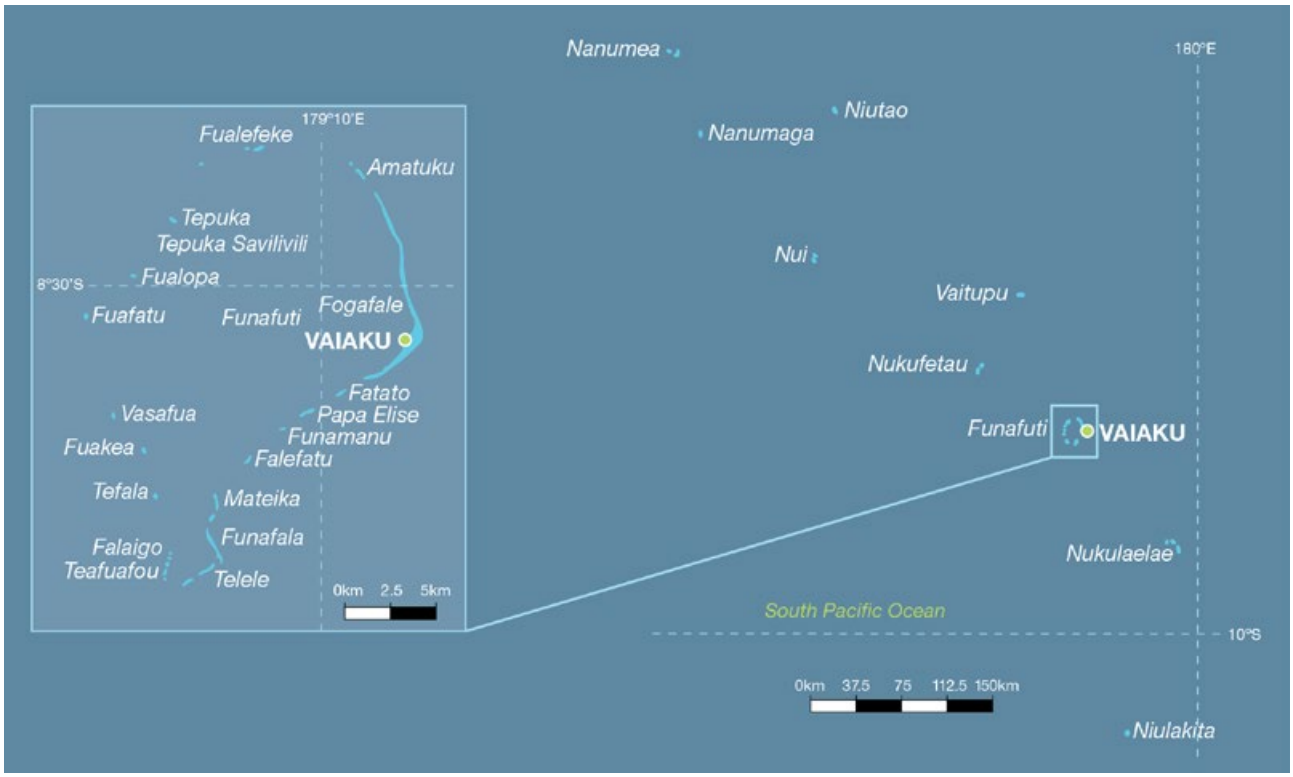

Figure 15.1: Tuvalu

15.3 Data Availability

There are nine operational meteorological stations in Tuvalu at the present time. Multiple observations within a 24-hour period are taken at four stations (Nanumea, Nui, Funafuti and Niulakita) and there are single observation rainfall stations at five locations: Nanumaga, Niutao, Nukufetau, Vaitupu and Nukulaelae. The Funafuti station has the longest record, with rainfall data available from 1927 and air temperature data from 1933.

Climate records for Funafuti and rainfall records for Nanumea for the period 1950–2009 have been used. The Funafuti climate station is located on the Fongafale islet on the eastern side of the Funafuti atoll in southern Tuvalu. Nanumea is the northernmost island in the Tuvalu group (Figure 15.1). Both records are homogeneous and more than 99% complete.

Monthly-averaged sea-level data are available from 1977 at Funafuti (1977–2001 and 1993–present). A global positioning system instrument to estimate vertical land motion was deployed at Funafuti in 2001 and will provide valuable direct estimates of local vertical land motion in future years. Both satellite (from 1993) and in situ sea-level data (1950–2009; termed reconstructed sea level; Volume 1, Section 2.2.2.2) are available on a global 1° x 1° grid.

Long-term locally-monitored sea-surface temperature data are unavailable for Tuvalu, so large-scale gridded sea-surface temperature datasets have been used (HadISST, HadSST2, ERSST and Kaplan Extended SST V2; Volume 1, Table 2.3).

15.4 Seasonal Cycles

Mean annual rainfall in the south of Tuvalu, including Funafuti, is around 3400 mm. Approximately 2900 mm per year falls at Nanumea in the north. The climate of Tuvalu is characterised by two distinct seasons: a wet season from November to April and a dry season from May to October (Figure 15.2). The wet season is shorter in Nanumea. This strong seasonal cycle is driven by the strength of the South Pacific Convergence Zone (SPCZ), which is strongest during the wet season. The West Pacific Monsoon can also bring high rainfall to Tuvalu during the wet season. Rainfall averages more than 200 mm each month of the year in Funafuti and more than 160 mm in Nanumea, reflecting the location of Tuvalu near the West Pacific Warm Pool, where convective rainfall occurs year-round.

Funafuti has virtually no seasonal cycle for maximum and minimum air temperature, with maxima averaging around 31°C and minima 25–26°C, all year round (Figure 15.2). Being on a small atoll island surrounded by ocean, air temperatures in Tuvalu are strongly related to sea-surface temperatures around the islands. Sea-surface temperatures around Nanumea are very similar to those around Funafuti and so air temperatures are similar there, although no long-term air temperature data at Nanumea are available.

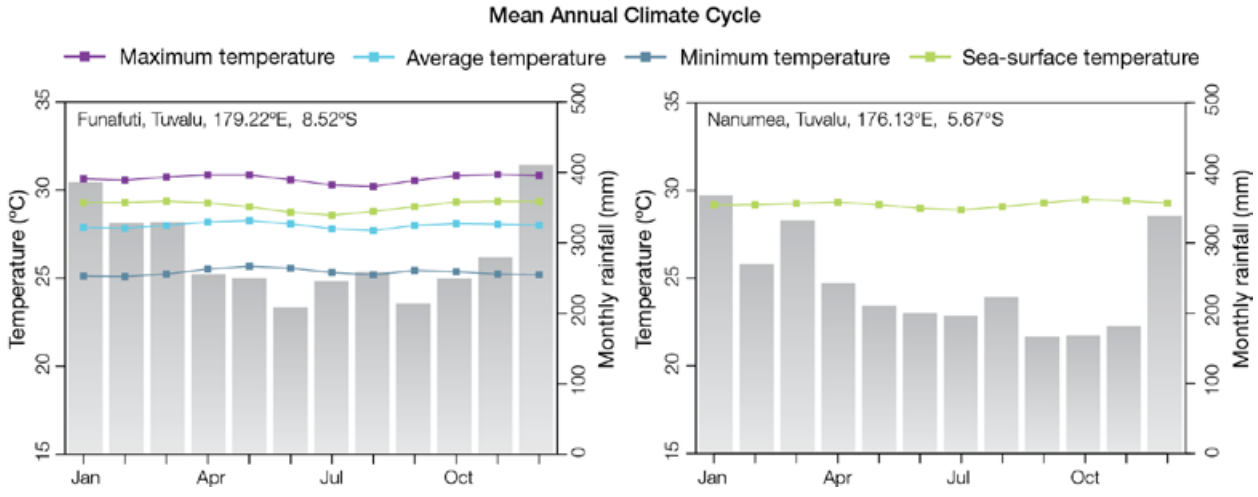

Figure 15.2: Mean annual cycle of rainfall (grey bars) and daily maximum, minimum and mean air temperatures at Funafuti (left) and Nanumea (right – rainfall only), and local sea-surface temperatures derived from the HadISST dataset (Volume 1, Table 2.3).

15.5 Climate Variability

High year-to-year variability in rainfall is observed in Tuvalu, mostly due to the impact of the El Niño-Southern Oscillation (ENSO; Figure 15.4). In the wettest years Funafuti receives about twice as much rainfall as in the driest years, while in Nanumea this can be as much as five times more. In an El Niño year, the SPCZ tends to move to the north-east over Tuvalu and so rainfall is higher. This impact is mainly seen in the dry season at Funafuti, but further north at Nanumea the effect is even stronger, especially in the wet season (Tables 15.1 and 15.2). At Nanumea the SPCZ tends to move over the island in El Niño years and away to the south-west in La Niña years, bringing severe drought. Considerable decadal variability is also evident in rainfall in Tuvalu, but the correlations with the Interdecadal Pacific Oscillation show only a weak relationship with wet-season rainfall in Nanumea.

In contrast to rainfall, interannual variability in average surface air temperatures is very small in Funafuti, although ENSO has some impact on air temperatures. Minimum temperatures are higher during El Niño years and lower in La Niña years, as are maximum air temperatures during the wet season. The influence is likely due to the warmer ocean temperatures around Tuvalu in El Niño years.

ENSO Modoki (Volume 1, Section 3.4.1) has a significant impact on rainfall and temperatures, but this impact is generally weaker than canonical El Niño and La Niña events. However, the impacts of ENSO Modoki events on maximum air temperatures and wet season minimum air temperatures are stronger. They also affect rainfall during the dry season in Funafuti and the wet season in Nanumea.

Table 15.1: Correlation coefficients between indices of key large-scale patterns of climate variability and minimum and maximum temperatures (Tmin and Tmax) and rainfall at Funafuti. Only correlation coefficients that are statistically significant at the 95% level are shown.

Climate feature/index		Dry season (May-October)			Wet season (November-April)		
		Tmin	Tmax	Rain	Tmin	Tmax	Rain
ENSO	Niño3.4	0.25		0.41	0.35	0.39	
	Southern Oscillation Index	-0.25		-0.47	-0.29		
Interdecadal Pacific Oscillation Index							
ENSO Modoki Index			0.28	0.27	0.41	0.60	
Number of years of data		64	64	76	63	63	77

Table 15.2: Correlation coefficients between indices of key large-scale patterns of climate variability and minimum and maximum temperatures (Tmin and Tmax) and rainfall at Nanumea. Only correlation coefficients that are statistically significant at the 95% level are shown.

Climate feature/index		Dry season (May-October)	Wet season (November-April)
		Rain	Rain
ENSO	Niño3.4	0.59	0.80
	Southern Oscillation Index	-0.58	-0.83
Interdecadal Pacific Oscillation Index			0.25
ENSO Modoki Index			0.50
Number of years of data		64	64

Training in *Pacific Climate Futures*, Funafuti

15.6 Observed Trends

15.6.1 Air Temperature

Warming trends are evident in both annual and seasonal mean air temperatures at Funafuti from 1950 (Figure 15.3 and Table 15.3), with the strongest trend in dry season mean air temperature (+0.24°C per decade). Trends in minimum air temperatures are slightly stronger than those calculated for maximum air temperatures.

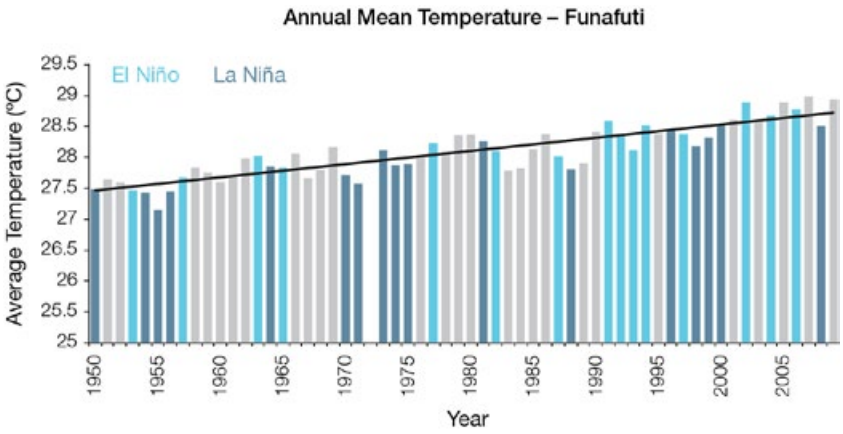

Figure 15.3: Annual mean air temperature at Funafuti. Light blue, dark blue and grey bars denote El Niño, La Niña and neutral years respectively.

15.6.2 Rainfall

Annual and seasonal rainfall trends for Funafuti and Nanumea for the period 1950—2009 are not statistically significant (Table 15.3 and Figure 15.4).

15.6.3 Extreme Events

The tropical cyclone season in Tuvalu is from November to April. Occurrences outside this period are rare. The tropical cyclone archive for the Southern Hemisphere indicates that between the 1969/70 and 2006/07 cyclone seasons the centre of 33 tropical cyclones passed within approximately 400 km of Funafuti. This represents an average of eight cyclones per decade. Tropical cyclones were most frequent in El Niño years (12 cyclones per decade) and least frequent in La Niña years (four cyclones per decade). The ENSO-neutral season average is six cyclones per decade. The interannual variability in the number of tropical cyclones in the vicinity of Funafuti is large, ranging from zero in some seasons to three in the 1997/98 season (Figure 15.5). This high variability makes it difficult to identify any long-term trends in frequency.

Tropical cyclones and spring tides are the main extreme events that affect Funafuti. In addition to high winds and rainfall, tropical cyclones also generate storm surge and swell, resulting in land inundation. This results in agricultural losses (especially taro) and damage to buildings and roads along the coast.

Table 15.3: Annual and seasonal trends in maximum, minimum and mean air temperature (Tmax, Tmin and Tmean) and rainfall at Funafuti and Nanumea for 1950–2009. Asterisks indicate significance at the 95% level. Persistence is taken into account in the assessment of significance as in Power and Kociuba (in press). The statistical significance of the air temperature trends is not assessed.

	Funafuti Tmax (°C per 10 yrs)	Funafuti Tmin (°C per 10 yrs)	Funafuti Tmean (°C per 10 yrs)	Funafuti Rain (mm per 10 yrs)	Nanumea Rain (mm per 10 yrs)
Annual	+0.21	+0.22	+0.21	-45	-2
Wet season	+0.18	+0.20	+0.19	-37	-4
Dry season	+0.24	+0.25	+0.24	-13	+1

15.6.4 Sea-Surface Temperature

Water temperatures around Tuvalu have risen gradually since the 1950s with the rate increasing over time. Since the 1970s the rate of warming has been approximately 0.13°C per decade. Figure 15.8 shows the 1950–2000 sea-surface temperature changes (relative to a reference year of 1990) from three different large-scale sea surface temperature datasets (HadSST2, ERSST and Kaplan Extended SST V2; Volume 1, Table 2.3). At these regional scales, natural variability may play a large role in determining sea-surface temperature in the region making it difficult to identify any long-term trends.

15.6.5 Ocean Acidification

Based on the large-scale distribution of coral reefs across the Pacific and the seawater chemistry, Guinotte et al. (2003) suggested that seawater aragonite saturation states above 4 were optimal for coral growth and for the development of healthy reef ecosystems, with values from 3.5 to 4 adequate for coral growth, and values between 3 and 3.5, marginal. Coral reef ecosystems were not found at seawater aragonite saturation states below 3 and these conditions were classified as extremely marginal for supporting coral growth.

In the Tuvalu region, the aragonite saturation state has declined from about 4.5 in the late 18th century to an observed value of about 4.0 ± 0.1 by 2000.

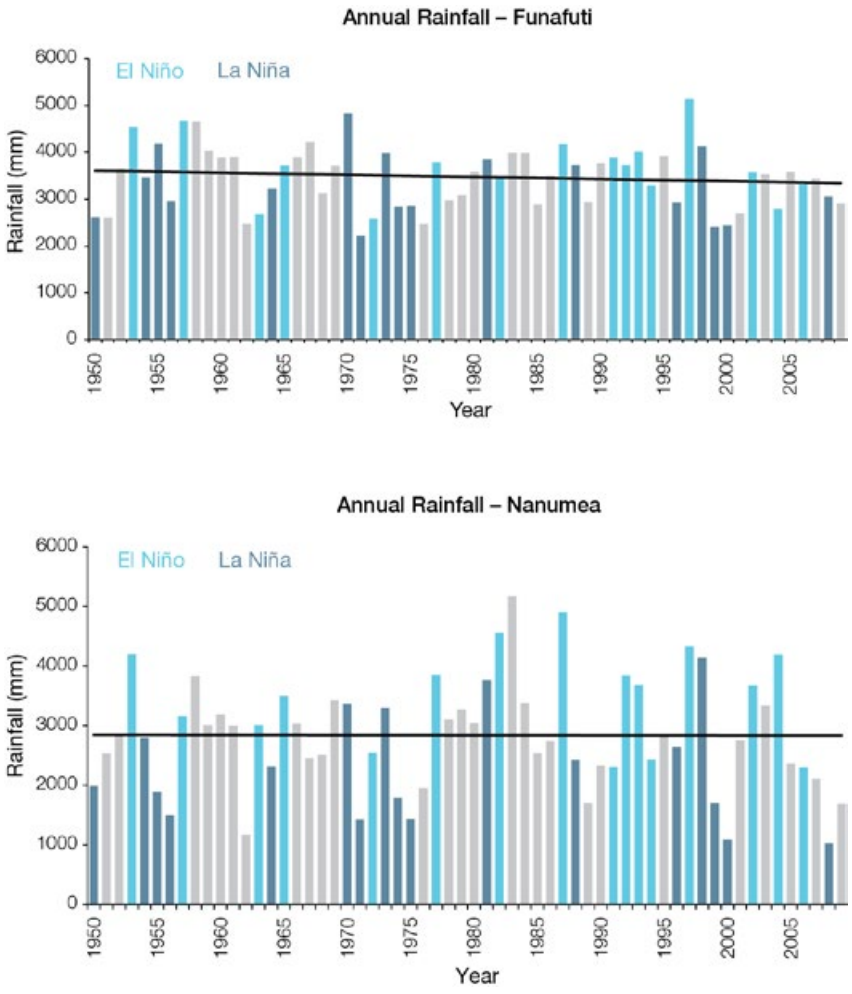

Figure 15.4: Annual rainfall for Funafuti (top) and Nanumea (bottom). Light blue, dark blue and grey bars denote El Niño, La Niña and neutral years respectively.

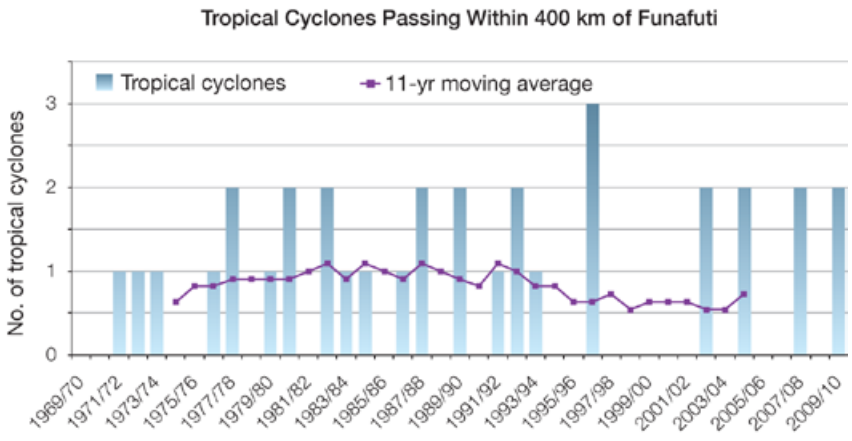

Figure 15.5: Tropical cyclones passing within 400 km of Funafuti per season. The 11-year moving average is in purple.

15.6.6 Sea Level

Monthly averages of the historical tide gauge, satellite (since 1993) and gridded sea-level (since 1950) data agree well after 1993 and indicate interannual variability in sea levels of about 26 cm (estimated 5–95% range) after removal of the seasonal cycle (Figure 15.10). The sea-level rise near Tuvalu measured by satellite altimeters (Figure 15.6) since 1993 is about 5 mm per year, larger than the global average of 3.2 ± 0.4 mm per year. This rise is partly linked to a pattern related to climate variability from year to year and decade to decade (Figure 15.10).

15.6.7 Extreme Sea-Level Events

The annual climatology of the highest daily sea levels has been evaluated from hourly measurements by tide gauges at Funafuti (Figure 15.7). Tides and short-term sea-level fluctuations create a tendency for highest annual water levels to occur during February through March. This is consistent with the timing of most of the top 10 highest sea levels recorded which all occur during these months. During La Niña years, there is a tendency for sea levels to be higher due to warmer ocean temperatures which influence the seasonal contributions (Volume 1, Section 3.6.3 and Figures 3.20 and 3.21) whereas short-term contributions to sea level due to the influence of weather events tend to be lower than the all-year averages. In other words, the seasonal and short-term influences appear to exert opposite influences on sea-level extremes. During El Niño, the seasonal contribution to extreme sea levels is lower whereas the short-term contribution is largely unchanged from the all-year averages. The top 10 events all occurred from February to April; six during ENSO-neutral years, three during La Niña years and one during El Niño. This suggests that tides exert a strong influence on the occurrence of sea-level extremes where as the influence of the ENSO cycle is less important.

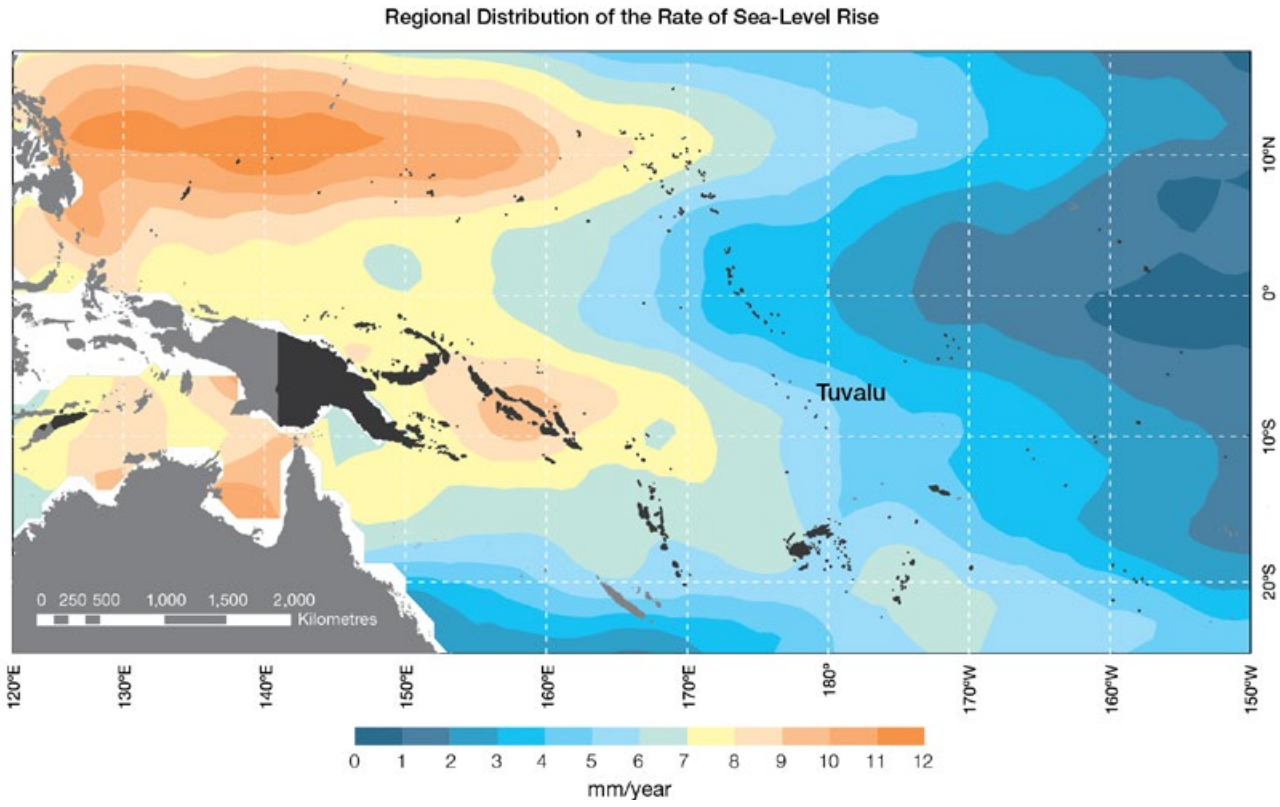

Figure 15.6: The regional distribution of the rate of sea-level rise measured by satellite altimeters from January 1993 to December 2010, with the location of Tuvalu indicated. Further detail about regional distribution of sea-level rise is provided in Volume 1, Section 3.6.3.2.

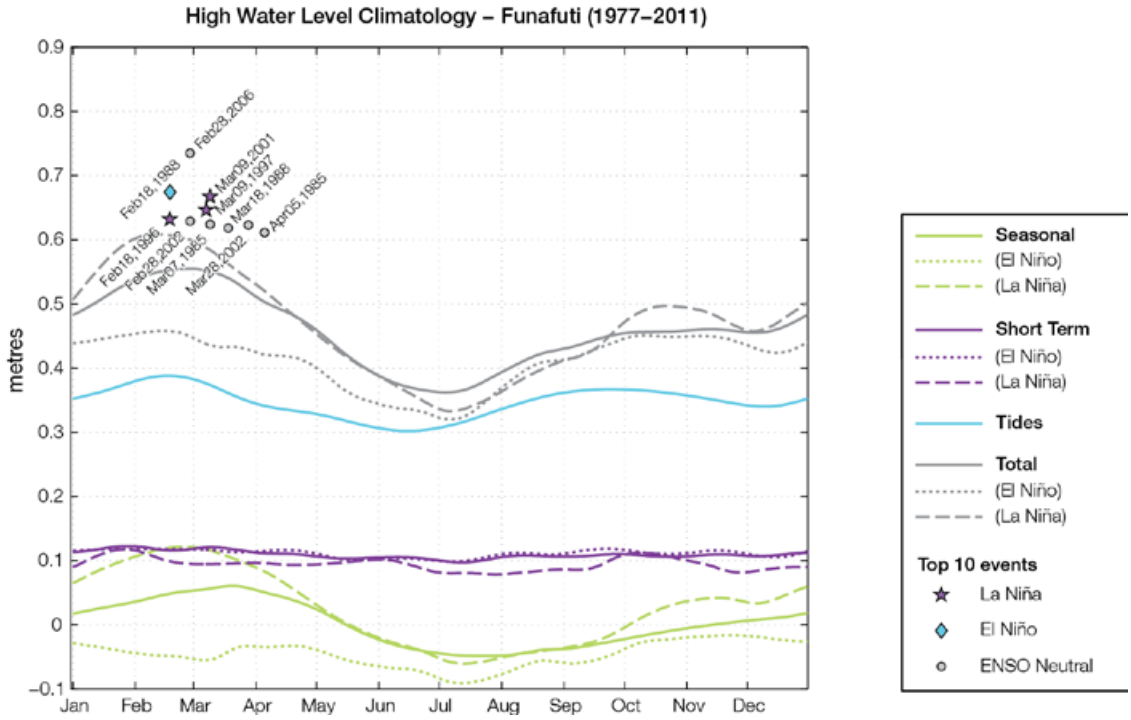

Figure 15.7: The annual cycle of high waters relative to Mean Higher High Water (MHHW) due to tides, short-term fluctuations (most likely associated with storms) and seasonal variations for Tuvalu. The tides and short-term fluctuations are respectively the 95% exceedence of the astronomical high tides relative to MHHW and short-term sea level fluctuations. Components computed only for El Niño and La Niña months are shown by dotted and dashed lines, and grey lines are the sum of the tide, short-term and seasonal components. The 10 highest sea-level events in the record relative to MHWW are shown, and coded to indicate the phase of ENSO at the time of the extreme event.

15.7 Climate Projections

Climate projections have been derived from up to 18 global climate models from the CMIP3 database, for up to three emissions scenarios (B1 (low), A1B (medium) and A2 (high)) and three 20-year periods (centred on 2030, 2055 and 2090, relative to 1990). These models were selected based on their ability to reproduce important features of the current climate (Volume 1, Section 5.2.3), so projections from each of the models are plausible representations of the future climate. This means there is not one single projected future for Tuvalu, but rather a range of possible futures. The full range of these futures is discussed in the following sections.

These projections do not represent a value specific to any actual location, such as a town in Tuvalu. Instead, they refer to an average change over the broad geographic region encompassing the islands of Tuvalu and the surrounding ocean (Figure 1.1 shows the regional boundaries). Section 1.7 provides important information about understanding climate model projections.

15.7.1 Temperature

Surface air temperature and sea-surface temperature are projected to continue to increase over the course of the 21st century. There is *very high* confidence in this direction of change because:

- Warming is physically consistent with rising greenhouse gas concentrations.
- All CMIP3 models agree on this direction of change.

The majority of CMIP3 models simulate a slight increase (<1°C) in annual and seasonal mean temperature by 2030, however by 2090 under the A2 (high) emissions scenario temperature increases of greater than 2.5°C are simulated by almost all models (Table 15.4). Given the close relationship between surface air temperature and sea-surface temperature, a similar (or slightly weaker) rate of warming is projected for the surface ocean (Figure 15.8). There is *high* confidence in this range and distribution of possible futures because:

- There is generally close agreement between modelled and observed temperature trends over the past 50 years in the vicinity of Tuvalu, although observational records are limited (Figure 15.8).

Interannual variability in surface air temperature and sea-surface temperature over Tuvalu is strongly influenced by ENSO in the current climate (Section 15.5). As there is no consistency in projections of future ENSO activity (Volume 1, Section 6.4.1) it is not possible to determine whether interannual variability in temperature will change in the future. However, ENSO is expected to continue to be an important source of variability for the region.

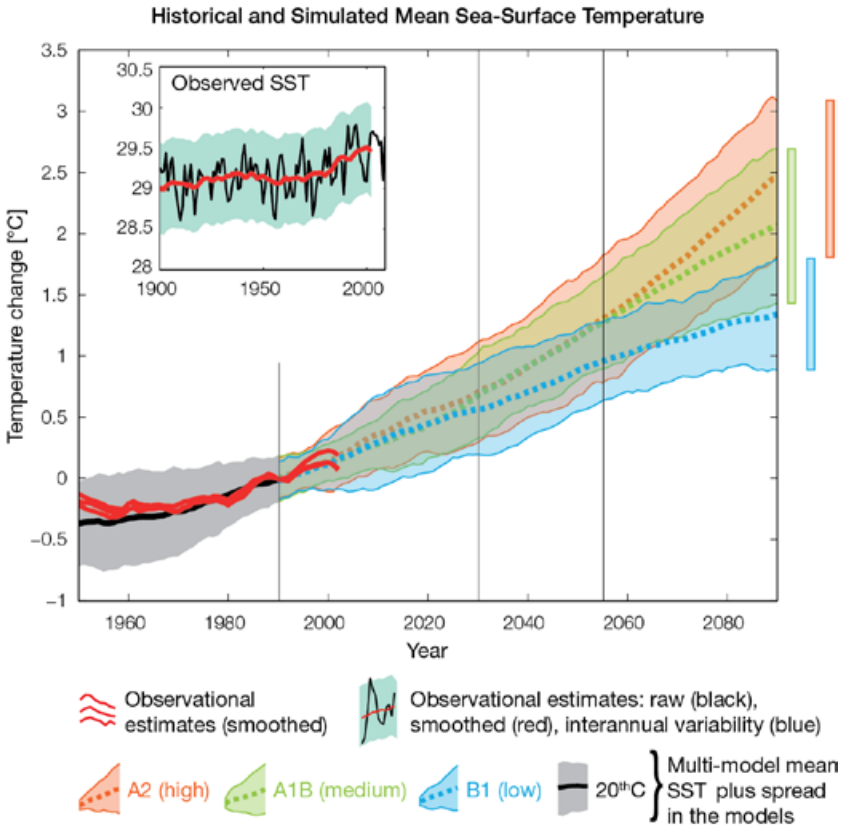

Figure 15.8: Historical climate (from 1950 onwards) and simulated historical and future climate for annual mean sea-surface temperature (SST) in the region surrounding Tuvalu, for the CMIP3 models. Shading represents approximately 95% of the range of model projections (twice the inter-model standard deviation), while the solid lines represent the smoothed (20-year running average) multi-model mean temperature. Projections are calculated relative to the 1980–1999 period (which is why there is a decline in the inter-model standard deviation around 1990). Observational estimates in the main figure (red lines) are derived from the HadSST2, ERSST and Kaplan Extended SST V2 datasets (Volume 1, Section 2.2.2). Annual average (black) and 20-year running average (red) HadSST2 data is also shown inset.

15.7.2 Rainfall

Wet season (November-April), dry season (May-October) and annual average rainfall are projected to increase over the course of the 21st century. There is *high* confidence in this direction of change because:

- Physical arguments indicate that rainfall will increase in the equatorial Pacific in a warmer climate (IPCC, 2007; Volume 1, Section 6.4.3).
- Almost all of the CMIP3 models agree on this direction of change by 2090.

The majority of CMIP3 models simulate little change (-5% to 5%) in wet season, dry season and annual mean rainfall by 2030, however by 2090 the majority simulate an increase (>5%), with up to a third simulating a large increase (> 5%) under the A2 (high) emissions scenario (Table 15.4). There is *moderate* confidence in this range and distribution of possible futures because:

- In simulations of the current climate, the CMIP3 models broadly capture the influence of the West Pacific Monsoon and the South Pacific Convergence Zone on the rainfall of Tuvalu (Volume 1, Section 5.2.3), although most models produce monsoon westerly winds that do not extend far enough east into the Pacific basin.
- The CMIP3 models are unable to resolve many of the physical processes involved in producing rainfall. As a consequence, they do not simulate rainfall as well as other variables such as temperature (Volume 1, Chapter 5).

Interannual variability in rainfall over Tuvalu is strongly influenced by ENSO in the current climate (Section 15.5). As there is no consistency in projections of future ENSO activity (Volume 1, Section 6.4.1) it is not possible to determine whether interannual variability in rainfall will change in the future.

15.7.3 Extremes

Temperature

The intensity and frequency of days of extreme heat are projected to increase over the course of the 21st century. There is *very high* confidence in this direction of change because:

- An increase in the intensity and frequency of days of extreme heat is physically consistent with rising greenhouse gas concentrations.
- All CMIP3 models agree on the direction of change for both intensity and frequency.

The majority of CMIP3 models simulate an increase of approximately 1°C in the temperature experienced on the 1-in-20-year hot day by 2055 under the B1 (low) emissions scenario, with an increase of over 2.5°C simulated by the majority of models by 2090 under the A2 (high) emissions scenario (Table 15.4). There is *low* confidence in this range and distribution of possible futures because:

- In simulations of the current climate, the CMIP3 models tend to underestimate the intensity and frequency of days of extreme heat (Volume 1, Section 5.2.4).
- Smaller increases in the frequency of days of extreme heat are projected by the CCAM 60 km simulations.

Rainfall

The intensity and frequency of days of extreme rainfall are projected to increase over the course of the 21st century. There is *high* confidence in this direction of change because:

- An increase in the frequency and intensity of extreme rainfall is consistent with larger-scale projections, based on the physical argument that the atmosphere is able to hold more water vapour in a warmer climate (Allen and Ingram, 2002; IPCC, 2007). It is also consistent with physical arguments which indicate that rainfall will increase in the deep tropical Pacific in a warmer climate (IPCC, 2007; Volume 1, Section 6.4.3).
- Almost all of the CMIP3 models agree on this direction of change for both intensity and frequency.

The majority of CMIP3 models simulate an increase of at least 20 mm in the amount of rain received on the 1-in-20-year wet day by 2055 under the B1 (low) emissions scenario, with an increase of at least 35 mm simulated by 2090 under the A2 (high) emissions scenario. The majority of models project that the current 1-in-20-year extreme rainfall event will occur, on average, four to five times per 20-year period by 2055 under the B1 (low) emissions scenario and six to seven times per 20-year period by 2090 under the A2 (high) emissions scenario. There is *low* confidence in this range and distribution of possible futures because:

- In simulations of the current climate, the CMIP3 models tend to underestimate the intensity and frequency of extreme rainfall (Volume 1, Section 5.2.4).
- The CMIP3 models are unable to resolve many of the physical processes involved in producing extreme rainfall.

Drought

The incidence of drought is projected to decrease over the course of the 21st century. There is *moderate* confidence in this direction of change because:

- A decrease in drought is consistent with projections of increased rainfall (Section 15.7.2).
- The majority of models agree on this direction of change for most drought categories.

The majority of CMIP3 models project that mild drought will occur approximately eight to nine times every 20 years in 2030 under all emissions scenarios, decreasing to six to seven times by 2090. The frequency of moderate and severe drought is projected to remain approximately stable from 2030 throughout the 21st century at once to twice and once every 20 years, respectively.

There is *low* confidence in this range and distribution of possible futures because:

- There is only moderate confidence in the range of rainfall projections (Section 15.7.2), which directly influences projections of future drought conditions.

Tropical Cyclones

Tropical cyclone numbers are projected to decline in the south-east Pacific Ocean basin (0–40ºS, 170ºE–130ºW) over the course of the 21st century. There is *moderate* confidence in this direction of change because:

- Many studies suggest a decline in tropical cyclone frequency globally (Knutson et al., 2010).
- Tropical cyclone numbers decline in the south-east Pacific Ocean in the majority assessment techniques.

Based on the direct detection methodologies (Curvature Vorticity Parameter (CVP) and the CSIRO Direct Detection Scheme (CDD) described in Volume 1, Section 4.8.2), 65% of projections show no change or a decrease in tropical cyclone formation when applied to the CMIP3 climate models for which suitable output is available. When these techniques are applied to CCAM, 100% of projections show a decrease in tropical cyclone formation. In addition, the Genesis Potential Index (GPI) empirical technique suggests that conditions for tropical cyclone formation will become less favourable in the south-east Pacific Ocean basin, for all analysed CMIP3 models. There is moderate confidence in this range and distribution of possible futures because in simulations of the current climate, the CVP, CDD and GPI methods capture the frequency of tropical cyclone activity reasonably well (Volume 1, Section 5.4).

Despite this projected reduction in total cyclone numbers, five of the six CCAM 60 km simulations show an increase in the proportion of the most severe cyclones. Most models also indicate a reduction in tropical cyclone wind hazard north of 20ºS latitude and regions of increased hazard south of 20ºS latitude. This increase in wind hazard coincides with a poleward shift in the latitude at which tropical cyclones are most intense.

15.7.4 Ocean Acidification

The acidification of the ocean will continue to increase over the course of the 21st century. There is *very high* confidence in this projection as the rate of ocean acidification is driven primarily by the increasing oceanic uptake of carbon dioxide, in response to rising atmospheric carbon dioxide concentrations.

Projections from all analysed CMIP3 models indicate that the annual maximum aragonite saturation state will reach values below 3.5 by about 2060 and continue to decline thereafter (Figure 15.9; Table 15.4). There is *moderate* confidence in this range and distribution of possible futures because the projections are based on climate models without an explicit representation of the carbon cycle and with relatively low resolution and known regional biases.

The impact of acidification change on the health of reef ecosystems is likely to be compounded by other stressors including coral bleaching, storm damage and fishing pressure.

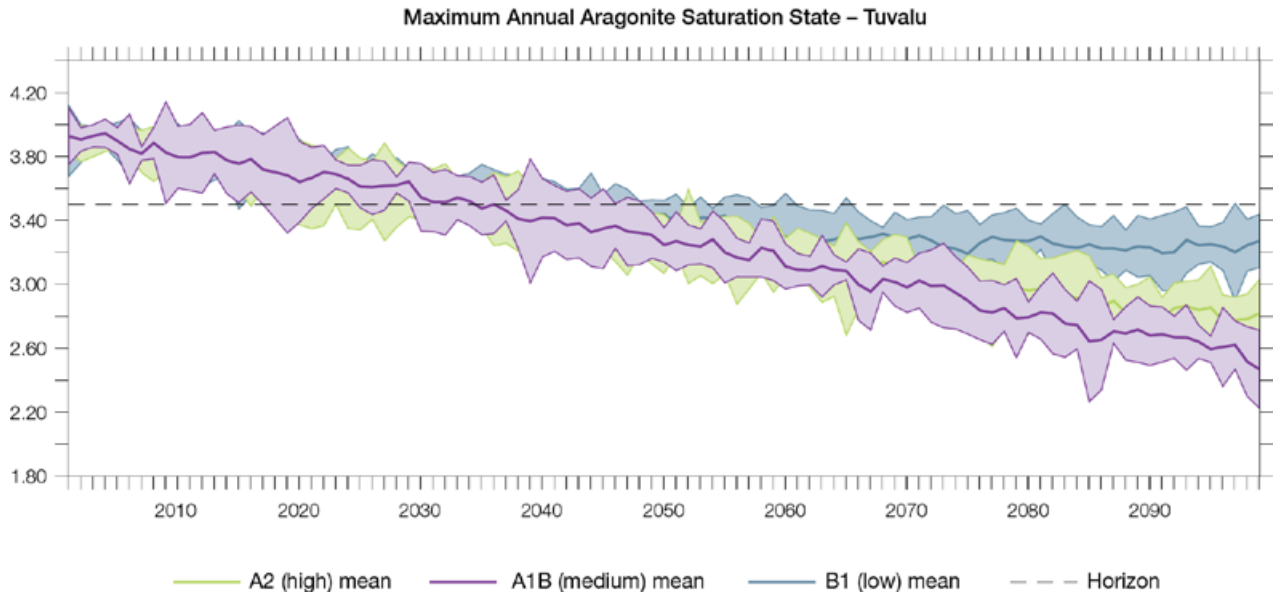

Figure 15.9: Multi-model projections, and their associated uncertainty (shaded area represents two standard deviations), of the maximum annual aragonite saturation state in the sea surface waters of the Tuvalu region under the different emissions scenarios. The dashed black line represents an aragonite saturation state of 3.5.

15.7.5 Sea Level

Mean sea level is projected to continue to rise over the course of the 21st century. There is *very high* confidence in this direction of change because:

- Sea-level rise is a physically consistent response to increasing ocean and atmospheric temperatures, due to thermal expansion of the water and the melting of glaciers and ice caps.
- Projections arising from all CMIP3 models agree on this direction of change.

The CMIP3 models simulate a rise of between approximately 5–15 cm by 2030, with increases of 20–60 cm indicated by 2090 under the higher-emissions scenarios (i.e. A2 (high) and A1B (medium); Figure 15.10; Table 15.4). There is *moderate* confidence in this range and distribution of possible futures because:

- There is significant uncertainty surrounding ice-sheet contributions to sea-level rise and a rise larger than that projected above cannot be excluded (Meehl et al., 2007b). However, understanding of the processes is currently too limited to provide a best estimate or an upper bound (IPCC, 2007).
- Globally, since the early 1990s, sea level has been rising near the upper end of the above projections. During the 21st century, some studies (using semi-empirical models) project faster rates of sea-level rise.

Interannual variability of sea level will lead to periods of lower and higher regional sea levels. In the past, this interannual variability has been about 26 cm (5–95% range, after removal of the seasonal cycle; dashed lines in Figure 15.10 (a)) and it is likely that a similar range will continue through the 21st century. In addition, winds and waves associated with weather phenomena will continue to lead to extreme sea-level events.

In addition to the regional variations in sea level associated with ocean and mass changes, there are ongoing changes in relative sea level associated with changes in surface loading over the last glacial cycle (glacial isostatic adjustment) and local tectonic motions. The glacial isostatic motions are relatively small for the PCCSP region.

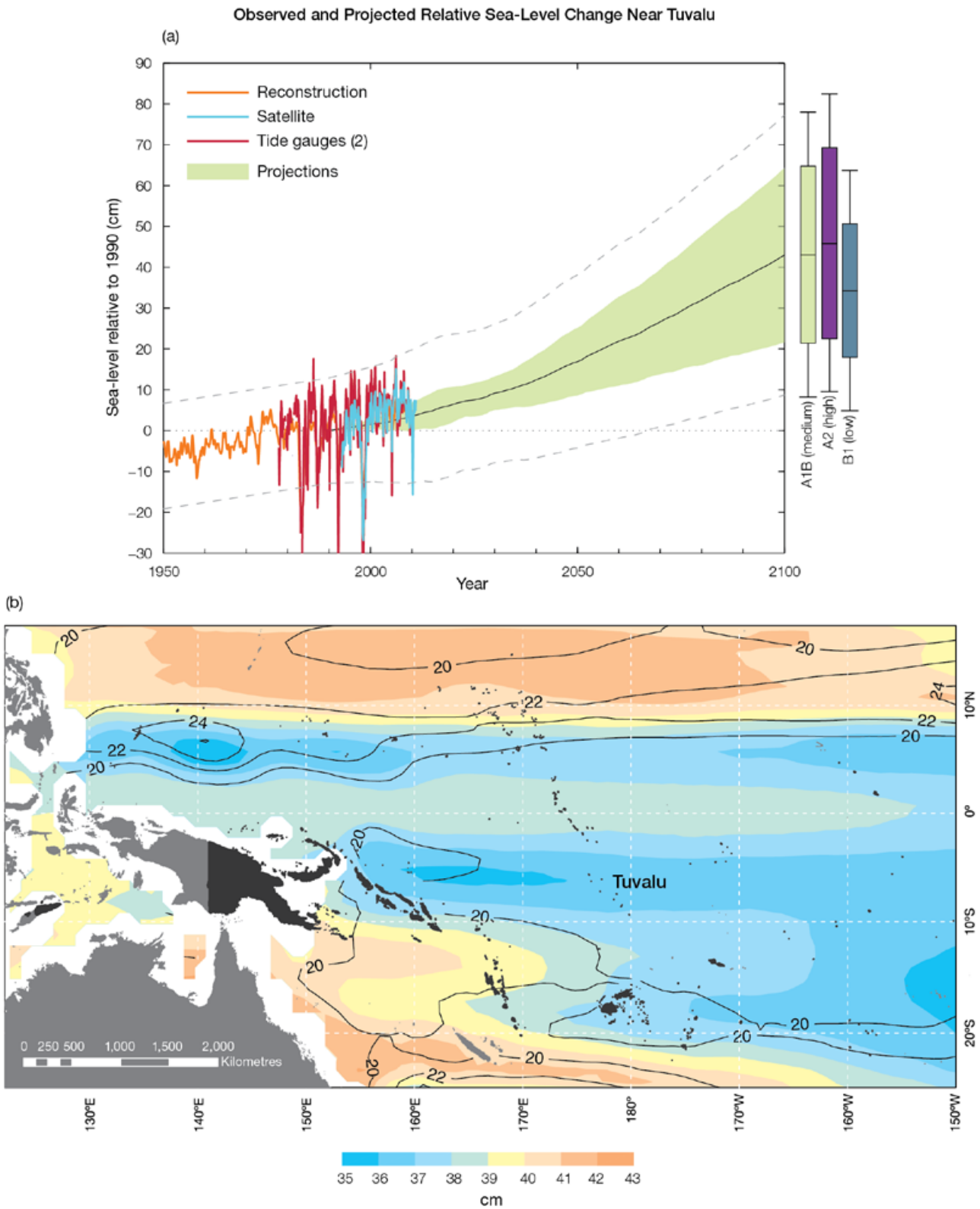

Figure 15.10: Observed and projected relative sea-level change near Tuvalu. (a) The observed in situ relative sea-level records are indicated in red, with the satellite record (since 1993) in light blue. The gridded sea level at Tuvalu (since 1950, from Church and White (in press)) is shown in orange. The projections for the A1B (medium) emissions scenario (5–95% uncertainty range) are shown by the green shaded region from 1990–2100. The range of projections for the B1 (low), A1B (medium) and A2 (high) emissions scenarios by 2100 are also shown by the bars on the right. The dashed lines are an estimate of interannual variability in sea level (5–95% range about the long-term trends) and indicate that individual monthly averages of sea level can be above or below longer-term averages. (b) The projections (in cm) for the A1B (medium) emissions scenario in the Tuvalu region for the average over 2081–2100 relative to 1981–2000 are indicated by the shading, with the estimated uncertainty in the projections indicated by the contours (in cm).

15.7.6 Projections Summary

The projections presented in Section 15.7 are summarised in Table 15.4. For detailed information regarding the various uncertainties associated with the table values, refer to the preceding text in Sections 15.7 and 1.7, in addition to Chapters 5 and 6 in Volume 1. When interpreting the differences between projections for the B1 (low), A1B (medium) and A2 (high) emissions scenarios, it is also important to consider the emissions pathways associated with each scenario (Volume 1, Figure 4.1) and the fact that a slightly different subset of models was available for each (Volume 1, Appendix 1).

Table 15.4: Projected change in the annual and seasonal mean climate for Tuvalu, under the B1 (low; blue), A1B (medium; green) and A2 (high; purple) emissions scenarios. Projections are given for three 20-year periods centred on 2030 (2020–2039), 2055 (2046–2065) and 2090 (2080–2099), relative to 1990 (1980–1999). Values represent the multi-model mean change ± twice the inter-model standard deviation (representing approximately 95% of the range of model projections), except for sea level where the estimated mean change and the 5–95% range are given (as they are derived directly from the Intergovernmental Panel on Climate Change Fourth Assessment Report values). The confidence (Section 1.7.2) associated with the range and distribution of the projections is also given (indicated by the standard deviation and multi-model mean, respectively). See Volume 1, Appendix 1 for a complete listing of CMIP3 models used to derive these projections.

Variable	Season	2030	2055	2090	Confidence
Surface air temperature (°C)	Annual	+0.7 ± 0.4 +0.8 ± 0.4 +0.7 ± 0.3	+1.1 ± 0.4 +1.5 ± 0.5 +1.4 ± 0.4	+1.5 ± 0.6 +2.3 ± 0.8 +2.7 ± 0.6	High
Maximum temperature (°C)	1-in-20-year event	N/A	+1.0 ± 0.6 +1.5 ± 0.6 +1.5 ± 0.5	+1.4 ± 0.7 +2.1 ± 1.1 +2.7 ± 1.3	Low
Minimum temperature (°C)	1-in-20-year event	N/A	+1.2 ± 1.8 +1.5 ± 2.0 +1.5 ± 1.8	+1.6 ± 1.8 +2.2 ± 2.0 +2.4 ± 1.9	Low
Total rainfall (%)*	Annual	+3 ± 8 +3 ± 8 +4 ± 8	+7 ± 11 +7 ± 10 +7 ± 12	+7 ± 12 +12 ± 14 +11 ± 18	Moderate
Wet season rainfall (%)*	November-April	+3 ± 10 +3 ± 9 +4 ± 8	+7 ± 9 +6 ± 11 +6 ± 10	+7 ± 11 +11 ± 14 +11 ± 16	Moderate
Dry season rainfall (%)*	May-October	+3 ± 10 +4 ± 11 +5 ± 13	+7 ± 16 +7 ± 16 +8 ± 19	+8 ± 18 +12 ± 23 +12 ± 26	Moderate
Sea-surface temperature (°C)	Annual	+0.6 ± 0.4 +0.7 ± 0.3 +0.7 ± 0.4	+1.0 ± 0.3 +1.3 ± 0.4 +1.3 ± 0.5	+1.3 ± 0.5 +2.1 ± 0.6 +2.5 ± 0.6	High
Aragonite saturation state (Ωar)	Annual maximum	+3.6 ± 0.1 +3.5 ± 0.2 +3.5 ± 0.2	+3.3 ± 0.1 +3.2 ± 0.2 +3.2 ± 0.1	+3.2 ± 0.2 +2.8 ± 0.2 +2.6 ± 0.2	Moderate
Mean sea level (cm)	Annual	+9 (4–14) +9 (5–14) +9 (4–14)	+17 (9–25) +19 (10–29) +19 (9–28)	+31 (16–45) +37 (19–56) +39 (19–58)	Moderate

*The MIROC3.2(medres) and MIROC3.2(hires) models were eliminated in calculating the rainfall projections, due to their inability to accurately simulate present-day activity of the South Pacific Convergence Zone and/or the West Pacific Monsoon (Volume 1, Section 5.5.1).

Eton Beach, West Efate

Chapter 16
Vanuatu

The contributions of Salesa Kaniaha and Philip Malsale from the Vanuatu Meteorology and Geo-hazard Department are gratefully acknowledged

Introduction

This chapter provides a brief description of Vanuatu, its past and present climate as well as projections for the future. The climate observation network and the availability of atmospheric and oceanic data records are outlined. The annual mean climate, seasonal cycles and the influences of large-scale climate features such as the South Pacific Convergence Zone and patterns of climate variability (e.g. the El Niño-Southern Oscillation) are analysed and discussed. Observed trends and analysis of air temperature, rainfall, extreme events (including tropical cyclones), sea-surface temperature, ocean acidification, mean and extreme sea levels are presented. Projections for air and sea-surface temperature, rainfall, sea level, ocean acidification and extreme events for the 21st century are provided. These projections are presented along with confidence levels based on expert judgement by Pacific Climate Change Science Program (PCCSP) scientists. The chapter concludes with a summary table of projections (Table 16.4). Important background information including an explanation of methods and models is provided in Chapter 1. For definitions of other terms refer to the Glossary.

16.1 Climate Summary

16.1.1 Current Climate

- Temperatures in the warmest months in Vanuatu (January-February) are about 4ºC higher than those in the coolest months (July-August).
- Vanuatu has a marked wet season from November to April.
- Vanuatu's rainfall is strongly influenced by the position and strength of the South Pacific Convergence Zone. During summer the South Pacific Convergence Zone intensifies and moves further south, bringing the higher rainfall of the wet season.
- Rainfall in Vanuatu varies greatly from year-to-year due mainly to the influence of the El Niño-Southern Oscillation.
- Warming trends are evident in both annual and seasonal mean air temperatures for Bauerfield Airport (Port Vila) for the period 1950–2009.
- The sea-level rise near Vanuatu measured by satellite altimeters since 1993 is about 6 mm per year.
- Annual and seasonal rainfall trends for Port Vila and Aneityum for the period 1950–2009 are not statistically significant.
- On average Port Vila experiences 23 tropical cyclones per decade, with most occurring in January and February. The high interannual variability in tropical cyclone numbers makes it difficult to identify any long-term trends in frequency.

16.1.2 Future Climate

Over the course of the 21st century:

- Surface air temperature and sea-surface temperature are projected to continue to increase (*very high* confidence).
- Wet season rainfall is projected to increase (*moderate* confidence).
- Dry season rainfall is projected to decrease (*moderate* confidence).
- Little change is projected in annual mean rainfall (*low* confidence).
- The intensity and frequency of days of extreme heat are projected to increase (*very high* confidence).
- The intensity and frequency of days of extreme rainfall are projected to increase (*high* confidence).
- Little change is projected in the incidence of drought (*low* confidence).
- Tropical cyclone numbers are projected to decline in the south-west Pacific Ocean basin (0–40ºS, 130ºE –170ºE) (*moderate* confidence).
- Ocean acidification is projected to continue (*very high* confidence).
- Mean sea-level rise is projected to continue (*very high* confidence).

16.2 Country Description

The island archipelago of Vanuatu lies between 13°S-21°S and 166°E–171°E and includes over 80 islands. The largest island is Espiritu Santo while the island of Efate is home to the capital, Port Vila and the Vanuatu Government. Vanuatu has an Economic Exclusion Zone of 710 000 km^2 which encompasses Vanuatu's total land area of 12 190 km^2. Larger islands are characterised by rugged volcanic peaks and tropical rainforests. The highest peak, Mount Tabwemasana on Espiritu Santo, is 1877 m above mean sea level.

Vanuatu's population in 2009 was estimated at 234 023 of which around 80% live in rural areas (Vanuatu Country Profile, SOPAC, 2000; Vanuatu National Statistics Office, 2010).

Most of Vanuatu's population relies on subsistence agriculture. Cocoa, copra and coffee exports contribute to Vanuatu's economy alongside tourism, logging and fishing. Revenue from mineral extraction is relatively new to the economy and may provide significant revenue in the future (Vanuatu Country Profile, SOPAC, 2000).

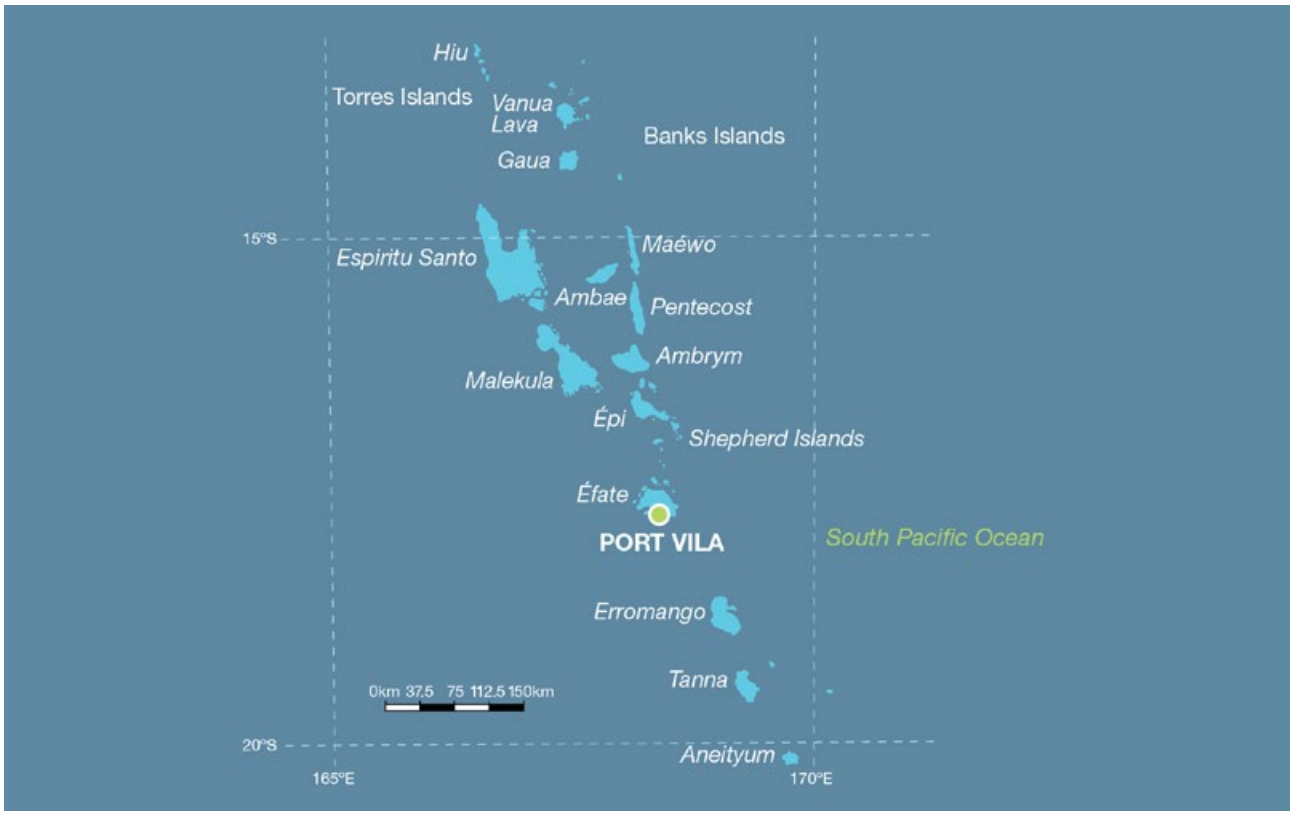

Figure 16.1: Vanuatu

16.3 Data Availability

There are currently 47 operational meteorological stations in Vanuatu. Multiple observations within a 24-hour period are taken at Sola, Pekoa, Saratamata, Lamap, Bauerfield, Whitegrass and Analguahat. At three climate stations, Lambubu, Lamap and Aneityum, and at 39 rainfall stations across the country a single observation is taken daily at 9.00 am local time. The primary climate stations are located at Port Vila and Bauerfield Airport on the island of Efate (Figure 16.1). Several stations, including Iririki (Port Vila), have rainfall data from the early 1900s. Iririki also has the earliest air temperature observations which began in the late 1940s.

Records used include a composite Iririki-Vila rainfall record, composite air temperature Iririki-Vila-Bauerfield record and single site record from Aneityum (southern Vanuatu) for the period 1950–2009. The Iririki-Vila-Bauerfield and Aneityum records are homogeneous and more than 95% complete.

Oceanographic records do not cover such a long time period. Monthly-averaged sea-level data are available from Port Vila (1993–present). A global positioning system instrument to estimate vertical land motion was deployed at Port Vila in 2002 and will provide valuable direct estimates of local vertical land motion in future years. Both satellite (from 1993) and in situ sea-level data (1950–2009; termed reconstructed sea level; Volume 1, Section 2.2.2.2) are available on a global 1° x 1° grid.

Long-term locally-monitored sea-surface temperature data are unavailable for Vanuatu, so large-scale gridded sea-surface temperature datasets have been used (HadISST, HadSST2, ERSST and Kaplan Extended SST V2; Volume 1, Table 2.3).

Climate data management training, Vanuatu Meteorology and Geo-hazard Department

16.4 Seasonal Cycles

The seasonal variations in rainfall and air temperature at both Port Vila (in the central region of Vanuatu) and Aneityum (in the south) are very similar (Figure 16.2). Being further south, mean monthly Aneityum temperatures are about 2ºC cooler than those in Port Vila. Both sites have highest temperatures in January-February, with the coolest months (July-August) about 4ºC cooler than the warmest months. The cooler winter air temperatures are due to weaker solar radiation and the influence of high pressure cells bringing cold winds from higher latitudes. Seasonal variations in sea-surface temperatures closely match those of air temperatures and have a strong influence on the air temperatures on the islands of Vanuatu.

Both sites have a marked wet season from November to April, with highest rainfall from January to March, and a dry season from May to October. The difference between seasons is slightly more marked in Port Vila as Aneityum receives more rainfall from extra-tropical influences such as cold fronts during the dry season. Vanuatu's rainfall is strongly influenced by the position and strength of the South Pacific Convergence Zone (SPCZ), which lies north of the country during the winter. During summer the SPCZ intensifies and moves further south, bringing the higher rainfall of the wet season. Low pressure systems embedded in the SPCZ often become tropical cyclones during the cyclone season. Topography also plays a role in the variations in rainfall across some islands. During the wet season, rainfall is particularly high on the windward (south-east) side of the mountain ranges of the bigger islands, and scarce during the dry season, especially on the leeward (north-west) sides.

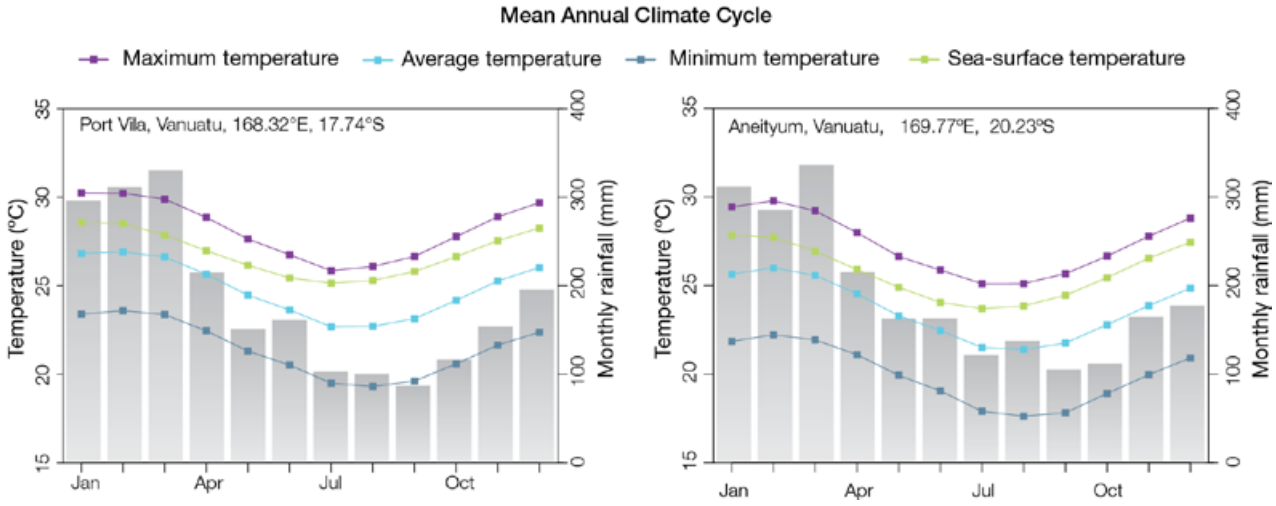

Figure 16.2: Mean annual cycle of rainfall (grey bars) and daily maximum, minimum and mean air temperatures at Port Vila (left) and Aneityum (right), and local sea-surface temperatures derived from the HadISST dataset (Volume 1, Table 2.3).

16.5 Climate Variability

Large variations in rainfall are observed in Vanuatu from year-to-year (Figure 16.4). The wettest years receive up to three times more than the driest years. Much of this variability is linked to the El Niño-Southern Oscillation (ENSO). There are significant correlations between ENSO indices and both rainfall and air temperature in Vanuatu (Tables 16.1 and 16.2). The impact of ENSO on climate in Port Vila and Aneityum are similar: El Niño events tend to bring a late start to the wet season and lower rainfall in both the wet and dry seasons, as well as cooler conditions in the dry season. Opposite impacts are usually observed during La Niña events. ENSO Modoki events (Volume1, Section 3.4.1) are as important as canonical ENSO events in Port Vila, and have much the same impacts, but are less influential further south in Aneityum. Long-term ENSO variability, seen in the Interdecadal Pacific Oscillation, appears to have a weak but significant influence on decadal rainfall variability in Port Vila during the dry season.

Table 16.1: Correlation coefficients between indices of key large-scale patterns of climate variability and minimum and maximum temperatures (Tmin and Tmax) and rainfall at Port Vila. Only correlation coefficients that are statistically significant at the 95% level are shown.

Climate feature/index		Dry season (May-October)			Wet season (November-April)		
		Tmin	Tmax	Rain	Tmin	Tmax	Rain
ENSO	Niño3.4	-0.41	-0.41	-0.45			-0.49
	Southern Oscillation Index	0.36	0.41	0.36			0.51
Interdecadal Pacific Oscillation Index				-0.28			
Southern Annular Mode Index							
ENSO Modoki Index		-0.40	-0.36	-0.26	-0.28		-0.45
Number of years of data		62	62	98	62	63	100

Table 16.2: Correlation coefficients between indices of key large-scale patterns of climate variability and minimum and maximum temperatures (Tmin and Tmax) and rainfall at Aneityum. Only correlation coefficients that are statistically significant at the 95% level are shown.

Climate feature/index		Dry season (May-October)			Wet season (November-April)		
		Tmin	Tmax	Rain	Tmin	Tmax	Rain
ENSO	Niño3.4	-0.51	-0.48	-0.43			-0.33
	Southern Oscillation Index	0.41	0.59	0.27			0.39
Interdecadal Pacific Oscillation Index							
Southern Annular Mode Index							
ENSO Modoki Index		-0.43	-0.45				
Number of years of data		59	58	61	55	53	60

16.6 Observed Trends

16.6.1 Air Temperature

Warming trends are evident in both annual and seasonal mean air temperatures at Bauerfield Airport (composite) and Aneityum for the period 1950–2009. Air temperature trends are stronger in the wet season when compared with the dry season, and minimum air temperatures trends are stronger than maximum air temperature trends at both sites (Figure 16.3 and Table 16.3).

16.6.2 Rainfall

Annual and seasonal rainfall trends for Port Vila (composite) and Aneityum for the period 1950–2009 are not statistically significant (Table 16.3 and Figure 16.4).

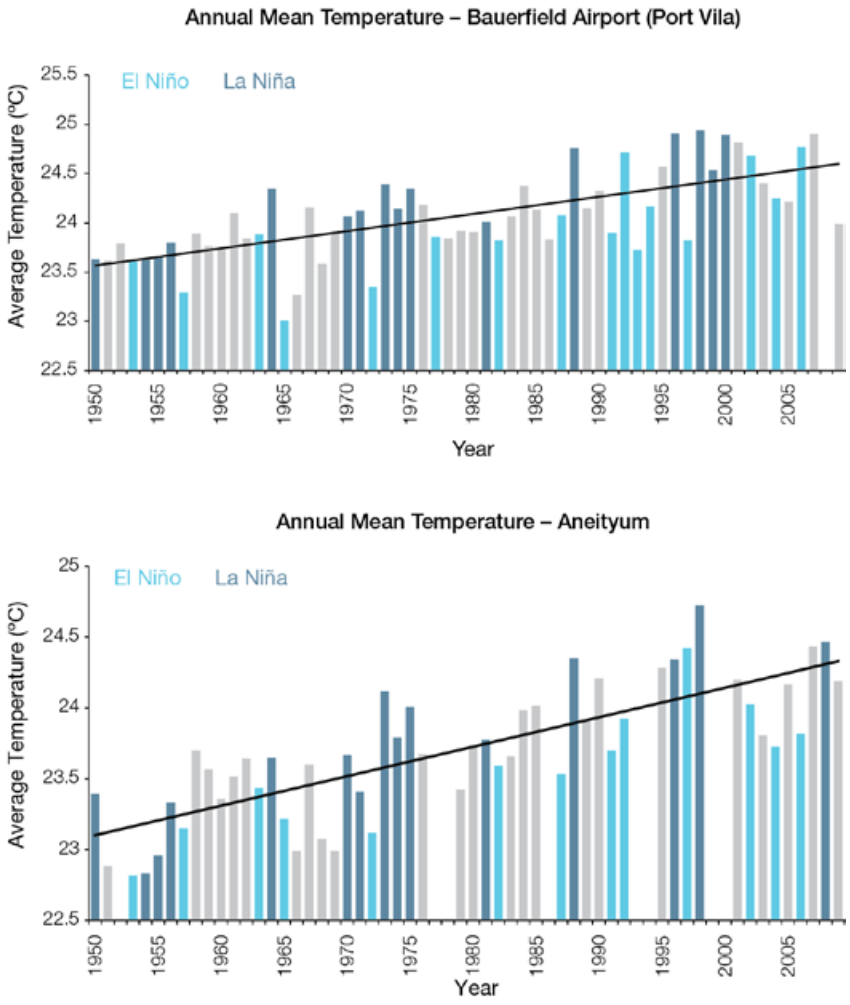

Figure 16.3: Annual mean air temperature at Bauerfield Airport (Port Vila) (top) and Aneityum (bottom). Light blue, dark blue and grey bars denote El Niño, La Niña and neutral years respectively.

Table 16.3: Annual and seasonal trends in maximum, minimum and mean air temperature (Tmax, Tmin and Tmean) and rainfall at Bauerfield Airport/Port Vila (composite) and Aneityum for the period 1950–2009. Asterisks indicate significance at the 95% level. Persistence is taken into account in the assessment of significance as in Power and Kociuba (in press). The statistical significance of the air temperature trends is not assessed.

	Bauerfield Airport Tmax (°C per 10 yrs)	Bauerfield Airport Tmin (°C per 10 yrs)	Bauerfield Airport Tmean (°C per 10 yrs)	Port Vila Rain (mm per 10 yrs)	Aneityum Tmax (°C per 10 yrs)	Aneityum Tmin (°C per 10 yrs)	Aneityum Tmean (°C per 10 yrs)	Aneityum Rain (mm per 10 yrs)
Annual	+0.17	+0.19	+0.17	-53	+0.18	+0.23	+0.21	-7
Wet season	+0.21	+0.21	+0.21	-40	+0.17	+0.25	+0.21	+4
Dry season	+0.13	+0.19	+0.15	-10	+0.16	+0.22	+0.19	-15

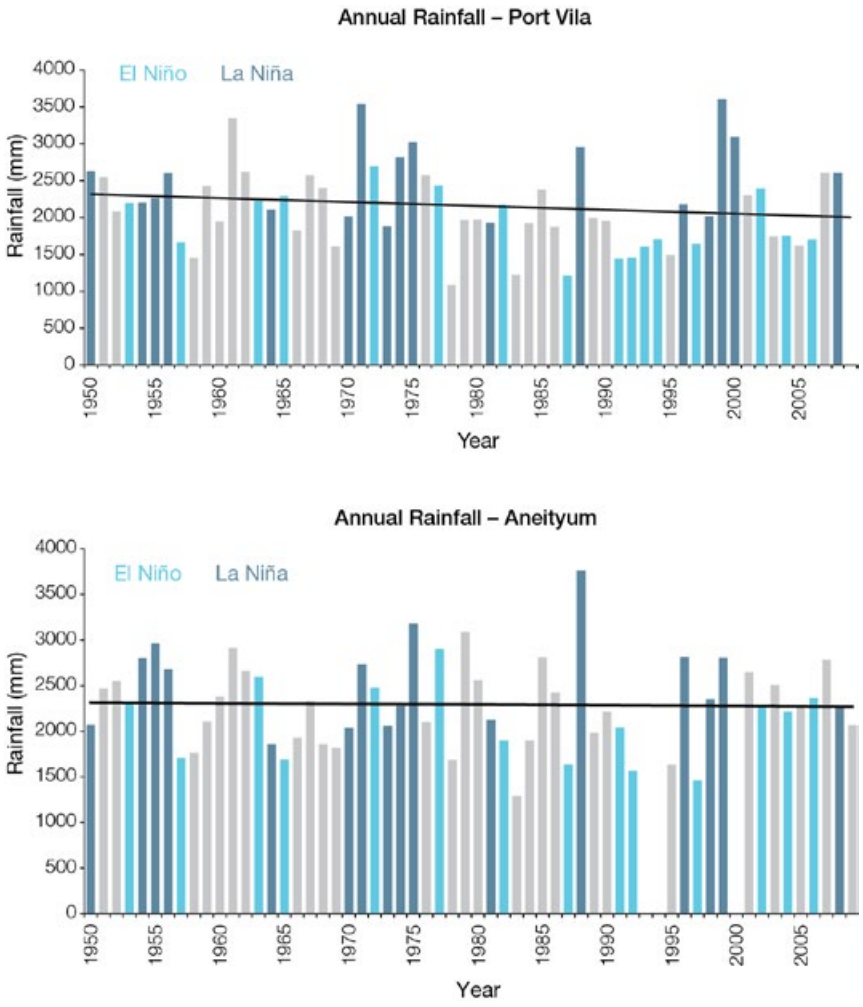

Figure 16.4: Annual rainfall at Port Vila (top) and Aneityum (bottom). Light blue, dark blue and grey bars denote El Niño, La Niña and neutral years respectively.

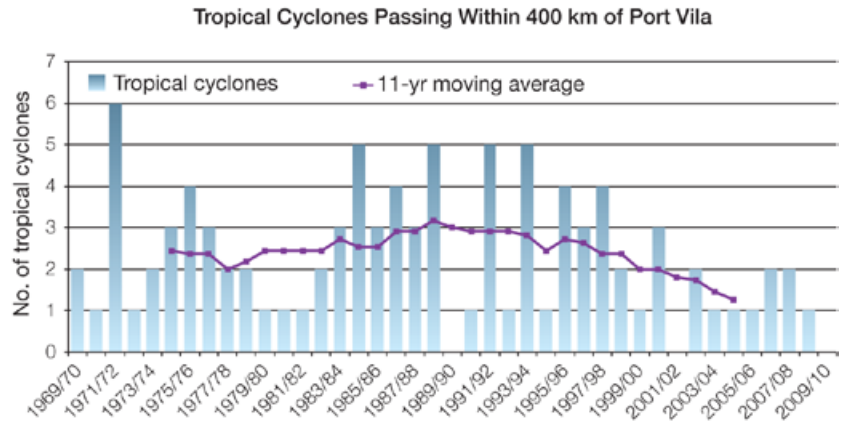

Figure 16.5: Tropical cyclones passing within 400 km of Port Vila per season. The 11-year moving average is in purple.

16.6.3 Extreme Events

The tropical cyclone season in the Vanuatu region is between November and April. Occurrences outside this period are rare. The tropical cyclone archive for the Southern Hemisphere indicates that between the 1969/70 and 2009/10 seasons, the centre of 94 tropical cyclones passed within approximately 400 km of Port Vila making this site the most impacted capital city in the PCCSP Partner Countries (Nuku'alofa, Tonga follows with 71 cyclones over the same period). This represents an average of 23 cyclones per decade. Tropical cyclone occurrence in El Niño, La Niña and neutral years are fairly similar (averages of 23, 25 and 22 cyclones per decade respectively). The interannual variability in the number of tropical cyclones in the vicinity of Port Vila is large, ranging from zero in some seasons to six in the 1971/72 season (Figure 16.5). This high variability makes it difficult to identify any long-term trends in frequency.

Impacts of climate variability and change are evident on most of Vanuatu's islands. ENSO-related drought and flooding are prevalent and continue to impact the socio-economic livelihood of the people of Vanuatu. For example, a flood event during the 2011 La Niña event washed through several villages on Emae Island, completely inundating agricultural land in Middle Bush, Tanna. Such occurrences are rare but the impacts can be devastating.

16.6.4 Sea-Surface Temperature

Historical changes around Vanuatu are consistent with the broad-scale sea-surface temperature changes of the PCCSP region. Water temperatures remained relatively constant from the 1950s to the late 1980s. This was followed by a period of more rapid warming (approximately 0.09°C per decade for 1970 to present). Figure 16.8 shows the 1950–2000 sea-surface temperature changes (relative to a reference year of 1990) from three different large-scale sea surface temperature datasets (HadSST2, ERSST and Kaplan Extended SST V2; Volume 1, Table 2.3). At these regional scales, natural variability may play a large role in the sea-surface temperature changes making it difficult to identify any long-term trends.

16.6.5 Ocean Acidification

Based on the large-scale distribution of coral reefs across the Pacific and the seawater chemistry, Guinotte et al. (2003) suggested that seawater aragonite saturation states above 4 were optimal for coral growth and for the development of healthy reef ecosystems, with values from 3.5 to 4 adequate for coral growth, and values between 3 and 3.5, marginal. Coral reef ecosystems were not found at seawater aragonite saturation states below 3 and these conditions were classified as extremely marginal for supporting coral growth.

In the Vanuatu region, the aragonite saturation state has declined from about 4.5 in the late 18th century to an observed value of about 3.9 ± 0.1 by 2000.

16.6.6 Sea Level

Monthly averages of the historical tide gauge, satellite (since 1993) and gridded sea-level (since 1950) data agree well after 1993 and indicate interannual variability in sea levels of about 18 cm (estimated 5–95% range) after removal of the seasonal cycle (Figure 16.10). The sea-level rise near Vanuatu measured by satellite altimeters (Figure 16.6) since 1993 is about 6 mm per year, larger than the global average of 3.2 ± 0.4 mm per year. This rise is partly linked to a pattern related to climate variability from year to year and decade to decade (Figure 16.10).

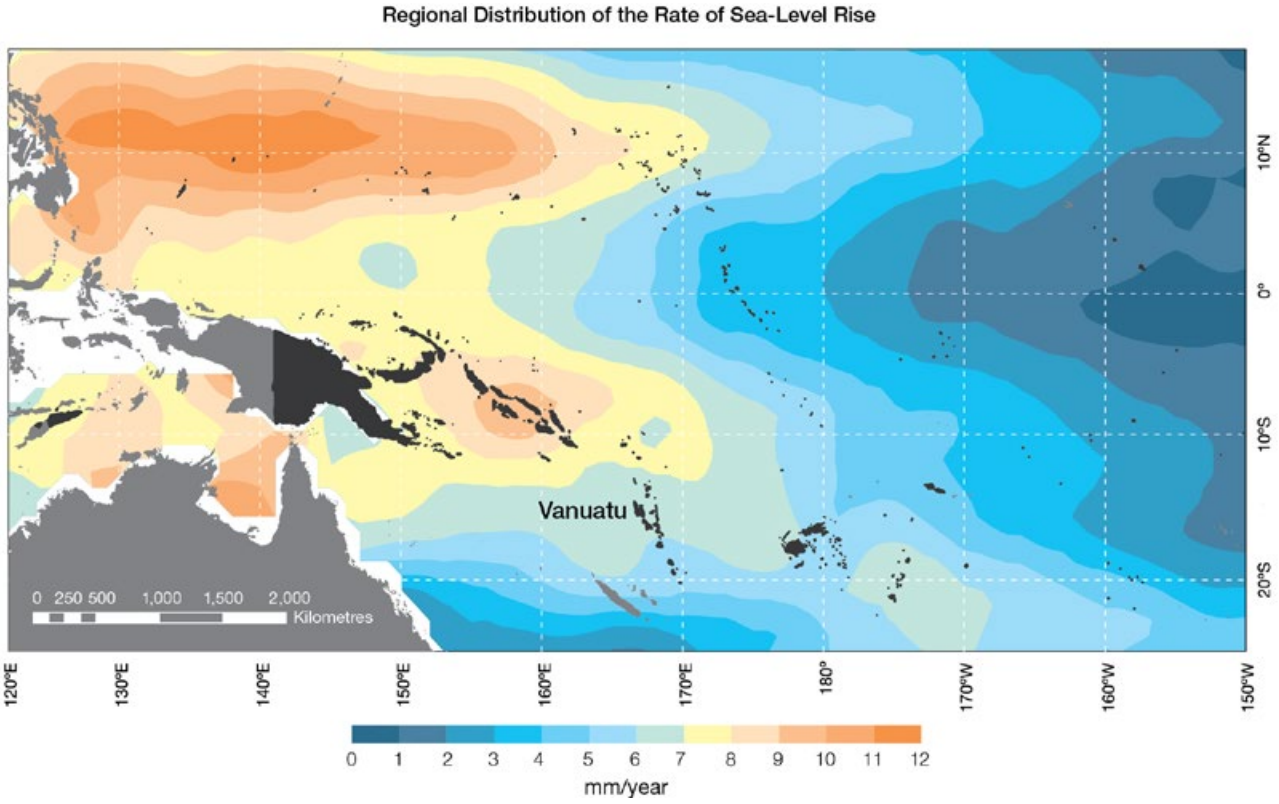

Figure 16.6: The regional distribution of the rate of sea-level rise measured by satellite altimeters from January 1993 to December 2010, with the location of Vanuatu indicated. Further detail about the regional distribution of sea-level rise is provided in Volume 1, Section 3.6.3.2.

16.6.7 Extreme Sea-Level Events

The annual climatology of the highest daily sea levels has been evaluated from hourly measurements by the tide gauge at Port Vila (Figure 16.7). High tides peak in November to January. Seasonal variations throughout the year are small. However, seasonal water levels tend to be higher during La Niña years and slightly lower during El Niño years (Volume 1, Section 3.6.3 and Figures 3.20 and 3.21). Short-term variations show evidence of a seasonal cycle, with a generally higher likehood of high water levels in December to March, roughly corresponding to the cyclone season. ENSO does not strongly affect short-term water level events. These tidal, seasonal and short-term components combine to produce a highest likelihood of extreme water levels from October through March. The top 10 water level events mostly occurred within this time frame during La Niña or ENSO-neutral conditions. Several were associated with a cyclone or tropical disturbance in the vicinity.

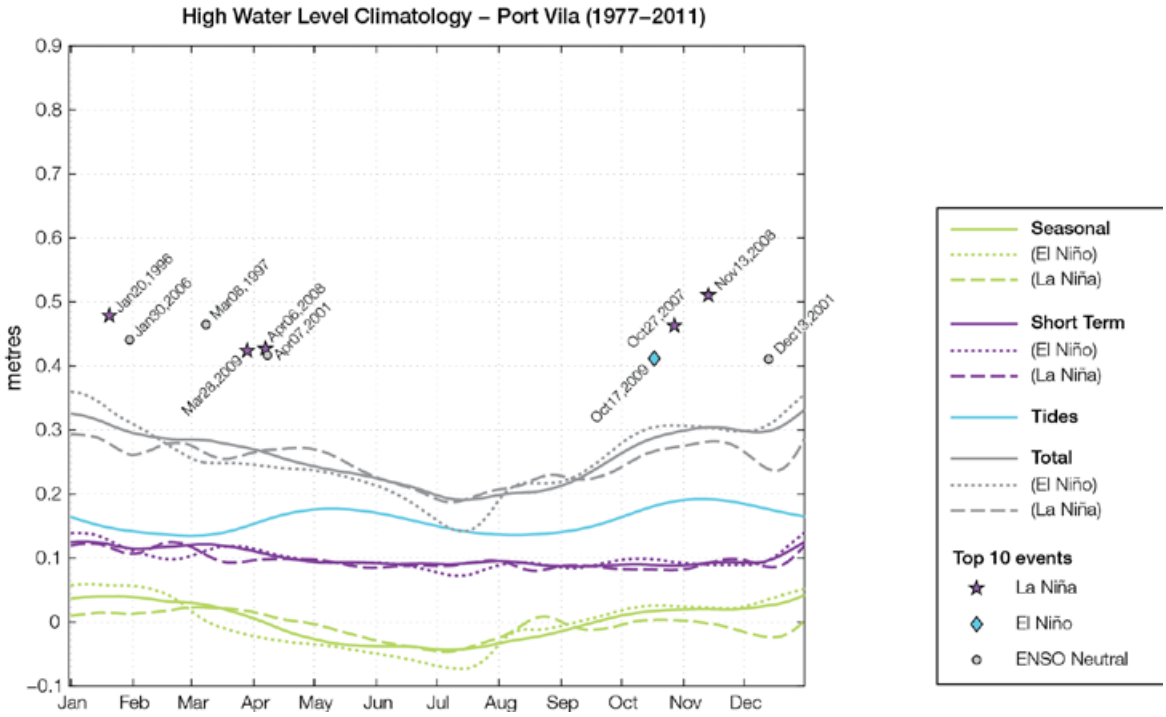

Figure 16.7: The annual cycle of high waters relative to Mean Higher High Water (MHHW) due to tides, short-term fluctuations (most likely associated with storms) and seasonal variations for Port Vila. The tides and short-term fluctuations are respectively the 95% exceedence levels of the astronomical high tides relative to MHHW and short-term sea-level fluctuations. Components computed only for El Niño and La Niña months are shown by dotted and dashed lines, and grey lines are the sum of the tide, short-term and seasonal components. The 10 highest sea-level events in the record relative to MHHW are shown and coded to indicate the phase of ENSO at the time of the extreme event.

16.7 Climate Projections

Climate projections have been derived from up to 18 global climate models from the CMIP3 database, for up to three emissions scenarios (B1 (low), A1B (medium) and A2 (high)) and three 20-year periods (centred on 2030, 2055 and 2090, relative to 1990). These models were selected based on their ability to reproduce important features of the current climate (Volume 1, Section 5.2.3), so projections arising from each of the models are plausible representations of the future climate. This means there is not one single projected future for Vanuatu, but rather a range of possible futures. The full range of these futures is discussed in the following sections.

These projections do not represent a value specific to any actual location, such as a town or city in Vanuatu. Instead, they refer to an average change over the broad geographic region encompassing the islands of Vanuatu and the surrounding ocean (Figure 1.1 shows the regional boundaries). Section 1.7 provides important information about interpreting climate model projections.

16.7.1 Temperature

Surface air temperature and sea-surface temperature are projected to continue to increase over the course of the 21st century. There is *very high* confidence in this direction of change because:

- Warming is physically consistent with rising greenhouse gas concentrations.
- All CMIP3 models agree on this direction of change.

The majority of CMIP3 models simulate a slight increase (<1°C) in annual and seasonal mean temperature by 2030, however by 2090 under the A2 (high) emissions scenario temperature increases of greater than 2.5°C are simulated by almost all models (Table 16.4). Given the close relationship between surface air temperature and sea-surface temperature, a similar (or slightly weaker) rate of warming is projected for the surface ocean (Figure 16.8). There is *high* confidence in this range and distribution of possible futures because:

- There is generally close agreement between modelled and observed temperature trends over the past 50 years in the vicinity of Vanuatu, although observational records are limited (Figure 16.8).

Interannual variability in surface air temperature and sea-surface temperature over Vanuatu is strongly influenced by ENSO in the current climate (Section 16.5). As there is no consistency in projections of future ENSO activity (Volume 1, Section 6.4.1) it is not possible to determine whether interannual variability in temperature will change in the future. However, ENSO is expected to continue to be an important source of variability for the region.

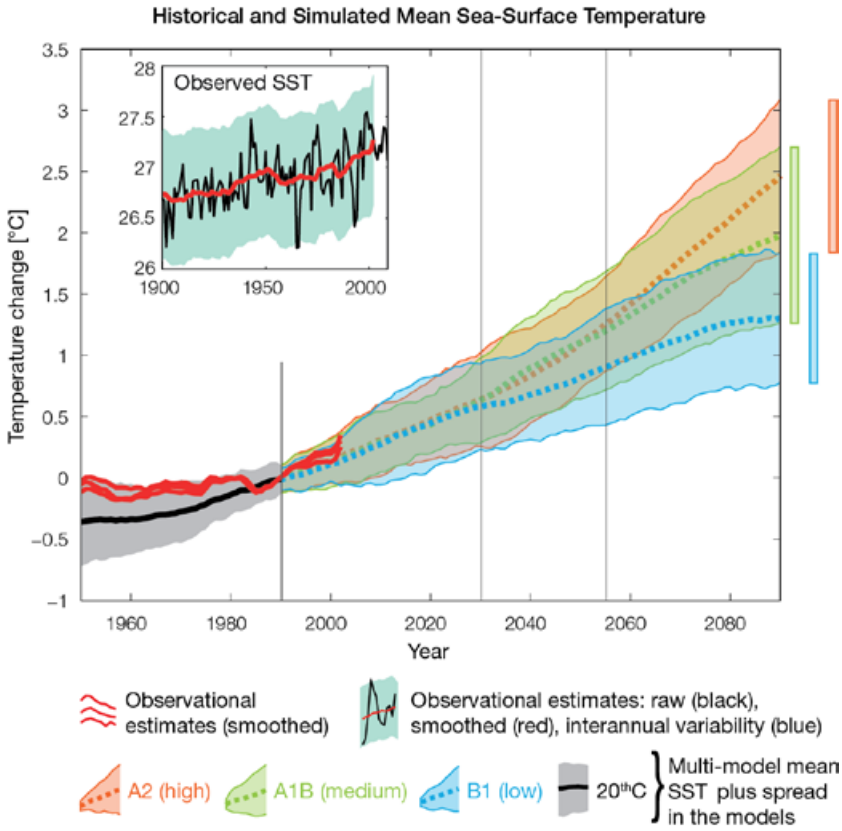

Figure 16.8: Historical climate (from 1950 onwards) and simulated historical and future climate for annual mean sea-surface temperature (SST) in the region surrounding Vanuatu, for the CMIP3 models. Shading represents approximately 95% of the range of model projections (twice the inter-model standard deviation), while the solid lines represent the smoothed (20-year running average) multi-model mean temperature. Projections are calculated relative to the 1980–1999 period (which is why there is a decline in the inter-model standard deviation around 1990). Observational estimates in the main figure (red lines) are derived from the HadSST2, ERSST and Kaplan Extended SST V2 datasets (Volume 1, Section 2.2.2). Annual average (black) and 20-year running average (red) HadSST2 data is also shown inset.

16.7.2 Rainfall

Wet Season (November-April)

Wet season rainfall is projected to increase over the course of the 21st century. There is *moderate* confidence in this direction of change because:

- An increase in wet season rainfall is consistent with the projected likely increase in the intensity of the South Pacific Convergence Zone (SPCZ), which lies over Vanuatu in this season (Volume 1, Section 6.4.5).
- The majority of CMIP3 models agree on this direction of change by 2090.

The majority of CMIP3 models simulate little change (-5% to 5%) in wet season rainfall by 2030, however by 2090 under the A2 (high) emissions scenario the majority simulate an increase (>5%), with the remainder simulating little change (Table 16.4). There is *moderate* confidence in this range and distribution of possible futures because:

- In simulations of the current climate, the CMIP3 models generally locate the SPCZ in the correct location relative to Vanuatu in the wet season (Brown et al., 2011).
- The CMIP3 models are unable to resolve many of the physical processes involved in producing rainfall. As a consequence, they do not simulate rainfall as well as other variables such as temperature (Volume 1, Chapter 5).

Dry Season (May-October)

Dry season rainfall is projected to decrease over the course of the 21st century. There is *moderate* confidence in this direction of change because:

- Approximately half of the CMIP3 models agree on this direction of change by 2090.

The majority of CMIP3 models simulate little change (-5% to 5%) in dry season rainfall by 2030, however by 2090 they tend to be approximately equally divided between a decrease (<-5%) and little change, with only a few models simulating an increase (>5%) (Table 16.4). There is *low* confidence in this range and distribution of possible futures because:

- In simulations of the current climate, some CMIP3 models have an SPCZ that extends too far east during the dry season, with too much rainfall over Vanuatu (Brown et al., 2011).
- The CMIP3 models are unable to resolve many of the physical processes involved in producing rainfall.

Annual

Total annual rainfall is projected to increase over the course of the 21st century. There is *low* confidence in this direction of change because:

- Projections of annual mean rainfall tend to be equally divided between an increase (>5%) and little change (-5% to 5%) by 2090, with only a few models simulating a decrease (<-5%).
- There is only moderate and low confidence in the range and distribution of wet and dry season rainfall projections respectively, as discussed above.

Interannual variability in rainfall over Vanuatu is strongly influenced by ENSO in the current climate, via the movement of the SPCZ (Volume 1, Section 5.5). As there is no consistency in projections of future ENSO activity (Volume 1, Section 6.4.1), it is not possible to determine whether interannual variability in rainfall will change in the future.

16.7.3 Extremes

Temperature

The intensity and frequency of days of extreme heat are projected to increase over the course of the 21st century. There is *very high* confidence in this direction of change because:

- An increase in the intensity and frequency of days of extreme heat is physically consistent with rising greenhouse gas concentrations.
- All CMIP3 models agree on the direction of change for both intensity and frequency.

The majority of CMIP3 models simulate an increase of approximately 1°C in the temperature experienced on the 1-in-20-year hot day by 2055 under the B1 (low) emissions scenario, with an increase of over 2.5°C simulated by the majority of models by 2090 under the A2 (high) emissions scenario (Table 16.4). There is *low* confidence in this range and distribution of possible futures because:

- In simulations of the current climate, the CMIP3 models tend to underestimate the intensity and frequency of days of extreme heat (Volume 1, Section 5.2.4).
- Smaller increases in the frequency of days of extreme heat are projected by the CCAM 60 km simulations.

Rainfall

The intensity and frequency of days of extreme rainfall are projected to increase over the course of the 21st century. There is *high* confidence in this direction of change because:

- An increase in the frequency and intensity of extreme rainfall is consistent with larger-scale projections, based on the physical argument that the atmosphere is able to hold more water vapour in a warmer climate (Allen and Ingram, 2002; IPCC, 2007). It is also consistent with the projected likely increase in the intensity of the SPCZ (Volume 1, Section 6.4.5).

- Almost all of the CMIP3 models agree on this direction of change for both intensity and frequency.

The majority of CMIP3 models simulate an increase of at least 15 mm in the amount of rain received on the 1-in-20-year wet day by 2055 under the B1 (low) emissions scenario, with an increase of at least 25 mm simulated by 2090 under the A2 (high) emissions scenario. The majority of models project that the current 1-in-20-year extreme rainfall event will occur, on average, three to four times per 20-year period by 2055 under the B1 (low) emissions scenario and four times per 20-year period by 2090 under the A2 (high) emissions scenario. There is *low* confidence in this range and distribution of possible futures because:

- In simulations of the current climate, the CMIP3 models tend to underestimate the intensity and frequency of extreme rainfall (Volume 1, Section 5.2.4).
- The CMIP3 models are unable to resolve many of the physical processes involved in producing extreme rainfall.

Drought

Little change is projected in the incidence of drought over the course of the 21st century. There is *low* confidence in this direction of change because:

- There is only low confidence in the range of dry season rainfall projections (Section 16.7.2), which directly influences projections of future drought conditions.

The majority of CMIP3 models project that the frequency of mild drought will remain approximately stable from 2030 throughout the 21st century at seven to eight times every 20 years, under the B1 (low) and A1B (medium) emissions scenarios. For the A2 (high) emissions scenario, a small decline from eight to nine times every 20 years in 2030 to seven to eight times by 2090 is projected. The frequency of moderate and severe drought is projected to remain approximately stable, at once to twice and once every 20 years, respectively.

Tropical Cyclones

Tropical cyclone numbers are projected to decline in the south-west Pacific Ocean basin (0–40ºS, 130ºE–170ºE) over the course of the 21st century. There is *moderate* confidence in this direction of change because:

- Many studies suggest a decline in tropical cyclone frequency globally (Knutson et al., 2010).
- Tropical cyclone numbers decline in the south-west Pacific Ocean in the majority assessment techniques.

Based on the direct detection methodologies (Curvature Vorticity Parameter (CVP) and the CSIRO Direct Detection Scheme (CDD) described in Volume 1, Section 4.8.2), 55% of projections show no change or a decrease in tropical cyclone formation when applied to the CMIP3 climate models for which suitable output is available. When these techniques are applied to CCAM, 100% of projections show a decrease in tropical cyclone formation. In addition, the Genesis Potential Index (GPI) empirical technique suggests that conditions for tropical cyclone formation will become less favourable in the south-west Pacific Ocean basin, for the majority (80%) of analysed CMIP3 models. There is *moderate* confidence in this range and distribution of possible futures because in simulations of the current climate, the CVP, CDD and GPI methods capture the frequency of tropical cyclone activity reasonably well (Volume 1, Section 5.4).

Despite this projected reduction in total cyclone numbers, five of the six CCAM 60 km simulations show an increase in the proportion of the most severe cyclones. This increase in wind hazard coincides with a poleward shift in the latitude at which tropical cyclones are most intense. Most models also indicate a reduction in tropical cyclone wind hazard north of 20ºS latitude.

16.7.4 Ocean Acidification

The acidification of the ocean will continue to increase over the course of the 21st century. There is *very high* confidence in this projection as the rate of ocean acidification is driven primarily by the increasing oceanic uptake of carbon dioxide, in response to rising atmospheric carbon dioxide concentrations.

Projections from all analysed CMIP3 models indicate that the annual maximum aragonite saturation state will reach values below 3.5 by about 2035 and continue to decline thereafter (Figure 16.9; Table 16.4). There is *moderate* confidence in this range and distribution of possible futures because the projections are based on climate models without an explicit representation of the carbon cycle and with relatively low resolution and known regional biases.

The impact of acidification change on the health of reef ecosystems is likely to be compounded by other stressors including coral bleaching, storm damage and fishing pressure.

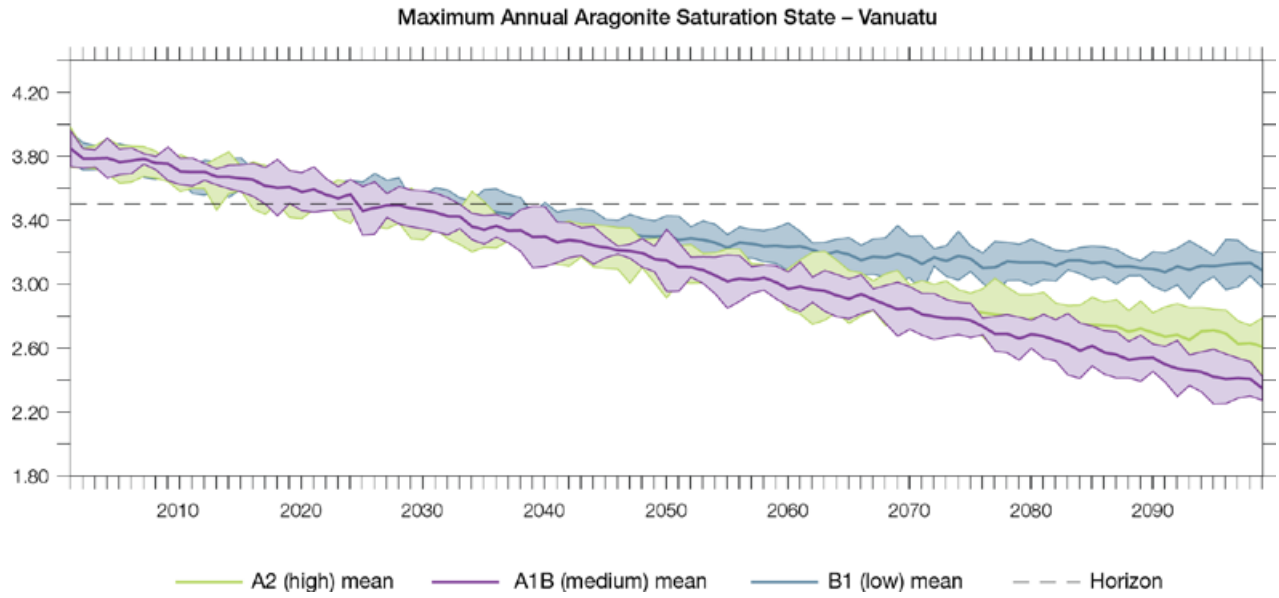

Figure 16.9: Multi-model projections, and their associated uncertainty (shaded area represents two standard deviations), projections of the maximum annual aragonite saturation state in the sea surface waters of the Vanuatu region under the different emissions scenarios. The dashed black line represents an aragonite saturation state of 3.5.

16.7.5 Sea Level

Mean sea level is projected to continue to rise over the course of the 21st century. There is *very high* confidence in this direction of change because:

- Sea-level rise is a physically consistent response to increasing ocean and atmospheric temperatures, due to thermal expansion of the water and the melting of glaciers and ice caps.
- Projections arising from all CMIP3 models agree on this direction of change.

The CMIP3 models simulate a rise of between approximately 5–15 cm by 2030, with increases of 20–60 cm indicated by 2090 under the higher emissions scenarios (i.e. A2 (high) and A1B (medium); Figure 16.10; Table 16.4). There is *moderate* confidence in this range and distribution of possible futures because:

- There is significant uncertainty surrounding ice-sheet contributions to sea-level rise and a rise larger than projected above cannot be excluded (Meehl et al., 2007b). However, understanding of the processes is currently too limited to provide a best estimate or an upper bound (IPCC, 2007).
- Globally, since the early 1990s, sea level has been rising near the upper end of the above projections. During the 21st century, some studies (using semi-empirical models) project faster rates of sea-level rise.

Interannual variability of sea level will lead to periods of lower and higher regional sea levels. In the past, this interannual variability has been about 18 cm (5–95% range, after removal of the seasonal signal; dashed lines in Figure 16.10 (a)) and it is likely that a similar range will continue through the 21st century. In addition, winds and waves associated with weather phenomena will continue to lead to extreme sea-level events.

In addition to the regional variations in sea level associated with ocean and mass changes, there are ongoing changes in relative sea level associated with changes in surface loading over the last glacial cycle (glacial isostatic adjustment) and local tectonic motions. The glacial isostatic motions are relatively small for the PCCSP region.

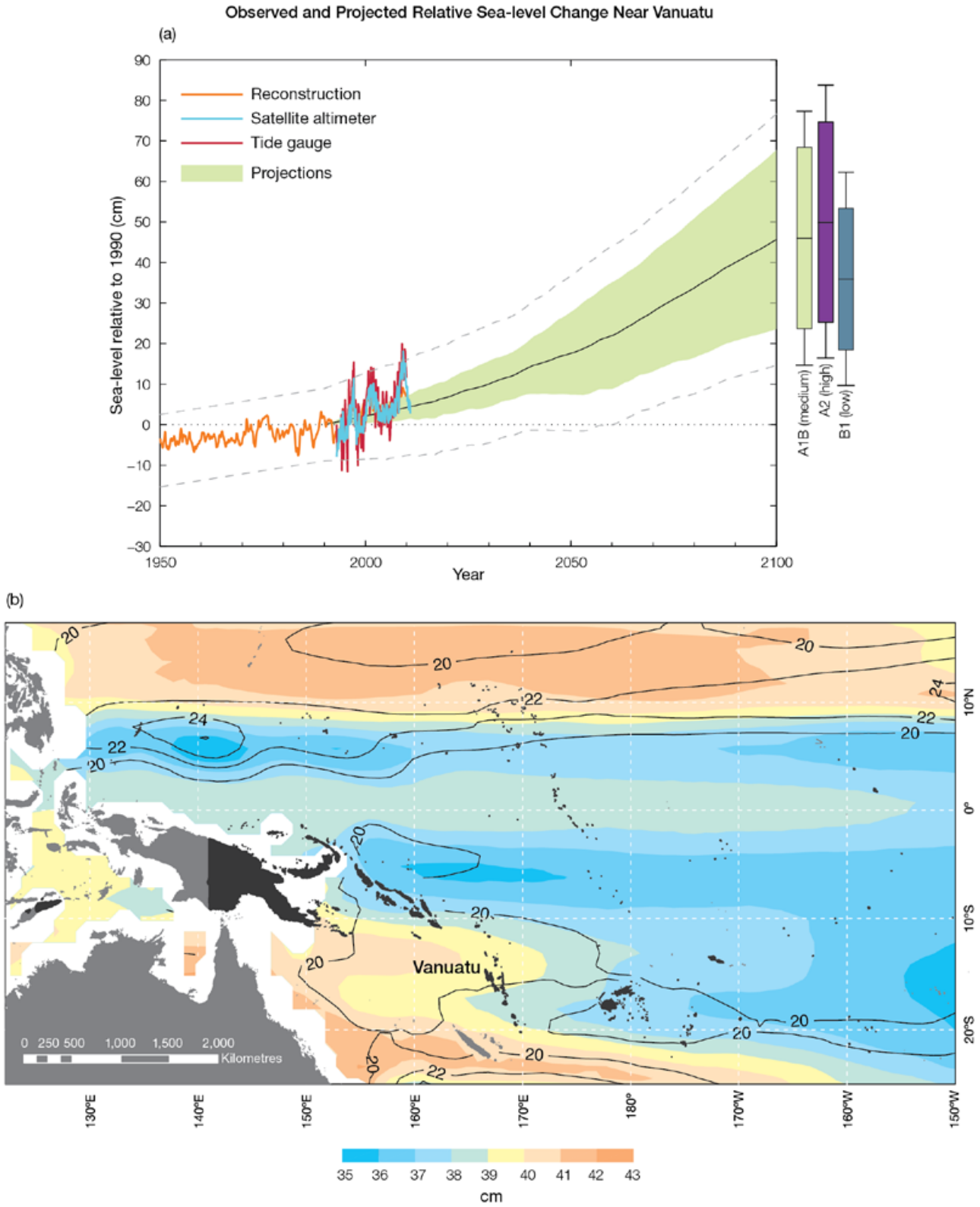

Figure 16.10: Observed and projected relative sea-level change near Vanuatu. (a) The observed in situ relative sea-level records are indicated in red, with the satellite record (since 1993) in light blue. The gridded sea level at Vanuatu (since 1950, from Church and White (in press)) is shown in orange. The projections for the A1B (medium) emissions scenario (5–95% uncertainty range) are shown by the green shaded region from 1990–2100. The range of projections for the B1 (low), A1B (medium) and A2 (high) emissions scenarios are also shown by the bars on the right. The dashed lines are an estimate of interannual variability in sea level (5–95% range about the long-term trends) and indicate that individual monthly averages of sea level can be above or below longer-term averages. (b) The projections (in cm) for the A1B (medium) emissions scenario in the Vanuatu region for the average over 2081–2100 relative to 1981–2000 are indicated by the shading, with the estimated uncertainty in the projections indicated by the contours (in cm).

16.7.6 Projections Summary

The projections presented in Section 16.7 are summarised in Table 16.4. For detailed information regarding the various uncertainties associated with the table values, refer to the preceding text in Sections 16.7 and 1.7, in addition to Chapters 5 and 6 in Volume 1. When interpreting the differences between projections for the B1 (low), A1B (medium) and A2 (high) emissions scenarios, it is also important to consider the emissions pathways associated with each scenario (Volume 1, Figure 4.1) and the fact that a slightly different subset of models was available for each (Volume 1, Appendix 1).

Table 16.4: Projected change in the annual and seasonal-mean climate for Vanuatu, under the B1 (low; blue), A1B (medium; green) and A2 (high; purple) emissions scenarios. Projections are given for three 20-year periods centred on 2030 (2020–2039), 2055 (2046–2065) and 2090 (2080–2099), relative to 1990 (1980–1999). Values represent the multi-model mean change ± twice the inter-model standard deviation (representing approximately 95% of the range of model projections), except for sea level where the estimated mean change and the 5–95% range are given (as they are derived directly from the Intergovernmental Panel on Climate Change Fourth Assessment Report values). The confidence (Section 1.7.2) associated with the range and distribution of the projections is also given (indicated by the standard deviation and multi-model mean, respectively). See Volume 1, Appendix 1 for a complete listing of CMIP3 models used to derive these projections.

Variable	Season	2030	2055	2090	Confidence
Surface air temperature (°C)	Annual	+0.6 ± 0.4 +0.7 ± 0.4 +0.7 ± 0.3	+1.0 ± 0.5 +1.4 ± 0.6 +1.4 ± 0.3	+1.4 ± 0.7 +2.2 ± 0.9 +2.6 ± 0.6	High
Maximum temperature (°C)	1-in-20-year event	N/A	+1.0 ± 0.6 +1.5 ± 0.7 +1.5 ± 0.5	+1.3 ± 0.5 +2.1 ± 0.9 +2.6 ± 1.2	Low
Minimum temperature (°C)	1-in-20-year event	N/A	+1.2 ± 1.8 +1.5 ± 1.9 +1.5 ± 1.7	+1.5 ± 1.8 +2.0 ± 1.9 +2.3 ± 1.8	Low
Total rainfall (%)*	Annual	+3 ± 9 +2 ± 11 +1 ± 17	+1 ± 12 +3 ± 15 +3 ± 16	+1 ± 16 +3 ± 19 +8 ± 20	Low
Wet season rainfall (%)*	November-April	+5 ± 8 +3 ± 11 +3 ± 17	+3 ± 12 +5 ± 15 +5 ± 15	+3 ± 15 +7 ± 19 +11 ± 18	Moderate
Dry season rainfall (%)*	May-October	0 ± 16 +1 ± 20 -2 ± 22	-4 ± 20 -1 ± 24 -1 ± 27	-2 ± 23 -4 ± 25 +2 ± 31	Low
Sea-surface temperature (°C)	Annual	+0.6 ± 0.4 +0.6 ± 0.3 + 0.6 ± 0.4	+0.9 ± 0.5 +1.2 ± 0.5 +1.3 ± 0.4	+1.3 ± 0.5 +2.0 ± 0.7 +2.5 ± 0.6	High
Aragonite saturation state (Ωar)	Annual maximum	+3.5 ± 0.1 +3.4 ± 0.1 +3.4 ± 0.1	+3.2 ± 0.1 +3.0 ± 0.1 +3.0 ± 0.1	+3.1 ± 0.1 +2.6 ± 0.1 +2.5 ± 0.1	Moderate
Mean sea level (cm)	Annual	+10 (5–16) +10 (5–16) +10 (3–17)	+19 (10–27) +20 (8–31) +19 (7–31)	+32 (17–47) +40 (20–59) +42 (21–63)	Moderate

*The MIROC3.2(medres) and MIROC3.2(hires) models were eliminated in calculating the rainfall projections, due to their inability to accurately simulate present-day activity of the South Pacific Convergence Zone (Volume 1, Section 5.5.1).

Funafuti lagoon, Tuvalu

References

Published References

Allen, M.R. and Ingram, W.J., (2002), Constraints on future changes in climate and the hydrologic cycle. *Nature*, 419, 224-232.

Brown, J.R., Power, S.B., Delage, F.P., Colman, R.A., Moise, A.F., and Murphy, B.F., (2011), Evaluation of the South Pacific Convergence Zone in IPCC AR4 Climate Model Simulations of the Twentieth Century: *Journal of Climate*, v. 24, p. 1565-1582.

Callaghan, J. and Power, S.B., (2010), Variability and decline in the number of severe tropical cyclones making land-fall over eastern Australia since the late nineteenth century: *Climate Dynamics*, v. 37, issue 3-4, p. 647-662.

Church, J. A. and White, N.J., (in press), Sea-level rise from the late 19th to the early 21st Century. *Surveys in Geophysics*, doi:10.1007/s10712-011-9119-1.

Church, J.A., Gregory, J.M., White, N.J., Platten, S.M., and Mitrovica, J.X., (2011), Understanding and Projecting Sea Level Change: *Oceanography*, v. 24, p. 130-143.

Coles, S., Bawa, J., Trenner, L., and Dorazio, P., (2001), An introduction to statistical modeling of extreme values: London, Springer, ix, 208 pp.

Folland, C.K., Parker, D.E., Colman, A.W. and Washington, R., (1999), Large scale modes of ocean temperature since the late nineteenth century. In: Navarra A., (ed), Beyond El Nino: decadal and inter-decadal climate variability. Springer, Berlin, Heidelberg, New York, p. 73-102.

Guinotte, J.M., Buddemeier, R.W., and Kleypas, J.A., (2003), Future coral reef habitat marginality: temporal and spatial effects of climate change in the Pacific basin: *Coral Reefs*, v. 22, p. 551-558.

IPCC, (2000): *Emissions Scenarios. Special Report of the Intergovernmental Panel on Climate Change*. Nakicenovic, N. and R. Swart, (eds). Cambridge University Press, UK. 570 pp.

IPCC, (2007): *Climate Change 2007: The Physical Science Basis. Contribution of Working Group 1 to the Fourth Assessment Report of the Intergovernmental Panel in Climate Change* [Solomon, S, D. Qin, M. Manning, Z. Chen, M. Marquis, K.B. Ayert, M. Tignor and H.L. Miller (eds.)]. Cambridge University Press, Cambridge, United Kingdom and New York, NY, USA, 996 pp.

Irving D.B., Perkins S.E., Brown J.R., Sen Gupta A., Moise A.F., Murphy B.F., Muir L.C., Colman R.A., Power S.B., Delage F.P., Brown J.N., (in press), Evaluating global climate models for climate change projections in the Pacific island region, *Climate Research*, doi: 10.3354/cr01028.

Kharin, V.V., Zwiers, F.W., and Zhang, X.B., (2005), Intercomparison of near-surface temperature and precipitation extremes in AMIP-2 simulations, reanalyses, and observations: *Journal of Climate*, v. 18, p. 5201-5223.

Kharin, V.V., Zwiers, F.W., Zhang, X.B., and Hegerl, G.C., (2007), Changes in temperature and precipitation extremes in the IPCC ensemble of global coupled model simulations: *Journal of Climate*, v. 20, p. 1419-1444.

Kirono D., (2010), Climate change in Timor-Leste – a brief overview on future climate projections. A report prepared for the Department of Climate Change and Energy Efficiency (DCCEE), Climate Adaptation Flagship, CSIRO, Australia.

Knutson, T.R., McBride, J.L., Chan, J., Emanuel, K., Holland, G., Landsea, C., Held, I., Kossin, J.P., Srivastava, A.K., and Sugi, M., (2010), Tropical cyclones and climate change: *Nature Geoscience*, v. 3, p. 157-163.

Kuffner, I.B., Andersson, A.J., Jokiel, P.L., Rodgers, K.S., and Mackenzie, F.T., (2008), Decreased abundance of crustose coralline algae due to ocean acidification: *Nature Geoscience*, v. 1, p. 114-117.

Kuleshov, Y., Fawcett, R., Qi, L., Trewin, B., Jones, D., McBride, J., and Ramsay, H., (2010), Trends in tropical cyclones in the South Indian Ocean and the South Pacific Ocean: *Journal of Geophysical Research-Atmospheres,* v. 115.

Lloyd-Hughes, B., and Saunders, M.A., (2002), A drought climatology for Europe: International *Journal of Climatology*, v. 22, p. 1571-1592.

Marshall, G.J., (2003), Trends in the southern annular mode from observations and reanalyses: *Journal of Climate*, v. 16, p. 4134-4143.

McGregor, J.L., and Dix, M.R., (2008), An updated description of the Conformal-Cubic atmospheric model: *High Resolution Numerical Modelling of the Atmosphere and Ocean*, p. 51-75.

McInnes, K.L., O'Grady, J.G., Walsh, K.J.E. and Colberg, F. (2011), Progress towards quantifying storm surge risk in Fiji due to climate variability and change: *Journal of Coastal Research*, SI64. 1121-1124.

Meehl, G.A., Covey, C., Delworth, T., Latif, M., McAvaney, B., Mitchell, J.F.B., Stouffer, R.J., and Taylor, K.E., (2007a), The WCRP CMIP3 multimodel dataset - A new era in climate change research: *Bulletin of the American Meteorological Society*, v. 88, p. 1383-1394.

Meehl, G.A., T.F. Stocker, W.D. Collins, P. Friedlingstein, A.T. Gaye, J.M. Gregory, A. Kitoh, R. Knutti, J.M. Murphy, A. Noda, S.C.B. Raper, I.G. Watterson, A.J. Weaver and Z.-C. Zhao, (2007b): Global Climate Projections. In: *Climate Change 2007: The Physical Science Basis*. *Contribution of Working Group I to the Fourth Assessment Report of the Intergovernmental Panel on Climate Change* [Solomon, S., D. Qin, M. Manning, Z. Chen, M. Marquis, K.B. Averyt, M. Tignor and H.L. Miller (eds.)]. Cambridge University Press, Cambridge, United Kingdom and New York, NY, USA.

Merrifield, M.A., Firing, Y.L. and Marra, J.J., (2007): Annual climatologies of extreme water levels. In: Aha Hulikoa: Extreme Events. Proceedings of the Hawaiian Winter Workshop, University of Hawaii at Manoa, January 23-26, 2007. SOEST, University of Hawaii, p. 27-32.

Parker, D., Folland, C., Scaife, A., Knight, J., Colman, A., Baines, P., and Dong, B.W., (2007), Decadal to multidecadal variability and the climate change background: *Journal of Geophysical Research-Atmospheres*, v. 112.

Perkins, S.E., (in press), Biases and model agreement in projections of climate extremes over the tropical Pacific: *Earth Interactions*, doi: 10.1175/2011EI395.1

Power, S., and G. Kociuba, (in press), The impact of global warming on the Southern Oscillation Index. *Climate Dynamics*, doi:10.1007/s00382-010-0951-7.

Power, S.B., and Smith, I.N., (2007), Weakening of the Walker Circulation and apparent dominance of El Nino both reach record levels, but has ENSO really changed?: *Geophysical Research Letters*, v. 34, issue 18.

Power, S., Casey, T., Folland, C., Colman, A., and Mehta, V., (1999), Inter-decadal modulation of the impact of ENSO on Australia: *Climate Dynamics*, v. 15, p. 319-324.

Power, S.B., Tseitkin, F., Torok S., Lavery, B., Dahni, R., and McAvaney, B., (1998), Australian temperature, Australian rainfall and the Southern Oscillation, 1910–1992: coherent variability and recent change: *Australian Meteorological Magazine*, 47, 85-101.

Rayner, N.A., Parker, D.E., Horton, E.B., Folland, C.K., Alexander, L.V., Rowell, D.P., Kent, E.C., and Kaplan, A., (2003), Global analyses of sea surface temperature, sea ice, and night marine air temperature since the late nineteenth century: *Journal of Geophysical Research-Atmospheres*, v. 108.

Troup, A.J., (1965), Southern Oscillation: *Quarterly Journal of the Royal Meteorological Society*, v. 91, p. 490.

Wolter, K., and M.S. Timlin, (1993), Monitoring ENSO in COADS with a seasonally adjusted principal component index: *Proceedings of the 17th Climate Diagnostics Workshop*, Norman, OK, NOAA/NMC/CAC, NSSL, Oklahoma Clim. Survey, CIMMS and the School of Meteorology, University of Oklahoma, 52-57.

Wolter, K., and M. S. Timlin, (1998), Measuring the strength of ENSO events - how does 1997/98 rank?: *Weather,* 53, 315-324.

Other References

Cook Islands

Cook Islands' First National Communication under the United Nations Framework Convention on Climate Change (UNFCCC), (2000). Government of Cook Islands. http://unfccc.int/resource/docs/natc/cisnc2.pdf

Cook Islands Statistics Office, (2010). http://www.stats.gov.ck/Statistics/Demography/popn_estimate.htm

Cook Islands Country Profile, (2000). South Pacific Applied Geoscience Commission (SOPAC). http://dev.sopac.org.fj/VirLib/CP0001.pdf

Cook Islands Country Statistics, (2011). Secretariat of the Pacific Community Applied Geoscience and Technology Division (SOPAC). http://www.sopac.org/index.php/member-countries/cook-islands

East Timor

East Timor Country Brief, (2011). Australian Department of Foreign Affairs and Trade. http://www.dfat.gov.au/geo/east_timor/east_timor_brief.html

Timor-Leste Country Statistics, (2011). Government of Timor-Leste. http://timor-leste.gov.tl/?p=547&lang=en

Federated States of Micronesia

Federated States of Micronesia's First National Communication under the United Nations Framework Convention on Climate Change (UNFCCC), (1997). Government of Federated States of Micronesia. http://unfccc.int/resource/docs/natc/micnc1.pdf

Federated States of Micronesia's Pacific Adaptation to Climate Change (PACC), (2006). Report of in-country consultations. http://www.sprep.org/att/publication/000661_Kosrae_FSM_NationalPACCReport_Final.pdf

Federated States of Micronesia Country Statistics, (2011). Secretariat of the Pacific Community Applied Geoscience and Technology Division (SOPAC). http://www.sopac.org/index.php/member-countries/federated-states-of-micronesia

Fiji

Fiji's First National Communication under the United Nations Framework Convention on Climate Change (UNFCCC), (2005). Government of Fiji. http://unfccc.int/resource/docs/natc/fjinc1.pdf

Fiji's Pacific Adaptation to Climate Change (PACC), (2009). Report of in-country consultations. http://www.sprep.org/climate_change/pacc/reports_detail_country.asp?id=668

Fiji Country Statistics, (2011). Secretariat of the Pacific Community Applied Geoscience and Technology Division (SOPAC). http://www.sopac.org/index.php/member-countries/fiji-islands

Kiribati

Kiribati's First National Communication under the United Nations Framework Convention on Climate Change (UNFCCC), (1999). Government of Kiribati. http://unfccc.int/resource/docs/natc/kirnc1.pdf

Kiribati's National Adaptation Program of Action (NAPA), (2007). http://unfccc.int/resource/docs/napa/kir01.pdf

Kiribati Country Statistics, (2011). Secretariat of the Pacific Community Applied Geoscience and Technology Division (SOPAC). http://www.sopac.org/index.php/member-countries/fiji-islands

Marshall Islands

Marshall Islands' First National Communication under the Framework Convention on Climate Change (UNFCCC), (2000). Government of Marshall Islands. http://unfccc.int/resource/docs/natc/marnc1.pdf

Marshall Islands' Pacific Adaptation to Climate Change (PACC), (2010). Report of in-country consultations. http://www.sprep.org/att/publication/000669_RMI_National_PACCReport_Final.pdf

Marshall Islands Country Statistics, (2011). Secretariat of the Pacific Community Applied Geoscience and Technology Division (SOPAC). http://www.sopac.org/index.php/member-countries/marshall-islands

Nauru

Nauru's First National Communication under the United Nations Framework Convention on Climate Change (UNFCCC), (1999). Government of Nauru. http://unfccc.int/resource/docs/natc/naunc1.pdf

Nauru's Pacific Adaptation to Climate Change (PACC), (2006). Report of in-country consultations. http://www.sprep.org/att/irc/ecopies/countries/nauru/41.pdf

Nauru Country Statistics, (2011). Secretariat of the Pacific Community Applied Geoscience and Technology Division (SOPAC). http://www.sopac.org/index.php/member-countries/nauru

Niue

Niue's First National Communication under the United Nations Framework Convention on Climate Change (UNFCCC), (2000). Government of Niue. http://unfccc.int/resource/docs/natc/niunc1.pdf

Niue's Pacific Adaptation to Climate Change (PACC), (2006). Report of in-country consultations. http://www.sprep.org/att/irc/ecopies/countries/niue/33.pdf

Niue Country Statistics, (2011). Secretariat of the Pacific Community Applied Geoscience and Technology Division (SOPAC). http://www.sopac.org/index.php/member-countries/niue

Palau

Palau's First National Communication under the United Nations Framework Convention on Climate Change (UNFCCC), (2002). Government of Palau. http://unfccc.int/resource/docs/natc/plwnc1.pdf

Palau's Pacific Adaptation to Climate Change (PACC), (2010). Report of in-country consultations. http://www.sprep.org/att/publication/000674_Palau_NationalPACCReport_Final.pdf

Palau Country Statistics, (2011). Secretariat of the Pacific Community Applied Geoscience and Technology Division (SOPAC). http://www.sopac.org/index.php/member-countries/palau

Papua New Guinea

Papua New Guinea's First National Communication under the United Nations Framework Convention on Climate Change (UNFCCC), (2000). Government of Papua New Guinea. http://unfccc.int/resource/docs/natc/papnc1.pdf

Papua New Guinea Country Statistics, (2011). Secretariat of the Pacific Community Applied Geoscience and Technology Division (SOPAC). http://www.sopac.org/index.php/member-countries/papua-new-guinea

Samoa

Samoa's First National Communication under the United Nations Framework Convention on Climate Change (UNFCCC), (2000). Government of Samoa. http://unfccc.int/resource/docs/natc/samnc1.pdf

Samoa's Second National Communication under the United Nations Framework Convention on Climate Change (UNFCCC), (2010). Government of Samoa. http://unfccc.int/resource/docs/natc/samnc2.pdf

Samoa Country Profile, (2000). Secretariat of the Pacific Community Applied Geoscience and Technology Division (SOPAC). http://dev.sopac.org.fj/VirLib/CP0015.pdf

Samoa Country Statistics, (2011). South Pacific Applied Geoscience Commission (SOPAC). http://www.sopac.org/index.php/member-countries/samoa

Solomon Islands

Solomon Islands' First National Communication under the United Nations Framework Convention on Climate Change (UNFCCC), (2001). Government of Solomon Islands. http://unfccc.int/resource/docs/natc/slbnc1.pdf

Solomon Islands Country Profile, (2000). South Pacific Applied Geoscience Commission (SOPAC). http://dev.sopac.org.fj/VirLib/CP0011.pdf

Solomon Islands Country Statistics, (2011). Secretariat of the Pacific Community Applied Geoscience and Technology Division (SOPAC). http://www.sopac.org/index.php/member-countries/solomon-islands

Tonga

Tonga's First National Communication under the United Nations Framework onvention on Climate Change (UNFCCC), (2005). Government of Tonga. http://unfccc.int/resource/docs/natc/tonnc1.pdf

Tonga's Joint National Action Plan (JNAP) on Climate Change Adaptation and Disaster Risk Management 2010–2015. Government of Tonga. http://www.sprep.org/att/IRC/eCOPIES/Countries/Tonga/66.pdf

Tonga's Pacific Adaptation to Climate Change (PACC), (2009). Report of in-country consultations. http://www.sprep.org/att/publication/000665_Tonga_National_PACCReport_Final.pdf

Tonga Country Statistics, (2011). Secretariat of the Pacific Community Applied Geoscience and Technology Division (SOPAC). http://www.sopac.org/index.php/member-countries/tonga

Tuvalu

Tuvalu's First National Communication under the United Nations Framework Convention on Climate Change (UNFCCC), (1999). Government of Tuvalu. http://unfccc.int/resource/docs/natc/tuvnc1.pdf

Tuvalu's Pacific Adaptation to Climate Change (PACC), (2009). Report of in-country Consultations. http://www.sprep.org/att/publication/000662_Tuvalu_National_PACCReport_Final.pdf

Tuvalu Country Statistics, (2011). Secretariat of the Pacific Community Applied Geoscience and Technology Division (SOPAC). http://www.sopac.org/index.php/member-countries/tuvalu

Vanuatu

Vanuatu's First National Communication under the United Nations Framework Convention on Climate Change (UNFCCC), (1999). Government of Vanuatu. http://unfccc.int/resource/docs/natc/vannc1.pdf

Vanuatu Country Profile, (2000). South Pacific Applied Geoscience Commission (SOPAC). http://dev.sopac.org.fj/VirLib/CP0014.pdf

Vanuatu National Statistics Office, (2010). http://www.vnso.gov.vu/

Federated States of Micronesia

Glossary

A

Anthropogenic

Resulting from or produced by human beings.

Anthropogenic emissions

Emissions of greenhouse gases, greenhouse gas precursors, and aerosols associated with human activities, including the burning of fossil fuels, deforestation, land-use changes, livestock, fertilisation, etc.

Anthropogenic forcing – see also **Forcing**

A **forcing** that is caused by human activities including changes in greenhouse gas and aerosol concentrations and land-use changes.

Anomaly

In climate science, a deviation from the normal value of a variable. It is usually the deviation of a variable from the average value at a specific place and time.

Aragonite saturation state – see also **Ocean acidification**

Aragonite is a form of calcium carbonate that makes up the shells and skeletons of key organisms in reef ecosystems, including reef-building corals. The saturation state of aragonite in seawater (known as Ω) is a measure of the potential for the mineral to form or to dissolve. When the $\Omega = 1$, the seawater is in equilibrium with respect to aragonite, so aragonite does not dissolve or precipitate. When $\Omega > 1$ seawater is supersaturated with respect to aragonite and aragonite will precipitate, and when $\Omega < 1$ aragonite will dissolve. Aragonite saturations states above about 4 are considered optimal conditions for healthy coral reef ecosystems, with values below 3.5 becoming increasingly marginal for supporting healthy coral reef growth.

Attribution

Attribution is the process of identifying the most likely causes for the detected changes in the **climate**.

B

Bias – see **Model bias**

C

Carbon cycle

The term used to describe the flow of carbon (in various forms, e.g. as carbon dioxide) through the atmosphere, ocean, terrestrial biosphere and lithosphere.

Climate

Climate in a wider sense is the state, including a statistical description, of the climate system. Climate in a narrow sense is usually defined as the average weather, (or more rigorously, as the statistical description in terms of the mean and variability of relevant quantities), over a period of time ranging from months to thousands or millions of years. The relevant quantities are most often surface variables such as temperature, precipitation and wind. The classical period for averaging these variables is 30 years, as defined by the World Meteorological Organization. In various parts of this publication different averaging periods, such as a period of 20 years, are also used.

Climate change – see also **Climate variability**

Climate change refers to a change in the state of the climate that can be identified (e.g., by using statistical tests) by changes in the mean and/or the variability of its properties, and that persists for an extended period, typically decades or longer. Climate change may be due to natural internal processes or **external forcings**, or to persistent **anthropogenic** changes in the composition of the atmosphere or in land use.

This definition is the same as the one used by the Intergovernmental Panel on Climate Change and differs from that used by the United Nations Framework Convention on Climate Change which makes a distinction between climate change attributable to human activities and **climate variability** attributable to natural causes.

Climate model – see **Global climate model**

Climate model drift – see **Model drift**

Climate projection

A projection of the response of the climate system to emission or concentration scenarios of greenhouse gases and aerosols, or radiative forcing scenarios, often based upon simulations by climate models. Climate projections are distinguished from climate predictions in order to emphasise that climate projections depend upon the emission/concentration/radiative forcing scenario used, which are based on assumptions concerning, for example, future socioeconomic and technological developments that may or may not be realised and are therefore subject to substantial uncertainty.

Climate variability – see also Patterns of variability

Climate variability refers to variations in the mean state and other statistics (such as standard deviations, the occurrence of extremes, etc.) of the climate on all spatial and temporal scales beyond that of individual weather events. Variability may be due to natural internal processes within the climate system (internal variability), or to variations in natural or anthropogenic external forcing (external variability).

Climatology

The description and scientific study of climate.

CMIP3

Coupled Model Intercomparison Project (Phase 3) is a set of climate model experiments from 17 groups in 12 countries with 24 models. Climate model output from simulations of the past, present and future climate was collected by Program for Climate Model Diagnosis and Intercomparison at Lawrence Livermore National Laboratory in the US, during 2005 and 2006. The resulting CMIP3 dataset was used to inform the Fourth Assessment Report of the Intergovernmental Panel on Climate Change.

CMIP5

The fifth phase of the Coupled Model Intercomparison Project (CMIP5). In September 2008, 20 climate modelling groups from around the world, agreed to develop a new set of coordinated climate model experiments which will provide a wider range of emissions scenarios, and improved models and simulations for the 5th Assessment Report of the Intergovernmental Panel on Climate Change.

Cold Tongue – see **Equatorial Cold Tongue**

Convection

Vertical motion driven by buoyancy forces arising from static instability, usually caused by near surface warming in the case of the atmosphere, and by near-surface cooling or increases in salinity in the case of the ocean.

Convergence

In meteorology where winds flow from different directions toward each other, thus meeting at one point or along one line. Similarly, in oceanography, where water currents flow toward each other and meet. Horizontal convergence usually forces vertical motion to occur, such as convection.

Coriolis Effect

Air or water that is in motion is deflected to the right (of the direction of flow) in the Northern Hemisphere and to the left (of the direction of flow) in the Southern Hemisphere as a result of the rotation of the Earth. The Coriolis Effect is largest at the poles and diminishes to zero at the equator.

D

Downscaling

Downscaling refers to techniques that derive small-scale (at a single location or region) information from data on larger spatial scales, such as Global Climate Model output. Two main methods are generally applied: dynamical downscaling (using fine-resolution global or regional climate models) and statistical downscaling (using statistical relationships).

Dynamical downscaling

Dynamical downscaling uses a finer resolution atmospheric climate model, driven by large-scale data from a global climate model to derive local or regional scale information. The fine resolution model provides better representation of topography and land/sea boundaries. This method is computationally intensive and the results are strongly dependent on the choice of both the global climate model and the atmospheric model.

Statistical downscaling

Statistical downscaling techniques develop statistical relationships that link the large-scale climate variables with local-scale or regional climate variables. This technique maintains important information regarding locally observed historical trends and variability, while also introducing important aspects of change from the global climate models.

Driver (of climate change)

Any natural or human-induced factor that directly or indirectly causes a change.

Dynamic response (of ice sheets)

Rapid disintegration of ice sheets through dynamic processes.

E

Ekman Currents

Wind driven currents in the upper few tens of metres of the ocean that flow at 90 degrees to the right of the wind direction in the Northern Hemisphere and to the left in the Southern Hemisphere.

El Niño – see also El Niño-Southern Oscillation, La Niña

This is the warm phase of the El Niño-Southern Oscillation. El Niño events occur on average once every two to seven years. They are associated with basin-wide warming of the tropical Pacific Ocean east of the dateline and a weakening of the Walker Circulation.

Canonical El Niño – see also El Niño, La Niña, El Niño Modoki

This is characterised by warming of waters in the central and eastern Pacific Ocean and cooling in a horse-shoe pattern in the western Pacific Ocean.

El Niño Modoki

El Niño Modoki, also called the Central Pacific El Niño, is a recurring pattern of variability in the tropical Pacific, in which the maximum warming occurs in the central tropical Pacific rather than in the east. This represents a variation on the Canonical El Niño.

ENSO Modoki Index (EMI)

This is the difference between the sea-surface temperature anomalies averaged over the central equatorial Pacific and the out-of-phase variations in the far eastern and far western Pacific.

El Niño-Southern Oscillation (ENSO) – see also El Niño, La Niña

The term El Niño was initially used to describe a warm-water current that periodically flows along the coast of Ecuador and Perú, disrupting the local fishery. It has since become identified with a basin-wide warming of the tropical Pacific Ocean east of the dateline. This oceanic event is associated with a fluctuation of a global-scale tropical and subtropical surface pressure pattern called the Southern Oscillation. This naturally occurring coupled atmosphere-ocean phenomenon, with time scales of approximately two to seven years, is known as the El Niño-Southern Oscillation (ENSO). The state of ENSO is often measured by the Southern Oscillation Index (SOI) and sea-surface temperatures in the central and eastern equatorial Pacific.

During an ENSO event, the prevailing trade winds weaken, reducing upwelling and altering ocean currents such that the sea-surface temperatures warm, further weakening the trade winds. This event has a great impact on the wind, sea-surface temperature and precipitation patterns in the tropical Pacific. It has climatic effects throughout the Pacific region and in many other parts of the world. The cold phase of ENSO is called La Niña.

Ensemble

An ensemble refers to a group of model simulations used for climate projections. It may refer either to a group of simulations from different models; or to a group of simulations run on the same model but using slightly different starting conditions.

Equatorial Cold Tongue

This is a region of relatively cool surface water in the equatorial eastern Pacific Ocean and along the west coast of South America.

Equinox

The times of the year when the Sun crosses the plane of the Earth's equator, occurring around March 21 and September 22 and making the length of night and day approximately equal all over the Earth.

Evapotranspiration – see **Potential evapotranspiration**

External forcing – see **Forcing**

Extreme weather event

An event that is rare at a particular place and time of year. Definitions of rare vary, but an extreme weather event would normally be as rare as or rarer than the 10th or 90th percentile of the observed probability density function.

F

Flux adjustment

In order to prevent drift in climate simulations older climate models and a minority of the CMIP3 models use flux adjustment. Flux adjustment involves making small corrections to heat, freshwater and momentum transfers between ocean and atmosphere models, in order to make sure that the climate remains relatively stable.

Forcing – see also Anthropogenic forcing, Natural forcing

An agent that causes a change in the climate system. External forcing refers to agents outside the climate system, such as changes in greenhouse gases or solar variations. Internal forcing refers to natural climate variations, such as the Interdecadal Pacific Oscillation. Radiative forcing refers specifically to external forcings that change the net radiation at the tropopause.

G

Global Climate Model (GCM)

This is a numerical representation of the climate system based on the physical, chemical and biological properties of its components, their interactions and feedback processes, and accounting for all or some of its known properties. Coupled Atmosphere-Ocean General Circulation Models provide a representation of the climate system that is near the most comprehensive end of the spectrum currently available. There is an evolution towards more complex models with interactive chemistry and biology.

Global surface temperature

The global surface temperature is an estimate of the global mean surface air temperature. However, for changes over time, only anomalies, as departures from a climatology, are used, most commonly based on the area-weighted global average of the sea-surface temperature anomaly and land surface air temperature anomaly.

Gridded data – see also Reanalysis

A set of climate data that are given for the same time or average period on a regular grid in space. Data at each grid point represent the average value over a grid box whose size is determined by the spacing between the grid points (also called the grid resolution). Global climate model and reanalysis data are produced as gridded data.

H

Hadley Circulation

The major vertical movement of heated equatorial air and its north-south transfer into the mid latitudes, first proposed by George Hadley in 1735 as an explanation for the trade winds. It consists of the equatorward movement of the trade winds between about latitude 30° and the equator in each hemisphere, with rising wind components near the equator, poleward flow aloft, and, finally, descending components at about latitude 30° again.

Halosteric – see also Steric

Sea-level changes induced by changes in water density are called steric. Density changes induced by salinity changes are called halosteric.

Holocene

The last 12 000 years of geological time.

Homogenisation

Observed climate variables sometimes show sudden shifts in the average values or variability. Not all of these shifts are caused by real changes in climate. Non-climate related shifts can be due to changes in instrumentation, observation site, surrounding environment and observation practices, or other factors.

Homogenous – see also Homogenisation

Climate data homogenisation aims to adjust data if necessary, so that all variations in the data series are caused by real changes in the climate, and not due to changes in the way the data have been recorded.

Humidity – see **Relative humidity**

I

Ice discharge (dynamical)

Discharge of ice from ice sheets or ice caps caused by the dynamics of the ice sheet or ice cap (e.g. in the form of glacier flow, ice streams and calving icebergs) rather than by melt or runoff.

Ice sheet mass balance – see **Mass balance**

Indian Ocean Dipole (IOD)

The Indian Ocean Dipole (IOD) is a coupled ocean and atmosphere phenomenon in the equatorial Indian Ocean that affects the climate of countries that surround the Indian Ocean basin, particularly rainfall. The IOD is commonly measured by the Indian Ocean Dipole (IOD) Index.

Indian Ocean Dipole (IOD) Index

The IOD index measures the difference in sea-surface temperatures between the western tropical Indian Ocean (50°E to 70°E and 10°S to 10°N) and the eastern tropical Indian Ocean (90°E to 110°E and 10°S to 0°S).

Index

A number representing a measure of a particular feature of the climate system at a given time, varying with time and used as some measure of variability.

Indices – see **Index**

Insolation

The amount of solar radiation reaching the Earth at a given location in a given time.

Interannual

From year to year.

Interdecadal Pacific Oscillation (IPO) – see also Pacific Decadal Oscillation (PDO)

The Interdecadal Pacific Oscillation (IPO) is a natural recurring pattern of variability in tropical Pacific Ocean sea-surface temperatures occurring on periods of about 15 years and longer. While defined differently the IPO and PDO (Pacific Decadal Oscillation) describe essentially the same variability.

Interdecadal Pacific Oscillation (IPO) Index

A measure of the strength and phase of the Interdecadal Pacific Oscillation pattern.

Internal forcing – see **Forcing**

Intertropical Convergence Zone (ITCZ)

An east-west band of low-level wind convergence near the equator where the Southeast trade winds of the Southern Hemisphere meet the Northeast trade winds of the Northern Hemisphere. It is co-located with the ascending branch of the Hadley Circulation and has a associated band of heavy rainfall as the winds converge and moist air is forced upward.

L

La Niña – see also El Niño, El Niño–Southern Oscillation

The most common of several names given to cold phase of the El Niño-Southern Oscillation. La Niña is the counterpart to the El Niño warm event, although La Niña events tend to be somewhat less regular in their behaviour and duration. La Niña is associated with large-scale cooling of the surface waters of the eastern tropical Pacific Ocean and a strengthening of the Walker Circulation.

M

Madden Julian Oscillation

The Madden Julian Oscillation (MJO) is a global-scale feature of the tropical atmosphere that is characterized as an eastward moving pulse of cloud and rainfall near the equator that typically recurs every 30 to 60 days, but it is not always present.

Maritime Continent

The Maritime Continent consists of parts of Southeast Asia and the islands of Indonesia and the Philippines on the western equatorial edge of the Pacific, and includes large areas of ocean as well as the islands.

Mass balance (of ice sheets)

The mass balance is the net gain or loss of ice and snow for an ice sheet. It is related to difference between snow accumulation versus melt, runoff and iceberg calving.

Mean High Water (MHW)

The average of all high waters observed over a sufficiently long period.

Mean Higher High Water (MHHW)

The mean of the higher of the two daily high waters over a period of time.

Mean sea level – see also **Relative sea level, Sea level change/rise**

Mean sea level is normally defined as the average relative sea level over a period, such as a month or a year, long enough to average out transients such as waves and tides.

Meridional – see also **Zonal**

In meteorology, a flow in a direction that is parallel to a line of longitude; along a meridian; northerly or southerly; as opposed to **zonal**.

Model bias

Model biases are spurious differences between climate model simulations and observations. These may be caused by a number of factors including a lack of model resolution or an insufficiently realistic representation of certain physical processes. Systematic biases are errors that are common to a majority the climate models.

Model drift

Model drift refers to spurious trends in climate simulations that are not caused by changing external **drivers** (such as increased greenhouse gases or changes in solar radiation). Instead these spurious trends arise as a result of the way that models are initialised or imperfections in the representation of physical processes. Under many circumstances drift only introduces a small error in the estimation of climate trends however it must be accounted for where it is large.

Model skill

Model skill is a measure of how well a climate model can realistically represent the climate system.

Multivariate ENSO Index (MEI)

A measure used to describe ENSO combining six observed variables over the tropical Pacific. These six variables are: sea-level pressure, zonal and meridional components of the surface wind, sea-surface temperature, surface-air temperature, and total cloudiness fraction of the sky.

N

Natural forcing – see also **Forcing**

A **forcing** in the climate system due to natural causes as opposed to **anthropogenic forcing**, Natural forcing includes changes in solar output, the Earth's orbit and volcanic eruptions.

NINO3 index

An average of sea-surface temperature anomalies in the Pacific Ocean over the area 5°N to 5°S, 150°W to 90°W.

NINO3.4 index

An average sea-surface temperature **anomaly** in the central Pacific (latitude 5°N to 5°S; longitude 170°W to 120°W).

NINO4 index

An average of sea-surface temperature anomalies in the Pacific Ocean over the area 5°N to 5°S, 160°E to 150°W.

O

Ocean acidification – see also **Aragonite saturation state**

Ocean acidification is the name given to the ongoing decrease in the **pH** of the Earth's oceans, caused by their uptake of **anthropogenic** carbon dioxide from the atmosphere. When carbon dioxide dissolves in the ocean it lowers the **pH**, making the ocean more acidic.

Oceanic NINO3.4 Index (ONI)

An average of sea-surface temperatures anomalies in the Niño 3.4 region (latitude 5°N to 5°S; longitude 120° to 170°W).

P

Pacific Climate Change Science Program (PCCSP)

A collaborative research partnership between Australian Government agencies, 14 Pacific island countries and East Timor, and regional and international organisations.

Pacific Climate Change Science Program (PCCSP) Region

The region defined by the coordinates: 25°S-20°N and 120°E–150°W (excluding the Australian region south of 10°S and west of 155°E).

Pacific Decadal Oscillation (PDO)

A naturally recurring pattern of variability in the tropical and northern Pacific characterised by warming and cooling sea-surface temperature, similar to that of ENSO, although broader in a north-south direction. Oscillations in the PDO take multiple decades usually 20–30 years.

Parameterisation

Representing in an approximate form processes that cannot be explicitly resolved at the spatial or temporal resolution of the model (e.g. cloud formation, ocean eddies).

Patterns of variability – see also **Climate variability**

Natural variability of the climate system, in particular on seasonal and longer time scales, predominantly occurs with preferred spatial patterns and time scales, through the dynamical characteristics of the atmospheric circulation and through interactions with the land and sea surfaces. Examples include the **El Niño-Southern Oscillation**.

pH

A measure of the acidity or alkalinity of a solution, numerically equal to 7 for neutral solutions, increasing with increasing alkalinity and decreasing with increasing acidity. The pH scale ranges from 0 to 14.

Potential evapotranspiration

Evapotranspiration is the sum of evaporation from the land surface (e.g. from the soil and bodies of water such as lakes and rivers) and transpiration from vegetation. Potential evapotranspiration is defined as the evapotranspiration that would take place if there was an unlimited water supply. It is a representation of the environmental demand for evapotranspiration.

Probability Distribution Function (PDF)

A PDF describes the likelihood that a certain event or outcome will occur based on prior experience. For example a PDF of daily temperatures would provide information on how likely it is to have an extremely hot or cold temperature.

Pycnocline

Moving downward through the ocean, the pycnocline is the region where there is a rapid increase in density with depth. It acts as a barrier to mixing between deep and surface waters.

R

Radiative forcing – see **Forcing**

Reanalysis – see also **Gridded data**

An analysis combining many irregular meteorological or oceanographic observations from close to the same time into a physically consistent, complete **gridded data** set for a given time and usually for the whole globe.

Relative humidity

Relative humidity is defined as the amount of water vapour in the air, relative to the maximum amount of water vapour that the air is able to hold, without it condensing (expressed as a percentage).

Relative sea level is sea level measured by a tide gauge with respect to the land upon which it is situated.

Relative sea-level rise – see also **Mean sea level, Sea level change/rise**

Relative sea level rise occurs where there is a local increase in the level of the ocean relative to the land, which might be due to ocean rise and/or land level subsidence.

Rossby wave

Also known as a planetary wave, it is a large, slow-moving, planetary-scale wave generated in the troposphere by ocean-land temperature contrasts and topographic forcing (winds flowing over mountains), and affected by the **Coriolis Effect** due to the earth's rotation. Rossby waves are also observed in the ocean.

S

Sea level change/rise – see also **Mean sea level, Relative sea-level rise, Thermal expansion**

Sea level can change, both globally and locally, due to; (1) changes in the shape of the ocean basins; (2) changes in the total mass of water and, (3) changes in water density.

Factors leading to sea level rise under global warming include both increases in the total mass of water from the melting of land-based snow and ice, and changes in water density from an increase in ocean water temperatures and salinity changes.

Sea-surface temperature

The temperature of the ocean surface. The term sea-surface temperature is generally representative of the upper few metres of the ocean as opposed to the skin temperature, which is the temperature of the upper few centimetres.

Solstice

The times of the year when the Sun is at its greatest distance from the equator, occurring around June 21, when the Sun reaches its northernmost point on the celestial sphere, or around December 22, when it reaches its southernmost point.

Southern Annular Mode (SAM)

The Southern Annular Mode (SAM) is the most important recurring pattern of natural variability in the Southern Hemisphere outside of the tropics. Oscillations in the SAM are associated with shifts in the position and strength of the mid-latitude westerly winds.

Southern Annual Mode (SAM) Index

Index measuring the difference in surface pressure between latitudes 40ºS and 65ºS. A positive SAM index corresponds to a southward movement and intensification of the sub-tropical westerly winds.

Southern Oscillation – see also **El Niño-Southern Oscillation**

Fluctuation of a global-scale tropical and subtropical surface pressure pattern.

Southern Oscillation Index (SOI)

The Southern Oscillation Index (SOI) is calculated from the monthly or seasonal fluctuations in the air pressure difference between Tahiti and Darwin.

South Pacific Convergence Zone (SPCZ)

A persistent and greatly elongated zone of low-level **convergence** extending from approximately 140°E near the equator to approximately 120°W at 30°S. The zone is not quite linear, but is oriented more west to east near the equator and has a more diagonal orientation (northwest to southeast) at higher latitudes.

SPCZ Position Index

The SPCZ Position Index is a measure of SPCZ location and is calculated as the normalised November-April difference in 9am (local time) in mean sea-level pressure between Suva and Apia. The SPCZ Position Index defines the latitude of the SPCZ between longitudes 180°W and 170°W.

Standardised Precipitation Index (SPI)

The Standardised Precipitation Index (SPI) is an **index** based on the probability of recording a given amount of precipitation. The probabilities are standardized so that an index of zero indicates the median precipitation amount. The index is negative for drought, and positive for wet conditions.

Statistical downscaling – see **Downscaling**

Steric – see also **Halosteric, Thermosteric**

Steric effects refer to the expansion and contraction of sea water.

Storm surge

The temporary increased height of the sea above the level expected from tidal variation alone at that time and place due to extreme meteorological conditions.

Stratosphere

The region of the atmosphere extending from the top of the troposphere at heights of roughly 10–17 km, to the base of the mesosphere at a height of roughly 50 km.

Sub-tropical High Pressure System

Areas of raised surface pressure between latitudes 20° and 40°.

T

Thermal Expansion – see also **Sea level change/rise, Mean sea level**

The increase in volume (and decrease in density) that results from warming water.

Thermocline

Moving downward through the ocean, the region where there is a rapid reduction in temperature with depth. The thermocline separates warm surface waters from cold deep waters.

Thermosteric – see also **Steric**

The expansion or contraction of sea water due to heating or cooling.

Time-series

The values of a variable generated successively in time. Graphically, a time series is usually plotted with time on the horizontal axis (x-axis), and the values of the variable on the vertical axis (y-axis).

Trade winds

The wind system, occupying most of the tropics that blow from the subtropical high pressure areas toward the equator.

Tropical cyclone

A tropical cyclone is a tropical depression of sufficient intensity to produce sustained gale force winds (at least 63 km per hour). A severe tropical cyclone produces sustained hurricane force winds (at least 118 km per hour). Severe tropical cyclones correspond to the hurricanes or typhoons of other parts of the world.

Troposphere

The lowest part of the atmosphere from the surface to about 10 km in altitude in mid-latitudes (ranging from 9 km in high latitudes to 16 km in the tropics on average), where clouds and weather phenomena occur.

Trough

An elongated region of low atmospheric pressure.

W

Walker Circulation

The Walker Circulation is the east-west circulation of air, oriented along the Equator, across the Pacific region.

Warm Pool (also known as **West Pacific Warm Pool** and **Indo-Pacific Warm Pool**)

An extensive pool of the world's warmest water, with temperatures exceeding 28–29°C extending from the central Pacific to the far eastern Indian Ocean. The PCCSP focuses on the region of the Warm Pool to the east of 120°E.

West Pacific Monsoon

A monsoon is a tropical and subtropical seasonal reversal of both surface winds and associated rainfall, caused by differential heating between a continental scale land mass and the adjacent ocean. The Western Pacific Monsoon is the eastern edge of the Indonesian or Maritime Continent Monsoon, and the southern extension of the larger Asian-Australian Monsoon system.

Z

Zonal – see also Meridional

In meteorology, latitudinal, that is, easterly or westerly; opposed to meridional.

www.pacificclimatechangescience.org

Australian Government
AusAID

Australian Government
Bureau of Meteorology

Australian Government
Department of Climate Change
and Energy Efficiency

CSIRO